2ICI

"SECOND INTERNATIONAL CONFERENCE ON ISOTOPES"

MILLENNIUM SYDNEY
12 - 16 OCTOBER 1997

CONFERENCE PROCEEDINGS

PAPERS 61 - 113

HOSTED BY THE
AUSTRALIAN NUCLEAR ASSOCIATION INC.

^{226}Ra MEASUREMENT BY THERMAL IONISATION MASS SPECTROMETRY : USE OF ^{226}Ra AND ^{14}C FOR GROUNDWATER DATING

L. DEVER[(1)] and C. HILLAIRE-MARCEL[(2)]

(1) Laboratoire d'Hydrologie et de Géochimie Isotopique UNIVERSITE PARIS-SUD 91405 91405 ORSAY , FRANCE.
(2) GEOTOP, UNIVERSITE DU QUEBEC A MONTREAL 1200 Saint Alexandre H3C3P8 MONTREAL, CANADA.

SUMMARY

The measurement of radium by TIMS allows analysis on small water samples (100 ml) . After Ra /Ba separation by chromatography the radium is measured by mass spectrometry with an uncertainty of 2 %. Radium with an half life of 1620 years is a very interesting radichronometer in a time range (0-5000) for which the radiocarbon datation on total dissolved inorganic carbon is quite difficult. Three sources of Radium has been identified: the radium coming from the dissolution of carbonates, the radium issued from ^{230}Th decay, ^{230}Th which is insoluble and absorbed on the grain surface and the radium produced by recoil effect.
In the unconfined aquifer with ages from 0 to 4000 the dissolution process is the major source. For older water in the confined part of the aquifer, the radium produced by the decay of the absorbed ^{230}Th cannot be neglected. The radium produced by recoil effect is very low. Through a geochemical model based on strontium concentration (which has the same chemical behaviour of radium) the three sources of radium are taken in account for an age calculation. The isochrone between radium and radiocarbon ages can be calculated: [age "^{14}C"] = 0,813 . [age "^{226}Ra"] with r = 0,91.

INTRODUCTION

^{226}Ra have an half life (1620 years) which is very interesting in hydrogeology for groundwater datation between a range covered by ^{3}H and ^{14}C. For many hydrological studies, datation by radiocarbon between 0 and 5000 B.P. is quite hazardous because of: the variation of the input fonction, the anthropogenic effects, the difficulty to assume a chemical steady state for radiocarbon models based on chemistry.

Under such conditions groundwater datation by ^{226}Ra can be useful for the validation of the radiocarbon age as ^{226}Ra and ^{14}C can be considered as two different tracers for matrix-water intercations. Since now over ten years attempts at using ^{226}Ra have often been made (1,2,3). Three methods have been investigated : (i) The radon emanation methods (^{222}Rn daugther product of ^{226}Ra) obtained by alpha scintillating counting (4,5), (ii) Direct measurement of ^{226}Ra by alpha spectrometry (6,7), (iii) Measurement of ^{226}Ra by Ge(Li) gamma ray sprectrometric method. All these methods need a large amount of water. ^{226}Ra measurement by Thermal Ionization Mass Spectrometry (TIMS) has been recently developped in uranothhorites and corals (8). Applying this method to natural low mineralised waters needs a 100 ml sampling only. The small amount of water necessary allows the measurement of ^{226}Ra concentration in groundwater, soil solid phase but also in water of the unsaturated zone. It's then possible to describe the ^{226}Ra behaviour in the water rock interactions during the mineralization of the water.

The main difficulty is the separation of Ra from Ba as Ba is 10^2 to 10^4 times more abundant than Ra in natural water samples.

the Ra-Ba separation can be obtained by ion-echange separation (9,10), in this study we develop a method based on a two-columns chromatography separation.

ANALYSIS

In order to calculate the efficiency of the Ra/Ba separation the water samples were spiked with ^{228}Ra. The spike is extracted from a Th nitrate and calibrated against a NBS ^{226}Ra standard.

After complete evaporation of the solution and dissolution in 2.5N HCl, the first stage of purification is to separate Ra and Ba from the bulk using a cation exchange resin. According to the method described previously (10) we introduce 3 ml 2.5N HCl sample on the resin and then wash it with 20 ml 2.5N HCl and 10 ml 6N HCl (flow rate 0.12 ml. min^{-1}). The ellution takes place with 22 ml 6N HCl, the eluted solution is then evapored.

A second column is used for the separation of Ra from Ba. The column is an inert substrate (Sr Spec from ElChrom ™) with a solution of 4,4'(5')bis-(tetra-buthylcyclohexano)-18-crown-6 in 1-octanol (11). The best separation of Ra and Ba is obtained with 0.3 ml of 3N HNO3 sample eluded by 0.7 of 3N HNO3. The Ra elution is then evaporated to dryness.

The sample is re-dissolved in 10 ml of 3N HNO3 and mixed with 2 ml of an activating solution (12). For TIMS measurement, the solution is loaded onto rhenium filament. Ra ionisation occurs between 1240-1350 °C after a pre-heating of 45 minutes at 1100°C for the elimination of the isobaric interferences. The mass ^{226}Ra gives between 600 and 3000 cps for a background of 4 cps. the overall analytical uncertainety is closed to 2%. U concentration and U-isotope ratios has been measured according to the routine procedure described by Gariépy et al. (13)

SAMPLING

Water samples of the Chalk aquifer in the Paris basin has been collected in severals wells used for public water supply. The chalk aquifer can be divided in two major parts: a) the unconfined aquifer located in the Chalk outcrop b) the confined aquifer under the tertiary layers. The water of the unsaturated zone have been sampling using in situ filtering devices. Soil and chalk profils has been also collected foir analysis. Chemical (majors and traces elements) and isotopic measurements ^{18}O,^{2}H,^{13}C,^{14}C, ^{234}U,^{238}U,^{226}Ra have been performed on the water samples and the solid phases.

RESULTS

The radium activities in the water vary from 0.045 to 4,096 dpm. $kg^{-1}$with a mean value of 0,26 dpm. kg^{-1} and 0,69 dpm. kg^{-1} for unconfined and confined aquifer respectively.Barium and Strontium have similar chemical behaviour with respect to Radium. In the chalk aquifer a strong relationship exists between Radium and Strontium concentrations (fig.1).

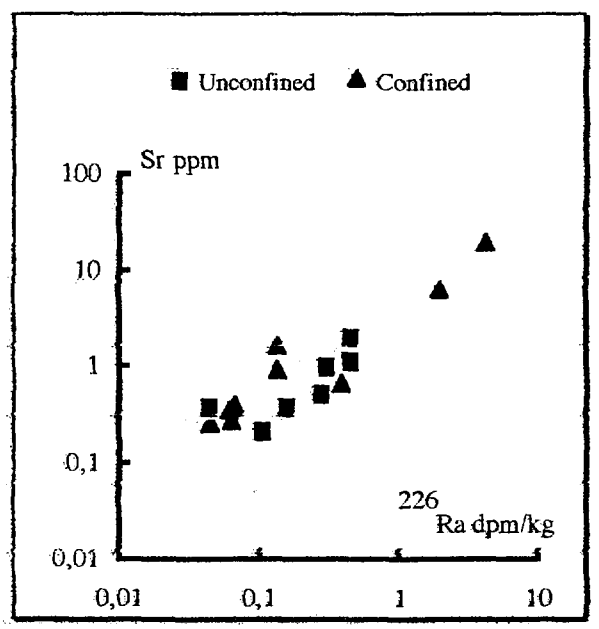

Fig. 1 : Relation between Stontium and Radium concentrations in the chalk aquifer.

In such diagram the correlation is different for the unconfined and the confined aquifer. Radium and Strontium concentrations are quite homogeneous in the solid phase, at the opposite the barium concentration is variyng largely in the chalk, by the way no correlation exists between Baryum and Radium. Radium is correlated to the ^{238}U concentration throught two relationships for unconfined and confined aquifer (Fig.2).

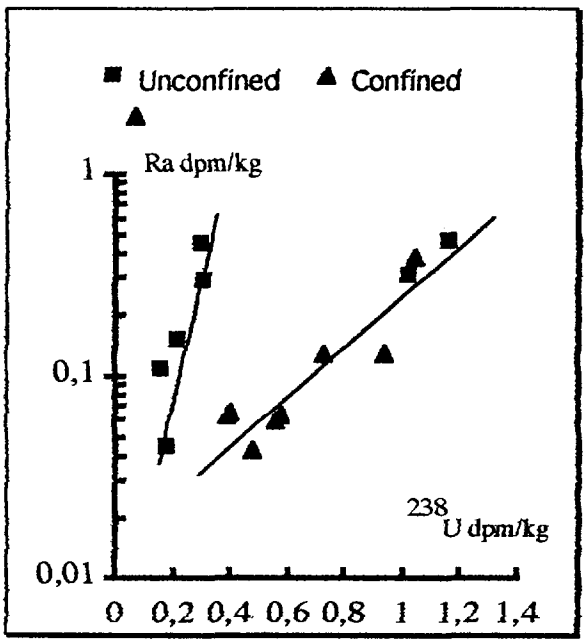

Fig. 2 : Relation between Radium and Uranium concentrations in the chalk aquifer.

In both cases the range of variation of Radium concentration are similar but the range of variation for 238U concentration is much wider for the confined than for unconfined aquifer.

DISCUSSION

The relation which takes place between Radium and Strontium indicates that dissolution of Radium is the main source for radium mineralization in the unconfined zone. By experience of dissolution of chalk in laboratory the radium coefficient distribution during dissolution precipitation processes has been measured. Kr_a is closed to 1(Hillaire Marcel et al. in prep.). Considering $[Ra]_L = [Sr]_L . [Ra]_S / [Sr]_S$ we can express the concentration of radium issue from dissolution as :

$$[Ra]_{diss} = [Ra]_S / [Sr]_S . [Sr]_L . e^{-\lambda 226 . t} \quad (1)$$

The secular equilibrium is attained between ^{234}U in the water and ^{230}Th. If we assume that the ^{226}Ra produced by ^{230}Th is dissolved, the radium concentration issue from desorption of the ^{230}Th absorbed on the solid phase can be written as :

$$[Ra]_{des} = K_{des} . [^{234}U]_S . \lambda_{226} . (1 - e^{-\lambda 226 . t}) \quad (2)$$

where K_{des} is a function of the specific surface of the solid phase.

The produced by recoil effect can be written as :

$$[Ra]_{rec} = K_{rec} . [^{230}Th]_S . \lambda_{230} . (1 - e^{-\lambda 226 . t}) \quad (3)$$

where K_{rec} is a function of the recoil effet which can be determined by assymptotic resolution.
Combining the equations (1),(2),(3) we obtain :

$$t = -1/\lambda_{226} \ln \{ Ra\ tot - (K_{des} . [^{234}U] . \lambda_{234}) - (K_{rec} . [^{230}Th] . \lambda_{230}) \} / \{ ([Ra]_S / [Sr]_S . [Sr]_L) - (K_{des} . [^{234}U] . \lambda_{234}) - (K_{rec} . [^{230}Th] . \lambda_{230}) \}$$

The "ages" calculated by "Radium model" can be compared to the ages obtained by radiocarbon (14). The radiocarbon ages have been calculated through a chemical and isotopic model corrected by trace elements partitioning during the dissolution precipitation process (Fig. 3).

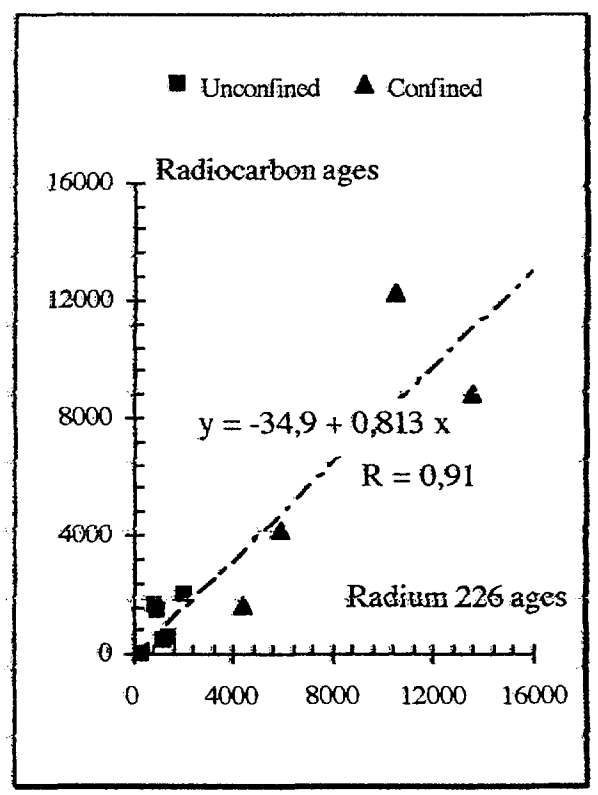

Fig. 3 : Correlation between radiocarbon and radium ages of the chalk aquifer.

The relation between radiocarbon ages and radium ages is good for the unconfined and confined aquifer, however the uncertainities are larger for ages up to 5000.

CONCLUSION

TIMS measurements of radium dissolved in the water allows a small water sampling. The radium concentration can be measured in the unsaturated, saturated zone and in the solid phase. The dissolved radium in the unconfined aquifer comes mainly from dissolution process and the radium concentration can be monitored by strontium one's. In the confined part, for much older ages, a part of the radium concentration is coming from the ^{230}Th which is absorbed on the grain surface. The recoil effect appears to be a very small contribution to the radium in solution. The three sources of radium are taking in account in a geochemical model based on the strontium concentration in water, and thorium and uranium concentration in the solide phase. An isochrone between radium and radiocarbon ages can be established. Through this model the radiocarbon ages calculated in a carbonated aquifer can be validated. The range for the best fit between the ages obtained by the two radiochronometer is from 0 to 5000. The interest of such study is evident for datation of the groundwaters using two different isotopic tracers.

REFERENCES

(1) Gellermann R., Fröhlich K., Jordan H. Groundwater studies with uranium series desequilibrium, in : Groundwater Monitoring and Management. Proceeding of the Dresden Symposium, march 1987. IAHS n° 173, pp 113-120, 1992.

(2) Osmond J.K., Ivanovich M. Uranium series mobilization and surface hydrology, in : Uranium series disequelebrium; Aplications eo Earth, Marine and Environmental Sciences. Ivanovich M., Harmon R.S. eds., pp 259-289, Clarendon Press, Oxford, 1992.

(3) Osmond J.K., Cowart J.B. Groundwater, in : Uranium series disequelebrium; Aplications eo Earth, Marine and Environmental Sciences. Ivanovich M., Harmon R.S. eds., pp 290-333, Clarendon Press, Oxford, 1992.

(4) Bhat S.G., Krishnaswami S., Rama D. Radon concentrations of air over the eastern Arabian sea. Proc. Indian Acad. Sci., 80, pp 109-116, 1974.

(5) Mathieu G.G. ^{222}Rn-^{226}Ra technique of analysis. Annual tech. Rep. C00-2185-0 to ERDA, Lamont-Doherty Geol. Obs., Palissades, NY, 1977.

(6) Koide M., Bruland K.W. The electrodeposition and determination of radium by isotopic dilution in sea water and in sediments simultaneously with other natural radionuclides. Anal. Chim. Acta. 75, 1-19, 1975.

(7) Rodrigez-Alvarez M.J., Sanchez F. Measurement of radium and thorium isotopes in environmental samples by alpha-spectrometry. J. of Radioanal.and Nuclear Chem.,191,1,3-13, 1995.

(8) Ben Othman D., Birck J.L., Allegre C. Detremination of 226/228 Ra and Ra concentration by spectrometry. Chem. Geol., 70, 172, 1988.

(9) Cohen A.S., O'Nions R.K. precise determination of femtogram quantities of radium by thermal ionisation mass spectrometry. Anal. Chem., 63, 2705-2708, 1991.

(10) Volpe A.M., Olivares J.A., Murrell M.T. Determination of radium isotopes ratios an abundance in geologic samples by thermal ionisation mass spectrometry. Anal. Chem., 63, 913-916, 1991.

(11) Chabaux F. Systématique ^{238}U-^{230}Th-^{226}Ra dans les roches volcaniques: développements analytiques et étude des processus de fusion. Thesis University Paris 7, Paris, pp339, 1993.

(12) Birck J.L., K,Rb, Sr isotopic analysis: application to Rb-Sr chronology, Chem. Geol., 56, 73-83, 1986.

(13) Gariépy C., Ghaleb B., Hillaire-Marcel C., Mucci A., Vallières S. Early diagenetic process in Labrador Sea sediments: Uranium-isotope geochemistry; Can. J. Earth Sci., 31, 1, 28-37, 1994.

(14)Klopmann., Dever L., Edmunds W.E. : Residence time of chalkgroundwaters in the Paris basin and the north German basin : a geochimical approach. . Accepted Applied Geochemistry, 1997.

Determination of ^{222}Rn in Water Samples from Wells and Springs in Tokyo by a Modified Integral Counting Method

Y HOMMA, Y MURASE, K HANDA and I MURAKAMI
Laboratory for Radiopharmaceutical Chemistry, Kyoritsu College of Pharmacy, 1-5-30, Shibakoen, Minato-ku, Tokyo 105, Japan.

SUMMARY. ^{222}Rn concentrations in water collected from private wells and springs in Tokyo were measured with a liquid scintillation spectrometer using a modified integral counting method. The ^{222}Rn concentrations ranged from 0.2 to 22.9 Bq/L and averaged 4.8 Bq/L. The errors due to the air luminescence counts and the interferences from ^{220}Rn and ^{219}Rn have been discussed and evaluated. ^{222}Rn samples of 0.2 Bq/L can be determined within an overall uncertainty of 3.1 %. The liquid scintillation method which agitate the sample water directly with a liquid scintillation cocktail was compared with this method and evaluated.

1. INTRODUCTION

Homma and Murakami have extended the integral counting method of liquid scintillation counting to the determination of the absolute disintegration rates of ^{226}Ra samples (1). In a preceding paper (2), we have measured the zero detection threshold of a liquid scintillation system, an average energy required to produce a measurable pulse, by measuring a standardized ^{3}H samples and proposed a high accuracy modified integral counting method by extrapolating the integral counting curve to the zero detection threshold.

With the aim of measuring natural occurring ^{222}Rn in natural waters, we have applied the modified integral counting method to analysis of ^{222}Rn samples of a wide variety of quench levels and obtained more accurate results than the conventional integral counting method and the efficiency tracing method (3).

In this study, the modified integral counting method has been applied to the determination of ^{222}Rn samples from private wells and springs in Tokyo. We have also examined and discussed the interferences from ^{220}Rn and ^{219}Rn and the effect of air luminescence counts on determination of ^{222}Rn by liquid scintillation counting.

2. EXPERIMENTAL

Sample preparation
To a 2 L of water sample in a 2.10 L plastic bottle, a 30 mL of toluene was added and the bottle was then capped and shaken vigorously for 5 min. Duplicate water samples were collected from each well and spring. The sample bottle was cooled to about 10 °C during transportation from the sampling site to our laboratory. After allowing the bottle to stand for 30 min at the room temperature, a 21 mL of the toluene in the bottle was transferred into a standard counting vial, in which PPO - 2,5-diphenyloxazole was placed in advance. The concentration of PPO in the toluene solution was 4 g PPO per litter toluene. The ^{222}Rn in the vial was allowed to remain for 3.5 h before measurement. During this time, the daughters ^{218}Po, ^{214}Pb, ^{214}Bi and ^{214}Po came to transient equilibrium with ^{222}Rn. Loss of ^{222}Rn during transportation from the sampling site to our laboratory (usually within 1-2 h) was negligible, because a large portion of ^{222}Rn is dissolved in cooled toluene and water in the air-tight bottle.

Solvent extraction of ^{222}Rn
By definition, the solubilities of ^{222}Rn in toluene and water are given by the relation, respectively:

$$\frac{A_t/V_t}{A_a/V_a} = \beta \qquad (1)$$

$$\frac{A_w/V_w}{A_a/V_a} = \beta' \qquad (2)$$

where A_t, is the activity of ^{222}Rn in the toluene, A_a the activity of ^{222}Rn in the air space above the toluene, A_w the activity of ^{222}Rn in the water, respectively, V_t is the volume of the toluene, V_a the volume of the air space, V_w the volume of

the water, respectively, and β is the Ostwald's coefficient of solubility of ^{222}Rn in toluene at the temperature of the sample water, β' the Ostwald's coefficient of solubility of ^{222}Rn in water at the temperature of the sample water, respectively. Combining the (1) and (2) gives

$$A_a : A_t : A_w = (V_a/\beta V_t) : 1 : (\beta' V_w/\beta V_t). \quad (3)$$

Then the total activity of ^{222}Rn in the sample water at the sampling time, A_T, is

$$A_T = A_a + A_t + A_w$$

$$\text{or } A_T = A_t(V_a/\beta V_t + 1 + \beta' V_w/\beta V_t). \quad (4)$$

In actual practice the numerical values to be substituted are β = 12.0, β' = 0.239 at 23 °C , V_a = 70 mL, V_t = 30 mL and V_w = 2000 mL. Using these values, we get,

$$A_T = A_t(0.194 + 1 + 1.328) = 2.52A_t. \quad (5)$$

Since about 40 % of ^{222}Rn dissolved in 2 L of sample water can be collected, it is clear that this method is successful for the measurement of low level ^{222}Rn in natural waters.

Measurements

The ^{222}Rn samples were measured with an Aloka liquid scintillation spectrometer, Model LSC-3500 (Aloka Co.Ltd.Tokyo, Japan) using a modified integral counting method (2). The measured integral counting curve was extrapolated not to the zero pulse-height, but to the zero detection threshold, of the liquid scintillation spectrometer. Based on analysis of the integral pulse-height spectra of standardized ^{3}H samples, it was determined to be 2.4 ± 0.10 keV below zero pulse-height. Samples were usually measured for 100 minutes.

3. RESULT AND DISCUSSION

Figure 1 shows the distribution of ^{222}Rn concentrations found in water samples collected from 163 private wells (A), 14 springs (B), and 163 private wells and 14 springs (C) in Tokyo. The average ^{222}Rn concentration for spring waters (8.5 Bq/L) is higher than that for private well waters (4.5 Bq/L) by a factor of 1.9. ^{222}Rn concentrations for all samples ranged from 0.2 to 22.9 Bq/L and averaged 4.8 Bq/L: About 63.9 % of all samples had ^{222}Rn concentrations of 5 Bq/L or less. The results of the duplicate measurements generally agreed to within 5 % and were averaged and reported one value.

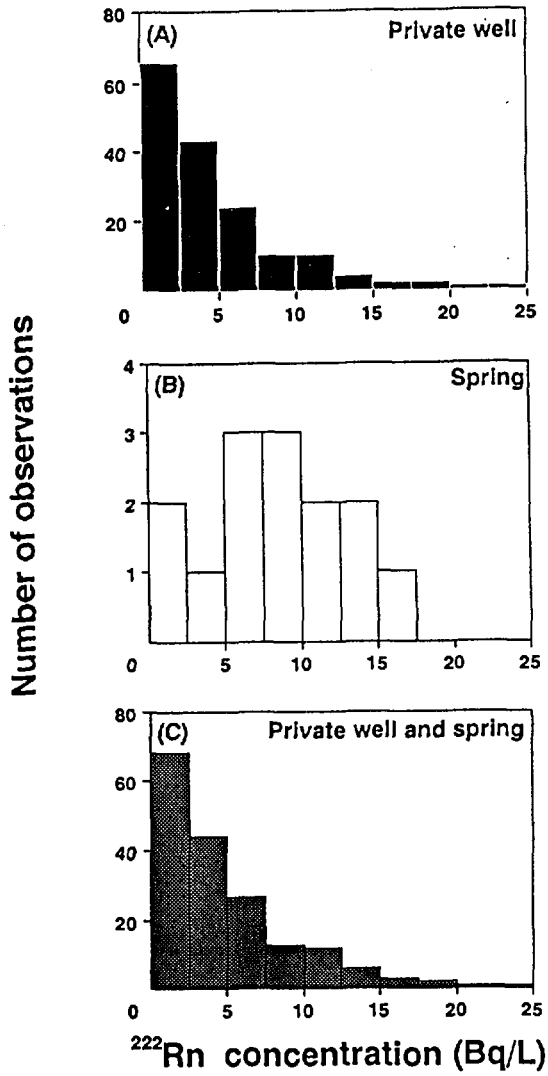

Fig. 1. The distribution of ^{222}Rn concentrations found in samples collected from (A) 163 private wells; (B) 14 springs; (C)163 private wells and 14 springs in Tokyo.

The highest ^{222}Rn concentrations were present in samples from wells and springs along the five rivers. These elevated ^{222}Rn concentrations, however, are still 2 orders of magnitude lower than the ^{222}Rn concentration found in the hot spring water at Misasa Hot Spring (1800 Bq/L), which is one of the most ^{226}Ra-rich areas in Japan. For comparison ^{222}Rn concentrations in public water supplies were also measured: The average concentration was 0.1 Bq/L, which is only 1/44 of the average ^{222}Rn concentration for all samples from wells and springs.

Interferences from ^{220}Rn and ^{219}Rn

Considering the abundance and half-lives of ^{232}Th and ^{238}U, it is reasonable to assume that, in most cases, ^{220}Rn (55.6 s) is possibly dissolved in toluene in the sampling bottle together with ^{222}Rn. However, ^{220}Rn and its daughter ^{216}Po (0.15 s) will have decayed completely by the time of measurements (usually 5-6 h after sampling). Moreover, the calculations based on the Bateman equations show that the sum of the activities due to the daughters of ^{218}Po (^{212}Pb, ^{212}Bi, ^{212}Po and ^{208}Tl), which is controlled by ^{212}Pb (10.64 h), is about 0.33 % of the initial activity of ^{220}Rn at the time of measurements. Therefore, it is clear that ^{220}Rn and its daughters would not have a large effect upon the determination of ^{222}Rn, even if the activity of ^{220}Rn is several times larger than that of ^{222}Rn. A large portion of ^{219}Rn is not allowed to diffuse out of earth and rock into environmental water samples due to its short half-life (3.96 s). Most of the daughters of ^{219}Rn, if present, will have decayed by the time of measurements, and they are seldom present at levels requiring measurement in the environment. Thus, interferences from ^{219}Rn and its daughters can be neglected too.

Air luminescence

As shown in Figure 2, ^{222}Rn and its α-emitting daughters in the air space above the liquid scintillator produce the air luminescence counts which lead to errors in quantitative determination of ^{222}Rn by liquid scintillation counting unless necessary corrections for the counts are made (4), (5): when we measure the ^{222}Rn in 9.0, 12.0, 15.0, 18.0, 21.0 and 22.0 mL of toluene-base scintillator solution, the estimated errors due to the air luminescence counts are: 5.3, 3.2, 2.0, 1.0, 0.3 and 0.2%, respectively (Table 1). The error can be eliminated spectrum analysis of ^{222}Rn sample. However, the most practical method for minimizing the error is to measure ^{222}Rn in a relatively larger volume of scintillator as is the case of this study.

Table 1. Distribution of ^{222}Rn and the daughters between the air space above the liquid scintillator and the liquid scintillator

Volume of air space (mL)	Volume of liquid scintillator (mL)	Percent of ^{222}Rn and daughters in the air space	Percent of ^{222}Rn and daughters in the liquid scintillator	Percent of air luminescence counts
14	9	11.5	88.5	5.3
11	12	7.1	92.9	3.2
8	15	4.3	95.7	2.0
5	18	2.3	97.7	1.0
2	21	0.8	99.2	0.3
1	22	0.4	99.6	0.2

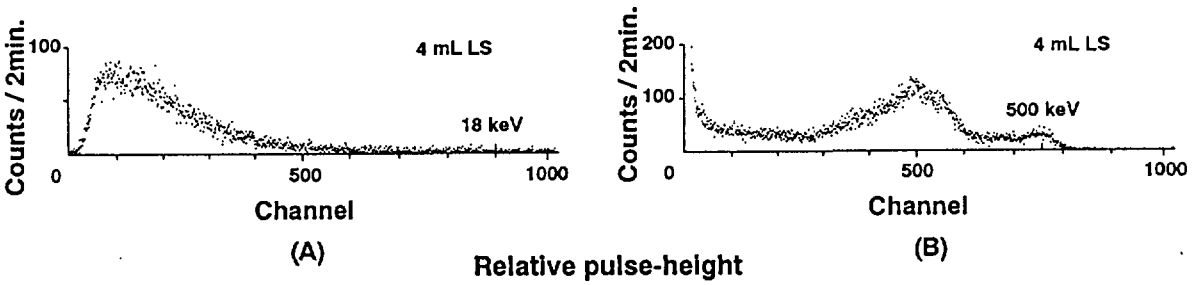

Fig. 2. Pulse-height spectra of ^{222}Rn sample measured with (A) 1024-channel analyzer of an Aloka LSC-3500 liquid scintillation spectrometer which was set to measure from approx. 1 to 20 keV; (B)another 1024-channel analyzer of LSC-3500 liquid scintillation spectrometer which was set to measure from approx. 1 to 500 keV. *LS=liquid scintillator

Advantages of the modified integral counting method

A method which agitates sample water (usually about 10 mL) with a liquid scintillation cocktail is rapid and practical when the activity of ^{222}Rn is high enough to obtain a statistically accurate value in a short time. However, it is not suitable for measurements of low level ^{222}Rn samples, because it can collect only 1.0 % of ^{222}Rn in 1 L of sample water. On the other hand, this method can collect about 40 % of ^{222}Rn dissolved in 2 L of sample water. It is clear, therefore, that this method is successful for the measurement of low level ^{222}Rn in natural waters.

More important, by adding 10 mL of water sample, it is possible also to add variable amounts of quench. In some cases sample water is preserved with nitric acid. Moreover, water itself is a strong quencher too. Therefore, an accurate quench correction method for strongly quenched samples is required. As shown in Fig.3, the slope of the integral counting rate curve increases as quench level of the ^{222}Rn sample increases. Therefore, it is clear that the modified integral counting method gives more accurate ^{222}Rn concentrations for water samples of a wide variety of quench than the conventional integral counting method (3).

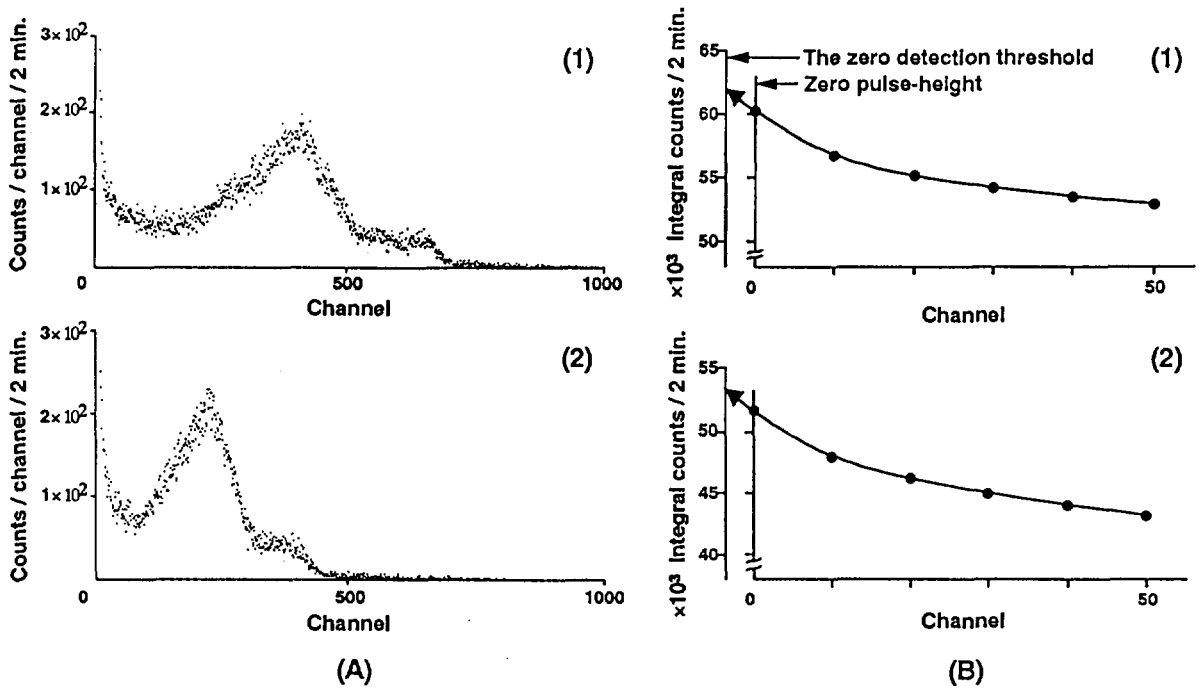

Fig. 3. Differential pulse-height spectra (A) and integral counting rate curves (B) for ^{222}Rn dissolved in a liquid scintillator. (1)for slight quench; (2)for strong quench.

Precision is calculated as the sum of the maximum estimates of possible errors. The principal errors are due to: sample preparation (<±0.7 %), estimation of the extrapolated value for the lowest concentration (0.2 Bq/L) of ^{222}Rn sample found in this study (<±3.0 %), the interferences from the daughter nuclides of ^{220}Rn (<±0.3 %), the air luminescence counts (<±0.3 %). Thus ^{222}Rn samples of 0.2 Bq/L can be determined within an overall uncertainty of 3.1 %.

4. CONCLUSIONS

(1) The average ^{222}Rn concentration for spring waters (8.5 Bq/L) is higher than that for private well waters (4.5 Bq/L) by a factor of 1.9. ^{222}Rn concentrations for all samples ranged from 0.2 to 22.9 Bq/L and averaged 4.8 Bq/L.

(2) The highest ^{222}Rn concentrations were present in samples from wells and springs along the five rivers.

(3) The modified integral counting method gives more accurate ^{222}Rn concentrations for water

samples of relatively strong quench than the conventional integral counting method.

(4) The elimination of the air luminescence counts which are produced ^{222}Rn and its α-emitting daughters in the air space above the liquid scintillator is should be eliminated.

(5) Interferences from ^{220}Rn, ^{219}Rn and their daughters can be neglected.

5. REFERENCES

(1). Homma Y. and Murakami Y. Study on the applicability of the integral counting method for the determination of ^{226}Ra in various sample forms using a liquid scintillation counter. 36, 173, 1977. J. Radioanal. Chem.

(2). Homma Y., Murase Y. and Handa K. The zero detection threshold of a liquid scintillation spectrometer and its application to liquid scintillation counting. 45, 341, 1994. Appl. Radiat. Isot.

(3). Homma Y., Murase Y. and Handa K. A modified integral counting method and efficiency tracing method for measuring ^{222}Rn by liquid-scintillation counting. 45, 699, 1994. Appl. Radiat. Isot.

(4). Homma Y., Murase Y. and Takiue M. Determination of ^{222}Rn by air luminescence method. 119, 457, 1987. J. Radioanal. Nucl. Chem. Lett.

(5). Murase Y., Homma Y. and Takiue M. Effect of air luminescence counts on determination of ^{222}Rn by liquid scintillation counting.40, 295, 1989. Appl. Radiat. Isot.

Determination of ^{222}Rn in Groundwater - Recent Applications for the Investigation of River Bank Infiltration

K FREYER, H C TREUTLER
UFZ - Centre for Environmental Research Leipzig-Halle Ltd.
Permoserstr. 15, D-04318 Leipzig, Germany

J DEHNERT, W NESTLER
Hochschule für Technik und Wirtschaft Dresden
P.O.B. 120701, D-01008 Dresden, Germany

SUMMARY. Radon-222 (^{222}Rn) can be used as a tracer to investigate exchange processes between surface water and groundwater. A reliable method for the representative collection of groundwater samples and the determination of ^{222}Rn in water samples using liquid scintillation spectrometry was developed for this purpose. The total error of the method is $< \pm$ 10 %. Groundwater measuring profiles near a waterworks extracting bank-filtered water near Torgau on the Elbe were used to study processes of exfiltration and infiltration. The passage of a flood wave across the bank was observed. The infiltration velocity of river water was determined.

1. INTRODUCTION

The noble gas radon-222 (hereafter simply referred to as radon) occurs naturally in all groundwater. With a half-life of 3.8 days, it makes an ideal tracer for tackling a whole range of problems in environmental research and hydrology. One important issue is describing the exchange processes taking place between surface waters and aquifers. For example, studies of how rivers are fed by groundwater have been performed by Ellins et al (1), Genereux and Hemond (2), Yoneda et al (3), and Hamada and Komae (4).

In 1989 Hoehn and von Gunten (5) proposed using the increase in radon activity concentration of infiltrating river water as it passes through the river bank to determine flow time. Similar studies have also been described by authors such as Bertin and Bourg (6), and Wilme et al (7).

The speed of infiltration is required in order to determine infiltration rates – which in turn are needed to size drinking water catchment facilities with artificial groundwater recharging and to study the alluvial meadow ecosystem. When dimensioning well intakes for the extraction of bank-filtered water, the infiltration speed is important because water quality must also be taken into account. A significant share of the pollutant degradation process takes place in the silting zone – a biologically highly active area which is just a few centimetres deep, and whose efficiency also depends on the infiltration speed.

In all cases, the radon activity concentration in the water must be determined using a suitable method. Radon's low activity concentrations in Pleistocene aquifers require high measuring accuracy. Owing to radon's high mobility, sampling itself must also be carried out carefully.

This paper describes a reliable sampling and measuring technique which uses liquid scintillation spectrometry for the fast, reproducible determination of the radon activity concentration in groundwater. The method also includes using radon to optimise the pumping times of groundwater gauging stations as described by Dehnert et al (8). The technique developed was used to study the infiltration of a river into the aquifer in the catchment area of a water works extracting bank-filtered water.

2. SAMPLING AND RADON-MEASURING TECHNOLOGY

2.1 Sampling

Sampling techniques depend on the kind and origin of the water sample. The representative collection of a groundwater sample in the field and its transportation to the laboratory are particularly difficult as radon escapes very easily. Suitable groundwater observation wells must be used. Although the best approach is to use "nests of observation wells", "bundles of observation wells" represent a good compromise between sample quality and construction costs.

Different water sampling devices (submersible pump, membrane pump, bailer) were compared to check their applicability. Assessed in terms of radon concentration, the fluctuations registered were below 1%. Furthermore it was found that a pumping rate of a submersible pump in the range between 0.15 and 1.92 m^3/h does not exercise any significant impact.

The sample vessel and the filling technique must take into account radon's tendency to escape. Consequently, the sampling device chosen was a glass mensure calibrated to one litre featuring a narrow neck sealed with a polyethylene stopper and a teflon gasket. First of all, 20 ml toluene scintillation cocktail is poured into the mensure. The water is then poured in through a glass tube specially made for radon measurement by underlying the scintillation cocktail without air contact. Sampling must be carried out free of turbulence and air bubbles. The filling technique used was tried out in several series of measurements. Radon loss after sampling and transport was below 2%.

2.2 Radon measurement

In view of the advanced state of liquid scintillation spectrometry, this measuring technique was selected as being the most suitable of the wide range of different options for determining radon activity as described for instance by Völkle and Borchardt (9).

The method detailed by Horiuchi and Murakami (10) was adapted and modified to determine activity concentration in water samples. The radon dissolved in the water is extracted by a toluene-based liquid scintillator cocktail. After extraction the toluene phase is separated from the water and the ^{222}Rn activity of this 20 ml cocktail is determined by liquid scintillation spectrometry using a TRI-CARB 2550 TR/AB (Packard), which works in low-level mode and has a special hardware and software option for α/β separation. The optimum measuring time is 60 minutes. The measuring error is < 3% for counting rates between 40 and 8,000 cpm. Using comparison measurement with gamma spectrometry, a calibration factor of $(8.3 \pm 0.7)\ 10^{-3}$ Bq/cpm was determined.

In order to check the correctness of the measurements, the TRI-CARB 2550 TR/AB also allows the alpha spectra measured to be evaluated by means of SPECTRAGRAPH software (Fig. 1). α/β separation can be used to calculate the α/β ratio – which in the case of

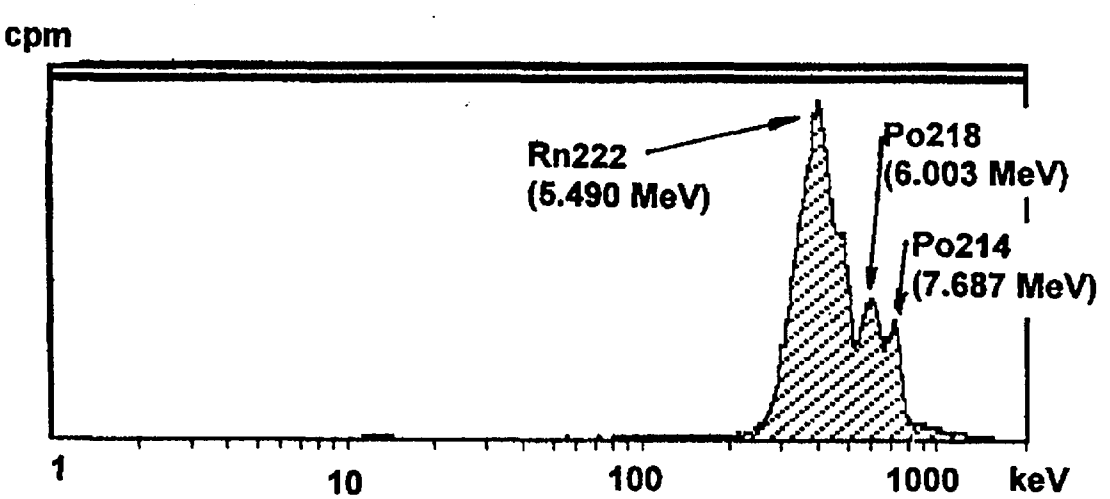

Figure 1: Alpha spectrum of ^{222}Rn and its daughter nuclides as shown by TRI-CARB SPECTRAGRAPH software

^{222}Rn ought to be 60:40. The radon activity at the time of sampling is calculated by regression following multiple measurements taken over a period of 6 days. The detection limit, calculated as 3 standard deviations of ten background measurements, is 0.05 Bq/l. The total error of the measuring method is $< \pm 10\%$.

3. INFILTRATION STUDIES

3.1 Method

The technique put forward by Hoehn and von Gunten (5) is based on the fact that river water only contains a small amount of radon because a turbulent current causes the mobile noble gas to escape. Radon is constantly emanated by the aquifer's grain structure in different concentrations (due to geogenous factors), entering the liquid phase of the water either via reaction effects during alpha decay or diffusion from the grain surface (Wilkening (11)). As infiltrating, low-radon river water flows through the aquifer, it continuously absorbs radon, so that an equilibrium between radon uptake and radioactive decay is established. If the equation for the increase of activity of a daughter nuclide until the state of equilibrium is reached is resolved in terms of time, the retention time of the infiltrate in the aquifer can be determined. Radon's half-life of 3.8 d enables this for a time window of up to 15 days after infiltration, but also requires ascertaining the radon activity concentration at the gauging stations once a state of equilibrium has been reached.

3.2 Study area

Work was carried out at a battery of wells at East Torgau Waterworks Ltd., where bank-filtered water is extracted as part of the long-distance water supply system covering the Elbe water meadows and the eastern Harz. The Pleistocene aquifer consists of fluviatile-glacifluviatile sediments and Holocene Elbe gravel, and is up to 55 m deep. The meandering Elbe is in direct hydraulic contact with the aquifer. In 1991/1992 two groundwater observation measuring profiles were set up for research purposes. The profiles, each of which is 2 km long, cross the Elbe and run along the central well of a battery of wells up to the hinterland. They enable depth-dependent sampling in up to 5 horizons using groundwater gauging stations and sunken membrane pumps. Moreover, three silting gauging stations enable sampling below the submerged river bed.

3.3 Optimising the pumping times of groundwater gauging stations

When measuring radon activity concentration in an aquifer, the optimum pumping time of the groundwater gauging station before sampling is of key importance. Owing to its short half-life of 3.8 days, the radon in the still water of the gauging station decays over 26 days to 1% of its original level. Incorrect pumping times lead to much more inaccurate results with radon than with other parameters. To eliminate this problem, a new and generally applicable technique for determining the optimum pumping times of groundwater gauging stations based on reaching constant radon activity concentration during pumping was developed and used (Dehnert et al (12)).

3.4 Results and discussion

The groundwater of the individual layers of the aquifer have characteristic radon activity concentrations of between 5 and 70 Bq/l. The petrographic structure of the aquifer and radon activity concentration in the groundwater largely correlate with each other. Although according to Hoehn and von Gunten (5), radon emanation needs to be macroscopically constant in order to determine durations of stay, this is not the case underground. Therefore the technique was modified such that the radon equilibrium concentration was determined for each gauging station by sampling the entire measuring profile during the slow exfiltration of the groundwater into the Elbe. This took place during the passage of a flood wave (Fig. 2). Further the passage of a flood wave across the bank could be observed by means of radon activity concentration. Fig. 3 depicts the situation at the crest of the flood. The sharp drop in radon activity concentration at all gauging stations indicates water infiltrated from the Elbe. Areas with activity concentrations < 8 Bq/l are shaded by way of illustration.

The durations of stay and the velocities of infiltration and flow can be calculated from the change in radon activity concentrations at the individual gauging stations over time compared to the equilibrium concentration. For example, an infiltrate retention time in the

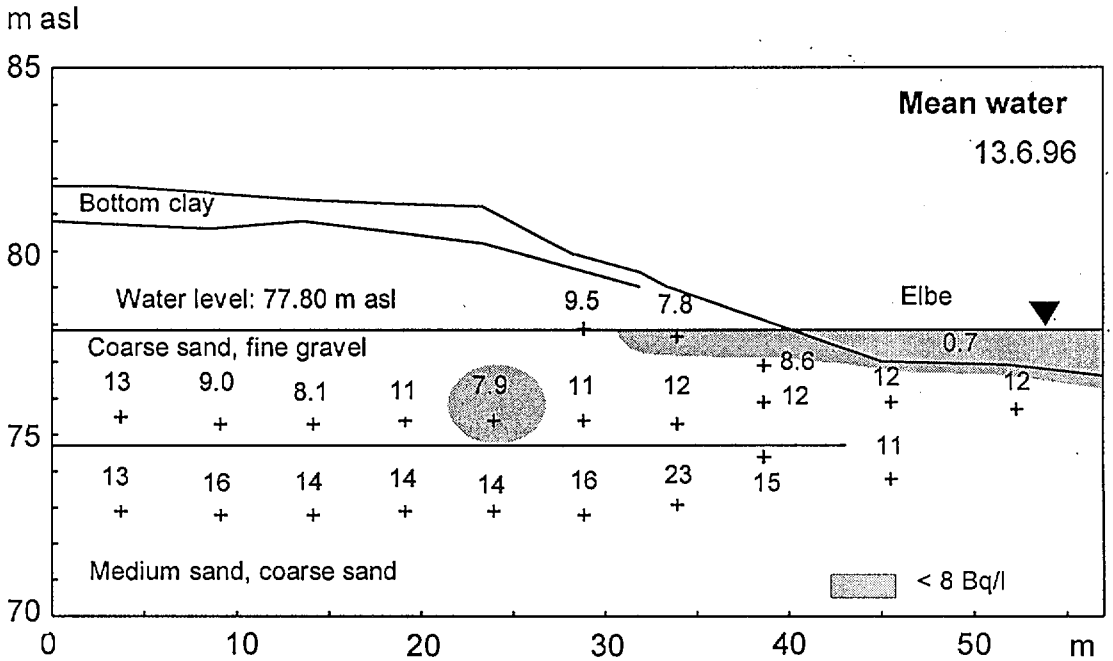

Figure 2: Radon activity concentrations in Bq/l in the measuring profile during exfiltration

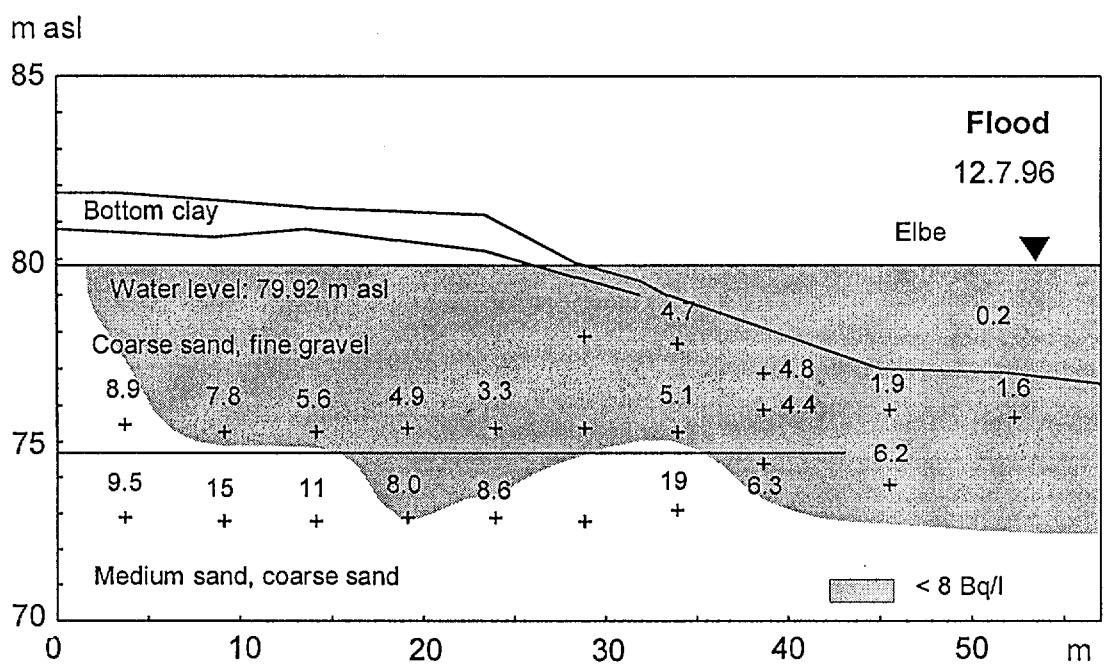

Figure 3: Radon activity concentration in Bq/l in the measuring profile during infiltration

aquifer during the passage of a flood wave of 0.5 d was determined for the silting gauging stations under the Elbe bed at an infiltration speed of 1.7 m/d. This value corresponds closely to estimates of quality parameters and geohydraulic calculations.

4. SUMMARY AND CONCLUSIONS

If ^{222}Rn is to be used as a tracer in water, a reliable technique for measuring radon must be used in view of its frequently low activity concentrations. The method chosen must also include a representative sampling technique, especially in the case of groundwater. The accuracy of the method described here with radon determination by liquid scintillation spectrometry has been proved and found to have a total error of $< \pm 10\%$. The precision of radon measurement is further improved by spectral analysis and α/β separation.
Extensive correlation was detected between the radon activity concentration of the groundwater and the petrographic structure of the aquifer at the Torgau aquifer studied here. Nevertheless, the existence of a radon activity concentration in the groundwater sufficiently representative of the flow path, which is required to determine the retention times of bank-filtered water, can probably not be counted on. The representative radon activity concentration in the equilibrium needed to ascertain the retention time of the infiltrate was determined separately for each gauging station by sampling the entire infiltration measuring profile during a phase of slow groundwater flow. The passage of a flood wave through the bank zone of an aquifer was observed. The infiltration speed of the Elbe could at first only be calculated for a silting gauging station beneath the bed of the Elbe. The results indicate that naturally occurring radon can provide under critical consideration of the boundary conditions a suitable parameter for describing infiltration by a river.

ACKNOWLEDGEMENTS

This work was carried out as part of the joint research project "Water extraction in valley aquifers in the Elbe catchment area" (02WT9454) funded by the Federal Ministry of Education, Science, Research and Technology. The authors would like to thank Mr Oese for his valuable assistance during sampling. We are indebted to Ms Scholz, Ms Petzold and Ms Bachmann for performing LSC measurement at the UFZ. Thanks also go to Fernwasserversorgung Elbaue-Ostharz Ltd. for their kind assistance, especially Mr Nitzsche (head of the Technical Office) and Mr Heilmann (the manager of East Torgau Waterworks).

REFERENCES

(1) Ellins K K, Roman-Mas A, Lee A: Using ^{222}Rn to Examine Groundwater/Surface Discharge Interaction in the Rio Grande De Manati, Puerto Rico. (1990), J.Hydrology 115: 319-341.

(2) Genereux D P, Hemond H F: Naturally Occuring Radon 222 as a Tracer for Streamflow Generation: Steady State Methodology and Field Example. (1990), Water Resour.Res. 26: 3065-3075.

(3) Yoneda M, Inoue Y, Takine N: Location of Groundwater Seepage Points into a River by Measurement of ^{222}Rn Concentration in Water Using Activated Charcoal Passive Collectors. (1991), J.Hydrology 124: 307-316.

(4) Hamada H, Komae T: Analysis of Exchange Between River Water and Groundwater Using Radon-222. (1994) XXV Congress of the International Association of Hydrogeologists, 21-25 Nov., Adelaide, South Australia, In: Water Down Under 94, Preprints of Papers 1: 115-120, The Institution of Engineers; Barton, Australia.

(5) Hoehn E, Von Gunten H R: Radon in groundwater: A tool to assess infiltration from surface waters to aquifers. (1989), Water Resour.Res. 25: 1795-1803.

(6) Bertin C, Bourg A C M: Radon-222 and Chloride as Natural Tracers of the Infiltration of River Water into Alluvial Aquifer in Which There Is Significant River/Groundwater Mixing. (1994), Environ.Sci.Technol. 28:794-798.

(7) Willme U, Schulte-Ebbert U, Hoehn E; Bestimmung von Grundwasserverweilzeiten mit geogenem ^{222}Rn bei künstlicher Grundwasseranreicherung und Uferfiltration in einer Trinkwassergewinnungsanlage. (1995), Wasser + Abwasser 136: 234-241.

(8) Dehnert J, Nestler W, Freyer K, Treutler H C, Neitzel P, Walther W: Radon-222 - ein neuer Leitkennwert zur Bestimmung optimaler Abpumpzeiten von Grundwasser-

meßstellen. (1997), Grundwasser 2(1): 25-33.

(9) Völkle H, Borchardt D (ed.): Messung von Radon und Radon-Folgeprodukten, (1991), Publikationsreihe Fortschritte im Strahlenschutz, Verlag TÜV Rheinland GmbH, Köln.

(10) Horiuchi K, Murakami Y: A new procedure for the determination of radium in water by extraction of radon and application of integral counting with a liquid scintillation counter. (1981), Int.J.Appl.Radiat.Isot. 32: 291-294.

(11) Wilkening H: Radon in the Environment.- Studies in Environmental Science 40, (1990), 137 p., Amsterdam-Oxford-NewYork-Tokyo: Elsevier.

(12) Dehnert J, Nestler W, Freyer K, Treutler H C, Neitzel P, Walther W: Bestimmung der notwendigen Abpumpzeiten von Grundwasserbeobachtungsrohren mit Hilfe der natürlichen Radonaktivitätskonzentration. (1996), in: Merkel B, Dietrich P G, Struckmeier W & Löhnert E P (ed.): Grundwasser und Rohstoffgewinnung.- 551 S.; Köln,GeoCongress 2, Verlag Sven von Loga, 40-45.

Effect of Duration of Exposure to $RaCl_2$ and to a Radium Apatite from Freshwater Mussels on Intestinal Transport and Bone Deposition of Radium

R. U. DOMEL[1] and A. M. BEAL[2]

[1]Australian Nuclear Science and Technology Organisation
Private Mail Bag 1, Menai, NSW, Australia, 2234
[2]Biological Science, University of New South Wales,
Sydney, NSW, Australia 2052

SUMMARY The freshwater mussel *(Velesunio angasi)* concentrates radium in its tissues as a phosphate compound. The uptake and tissue incorporation of the mussel radium salt was assessed in rats using jejunal transport studies *(in situ, in vivo,* ligated segment of anaesthetised animals) and feed trials. The results were compared to similar experiments with radium chloride. In addition, the influences of age and duration of dosage (hours in the case of the jejunal transport and weeks in the feed trial studies) were investigated.

Mussel radium transport across the jejunum of adults and juveniles (< 0.3% injected dose) was very small when compared to radium chloride (> 50% injected dose). The amount of mussel radium available for intestinal uptake in the feed trials was also low (< 0.5%) when compared to the uptake of radium chloride (< 1.5%). Incorporation of mussel radium into bone was less than that of radium chloride ($p = 0.0001$) for both adults and juveniles.

Extrapolation of the data from the animal model to humans suggests that eating these mussels, carries with it only a low risk of exceeding the Annual Limit of Intake (ALI) set for members of the public, even in juveniles.

INTRODUCTION

The Northern Territory's Uranium Province is named for the sizeable uranium ore deposits found in the area. Natural leaching of these ore deposits has resulted in elevated levels of uranium decay chain products such as ^{226}Ra in some surrounding waterways and mining has the potential to accelerate the movement of these pollutants into waterways. The freshwater mussel, *Velesunio angasi,* accumulates high concentrations of the non-essential, alpha-emitting radionuclide, ^{226}Ra, in its tissues. Together with other ions (Ca, Ba, Mg, Fe, Al), the radium is present mainly in mineral granules (of *approx.* 1μm in diameter) as a phosphate compound (1, 2). These mussels are a traditional dietary item for Aboriginals who harvest them from billabongs downstream of the Ranger ore body. The ^{226}Ra concentrations in mussel tissue and thus human ^{226}Ra intake from mussel consumption could be increased by release of mine effluent. The magnitude of the radium dose that members of the public (adults and children) might receive from the ^{226}Ra in the mussels is uncertain.

Based on human uptake and metabolism of radium, both from natural sources (3) and from accidental or iatrogenic sources (4) and on animal studies where human data was not available (5), the International Commission on Radiological Protection (ICRP) (6) recommends that occupational exposures be limited to an effective dose to 0.1 Sv in a five year period (≡ average annual value of 0.02 Sv). For internal exposure, the annual limit of intake (ALI) is based on a committed effective dose of 0.02 Sv which, for workers, corresponds to an ingested ALI of 90,000 Bq of ^{226}Ra. For members of the public, the ICRP recommends a principal limit of exposure of 1 mSv in a year excluding natural radiation and patient exposure in medical use of radiation but permits a subsidiary dose limit of 5 mSv in a year for a number of years with the provision that the average annual effective dose equivalent over a lifetime does not exceed 1 mSv (7). However, these ALIs are based on a standard 70 kg man and are not appropriate for persons of smaller stature nor for the young (8).

The ICRP (9) recommends a gut transfer (f_1- a fractional value relating to a total of 1) for adults of 0.2 for all compounds of radium. Derived values for the absorption of radium in the adult gastrointestinal tract are in the range of 0.15-0.21 (10). However, uptake of radium chloride from the gastrointestinal tract of rats is higher in 14-18 day-old animals ($f_1 = 0.79$) than in 60-70 week-old adult animals ($f_1 = 0.032$) (11) Also, the presence of calcium may depress

radium uptake, possibly due to competition for gut transport sites (12). Thus, current ICRP recommendations are of limited application having been derived from a data base for the retention and excretion of radium in adults only. Additional data are needed on the metabolism, retention and excretion of radium during both short and long exposures in young and adolescent populations, where the expected increase in calcium requirement for skeletal growth could lead to increased absorption of radium.

The following experiments were done using a standard laboratory animal model (rat) and were designed to determine radium uptake and retention by bone of both juvenile and adult animals over different lengths of exposure. Two species of radium were used; radium chloride and radium apatite from freshwater mussels obtained on the Magela flood plain of the Northern Territory. Three comparisons were made: i) Radium chloride uptake with mussel radium uptake for short-term exposure (up to 3 hours); ii) Radium chloride uptake with mussel radium for longer-term exposure (up to 8 weeks); iii) Uptake during short-term exposure with uptake during long-term exposure to radium chloride or to the mussel radium salt.

METHODS

Materials

The rats: The experimental animals were specific pathogen-free female rats of the Australian Albino Wistar strain. Two age groups were used; juveniles (4-6 weeks of age) and adults (over 12 weeks) Within each age group, the animals had similar body weights. The rats were kept under a 12/12 lighting regime and at an environmental temperature of 24°C. Before experimentation (acclimation) the animals were fed standard laboratory rodent pellets with distilled water being available *ad libitum*.

The cages: Standard polycarbonate rodent cages each with a filter top and raised metal grid bottom (to prevent coprophagy and external contamination) were modified to accept the feeder trays commonly used with metabolic cages. This allowed refilling of the daily food and radium dose with minimum disturbance to the animals. The bottom of the cage was lined with blotting paper, changed weekly, to absorb the urine. The cages were cleaned and sterilised after each experiment or weekly during the longer experiments. To minimise contamination the control animals were kept in cages towards the top of the cage rack.

Radium preparation 1. The freshwater mussels were collected from billabongs downstream of the Ranger mine and shipped live to ANSTO, Sydney. The mussels were kept in tanks of simulated Magela Creek water, fed cultured algae and dosed with $^{226}RaCl_2$ daily so that the radium content of the mussels was elevated sufficiently to give meaningful biodistribution results. After two weeks, the mussels were removed from the tanks, opened, the tissue dried in an oven at 30 °C and then powdered in a blender. Weighed samples of the mussel tissue batches were treated the same as the rat tissue samples (see ^{226}Ra, analytical procedures) and counted to allow dose calculation.

Radium preparation 2. The ^{223}Ra species was chosen for its short half-life (11.43 days) and abundant gamma emissions which allowed measurement without the processing necessary for the liquid scintillation counting (for ^{226}Ra samples). This radium species was obtained when needed by organic extraction, in acidified isotonic saline, from an ^{227}Ac generator. Its purity was maintained by counting the gamma emissions of a sample, at known energy peaks, on a pure germanium detector, and comparing the energy peaks obtained, to those of possible contaminants.

The food.. Standard rodent pellets were powdered in a blender and sieved through a fine mesh cloth to obtain even particle size with no lumps. The calcium content was 1.15%. Distilled drinking water was used for the animals to minimise contaminants that may alter intestinal transport of radium.

Experimental Procedures

Feed Trials; Exposures of 1, 2, 4 or 8 weeks: Five experimental animals and three control animals were used for each period of exposure. Each animal was kept in a separate cage and dosed daily; faeces were collected daily or weekly and weighed; urine was collected weekly. The dose (0.5-1 gram dried, powdered mussel tissue or 0.1 ml of radium chloride solution) and the powdered rodent food (10-20 grams) were dispensed daily into feeder trays; the radium dose was mixed evenly with the rodent food and the animals fed directly from the feeder tray with minimum contamination of the cage bottom. The liquid radium chloride was mixed dropwise with the powdered food to avoid large lumps. Distilled water was available *ad libitum.*

At the end of the specified period of dosage, the animals were fasted for 24 hours with distilled water being available *ad libitum,* killed by ether overdose and dissected for the biodistribution studies. Tissues and organs were sampled into glass vials and weighed, dried, ashed and acid digested for ^{226}Ra analysis by liquid scintillation counting, or into plastic tubes for ^{223}Ra analysis by gamma counting The data was used to

calculate the tissue biodistributions for radium and the *total fed dose or total injected dose* for each individual animal was used as the reference standard for that animal against which the biodistribution for each tissue type was calculated.

Jejunal Transport Experiments; Exposures of 1, 2 or 3 hours: Experiments were done in a biohazard cabinet (Class II Gelman) maintained at 30°C with large 250W globes. Anaesthesia was induced (in a fume cupboard) with ether and maintained by an intravenous injection of 5-ethyl-5(l'-methyl-propyl)-2-thio-barbituric acid *(Inactin,* Promonta, Hamburg) into the tail vein at 100 mg/kg body weight. While under anaesthesia, the body temperature of the animals was maintained at 37±1°C. Temperature was monitored with a rectal probe attached to a digital thermistor (Accurex 9001c). Through a midline abdominal incision, the intestine was ligated 10-12 cm below the pyloric sphincter and double ligated a further 10-12 cm posterior to the first ligature thereby isolating a segment of upper jejunum. Isotonic saline containing radium (osmolality 250-300 mosmols/kg) or the mussel radium slurry was injected into the jejunal segment at its anterior end by inserting hypodermic needle through the intestinal wall just below the single anterior ligature. A second ligature was applied around the needle and, after completion of the injection, tightened to seal the jejunal segment.

In adult rats, 1mL of ^{223}Ra chloride solution (having 1-2x10^5 counts/min; specific activity of 7.4kBq/mL) was injected into the segment, whereas in juvenile rats, 0.5mL of radium solution having the same range of counts/min was injected, thus avoiding excessive distension of the intestine. For the mussel radium slurry, the quantities injected were the same as above. The intestine was returned to the abdomen, and the abdominal incision was closed with surgical staples. If a blood vessel belonging to the experimental segment was ruptured during preparation, the animal was rejected because such damage might compromise transport by the segment. The procedure caused minimal disturbance to the small intestine and other viscera. Circadian variations in drug absorption have been documented (13). Consequently, these studies were all done in the late afternoon/evening period to maximise absorption at a time when the rats would have been most active and feeding.

Analytical procedures

^{223}Ra, gamma counting: The tissue samples were counted for 10 minutes in the gamma counter (Packard model 5650) using a 2" NaI crystal. The tissue sample counts were obtained as close to the injection time as possible and corrected for decay time between injection and tissue counting.

^{226}Ra, liquid scintillation counting: After dissection, the tissue samples in pre-weighed Packard liquid scintillation vials were weighed, dried and reweighed and then ashed at 450-470° C for 3 to 5 days (to obtain a white ash). The ashed samples were reweighed when cool and acid digested in the vial with concentrated HCl. Hydrogen peroxide was used to bleach colour from the samples where necessary. The digested samples wore evaporated close to dryness, 10mL of 0.1 molar HCl added to each vial, sealed with a screw cap (with a viton disk inserted) and shaken. The following day 10 mL of toluene containing 5g/L 2,5 Di Phenyloxazole (PPO - Ajax Chemicals, Australia) was added to each sample vial and shaken. This 2 phase cocktail was adopted for all ^{226}Ra tissue counting (14). The samples were left for one month to allow the radon daughters to grow into equilibrium with the radium parent and then each vial counted for 30 minutes with counts per minute recorded on a Liquid Scintillation Analyser (United Technologies Packard 2000CA Tri Carb) in the region of 150 to 1500 thousand electron volts (keV). Sample counts were the average of three counting cycles with the background subtracted. A predetermined quenching coefficient was recorded for each sample.

Biodistribution calculations-. The sample masses and counts, after correction for background and decay (in the case of ^{223}Ra), were used to determine the distribution of the fed (FD) or injected dose (ID) in each animal, in relation to its whole body weight and the radioactivity of the total dose. All major tissues and organs as well as faeces and urine were analysed for the full biodistribution study (15). For bone, the major target organ for absorbed radium, factors based on the whole body weight of the animal determined the organ mass. The activity in the bone of each animal is presented as a percentage of the total activity either fed to that animal or injected into the jejunal segment.

Statistical procedures

The mean and standard error for the tissues were calculated for each set of animals. Analysis of variance (anovar) was used for comparing variation between the groups.

RESULTS

i) Comparison of radium chloride uptake with mussel radium uptake during short-term exposure

When the radium was given as the chloride salt (Fig. 1), radium uptake onto bone after 3 hours exposure in juveniles (41.1±3.21%ID) was greater than that in adults (31.8±1.12%ID, $P<0.05$). Juvenile bone uptake was also higher, $P<0.05$, than that of the adults at both the 2 and 1 hour time intervals. Conversely, when the radium was derived from mussels (Fig. 2),

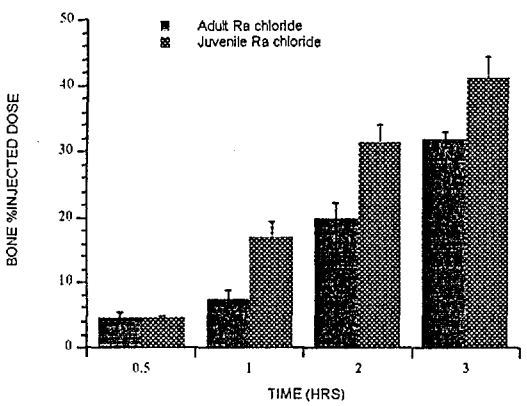

Fig. 1 Radium uptake in bone for adult and juvenile rats during short-term exposure to radium chloride.

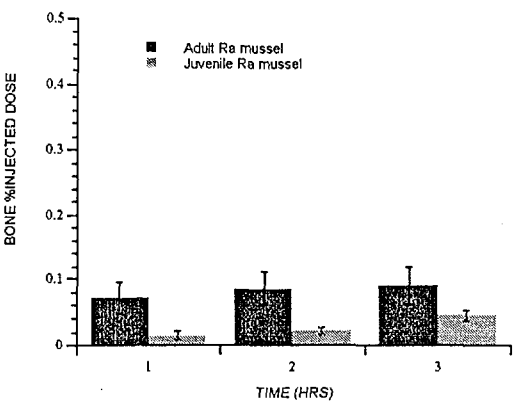

Fig. 2 Radium uptake in bone for adult and juvenile rats during short-term exposure to mussel radium.

radium uptake onto bone after 3 hours exposure in juveniles (0.045±0.009%ID) was lower ($P<0.01$) than that in the adults (0.091±0.029%ID). Overall, bone uptake of radium supplied as radium chloride was more than three orders of magnitude greater than when the radium was supplied as the mussel radium salt (Fig. 1 & 2). The data for the mussel radium uptake was also more variable possibly because the values were very low and thus close to the detection level of the counter.

ii) Comparison of radium chloride uptake with mussel radium uptake during longer exposure

Rats were exposed to radium chloride in the diet for one week and to the mussel radium salt for up to 8 weeks (Fig. 3). In adults, bone uptake after 1 week of mussel radium treatment was 0.30±0.015%FD, which was less ($P<0.0001$) than uptake after 1 week of radium chloride treatment (0.59±0.022 %FD). Similarly, bone uptake in juvenile rats after 1 week of mussel radium treatment was 0.28±0.007% which was less ($P<0.01$) than uptake after 1 week of radium chloride treatment (1.19±0.067%FD).

In adults, mussel radium uptake by bone as a % of the amount fed peaked at 2 weeks (0.35±0.008%FD) and by 8 weeks had fallen ($P<0.01$) to 0.25±0.018%. In contrast, uptake of mussel radium onto bone in juveniles increased progressively from week 1 to 0.48±0.018%FD at 8 weeks. In juveniles, the accumulation of radium in bone as a proportion of the dietary intake was linearly related with the duration of exposure ($R = 0.983$; $P<0.01$) whereas in adults, bone uptake/retention was negatively correlated ($R = 0.781$; $P<0.01$) with time over the 8 weeks of dietary exposure to the radium salt from mussels.

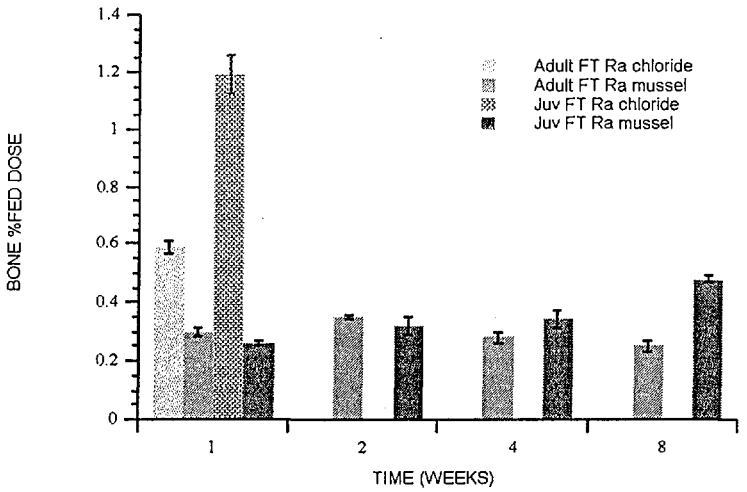

Fig. 3 Radium uptake in bone for adult and juvenile rats with mussel radium and radium chloride.

iii) Uptake during short-term exposure with uptake during long-term exposure to radium chloride or to the mussel radium salt.

Bone accumulation of radium during short-term exposure to radium chloride in both adults ((31.8±1.12%ID) and juveniles (41.1±3.21%ID) was greater (P<0.01) than that after 1 week's exposure to radium chloride in the diet (adults: 0.59±0.022%FD; juveniles: 1.19±0.067%FD) (Fig. 4). Bone uptake at 3 hours in the jejunal transport experiment exceeded uptake from feeding by more than two orders of magnitude. In contrast, radium accumulation in bone, from feeding the mussel radium salt to both adults and juveniles for 1 week, was higher (P<0.01) than that after 3 hours exposure during assessment of jejunal transport and remained so for the 8 week period in which mussel radium was fed (Fig. 5).

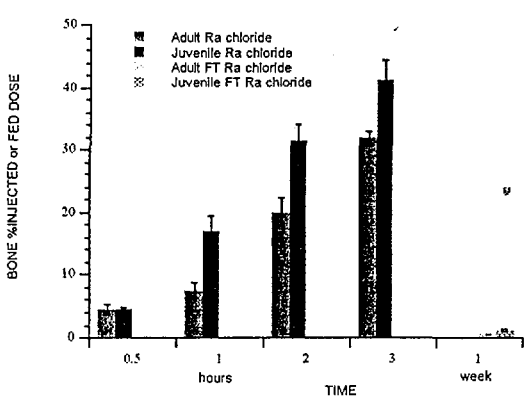

Fig. 4 Radium uptake in bone for adult and juvenile rats from radium chloride.

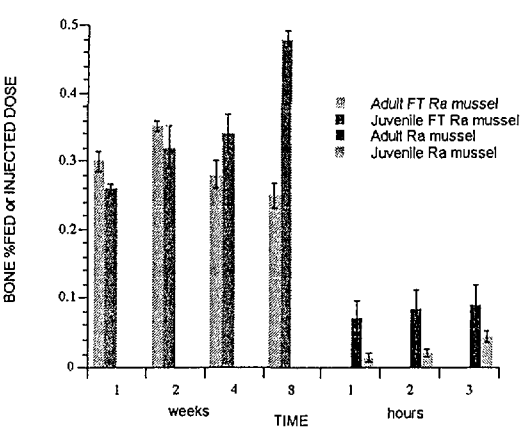

Fig. 5 Radium uptake in bone for adult and juvenile rats from mussel radium.

DISCUSSION AND CONCLUSIONS

In biological systems, divalent ions tend to be membrane-impermeant. Thus the high rate of absorption of radium, as the chloride salt, from the isolated jejunal segment indicates the presence of a transport mechanism in the jejunal wall. The calcium transport system has been postulated as a mechanism for radium absorption from the intestine (12). If so, dietary calcium in the feeding trials would compete with radium for this transport mechanism causing a proportionate reduction in radium absorption from the gut which would be related to the concentrations and the affinities of the transport mechanism for the two ions. Results from additional studies have shown this to be the case (15). Such competition would, in part, also explain the substantially lower % of the fed radium chloride dose found in bone relative to that for the jejunal transport studies where the radium solution contained no calcium. In addition, absorbed calcium would compete with radium at the bone deposition sites thereby reducing bone uptake and retention.

In the jejunal transport experiment, radium absorption from the mussel radium salt, as indicated by bone uptake, was minimal, being about 1 % of that for radium chloride after 3 h exposure in both age groups. In contrast, the difference in bone retention after 1 week of feeding of the two radium salts was much smaller; radium chloride retention being twice that of mussel radium in adults and four times in juveniles. These differences in bone uptake/retention of the two radium salts are explained by several factors which impact differentially on the bioavailability and intestinal transport under the two experimental regimes. i) The radium granules from mussels contain calcium and possibly other cations which compete with radium for gut absorption and bone deposition. The impact of this would be most obvious in the jejunal transport experiments. ii) Mussel radium incorporated into the diet will be made more available by its passage through the stomach where the very low pH increases solubility by encouraging ionization of the radium. In addition, proteolytic enzymes in the gastric secretion would break down the protein matrix which is typical of such molluscan granules (16,17) and on which the radium was precipitated. iii) In the jejunal transport experiments, the radium chloride was presented as a simple solution and thus was readily available for transport. Also, osmotic absorption of water following the absorbed radium would tend to maintain a high radium gradient between the jejunal lumen and the blood. iv) In the radium chloride feed trials, the radium concentration in the ingested food was reduced by intestinal secretion and the presence of food provided an opportunity for radium to bind to non-digestible components in the diet, both of which would lower the radium gradient between gut and blood.

Using *in vitro* techniques, Karbach and Feldmeier (18) found that caecal calcium absorption was six times that reported for other intestinal segments. How the level of jejunal absorption of radium compares with other intestinal regions has not been established. Likewise, the effect of calcium concentration on radium absorption from various intestinal segments and on radium deposition at the bone needs further investigation.

In both adult and juvenile rats, the $f1$ for radium chloride had surpassed the ICRP limit (0.2) for intestinal absorption of radium after only 2 h exposure. However, the conditions necessary for this rate of absorption would rarely if ever occur naturally. From the results for mussel radium, we conclude that individuals (adults and children) who use freshwater mussels from the Magela flood plain (radium content up to 4 Bq each) as a staple dietary item, would be in a category of very low risk of exceeding the ALI recommended for members of the public.

REFERENCES

(1) Jeffree R.A. (1984) The accumulation of radium-226 by populations of freshwater mussel, Velesunio angasi, from the Alligator Rivers Uranium Province, Northern Territory, Australia. *Verh. Internat. Verein. Limnol.* **22**, p2486-2492.

(2) Jeffree R.A. and Davy D.R. (1983) The transfer of Radium-226 via mussels to man in the Alligator Rivers Uranium Province, Northern Territory, Ausralia. *Paper to IAEA Seminar* 17-21st October, Brussels, Belgium.

(3) Globel B., Muth H. and Berlich J. (1982) Age dependent radiation dose rate from ^{226}Ra in human bone and some transfer factors from diet to human tissues. From: *Radiological Protection: vol. I. Advances in Theory and Practice. Proc. of the 3rd International Symposium in Inverness, Scotland.* 6-11 June, p381-386.

(4) Evans R.D. (1974) Radium in Man. *Health Physics* **27** (Nov.).

(5) Bruenger F.W., Smith J.M., Atherton D.R., Jee W.S.S.,Lloyd R.D. and Stevens W. (1983) Skeletal retention and distribution of ^{226}Ra and ^{239}Pu in Beagles injected at ages ranging from 2 days to 5 years. *Health Physics*, **44** (Suppliment No.1):p513-527.

(6) International Commission on Radiological Protection (1991). Annual Limits on Intake of Radionuclides by Workers Based in the 1990 Recommendations. *ICRP publication 61.* Pergamon Press, Oxford.

(7) International Commission on Radiological Protection (1985). Quantitative Bases for Developing a Unified Index of Harm. *ICRP publication 45.* Pergamon Press, Oxford.

(8) International Commission on Radiological Protection (1989). Age - dependent Doses to Members of the Public from Intake of Radionuclides *ICRP publication 56.* Pergamon Press, Oxford.

(9) International Commission on Radiological Protection (1972). Alkaline earth metabolism in adult man. *ICRP publication 20.* Pergamon Press, Oxford.

(10) Stehney A.F. and Lucas H.F. (1956) Studies on the radium content of humans arising from the natural radium of their environment. *Proc. UN Conf. P.U.A.E.*, **11**, 49-54.

(11) Taylor D.M., Bligh P.H. and Duggan M.H. (1962) The absorption of calcium, strontium, barium and radium from the gastrointestinal tract of the rat. *Biochem. J.* **83**, p25-29.

(12) Norris W.P., Speckman T.W. and Gustafson P.F. (1955) Studies on the Metabolism of Radium in Man. *Am. J. Roentgenol. Radiat. Therapy and Nuclear Med.*, **73**:785-802.

(13) Goo R.H., Moore J.G., Greenberg E. and Alazraki N.P. (1987) Circadian Variation in Gastric Emptying of Meals in Humans. *Gastroenterology* **93**:515-8.

(14) Williams A. R. (1988) The role of aquatic plants and sediments in radium cycling in a tropical wetland. Thesis (M. Sc.) Maquarie University Library, NSW, Australia.

(15) Domel R.U. (1996) Intestinal Transport and Biodistribution of Radium. PhD Thesis. University of New South Wales, Australia.

(16) Howard B., Mitchell P.C.M., Ritchie A., Simkiss K and Taylor M.G. (1981) The composition of intracellular granules from the metal-accumulating cells of the common garden snail *(Helix aspersa). Biochem J.*, **194**: 507-511.

(17) Taylor M.G., Simkiss K., Greaves G.N. and Harries J. (1988). Corrosion of intracellular granules and cell death. *Proc. Roy. Soc.*, **234B**: 463-476.

(18) Karbach U. and Feldmeier H (1993) The Cecum Is the Site with the Highest Calcium Absorption in Rat Intestine. *Digestive Diseases and Sciences* **38** (10): 1815-1824

66/31

Radiation Safety Aspects in application of Isotopes for Industrial Radiography in Bangladesh

D BAKHT
Titas gas T & D Co. Ltd 105, Kazi Nazrul Islam Avenue
Kawran Bazar C/A Dhaka-1215, Bangladesh.

SUMMARY. Industrial Radiography arose out of the wide spread applications of X-Rays pioneered by Roentgen about 100 years back. It is routinely used in studying the integrity of structural materials and like most countries of the would, its use in Bangladesh is increasing at a faster rate. While doing benefits to the industries, the uncontrolled use or misuses of the technology may cause harm to the operators and the public. In order to ensure safety & radiation protection, Nuclear Safety & Radiation Control Act 1993 has been promulgated. The current state of the art so far as safety aspects in application of isotopes are concerned has to be dealt with recommendations likely to strengthen the safety of sources & protection of the occupational workers & the public. The role of Bangladesh Atomic Energy Commission (BAEC) & Bangladesh Society for Non-Destructive Testing (BSNDT) in collaboration with international agencies are also important in achieving the desired objectives in these spheres of activities in furthering the safe industrialization process.

1. INTRODUCTION

Bangladesh is a developing country of 3rd world located in South East Asia covering a territory of 147,750 sqkm with 115.5m population. In the backdrop of agrarian poverty ridden economy, its population may exceed 125m by 2000 AD leaving some 12m people unemployed. To support them, therefore, immense activities are activated in different sectors. Accordingly increasing importance on NDT is given. In most cases particular application of Radiography is preferred using Ir-192 isotopes for quality production, construction & maintenance of industries, power plants, oil and gas pipelines & plants, railway, aviation systems, naval structures and vessels, etc.

Consequently the points of implications of isotopes are in Open Field & Inservice Inspection Radiography, Handling of Radiation Emergencies, Safe Transport of Radioactive Materials and Hazardous Effects & Risk of Ionizing Radiation. etc. Accordingly over exposure of Ir-192 Radionuclides, Accidents & Unusual Occurrences : Case Studies, Nuclear Safety& Radiation Protection Act 1993, Training Courses on Safety & Regulation of Sealed Sources and Radioactive Materials, Licenses for Radiography Operation including Safe Disposal of Isotopes are the salient issues to be viewed in appropriate perspectives.

Further, it is also pertinent to overview the essential status, need and strategies of Bangladesh in these fields in view of regulations and recommendation of Inter-national Atomic Energy Agency (IAEA) & BAEC. etc in an attempt to draw analogies highlighting the eventuatilies & priorities so far asisotope is concerned. The role played by Bangladesh Society for Non-Destructive Testing(BSNDT) in collaboration with other members of the International Committee for NDT (ICNDT) and achievement made so far may also be taken in to account.

2. NDT TECHNIQUES BASED ON IONIZING RADIATIONS.

Ionizing radiations, as the name implies involves the use of charged particle radiations as protons, electrons, positrons etc. and electromagnetic radiations such as X-rays and gammarays. It was shown by Raj et al (1) that the essential difference between X and gamma rays and the other electromagnetic radiations as light, UV and Infrared waves from the view point of testing and evaluation is that X- and gamma rays and able to penetrate matter which is opaque to light and have a pholotraphic action similar to light.

The basic advantage of the use of ionizing radiation in non-destructive testing arises from the fact that the objects which can be examined can range in sizes and shapes from microminiature electronic parts to mammoth missiles or power plant structures. Further ionizing radiations can be used

for testing a wide variety of materials ranging from light elements as aluminum, beryllium, and magnesium to steel, nickel and other heavy elements. The manufactured forms inspected by these radiations include a wide variety of castings, weldments, composites and assemblies. No prior preparation of the surfaces of the specimen is necessary. However, since indiscriminate exposure to ionizing radiation can produce biological damage, strict control of human exposure to these radiations is essential.

3. CONVENTIONAL & GAMMA RADIOGRAPHY

It has been further Stated by Raj et al(1) that, in the widely used conventional radiography, the source of radiation is an X ray tube consisting of a source of electrons, an accelerating potential and a heavy element target with which the acce-lerated electrons interact to produce X-rays. In 1913, Coolidge built an X-ray tube which used a heated filament to produce electrons & not much change in the structure of the tube has taken place. But highly automated self propelled X-ray mini Crawlers which travel within pipelines to take radiographs of pipelines from inside are now available. The control for posi-tioning along the length is by means of a small radioisotope source which emits a colli-mated beam of radiation down through the pipe wall. Such systems,designed for remote control, would be suitable for on-shore & off-shore structures including oil, gas and other fluid handling networks with pipelines down to 250 mm bore.

In contrast to X-ray machines which emit radiation with a spectrum of energies, gamma ray sources emit one or a few discrete energies. Radiography with gamma rays has the advantages of simplicity of Radioactive materials and radiation sources can do harm to the users or persons around, unknowingly. Radiation burns were first identified in 1896 within a month of Roentgen's discovery of X-rays. Iionizing radiation prima-rily includes : X-rays, gamma rays, beta, alpha, neutrons, positrons etc. Such radiations while passing through living cells ionize the molecules and in the process may damage, cause chemical changes or modify them. Radiation breaks large DNA molecules and causes structural changes. The damage is proportional to the does deli-vered by incidental radiation. *Modified cells may eventually be developed into* the apparatus used, compactness of radiation source, and indepen-dence from outside power. This facilitates the examination of pipe , pressure vessels and other assemblies in which access to interior is difficult 3.1 **SOURCES FOR GAMMA RADIOGRAPHY & IRIDIUM 192**

The four most popular radiographic sources are :Cobalt 60 (Co-60),Cesium 137 (Cs-13), Thulium 170(Tm-170) and Iridium 192 (lr 192). The once popular Radium 226 (Ra-226) is no longer used. Among these, Iridium-192 is mostly used in *Bangladesh for Industrial Radiography. Iridium is a* naturally occurring element belong-ing to the platinum family with a density of 22.4 gm/cc.It has two stable isotopes Ir-191 and Ir-193 with natural abundances of 37.3% and 62.7% respectively. When elemental Iridium is exposed to neutrons, radioisotopes Ir-192 and Ir-194 are produced. While Ir-192 has a half life of 74.3 days,the half life of Ir-194 is only 19 hours.

The gamma ray spectrum of Ir-192 is quite complex containing at least 24 spectral lines in the energy range 0.2 to 0.7 MeV. Its relatively low energies permit the use of lead shields weighing less than 50 kg for source strengths of 2000-4000 GBq making the isotope ideal for field work where portability and small size are desirable. This isotope is principally used for the radiography of steel upto 100 mm. In an overview of wide spread applications of radio-isotopes gauges and radiation sources to industry, it has been stated by Airey et al (2) that a number of polential applications are being developed in the field of treatment of waste water & sewage and flue gases as well.

4. RADIATION EFFECTS

malignancies. Since such modified cells may include the germ cells which transmit genetic information, it is also conceived that it may cause genetically transmitted hereditarily defects. Large exposures to the embryo and foetus during the early pregnancy have been found to cause leukemia, ssevere mental retardation & large congenital malformations. Radiation effects are sensitive to age & sex of a person.Children exposed to radi-ation in uterus during first 8-15 weeks of preg-nancy were found downward shift in distri-bution of IQ with increasing dose. Besides different organs have *different sensitivities to radiations.*

Large radiation dose may cause harmful effects or even deaths within hours or weeks. This is known as prompt effect. Prompt effects include radiation burns, radiation sickness, nausea, vomiting, loss of appetite, general sickness, diarrhoea, fever etc. Exposures to low doses can cause late effects referred to as somatic effects or to the future generation called genetic effects. Delayed effects are cancer, loss of hair etc. Prompt effects has a threshold value (approx 200 mSv), below which it is barely detectable. The delayed effects have no threshold. The proba-bility of harms to be caused, except for very low doses, is linearly proportional to the total amount of dose received during the life span. Late effects can be seen between 2 to 20 years after the exposures. It is also possible that genetic change caused by radiation is beneficial but the probability of such good effect is very low.

5.BIOLOGICAL EFFECTS OF RADIATION

Chowdhury(2)has identified the effects as follows :

Dose	Probable Effect
0.25 rems*	No obvious injury (safe)
26-50 "	Possible change in blood composition but no serious injury
51-100 "	Blood cell changes, some injury, no disability
101-200 "	Serious injury, possible disability
201-400 "	Injury and disability certain, death possible
Above 400	fatal

* Rem = Roentgen Equivalent Man

For X- ray and Gamma Rays

I Roentgen = 1 Rem, usually quoted as thousands of a rem= millirem (mrem)

Radiation doses should be kept to a minimum, but must never exceed 5 Rems per year. This works out at 100 millirems per week. The does rate, therefore, at the barriers of a work site must not exceed 2.5 millirems per hour. The does rate is determined by a radiation monitor, the accumulated does is determined by a film badge or a pocket dosimeter.

In radiographic operation that use X-ray machines or radioisotopic sources, the magnitude of the radiation hazards to personnel and other persons in the vicinity depends on a number of factors such as:Type and energy of the radiation,Total doses, Dose rate,Part of the body irradiated,

Species, Strain, Age, Sex & Nutritional Condition

6. RISKS IN RADIOGRAPHY & CAUSES OF ACCIDENTS

As stated earlier,the X-rays and gamma rays are most common types in industrial radiography. The radiations used in the radiography are highly penetrating and intense. The jobs are often carried out at open sites or in industrial environment. Radiographer some times have to perform in difficult job positions and circum-stances. It has been shown by Molla et al(4) that all these adverse circumstances put the radiography supervisors and technicians at high risks. Accidental exposures can easily occur unless the jobs are done properly and the working rules are rigoroulsy followed. Besides, accidents do occur during the transportation and storage of the gamma sources. Such accidents took place mostly due to the failure in comply-ing the prescriptions of the working rules. Serious accident involving radiography source occurred in many countries e.g. Mexico(1962), Algeria (1978),India (1968), Morocco (1984) and even in Bangladesh (1985). The 10 years data (1970-80) of the USA show that 60% of all the high overexposure and 70% of all the very high overexposure occurred in industrial uses of radia-tion, were related to the gamma radiography.

Among various reasons of radiography accidents, followings may be identified as significant ones:

*Radiography sources was left out at the exposed position.

*Survey meter has not been used or used improperly.

*Source has not been locked in the safe positions.

*Lapses in the training of the operator.

*Defective equipment and meters.

Any action towards taking care of the above mentioned issues shall lead to the improvement of safety situation.

7. GENERAL SAFETY REQUIREMENTS FOR INDUSTRIAL RADIOGRAPHY

of the body. Such operations can be quite safe if carried out by trained personnel using the proper equipment in installation designed for the purpose. For this to be satisfied, the following requirements are mandatory.

8.TRAINING OF PERSONNEL & MEDICAL REQUIREMENTS

Persons using radioisotopes or X-rays in industrial radiography should receive train-ing that will give a full understanding of :

* fundamentals of radiation protection
*proper operation of devices & equipment
* use of protective equipment
* Govt. regulations pertaining to the use of radioisotopes and X-ray in Industrial Radiography
*procedures to be followed in the event of accident or fire involving a radioactive source.

Each radiographer is to be given medical examinations of such nature and at such intervals as the Bangladesh Atomic Energy Commission Control Board may require on the advice of the health authorities.

8.1. SAFETY EVALUATION OF RADIOGRAPHIC EQUIPMENT

Every radiographer should understand the work-ing principles and operation of each radiographic unit that he will be using. The equipment should be checked before taking it out to the field and before using it, to ensure that it is functioning satisfactorily. This will enable the radiographer to deal with emergencies with minimum delay and to limit personal radiation exposure.

8.2 MONITORING DEVICES

Every person using sources of ionizing radiation must ware a Therme Luminance Dosimeter whenever high radiation fields are prevailing. As outlined by Chowdhury(2),it has to:

*be used frequently during each operation
*have a range such that radiation fields from 2 mR#/h to IR#/h can be measured within + 2-% of the true intensity
*preferably be of ion- chamber type

#R = Roentgen

All monitoring equipment should be properly maintained & calibrated for the energy of gamma radiation emitted by the radioactive source.

8.3.OPERATION SAFETY PROCEDURES MANUAL

Each company should have an operating safety procedure manual for routine operations and emergency procedures to keep its operations within the framework of the Bangladesh Atomic Energy Commission Control Regulations. The relevant items of information on health and safety should be included in the manual.

9. SAFETY STANDARDS & PROCEDURES

The radiation dose received should not exceed :

*5 rems in one calendar year or in any period of 52 consecutive weeks for those engaged in radiographic or associated work.
* 3rems in one calendar quarter of a year or any period of 13 consecutive weeks for those engaged in radiographic or associated work.
*500 mrem in one calendar year or 10 mrem per week for those whose regular duties do not require them to work with radioisotopes or X- rays. It is desirable to exclude such persons from areas where the radiation intensity is likely to exceed 10 mR/h.

10. GENERAL SAFETY WORKING PROCEDURE

The choice of the safest working procedure will depend on the nature of the job and the equipment used. However, observance of the rules set out will reduce the possibility of excessive exposure. The aim of the radiographer should be to reduce to a minimum the exposure of himself and others to radiation, by distance and working time.

11. PRELIMINARY STEPS & BASIC SAFETY MEASURES.

*Select type and strength of the radioactive source in accordance with the job to be performed.
*In field operations, always use appropriate directional shields whenever practicable
*Make sure the source capsule or pencil is appr-oved for use in the camera to be employed. i,e. Source capsules or pencils designed and approved for use in one type of camera must not be used in any other type without prior authorization by the Atomic energy Control Board.

*Perform radiographic operations whenever possible during that time of day when a minimum number of people are in the vicinity.

In order to keep the occurrences of accident/ overexposure within the acceptable limits it is essential that the regulatory requirements and the prescriptions of the applicable codes and standards

*Ensure that survey meter is in working order and that all persons involved are wearing film monitors.
*With source in camera and shutter closed take measurements in three mutually perpendicular planes at a distance of 150 mm from the surface of the camera, if the radiation intensity exceeds 50 mR/h, do not use the camera.

are strictly followed. The basic safety measures, however, require :

* written operating procedures covering details of what shall be done and what shall not be done and that the oprators shall comply the instructions,

*Operators must understand the need and importance of time , distance and shielding and

*Shall implement emergency response plan about which,a operator must be aware of.

12. **EMERGENCY SAFETY PROCEDURES**

Accidents are likely to induce panic. Therefore comprehensive procedures anticipating various possible modes of accident are to be prepared in advance to cope with possible accident situations and copies should be available at site of every radiography operations. Serious situations endangering safety may develop from but not limited to improper storage,handling, disposal, changing, sources & malfunctioning of equipments etc.

Further , sources not returning to camera, source capsule found damaged or leaking, vehicle carrying source meeting accident or source involved in fire etc are other causes to generate emergency situations calling for special safety measures for which afore mentioned prescribed emergency plans are to be followed. Particularly, much caution has to be exercised against. contamination or possibility of ingestion of radioactive material by any person. In certain cases auxiliary protective devices like lead-sheeting or mobile screen may also be used in a manner so as to avoid creep and to protect it from mechanical change.

13. **REGULATORY CONTROL**

Bangladesh Nuclear Safety kind Radiation Control Act No. 21 was promulgated in July 1993. The BAEC has been entrusted with the power to implement the law. As referred to by Awal(5), education & training program is under preparation It may be noted that BSNDT established in 1990 has been enrolled as the member of International Committee for Non- Destructive Testing(ICNDT) in the 14th world congress held in New Delhi, December 1996. Earlier BSNDT has signed bilateral agreements for co-operation with similar societies of Japan, Australia, Indonesia, Srilanka, Malaysia, Canada and India. It has been keeping close contact with those countries to play pioneering role in development and application of NDT in Bangaldesh. Further, with continuous assistance and in the light of same. The section 4 of the Act provids that all nuclear and radiation activities including the radiography shall require license from the BAEC to operate in Bangladesh. The regulations which will provide detailed requirements are now under preparation. Once the regulations are gazetted, the law will be put to force. Besides the regulations, there are codes of practice and guides published by the International Agencies and National Government which provide guidance for complying the provisions of the law/regulations and promote safety and protection of the radiation sources. It has been observed by Ahmad(6) that health & safety implies not only health profection & health promotion but also freedom from risks arising out of or in the course of occupation. Keeping this in view, the regulations and the codes applicable to radiography specify, among others,the following topics :

- delineation of the responsibilities of licensee and workers.
- Safety procedures
- design, construction and maintenance of equipment
- protective barrier, interlock and other safety features
- storage of radioactive sources
- radiation dosimetry and radiation monitoring requirements (and their calibrations and standardization)
- comprehensive working procedures
- training and certification of radiographer
- emergency response plan.
- use of warning labels, notices, barriers and markings
- recording and reporting requirements.

14. **ROLE OF BSNDT**

support from BAEC, it has been working to dissiminate different aspects of NDT technology with particular contrast to industrial radiography and for that matter radiation safety. BSNDT has already trained about 100 officials of different organization of the country in these fields and has been organizing workshops seminars including publishing News letters & proceedings etc since its inception. Recently it has also introduced BSNDT-Award to honour individuals & organizations to recognise outstanding performance & contributions

in these fields.

15. CONCLUSION

The experience in use of isotopes in industrial radiography has been marked in one occassion with stealing of an Iridium 192 Source contained from storage pit surrounded by barbed wire with cautionary signs duly displayed. This was out of silly idea of selling the container as scrap material.This was done in late 80" s by a mem-ber of local people due to shear ignorance & illiteracy causing a hazardous situation to himself too.Similarly growth of industrializ-ation employing the labours & work forces coming from villages with farming & cultivation back grounds of rural Bangladesh can not be expected to know all rules and regulation & consequential effects over night as required particularly in this profession. But it is important to note that though there is stringent rules to follow, yet due to lack of strict compliance by both employer and employee due to ignorance and inexperience they may, at times, be subjected to risk of hazards and accident which may increases and reach to an alarming level unless adequate steps are taken with due importance.

Radiation is harmful. Industrial radiography is potentially more hazard prone than to any other industrial use of ionizing radiation. Complexities arising out of safety even calling for the need of alternate applications of NDT methods has been foreseen by Bakht(7) in certain situations. Howaver, strict compliance to the written procedures and regulatory prescriptions are essential to ensure adequate safety and protection of the workers and the members of the public. Mere existence of law and regulations are not enough to ensure safety. Close cooperation between the regulator and the licensees are also needed. Besides the safety culture has to be promoted to keep the standards of the safety and protection high.

16. ACKNOWLEDGEMENT

The author wishes to acknowledge with thanks the inspiration received from Dr. M. Sana Ullah & Dr.S.M.M.R. Chowdhury, Dr Peter L. Airey & Dr. Bal Dev Raj for development the paper. Sincere thanks are also due to colleagues at Titas Gas & BSNDT for the suport. Gratitude are also recorded in favour of TGTDCL & Petrobangla Management for their kindly permission to publish the same.

17. REFERENCES

1.Raj, B, & Venkatraman,B,Ionising Radiations for Non- Destructive Evaluation ISRP, Kalpakkam Chapter, India 1989.

2.Chowdhury, S.M.M.R. Safety Aspects in NDT operations, Training Programme on Radiation Protection, BAEC Dhaka 18-29 March, 1994.

3.Airey,P& ANSTO,Industrial Applications of Isotopes and Radiation,IAEA/RCA. Regional Seminar Bangladesh 23 Feb.1997.

4.Molla, E., Radiation Protection in Industrial radiography:Bangladesh Perspective,Course notes on NDT Appreciation BSNDT, BAEC,23-28 July 1994.

5.Awal, K.O., Education & Training Requirements for Medical uses of Ionizing radiation from Regulatory Perspective : An Outline. Workshop on Safe Use & Control of Ionizing Radiation in Medical Fields, BAEC Dhaka 14-15, Dec, 1994.

6.Ahmad,S.A.Occupational Health & Safety Services, National Workshop on Occupational Health & Safety,IEDCR,Dhaka 29-31 May,1995.

7.Bakht, D., Complexity Evaluation in NDT Application for Inservice Inspection and Energy System Maintenance in Bangladesh, Conference Proceeding Vol.2, 14th International Conference on NDT, New Delhi, 8-13 th December, 1996.

How to Understand the Radiation Effects of Small Dose --Some Critical Comments on ICRP Recommendations

TATSUO MATSUURA
Radiation Education Forum, Sanwa Daiichi Building, 1-17-2, Nishi-Shimbashi, Minato-ku, Tokyo, 105 JAPAN

SUMMARY The widespread "radiophobia" by the public is mostly based on the "linear no-threshold hypothesis" adopted by ICRP for the risk of ionizing radiation. This hypothesis, which assumes even a single beam of radiation can be harmful and is now regarded as if a fact for non-professionals, has now become one of the controversial scientific topics. In this paper, some critical comments on this hypothesis were presented from several points. First point is the question of assessment of individual radiation dose by the atomic-bomb survivors used in the present epidemiological data. Secondly, a brief review was given on the radiation effect at the level of background radiations, including the information on radiation hormesis, which is effect that cannot be anticipated from the data of higher dose. The importance of dose rate effect was explained by using a simple mathematical analysis of typical data. Finally, a proposal of adopting a new type of radiation paradigm, by estimating scientifically reasonable "de minimis" level both for dose and dose rate, under which value the radiation effect is practically harmless.

1. INTRODUCTION

At present, the general public in all over the world have an excessive fear and concern for the risk of radiation and radioactivity. If things will be left as they are, not only the sound development of peaceful uses of nuclear technology and use of ionizing radiations in various fields will be hindered and may lead to earlier global energy crisis, but also not a few innocent people will never cease to suffer from the psychological stress by unnecessary fear for the risk of very minor amount of radiation, due to ignorance of true scientific facts.

As a scientist who had been engaged in a specialized research of radioisotopes but is now engaged in an activity of proliferating the correct knowledge of ionizing radiation and nuclear technology in various ways (1,2,3), I would like to present some ideas of how to understand the effect of low-level radiation especially at low dose rate, as a form of critical comments to the recent ICRP recommendations (4).

As all of us are well aware, we human beings have been continuously exposed to small dose of natural background radiation since our birth on Earth, and this radiation level depends from site to site, i.e., in Japan it varies from ca 4 μR/hr to ca 17 μR/hr (5,6). We believe humans must be endowed with resistance to this small amount of ionizing radiation although its large amount is harmful, just as for other various toxic substances existing in our environment. Also, our common sense expects that even if an additional small exposure is given within the variation of natural level, it will do no harm to human body.

In reality, it has recently been found experimentally that the small dose of ionizing radiation is necessary for cell proliferation (7), and there are many epidemiological and experimental data which indicate that a small dose of radiation seems to have rather a beneficial effect for living matters (8~12). Thus the concept of "RADIATION HORMESIS" as emerged. "Hormesis" is the name given to "any physiological effect which occurs at low doses and which cannot be anticipated by extrapolation from toxic effects noted at high doses" (8) or "the stimulating effects of small doses of substances that in larger doses are toxic" (12).

Many scientists nowadays point out that ICRP recommendations are responsible to the present situation of "radiophobia" of the general public, and now there appear not a few papers which explicitly criticize the underlying principle of ICRP--the linear non-threshold model (11~16), although if such opinion is disclosed in a popular journal such as ref. 13 it readily is attacked by some opposing opinions (17). However, the present ICRP recommendations for radiation protection regime are made "by extrapolating the scientific facts observed at high and medium levels to low dose, and by adding some social consideration" (18). The "extrapolation" assumes that quite the identical mechanism governs in every dose level, and that there is no threshold (under which there is no harm) in every type of cancer, and the dose-response relationship is linear to zero dose at very low level (19). This linear no-threshold model of ICRP is a HYPOTHESIS adopted since 1958 from the standpoint of radiation protection (20). This very understandable concept, that radiation of a single track can be injury to the cells of

living matters and be harmful, has been accepted as if a FACT by the majority of people, and frequently exaggerated by mass media, the phrase "radiation is very dangerous even at small amount" has now become the common sense as is described in many school textbooks (1,2,3).

We recognize this concept served, as a merit, for establishing the "safety culture" for radiation protection and providing the complete regulatory regime for ionizing radiation in every country. On the other hand, it has brought several demerits. The widespread, never-ceasing anti-nuclear emotion by the public will bring enormous economical cost for energy production, and many people in general feel anxiety for the nuclear installations and the related event, sometimes an extreme psychological stress by the people involved in some nuclear accident induced several tragedies. For example, it has been reported that many residents living in the contaminated area near Chernobyl got ill from mental stress, and the number of abortions in a country far from Chernobyl increased after the accident (21). We hope ICRP will not only re-assess the risk of low-level radiations based on many recent experimental evidences, but also pay much sociological consideration on the majority of innocent people worried by incorrect information.

Government in every country, which has been "recommended" to adopt the newest recommendations (1990 ICRP recommendations), is now in the procedure of considering to incorporate them to some extent into each own radiation regulation regime. In Japan, the Radiation Council of the government has recently disclosed a memo reporting the process of discussion in the meeting openly and has collected public opinions. Thus in Japan, this issue, whether there is a threshold dose or not for "probabilistic effects" (carcinogenicity and mutanogenicity), including the fundamental mechanism of carcinogenesis, has become one of the important topics of scientific discussion (19, 22). Several researchers have recognized that recent scientific (both epidemiological and experimental) data suggest that quite different mechanisms are working at low doses from those at high doses, such as an "adaptable response" observed at cSv levels and enhanced immunocompetence as some forms of radiation hormesis (10,12,23,24). However, the "most of the radiation protectionists are conservative", and it seems a long way until the ICRP will in some near future amend its basic principle from the present "old paradigm" to "new paradigm", by discarding the "linear no-threshold relationship" model (15).

As for the mutanogenicity--genetic hazards, it was very happy for us, including our Japanese A-bomb survivors, that the recent epidemiological studies show that "no significant increase in genetic damage has been observed" among the children from atomic-bomb (A-bomb) survivors of Hiroshima and Nagasaki (25).

Here is one recent topics. As for shortening of life after radiation exposure, the recent TIME magazine (26) briefly reports "the A-bomb survivors seem to be by some measures outliving contemporaries who were not exposed", and it was criticized by the scientist who was interviewed by the magazine writer that "the article is bad" (27), and opposing comments appeared soon in later issue of that magazine (28). In reality, a report on the possible longevity of A-bomb survivors appeared in an authoritative Japanese academic journal, in which a hormetic tendency was observed in a limited small dose level, only in male survivors (29). Thus, although it seems to me this is one of the controversial topics, an expert says that there is a definite threshold for the longevity induced by low dose of radiation (30,31). So the present controversy seems to be only focussed to the cancer risk.

Although I am not an expert of radiology but only a new-comer in this field, I have a keen interest in this important topic, i,e, how to understand and explain the effects of radiation at low dose to as many non-professionals as possible. In this paper, as a form of critical comments on the ICRP recommendations, a few topics of which I have recently learned are presented. These include a new aspect on the dose-response relationship of the epidemiological data of A-bomb survivors, a brief summary of data of natural, high background area, the dose rate effect, and the proposal of revising the present paradigm by adopting the "de minimis " or exemption level for low dose especially at very low dose rate. For the purpose of demonstrating that an animal in general has a repairability of radiation damage, an example of a simple mathematical analysis of dose-rate effect on the lethality data of mice (32,33) was added as Appendix.

2. COMMENTS ON THE DOSE-RESPONSE RELATIONSHIP AT LOW DOSE

2.1 On "Linear No-Threshold Relationship" at Low Dose

The actual process occurring in living matters is very complex, and many researchers are studying the mechanism of carcinogenesis induced by radiation and other carcinogen. Here, we only discuss the overall dependence of probability of appearance of cancer upon radiation dose and dose rate, especially at their respective low values.

The general dose response relationship for whole dose range assumed by ICRP is as shown in Fig. 1 (4), which shows no threshold. This curve has various slopes of the linear part at zero dose, depending on the ways of extrapolation, i.e, from high, medium, or low dose level. The slope represents the risk coefficient per unit dose. The ICRP text allows further reduction of the slope depending on dose rate. The reduction coefficient is called DDREF (dose and dose rate effectiveness factor), which value may be assumed to be 2 ~10 according to ICRP and other official reports. However, in ICRP recommendations 2, the most conservative value, is adopted "for the sake of radiation safety" (4).

What we have interest is:
(1) Is "no-threshold" concept for induced carcinogenesis scientifically correct?
(2) When dose rate becomes lower and lower up to the level of natural background radiation, how much is the proper value for DDREF?
In this paper a few comments will be stated in connection with these questions.

2.1.1 On the dose-response relationship of A-bomb survivors

Some of the most recent epidemiological data at low dose level for A-Bomb survivors are as shown in Fig. 2 (34) and Fig. 3 (31), which are considered to be very authentic, because these data are based on much elaborated studies for many years. The experts of radiology conclude that "these data do not show statistically significant evidence of presence of threshold" (22). However, I have a fundamental question for these data, as to the actual dose received by A-Bomb survivors.

I remember that, as one of air-raid sufferers in another city in Japan in that period, many sufferers lived for many years in temporarily constructed houses at the same places as they lived before soon after their houses were burnt down. I believe that a considerable number of Hiroshima and Nagasaki survivors lived in this way, that means, they must have received some additional chronic exposure from elevated background radiation due to fall-out or neutron-induced radioactivities in the surrounding ground. If this contribution could be estimated and added to the radiation dose already estimated at the instant of A-bomb explosion (as "T65D" or "DS86"), the total doses actually received by the survivors become higher than those shown in Figs. 2 and 3. Then, all the plots of Figs. 2 and 3 will shift rightward, the whole picture of which is schematically shown in Fig. 4 (a and b).

If the additional dose is the same for the whole people studied, the resulting revised dose-response relationship will be as shown in Fig. 4-a, and the extrapolation will probably give a threshold value. However, the real picture will, with the erratic point as stated in the next paragraph, probably be as shown in Fig. 4-b, because the additional dose depends on the place where the survivor lived. The nearer he/or she was in relation to the site of explosion and received the higher instantaneous dose, in general, the higher must have been the level of the surrounding activity, thus the larger the additional integrated exposure. So, this consideration may not help to show the presence of a threshold. However, it will very probably serve the lowering of the slope of the curve or the straight line, and lower the risk coefficient.

Fig 4-b includes the erratic point, where the contribution of the additional exposure is relatively high compared with the intensity of instantaneous exposure. This is such a case as the residents at Nishiyama District (located 3 km from the site of explosion) in Nagasaki. There, the instantaneous radiation was shielded by mountain but the "black rain" containing the fall-out nuclides gave the 280 residents a chronic exposure of as much as 0.2 Sv and caused an abnormal increase in leukocytes of most residents for several months (35,11). It is well known that the "black rain" fell also in Hiroshima. Thus it is possible that the proportionality of the additional dose to the instantaneous dose may not in general be so good as stated in the preceding paragraph, and this might cause the appearance of a threshold with a little higher probability.

An additional aspect as to the dose of A-bomb survivors, which has been pointed out by Prof. Sugahara (36), is the fact that the doses for the exposed group below 0.01 Gy has until quite recently been treated as "zero dose group" such as in ref. 34. Since 1996, such as in ref. 33, "zero" means <0.005 Gy. I agree with the opinion of this expert that it is a question to discuss the effects of

epidemiological data of Hiroshima from such treatment of the data for "zero dose". Namely, since this zero dose value represents the control, if a hormetic effect actually had occurred within this dose level, every other value at higher dose will show only positive risk.

2.1.2 Effect of radiation at natural background level

At present a detailed map of natural background data (the cosmic ionizing radiation and earth's crust gamma rays) in many districts in Japan is available (5,6) and the level ranges from ~4 μR/hr to ~17μR/hr. The epidemiological studies were done to investigate the relation between the natural background level and the standardized mortality ratio (SMR) by various cancers (6). The conclusion drawn is that the observation as a mass afford no correlation.

Another important finding is the epidemiological data of Misasa spa district in Tottori Prefecture of Japan, which is famous for one of the highest content of radon. According to Dr. Tanooka and his collaborators (37), the carcinogenic rate in stomach in the residents at high background level of radon concentration at Misasa is smaller than those of control area. Such observation suggests the hormetic effect of small amount of radon. This result is very interesting because the radon content in the air in the uranium mine and also in ordinary residence has once been reported harmful in U. S. A. (38), although the data were analyzed by Prof. Kondo as hormetic (11). According to the recent UNSCEAR report 1994 (39), "there is little direct evidence on the risks of lung cancer resulting from residential exposure by radon".

2.1.3 Epidemiological studies of high background radiation area (HBRA)

According to the recent Japan-China collaborative studies (leaders: Dr. L. Wei and Prof. T. Sugahara) for HBRA in Kanton District in China, it has been concluded that there is no statistically significant association between cancer mortality rate at the high background area (HB) and that at CA (control area), where the background radiation level of HB is about 3 times higher than CA (16).

It has been pointed out that although the cancer rate is not increased in HBRA, the frequency of chromosome aberration is significantly increased (40). So the investigators conclude that the chromosome aberration can be a sensitive index of cumulative dose received, and the mechanism of carcinogenesis is not identical with that of chromosome aberration.

In India also, there is a district (Kerala) where the natural background is much higher than other places, and the recent study reports that there is no difference in the cancer rate between the higher background and the control area (16,41).

It should be added here that the results of epidemiological study should be treated carefully, because there are several difficulties for obtaining reliable data (42).

2.2 On the Dose Rate Effect

It is well known in animal experiments that when the same dose of the same kind of radiation is given, the effect is usually small when the exposure is at low dose rate. This is understood by the recovery action of damaged cell in living matters during exposure, and called "dose rate effect". Similar recovery has been observed as "Elkind type recovery", where the sublethal damage is recovered and lethality becomes lower when the same dose was given in fractionation for mammalian cell (33,43.44).

For high LET radiations these effects are usually small, because they induce much more unrepairable damage than low-LET radiations. I once had an interest in the nature of LET effect for various chemical (and biological) systems, and has proposed a "high local temperature model " for high LET radiations (45), which can favor the chemical reaction with high activation energy. This concept might be applicable also to the case of very high dose rate of low LET radiation, by the mechanism of overlapping of tracks.

Here, in the opportunity of writing this paper, a mathematical analysis for phenomenologically interpreting the typical data of dose rate effect of ionizing radiation illustrated in a text-book (33). The purpose is only to show that there is a recovery action in the radiation effect in living matters. The analysis is shown in Appendix. There is a conclusion in the analysis that the dose rate effect was interpreted only by introducing "linear-quadratic model" for the range of high dose rate region as written in a text-book (32). However, the assumed physical meaning may not be true, because the actual processes occurring by exposure of radiation to death of an animal are very complicated.

Recently, an expert team of radiologists headed by Prof. Sado (22) as well as Prof.

Kondo (46) proposed for radiation carcinogenesis the high probability of presence of a threshold dose-rate region, below which any harmful effects of radiation cannot be detected above the control level. In a review of Prof. Kondo (46) are included as the example Ootsuyama and Tanooka's results, showing a threshold dose rate of ca 2 Gy/week for skin cancer of mice repeatedly irradiated with beta rays from ^{90}Sr-^{90}Y (47,48).

2.3 Proposal of Amending "Old Paradigm"

The problem with which we are now confronted seems to be where we should draw a line between "safe" and "hazardous" for radiation dose and for dose rate. As for the least detectable dose for cancer risk in the epidemiological data of A-bomb survivors, i.e. 0.2 Gy, the dose rate can be calculated to be ca 720 Sv/ hr, if it is assumed the dose was given almost instantaneously, during 1 sec. On the other hand, the maximum natural background level (Kerala, India), 10 mSv /y, corresponds to 1.14 μSv/hr. The ratio of 720 Sv/hr (barely possibly hazardous) versus 1.14 μSv/hr (quite safe) is 6.3 x 10^8. Unfortunate thing is that for humans we have no reliable data of dose and dose rate between these extremely apart dose rate ranges. I believe, just as the probable presence of threshold value for dose, there must be some threshold dose rate. We expect that useful data will be available by experiments using animal. However, It is natural that the threshold dose values may depend on dose rate, so to obtain threshold dose value with much reproducibility and reliability may be considerably difficult, owing to the dose rate effect.

I agree with Prof. Sado's opinion that too much emphasis was given on the epidemiological data of A-bombs for the risk estimation of low dose (22). The epidemiological data themselves should not be regarded "authentic" but need careful reestimation. However, it is probably very difficult to obtain better epidemiological data than the present ones, which do not tell us definitely the presence or absence of thresholds. And, as Prof. Sugahara states, "a long debate will continue among scientists who support a new model and who insist on the old one, and it will take a long time before the new paradigm will be accepted", and he suggests a compromised amendment (15,20) for the time being. This is surely an idea. However, I think that as far as the linear model is assumed however small is the risk coefficient, the general public will never cease to believe that "even a small dose of radiation is dangerous", because they tend to consider everything qualitatively, not quantitatively.

I have a naive question: "Does the natural background radiation act as the cause of naturally occurring cancer?" According to the study by Doll and Peto (49), in U. S. A. 35% and 30% of cancer are caused by food and tobacco, respectively, and only 3% is caused by "physical factor", including radiation. My personal opinion is the contribution from natural background radiation is almost negligible. It seems worthwhile calculating the incidence rate of cancer by the present risk coefficient for overall exposure or radiation, including medical exposure.

Among the discussion of ICRP, it has been reported that there is an idea of the "de minimis dose", or "exemption dose", under which value we cannot observe practically any harmful effect of radiation, so no regulation on action or source is necessary, and tentatively the values of 10 μ Sv/y and 1 man Sv/y are presented (18). I hope much more higher values of the "de minimis level" for both dose and dose rate will be settled by some plausible scientific reasoning, hopefully using recent experimental and epidemiological evidences. I think the adoption of this concept, which may be one new type of radiation paradigm, will contribute to save much money and energy from costly control of radiation and to ease the fear for radiation cherished by the majority of people in the world.

In accordance with this concept, the author has learned very recently the suggestion for "Setting standards for radiation protection" (16). The paper reports with many references that "heterogeneous groups of humans have, without observed ill effect, tolerated chronic radiation exposure of at least 6 mSv y^{-1} and can tolerate acute exposure of at least 0.1 Sv, also with no effect," and that Health Physics Society's position statement (50) recommends that "estimates of risk should be limited to individuals receiving a dose of 5 rem in one year or a lifetime dose of at least 10 rem in addition to natural background. Below these doses, risk estimates should not be used." I sincerely hope ICRP, as well as every government, will earnestly consider these suggestions.

3. APPENDIX. EXAMPLE OF A PHENOMENOLOGICAL ANALYSIS OF THE DOSE RATE EFFECT

Some phenomenological approach to interpret

the dose rate effect was attempted, on the data shown in a literature (32,33) The original data is as shown in Table 1, in which almost the same total dose was given to mice at different dose rate.

Table 1. $LD_{50(30)}$ values of mice which were irradiated by X-rays at various dose rate

Dose rate (rad/min)	Irrad. time	$LD_{50(30)}$	1 / $LD_{50(30)}$
706	1 min	788 ± 24	1.269×10^{-3}
68	11 ~13.5 min	850 ± 12	1.176×10^{-3}
8	2 hr	948 ± 8	1.055×10^{-3}
4.5	4 hr	1030 ± 10	9.71×10^{-4}
3	6 hr	1040 ± 12	9.62×10^{-4}
2.5	8 hr	1097 ± 31	9.12×10^{-4}

The following assumptions were made:
(1) Ionizing radiation produces partially damaged or unstable cells in proportion to the dose delivered per unit time, but the number of the partially damaged (or unstable) cells (N_P) decrease at the same time with a definite decay rate (λ) by some disappearing mechanisms, such as repairing or apoptosis (self-suiciding action) during irradiation.
(2) The number of partially damaged cells at the end of irradiation is proportional to the number of lethally damaged cells (N_{LD}).
(3) Number of lethally damaged cells (N_{LD}) is proportional to the reciprocal of $LD_{50(30)}$ value, i.e. to 1 / $LD_{50(30)}$.

These assumptions can be expressed by the following formulas, where D is dose rate:

$$\frac{dN_P}{dt} = kD - \lambda N_P \quad (1)$$

$$N_{LD} \propto \frac{1}{LD_{50(30)}} \propto N_P \quad (2)$$

By solving eq. (1) and using eq. (2),

$$N_P = \frac{kD}{\lambda}(1-\exp[-\lambda t]) \quad (3)$$

$$\frac{1}{LD_{50(30)}} = k'D(1-\exp[-0.693/T_{1/2}t]) \quad (4)$$

where $T_{1/2}$ is half life of disappearing of the damaged cells, t is time during irradiation, and k, k' are constant. Although the number and quality of the damaged cells may change after the end of irradiation, here assumed that the change is equal for every condition.

We calculated a better-fit parameter for $T_{1/2}$ among several discretely selected values. It has proved to be 200 min, as shown in Table 2. However, as shown in the table, the relative relation between the two $LD_{50(30)}$ values at high dose rate cannot be analyzed by eq. (4), i.e., only by linear term of D. So we introduced additional quadratic term for dose rate, i.e $(D + k''D^2)$ instead of D. This analysis is also included in the Table 2, in which an additional adjustable parameter k'' was chosen to fit the relative values of two values at high dose rate, here $k'' = 1.11\times10^{-6}$.

Table 2. Analysis of data of Table 1 by assuming a model with best-fit parameters of $T_{1/2}$ and k''

D(rad/min)	t(min)	D x exp[$-0.693/T_{1/2}t$]*		$(D + k''D^2)$x exp[ ] *		1 / $LD_{50(30)}$*
706	1	2.436	(0.88)	2.980	(1.076)	(1.079)
68	12	2.762	(1)	2.767	(1)	(1)
8	120	2.716	(0.983)	2.716	(0.982)	(0.897)
4.5	240	2.537	(0.918)	2.537	(0.917)	(0.826)
3	360	2.135	(0.773)	2.135	(0.772)	(0.818)
2.5	480	2.024	(0.733)	2.024	(0.731)	(0.775)

*The parentheses show the values of ratio normalized to the value at 68 rad/min.

Tentative conclusions from this simple analysis are as follows:
(1) Among several values, 60, 100, 200, and 300 min., which were chosen for the parameter $T_{1/2}$, 200 min (ca 3 hr) gave the best agreement with the observed values. This value might have correlation with the time interval (12 hr) for which "Elkind type recovery" becomes apparent for Chinese hamster cells (33).
(2) The necessity of introducing the quadratic term of D for fitting the observed data may

mean the mutual interaction of the initially formed, partially damaged species, or the interaction of the damaged species with some radiation-induced product of intracellular components (such as the free radicals produced by the radiolysis of intracellular water), can play an important role in the high dose rate levels, corresponding to the spatially increased concentration of the damaged cells with increasing dose rate.

4. CONCLUSION

(1) Critical comments on ICRP recommendations were made from several points. The recommendations should be amended, both by honestly adopting the recent scientific findings and by carefully considering several non-scientific factors which influence the feelings of majority of people and economy for keeping radiation safety, from the global point of view.
(2) As for the determination of presence or absence of threshold and assessment of risk coefficient at low dose from epidemiological data, it seems necessary to re-estimate the individual dose of A-bomb survivors by considering their additional chronic exposure due to living after explosion at the contaminated area, and to reconsider the treatment of data of "zero-exposure" group.
(3) Recent experimental data at the background level radiation show several evidences of no harm or hormetic effects at low dose and low dose rate exposure.
(4) The dose rate effect should thoroughly be investigated, and the risk coefficient at various conditions should be re-estimated. For an educational purpose, a mathematical analysis of an example of dose rate effect for an experimental animal was illustrated.
(5) A new paradigm for radiation effect is hoped to be established by adopting some suitable "de minimis" levels both for dose and dose rate, and recently suggested values for setting standards in accordance with this concept were shown.

ACKNOWLEDGEMENTS

The author wishes to express his sincere thanks to Professor Emeritus Kodi Husimi, Professor Emeritus Eizo Tajima, Professor Emeritus Tsutomu Sugahara, Professor Emeritus Nobufusa Saito, Professor Emeritus Masanobu Sakanoue, Professor Emeritus Sohei Kondo, Dr. Masashi Imamura, Mr. Yoshiharu Shinozaki, Professor Emeritus Shigefumi Okada, Professor Hikoyuki Yamaguchi, Dr. Hiroshi Tanooka, Professor Emeritus Tsugio Shiroya, Professor Emeritus Ryota Miki, Dr. Toyojiro Fuketa, Professor Akiko Kubodera, Professor Kazuaki Kato, and several colleagues of Radiation Education Forum, for their warm encouragements from all people and for helpful suggestions from several people, especially Prof. Sugahara, Prof. Kondo, Prof. Yamaguchi, and Dr. Tanooka.

REFERENCES

1. T. Matsuura, "How to Improve the Education of Radiation and Radioactivity", Proc. of 1996 SERNIA (Symposium on Environmental Radioactive Nuclides Impact in Asia), Taipei, 6-8 Sept., 1996, pp.3-11.
2. T. Matsuura, "Toward Improvements of the Education Concerning Radiation, Radioactivity, and Nuclear Energy in High Schools in Japan", Proc. of 10th Pacific Basin Nuclear Conference, Kobe, Japan, 20-25 Oct. 1996, pp.969-978.
3. T. Matsuura, "Activities of "Radiation Education Forum"--Toword Improvements of the Education of the Science Subject in Schools in Japan and Towards Removal of the Widespread Feeling of the "Radiophobia" by the General Public", Hokenbutsuri, 32(2), 235-239 (1997). (in Japanese)
4. ICRP Publication 60, "1990 Recommendations of the International Commission on Radiological Protection, Adopted by the Commission on November 1990", Annals of the ICRP,Vol. 21, Nos. 1-3 (1991); (Japanese version, published by Japan Isotope Association, 1991).
5. M. Sakanoue, "Comparison of Radiation Level in Japan by Carborne Monitoring", Radioisotopes, 44, 459-463 (1995). (in Japanese)
6. Nuclear Safety Research Association, "Environmental Radiation and Cancer", Report of study group (Chairman: I. Miyanaga), March 1997, pp. 61. (in Japanese)
7. H. Planel, J. P. Soleilhavoup, R. Tixador, G. Richoilley, A. Conter, F. Croute, C. Croute, C. Caratero, Y. Gaubin, "Influence on Cell Proliferation of Background Radiation or Exposure to Very Low, Chronic γ Radiation", Health Physics, Vol. 52, 571-578. (1987).
8. L. A. Sagan, "What is Hormesis and Why Haven't We Heard About it Before?", Health Physics, Vol. 52, No. 5, 521-525 (1987).
9. T. D. Luckey, "Physiological Benefits from Low Levels of Ionizing Radiation", Health Phys., Vol. 43, 771-789 (1982); T. D. Luckey, "Hormesis with Ionizing Radiation", CRC Press, Boca Raton, 1980; T. D. Luckey, "Radiation Hormesis", CRC Press, Boca Raton, 1991. (These two books have the Japanese-translated versions.)
10. K. Ishida, "Radiation Hormesis Effect--Recent Studies",

Genshiryoku-kogyo, 43 (1), 89-76 (1997). (in Japanese)
11. S. Kondo, "Health Effects of Low Level Radiation", Kinki University Press, Osaka, Japan, 1993.
12. T. Yamada, "Radiation Hormesis: the Stimulating Effects of Low Level Ionizing Radiation", 1995 International Chemical Congress of Pacific Basin Societies [PACIFICHEM '95], Dec. 17-22, 1995, Honolulu.
13. M. Goldman, "Cancer Risk of Low-Level Exposure", Science, Vol. 271, 1821-1822 (29 March, 1996).
14. M. Kaneko, "Status of ICRP Recommendations at Nuclear Power Plants", Hokenbutsuri, 31(4), 426-429 (1996) (in Japanese); M. Kaneko, "Low Level Radiation Effects and Concept of Safety", Proc. of 22nd Japan Conference on Radiation and Radioisotopes", Yokohama, Dec. 17-19, 1996, A651.
15. T. Sugahara, "Hiroshima and Nagasaki: From Fear through Science to Risk Assessment, 100 Years of X-Rays and Radioactivity (RON-BEC100), D. D. Sodd et al eds., Bhabha Atomic Research Centre, India, 1996, pp. 367-376; T. Sugahara, "The Radiation Paradigm Regarding Health Risk from Exposures to Low Dose Radiation", in "High Levels of Natural Radiation 1996, Radiation Dose and Health Effects", L. Wei and T. Sugahara, eds., Elsevier, 1997, pp.331-339.
16. H. W. Patterson, "Setting Standards for Radiation Protection: the Process Appraised", Health Phys., 72, 450-757 (1997).
17. J. S. Puskin, N. S. Nelson, "Risks from Low Doses of Radiation", Science, Vol. 272, 631 (3 May 1996); R. H. Nussbaum, Science, Vol. 272, 632 (3 May 1996); D. A. Pierce, D. L. Preston, Science, Vol. 272, 632 (3 May 1996).
18. E. Tajima, "What the Radiation Protection Standard Means", Nuclear Safety Research Association, Primar No. 1, (1994). (in Japanese)
19. S. Okada, "Dose-Effect Relationship in Low Dose Range", in panel discussion "On Linear Hypothesis of Dose-response Relationship", Proc. 34th Meeting of Isotopes, 260-263 (1997). (in Japanese)
20. T. Sugahara, "What the Discovery of X-rays has Brought us--A Perspective for 100 Years", Environment and Health, 8, (6), 233-240 (1995). (in Japanese)
21. D. Tricopoulos, X. Zavitsanos, C. Kontis, P. Drogari, C. Proukakis, E. Petridon, "The Victims of Chernobyl in Greece: Induced Abortions after Chernobyl", Br. Med. J., 295, 1100 (1987).
22. Nuclear Safety Research Association, "Studies on the Threshold Problems for the Cancers Induced by Radiation", Report of study group (Chairman: T. Sado), March 1997, pp. 213. (in Japanese)
23. T. Sugahara, O. Nikaido, M. Watanabe, T. Niwa, "Various Problems of Radiation Paradigm", Environment and Health, 8, (1), 1-8 (1995). (in Japanese)
24. M. Watanabe, "Peculiarity of Biological Effect of Low Dose Radiation Related to Carcinogenesis", Proc. of 22nd Japan Conference on Radiation and Radioisotopes", Yokohama, Dec. 17-19, 1996, A620.
25. J. V. Neel, W. J. Schull, A. A. Awa, C. Satoh, H. Katoh, M. Otake, Y. Yoshimoto, "The Children of Parents Exposed to Atomic Bombs: Estimates of the Genetic Doubling Dose of Radiation for Humans", Am. J. Hum. Genet., 46, 1053-1072 (1990); J. V. Neel, W. J. Schull, "The Children of Atomic Bomb Survivors", National Academy Press, Washington, D. C. (1991).
26. D. Thompson, "A-Bomb Fallout--Radiation Kills, but not as Effectively as We Thought", Time, June 23, 1997, p. 54.
27. A comment by Dr. E. Douple, delivered by a private communication from Dr. Mitio Inokuti.
28. D. Preston, K. Mabuchi, "Effects of Radiation Exposure", Time, Aug. 4, 1997, p.3; A. Shardt, Time, Aug. 4, 1997, p.3.
29. H. Okumura, M. Mine, S. Honda, H. Kondo, "Relative Risk of A-Bomb Radiations", in "Verification of Radiation Hormesis" eds, by J. Misonoh and T. Yamada, J. of the Atomic Energy Society of Japan, 39 (7), 528-531 (1997). (in Japanese)
30. Y. Shimizu, H. Kato, W. J. Scull, D. G. Heal, "Life Span Study Report II. Part 3, Noncancer Portality, 1950-85, Based on the Revised Doses (DS86)", Radiation Res., 130, 249-266 (1992).
31. Y. Shimizu, H. Kato, W. J. Schull, K. Mabuchi, "Dose-Response Analysis among Atomic-Bomb Survivors Exposed to Low-Level Radiations", in "Low Dose Irradiation and Biological Defence mechanisms", T. Sugahara et al eds., Elsevier Science Pub., Amsterdam, 1992, pp.71-74.
32. F. E. Neal, "Variation of Acute Mortality with Dose-rate in Mice Exposed to Single Large Doses of Whole-body X-irradiation", Int. J. Radiat. Biol. 2, 295 (1960).
33. Japan Nuclear Energy Society, Special Committee for the Effect and Safety Assessment of Low level Radiations, "Terms and Health Effect of Radiations for Nuclear Engineers", Aug. 1992. (in Japanese)
34. D.A. Pierce, Y. Shimizu, D. L. Preston, M. Vaeth, K. Mabuchi, "Studies of the

Mortality of Atomic Bomb Suvivors. Report 12, Part I, Cancer: 1950–1990", Radiation Res., 146, 1–27 (1996).
35. S. Nakashima, and others (23 researchers), "Studies of Atomic Bomb Effects on Residents in Nagasaki", in "Genshibakudan Saigai Chosa Hokokusho (Atomic Bomb Disaster Survey Compiled Reports), Nihon Gakujutsu Kaigi, ed., Nihon Gakujutsu Shinkokai Publisher, Tokyo, 1953, pp. 949–978 (in Japanese).
36. T. Sugahara, private communication.
37. M. Mifune, T. Sobue, H. Arimoto, Y. Komoto, S. Kondo, H. Tanooka, "Cancer Mortality Survey in a Spa Area (Misasa, Japan) with a High Radon Background", Jpn. J. Cancer Res., 83, 1–5. 1992.
38. P. H. Abelson, "Uncertainties about Health Effects of Radon", Science, 250, 353 (1990).
39. UNSCEAR, "Sources and Effects of Ionizing Radiation", UNSCEAR 1994 Report, United Nations, New York, 1994.
40, I. Hayata, "Advanced Cytogenetical Techniques Necessary for the Study of Low Dose Exposures", in "High Levels of Natural Radiation 1996, Radiation Dose and Health Effects", L. Wei and T. Sugahara, eds., Elsevier, 1997. pp.293–300; S. Nakai, T. Jiang, D. Chen, I. Hayata, Y. Yuan, N. Morishima, S. Fujita, T. Sugahara, L. Wei, "Effect of Low Dose Rates on the Production of Chromosome Aberration under Lifetime Exposure to High Background Radiation", in "High Levels of Natural Radiation 1996, Radiation Dose and Health Effects", L. Wei and T. Sugahara, eds., Elsevier, 1997. pp.307–315.
41. M. K. Nair, ed., "Natural Background Radiation Cancer Registry", Regional Cancer Centre, Trivanderum Technical Report–1 (1990 – 1994), 1996.
42. T. Sugahara, "Difficulty in Epidemiology", Environment and Health, 8, (5) 163–167 (1995) (in Japanese); H. Kato, "Problems in Epidemiological Studies", Environment and Health, 8, (5) 201–208 (1995). (in Japanese)
43. M. H. Elkind, H. Sutton, "Radiation Response of Mammalian Cells Grown in Culture. I. Repair of X–Ray Damage in Surviving Chinese Hamster Cells", Radiat. Res., 15, 556–593 (1960).
44. J. Kiefer, "Biological Radiation Effects", Springer Verlag, Berlin–Heidelberg, 1990; (Japanese version) translated by T. Shiroya, H. Oyama, J. Suhara, T. Yamada, Springer Verlag, Tokyo, 1993.
45. T. Matsuura, K. Sasaki, "On the Primary Retention in Neutron Irradiated Chromium Trisacetylacetonate", Radiochim. Acta, 49, 17–23 (1990).
46. S. Kondo, "Tissue–Repair Error model for radiation Carcinogenesis", Proc. 12th Congr.Photobiology, Vienna, 1997, in press.
47. A. Ootsuyama, H. Tanooka, "One Hundred Percent Tumor Induction in Mouse Skin After Repeated Irradiation in a Limited Dose Range", Rad. Res., 115, 488–494 (1988).
48. A. Ootsuyama, H. Tanooka, "Zero Tumor Incidence in Mouse Skin After Repeated Life–time Exposure to 0.5 Gy of Beta Radiation", Rad. Res., 134, 244–246 (1993).
49. R. Doll, R. Peto, "The Causes of Cancer––Quantitative Estimates of Avoidable Risks of Cancer in the United States Today", J. Natl. Cancer Inst., 66, 1101–1308 (1981); "The Causes of Cancer", Oxford University Press, 1981. (Japanese translated version, by K. Aoki, Y. Ohno, Nagoya Univ. Press, 1991).
50. K. L. Mossman, M. Goldman, F. Masse, W. A. Mills, K. J. Schiager, R. J. Vetter, "Radiation Risk in Perspective", Health Physics Society Position Statement", Health Phys. Newsletter, 24, (3), 1996.

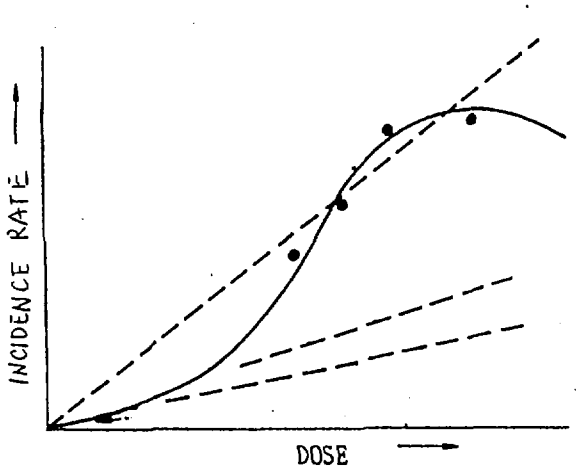

Fig. 1. The schematic curve of dose-response relationship (Ref. 4, NCRP, 1980)

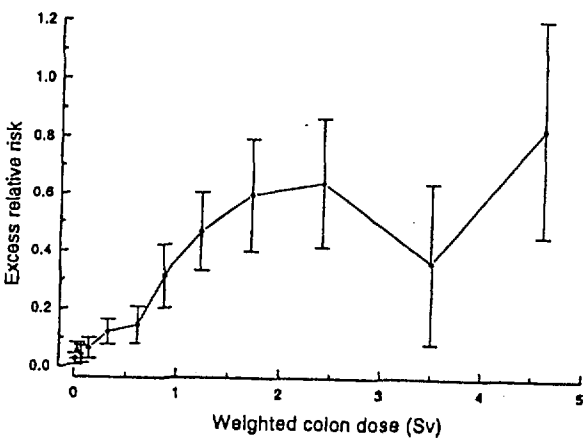

Fig. 2. Shape of the dose response for solid cancer for A-bomb surviviors, shown in terms of excess relative risk, adjusted to males of age 30 at exposure. (Error bars show 95% reliability region.) (Ref. 33) → (34)

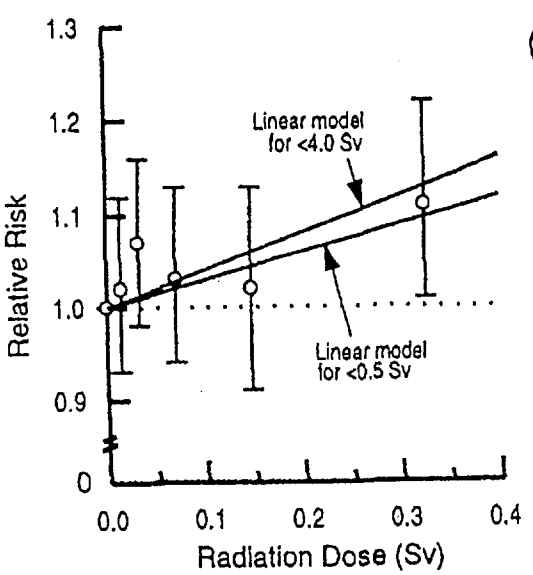

Fig. 3. Shape of the dose response for solid canoer for A-bomb surviviors at low dose region. (Error bars show 95% reliability region.) (Ref. 34) → (31)

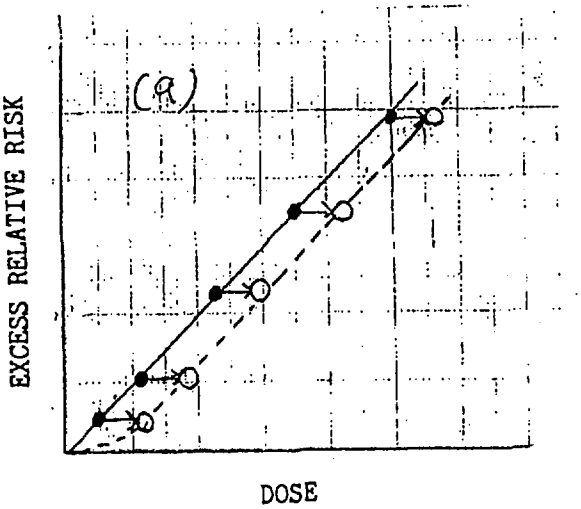

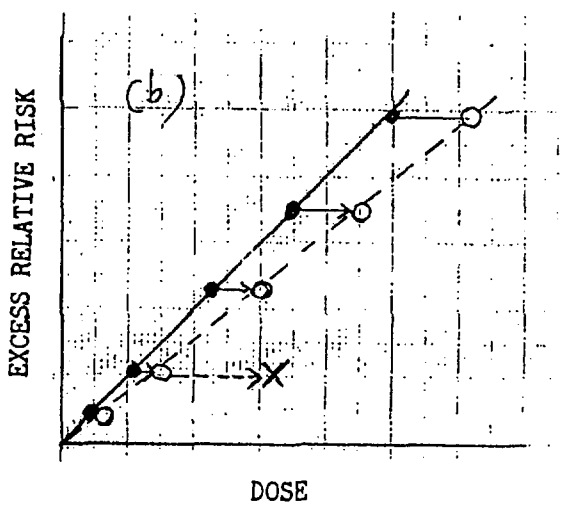

Fig. 4. Schematic representation of re-estimation for dose-response relationship for A-bomb survivors.
●: present plots,
○: corrected plots including the chronical exposure from elevated background radiations,
a: when the additional dose is the same for all people studied,
b: more probable case, point x represents the possible erratic plot due to "black rain"

AU9817369

Important Radiation Protection Aspects of the Operation of a Commercial Medical Cyclotron

BHASKAR MUKHERJEE
ANSTO, Safety Division, Radiation Protection R&D Section
PMB 1, Menai, NSW 2234, Australia

SUMMARY. The routine operation of Medical Cyclotrons generating a high yield of radioisotopes results in the accumulation of induced radioactivity in various critical cyclotron components, caused by the neutrons produced during target bombardment with energetic protons. Evidently, the activated cyclotron components impact on the personnel radiation exposure of the workers during the routine maintenance and emergency repair procedures. Since the adherence to the principle of ALARA (As Low As Reasonable Achievable radiation exposure) constitutes a major objective of the cyclotron management, it became imperative to investigate the effects of the induced radioactivity prevailing in the cyclotron target cave and the decay (cool down) time thereof on the personnel radiation exposure. By utilising the health physics survey database collected during the 1994-1996 period and experimental results, important guidelines have been developed to achieve the optimum personnel dose minimisation. This paper highlights the practical radiation protection aspects of these guidelines.

1. INTRODUCTION

Since July 1991 the Radiopharmaceutical Division of the Australian Nuclear Science and Technology Organisation (ANSTO) has operated a 30 MeV H^- ion Medical Cyclotron (Model: CYCLONE 30, Manufacturer: Ion Beam Applications, Louvain La Neuve, Belgium). During routine isotope production operations at the cyclotron a thick copper substrate plate electroplated with thin layer of selected enriched target material is bombarded with a 30 MeV proton beam current up to 450 μA. The nuclear reaction of protons with the copper atoms result in the production of prompt evaporation neutrons with a peak energy of ~1.8 MeV. These evaporation neutrons slow down via multiple collisions with the concrete shielding walls of the target cave, bounce back to the interior space of the cave activating the cyclotron parts, beam tube components and other utilities installed in the irradiation cave.

At our cyclotron facility gamma dose equivalent rates of $\sim 10^5$ $\mu Sv h^{-1}$ were measured at contact with the target stations and beam collimators after the completion of the routine weekly 60 hour isotope production run. Evidently, these gamma rays emitted from the activated cyclotron components impose a crucial radiation exposure problem for the cyclotron maintenance technicians (1).

At our Health Physics laboratory, experiments had been carried out in order to identify the specific path-ways of cyclotron component activation and to assess the probable personnel radiation exposure during handling of the activated cyclotron parts (2). The cool-down (radioactive decay) characteristics (3) of the activated cyclotron components were estimated experimentally at different target bombardment conditions using the wall mounted gamma area monitors interfaced to the Health Physics Datalogger (4).

The gamma dose equivalent rates at contact with various locations of interest at the target irradiation station and at the typical work areas of the maintenance personnel were carefully measured with a radiation (gamma) survey instrument during the routine weekly health physics survey procedure for the past the three years (1994 - 1996) operation period of the cyclotron, and included in a database. By utilising this large health physics database and the recent experimentally estimated cool-down characteristics (3), a simple physical model has been developed. The model was used with a view to predicting the personnel radiation exposure prior to a particular active maintenance work being undertaken in the cyclotron target cave, and to provide a valuable decision making aid to minimise occupational radiation exposure to cyclotron technicians.

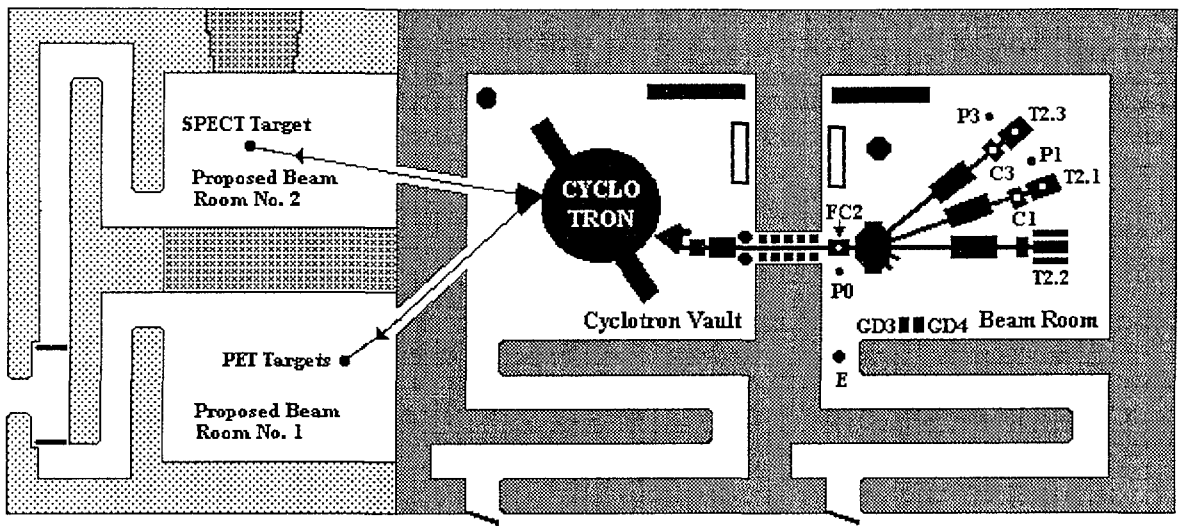

Figure 1: Schematic diagram of the 30 MeV (H^- ion) Medical Cyclotron Facility of ANSTO showing the Cyclotron Vault and Beam Room housing the Cyclotron and the Target Irradiation Stations as well as the proposed PET and SPECT beam rooms. The diagram is explained in the text.

2. MATERIALS AND METHOD

In course of routine Health Physics surveys, the gamma dose equivalent rates at various selected work areas were assessed with a wide-range gamma dose rate meter (Figure 1) and the results were entered in a database. The routine Health Physics surveys are usually conducted on Monday mornings (7.30 - 8.30 AM) allowing the decay of the induced component-radioactivity during weekends, hence minimising the personnel radiation exposure to Health Physics technicians. In this investigation the gamma dose rates at contact with the Faraday-cup FC2, solid target stations T2.1 and T2.3, the collimators C1 and C3, the work areas P0 (50 cm from Faraday-cup), P1 (50 cm from target station T2.1) and P3 (50 cm from target station T2.3) and the entrance point E of the beam room have been taken into account (Figures 2a, 2b, 2c, 2d and 2e).

It became evident that the decay characteristics of the beam room radiation field (gamma dose equivalent rate) could not be explicitly assessed from the gamma dose rates recorded at various locations of interest in the beam room during the routine Health Physics survey. Hence, the cool-down characteristics of the induced gamma radiation field were determined experimentally as follows: The gamma area monitors GD3 and GD4 at the entrance of the beam room (Figure 1) was switched on at 07:59AM, immediately after the transfer of the target shuttle (irradiated with 30 MeV protons for 12 hours in target station T2.3) to the radiochemistry cell. The gamma dose rates were sampled with the Health Physics Watchdog (4) for every minute till 11: 49 PM and shown in Figure 3.

During the operation period 20 March - 30 June 1995 no health physics survey was performed and the target station T2.1 and the collimator C1 were removed. This is clearly indicated by the absence of data points in Figures 2b and 2c.

3. RESULTS AND DISCUSSION

The gamma dose rates at contact with Faraday-cup FC2, at the spots P0 and at E over the operation period 12 December 1994 - 25 February 1996 are shown in Figure 2a. The gamma dose rates at contact with target station T2.1, at the spots P1 and at E over the same operation period are shown in Figure 2b. The gamma dose rates at contact with the collimator C1 and at the beam room entrance E over the same period are shown in Figure 2c. Similarly, the gamma dose rates at contact with the target station T2.3, at the spots P3 and at E are shown in Figure 2d. The gamma dose rates at contact with collimator C3 and at entrance point E are shown in Figure 2e. It is evident from the routine health physics survey data

recorded on every Monday morning between 7.30-8.30 hr that the gamma dose rates prevalent at contact with the cyclotron targets (2.1 and 2.3), beam collimators (2.1 and 2.3), Faraday Cup (FC2) as well as the dose rates at a distance of 50 cm therefrom and at the Beam room entrance (E) remained unchanged during the entire data collection period from December 1994 - February 1996. This finding was confirmed by the "plateau nature" of the graphs presented in Figures 2a, 2b, 2c, 2d and 2e. The target station 2.1 was removed on 23 March 1995 and replaced with an upgraded high performance target station (suitable for a beam current up to 450 μA) on 30 June 1995 as indicated by the missing data points in Figures 2b and 2c.

The gamma doses rate at contact and at a distance of 50 cm for each work area were represented in terms of the dose rate at Beam room entrance (E):

$$D_i(t_d) = k_i D_e(t_d) \quad (1)$$

Where,

D_i [μSvh^{-1}] = gamma dose rate at i^{th} work area after the delay period of t_d

$$k_i = D_{pi}/D_e \quad (2)$$

Where,

D_{pi} = Plateau dose rate at work area of type i

D_e = Plateau dose rate at the Beam room entrance (Figures 2b, 2c, 2d, 2e).

The results are summarised in Table 1.

In order to assess the effect of the time delay (cool down time) of the inducted radioactivity in the beam room and the subsequent reduction of the personnel dose explicitly, the decay curve shown in Figure 3 was constructed. The decay curve was unfolded into four exponential functions representing the presence of four major radioactive species generated in the beam room during the isotope production process (3):

1) $A_1(t_d) = 0.65 \exp(-0.693t_d/4)$ (3a)
2) $A_2(t_d) = 0.20 \exp(-0.693t_d/156)$ (3b)
3) $A_3(t_d) = 0.06 \exp(-0.693t_d/900)$ (3c)
4) $A_4(t_d) = 0.09 \exp(-0.693t_d/64224)$ (3d)

Where, $A_1(t_d)$, $A_2(t_d)$, $A_3(t_d)$ and $A_4(t_d)$ represent respectively the normalised activity of ^{27}Al ($T_{1/2}$ = 4 min), ^{55}Mn ($T_{1/2}$ = 156 min), ^{23}Na ($T_{1/2}$ = 900 min = 15 h) and ^{58}Fe ($T_{1/2}$ = 64224 min = 44.6 d) induced in the various cyclotron components.

Hence, the gamma dose rate at the Beam room entrance D_e after the delay period of t_d could be calculated as:

$$D_e = D_0 [A_1(t_d)+A_2(t_d)+A_3(t_d)+A_4(t_d)] \quad (4)$$

Where, D_0 = Gamma dose rate detected immediately after the removal (t_d = 0) of the irradiated target = 9000 μSvh^{-1} (Figure 3).

Table 1: Showing the maximum gamma dose rate D_{max} and the ratio (k_i) between the plateau and entrance dose rate for selected work areas in the cyclotron Beam room (Figure 1).

Work area	D_{max} [μSvh^{-1}]	k_i
FC2 (at contact)	2000	10
FC2 (at 50 cm)	550	2.7
T2.1 (at contact)	30000	150
T2.1 (at 50 cm)	5000	25
T2.1 (Collimator)	100000	500
T2.3 (at contact)	80000	400
T2.3 (at 50 cm)	10000	50
T2.3 (Collimator)	100000	500

By substituting the values of D_e from equation 4 and the k_i from Table 1 in equation 1, the gamma exposure (dose) rate to cyclotron technicians at various critical work locations in the beam room after a delay period of 1, 7, 14 and 30 days were calculated (Table 2).

Using the radiation survey data collected during the 1993 - 1996 period a simple dose optimisation model has been developed. The cyclotron radiation worker dose optimisation (ALARA) model is basically comprised of two constraints:

a) Personnel dose reduction constraint

$$D_p = \Sigma r_i D_i(t_d) T_i/n_i \quad (5a1)$$
$$D_p \text{ (max)} \leq 150 \ \mu Sv \quad (5a2)$$

Where,

D_p = daily maximum allowable dose [μSv] of any one worker authorised by the Statutory Authority

n_i = number of workers for the work of type i

r_i = instrumental dose reduction factor for the work of type i (erection of local shielding, use of special handling tool)

$D_i(t_d)$ = extrapolated work area specific dose rate after the delay time t_d (equation 1)
T_i = execution time of the work of type i

b) Isotope production cost constraint

$$\eta = 1-\Delta R/(\Delta c_d+\Delta c_s+\Delta c_i+\Delta c_t+\Delta c_w) \quad (5b1)$$
$$\eta\ (max) \rightarrow 1 \quad (5b2)$$

Where,
η = Overall performance (efficiency) factor
Δc_d = increment in the organisational (social) cost of dose reduction [$]
Δc_s = increment in the cost of extra shielding installation [$]
Δc_i = increment in the cost of instrumental dose reduction [$]
Δc_t = increment in the cost of down time [$]
Δc_w = increment in the cost of worker's wage/overtime payment [$]
ΔR = Reduction of the daily net revenue earned from the radioisotope sale [$]

4. CONCLUSION

Unlike conventional positive ion cyclotrons, (3) negative ion Medical Cyclotrons, like the CYCLONE 30, possess close to 100% beam extraction efficiency (5). This allows the operation of such cyclotrons of a very high beam current level (~ 850 μA) producing a high yield of radioisotopes. On the other hand, the high beam currents result in the activation of targetry, beam lines and other ancillaries located in the beam room (target cave) and thereby cause high potential radiation exposure to cyclotron technicians during the maintenance or repair work. The aim of the optimisation model presented in this paper is to assist the cyclotron management in achieving a high production performance (criterion 5b2) with the lowest accumulated personnel dose (criterion 5a2). ALARA prevails.

5. REFERENCES

1. Dickie, W.J., Stevenson, N.R. and Szlavik, F.F., 1993, Nuclear Instruments and Methods, Vol B79, pp 919-932.
2. Mukherjee, B., 1994, Proceedings of the 9th Pacific Basin Nuclear Conference, Sydney, Australia, May 1-6, pp 645-649.
3. Mukherjee, B., 1997, Applied Radiation and Isotopes, Vol 48, pp 735-738.
4. Mukherjee, B., 1992, Proceedings of the 13th International Conference on Cyclotrons and their Applications, Vancouver, Canada, July 6-10, pp 252-254.
5. Bol, J.L. Chevalier, A., Conard, M., Jongen, Y, Ladeuze, M., Lannoye, G., Ledocte, T., Lacroix, M., Ninane, A., Ruckewaert, G. and Zaremba, S., 1989, Proceedings of the 12th International Conference on Cyclotrons and their Applications, Berlin, Germany, May 8-12, pp 149-151.

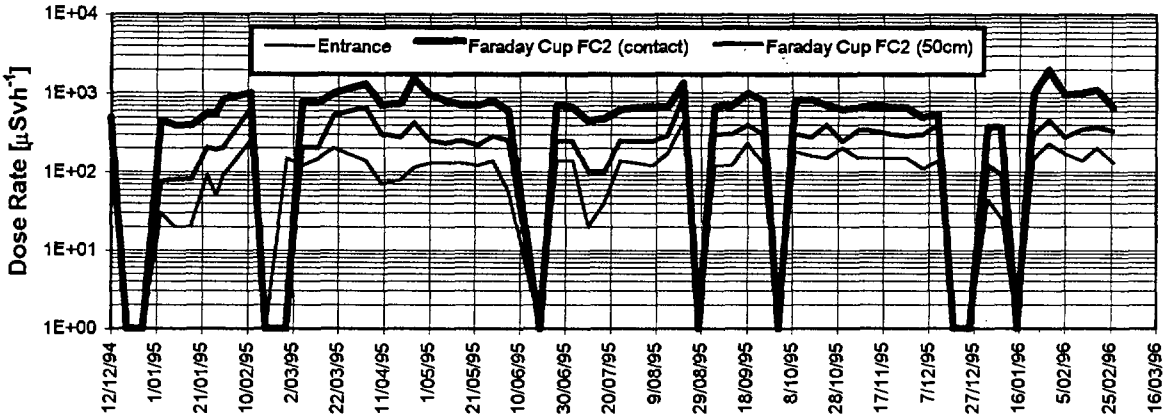

Figure 2a: Gamma dose rates at contact with Faraday-cup FC2 and at P0 (50 cm from FC2) and at the entrance point E of the beam room recorded during the weekly Health Physics Survey over the period of 12 December 1994 - 25 February 1996.

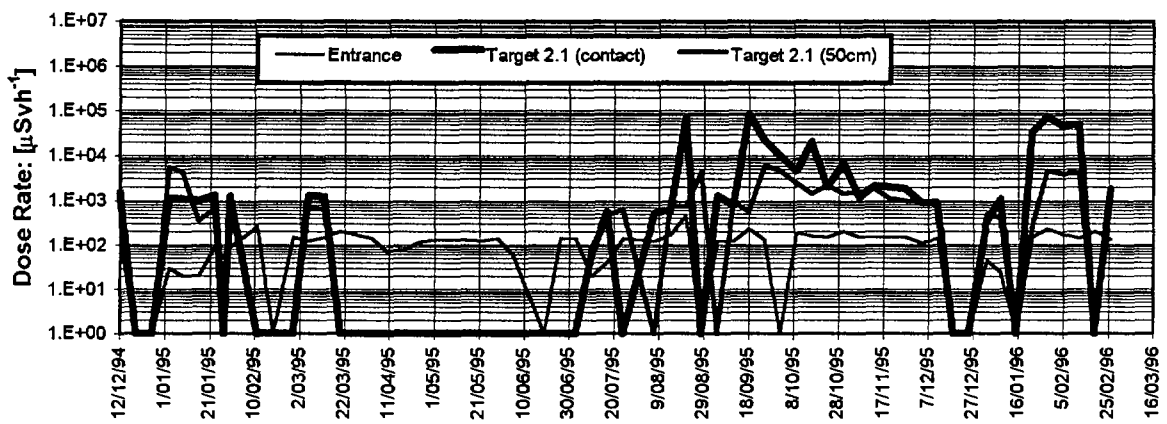

Figure 2b: Gamma dose rates at contact with Target Station T2.1 and at P1 (50 cm from T2.1) and at the entrance point E of the beam room recorded during the weekly Health Physics Survey over the period of 12 December 1994 - 25 February 1996.

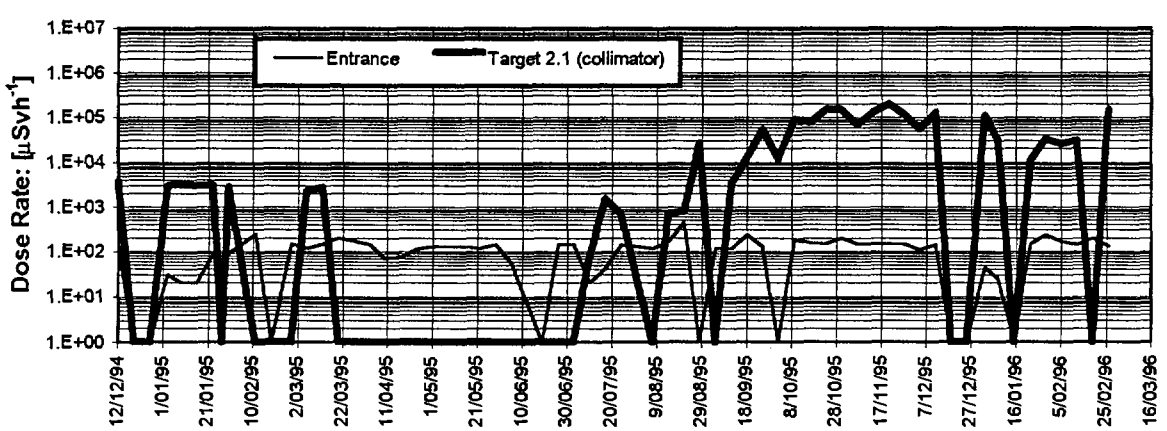

Figure 2c: Gamma dose rates at contact with the Collimator C1 of Target Station T2.1 and at the entrance point E of the beam room recorded during the routine weekly Health Physics Survey over the period of 12 December 1994 - 25 February 1996.

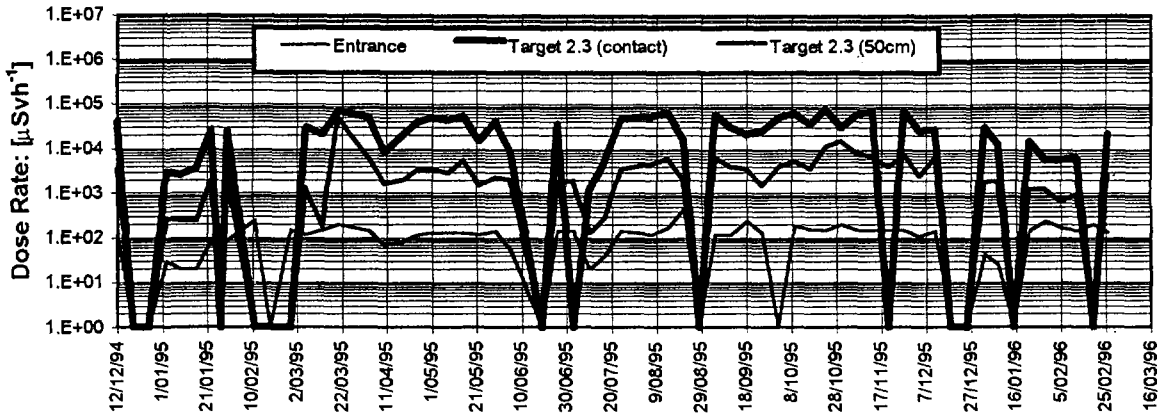

Figure 2d: Gamma dose rates at contact with Target Station T2.3 and at P3 (50 cm from T2.3) and at the entrance point E of the beam room recorded during the weekly Health Physics Survey over the period of 12 December 1994 - 25 February 1996.

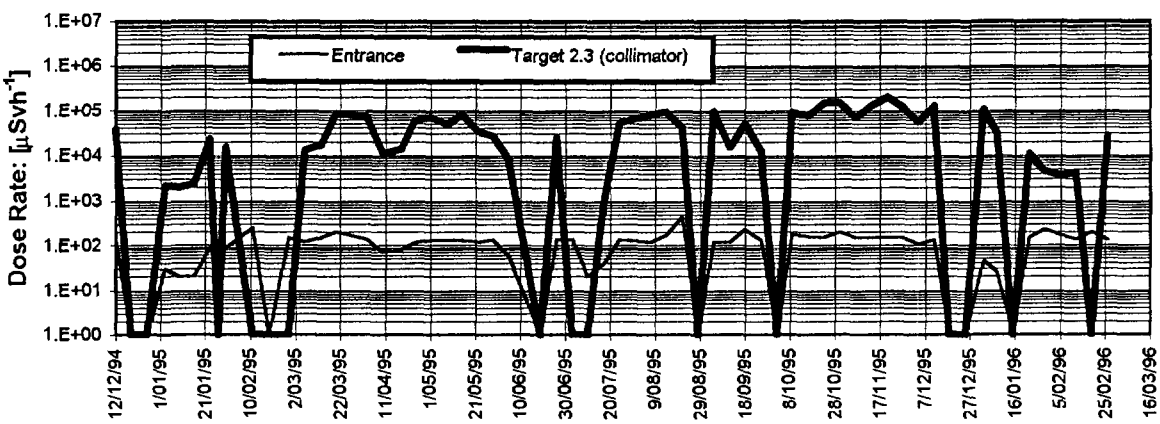

Figure 2e: Gamma dose rates at contact with the Collimator C3 of Target Station T2.3 and at the entrance point E of the beam room recorded during the routine weekly Health Physics Survey over the period of 12 December 1994 - 25 February 1996.

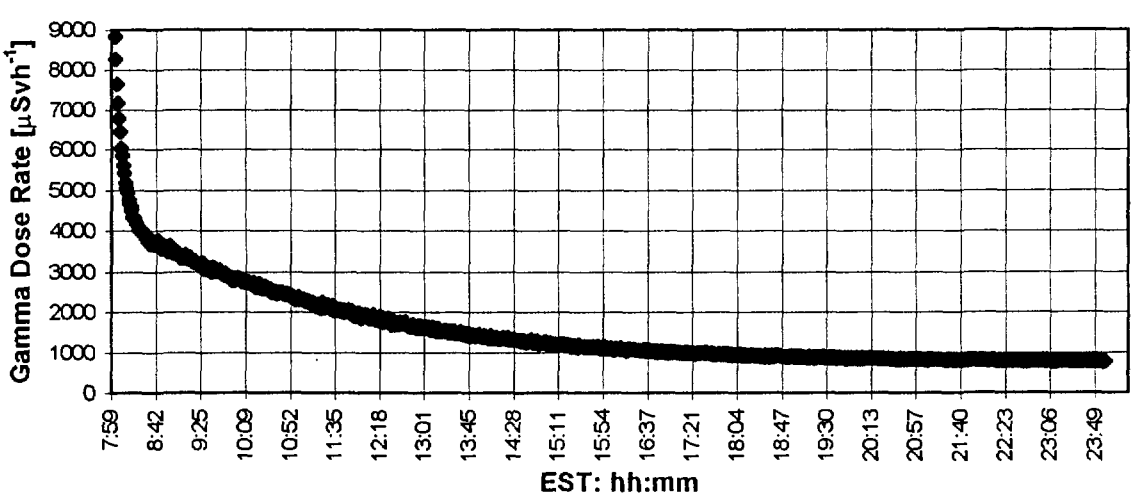

Figure 3: Average gamma dose rate in the beam room detected with the gamma area monitors GD3 and GD4 located at the beam room entrance (Figure 1) is shown as a function of the elapsed (cool down) time of the radiation field prevailing in the Beam (target) room.

Table 2: The work specific personnel radiation exposure to cyclotron maintenance technicians calculated with the ALARA model (equations 5a2 and 5b2) for the delay period of 1, 7, 14 and 30 days after the cyclotron shutdown, the execution time (approximate) of the radiation work (column 2) and the location of the particular work (column 3) area are shown. The average gamma dose rate recorded with the area monitors GD3 and GD4 (Figure 1) on maintenance was found to be $200\mu Svh^{-1}$.

Brief description of the Radiation Work at the NMC	**Duration of Work [minutes]**	**Location of Work (Figure 1)**	**Work specific personnel radiation exposure [μSv/person] after the delay period of:**			
			1 day	**7 days**	**14 days**	**30 days**
Target 2.1 Collimator removal	10	C1	6863	1212	161	1.6
Target 2.1 Collimator replacement	20	C1	13646	2424	323	3.2
Target 2.3 Collimator replacement	20	C3	2099	373	50	0.5
Perforated Beam line, VAT Valve removal	40	P1	1924	342	46	0.1
Perforated Beam line, VAT Valve removal	40	P3	595	106	14	0.1
Target 2.1 Ram failure, Trouble shooting	5	P1	241	43	6	0
Target 2.3 Ram failure, Trouble shooting	5	P3	74	13	2	0.1
Target 2.1 Ram failure, Cleanup procedure	5	P1	241	43	6	0.1
Target 2.3 Ram failure, Cleanup procedure	5	P3	74	13	2	0
Target 2.1 Cylinder removal	10	P1	481	85	11	0
Target 2.3 Cylinder removal	10	P3	149	26	4	0
Target 2.1 Vacuum pump replacement	2	P1	96	17	2	0
Target 2.3 Vacuum pump replacement	2	P3	30	5	1	0
Perforated Faraday Cup removal	5	FC2	105	5	1	0
Perforated Faraday Cup replacement	20	P0	31	19	2	0

Radiation Processing for Environment-friendly Industrial Applications

A B MAJALI and S SABHARWAL
Isotope Division, Bhabha Atomic Research Centre, Trombay, Mumbai 400 085, India.

SUMMARY. Radiation processing techniques are increasingly being applied to minimize the environmental pollution associated with many industries. In the present paper, three such processes are discussed that utilize high energy electron beam (EB) radiation for minimizing environmental pollution. Emission of sulphur containing toxic gases like H_2S is an undesirable side product of viscose-rayon process. EB irradiation can significantly decrease the pollution levels associated with the process by reducing the CS_2 requirement by 40%. EB based additive-free process can be utilized for converting the polytetrafluroethylene (PTFE) scrap into industrially useful microfine powder. Development of fast-response temperature-sensitive hydrogels that swell or shrink in response to small temperature changes in the environment is being sought to reduce the energy consumption levels of many processes. EB crosslinked poly(vinyl methyl ether) gels that swell/shrink about 100 times faster than conventionally crosslinked gels have been developed.

1. INTRODUCTION

The adverse environmental impact of increasing industrialization and use of energy intensive processes have stimulated search for new industrial processes to eliminate or minimize environmental hazards and at the same time produce better materials using less energy. High energy ionizing radiation, with its unique ability to induce chemical reactions in solid, liquid or gas phase at any desired temperature without any catalyst, has many advantages. These include ability to process products in their final form, production of additive-free polymeric materials and energy savings. Thus, radiation technology, by producing better quality products, imparting unique properties to materials and increasing energy efficiency has always been *indirectly* an environment friendly process. However, in recent years this technology is being addressed to *directly* provide answers to many environmental challenges viz. flue-gas treatment, Sato et al. (1), waste water treatment, Chmielewski et al. (2) and plastic waste disposal, Ait et al. (3). Our efforts have been aimed at utilizing the benefits of radiation technology for specific processes of importance to Indian industry. The results of some of these studies are presented.

2. PROCESS STUDIES AND RESULTS

2.1 Viscose-rayon Process

Due to a very tight hydrogen-bonded structure, cellulose can neither be easily dissolved, nor melted and hence this technology depends upon a very convoluted process where cellulose chains are forced apart by reaction of carbon disulphide (CS_2) with soda cellulose, which subsequently decomposes in acid bath to yield rayon fibre; the process generates sulphur containing decomposition products of xanthates which pollute the atmosphere. Rayon manufacture around the world has diminished over the last few years for this reason. The industry is therefore examining appropriate ways to reduce the levels of these emissions in atmosphere. It has been observed that the radiation treatment of paper pulp, increases its sensitivity to enzymatic hydrolysis and its solubility in CS_2; this markedly reduces the quantity of CS_2 required in the viscose process, Charlsbey (4). We have studied the effect of EB treatment on indigenous paper pulp on a laboratory scale to standardise the conditions to obtain the desired degree of polymerization. The effect of radiation dose on the various chemical properties of the paper pulp

is presented in Table 1. The results clearly indicate that a dose of 5 to 10 kGy can reduce the degree of polymerization (DP) of pulp from 625 to about 400-450. In the conventional process, this is achieved by steeping the pulp with alkali for long durations. For the EB treated paper pulp, the quantity of CS_2 required is reduced by about 40% ; a plant consuming about 300 tons of pulp per day can reduce the CS_2 consumption by 40 tons a day.

2.2 Radiation Degradation of Polytetrafluoroethylene (PTFE)

The microfine PTFE powder, due to its outstanding anti-friction properties and non-toxic nature, is extensively used as a non-stick coating material for kitchenware and electric appliances. The polymer, however, is extremely resistant to pulverization and when pulverized by cooling it to -180°C, the high molecular weight powder thus produced has a tendency to progressively agglomerate. It is well known that PTFE predominantly undergoes chain scission on exposure to radiation, therefore its molecular weight can be significantly reduced by irradiation. It was observed that an EB dose of 1-2 MGy was adequate for producing a low molecular weight (1×10^4 - 1×10^5) product amenable to conventional high speed grinding.

Figure 1 shows the particle size distribution of PTFE powder produced by this process using conventional high speed grinding techniques.

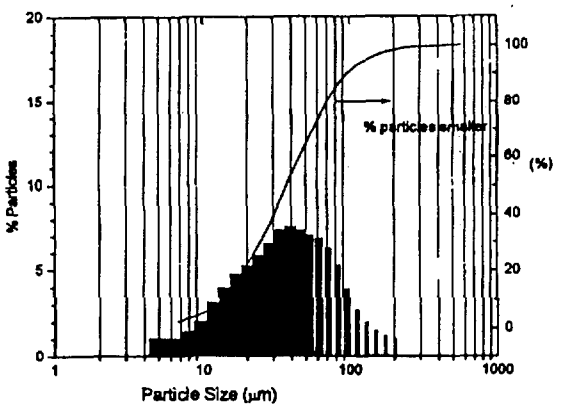

Figure 1: Particle size distribution of EB radiation degraded PTFE.

2.3 EB Crosslinked Fast Response Temperature Sensitive Hydrogels

Generally, aqueous solutions are concentrated by evaporating the water at high temperatures. This is an energy consuming process. Environmentally sensitive polymer gels are an alternative for concentrating many biological slurries near room temperature. These gels display phase transitions in response to small environmental changes, viz. pH, temperature, solvent composition and electric field.

Table 1. Effect of EB radiation dose on the properties of paper pulp for rayon.

Property	EB Irradiation Dose (kGy)				
	0	5	10	15	20
Viscosity, cp	10.84	7.26	6.30	5.13	4.33
Degree of Polymerisation	635.0	461.0	399.0	310.0	236.0
Alpha Cellulose, %	95.13	94.18	92.69	91.63	87.61
Beta Cellulose, %	3.61	4.44	5.70	6.67	10.63
Gamma Cellulose, %	1.26	1.38	1.60	1.70	1.76
Rayon Yield, %	97.52	97.07	97.06	96.79	96.02

Temperature sensitive gels are produced by crosslinking linear polymers that display lower critical solution temperatures (LCST), e.g. poly (vinyl methyl ether) (PVME) and poly (N-isopropyl acrylamide) (PNIPAm). However, the conventional method of crosslinking these polymers by thermochemical route, leads to the formation of homogeneously crosslinked material with an extremely slow response, rendering them unsuitable for industrial applications. For instance, a conventionally crosslinked 1 mm thick sheet of temperature sensitive PNIPAm hydrogel takes more than 24 hours to swell or shrink to equilibrium, Hoffman et al (5). This slow response is due to the fact that the conventionally crosslinked gels are homogeneous to atleast a submicron level. Our recent pulse radiolysis results have shown that by irradiating the aqueous solutions of these polymers at high dose rates with EB accelerators, inhomogeneous crosslinking can be induced, resulting in the formation of fast-response hydrogels, Sabharwal et al, (6,7). We have used irradiation to create inhomogeneous crosslinking of a temperature sensitive polymer- PVME, so as to produce a fast response hydrogel which undergoes a phase transition at 37°C. Figure 2 shows the swelling behaviour of a few hydrogels at various temperatures. The curve clearly indicates a

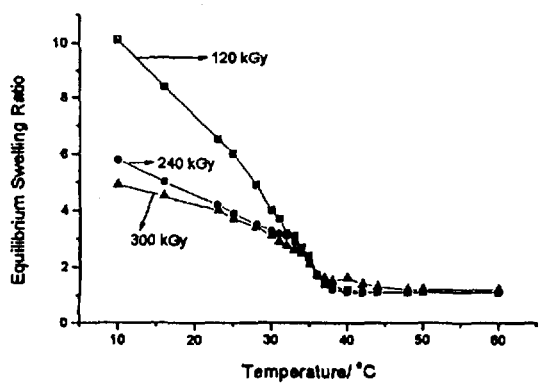

Figure 2: Equilibrium swelling behaviour of EB crosslinked PVME hydrogels at different temperatures.

transition point at 37°C. The hydrogel is produced by irradiating linear PVME to a dose of 300 kGy. The coefficient of diffusion of polymer(D) into water matrix has a value of about 10^{-5} cm^2s^{-1} as compared to conventional hydrogels which generally have (D) value of about 10^{-7} to 10^{-8} cm^2s^{-1}. EB processed gels therefore exhibit faster response time.

The swelling and deswelling response of these hydrogels, shown in Figure 3, clearly indicates that these hydrogels require just a few seconds to reach equilibrium swelling.

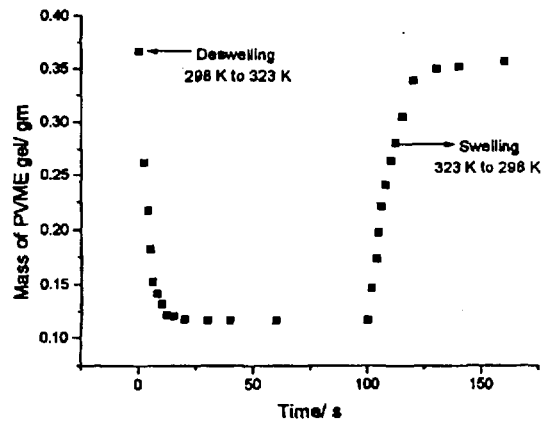

Figure 3: Swelling and shrinking kinetics of EB crosslinked PVME hydrogel.

These materials could be beneficial in reducing the energy requirements for a variety of applications, such as concentrating biological or coal slurries. We have studied the use of those hydrogels for concentrating dilute sewage sludge. In this study, the sludge (2% solids) from input line of Sludge Hyginisation Research Irradiator (SHRI) was used. The PVME gel equilibrated at the temperature of 323K was added to the sludge at 298K and allowed to swell to equilibrium for varying lengths of time (15s to 120s). The gel samples were then taken out, equilibrated at 323K for the same length of time as for swelling, so that they shrink and desorb water. The process was repeated for 10 cycles; the amount of water desorbed by the gel was estimated gravimetrically. The results of this study, shown in Figure 4, indicate that 1 g of gel could remove 9 to 12 g of water from 25 g of sludge, in ten cycles.

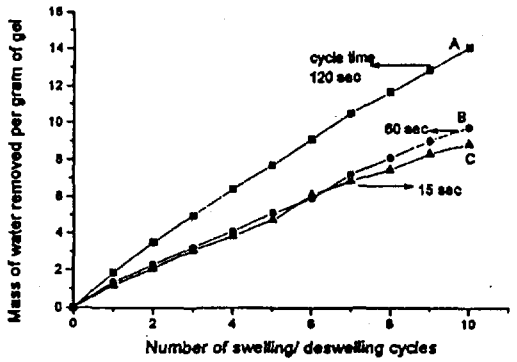

Figure 4: Dewatering behaviour of sewage sludge with PVME gels.

3. CONCLUSIONS

Radiation processing has great potential to reduce environmental pollution from chemical processing industries. EB treatment of pulp for viscose rayon industry, for recycling polymeric wastes and production of fast response temperature-sensitive polymers are promising areas wherein radiation technology can play a major role, provided reliable, high power and cost effective EB machines are available.

4. ACKNOWLEDGEMENTS

The post irradiation viscometry of paper pulp was carried out by Mr. Manish Jain and Mr. Sharad K. Jain at Grasim Industries Ltd., Nagda and Mr. S.K. Roymaulik of Birla Research Institute for Applied Sciences, Nagda. We thank M/s Grasim Industries Ltd. for their help.

5. REFERENCES

(1) Sato, S., Tokunaga, O., Arai, H. and Hashimoto, S., Electron Beam irradiation technology for environmental Conservation, Proceedings Symposium IAEA-SM-325, International Atomic Energy Agency, Vienna, 1992.

(2) Chmielewski, A.G., Zimek, Z., Bryl-Sandelewska, T., Kosmal, W., Kalisz, L. and Kazmiercruzk, Radiat. Phys. Chem., 46, 1995, 1071.

(3) Ait, S.I., Mamar, S. and Hadjadj, A., Radiat. Phys. Chem., 35, 1990, 451-455.

(4) Charlsbey, A., Atomic Radiation and Polymers. Pergamon Press, Oxford, 1966.

(5) Hoffman, A. S., Afrassiabi, A. and Dong, L. C., J. Controlled Release, 4, 1986, 174.

(6) Sabharwal, S., Mohan, H., Bhardwaj, Y. K. and Majali, A. B., J. Chem. Soc. (Faraday Transactions), 92, 1996, 4401.

(7) Sabharwal, S., Bhardwaj, Y. K., Sarma, K. S. S. and Majali, A. B., Synthesis of crosslinked fast response temperature sensitive poly (vinyl methyl ether) hydrogels by electron beam irradiation, Proceedings RadTech Asia 95, Workshop and Symposium, Chylalongkorn University, Bangkok, Thailand, December 1995, 303-310.

The Design and Application of a Radiological Consequence Model for Tropical and Subtropical Regions

R.U. DOMEL, F.F. HARRIS AND J. CRAWFORD
Australian Nuclear Science and Technology Organisation
PMB 1 MENAI NSW 2234
Renate.Domel@ansto.gov.au

Key words: Radiological consequence, tropical, subtropical, exposure pathways, dose assessment

SUMMARY The post Chernobyl era has seen the development of a plethora of radiological consequence models. The information used in these models pertains mostly to temperate and cold climate data, with these data mostly being hard-wired into the body of the model. At the Australian Nuclear Science and Technology Organisation (ANSTO), a model is being developed with a user-friendly interface which will assess the radiological consequences, after an incident, in tropical and sub-tropical climates. The model combines specific regional data with transfer parameters (soil to plant, plant to animal) obtained for tropical and sub-tropical regions. Where the relevant data are not available default temperate data are used whilst specific research will be initiated to determine the information required.

INTRODUCTION

The use of a model as a tool to aid in the assessment of the effects on the environment and humankind, inclusive of the effects of industrial incidents or accidents, can be very valuable for emergency response, evaluation, planning and research. The model needs to be able to handle the complexity of environmental situations whilst allowing the operator to alter parameters as required to meet specific needs.

The post Chernobyl era has seen the development and assessment of many radiological consequence models dealing with nuclear accidents and incidents including planned discharges and waste repositories. The major studies have been mainly in the temperate regions of the world and so the information used in these models pertains mostly to temperate and cold climate studies with these data mostly being hard-wired into the body of the model. This left a large proportion of the worlds population, resident in the tropical and sub-tropical regions, without such a tool.

At ANSTO, a model is being developed with a user-friendly interface which will allow the user to determine the radiological consequence in the event of a release of radionuclides in tropical and subtropical climates. The model was focussed on the major pathways by which dose assessment to humans is made. These pathways include inhalation, groundshine, cloudshine and the transport of radionuclides in the food chain, with atmospheric dispersion being modelled separately and made available to the program. Preprocessing of the output produced by the dispersion model is required to select the appropriate data and to store it in a format suitable for the program. Further, for the current implementation, physical processes such as leaching, runoff and groundwater transport are not considered, although the concentration data can be preprocessed by such models if available.

METHOD

Data Acquisition

The initial data acquisition was based on locally available publications and ANSTO expertise to ascertain the amount of relevant material available on site. Various people had information to impart relating to the type of models used overseas, their structure and type of data used within these models. Post Chernobyl, many countries are using the information specific to their own environment to model the radiological consequences and verify

the model response against measured data. Literature relating to many such models has been obtained during the data acquisition process. Two of these, found to be very valuable are: i TAME - The Terrestrial-Aquatic Model of the Environment (1), ii Individual Evaluation of Model Performance for Scenario S (2). Other information gathered consisted of lists of possible contacts, as well as related studies. These included the International Atomic Energy Agency (IAEA) initiated Cooperative Research Program (CRP) collating transfer parameters for tropical and semi-tropical environments. An ANSTO library search of books, databases and journals was conducted. Relevant books in the library included proceedings of conferences and seminars on environmental radioactivity. These were mainly of the 1970's and 1980's studies associated with weapons testing radiological consequences but still provided good background data. The IAEA Technical Report Series, Safety Series and the Annals of the International Commission on Radiological Protection (ICRP) all provided important sources of information. The various annals of the ICRP are important sources for the Reference Man (Caucasian) data needed in the model, including the recent ICRP Publication 71 'Age Dependent Doses to Members of the Public from Intake of Radionuclides: Part 4 Inhalation Dose Coefficients' (3). An IAEA Technical Document is currently being prepared which presents Reference Asian Man data. In conjunction with the library staff, a search of the International Nuclear Information System (INIS) was conducted. The references of interest from the INIS searches were then used to assemble the data or default values for the model.

Demographic and geographic data were not available at ANSTO. Much of the statistical information required for the South East Asian region was obtained from the United Nations (UN) library in Sydney. This required personal visits to the library to search for and copy the data. The internet was another source for retrieval of demographic information on a country basis. Most countries have a web page, some with comprehensive information relating to climate, topography and population as well as economic statistics.

Pathway diagrams were drawn to incorporate all the factors contributing to the dose to man from nuclear incidents producing airborne contaminants. This allowed the model to be constructed in a systematic sequence where all the selected pathways were addressed.

Model Development

The model is implemented in the Java programming language. Java was chosen because a toolkit is available to build graphical user interfaces, which was one of the requirements of the project. Java also allows portability across computer platforms such as Unix, PCs or Macs, and the language enforces modular code development which is well suited to this project.

The main components are as follows:

i. The source of the release:- to simulate the source, a number of release scenarios were formulated. These include the choice of such parameters as: radionuclides released, release heights and duration of the release.

ii. An atmospheric transport mechanism:- For this project the interest was in tracing the dispersion of the released radionuclides in the atmosphere and the amount deposited on the ground. This component was modelled by the Bureau of Meteorology (BoM), although data from any dispersion model may be used. On supplying the release amounts and locations, the BoM supplied ANSTO with the air concentration and ground deposition over the affected region, which was estimated using BoM's atmospheric transport models.

iii. Transport in the pathways:- Deterministic mathematical formulae describing the pathways that lead to the dose received by humans were adapted from existing models with required modifications. The computer program was implemented to:

- facilitate the viewing of the ground deposition and airborne concentration of each radionuclide over the affected two-dimensional region for each time period
- set optional parameters in the pathways that lead to the humans acquiring a dose

calculate the effective dose to humans and graphically display the results, as well as allowing the user to view the total dose from the

selected scenario at a grid location and a time period. In addition breakdown of dose contribution from each of the pathways in the scenario is given for each of the radionuclides.

Effects on foodchains in large volumes of water or moving streams are not modelled in this initial version. Sensitivity and uncertainty analyses are yet to be implemented.

Assumptions: As with any mathematical model of physical processes, a large number of simplifying assumptions need to be made. The majority of the assumptions made for the implementation of this model are conservative, and their importance will be assessed during the sensitivity/uncertainty analysis. A local production and consumption approach is considered, i.e. food produced in a grid location is assumed to be consumed in that grid location, there is no transfer between grid locations. Radionuclide decay is taken into consideration, but daughter product buildup is yet to be implemented.

RESULTS

Computer Program (RadCon)

The task was to design and implement a computer program to integrate data from the various sources and calculate the effective dose to humans and presentation to the user (Fig 1). The mathematical models define the transport processes that utilise the input data to determine a spatially and time varying dose according to user selected options. The BoM simulation generates the ground and airborne concentrations over the two dimensional region of interest over a specified time period.

A regional map is included for visualisation purposes. The dose is calculated for the affected region, which is then displayed superimposed on the map so that the user can easily identify affected regions. The dimension of the BoM simulation determine the dimensions to be used by RadCon.

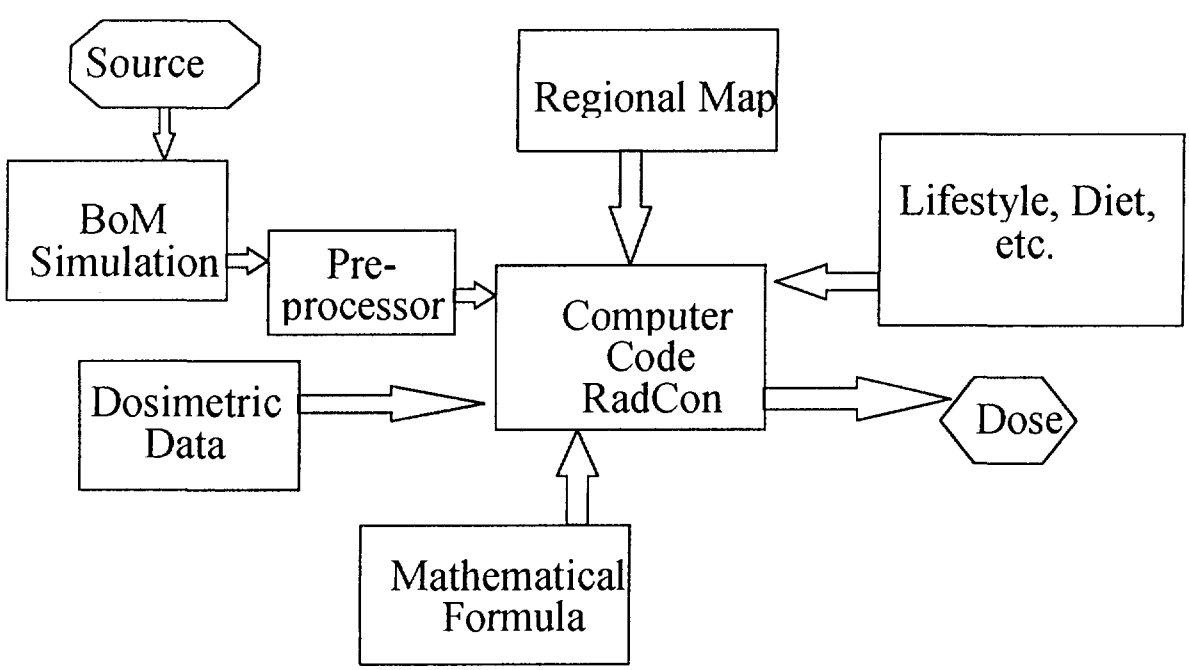

Fig. 1: Function of Computer Code

For the purpose of this project the interest was only in the ground deposition and the first layer (up to 10 m height) of the airborne concentration. The file as supplied by the BoM contains a number of vertical levels of the airborne concentration. In order to reduce both the disk space and computational time requirements for the processing of the data, a pre-processor was written which reads the BoM file, extracts the required information and writes it in a format suitable for input to the RadCon program. In addition, the program can optionally select subsets of the region over which the simulation is carried out.

Mathematical Models of Pathways

The main focus of this project is the study of transfer processes (or pathways) of radionuclides in the environment (*i.e.* ground deposition and airborne concentration following an accidental release in the atmosphere) to humans.

From the large number of regional models available, segments of the mathematical formulae used in these computer codes were taken and the parameters and assumptions specific for this study were incorporated, *e.g.* race dependency, vegetation and animals used as food in the region, etc. Once the mathematical formulae within the selected pathways are fully developed and implemented a sensitivity analysis will be carried out to identify the most critical parameters so that studies can be initiated into measuring these parameters more accurately.

The major pathways to be considered were:

Short term:-

- External irradiation from material in the cloud. (Cloud Shine)
- External irradiation from material deposited on the ground. (Ground Shine)
- Internal exposure following inhalation.
- Ingestion of short lived radionuclides such as iodine (yet to be implemented).

Long term:-

- Ground shine.
- Internal exposure from ingestion of contaminated food.
- Re-suspension, (*i.e.* contaminated material re-entering the atmosphere, say through agricultural practices or wind) to be considered.

Pathway Parameters

The parameters to be considered in this project have been identified and are included in the mathematical formulae adapted for the project. One of the main modifications has been to introduce race (Caucasian, Asian, Indian, Islander) into the equations. For each race defined in the system, dose effect can be calculated selectively for standard groups (*e.g.* man, woman, infant, child). Further, the values of the parameters are not directly accessible by the user but a set of predefined options are offered for the user to select.

A full report on the mathematical development of all the pathways is available at ANSTO. Only one of the pathways is presented in this paper and is representative of the procedure adopted for all the other pathways.

Ground Shine

External irradiation in the time interval (t-Δt,t) from radioactive material deposited on the ground is modelled by the following mathematical formula (equation 1):

$$GS(r,t) = GD(r) * S * SF * D(r) * \int_{t-\Delta t}^{t} e^{-\lambda x} dx$$

Table 1. gives a short description of the parameters in this equation, their units and dependencies.

Table 1: Ground Shine Parameters

Parameters	Description	Unit	Depends on
$GS(r,t)$	dose to person from radionuclide r, at time t from deposit	Sv	radionuclide, time from deposit
$GD(r)$	ground deposition	$\frac{Bq}{m^2}$	radionuclide(as supplied by BoM)
S	reduction factor	dimensionless	soil type
SF*	shielding factor	dimensionless	lifestyle**, shielding
$D(r)$	dose conversion factor	$\frac{Sv}{Bq*h/m^2}$	radionuclide
Δt	interval of exposure	day	
t	elapsed time	day	time from deposition
λ***	decay constant	day^{-1}	radionuclide

* SF = Fraction of Time Out Doors * Out Doors Shielding Factor +
Fraction of Time In Doors * In Doors Shielding Factor

** Lifestyle combines rural/urban housing types and indoor/outdoor occupancy factors.

*** $\lambda = \frac{\ln(2)}{halflife}$

Assumptions for Ground Shine

The mathematical formula for the Ground Shine pathway has been adapted from Krajewski (2). It was assumed that:

- Gamma radiation only is considered.
- Allowance is made for the attenuation of gamma radiation by buildings. In the current implementation, three building types are considered (user selectable), one for rural, one for residential and the other for urban areas. Thus a shielding factor is required for each of the three types of buildings.
- Indoor and outdoor occupancy factor is also required to estimate the overall shielding factor to account for the attenuation.
- The dose conversion factor is age and race independent.
- The gamma dose rate is calculated for one metre above ground.
- A factor is included to account for the different migration rates of radionuclides in different soil types. This results in varied effective deposition contributing to gamma radiation to people.

Depending on user selection, the shielding factor will use values specified for rural or urban building types and indoor or outdoor occupancy factors.

Total Dose to Humans

For the current implementation, where only contribution of crop and animal product consumption are considered, the total dose to humans from the ingestion pathway at time t is given by equation (2), where P and M are the number of crop and animal products consumed respectively and N is the number of radionuclides.

$$TotalDose(t) = \sum_{r=1}^{N} \left(\sum_{p=1}^{P} DP(r,p,t) + \sum_{m=1}^{M} DM(r,m,t) \right) \qquad \text{equation (2)}$$

CONCLUSIONS

Both the wide ranging literature search and the model development have highlighted the gaps in the data. These gaps include information on the physical activity rates of the people of South East Asian countries, the time spent indoors/outdoors, the amount and type of food consumed per day in the individual countries, food processing, shielding factors for the houses and various geographical parameters. At present, default data or data for temperate climates is used. This information will enable the research to be stringently focussed to filling the most significant gaps in terms of consequence, for the remainder of this project.

In running the model it becomes immediately obvious that it is focussed on the South East Asian region but flexibility has been incorporated into the design to allow application in other regions. A geographic information system is used for the display of input and output data allowing quick access to not only the results but also the underlying assumptions.

We currently have a working program which implements many of the features we require. It can be used to evaluate and view consequences on the basis of time, pathway and radionuclide. It provides an easy tool for selection of data analysis for specific regions, setting scenario parameters, calculating dose to humans and visualising the results and their underlying assumptions. The focus has been on getting the system up and running using the available tools. Although a number of improvements can be made, the implementation of sensitivity and uncertainty analysis will be the next step. A future extension will allow viewing and modification of data files via the program. Currently this is carried out using system supplied tools.The model has portability across platforms and future extensions for a scaled down version to operate solely on a PC are planned.

Acknowledgements
The project team thankfully acknowledges the assistance of Murray Haywood, David Hambley, John Twining and the ANSTO library staff with this stage of the project.

References

(1) Klos R.A., Müller-Lehmans H., van Dorp F. and Gribi P. 'TAME - The Terrestrial-Aquatic Model of the Environment: Model Definition' Paul Scherer Institute publication No. 96-18, 1996, Switzerland.

(2) Krajewski, P. Individual evaluation of model performance for Scenario S, 1993/1994 IAEA Exercise in Validation of Model Predictions (VAMP), Central Laboratory for Radiological Protection, Poland, 1994 (CLRP).

(3) ICRP Publication 71 'Age Dependent Doses to Members of the Public from Intake of Radionuclides: Part 4 Inhalation Dose Coefficients'. Vol. 25 Nos 3-4, 1995.

Secondary UV Radiation from Biota as a Proof of Radiation Hormesis and Gurwitsch Phenomena

W. GORACZKO
Radio- and Photo-chemistry Department, Technical University Poznan
60-965 Poznan, Piotrowo 3, Poland
GORACZKO@SOL.PUT.POZNAN.PL

SUMMARY. The results of the present research demonstrate that the excitation of living systems by γ-quanta (high energy, low doses) initates prolonged secondary emission that influences biota and activates many important processes in biological systems. The spectral analysis of this secondary emission confirmed the contribution of the UV component to the total emission. The data obtained (by using SPC-single photon counting method) make possible at least a parcial understanding of the radiation hormesis phenomenon and suggest closer relationship to so-called mitogenetic radiation (UV emission from biological systems during mitotic processes).The experiments confirm the author hypothesis that γ-irradiated biological objects are capable to emit secondary biogenic radiation. This secondary radiation plays very important role in the intercellular communication. The paper proposes a common denominat for mechanisms of UV and ionizing radiation interacting with living cells, underlying both mitogenetic effect and hormesis.

1. INTRODUCTION

Ionizing radiation (IR) is only one form of electromagnetic radiation in which both biological and not-biological systems are diving. It is well known chat other forms of electromagnetic waves as US, USV, micro-waves or infra-red play significant part in living systems.

And what about IR ? Does IR plays any part in living systems ? Does IR is an important factor in human live ?

Great deal of scientific researches confirmed that high (large) and low (small) doses of IR consistently induce opposite physiologic effects in biological systems (1,2,3,4). What does it means low-level dose of IR ? This dose is defined as a value from of more than ten times of Natural Background Radiation (NBR) to 1/100 LD (lethal dose); i.e.40-50 mGy (5). Stimulation (bio-positive effect) by low level doses of any agent is called hormesis (1,2,3,4,5). Luckey (1,2) in his works transfered this notion to IR and defined radiation hormesis (RH) as a bio-positive effect of low-level doses of IR.

RH is found in plants and both invertebrate and vertebrate animals. The data show increased or accelerated respiration, germination, growth, development and maturation, reproduction, resistance to disease and subsequent irradiation and average longevity. Under the irradiation of gamma rays the increasing of mitosis index is observed. Hormesis evokes increased vigor and strength in individuals subjected to suboptimum conditions.

The hormetic dose varies with subject, conditions, physiologic function measured, dose rate and total exposure. The type of radiation seems to be less important than the rate at which it is administrated. Next, the dose rate is probably more significant than total dose in radiation damages. The same total dose irradiated in long or short time effects differently in living organisms (1,2).

RH following whole-body irradiation was established in animals for growth and development, fecundidty, immune

competence, decrease mortality rates from infection and average life span. RH is regularly noted in independent microbes such as bacteria, yeasts and algae. Whole-body human exposure to low-level doses of IR cansistently results in decreased cancer death rates (1,2,4).

Man appears to be one of the most radiosensitive species. The magnitude of LD_{50}^{30} for man equals to about 2.6 Sv and this value is at least one order of magnitude smaller than the corresponding value for other living organisms (1,2). We can realistically estimate total dose which a man is exposed to equals about 1 mGy/y. But there are some regions of the Earth where the NBR is much higher than so-called normal level. For example : in Brazil, beaches of Guarapari - 263 mGy/y, Guapara 10-18 mGy/y and Apaxi 35 mGy/y; Iran, Ramasari 7-480 mGy/y; India - Kerela coast - 4-23 mGy/y; several thousend people in Espirito Santos - 30 mGy/y; Caucasus and Himalaya mountaineers - 35 mGy/y. People from Nagasaki or Hiroshima who during A-bomb explosion received doses of 60 to 700 mGy appear to live longer than those who received either higher dose or none (1,2).

Till 1990 the information on low-level doses of IR in scientific literature had only little meaning however a great deal of data show that high and low-level doses induced opposite results in microbes, plants, a variety of invertebrates and many mammal, including humans. The effects of low level doses cannot be inferred by interpolation between the results from samples exposed to high doses and controls irradiated only by NBR.

The development of A-bombs and political situation in the World ("cold war", existing of two opposite political and military systems) led to extensive researches only on the damage effects of high-level doses and forced the concept that all doses of IR are harmful. "Harm dominated the last half century of radiobiologic research" - as Luckey has written (2). Even today RH hypothesis is still controversial.

In the 1920's Gurwitsch examined the influence of rapidly dividing cells on other cells not undergoing the mitosis process. Under certain circumstances dividing cells (inductors) were stimulating the division process in other, neighbouring cells (detectors). Gurwitsch claimed that dividing cells emit a very weak radiation which is able to stimulate the mitosis process in other cells. He termed it- "mitogenetic radiation" MR (7).

These first experiments were carried out on onion roots, both as the inductor and detector. Using mirrors and particular optical filters made of glass and quartz (simple spectral analysis) he demonstrated that the mitogenetic effect is brought by ultraviolet light. These experiments have been verified by using other natural inductor and detector systems (for example - onions, malt yeasts, regenerating cornea of frog's eyes, blood cells). Using quartz spectrographs and biological detectors two spectral regions of the MR : 180 - 280 nm (UV-C) and 300 - 330 nm have been found (6).

Gurwitsch claimed that the MR exhibits two significant properties :

- secondary radiation SR - the secondary MR was emitted only by cells which absorbed either the so-called "primary" MR from the surface or secondary MR from neighbouring cells. Secondary radiation SR is also able to induce mitosis.
- degradation radiation DR - if cells of the inductor are killed by cooling, poison or mechanically, the detector cells show a clear mitogenetic effect. It has been claimed that dying cells emit the so-called "degradation radiation" (necrobiotic). This radiation has higher intensity than SR but exists for shorter time. Many experiments

have confirmed the existence of necrobiotic radiation (8,9).
Some authors have proved the existence of this radiation, whereas others have been unable to find such significant effect although they have been working with the same measurement equipment and objects. Very reliable systematic research was made by the Quickenden group (10,11).
In recent years the MR has been studied by many researchers by using typical high-developed physical equipment - i.e. photoncounter photomultipliers and CCD (charge coupled device) photon image cameras (12,13).
Even today research of the MR is still very controversial. Primary controversy which referred to the existence of MR has changed and now we are trying to answer the question : does MR can stimulate mitosis, and if so, how ? What part of a cell can create MR ? What is the nature of MR ? (for review see 6).

2.IR AND MR - TWO LINKS OF THE SAME ENERGETIC CHAIN

In my opinion there is a close relationship between IR and MR. I postulate the above hypothesis based on the principal biological fact - the process of cell division (mitosis) is conditioned by two factors, namely : by metabolic processes which lead cells to dividing stand-by, and by "impuls" (stimulant) which start (in motion) deviding process.
I suggest that this so-called "starting impuls" is nothing else as mitogenetic radiation MR. Even low density flux of UV-C (180-220 nm) or a few quanta can start mitosis (14). On the other hand under the irradiation of gamma rays the increasing of mitosis index is observed, i.e increasing of MR.

3.THE EXPERIMENT AND RESULTS

As we know from radiation chemistry the formation of H_2 and H_2O_2 are equally pos-sible in aqueous solutions irradiated by ionizing radiation. The primary ionizing of the water molecule is followed by recombination and fast dissociation : $H_2O \rightarrow H_2O^+ + e^- \rightarrow H_2O^*$. Part of the excited water molecules dissociate into radicals : $H_2O^* \rightarrow H^* + OH^*$. Molecular products are formed through the recombination of radicals : $H^* + H^* \rightarrow H_2$ and $HO^* + OH^* \rightarrow H_2O_2$. The above combination processes take place at the beginning of the life clusters when the local radical concentrations are still high. Chemical or radiochemical results which we observed usually followed as a consequence of the chemical reaction between water radiolysis products (hydrogen peroxide, radicals) and cell compounds.
Therefore when the water solution was irradiated as the product of radiolysis, some concentration of hydrogen peroxide has been received. This chemically reactive compound effects on another bio-important compounds.

I took into consideration the simplest amino-acid (endogennic), an element of proteins. The reaction of hydrogen peroxide on glycine has been examinated. Hydrogen peroxide produced may in turn continue oxidation :

$$H_2NCHR - COOH \xrightarrow{H_2O_2,NH_3} \rightarrow O = CR - COOH + h\nu$$

During this process some secondary emission has been detected - Figure 1.

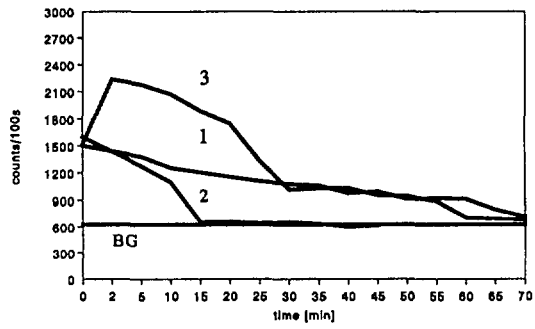

Figure 1 *Secondary emission from Gly (different ammonia concentration)*
1:Gly-0.87M,hyd.per-0.7M,amm-0.7M
2:Gly-0.87M,hyd.per-1.125M,amm-0.875
3:Gly-0.9M,hyd.per-0.9M,amm-0.7M

The spectral analysis indicates that the latter emission belongs to the UV range of spectrum. It was interesting to investigate for how long time it is possible to reveal this secondary radiation. The results presented in Figure 2 show that the effect was quite high within 20-30 minutes for the beginning of the experiment (after adding NH_3). Then it decreased by the next 1 hour (15).

If we irradiated water solution of glycine by gamma rays we received the following :

$$\gamma + H_2NCHR - COOH \xrightarrow{H_2O,NH_3} \rightarrow O = CR - COOH + h\nu$$

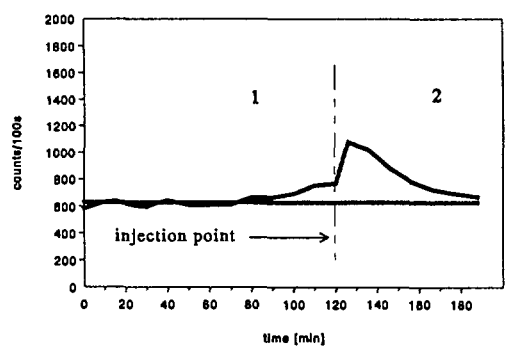

Figure 2 *Gly emission as a function of ammonia concentration.*
1:Gly-0.87M,hyd.per-0.7M,amm-0.35M
2:Gly-0.8M,hyd.per-0.67M,amm-0.67M

I conclude chat this UV quantum is nothing else as the mitogenetic radiation. Now I am preparing experiment in which I will stimulate mitosis process by this quantums in yeast after gamma irradiation.

4.HOW TO EXPLAIN CREATION OF MR AFTER IRRADIATION OF MR ?

If we irradiate some living objects with low-level doses of IR macromolecules of DNA, RNA, proteins will probably turn to excited states. As a result of these processes the polaritons are created. Polaritons create the subsequent coherent radiation from DNA. This secondary radiation (the so-called DNA fluorescence) has much longer wavelenght than primary radiation which excited DNA molecules. This secondary radiation is analogous to postulated mitogenetic radiation MR.

Therefore, we deduce that IR can create MR. On the basis of this conclusion we can understand why IR and MR (or UV) affect the same processes inside the living matter. On the other hand, only IR without excessive reduction can penetrate a deep region of a macroorganism, because MR is easily absorbed by biological tissue.

It is well-known that both litosphere and biological systems contain some radioisotopes. It is highly probable that MR arises in susceptible biological molecules either by cosmic radiation or by the far UV Cerenkov radiation excited by the cosmic rays, or from the NBR. Because Cerenkov radiation is totally absorbed inside cells, consequently this photons must play very important part in energetic balance in living organism. I expect that Cerenkov radiation may converse - like IR - into UV photons. In my opinion this is very important problem because a simple calculation shows that for ^{40}K about 10 Cerenkov photons will be created during 1 second in 1 mm of

water's layer. Consequently for adult (70 kg) we should measure more than 0^8 Cerenkov photons per 1 second. For ^{32}P and ^{4}C less but still very high number.

5.MEDICAL ASPECTS OF RH AND MR

It is well-known fact chat even for the developed organism there can be found a certain balance between destructive and creative processes. When the quantities or intensities of of the creative processes are higher than degradations, the biological system is developing. Otherwise, the organism is dying.

The MR rays of dying cells stimulating other cells to enter phase of mitosis may be part of a control circuit to keep the number of cells in a "healthy" organism constant. In case of the developed, young organism we can expect more intense MR (i.e; primary MR and SR) in comparison with "normal" or „adult" one. Consequently, in the case of so-called "old" or „ill" organism, the intensity of DR will be higher. Maybe, in the nearest future, measurement of MR, in particular the ratio of (SR/DR), will enable us to estimate the ability of a whole organism (or its part or organs) with regards to their fundamental, biological function. Some unnormal intensities, both lower or higher than the so-called "normal", indicate some destructive processes. To make this idea more realistic, first of all, we should measure and collect the data for preparing the photon emission medical atlas for certain organs and whole human body, and define the notion "normal" photon emission PE, i.e; from healthy organism.

We know epidemiological evidence which show that human cancer mortality rates are lower in areas of high NBR than in low-level radiation regions. Some physicians postulated that low-level doses of whole-body irradiation may reduce cancer induction (1,2). This hormetic phenomenon appears in this respect as a possible new method of therapy. Maybe in the near future we will irradiate our children like now we are inocullating them. It is surprising proposal but if we remember how vaccine works in human organism we understand easily the idea of hormetic therapy. Based on the experiments and epidemiological evidences the following doses are recomended : 20 mGy/y for selected organs and 100 mGy/y for whole-body chronically irradiation (2).

I think researches on both the influence of Cerenkov, natural background radiation and radiation hormesis on living systems should be advanced. Maybe there are among the other important factors not only in the evolution of biological systems but in the creation of Earth's life in general.

6. REFERENCES

1.T.D.Luckey,Hormesis With Ionizing Radiation, CRC Press Inc;Boca Raton, Fla.1980.

2.T.D.Luckey,Radiation Hormesis,CRC Press Inc;Boca Raton, Fla.1991

3.H.Planel, *Health Phys.*, 1987, **52**,571.

4.A.M.Kuzin, *Radiobiologia* (Rus), 1994, **34.3**, 398.

5.United Nation Scientific Committee on the Effects of Atomic Radiation, UNSCEAR 1994 Report - Sources and Effects of Ionizing Radiation, United Nations, New York, 1994.

6.W.Goraczko,*Current Topics in Biophysics*,1996, **19**,33.

7.A.G.Gurwitsch,`Das Problem der Zellteilung Physiologisch Betrachtet,Springer Verlag, Berlin, 1926.

8.Reiber H.(1989). Low-level Luminescence from Disintegrated Brain Cells Subcellular Distribution and Kinetics of the Biophysical Radiation, in : Proc.First Intern.School - Biological Luminescence, Eds.B.Jeżowska-Trzebiatowska, B.Kochel, J.Slawiński, W.Strek, World

Scientific, Singapore-New Jersey-London-Hong Kong, 224-233.
9. Sławiński J.(1990). Necrotic Photon Emission in Stress and Lethal Interaction,Current Topics in Biophysics, **15** (1), 8-27 (English translation).
10. Quickenden T.I. & Que Hee S.S. (1981).On the Existence of Mitogenetic Radiation, *Speculation in Sci. Technol.*,Vol.4, 453-464.
11. Quickenden T.I. & Tilbury R.N. (1983).Growth Dependent Luminescence from Cultures of Normal and Respiratory Deficient Saccharomyces cerevisiae , *Photochem.Photobiol.* **37**, 337-344.
12. Scott R.Q.,Usa M. & Inaba H.(1989). Ultraweak Emission Imagery of Mitosing Soybeans, *Appl.Phys.*, B **48**, 183-185.
13. Inaba H.(1988). Super-high Sensitivity Systems for Detection and Spectral Analysis of Ultraweak Photon Emission from Biological Cells and Tissues, *Experientia*, **44**, No.7, 550-559.
14. *Kossakowski*
15. Goraczko W. Ionizing Radiation as a Source of Secondary UV Radiation in Biota, 12-Th Symposium on Microdosimetry, An Interdisciplinary Meeting on Radiation Quality, Molecular Mechanusms, Cellular Effects and Health Consequences of Low Level Ionising Radiation, Kieble College, Oxford, UK, 1996.

Second International Conference on Isotopes, Sydney, 12-16 October 1997

On-Line Bulk Analysis of Hot Reduced Iron Ore

C.S. LIM, B.D. SOWERBY AND S. RAINEY

Division of Minerals
Commonwealth Scientific and Industrial Research Organisation (CSIRO)
Private Mail Bag 5, Menai NSW 2234, Australia

SUMMARY. New technologies such as direct reduction and smelting reduction processes are increasingly being used to supplement conventional blast furnace ironmaking technology. The critical product quality parameters in many of these processes are the degree of pre-reduction (PRD) (or the degree of metallisation) and the carbon and silica contents. However, on-line measurements need to be made on hot ore (up to 1000° C) in circumstances where access to representative sample streams is very difficult. An on-line gauge based on the measurement of neutron inelastic scatter gamma-rays was installed and calibrated at a plant in Western Australia. The gauge uses an ^{241}Am-Be neutron source and a bismuth germanate (BGO) detector inside a water-cooled tube surrounded by hot iron ore. The gauge monitors the iron, oxygen, carbon and silica contents of the ore based neutron inelastic scatter gamma-rays at 0.85, 6.13, 4.43 and 1.78 MeV respectively. In plant trials the gauge determined iron, oxygen, carbon, silica and PRD to within 2.2 wt.% (4% relative), 0.6 wt.% (2% relative), 0.5 wt.% (25% relative), 1.0 wt.% (9% relative) and 0.4% (1% relative) respectively.

1. INTRODUCTION

The critical product quality parameters in the direct reduction (DR) and smelting reduction (SR) ironmaking processes are the degree of pre-reduction (PRD) (or the degree of metallisation) and the carbon and silica contents (1). The pre-reduction degree, expressed as a percentage, is defined by the following equation:

$$PRD = 100.0 - 232.7\ O_{Fe}/Fe_{tot} \qquad (1)$$

where Fe_{tot} = total iron; O_{Fe} = oxygen in the iron oxide = (O_{tot} - O_{gangue}); O_{tot} = total oxygen; and O_{gangue} = oxygen in the gangue (i.e. the non-iron oxide component), all expressed as weight percent on a dry basis. Gas-based DR processes, which are used in over 90% of DR plants, usually aim to achieve metallisation levels of 85-93% and carbon contents of 1.0-2.5%. Independent control of these quantities can be achieved by selection of appropriate reduction temperature and gas composition. In the remaining coal-based DR processes, carbon control is difficult to achieve. Silica is the predominant component of the gangue.

Currently available methods for PRD measurement are off-line and too slow for control purposes. However on-line measurements have to be made on hot ore, with sample temperatures of up to 1000°C, in circumstances where access to representative sample streams may be difficult.

Work has recently been carried out by CSIRO Minerals on the development and plant-testing of a gauge at a plant in Western Australia, for the on-line monitoring of PRD, carbon and silica contents of hot iron ores using the neutron inelastic scatter gamma-ray technique (2). This work represents the first reported industrial application of neutron techniques to the on-line bulk elemental analysis of hot iron ores.

2. TECHNIQUE

The neutron inelastic scattering (NIS) technique involves bombarding a sample with fast neutrons and analysing the gamma-rays promptly emitted as the sample is being irradiated (3). The technique is well suited to the analysis of

elements of concentration greater than about 1 wt.%. The accuracy obtained depends on inter-element interferences, scattering cross sections and background, and high accuracy can be achieved in favourable cases, such as the determination of carbon in coal (4,5). The NIS technique is well suited to the accurate determination of elemental ratios, as the ratio of gamma-ray yields calculated from peak areas is much less affected by changes in bulk density or geometry than the individual peak areas. The technique has the advantages of using highly penetrating radiation so that measurements can be made on bulk samples through the walls of vessels, of allowing the simultaneous quantitative measurement of many elements, and of being independent of temperature.

Nuclear methods such as NIS can only determine elemental compositions and cannot discriminate between chemical species. Thus, in the case of PRD measurement, the level of oxygen measured includes all oxygen contained in the sample, whether it be in the form of iron oxide or some other form of oxide, such as alumina or silica. Since PRD is defined in terms of only two parameters - total iron and oxygen in iron oxide - other sources of oxygen need to be taken into account. This can be done by directly measuring the other oxides present or by inferring these oxides from iron and silicon measurements. In the case of this particular application, the proportion of oxygen in the gangue only varies within a limited range (typically 0.5 wt.% under normal operating conditions); it can be shown that as a consequence the effect on PRD (equation 1) should be negligible.

3. LABORATORY TESTS AND GAUGE DESIGN

Initial laboratory tests were carried out to investigate the effect of measurement geometry, the sample container material, the effect of bulk density and the sensitivity of the NIS technique to a range of elements at levels typically expected in the plant. Results (6) indicated that:
(i) in a backscatter geometry, using a 370 GBq (10 Ci) ^{238}Pu-Be source in conjunction with a 3"x3" bismuth germanate (BGO) detector, with a counting time of 20 live minutes, PRD, iron content and carbon content could be determined with accuracies of 1.3% (11% rel.), 0.5 wt.% (1% rel.) and 0.25 wt.% (12% rel.) respectively;
(ii) construction materials such as some nickel alloys, containing relatively low amounts of iron and capable of withstanding high temperatures, are preferred in areas "visible" to the gauge;
(iii) bulk density effects could be significant unless corrections are made.

In the plant, the NIS gauge needs to be surrounded by a radiation shield to reduce the neutron and gamma surface dose rates to acceptable levels. In the present application, choice of material for the radiation shield was restricted by the application-specific requirements of minimum oxygen content, non-flammability and a relatively high melting point. The most suitable shield material under these circumstances is polycast (borated polyethylene in a binder material), which has a recommended temperature limit of 80-100°C and is widely used as a neutron shield in industrial applications.

After consideration of a number of alternative gauge locations, it was decided to develop and install a gauge to directly analyse hot ore extracted from the side of the pre-reduction system (PRS). A schematic diagram of the gauge installation at the plant is shown in Figure 1. The gauge was located at a point where some material from the bed fell into the sample chamber. A fluidising plate was fixed to the base of the chamber so that the material could be blown back into the PRS when the measurement was complete. A 370 GBq ^{241}Am-Be source, tungsten shield and BGO detector were placed inside a water-cooled annular horizontal pipe inside a sample chamber. The inner polycast shield was also water cooled. Tests were carried out to determine the optimum diameter of the pipe and the minimum desirable sample thickness. A gamma-ray transmission level gauge was positioned at the top of the sample chamber to provide a means for ascertaining when the chamber was full. A sample bottle was located at the bottom of the sample chamber for the collection of small (~1 kg) samples for chemical laboratory analysis.

Eleven 80-90 kg iron ore samples were provided for laboratory testing of the gauge shown in Figure 1. These samples cover a range of PRD values from 0 to 29.4% and Fe values from 55.8% to 68.7 wt.%. The samples had been crushed to a particle size of less than 200 microns. Two sets of laboratory measurements were taken using the gauge, each with collection times of 600 and 1200 live seconds. Intensities of the 0.51 (pair production), 0.85 (iron), 4.43 (carbon) and 6.13 (oxygen) MeV gamma-rays were measured. The r.m.s. errors between gauge measurements and chemical laboratory analyses were 1.0 % (7% rel.) for PRD and 0.7 wt.% (1% rel.) for total iron. The range of values for carbon content in the samples provided was too small (0.6 wt.%) for a sensible correlation to be obtained.

4. PLANT TRIAL MEASUREMENTS

The gauge was installed in the plant for testing and on-line calibration. A survey of radiation dose levels around the gauge by the WA Radiation Health Department after installation found that the maximum dose rate was 3 μSv/hr at a distance of 1 m from the gauge surface, well below the legally required limits.

Data was collected over a period of 8 days, using a counting time of 600 live seconds for each spectrum. Of these data, there were a total of 17 spectra for which there was a matched chemical laboratory sample, including 5 spectra which had been collected for the one chemical laboratory sample. The data were analysed for PRD, Fe, O, C and SiO_2 and r.m.s. errors of 0.4% (1% rel.), 2.2 wt.% (4% rel.), 0.6 wt.% (2% rel.), 0.5 wt.% (25% rel.) and 1.0 wt.% (9% rel.) respectively were obtained as shown in Table 1. The 0.51 MeV gamma-ray was used to compensate for bulk density. The correlation between gauge and chemical laboratory data for PRD is shown in Figure 2.

Although the relative error for PRD in the plant trial measurements was much better than that obtained in the laboratory (1% compared to 7%), the range of PRD values available from the field trial data was relatively small (only 5.6% compared with almost 30% for the laboratory data). On the other hand, the relative error for Fe was significantly higher for the plant trial, reflecting a much wider range of Fe values.

The sampling line through which samples were extracted from the measuring chamber for chemical laboratory analysis could not be positioned easily to provide representative samples. However, the good agreement between the gauge and laboratory assays indicates that the material in the measuring chamber was fairly homogeneous.

Table 1 Summary of results of the plant test of a NIS gauge of hot pre-reduced ore.

Parameter	Range*	R.m.s. error*	Correl. coeff.
PRD	24.3-29.9	0.4	0.98
Fe	40.6-61.5	2.2	0.95
O	21.2-30.2	0.6	0.98
C	0.1-4.12	0.5	0.85
SiO_2	6.1-15.5	1.0	0.94

* wt.% except for PRD which is expressed as %.

5. DISCUSSION

The work presented describes the successful development and testing of a gauge for the continuous on-line bulk elemental analysis of hot iron ores. This gauge can be used in, but is not limited to, DR and SR processes where real-time monitoring of quantities such as PRD, iron, carbon or silica content can lead to improvements in process control and efficiency. In this particular case, a by-line gauge with an annular geometry to maximise detection efficiency was used. This approach has the advantages that the gauge can be located anywhere in the plant where there is a suitable exit point for the sample, and that the sample density should be fairly reproducible. However, the disadvantages of such an arrangement are the sample handling issues and the need to ensure that the portion of the ore which is diverted into the sample chamber is representative of the total stream. An alternative approach would be to modify the gauge to be used at a location where the stream could be continuously monitored,

such as on a pipe. In this case, a backscatter geometry would probably be preferred.

6. ACKNOWLEDGMENTS

The authors would particularly like to thank G.J. Hardie for his contributions and support throughout this work. Thanks are also due to M. Dunne, C. Prickett, P. Rafter and V. Sharp for their contributions.

7. REFERENCES

1. J.K. Wright, I.F. Taylor and D.K. Philp, "A review of progress of the development of new ironmaking technologies", Minerals Engineering 4(1991)7-11

2. Lim, C.S., Sowerby, B.D., Rainey, S. and Hardie, G.J., "Plant trial of a neutron inelastic scatter gauge for the on-line analysis of hot reduced iron ore", Proc. International Conference on Neutrons in Research and Industry, Crete, Greece, 9-15 June 1996, (SPIE Proceedings Series, Vol. 2867, ed. G. Vourvopoulos), 211-214.

3. B.D. Sowerby, "Elemental analysis by neutron inelastic scattering gamma-rays with a radioisotope source", Nucl. Instrum. Methods **166** (1979) 571-579.

4. B.D. Sowerby, "Measurement of specific energy, ash and moisture in bulk coal samples by a combined neutron and gamma-ray method", Nucl. Instrum. Methods **160** (1979) 173-182.

5. N.G. Cutmore, C.S. Lim, B.D. Sowerby, V. Yip and A.L. Ottrey, "On-line analysis of low-rank coal", J. Coal Quality **12** (1993) 85-93.

6. C.S. Lim and B.D. Sowerby, "Neutron techniques of on-line analysis in the Australian mineral industry", 4th Internat. Conference on Applications of Nuclear Techniques, Crete (Greece), 12-18 June 1994.

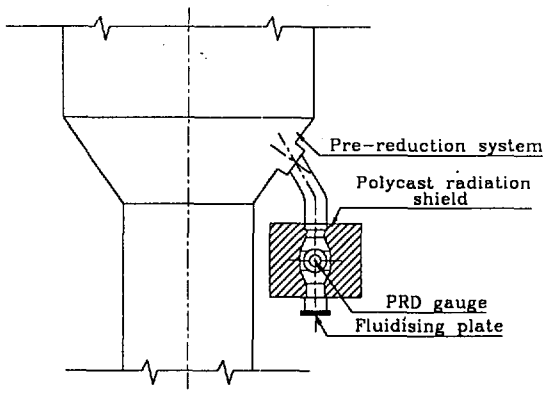

Figure 1. Schematic diagram of the neutron inelastic scatter gauge installed on the plant in Western Australia.

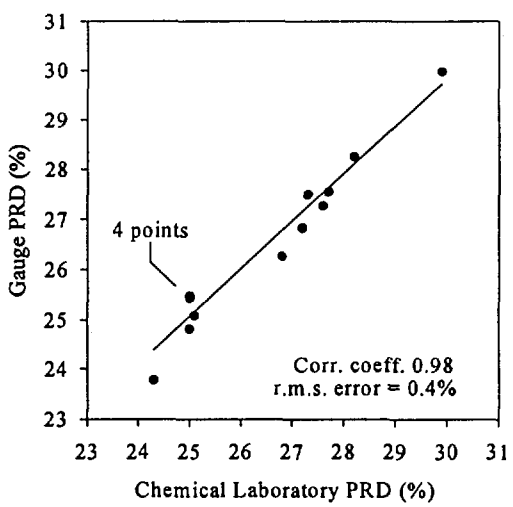

Figure 2. PRD correlation between chemical laboratory assay and NIS gauge measurements during plant trial.

Combining Computational Modelling with Radioisotope Technology for a more Cost-Effective and Time-Efficient Method of Solving Multiphase Flow Problems.

J. F. Easey[1], J. Y. Tu[1] and W. M. Burch[2]

[1]Australian Nuclear Science & Technology Organisation (ANSTO)

Private Mail Bag 1 Menai, NSW 2234, Australia

[2]John Curtin School of Medical Research, Australian National University, Canberra, ACT 0200, Australia.

SUMMARY. The recent rapid advances and growth in computing power has made access to powerful computer hardware both feasible and affordable for the wider technological and scientific community. The emergence of cost-effective and time-efficient computational simulation. of industrial phenomena and processes as an alternative to either the traditional experimental or analytical methods of investigation can be seen as an illustration of this breakthrough. An essential link in the establishment of the process models is the important verification and validation process. For the computational models of complex industrial processes, this can be a very exacting process. In many cases there are very precise and restrictive requirements on the physical and chemical properties of the tracer materials needed for the validation experiments. Radioisotope tracers have a long history of being used as tools for process investigations in Industry and Medicine and are well-suited to these investigations. New developments in the formulation of encapsulated radioisotopes are being made that will open up the use of radiotracer applications for such wider ranging validation work, not only in industrial but also in medical investigations and will greatly assist the important area of multiphase flow.

1. INTRODUCTION

The rapid growth in computing power in the 1980's has seen the emergence of the computational simulation. of multiphase flow as a cost-effective and time-efficient alternative to either the traditional experimental or the analytical methods of investigation. This trend has been accelerating in the 1990s, providing opportunities for integrating aspects of computational science to provide computational design and management as well as stimulating more fundamental computational science investigations. Multiphase flow is an important phenomenon that encompasses human activity from the act of breathing to the operation of complex industrial processes.

Concerning potential medical applications, in the past insufficient attention has been paid to achieving a thorough understanding of the various phenomena involved in inhaling aerosol particles, although breathing dust particles has been widely studied in an industrial context (e.g. pneumoconiosis). As pointed out by Stewart and Demetri (1), the two aspects are not necessarily identical. In particular, little emphasis has been placed upon the scientific background of aerosol therapy, and little attention paid to the aerodynamic behaviour of therapeutic aerosols. For example, there is need to determine the effects of particle size, breathing patterns, and airway calibre on the spatial distribution of particles within the respiratory tract. Other examples of deficiencies in our knowledge of this area include:

- the inadequate characterisation of therapeutic aerosols;
- the need to quantify the smallest drug dose which will give an optimal therapeutic effect; and,

- the importance of correlating the site of deposition of aerosols or drugs with the location of the relevant receptor sites.

In trying to address these problems, computational modelling will be able to play an important role. This is because of the diverse geometries involved and the wide variation in the physical and chemical properties of solid and liquid making up the aerosols. Experimental evaluation of each specific type of aerosol is not a practical consideration and cannot be undertaken as a realistic measure. Thus predictive models are required to assess both the total rate of deposition and its internal distribution. Progress toward achieving this goal will be accelerated by a better understanding of aerosol transport mechanisms in the complex geometries present in human airways.

The extension of the modelling of particle flow and deposition within human airways requires experimental measurements to both validate the computational predictions and calibrate the terms modelling fluid-particle interactions and particle deposition distributions. Studies using radioaerosol imaging techniques have so far produced some of the most reliable data on the deposition of inhaled particles in airways and much of this information would have been difficult, if not impossible, to obtain by other means. Imaging of radioactive aerosols can define their deposition in the central airways or lung. Thus the validation of these models is crucial and the new radionuclide tracers currently being developed will be needed to provide the essential data for model development and refinement. Once obtained, these validated models should be able to provide unprecedented information about such factors in the airways and lungs as: wall-shear stress; recirculation zones; mass and heat transfer rates; particle deposition sites; effects of particle shape and size; and, other important fluid and particle transport phenomena, which can be used to effect for greatly improved diagnoses.

In industry, in spite of the ready availability and affordability of powerful computer hardware, there is a extreme shortage of reliable computational models capable of simulating the increasingly complex tasks they require. Although some mathematical models are available for predicting industrial flow characteristics, their reliability is sometimes questionable, particularly where multiphase flow transport processes are involved, due to a lack of fundamental knowledge about the fluid-particle interaction mechanisms. Some scale-model studies of specific cases have been conducted in the laboratory but they are not capable of simulating all flow conditions that might be present in a real industrial environment, for example, the multiphase flow regimes operating in a power utility boiler. In such cases, actual field studies are the essential links to provide the necessary verification and validation of the computational models of the complex industrial processes. Overcoming this shortage of validated computational models through a programme of concerted efforts in model development and verification is a major challenge for the remainder of the 1990's.

Radioactive tracers and radioisotope gauges have been used for many years in industry for process optimisation and control, and for assessing the operational efficiency of plant and its compliance with specifications (2). The technology has been evolving over the years in response to the demands of industry and the new opportunities presented by modern data processing systems. There has been a growing demand for this technology to be established in the Asia Pacific region and this has been addressed through assistance programmes such as the IAEA's technical cooperation programme, the Regional Cooperative Agreement (RCA) for Asia and the Pacific and various bilateral assistance programmes (3,4).

2. EXAMPLES OF THE SCOPE FOR MATHEMATICAL MODELING OF MULTIPHASE PROCESSES

2.1 Medical Applications

Accurate estimation of aerosol deposition in human airways is necessary for efficient and effective targeting of aerosolized drugs for diseases such as asthma. Improved knowledge gained about particle deposition and distribution has important implications for aerosol therapy and the achievement of more effective and efficient clinical management of the condition.

The physical processes of aerosol particle deposition are mainly
(i) diffusion - this results from a balance between inherent thermal energy and the frictional restraining force of air on the particle surface.
(ii) gravitational settling - the rate of sedimentation is driven by gravitational force and opposed by air friction., and
(iii) inertial impaction - the inertia of a particle depends directly on its mass.
Other factors which may be significant include the electrical charge, hygroscopic behaviour, and chemical composition.

The deposition of inhaled particles in the human airways is determined not only by the physical characteristics of the particles themselves, but also by the nature of the air flow in the various regions, such as turbulence due to a reduction in diameter, or partial obstruction of airways as seen in diseases such as asthma.

A number of studies using computational fluid dynamics (CFD) codes on flow field and particle deposition in human airway bifurcations have recently been performed by different groups of researchers. (5-11). One of the difficulties has been the calculation of the gas and aerosol particle flows in a realistic airway geometry, such as the multiple-branching airways that are present in human lung. This is due to the factors such as:

- the difficulty of constructing a computational domain for the airway geometry, using the conventional numerical techniques like using a single structured grid;
- the high cost of studying the particle trajectories in a multiple-branching airway using the particle trajectory methods mentioned above.

To overcome these difficulties, more sophisticated numerical techniques and methods are being developed that are capable of predicting gas and particle deposition for such conditions.

Tu and Fuchs (13) have developed a novel numerical methodology for dividing a multiple-branching domain into a number of single branches where the computational grids can be easily constructed using conventional techniques. The mathematical interface between the connecting branches in the flow calculation has not yet been developed. Recently, a computationally economic two-fluid model Eulerian approach for gas-particle two-phase flow (14) has been combined with the Lagrangian method, (15) permitting simulation of both gas and particle flows in multiple-component domains such as the multiple-branching in human airways without difficulty.

Single-phase (gas phase) turbulence modelling is now reasonably reliable and economical in computing time (16) for predicting the mean-flow character. Turbulence modelling for the particle (dispersed) phase is not yet so developed as the single phase flow but some progress has already been made (14).

An enhanced understanding of the fundamental behaviour the dynamic characteristics of aerosol particles within the human airways and lungs has to be developed to allow better understanding of the processes involved and to achieve better and more effective medical treatments. The advances in computational techniques combined with the new controlled size particulate radioisotope formulations can be used, for example, to investigate, computationally

and experimentally, the dynamic behaviour of aerosol particles in critical size ranges and to quantify particle deposition in multiple-branching airways. From such work it will be possible to develop enhanced procedures for radioaerosol imaging techniques for the lungs and the airways, based on real-time analysis.

2.2 Industrial Processes

Multiphase flow operations feature in all major process industries, including coal-fired power generation and metallurgical processing, and thus, are of prime economic importance to the national economies of many countries. In the past, empirical approaches have had to be used to assist in the design of such systems, because of the complexity of the fluid mechanics of multiphase processes. These approaches have inevitably been non-optimal and expensive. The readily availability of affordable high power computational hardware coupled with the development of more sophisticated measurement techniques, provides the tools to improve the understanding and characterisation of multiphase flows, ultimately leading to the development of reliable predictive models that will greatly facilitate the design and optimisation of such systems.

The problem of deposition of particles and erosion of material, through the impaction of particles in the fluid stream, is one important problem found in many industrial multiphase flow systems. Examples of this problem are found in a large number of major process industries such as - agricultural production, food, energy, minerals production and metallurgical processing, all of which are fundamental to the Australian and other national economies.

In the example of the coal-fired power generation industry, it has been established that fly ash from the hot combustion gases can deposit and build-up (fouling) on boiler tubes, causing erosion of the tubes and reduced their heat transfer performance. In the past, the complex fluid mechanics of the gas-particle flow processes causing the tube erosion and the deposition of fly ash have had to be dealt with using empirical approaches. A combination of computational and experimental techniques, can be used to model the complex physical processes causing erosion and deposition so that the mechanisms can be much better understood. Tu (17) has recently developed a computational component that takes advantage of the Lagrange-equivalent solid surface particulate boundary conditions and now allows very precise determination of the near surface turbulent gas solid phase interaction processes. Physical models describing the particle erosion and deposition mechanisms associated with turbulent gas-particle flow in power boilers (18) can also be extended.

3. DEVELOPMENTS IN RADIOISOTOPE TRACERS

The introduction and use of new formulations of encapsulated radioisotopes, currently being researched at ANSTO, will open up further possibilities for the utilisation of radiotracer applications for a wider range of validation work not only in medical but also in industrial investigations.

Examples of current progress are the development of encapsulated noble gases in carbon matrices. It has been shown that the noble gases argon, krypton and xenon can be incorporated into the interstitial sites in C_{60} fullerene to form stoichiometric compounds of the type X_1C_{60}, where X is the noble gas(19-21). This has been achieved using Hot Isostatic Pressing and for argon the typical conditions are a pressure of 1.7 kbar and temperatures of 200° or 400°C. The noble gas is trapped in an interstitial well in the fullerene matrix and is at a concentration that is equivalent to a gas pressure of

around 50 atmospheres. The resulting compounds are stable at room temperatures and can be irradiated without major decomposition (22). Examination of the irradiated compounds has indicated that there is a small proportion (1-2%) of transfer of the noble gas through a gamma recoil mechanism, from the interstitial position into the C_{60} cage to produce an endohedral compound (23).

It has also been demonstrated that carbon nanotubes can be filled with argon (24) using HIP at 650°C at a pressure of 170 MPa. There is little observed gas loss from the product over a period of several months and the Ar pressure inside these nanotubes at room temperature is equivalent to 60MPa.

The preparation of these compounds and the development of analogous materials will open up the possibilities for studies in the petrochemical and chemical industries which have been restricted because of the absence of a suitable short lived radioisotope of carbon. By placing a carbon shell, such as the fullerene molecule, or other impervious materials around the radionuclide of another element that has the required half-life and gamma emitting properties and combining this with the ability to produce particulate materials of reproducible and narrow size range, it will be possible to produce a synthetic carbon tracer able to monitor the behaviour of specific phases in multiphase flow.

4. CONCLUSION

The exploitation of the recent advances in computational hardware and software for the solution of multiphase flow problems in medicine and industry is linked to the availability of suitable radioisotope tracer materials to calibrate and validate the models. Work being carried out at ANSTO in both areas will be able to contribute to the advancement of multiphase flow studies.

References:

1. Stewart, W.C. and Demetri P. (Ed.), Aerosols and the Lung: Clinical and Experimental Aspets, London, Butterworth, (1984).
2. Easey, J. F, Applications of Tracer Techniques to Industrial Troubleshooting and Environmental Pollution Control, in Isotopes and Radiation Technology in Industry, ed S. M. Rao and K. M. Kulkarni, pub NAARRI, Bombay, India (1994), pp215-229.
3. Easey, J. F, The contribution of the UNDP/RCA/IAEA Programmes to the Development of Nuclear Technology in the Asia Pacific Region, Proceedings 9th Pacific Basin Nuclear Conference, Sydney, Australia, Vol 1, May 1994, pp23-26.
4. Easey,J. F, The Achievements of the Regional Co-operative Agreement (RCA) for Asia and the Pacific, International Conference on Isotopes, Beijing, (May 1995).
5. Balashazy and Hofmann, Particle deposition in airway bifurcations –I. Inspiratory flow, J. Aerosol Sci., 24, (1993), pp 745-772.
6. Balashazy and Hofmann, Particle deposition in airway bifurcations –II. Expiratory flow, J. Aerosol Sci. 24, (1993),pp 773-786.
7. Balashazy and Hofmann, Deposition of aerosols in asymmetric airway bifurcations, J. Aerosol Sci., 26, (1995), pp 273-292.
8. Asgharian and Anjilvel, Inertial and gravitational deposition of particles in a square cross section bifurcating airways, Aerosol Sci. Technol., 20, (1994), pp 177-193.
9. Hofmann, W., Balashazy, I, Heistracher, T., Koblinger, L., The significance of particle deposition patterns in bronchial airway bifurcations for extrapolation modelling, Aerosol Sci., Technol., 25, (1996), pp 305-327.

10.Lee, J. W., Goo, J. H., and Chung, M. K., Characteristics of inertial deposition in a double bifurcation, J. Aerosol Sci., 27, (1996), pp 119-138.

11.Yu, G., Zhang, Z., and Lessmann, R., Computer simulation of the flow field and particle deposition by diffusion in a 3-D human airway bifurcation, Aerosol Sci. Technol., 26, (1996), pp 338-352.

12. Zhang, L., Asgharian, B., and Anjilvel, S, Inertial deposition of particles in the human upper airway bifurcations, Aerosol Sci. Technol., 26, (1997), pp 97-110.

13.Tu, J.Y. and L. Fuchs, Calculation of Flows Using Three-Dimensional Overlapping Grids and Multigrid Methods, Int. J. Numer. Methods Eng. 38, (1995), pp. 259-282.

14.Tu, J.Y., Computation of Turbulent Two-Phase Flow on Overlapped Grids, Numerical Heat Transfer B, in press.

15.Tu, J.Y. and C.A.J. Fletcher, Numerical Computation of Turbulent Gas-Solid Particle Flow in a 90° Bend, AIChE Journal, 41 (10), (1995), pp.2187-2197.

16.Wilcox, 1993, Turbulence models in CFD, New York.

17.Tu J. Y., C. A. J. Fletcher, M. Behnia, J. A. Reizes, D. Owens and P. Jones., Prediction of Flow and Erosion in a Coal Fired Power Boiler and Comparison with Measurement, J. Eng. Gas Turbines & Power, 119, (1997), pp709-716.).

18.Tu J.Y., C. A. J. Fletcher and M. Behnia, Numerical Modelling of Three-Dimensional Flyash Flow in Power Utility Boilers, Int. J. Numer. Methods Fluids, 24, (1997), pp787-807.

19.Lee, B.Y. and Tu, J. Y., Eulerian Modelling Particle-Wall Interaction for Predicting Tube Erosion and Deposition, in press ASME J Fluids Engng.

20.Gadd, G. E., M. James, S. Moricca, P. J. Evans and R. L. Davies, Structural Characterisation of the new Fullerene-Rare Gas Compound Ar_1C_{60}, Fullerene Sci & Technol., 4(5), (1996), pp853-862.

21.Gadd, G. E., P. J. Evans, S. Moricca, and M. James, The Intercalation of Ar into C_{60} Films, J Mat Research, 12(1), (1997), pp1-4.

22.Gadd, G. E., P. J. Evans, D. J. Hurwood, J. Wood, S. Moricca, M. Blackford, M. Elcombe, S. Kennedy and M. James, Neutron Irradiation of Ar_1C_{60}, Chem Phys Letters, 261, (1996), pp221-227.

23.Gadd, G. E., P. J. Evans, D. J. Hurwood, P. L. Morgan, S. Moricca, N. Webb, J. Holmes, G. McOrist, T. Wall, M. Blackford, D. Cassidy, M.Elcombe, J. T. Noorman, P> Johnson and P. Prasad, Endohedral Fullerene Formation through Prompt Gamma Recoil, Chem. Phys. Letters, 270, (1997), pp108-114.

24.Gadd, G. E., M. Blackford, S. Moricca, , N. Webb, P. J. Evans, A. M. Smith, G. Jacobsen, S. Leung, A. Day and Q. Hua, The World's Smallest Gas Cylinders?, Science, 277, August (1997), pp933-936.

The Cobalt-60 Container Scanner

AN Jigang, ZHOU Liye, LIU Yisi, WU Haifeng, WU Zhifang, WANG Liqiang, ZHENG Yuanshui, XIANG Xincheng, LI Furong, GAO Baozeng,SHENG Chunfa
The Institute of Nuclear Energy Technology(INET),
Tsinghua University, Beijing, 100084,China

SUMMARY. The container(or cargo) scanners using digital radiography are very effective in the fight against contraband. This paper presents a special container(or cargo) scanner, which uses the commercial industrial radiography Cobalt-60 source of 100-300Ci. Depending on the adoption of high sensitive array detector, which is invented by INET, and other technical solutions, the characteristics of Cobalt-60 scanner are good enough for container(or cargo) inspection. Its "Contrast Indicator(CI)" and "Image Quality Indicator(IQI)" for 100mm steel are equal to 0.7% and 2.5% respectively and the "Steel Penetration(SP)" is about 240mm .The cobalt-60 container scanner is much cheaper and more reliable than those scanners using accelerator source, and its penetration ability is much better than that of x-ray machine scanner. The total composition, main difficulty and technical solutions, inspection characteristics and the application prospect of the Cobalt-60 scanner are presented with an emphasis.

1 INTRODUCTION

Since 1990, Schlumberger Industries (French) [1], Heimann Company(German) and Aerospace Company (British) have produced and sold several sets of container (or cargo) scanners using static or linear electron accelerator as high energy x-ray source. Tsinghua University (Chinese) also has researched and constructed one set of container or cargo scanner in Beijing, which x-ray source is a 9 Mev electron linear accelerator too [2].These scanners have very nice inspection characteristics and have been being strong weapons in the fight against drugs, arms and conventional contraband.

Nevertheless, these kinds of accelerator container scanner still have not been applied widely. The main reasons for such situation are as following :

a) Too expensive
The cost of the equipment is about ten million USD or more now.

b) Very high radiation intensity
The output of the accelerator used is as strong as 3000-4000 cGy/min.m. A lot of money have to be paid for shielding so strong radiation.

c) Large area
Because the length of inspection tunnel must be longer than 50m to prevent the radiation escape and the distance from accelerator target to array detectors is more than 12m, the total area of this kind of scanner is very large.

d) Complex maintenance
Especially for the accelerator , the maintenance is complex and difficult. The users have to pay 10-20% of the equipment cost per year for maintenance.

Therefore, a lot of work have been done to find out other container scanner designs which are much cheaper, easier to shield and can be installed in a much smaller area.

Several companies have tried to use x-ray machine as the radiation source. Nevertheless, because of the highest energy of the x-ray is just only several hundred keV, the steel penetration of these x-ray machine scanner is very poor($\leqslant$ 100mm steel).

The penetration ability of Cobalt-60 isotope source (E_r=1.17,1.33MeV) is much higher than that of x-ray machine and is similar to that of the electron accelerator of 4-5MeV. But the radiation output of ordinary radiography cobalt-60 source is much smaller than accelerator's. By using very high sensitive array detector , low noise level front-end circuit and special signal and image treatment method, we have successfully designed and constructed a Cobalt-60 scanner, which uses the widely adopted industrial radiography Cobalt-60 source of 100-300 Ci. The steel penetration and other characteristics of the Cobalt-60 scanner are similar to those of 4 ~ 5 MeV accelerator scanner, but its cost is much cheaper . It is easy to operate and maintain and only need much smaller area for installation and operation.

The following article will present the Cobalt-60 container scanner with an emphasis on the total composition , main difficulty and technical solutions , inspection characteristics and the application prospect.

2. SYSTEM COMPOSITION

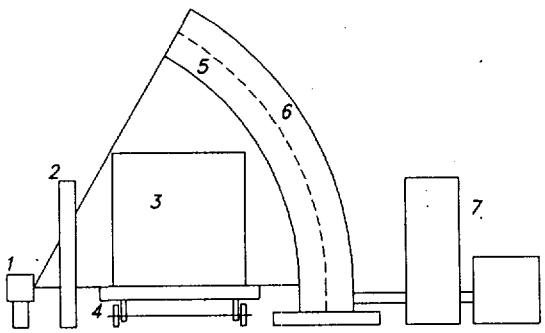

fig.1 system composition

The system composition of cobalt-60 container scanner is shown in fig 1. It consists of following main components:

a)Radiation source ①
The commercial industrial gamma radiography cobalt-60 source projector is used. The source activity is 100 ~ 300 Ci. The active dimensions of the source are ϕ 4 × 4mm. The total weight of the projector is less than 250kg. This kind of cobalt-60 source have been adopted widely in industrial non-destructive testing and have been proved to be very reliable, safe and convenient.

b)Front and back collimators ②⑤
The γ radiation of cobalt-60 source is collimated by the front and back collimator into a very thin slice type and then aims the array detector.

c)Conveyer system ④
It is used to pull the object-container to pass through the slice type radiation zone with a settled speed.

d) Array detector ⑥

The special gas-pressurized array ion-chamber invented by INET[3] is used. Because of special construction and gas-mixture, the ^{60}Co efficiency and sensitivity of this array detector are as high as 40% and 4×10^5pC/cGy respectively. This is the key technique of cobalt-60 container scanner.

e)Detection electronics and image processing subsystem ⑦

The very low noise front-end circuits are used to get large dynamic range . The signals are digitized on 16 bits after integration .The image processing subsystem acquires the digitized signals coming from the detection electronics, builds up the radioscopic images and displays them on the screen for examination by the operators.

3. THE MAIN DIFFICULTY AND THE TECHNICAL SOLUTIONS

The energies of ^{60}Co γ photons are never changed . Their intensity is also very stable in the period of measurement , because the half -life time of Cobalt-60 is as long as 5.3 year. The ^{60}Co gamma radiography projector possesses yet more merits , such as reliability, easier operation and convenient maintenance.

Nevertheless, the radiation output of the Cobalt -60 gamma projector with the activity of 100-300 Ci is much lower than that of the accelerator . It is equal to or less than 0.1% of the latter's. This is the main difficulty for cobalt-60 container scanner to possess nice inspection characteristics.

The main technical solutions of this difficulty are as follows:

a) The high efficiency and sensitivity array detector has been adopted.

As shown before , the efficiency and sensitivity of INET's gas - pressurized array ion-chamber for ^{60}Co γ -rays are equal to or higher than 40% and 4×10^5pC/cGy respectively. So the maximum signal current of the cobalt-60 scanner can be as large as several nA, and the statistical fluctuation can be kept low enough to insure nice inspection characteristics of the scanner.

b) The special low noise front amplifier has been designed and constructed. Its noise current level is less than 1×10^{-13}A. So the real total signal dynamic range of the measurement subsystem is higher than 2×10^4. This will deduce to nice contrast indicator and larger steel penetration.

c)Much shorter distance from source to array detector (e.g. 5-7m) can be chosen ,because the space distribution of Cobalt-60 gamma radiation is homogeneous .

d) The conveyer speed will be a little bit slower (e.g. 20cm/s).

Because the auxiliary inspection time of the Cobalt-60 scanner is much shorter than that of the accelerator scanner, its total throughput can be not less than the latter's in spite of the slower conveyer speed.

Depending on these technical solutions, the main difficulty of low radiation intensity is overcome and the inspection characteristics of Cobalt-60 scanner can be similar to those of the accelerator scanner.

4. MAIN INSPECTION CHARACTERISTICS

Five key indicators allow to quantify the performances of a radiation container scanner:

a) The "Image Quality Indicator (IQI)."
It is obtained by determining the diameter of the thinnest steel wire detectable behind a steel screen of a given thickness.

b)The "Contrast Indicator(CI)"
It represents the smallest overthickness detectable on a steel screen of a given thickness.

c) The "Steel Penetration (SP)"
It is the maximum thickness of steel behind which a totally absorbent object is still visible.

d) The "Maximum Dose Absorbed per Scanning"

e) The "Throughput " of radioscopy that can be achieved by the scanner.

The following performances of the cobalt-60 container scanner are achieved at INET (Tsinghua University):

-IQI: 2.5% behind 100 mm of steel
-CI: 0.7% behind 100 mm of steel
-SP: 240 mm of steel
-Maximum Dose per Scanning :0.02mGy
-Throughput : 20 40-foot containers per hour.

Fig.2 shows the radioscopic image of a motorcycle realized at the Cobalt-60 container scanner. A 1kg pack of sugar was hidden behind the oil box of the motorcycle, and is already visible on the image.

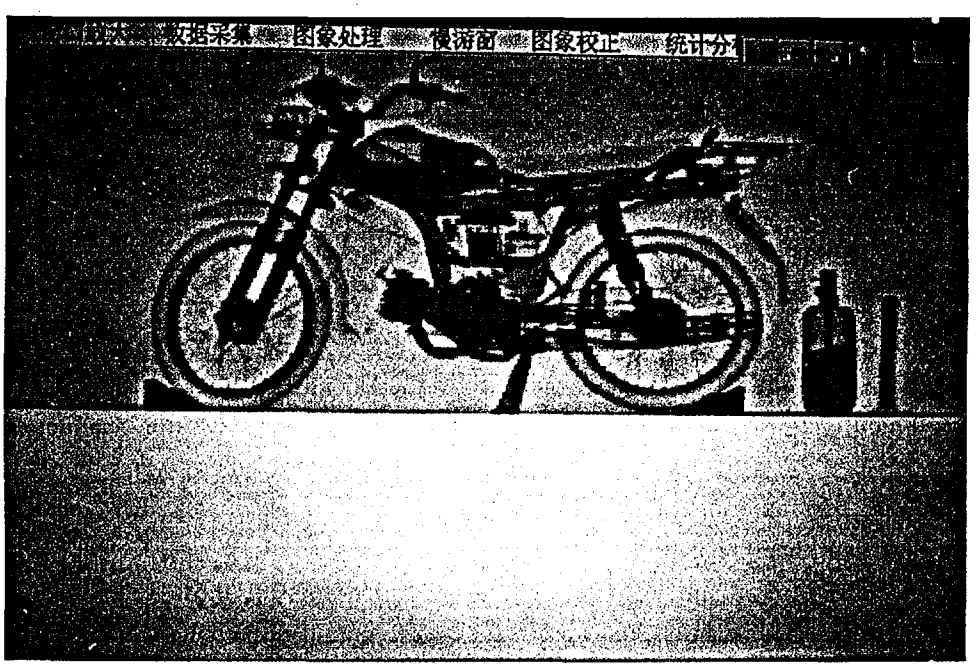

Fig.2 radioscopic image of a motorcycle

5. SPECIAL FEATURES AND APPLICATION PROSPECT.

A comparison of the inspection characteristics between the cobalt -60 scanner and the static accelerator scanner is shown in table 1.

Table 1. A comparison of inspection characteristics

indicator / scanner	IQI (100mm steel)	CI (100mm steel)	SP (steel)	Maximum Dose Absorbed per Scanning	Throughput
static accelerator scanner (2.5Mev)	2.5%	0.4%	240mm	0.4mGy	60 10-foot containers per hour
static accelerator scanner (5 Mev)	3%	0.75%	280mm	1mGy	20 trucks per hour
Cobalt-60 scanner	2.5%	0.7%	240mm	0.02mGy	20 40-foot containers per hour

As shown in table 1, the inspection characteristics of Cobalt-60 container scanner are similar to those of accelerator scanner. On the other side, the former possesses many other special features which are much better than the latter's :

a) Cheap price

The price of the Cobalt -60 scanner produced by INET will be about one or two tenths of the accelerator scanner's .

b) Low radiation intensity

Because the radiation output of the radiography Cobalt -60 source used is less than 0.1% of the accelerator's , the radiation protection problem is much easier to solve. There will be a lot of money to be saved on the radiation shielding building.

c) Small building area.

The inspection tunnel length of 6-8m is long enough for the Cobalt-60 scanner. The distance from source to detector is 5-7m. So the building area for Cobalt-60 scanner will be much smaller than that of accelerator scanner.

d) Simple operation and convenient maintenance.

The radiography Cobalt-60 source is easy to operate and maintain . So the operation and maintenance fee for Cobalt -60 scanner will be much lower.

e) Reliability and Stability

The energies of Cobalt-60 gamma rays are never changed and its intensity can also be considered to be constant during the scanning period . These are very beneficial for the signal and image processing . Because there is no high voltage, strong microwave and large electric power equipment etc. in the system , the cobalt-60 scanner is very reliable and stable .

Because of these special features and the nice enough inspection characteristics , the cobalt-60 container scanners are more suitable to be applied widely. This kind of scanner is satisfied for boundary customs, seaports, airports and railway stations etc..

6 CONCLUSION

A Cobalt-60 container(or cargo) scanner,which radiation source is a commercial radiography cobalt-60 source of 100-300Ci, has been designed and contrusted successfully by INET of Tsinghua University.

The inspection characteristics of this Cobalt-60 scanner are similar to those of the accelerator scanner. But its price is much cheaper and the building area needed for installation and operation is much smaller. The low radiation intensity, the simple operation and convenient maintenance, the reliability and stability etc. are the other merits of the Cobalt-60 container scanner.

The high properties and the low price will make Cobalt-60 container scanners have much better application prospect.

REFERENCE

[1] J.-F. Bouisset, A. Blis, A.-P. Lilot etc., "The Roissy - charles -de-Gaulle SYCOSCAN: a Reality"
in proceedings of the "Contraband and Cargo Inspection Technology" International Symposium Washington D.C. , October 28-30, 1992.

[2] AN Jigang, "Research and Construction of the Container Radiation Scanner"
Isotopes , Vol.8 . No. 1 p16-20(1995)(Chinese)

[3] AN Jigang, WU Heifeng , "Device of Gas Ionization Array Detectors for High Energy X or γ -rays Radiography", Chinese Patent.No. 93102728.4(1993)

Investigations of the Influence of the H_2O_2 and NaF on the Corrosion on Valve Metals and Steel in Systems of Pratical Importance by Use of Radioisotopes.

G. MARX; C. NEHM; M. LASKE; A. KUPFER
Freie Universität Berlin, Institute of Inorganic and Analytical Chemistry,
Radiochemical Division, Fabeckstraße 34-36, 14195 Berlin, Germany

SUMMARY

In order to investigate the corrosion on materials, pollux containers for direct radioactive waste disposal shall consist of, Ti; Ti99.8Pd; TiCode12 and steel (TSTE335) were investigated in brines (saturated NaCl solution, Solution 3 and Q-brine) by use of the RadioIsotope Method (RIM), using ^{59}Fe as isotopic and ^{46}Sc and ^{58}Co as nonisotopic tracers. Especially the influence of the radiolytic products H_2O_2 and ClO^- on corrosion were studied in these specific media, not only at rest potentials but also at various potentials applied. Furthermore the influence of temperature (25°C; 55°C and 80°C) was taken into consideration.
The results obtained indicate that the pollux container will withstand corrosion in brines for at least 500 years. The concentrations of the radiolytic products H_2O_2 and ClO^- existing under practical conditions of a waste repository do not influence corrosion on titanium and Ti99.8Pd at all. The influence of H_2O_2 on Ti and Ti99.8Pd corrosion is identical at higher concentrations. The corrosion on zirconium can be compared with that on titanium in brines.
In NaCl solutions the corrosion rate on steel (TSTE335) is very small, at constant pH=5.5, although this specific steel is in the active range. The steel corrodes homogeneously with respect to its surface without any remarkable pit corrosion.

1. INTRODUCTION

Germany decided the direct disposal of radioactive waste in salt diapirs to be an option to cope with the problems of waste management. Since the relevant cascets, the spent fuel elements shall be put in, are pollux containers, optionally consisting of two sections of steel, the inner one being plated with titanium and its alloys TiGr.7 and TiCode12, the corrosion on these materials had to be studied under practical conditions, that means in brines and bentonite pore water. The brines might result from intrusion of water into salt domes, which is still a hypothetical event. The titanium layers of the cascets shall increase the resistance of these containers towards corrosion, so that they are able to withstand corrosion for at least 500 years. After that time the ironoxide produced will act as scavenger forming mixed potentials. The main interest of the investigations was focused on the influence of the products of radiolysis, H_2O_2 and ClO^-, because of their oxidising behaviour, which drastically changes the rest potentials of the various systems under investigation. In addition the influence of NaF on corrosion was studied out of theoretical reasons. Quite a lot of parameters, therefore, must be known in detail to obtain reliable data for modelling the physico-chemical conditions in a waste repository, these conditions being extrapolated to time periods, hardly to be imagined.

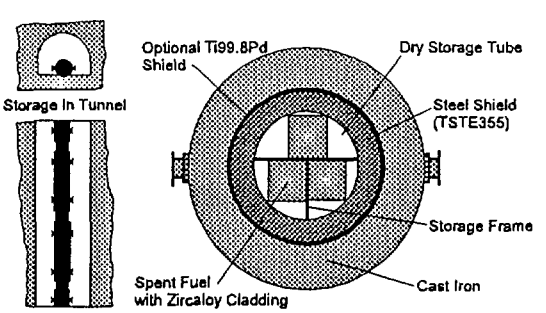

Figure 1
Pollux container

2. EXPERIMENTAL DETAILS

Titanium (99.98%), Ti99.8Pd and TiCode12 (Mo: 0.29%; Ni: 0.89%; Fe: 0.11%), were investigated in saturated NaCl solution, Solution 3 and Q-brine[1] at 25°C, 55°C and 80°C at rest potentials and different applied potentials within the range from -1000 mV to +1000 mV the first two metals mentioned also in presence of H_2O_2 at various concentrations (from $7 \cdot 10^{-4}$ to $7 \cdot 10^{-2}$ $mol \cdot l^{-1}$). At the beginning of the experiments the definite H_2O_2 concentrations were determined spectroscopically from the relevant TiO_2^{2+}-ion concentrations by use of an UV/VIS spectrometer (Perkin Elmer 330 Spektrophotometer).
The method applied to the corrosion measurements was the RadioIsotope Method RIM[2] joining electrochemical and radiochemical procedures combined with impedance measurements. Automatically working RIM needs an ordinary electrolytic cell with reference (Ag / AgCl), counter (Pt) and working electrode, consisting of the neutron activated material under investigation and in addition a potentiostat (FUB) for carrying out potentiostatic and potentiodynamic measurements. The corrosion rates were γ-spectroscopically (MCA Silena Cicero) determined from the activity of the relevant solutions, continuously passing the GeLi-detector (PGT), the specific γ-rays being not only emitted from isotopic but also from nonisotopic tracers (Ti ≅ ^{46}Sc; Ni ≅ ^{58}Co)
Furthermore the corrosion rates were independently calculated from the measured current densities by use of Faraday's law.
A frequency generator (Zahner IMD5) permitted impedance measurements to be simultaneously carried out, which informations on the protecting oxide layers of the studied valve metals (thickness; electrical conductance, dielectric numbers) were obtained from.
In addition the corrosion on zirconium, Zircalloy-4 and steel (TSTE 335) was studied by RIM in the same media, steel also by using AAS; titration and mass loss. The radioisotopes applied were ^{95}Zr and ^{59}Fe.

3. RESULTS AND DISCUSSION

3.1 RESULTS FROM MEASUREMENTS ON TI AND TI99.8PD

The relevant results are listed up in the following tables and figures. The data indicate that H_2O_2 drastically increases the corrosion on Ti and Ti99.8Pd by destroying their oxide layers forming TiO_2^{2+}-ions due to the equations (1) and (2).

$$Ti + 2H_2O_2 \rightarrow TiO_2 + 4H^+ + 4e^- \text{ eg. (1)}$$

$$TiO_2 + H_2O_2 + 2H^+ \rightarrow TiO_2^{2+} + 2H_2O \text{ eg. (2)}$$

3.1.1 MEASUREMENTS AT REST POTENTIALS

The results obtained at the relevant rest potentials (350 - 450 mV (SHE)) prove that in the different media the corrosion rates are proportional to the relevant H_2O_2 concentrations (cf. table 1).

Table 1
Influence of H_2O_2 on the corrosion of Ti99.8Pd at rest potential (sat. NaCl; 25°C)

H_2O_2-concentration mol/l	Corrosion rates µm/a
$7.0 \cdot 10^{-2}$	18 ± 2
$3.5 \cdot 10^{-2}$	9 ± 1
$7.0 \cdot 10^{-3}$	3 ± 1
$7.0 \cdot 10^{-4}$	0.8 ± 0.2
$7.0 \cdot 10^{-5}$	0.7 ± 0.2
0	0.4 ± 0.2

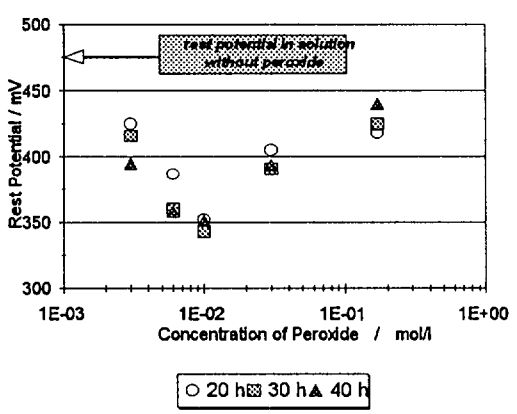

Figure 2
Rest potential of Ti99.8Pd (sat NaCl / 25°C)

In saturated NaCl solution at 25°C the corrosion rate is 22 $\mu m \cdot a^{-1}$ for $6 \cdot 10^{-2}$ $mol \cdot l^{-1}$ H_2O_2 and 0,5 $\mu m \cdot a^{-1}$ for $6 \cdot 10^{-4}$ $mol \cdot l^{-1}$ H_2O_2, the last

value equalling that one obtained in solutions, free from H_2O_2 (0.3 ± 0.2) $\mu m \cdot a^{-1}$. H_2O_2 concentrations smaller than 10^{-4} $mol \cdot l^{-1}$ have no influence at all on the corrosion on Ti99.8Pd ($r_{corr.} < 0.5$ $\mu m \cdot a^{-1}$). The curve rest potential on Ti99.8Pd vs. H_2O_2 concentration passes a minimum, which is due to the fact, that H_2O_2 decomposes into H_2O and O_2. Higher corrosion rates increases the partial anodic current density, shifting the rest potential to more negative values. The increasing O_2 content in the solution on the other hand increases the partial cathodic current density, these two effects opposing each other. All relevant rest potentials on Ti and Ti99.8Pd are in the passive range (cf. Figure 3)

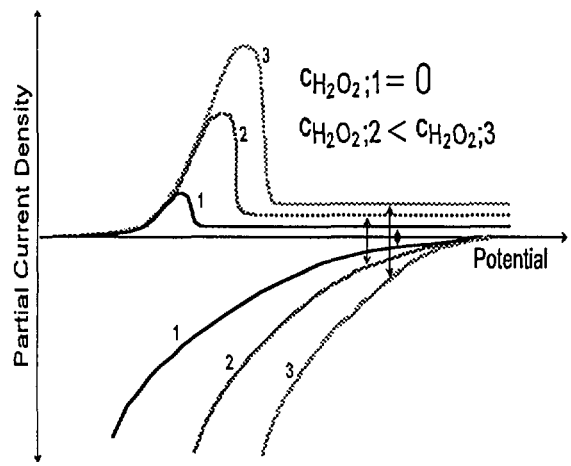

Figure 3
Shift of rest potential in presence of H_2O_2

3.1.2 POTENTIOSTATIC MEASURMENTS ON Ti AND Ti99.8Pd

Potentiostatic measurements on Ti99.8Pd were performed in saturated NaCl solutions at 25°C containing $7 \cdot 10^{-2}$ $mol \cdot l^{-1}$ H_2O_2 within the potential range from -1000 to +1000 mV. In the active range corrosion rates were obtained in the medium aforementioned from 1000 to 1500 $\mu m \cdot a^{-1}$. In saturated NaCl solutions containing only $7 \cdot 10^{-3}$ $mol \cdot l^{-1}$ H_2O_2 on the other hand the corrosion rates are definitely smaller (30 - 40 $\mu m \cdot a^{-1}$). Even the corrosion rates in the active range can be neglected from the practical point of view. At $7 \cdot 10^{-2}$ M H_2O_2 the corrosion rates of Ti equal that of Ti99.8Pd.

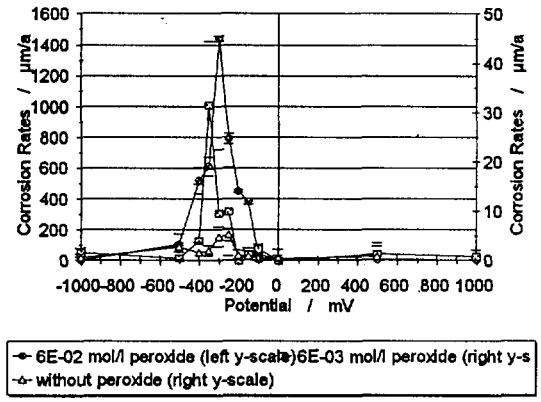

Figure 4
Corrosion rates vs. potential (Ti99.8Pd / sat. NaCl / 25°C)

Figure 5 shows the influence of temperature on the corrosion rate at various potentials applied. A significant influence of temperature on corrosion is only to be seen in the active range.

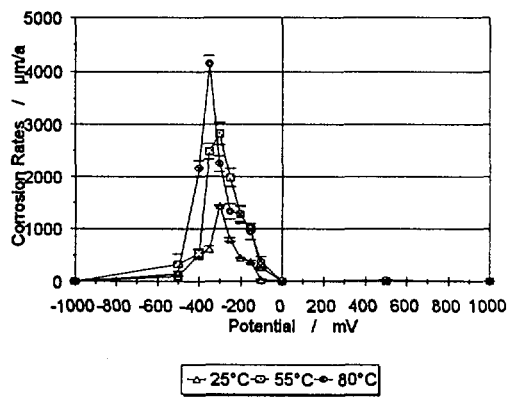

Figure 5
Corrosion rate of Ti99.8Pd at various temperatures (sat. NaCl / $7 \cdot 10^{-2}$ $mol \cdot l^{-1}$ H_2O_2)

3.2 CORROSION ON Ti99.8Pd UNDER THE INFLUENCE OF NaF AT REST POTENTIALS

A non decomposing complexing agent as NaF increases Ti corrosion by forming TiF_6^{2-} and therefore shifts the rest potential to more negative values (cf. table 2) approaching the relevant active range, without reaching it.

Table 2
Influence of NaF on the corrosion on Ti99.8Pd at rest potential (sat. NaCl; 25°C)

NaF-concentration	rest potential	corrosion rates
mol/l	mV	µm/a
$6.7 \cdot 10^{-2}$	304	14 ± 2
$3.3 \cdot 10^{-2}$	294	7 ± 1
$6.7 \cdot 10^{-2}$	-194	0.6 ± 0.2
$3.3 \cdot 10^{-2}$	-308	0.2 ± 0.2

3.3 CORROSION ON Ti99.8Pd UNDER THE INFLUENCE OF ClO^-

In order to take the second radiolytic product of interest into account the influence of ClO^- on Ti99.8Pd corrosion was studied in saturated NaCl solution, containing $8 \cdot 10^{-2}$ mol·l^{-1} ClO^-, in the active range (-250 mV) at 25°C. Although these conditions are the worst case from the corrosion point of view, there was no increase of corrosion on Ti99.8Pd to be detected radioanalytically (3 ± 2 µm·a^{-1}) with respect to that corrosion obtained in ClO^- free solution (5 ± 2 µm·a^{-1}). These results were verified electrochemically by performing cyclovoltammogrammes, which indicate that the relevant oxide layer is not destroyed under these conditions.

4. MEASUREMENTS ON CORROSION ON ZIRCONIUM IN BRINES

The results from the measurements on zirconium in saturated NaCl solution (cf. table 3) and in Q-brine (cf. table 4) at rest potentials indicate a similar behaviour with respect to the corrosion on this valve metal compared with that on titanium.

Table 3
Corrosion rate of titanium, zirconium and Ti99.8Pd in sat. NaCl solution

Material	Corrosion rate µm·a^{-1}		
	25°C	55°C	80°C
Zirconium	0.4 ± 0.1	0.2 ± 0.1	
Titanium	0.4 ± 0.2	0.3 ± 0.2	0.3 ± 0.2
Ti99.8Pd	0.4 ± 0.2	0.3 ± 0.2	0.4 ± 0.2

Table 4
Corrosion rate of titanium, zirconium and Ti99.8Pd in Q-brine

Material	Corrosion rate µm·a^{-1}		
	25°C	55°C	80°C
Zirconium	0.3 ± 0.1		
Titanium	0.4 ± 0.2	0.2 ± 0.1	0.2 ± 0.1
Ti99.8Pd	0.3 ± 0.2	0.4 ± 0.2	0.3 ± 0.2

4.1 MEASUREMENTS ON CORROSION ON STEEL (TSTE335) IN NaCl SOLUTIONS AT REST POTENTIALS

In NaCl solutions the corrosion rate at constant pH =5.5 on steel TSTE335 depends on NaCl concentration and temperature (cf. figure 6). Under the prevailing conditions the steel is in the active range but at these high Cl^--concentrations (5.4 mol·l^{-1} ≅ saturated NaCl solution) the corrosion on steel is comparatively small (70 µm·a^{-1}) due to the low solubility of O_2 in the medium, the reduction of O_2 to H_2O being the counter reaction. From the reproducibility of the experimental data and also from microscopic investigations it can be seen that this steel corrodes homogeneously with respect to its surface without any remarkable pit corrosion.
The curve corrosion rate vs. temperature passes a maximum, which is caused by two opposing effects, the decrease of O_2 concentration in the solution with rising temperature and the increase of the velocity rate constant due to Arrhenius' law. Due to the small O_2 concentration the cathodic Stern-Geary-factor[3] has a very high value so that the anodic Stern-Geary-factor becomes the proportional factor between polarisation resistance and inverse anodic current density at rest potential allowing the specific anodic current density to be calculated from impedance measurement alone.

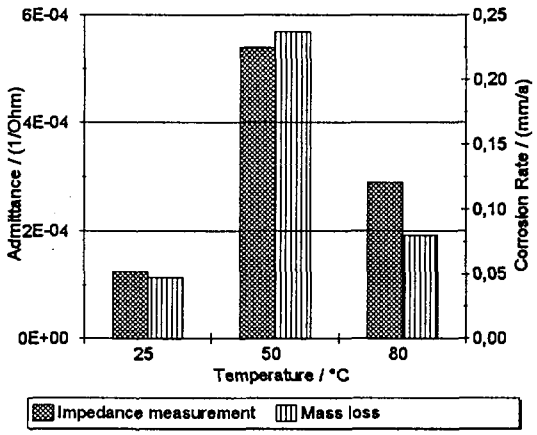

Figure 6
TSTE335 in 5.4M NaCl solution at rest potential

5. CONCLUSION

The results obtained from the corrosion measurements on the materials the pollux containers shall optinally consist of, indicate that the pollux container will withstand corrosion in brines for at least 500 years. The concentrations of the radiolytic products H_2O_2 and ClO^- existing under practical conditions of a waste repository do not influence corrosion on titanium and Ti99.8Pd at all. The influence of H_2O_2 on Ti and Ti99.8Pd is identical at higher H_2O_2 concentrations.
Corrosion on Ti and Ti99.8Pd is not effected by higher temperature in the passive range, it is slightly increased by rising temperature in the active range.
The corrosion on zirconium can be compared with that of titanium under the conditions aforementioned.
In NaCl solution the corrosion rate at constant pH=5.5 on steel TSTE335 depends on concentration and temperature and is very small in saturated NaCl solution (70 $\mu m \cdot a^{-1}$) due to the low solubility of O_2 in the medium, the reduction of O_2 to H_2O being the counter reaction. The steel corrodes homogeneously with respect to its surface without any remarkable pit corrosion.

6. ACKNOWLEDGEMENT

The financial support of European Community (F14W-CT95-0002) is gratefully acknowledged.

[1] Braitsch, O., Entstehung und Stoffbestand der Salzlagerstätten, Springer-Verlag Berlin, 1962, 86ff
[2] Wegen, D.; Heppner, P.-M.; Nehm, C.; Marx, G.; Das Korrosionsverhalten von Titan und UO_2 im Rahmen der Wiederaufarbeitung und der direkten Endlagerung von Kernbrennstoffen, DECHEMA-Monographie Vol. 128, 1993, 511 - 531, VCH Verlagsgesellschaft.
[3] Stern, M., Geary A.L., Electrochemical Polarisation I. Shape of Polarisation Curves, J. Electrochem. Soc. 104, 1957, 56

AU9817377

The ANTARES Accelerator: A Facility for Environmental Monitoring and Materials Characterisation

C TUNIZ, Australian Nuclear Science and Technology Organisation
PMB 1 Menai 2234 NSW Australia

SUMMARY ANTARES is a facility dedicated to accelerator mass spectrometry and ion beam analysis. Research programs based on the AMS spectrometer include applications of ^{14}C, ^{10}Be, ^{129}I and other long-lived radionuclides in quaternary science studies, global climate change and environmental monitoring for nuclear safeguards. Ion beam analysis methods based on elastic recoil detection are used for the *in-situ* determination of specific elements or isotopes in surface materials. New analytical systems are under construction, including an AMS beamline for the measurement of actinide isotopes and a heavy ion microprobe for elemental imaging with micron resolution.

1. INTRODUCTION

The ANTARES accelerator is based on the FN tandem accelerator originally built by High Voltage Engineering for Rutgers University (New Jersey, USA). Since its arrival in Australia, in 1989, the accelerator has undergone a complete refurbishment and upgrade. During the first phase, major items in this transformation have been new spirally-inclined accelerator tubes, a 60-sample high-intensity sputtering source and a high resolution injection magnet (1). Several major elements of the accelerator structure were to improve both the energy stability and the focal properties of the particle beam. The most significant recent upgrades have been the installation of a recirculating gas stripper and a new Pelletron charging system. As a consequence, operations at eight million volts is now possible. Versatility is allowed by multiple beamlines for AMS and IBA applications (Fig. 1)

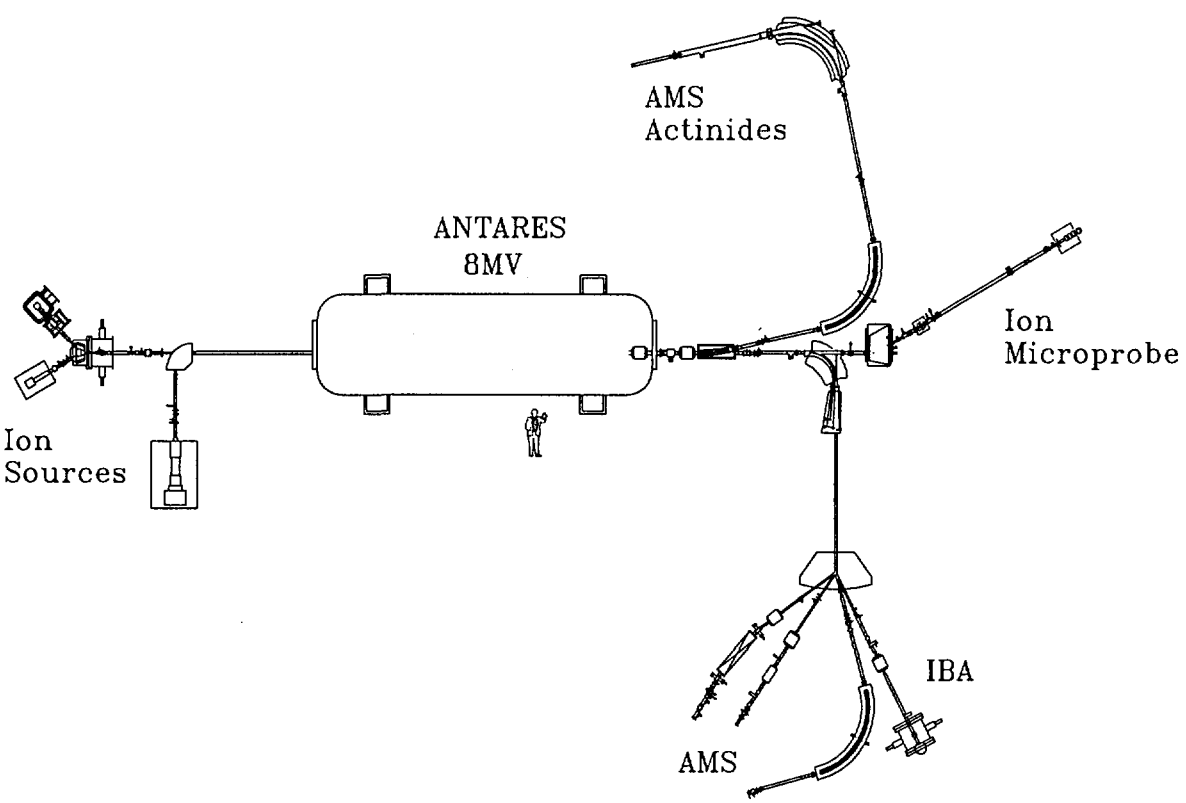

Figure 1 – Layout of the ANTARES facility.

1.1. The ANTARES AMS spectrometer

The ANTARES AMS facility performs ultrasensitive analysis of the long-lived radioisotopes ^{14}C, ^{10}Be, ^{26}Al, ^{36}Cl and ^{129}I.

The chemistry laboratories for target preparation are an integral part of the ANSTO AMS facility. Samples containing 0.2 mg or more of original carbon are processed routinely for radiocarbon analysis. The current ^{14}C chemistry background for 1 mg carbon is about 0.2-0.3 percent of modern carbon. With the increasing demand for measurement of extremely small samples, we are currently developing methods for the preparation of targets containing tens of micrograms of carbon. Several unknown samples with masses as low as 50 μg carbon have been recently analysed. We are presently expanding the capabilities of the chemistry laboratories to encompass the preparation of ^{10}Be, ^{26}Al and ^{36}Cl from a variety of environmental samples. Procedures for the extraction of iodine from water, sediments, soils and biota are being developed for ^{129}I analyses.

After chemistry processing, AMS targets are loaded in the sputter ion source of the ANTARES accelerator. High precision AMS analysis is carried out by rapid sequential injection of the isotopes of interest, in order to overcome variability in source output and accelerator transmission. Following injection into the accelerator, negative ions are attracted by the positive voltage at the terminal and thereby accelerated to high energies (e.g. 6 MeV during ^{14}C analysis), at which point they pass through a gas or a foil stripper located at the terminal. The same positive voltage then further accelerates the multi-charged positive ions on the terminal. Following the acceleration, combinations of magnetic and electric fields select charge, momentum, energy and velocity of the ions. The beamlines dedicated to AMS are equipped with a Wien filter, a 22° electrostatic analyser and a 90° electrostatic analyser, which provide the selectivity necessary to separate the radionuclide of interest. The final identification of the rare radionuclide is performed in the ion detector by measuring one or more of the following parameters: total energy, stopping power, range and velocity. Depending on the isotopes to be counted, a variety of detectors are available for this final stage at the ANTARES AMS spectrometer, including a multi-anode ionisation chamber, a Bragg detector and a time-of-flight system.

2. AMS APPLICATIONS

Long-lived radionuclides are used as tracers and chronometers in many disciplines: geology, archaeology, astrophysics, life and materials science. Low-level decay counting techniques have been developed in the last half-century to detect the concentration of cosmogenic, radiogenic and anthropogenic radionuclides in a variety of specimens. The radioactivity measurement for long-lived cosmogenic radionuclides, such as ^{10}Be, ^{14}C, ^{26}Al, ^{36}Cl, is made difficult by low counting rates and in some cases the need for complicated radiochemistry procedures and efficient detectors of soft beta particles and low energy x rays. AMS can measure cosmogenic radionuclides in geological samples up to 10^6 times smaller then those required for conventional techniques, allowing novel applications in geology and environmental science.

2.1 Global climate change

The ANTARES AMS spectrometer is a key facility for reserch programs based on the application of nuclear science and technology to the understanding of natural processes. Some of the projects carried out at ANSTO are discussed in the following.

2.1.1 Long-lived radionuclides in Antarctic ice

Ice cores are providing the best source of preserved air from which to reconstruct levels of greenhouse gases over recent centuries to millennia. Ice cores from Law Dome, East Antarctica, characterised by high accumulation rates but minimal summer melting, provide an unparalleled time resolution through the Holocene and possibly beyond. In addition, air extracted from the firn permits direct comparison of entrapped trace gas concentrations with modern records. One of the problems is that recent CO_2 growth rate variations are difficult to interpret due to the smearing of ice-core signals induced by the diffusion of air in the firn. In collaboration with the CSIRO Division of Atmospheric Research, ANSTO researchers recently succeeded in using the ^{14}C "bomb spike" to determine the age spread and age of CO_2 in Antarctic ice and firn (3).

Future research will include studies of the last glacial/interglacial transition, search for a Younger Dryas in the Southern Hemisphere and investigations on changes in CO_2 and CH_4 in the Holocene period, concentrating on particular periods of interest such as the Maunder Minimum.

^{10}Be measurements at annual resolution are planned in cores of known chronology from Low Dome spanning up to several solar cycles to determine the magnitude of the solar modulation and to compare the data with neutron flux records.

An important greenhouse gas is methane, but the anthropogenic contribution to the global methane budget is not well understood. In fact, it is difficult to obtain atmospheric samples prior to the nuclear era for the measurement of ^{14}C and the determination of the methane budget. The large volumes of atmospheric gas trapped in the porous firn overlying the ice offer a solution and a sampling expedition is planned to investigate the feasibility of this approach.

2.1.2 Southern hemisphere glaciation project

Cosmogenic radionuclides such as ^{10}Be, ^{26}Al and ^{36}Cl produced in rocks can provide information on glacial histories in the southern hemisphere. The ANSTO research program is targetting three geographic regions that show distinct glacial formations and deposits: Tasmania, New Zealand and Antarctica. The ANTARES AMS spectrometer is used to analyse glacially polished bedrock surfaces, large erratics and boulders deposited on lateral and terminal moraines and within glacial outlet valleys.

2.1.3 High resolution palaeoclimate records

The aim of this project is to improve the chronologies of key palaenvironmental records in the Asian, Australian and Antarctic regions spanning the last 350,000 years. This project will complete the transect of records for climate change across the southern hemisphere and provide past climate patterns. The research is centred on sediment cores which will be used to reconstruct changes in salinity, temperature, nutrient levels, ice cover and productivity in the region from evidence provided by diuatom records, thorium/polonium ratios, carbon-13 values and grain size analysis. Dating of cores is being carried out using AMS radiocarbon techniques and lead-210 dating.

2.2 Monitoring nuclear activities

ANSTO is involved in IAEA programs, supported by the Australian Safeguards Office, to develop new methods for environmental monitoring for nuclear safeguards.

Nuclear activities such as reactor operation and fuel reprocessing introduce into the environment long-lived radionuclides such as ^{129}I and ^{36}Cl. AMS is the analytical technique of choice for the practical analysis of these radionuclides in natural specimens (4). Isotopic concentrations of 10^6 atoms per gram can be detected in samples taken from a variety of environmental materials such as water, air, soil and biota. In collaboration with the IAEA, the ANSTO AMS group has recently analysed ^{129}I in waters and sediments collected by IAEA inspectors at various locations from a nuclear reprocessing plant. ANSTO researchers are also analysing ^{129}I and other long-lived radionuclides in water specimens from the Mururoa lagoon, contributing to an international project aimed at determining the environmental impact of the underground nuclear tests in the Pacific atolls.

3. ION BEAM ANALYSIS

Ion accelerators can provide a variety of high-energy ion beams to probe the structure of materials and their composition. Ions penetrating the surface of a material specimen lose energy by ionization processes caused by the Coulomb interactions between the projectile and the target electrons and also by nuclear scattering. The range of ions in materials is short, with a relatively well defined end point. By comparison, x-ray and neutron beams are attenuated according to an exponential law and sample a much greater amount of material. Ion beams are applied to trace element determinations using the characteristic x-rays produced in the ionization process. Nuclear reactions, including elastic and inelastic scattering or Coulomb excitation, are useful to identify specific elements and nuclides present in the sample. Concentration measurements of individual elements or isotopes as a function of depth are determined using narrow nuclear resonances and energy loss of ions as they penetrate the material.

An IBA system based on elastic recoil detection (ERD) is available on one of the ANTARES beamlines. In elastic scattering processes, the target atoms gain momentum in a forward direction. By detecting the atoms leaving the target in a forward direction, information on the concentration and depth distribution of various elements can be obtained Measurements of time of flight and energy provide unambiguous identification of the knocked-on nuclides. ERD is being used by ANSTO groups in studies related to Synroc. This material has a high leach resistance in aqueous media, but it is difficult to use H_2O to measure the hydrogen incorporated in leached Synroc, due to the ubiquitous presence of hydrogenous surface contamination. The use of D_2O provides a more sensitive and reliable method for this kind of studies. ERD techniques using heavy ion beams are used at ANSTO to study deuterium depth penetrations and concentrations in Synroc samples

and to evaluate the chemical reactions taking place during the dissolution of this material at different temperatures (5).

4. FUTURE DEVELOPMENTS

As described in the previous sections, the ANTARES accelerator is presently used for the AMS analysis of commonly used long-lived radioisotopes and for the IBA characterisation of materials surfaces. Two new facilities, an ion microprobe and a system for AMS analysis of *heavy* rare isotopes, are under construction and will expand present capabilities.

4.1. The heavy ion microprobe

Ion microbeam analysis uses an ion beam focussed to μm dimensions for elemental imaging of materials surfaces. This can be performed by using secondary radiation induced by the primary ion beam, such as x-rays and nuclear reaction products, or by using the energy loss of transmitted primary ions. Pioneering studies with proton microbeams (50 μm diameter) were performed in the mid sixties at the Lucas Heights 3-MV accelerator (6). These first experiments paved the way for the modern nuclear microprobes, characterised by sub-micron lateral resolution (7). A heavy-ion microprobe for surface imaging and depth profiling is presently being developed at ANTARES,. This nuclear microprobe is designed to focus a variety of ion beams, including iodine, to lateral dimensions of about 10 microns or less.

4.2. AMS of actinides

A new facility is being constructed at ANTARES to analyse rare heavy radionuclides, such as ^{236}U, $^{229,230}Th$ and ^{244}Pu, in natural samples with ultra-high sensitivity. The main use of this facility will be for the ANSTO program in environmental monitoring and nuclear safeguards. An electrostatic quadrupole doublet has been installed on the high-energy end of the accelerator to provide mass independent focussing of the beam at an external gas stripper, where stripping to higher charge states will allow rejection of molecular fragments having similar M/Q. Momentum and E/Q analysis will be performed with a new analysing magnet (mass-energy product = 250 MeV.amu) and an electrostatic analyser (ESA). The 90° spherical ESA, manufactured by Danfysik, has a radius of 2.5 m and a nominal maximum rigidity of E/Q = 7.6 MV and an energy dispersion of 5000 in the image plane.

5. CONCLUSIONS

ANSTO is promoting an advanced research and development program in a variety of topics of high international significance such as global climate change and environmental monitoring for nuclear safeguards. Other research projects are related to the processing of novel materials for use in functional devices. The analytical facilities available at ANTARES provide essential capabilities for the development of this program.

ACKNOWLEDGMENTS

This paper presents a summary of the activities and programs performed at ANTARES by the ANTARES Operations Group, the AMS Group and the Accelerator Applications Group in the Physics Division.

Part of the research illustrated in this paper is funded by the Australian Institute of Nuclear Science and Engineering, the Australian Research Council, the National Greenhouse Advisory Committee and the Australian Safeguards Office.

REFERENCES

(1) Tuniz, C., Fink, D., Hotchkis, M.A.C, Jacobsen, G.E., Lawson, E.M., Smith A.M. and Hua, Q. (1997) Research and measurement program at the ANTARES AMS facility, Nucl. *Instr. and Methods in Phys. Res.*, Vol 123, pp 73-78.

(2) Tuniz, C., Bird, J.R., Fink, D. and Herzog, G.F. Accelerator Mass Spectrometry: ultrasensitive analysis for global science, *CRC Press, LLC*, in press.

(3) Levchenko, V.A., Francey, R.J., Etheridge, D.M., Tuniz, C., Head, J., Morgan, V.I., Lawson, E.M. and Jacobsen, G.E. (1996) The ^{14}C "bomb spike" determines the age spread and age of CO_2 in Law Dome firn and ice, *Geophysical Research Letters*, Vol 23, pp 3345-3348.

(4) Tuniz, C. and Hotchkis, M.A.C. (1997) Accelerator Mass Spectrometry to identify signatures of nuclear activities, *Proc. International Workshop on the Status of Measurement Techniques for the Identification of Nuclear Signatures, Belgium*, in press.

(5) Dytlewski, N., Vance, E.R. and Begg, B.D. (1996) Energy-recoil analysis of deuterium incorporated in Synroc by reaction with D_2O at 120 and 190 °C, *Journal of Nuclear Materials* Vol 231, pp 257 -259.

(6) Breese, M.B.H., Jamieson, D.J., King, P.J.C., Materials analysis using a nuclear microprobe, *John Wiley & Sons, Inc., New York,* 1996.

(7) Mak, B.K., Bird, J.R. and Sabine, T.M. (1966) Proton microanalysis, *Nature* Vol 211, pp 738-739.

Biomedical Applications of Accelerator Mass Spectrometry at ANU

L.K.FIFIELD, M.L.di TADA, KEXIN LIU and R.G.CRESSWELL
Department of Nuclear Physics, RSPhysSE, Australian National University
Canberra, ACT 0200, Australia

J.P.DAY, C.L.OLDHAM, J.POPPLEWELL and R.CARLING
Department of Chemistry, University of Manchester
Manchester M13 9PL, UK

Radioactive isotopic tracers are widely used in biomedical research, but for some elements of much current interest such as aluminium, silicon and plutonium, suitable isotopes for radioactive decay counting are not available. Each of these elements, however, possesses a long-lived isotope which could in principle be used if a suitable atom-counting detection technique were available. Accelerator Mass Spectrometry (AMS) is such a technique.

AMS can provide ultra-sensitive detection of fewer than 10^6 atoms of isotope, thereby enabling tracer experiments with human subjects without adding significantly to radiation body burdens. It achieves this by adding a high-energy acceleration stage to a conventional mass spectrometer, and then uses the ion-identification techniques of nuclear physics to count individual atoms.

The AMS system based on the fifteen-million-volt 14UD accelerator at the ANU was further upgraded a year ago with the installation of a 32-sample SNICS ion source which provides beams with higher intensities than previously. It also requires fewer openings of the source due to the possibility of loading 32 samples at a time. A new stripper assembly in the high-voltage terminal of the accelerator has just been installed. Its role is to strip electrons off the negative ions after the first stage of acceleration, and to break up any molecular ions. Depending upon the application, either a thin carbon foil or a gas stripper may be required, and the new assembly incorporates a much improved gas stripper which is differentially pumped by a pair of turbomolecular pumps and two ion pumps. Finally, a Wien velocity filter was added to the AMS line which provides a great improvement in ion selection before detection.

AMS is being applied at ANU to a number of biomedical projects using ^{26}Al, ^{32}Si and the isotopes of plutonium as tracers. These are outlined below.

^{26}Al ($T_{½}$ = 720,000 a)
We have been using ^{26}Al to study the kinetics of aluminium absorption and excretion in humans under a range of conditions. The impetus for this work comes from the now well-established toxicity of aluminium in sufficiently large amounts as observed in some kidney dialysis patients. The partitioning of aluminium among the various components of the blood has also been determined. It is found that:

- Only a small fraction, typically 0.1%, of ingested aluminium is absorbed from the gut.
- Of this fraction, more than 90% is excreted within 2 days.
- In the blood, >80% of the aluminium is bound to the high molecular weight transferrin protein.
- The kinetics of the excretion process are well described by a simple 4-component box model.
- Absorption of aluminium from the gut depends strongly on the chemical form in which it is ingested. Insoluble aluminium hydroxide (used in some antacids) is very poorly absorbed, whereas as much as 1% of the much more soluble aluminium citrate can be absorbed.

In these studies, the biological samples are first digested to convert them to inorganic form (after addition of ^{27}Al carrier) and the aluminium is extracted and converted to Al_2O_3. This is mixed with silver powder for thermal and electrical conductivity and pressed into the sample holders which are loaded into the ion source wheel. For most of these studies, where the anticipated $^{26}Al/Al$ ratio is between 10^{-11} and 10^{-9}, an older ion source has been used in order to avoid contamination of the new high-intensity source. The latter has been reserved for lower-level samples where the higher been intensities confer a significant benefit in precision. The Al^- ions are accelerated to 11 MeV, stripped to Al^{7+} in the high-voltage terminal of the 14UD, and further accelerated to 88 MeV. At these energies it is straightforward to separate ^{26}Al ions from any other ions that reach the detector. The Wien filter, by rejecting many ions that would otherwise arrive at the detector, further improves sensitivity.

^{32}Si ($T_{½}$ = 150 a).

It has long been suspected that silicate may play an important role in suppressing aluminium absorption and enhancing aluminium excretion. A suitable tracer for testing this hypothesis would be ^{32}Si, which could also be used in double tracer experiments with ^{26}Al. The principal difficulty confronting AMS measurements of ^{32}Si is a very high counting rate of the ^{32}S isobar. In order to overcome this problem, we have supplemented the normal AMS method with a gas-filled magnet in order to suppress this isobaric interference. For these measurements, it was possible to use an existing split-pole spectrometer and its associated focal plane detector. The principle of this technique is based on the fact that the trajectories of heavy ions with a distribution of charge states merge into one when they are subject to a magnetic field in a gas filled region. As this new trajectory is defined by the mean charge state of the distribution, which depends on the atomic number of the ions, isobars will travel along different trajectories, allowing their separation at the focal plane detector. The experiments were performed by filling the magnet with Nitrogen at a pressure of 6 torr, and using a removable flap to prevent ^{32}S ions from entering the focal plane detector. The rejection factor of this assembly is 10^6. Residual ^{32}S ions which do reach the detector are readily discriminated from ^{32}Si ions, providing an additional rejection factor of 10^6. With this set-up it was possible to measure $^{32}Si/Si$ ratios as low as 10^{-15}, and therefore to use ^{32}Si as a tracer in human studies. It is found that absorption and excretion of silicate are very different from aluminium. About 36% of the ingested silicate was absorbed from the gut, and its removal by the kidneys was very rapid - >90% had been cleared after 6 hours.

Plutonium: (Four isotopes, $^{239,240,242,244}Pu$ with half lives between 6000 and 8×10^7 years)

Concerns about the effects of plutonium on people living near reprocessing or former nuclear-weapons production plants have led to demand for a means of measuring Pu levels in at-risk groups. Levels in urine are too low for alpha-particle counting, but may be within the reach of AMS. The principal challenges facing AMS measurements on plutonium are its large mass, necessitating gas stripping and powerful bending magnets, the lack of stable isotopes for normalisation and system set-up, and the difficulty of detecting these heavy, slow-moving ions. The normalisation problem is solved by spiking at low levels with another isotope of plutonium, while set-up is done with a ^{232}Th beam. Because the elemental Pu^- ion is only weakly produced, it is necessary to inject the more prolific PuO^- ion into the accelerator. The accelerator is operated at a very modest 4.5 MV, and the 6^+ charge state is selected after acceleration. Overall transmission from ion source to detector is 1%. A special detector was developed for these measurements. It consists of a gas-filled ionisation chamber, using propane at 80 Torr, with the charge-collecting electric field oriented parallel to the track of the incoming ion. With these new techniques we achieve sensitivities of fewer than 10^6 atoms. A first measurement, using ^{242}Pu, of plutonium absorption by a human subject has been completed. Urine was collected during 7 hours after the ingestion, by a healthy male subject, of 10 Bq (1.7×10^{14} atoms) of ^{242}Pu. The $^{242}Pu/^{244}Pu$ ratios were measured and a preliminary estimate of $\sim5\times10^{-5}$ for the gut uptake factor for Pu can be made. A program of measuring plutonium levels in a group near the reprocessing plant at Sellafield (U.K.) is underway.

Paper 78/190

Applications of Cosmogenic Radio-Isotopes, ^{10}Be, ^{26}Al and ^{26}Cl in the Earth Sciences Using AMS at ANSTO

DAVID FINK and GREG ELLIOT
ANSTO, PMB 1, Menai NSW 2234, Australia

Production of long-lived cosmogenic radionuclides (CRN) is dominated by cosmic ray interaction in the upper atmosphere. Through atmospheric transport and precipitation, they become distributed over the Earth's surface, and participate in various geochemical and geophysical global processes. An alternate production mode of CRNs is in the Earth's lithosphere, particularly in exposed rocks and surfaces. The production rate of these in-situ produced CRNs depends primarily on the reaction mode and type of target material. Although production is small - a few tens of atoms per gram per year - the built-up in concentration even after a few thousand years of exposure can be measured using the technique of Accelerator Mass Spectrometry. Concentrations of *in situ* nuclides in the near-surface zone allows a "surface exposure history" to be estimated resulting in a measure of exposure ages and erosion rates. With a range in half-lives from 0.3-1.5 Ma, in-situ produced CRNs are ideally suited as geochronometers and tracers in Quaternary geomorphology related to paleoclimate change.

Using concentrations of ^{10}Be and ^{26}Al produced in-situ in quartz grains, and ^{36}Cl in select K- and Ca-rich minerals, one can successfully model the exposure history of the rock surface. Generally, meaningful measurements can be made with as little as 10-20 grams of quartz or granite exposed at sea-level for as short a period as 5-10 ky. This model has been applied in a variety of geomorphic contexts: glacially polished bedrock, tills and moraine boulders, meteorite impact craters, alluvial fans, beach terraces, desert sands and palaeoseismic events. Parameters characterizing the exposure history are effective exposure and burial ages, time-averaged erosion rates, depositional and uplift rates. Determination of absolute production times, prerequisites to calibrate the model, have been addressed by using surfaces of known age from different and well-selected sites.

In parallel with a successful ^{14}C AMS program, routine measurements of ^{10}Be, ^{26}Al, and ^{36}Cl have been demonstrated at ANTARES. With this capability, ANSTO is coordinating and leading a comprehensive multi-faceted program in the application of in-situ CRNs to study southern hemisphere Quaternary climate change. The sub-projects within the program are based on strong university collaboration and range in environment from arid central Australia, alpine Tasmania and frozen Antarctica. An extensive geochemistry laboratory, funded by ANSTO, for sample processing has been completed and is now operational. Some of these projects are listed:

(a) Glacial history of the Prince Charles Mnts, Antarctica, using ^{10}Be and ^{26}Al in bedrock and erratics to estimate exposure ages (with Barrie McKelvey, Univ of New England);

(b) Pleistocene ice-cap and glacial history in central and west Tasmania using ^{36}Cl in moraine (dolerite) boulders, ^{10}Be, ^{26}Al in quartz-rich glacial pavements and ^{14}C in sub-algal lake deposits (David Hannon, Univ of Tasmania, an Eric Colhoun, Univ of Newcastle);

(c) Glacial history of fiordland, South island, and evidence for the Younger Dryas in New Zealand (Paul Williams and Paul Augustinus, Univ of Auckland);

(d) Using ^{10}Be in cores from coastal sandstone escarpments of the Victorian Plateau, southwest Western Australia, to differentiate between processes of local laterization and accumulation of transported material (David Newsome, Murdoch Univ, WA);

(e) Dating the advance of weathering fronts in pediment surfaces at the Flinders Ranges, stepped granite bornhardts on the Eyre Peninsula, and paleosiesmic events such as avalanches, slab fractures in central Australia (Rowl Twidale, Univ of Adelaide, SA);

(f) Comparing long term erosion estimates based on apatite fission tracks with cosmogenic in-situ erosion rates over the past million years on eroding surfaces in central Australia (Rod Brown, Latrobe Univ).

This paper will briefly outline principles and techniques of ^{10}Be, ^{26}Al and ^{36}Cl in-situ methods and describe some of the above projects related to the unique geomorphology of the Australian and Antarctic continents.

ITEP ElectroNuclear Neutron and Proton Facility.

Report for Second International Conference on Isotopes,
Sydney, Australia, October 12-16, 1997

O.V.Shvedov, M.I.Igumnov, M.M.Katz,A.A.Kolomietz,A.M.Kozodaev,
N.V.Lazarev,V.V.Vasilyev,E.B.Volkov,G.V.Shymchuk

State Science Center of Russian Federation
Institute of Theoretical and Experimental Physics.
117261 Moscow, Russia, B.Cheremushkinskaya, 25
phone/fax:(095)1270543

Abstract

Construction and current stage of the ITEP Subcritical Facility on the base of proton accelerator, target and subcritical blanket. The facility uses linac working in pulse mode with proton beam 200 mA in pulse and enrgy of protons 36 MeV, Be neutron producing target and heavy water subcritical blanket. Neutron and proton beam parameters of the facility are listed. Special attention is devoted to isotope production and isotope application for electron-positron tomography.

1. Introduction.

ElectroNuclear Systems (ENS)[1] including an accelerator, a neutron producing target and a subcritical blanket is more steadily considered for the last years as possible base for the future transmutational and energetic facilities [1]. Some problems of ENS substantiation may be solved with the help of a low energy prototype united a middle energy proton accelerator, a light metal target and channel type subcritical blanket consisting enriched uranium in a heavy water moderator. There are unique conditions for solving this problem in SSC ITEP where the linear proton accelerator (LPA) "ISTRA-36" is constructed and the body, equipment, heavy water and fuel reserves of the decomissioned ITEP HWR are in hand. The Subcritical ElectroNuclear Neutron Source (SENNSe) is constructed on this basis. It will be one of a few electronuclear systems driven by proton beam in the world. By the way dismountling a reactor down to a "meadow" (for instance, ITEP HWR in Moscow) is impracticable now because of a great cost and a great ecological danger of this work. ITEP's alternative proposal is to transform the ITEP HWR into a subcritical neutron source neutron source with the highest level of safety. This work may be good example of a decomissioned reactor utilization.

[1]Note of the reporter: Term ElectroNuclear System is used in Russian technical literature. Other term "Accelerator Driven System" is used in world literature usually.

2. Subcritical neutron source structure chart.

SENNSe will be one of a few first electronuclear systems, which allows to solve many fundamental and applied problems. Also it will serve as prototype of full-scale electronuclear facility of high energy (≈1 GeV).

The main SENNSE design parameters are:

Table 1.

- proton energy	36 MeV
- average proton beam current	0.5 mA
- intensity of fast neutrons from target	$1.4 \cdot 10^{14}$ n/s
- thermal neutrons flux in reflector	$(1.5\text{-}3.0)\times 10^{12}$ n/cm^{2}s
- blanket multiplication	0.95-0.97

SENNSe structure chart is shown in the fig.1.

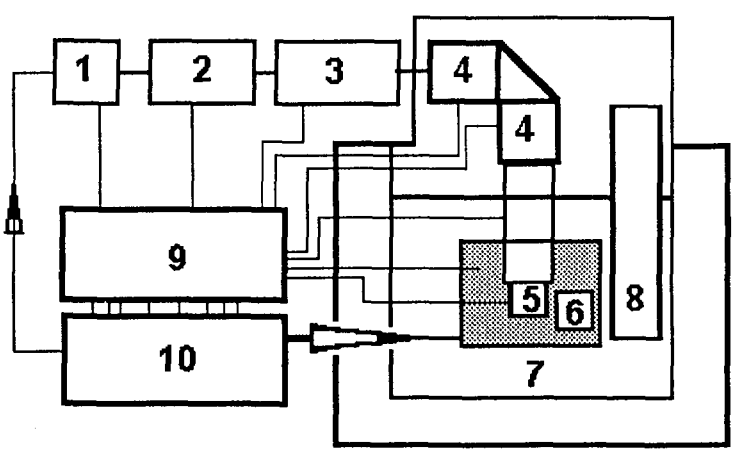

Fig.1. SENNSe block chart.

The ion source 1, accelerating structures 2,3 and the transport channel 4 provide ion generation, acceleration and transportation from the horizontally arranged

accelerator to the vertical part of the ion guide tube. The bottom of this tube is the target 5, disposed in the centre of the neutron multiplicating blanket 6. A peculiarity of a heavy water reflector 7 is extensive thermal neutron maximal flux region where large experimental devices 8 may be disposed. A Control and Safety System (CSS) 9,10 is an important SENNSe part for providing the assigned level of subcriticality in an operational state.

3. Accelerator.

Proton Linac ISTRA-36 was constructed in ITEP as a pulse prototype of high-current accelerator [2] for solving of nuclear power problems will serve as well as subcritical blanket driver.The Linac will have proton output energy of 36 MeV, average beam current 0.5 mA at average its power 18 kW in next pulse mode:

- pulse beam current 150 mA - pulse beam power 5.4 MW
- pulse length 150 μs - pulse repetition rate 25 Hz

It is possible in future to increase average beam current up to 5-10 mA.
The Linac ISTRA-36 will be disposed on two levels near the HWR body. On the ground floor the injector with the ion source, sections of RFQ and DTL-1 are placed. Then 10 MeV proton beam is directed by 90° bending magnets and beam transport line to the first floor changing beam direction backwards. After acceleration in DTL-2 cavity 36 MeV proton beam is fed by HEBT to the Be target. Bending magnets (M), quadrupole (Q) and octupole (O) lenses ensure optimal beam transportation. About 98-99 % of output 36 MeV beam hit the target built into subcritical assembly.

4. Target and Blanket.

Berillium was chosen as material for the target due to a sufficient heat conductivity, high melt temperature and as suitable for machining. The neutron yield in Be(p,n) and accompaning three particle reactions will be equal to $1{,}5 \cdot 10^{14}$ n/s as preliminary estimation has shown. There is a problem to coat berillium to prevent direct contact with the heat carrier but it is solvable with the help of vacuum deposition technique. The experience of Berillium target manufacturing demonstrated that the thickness of the hollow cone (24^0) must be not less than 6 mm to provide mechanical strength when processing and leak-proofness in operation. 36 Mev protons are absorbed in the first 2 mm. The rest of thickness is used as a fast neutron multiplier due to the reaction Be(n,2n). The fast neutron flux from the target increases by 20-25% due to the multiplication.
The multiplying blanket has to guarantee the following:

- nuclear safety (due to properly chosen structure, technology and methods of control);
- maximum of thermal neutron flux in experimental channel;
- maximal cross-sections of some experimental channels for inserting experimental devices like cryogenic moderators and converters;
- great scope of possibilities for irradiating experiments with uniform distribution of

neutron flux density over a sample irradiated. The blanket main parameters are listed in Table 2. These requirements are satisfied to a great extension in the blanket containing the following set of components: - a combined reflector consisting of heavy water and grafite;
- a compact active core with enriched uranium; - heavy water heat carrier and moderator. The following blanket structure was selected taking into attention the ITEP great experience in exploitation of the experimental heavy water reactors:
- the heat releasing assemblies (HRA) are distributed around the target forming the triangle lattice with step of 110 mm; HRA is a fuel channel combining the standart fuel elements of

Table 2. Main Blanket parameters.

nn	Feature, parameter	unit	value
1.	K_{eff} interval in operation		0.95-0.97
2.	Fuel assembly number		16-17
3.	U-235 load	kg	1,29-1,37
4.	U-235 fuel enrichment	%	90
5.	Fuel lattice step	mm	110
6.	Fuel assembly height	mm	1110
7.	Moderator , Coolant (heat carrier)		D_2O
8.	Reflector		D_2O, graphite
9.	Fast neutron flux from the target	n/s	$3{,}0 \cdot 10^{14}$/mA
10.	Averaged thermal neutron flux in experimental channels	$n/(cm^2 s)$	$1{,}5 \cdot 10^{12}$
11.	CSS unit weights:- compensating element (1) - automatic regulation element (1) - shut-down rod (2)	%(ΔK/K)	0,40 0,40 4,60
12.	Fission heat power (K_{eff}=0.95)	kW	76
13.	Blanket unit weights: - fuel channel - vertical experimental channel - ∅ 250 mm. - ∅ 100 mm . - ∅ 42 mm.	%(ΔK/K)	2,0 1,23 0,32 0,09
14.	Reactivity effects: - quick temperature reactivity coefficient - coolant density temperature coefficient of reactivity - moderator density temperature coefficient of reactivity - heat carrier loss - static poisoning -fuei burning down in 6 years at nominal power	%(ΔK/K) %/ °C %	 $1{,}7510^{-4}$ $7{,}86 \cdot 10^{-3}$ $-3{,}70 \cdot 10^{-2}$ -2,0 -1,6 -1,8

grommet (bushing) type with ^{235}U enriched fuel (90%); the active HRA length is 1110 mm; the total amount of HRA simultaniously loaded in the blanket is 16-17;
- it is supposed to use two rods containing B_4C as actuators of the CSS protection system
and two cylindrical rods with aluminium as actuators for handle and automatic regulation with the active part of 38 mm in diameter; the actuators are disposed in the fuel lattice points;
- the vertical experimental channels of different sizes are disposed in the blanket reflector; they are to be loaded by experimental devices; three types of these channels of 250-400, 100 and 42 mm in diameter are considered to be used; the channels are placed in the lattice points; three channels of great cross-sections are located in the region of maximal thermal neutron density;
- the construction of the bottom spacing lattice provides heat carrier pumping through the HRA and the target unit; it is possible to install the HRA instead of small vertical channels with necessary heat removal if a new active core configuration is needed for actual problem treatment.

5. Opportunity of short-lived radionuclides production and other applications.

The rise of radionuclide's productions for medical application is observed in connection with wide development of radioisotope's diagnostic procedures. Especially the radionuclides for medicine of as so named "cyclotron's" are used very often now. Specialists of SSC ITEP were considered the opportunity of "cyclotron's" radionuclides production by the use of linear proton accelerators for different energy of protons. The basis of this consideration was the main field for the application of short- and middle-lived "cyclotron's" radionuclides at diagnostic radioisotope's procedures. The main field of medical application for cyclotron's" radionuclides are presented in Table 3.

Table 3. Main field of medical application for "cyclotron's" radionuclides

Radionuclide	$T_{1/2}$	Main field of medical application
^{67}Ga	3,261 days	Definition of malign bumps
^{81m}Kr (from ^{81}Rb)	13 s (4,58 hours)	Investigations of lung's ventilation and cardiac activity
^{111}In	2,807 days	diagnostics of new bumps and check of bump's increasing, detection of kidney diseases and so on
^{123}I	13,2 hours	Detection of thyroid glands and heart function and other
^{195}Au (from ^{195m}Hg)	30,055, s (1,73 days)	Estimation of heart function and so on
^{201}Tl	3,046 days	Detection of activity heart, early diagnostics for heart-diseases and so on

^{68}Ga (from ^{68}Ge)	1,135 hour (270,8 days)	for positron-emission tomography

According to this investigation there are 3 type of proton accelerators which can produce the medical and industrial radionuclides with different energies: 1. 10-17 MeV; 2. 30-40 MeV; 3. more 40 Mev. The proton accelerator with proton energy 10-17 MeV and average current beam 30-80 μkA can produce the following main medical radionuclides for positron-emission tomography: ^{11}C, ^{13}N, ^{15}O, ^{18}F, ^{19}Ne, ^{45}Ti, ^{62}Cu, ^{76}Br, ^{110}In. The proton accelerator with proton energy 30-40 MeV and average current beam approximately 1 mA can produce all medical and industrial radionuclides, including abomentioned. So energy of protons 36 MeV is possible to make almost whole spectrum radionuclides for medical-biological application and significant part radionuclides for industrial application. The proton beam with energy 10 MeV is convenient for manufacture of the main short-lived radionuclides, used for positron tomography. List of of radionuclides produced by SENNSe is given in Table 4.

Table 4. List of radionuclides which can be to produce by SENNSe.

Radionuclide	Half-life	Energy of protons, MeV	Nuclear reaction
^{55}Co	18,0 hours	15-40	^{56}Fe(p,2n)
^{67}Ga	78,3 " "	15-35	^{68}Zn(p,2n)
^{68}Ga	68 min	"	^{69}Ga (p,2n)
^{68}Ge	288 days	"	"
^{81}Rb	4,7 hours	16-32	^{82}Kr(p,2n)
^{82}Sr	25,5 days	32-70	^{85}Rb((p,4n)
^{82}Rb	6,3 hours	"	"
^{87}Y	3,3 days	15-33	^{88}Sr(p,2n)
^{87}Sr	2,8 hours	"	"
^{123}I	13,3 hours	10-30	^{124}Xe(p,2n)
^{201}Tl	73 hours	14-35	^{202}Hg(p,2n)
^{203}Pb	52,1 hours	20-35	^{205}Tl(p,3n)

The started targets for the production of ^{67}Ga, ^{68}Ge, ^{111}In, ^{195m}Hg , ^{201}Tl are as solid metallic substrates, for the production of ^{81}Rb and ^{123}I - as gas in special ampoules. These targets are cooled by water or gas coolant during process of irradiation.
These investigations and other reason were the basis to make the choice of proton accelerator with abovementioned characteristics. The use of this proton accelerator allows the production of radionuclide with different activity (see Table 5).

Table 5 . Total radioactivity per year for some radionuclides.

Radionuclide	Activity,	Amount of	Consumption of	Total activity	Total

	Cu	targets per year	work of accelerator hours/year	in targets Cu/year	productivity for radionuclide Cu/year
^{67}Ga	5	40	400	200	70
^{68}Ge	0,5	2	500	1	0,7
^{81}Rb	1,5	200	600	300	60
^{111}In	4	40	800	160	50
^{123}I	10	100	1000	1000	200
^{195m}Hg	2	10	<100	20	6
^{201}Tl	2,5	100	1600	250	100

Besides these radionuclides there is the possibility to produce near 500 Cu/year of different radionuclides, indicated in Table 4. Total activity per year of all radionuclide from Table 5 by use Accelerator Driven System of ITEP is approximately 2500 Cu/year.

The presence in ITEP of department of medical physics with a active service of patients will allow to organize fast use received shortly and ultra-short-lived radionuclides in medical radiating diagnostics.

The protons with energies 3 Mev and 10 Mev can be used for realization of element activation analysis, where with their help it is possible to define a impurity of one metals in other, to find out small gas impurity C, N, O, Cl in substances (sensitivity on a nitrogen, for example, 10^{-5} %), to define quantity boron in semi-conductor silicon (sensitivity 10^{-6} %), to measure quantity are grey in petroleum products (threshold of sensitivity of 0,01 %). The proton fluxs with energies 3, 10 and 36 Mev can be used in study of radiating resistance of substances, materials, components and finished products, in particular, for the decision of some problems, which arise at development of space, as far as in the interplanetary space from positively charged particles prevail protons with energy, not exceeding by 10-20 Mev, and in the near earth space -protons with energy not above 70 MeV.

6. Current stage.

To-day the technical design of the heavy water blanket is ready. There are all principal units of linac equipment on site to-day, the readiness of technology systems is about 60-70 %. Tentative variance of RFQ section have started up. The 3 MeV pulse proton beam was obtained with current up to 245 mA. Particle losses are near to zero in the current range of 0-100 mA, output beam consists of 95 % accelerated particles. The physical launching of the first phase of the Linac including sections RFQ and DTL-1 have been carried out, the nominal pulse current was obtained at the energy of 10 MeV, output current practically do not contain unaccelerated particles. The next stages are: the reactor building upgrade, the manufacturing of the subcritical pile, a completion of the Linac ISTRA-36 construction with simultaneous reconstruction of modulators and RF power supply system to step average output current up to 500 mA.The ITEP technical base together with the presence of the high qualified scientific potential - scientists in

nuclear reactors, neutron physics, charged particles accelerators study makes the construction and utilization of the SENNSE quite realistic.

The nearest plans are connected with the experimental substantiation of SENNSe design. The method of full-scale physical modelling will be apply to perform the experiments on available neutron source parameters substantiation and to substantiate the neutron source safety and for testing CSS elements. All of these will be done at the "MAKET" stand (zero power reactor) which is in operation now. The stand is designed for heavy water reactors (industrial including) and multiplying assemblies neutron physical parameters research.

The full-scale blanket model for testing and investigation of CSS model will be worked out according with the computer simulation, fabricated and installed in the stand. While CSS conceptual design developing a possibility to analyse the blanket from the parameters of neutron pulses will be investigated. The neutron pulses arise into the blanket as a result of spreading and moderation of fast neutrons emitted by the target bombarded by the proton pulses. For neutron pulses imitation the D-T neutron tube early installed at "MAKET" will be used. As the base for working out the "MIRAGE" system is adopted which was developed for research reactors by SE "RED STAR" and MEPhI. The real target neutron yield and neutron spectrum measurements will be fulfilled at a cyclotron.

The work was partly supported by Russian Foundation of Fundamental Investigations (RFFI).

References.

1. F.Carminatty et. al. An energy amplifier for cleaner and unexaustible nuclear energy production driven by a particle beam accelerator. *CERN/AT/94-47(ET)*, pp.1-47.

2. I.M. Kapchinsky. High current linear ion accelerators. *Successes in Physical Sciences*. 1980, v.**132**, rel.4, p.639.

3. V.V. Vassiliev, A.A.Dejurny, M.M.Igumnov et.al. *ElectroNuclear Generator of Ultracold Neutrons. ITEP Preprint* **9-95**, 1995, pp.1-28.

4. V.V. Vassiliev. *Nuclear Physics*, v.**53**, rel. 6, pp.1586-1590, 1991.

5. J.M.Doyle, S.K.Lamoreaux. *//Europhys.Lett.*1994. V.**26** (4),ð.253-258

Paper 80/135

Exploration of New Tritium Labelling Methods

HENDRIK ANDRES, DEVENDRA K JAISWAL, HIROMI MORIMOTO
MANOUCHEHR SALJOUGHIAN, CHIT THAN,
PHILIP G WILLIAMS and ELIZABETH M ZIPPI
National Tritium Labelling Facility and Structural Biology Division
E O Lawrence Berkeley National Laboratory
One Cyclotron Road, Berkeley, CA 94720, USA

A great deal of elegant chemistry is available for hydride transfer reactions, and could be adapted for tritium labelling. Nevertheless, most high level tritiation reactions still involve either hydrogenation (alkene or alkyne precursor) or catalytic dehalogenation. In the last decade we have endeavoured to propose and popularize alternative labelling techniques and reagents, including: i) the synthesis of new precursors for the production of methyl iodide;[1a] ii) the synthesis of methylene diiodide;[1b] iii) the production and use of T_2O, and solvents made from it, eg. CH_3COOT, CF_3COOT;[1c] iv) high specific activity hydride reagents, eg. $LiAlT_4$,[2a,b] $LiEt_3BT$;[2a,b] $(Bu^n)_3SnT$,[2c] $ZrCp_2ClT$,[3a] LiT,[3b] $Li(OCH_3)_3BT$,[3b] Ph_2SiT_2,[3c] BT_3-THF,[4a] Li/Na/KBT_4;[4b,c] v) reduction with diimide;[5a] vi) use of T_2O in special reactions such as the Shapiro reaction [5b] and Brook rearrangement;[5c] and vii) developments of a new acetylation reagent.[6] We have also initiated and continued a number of innovative applications of tritium NMR spectroscopy.

Many of these projects have grown out of User or Collaborator requirements at the NTLF. We regard this stimulus to develop and refine both tritiation and NMR techniques as healthy and challenging.

References

1. (a) M Saljoughian *et al, J Chem Soc, Perkin Trans 1*, 1990, 1803-1808; (b) M Saljoughian *et al, J Chem Soc Chem Commun*, 1990, 1652-1653; (c) H morimoto and P G Williams, *Fusion Technology*, 1992, **21**, 256-261.
2. (a) H Andres *et al, J Chem Soc, Chem Commun*, 1990, 627; (b) H Andres *et al*, US Patent: 5,186,868, 1993; (c) D K Jaiswal *et al, J Chem Soc, Chem Commun*, 1993, 907.
3. (a) E M Zippi *et al, Synth Commun* 1994, **24**, 1037-1044; (b) E M Zippi *et al, Synth Commun*, 1995, **25**, 2685-2693; (c) E M Zippi *et al, J Labelled Radiopharm Compd*, 1996, **38**, 693-711; (c) C Than *et al, J Org Chem*, 1996, **61**, 8771-8774.

Paper 81/175

Sodium Triacetoxyborotritide: Its Preparation and Use

HIROMI MORIMOTO, PHILIP G WILLIAMS, CHIT THAN, KAREEM CHEHADE* and PETER SPIELMAN*
National Tritium Labelling Facility and Structural Biology Division
EO Lawrence Berkeley National Laboratory
One Cyclotron Road, Berkeley, CA 94720, USA
*Department of Biochemistry, University of Kentucky,
Chandler Medical Center, Lexington, KY, USA

Tritide reducing agents provide attractive approaches for the preparation of tritiated molecules of high specific activity. During the last decade we have demonstrated the synthesis and use of fully tritiated highly reactive tritide reagents such as lithium triethylborotritide. Lithium aluminium tritide and borane. Recently, the biological molecules of interest have become more complex and the appropriate labelling reagents have become more selective and sophisticated.

Sodium triacetoxyborohydride is a very mild and highly selective reducing agent, capable of reducing aldehydes selectively in the presence of ketones. It also reduces indole double bonds, acid chlorides and lactones. It is the reagent of choice for the reductive amination of aldehydes, and saturated aliphatic ketones with primary and secondary amines.

Over the past year, we have developed simple, convenient and efficient methods for the labelling of metal borohydrides by exchange with tritium gas. Direct treatment of $NaBT_4$ with glacial acetic under mild conditions produces sodium triacetoxyborotritide. This reagent was characterized by proton, tritium, and boron NMR spectroscopy. Its utility was demonstrated by its ability to reduce an aldehyde in the presence of a ketone, and by a reductive amination of farnesal acetate and aniline.

Paper 82/196

Tritium Nuclear Magnetic Resonance Spectrosopy - An Update

PHILLIP G WILLIAMS
National Tritium Labelling Facility and Structural Biology Division
EO Lawrence Berkeley National Laboratory
One Cyclotron Road, Berkeley, CA 94720, USA

Tritium NMR spectroscopy has become a mature technology, with a large number of published papers, several books or book chapters, and a healthy quantity of reviews describing its use. Since the first publication in the 1960s, high resolution ^3H NMR has progressed to become firmly established in several important applications. It is an essential tool for the characterization of ^3H labelled materials, and most ^3H synthesis papers should now include such analyses.

Aside from routine high resolution ^3H NMR analyses, there are many other non-routine applications, and they may be used to provide exquisitely detailed information on a hose of chemical and biological problems. Recent work and publications have addressed such fundamental issues as the size and mechanism of couplings, chemical structure and stereochemistry in liquids, liquid crystals and solids, the mechanism of rapid proton exchange processes, and the strength and symmetry of hydrogen bonds. Intricate details of biochemical processes may also be gleaned from ^3H analysis of enzymatic reaction products, ^3H NMR study of ligand binding, and study of metabolic processes in progress.

The applications of ^3H NMR spectroscopy will continue to expand as the sensitivity of NMR instrumentation improves, selective labelling techniques advance, and increasingly detailed knowledge of hydrogen dynamics or disposition is required.

Tritated mixed waste: how can we deal with it?

CHIT THAN, LI-YANG CHANG,* HIROMI MORIMOTO and PHILIP G WILLIAMS
National Tritium Labelling Facility and Structural Biology Division
*Environment, Health & Safety Division
EO Lawrence Berkeley National Laboratory
One Cyclotron Road, Berkeley, CA 94720, USA

There is currently no satisfactory disposal or recycling route for tritiated mixed waste of high tritium content. With mounting concerns in the US regarding land burial and potential environmental releases (atmospheric, vegetation, surface water, and ground water), it is essential to develop processes for ensuring that contaminated materials may be disposed in an environmentally benign manner. this problem exists on a large scale in the US Department of Energy (DOE) weapons complex, and to a lesser extent in the pharmaceutical industry where isotopes such as tritium and carbon-14 are regularly used in research and drug development projects, and process solvents are contaminated. On a smaller scale, academic institutions conducting life science and biomedical research invariably produce mixed waste. In general, the mixed waste streams of concern to the National Tritium Labelling Facility (NTLF) have organic or biological hazardous components, and are radioactively contaminated with tritium.

It is so widely recognized that there is insufficient capacity for mixed waste treatment and disposal that the US Environmental Protection Agency (EPA) has a policy of low priority enforcement against the storage limitations in the Resource Conservation and Recovery Act regulations. As a direct result, mixed waste is accumulating in all research institutions across the US, with little hope for resolution. As a step towards providing leadership, the Federal Facilities Compliance Act requires federal facilities to develop Site Treatment Plans (STP), which commit to schedules for identifying unique waste streams and solutions. Although the DOE has built various advanced incineration devices to address mixed waste (Mixed Waste Disposal Facility, INEEL), the fact that the radioactive isotope in tritiated mixed waste would be released with the incineration products (ie. as tritiated water) rather than retained in the ash makes these approaches environmentally unsound for tritium.

Since a disposal route exists for radioactive aqueous waste, free of hazardous materials, one solution to the problem could be efficient conversion of the hazardous organic components to water and CO_2. A number of traditional methods exist for converting organic solvents to water and CO_2, and the processes should be adaptable to use with chemicals containing tritium or carbon-14. We have embarked on a study of the treatability of tritiated mixed waste by catalytic chemical oxidation (CCO), which will yield the products HTO and CO_2. CCO technology has been successfully applied to destroy hazardous organic chemicals for many remediation projects.

With a mature waste treatment technology, the major roadblock to the widespread use of such processes is regulatory; specifically, materials derived from a listed waste are listed in perpetuity. These types of legal problems need to be squarely addressed by groups such as the DOE Tritium Focus Group, the International isotope Society, and other professional societies whose members feel the negative impact of such unproductive and restrictive legislation. At the very least, catalytic oxidation technology can reduce or eliminate the hazardous nature of mixed wastes (ie. their "characteristic"), thereby allowing more flexible management of these materials. With some thought, planning and co-operation between institutions, some tritiated mixed waste streams might cease to exist, and the tritium they contained could be made available for recycling.

Radiopharmaceuticals to Monitor the Expression of Transferred Genes in Gene Transfer Therapy

LEONARD I. WIEBE
Noujaim Institute for Pharmaceutical Oncology Research, 3118 Dentistry-Pharmacy Centre, University of Alberta, Edmonton, Canada T6G 2N8.

SUMMARY. Gene transfer therapy is a new therapeutic modality that holds promise for effective treatment of disease by modification of the diseased cell's genetic structure. The genetic modification may involve replacement of a deficient or poorly-expressed normal gene, or the introduction of a foreign gene that will enhance the cell's sensitivity or resistance to specific therapeutic agents. Imaging provides the only realistic, non-invasive *in vivo* means by which to evaluate the success of the gene transfer, transcription and translation, and by which to detect unwanted transfer to non-target tissues. This paper briefly reviews the classical approaches to radiopharmaceutical design, and develops the concept of 'molecular' radiopharmaceuticals, with emphasis on gene therapy imaging. The Herpes simplex type-1 thymidine kinase (HSV-1 *tk*$^+$) gene, used initially as a suicide gene for gene therapy of glioma, is used as a model to focus the theme of scintigraphic imaging to monitor gene expression *in vivo*.

1. INTRODUCTION

Radiopharmaceuticals for *in vivo* scintigraphic imaging were initially used to obtain anatomical images based on physiological function that depended on blood flow, perfusion or clearance in a target region or organ. Early radiopharmaceuticals produced images attributable to vascular trapping (e.g. micro- and macro-aggregates) and reticulo-endothelial uptake (e.g. colloids), while others reflected physiological functions such as renal (e.g. iodo-aromatic acids and hydrophilic ^{99m}Tc-chelates) and hepatic (e.g. lipophilic ^{99m}Tc-chelates) clearance. (Table 1). From the beginning, there was substantial scientific interest in using radiotracers for imaging metabolic processes, including nucleoside antimetabolites directed against DNA synthesis. An example is the use of 5-iododeoxyuridine (IUDR), a thymidine analogue, to delineate tissues that have high mitotic indices (1). Modern imaging technologies, including x-ray CT and magnetic resonance imaging (MRI), have vastly superior spatial resolution compared to radiopharmaceutical scintigraphy (planar and tomographic imaging using single photon and positron emitters). It is the highly sensitive, quantitative functional measurements that provide the unique information that makes nuclear medicine imaging an invaluable diagnostic technique.

Table 1.Tracer accumulation mechanisms exploited in functional *in vivo* imaging (types of radiopharmaceutical are shown in parentheses).

- capillary blockage (aggregates)
- secretion / excretion (small molecules)
- phagocytosis (colloids, particulate & cellular immune reagents)
- diffusion / partition /pH (amines)
- receptor binding (steroids)
- protein binding (aptamers; non-specific binding agents)
- ionic substitution (anionic & cationic molecules & elements)
- transport (metabolic substrates)
- metabolic trapping (enzyme substrates)
- immune recognition (antibodies, fragments)
- nucleic acid binding (oligonucleotides)

The list of exploitable molecular targets for imaging has expanded immensely during the past two decades. Approaches to imaging molecular targets in membranes, and in extracellular, cytoplasmic and nucleoplasmic compartments, continue to exploit the sophisticated techniques developed in the basic sciences of molecular biology and genetic engineering.

In the 1970's, the new fields of molecular biology and genetic engineering created unanticipated opportunities for biomedical research. The immunological applications captured major attention in the early 1980's, and even today, a large, important component of experimental and clinical radiopharmaceutical science and nuclear medicine is based on radiolabelled monoclonal antibodies and monoclonal antibody fragments. Immunological research has stimulated strong therapy programs, including radiotherapy.

A number of fundamental barriers challenge the intracellular delivery of targeted, macromolecular radiopharmaceuticals (Table 2). Although many of these factors apply to all drugs, the macromolecules, especially the proteins, may also evoke an immunological response.

Table 2. *In vivo* barriers to the effective application of radiopharmaceuticals

- vascular and intracellular
  - * hydrolytic enzymes
  - * antibodies
  - * proteins (non-specific)
- lymphocytes
- reticuloendothelial cells
- membranes
  - * plasma
  - * nuclear & mitochondrial

Innovative *in vivo* delivery of 'biological' radiopharmaceuticals, whether they are monoclonal antibodies (MABs), MAB fragments, peptides or oligonucleotides remains a major challenge for scientists in this field. The *in vivo* instability of these substances, their frequently exaggerated (too fast or too slow) clearance kinetics and the difficulty in moving through biological membranes are among the challenges. The timely advent of solid phase and combinatorial synthetic chemistry has facilitated the move from these difficult to handle, large biomolecules to smaller, rigid chemical structures that are more 'tuneable'. Undoubtedly, although the molecular targets of today's macromolecular radiopharmaceuticals are unlikely to disappear, there is already a revival of small-molecule radiopharmaceuticals for diagnostic imaging.

Gene therapy represents the ultimate approach to the intracellular delivery of macromolecules. It by-passes the normal barriers to drug delivery, by genetically coding for the intracellular production of the desired substance in the target cell. Although this does not solve the problems of delivering a macromolecular radiopharmaceutical, it does pave the way for creation of unique molecular targets. The following paragraphs provide a brief review of the objectives and mechanics of gene therapy, after which some possible applications of imaging technologies are presented. A short **vocabulary** is included (Appendix A) as a guide for those less familiar with the field.

2. GENE THERAPY

Gene transfer therapy, directed *in situ* at the root-cause of disease within the host genome, has already been applied to a number of pathologies (Table 3). The first clinical trial in humans was started in 1990. The Recombinant DNA Advisory Committee of the US FDA has subsequently approved more than twenty gene therapy protocols that support upwards of 200 clinical trials world-wide. The current consensus is that the process needs substantial improvement, that there are risks and that there have not been any unequivocal cures (2).

Table 3. Applications of gene therapy.

- proliferative disease (e.g. atherosclerosis)
- enzyme deficiencies (e.g. ADA deficiency)
- infection (e.g. HIV)
- oncology (e.g. glioma)

International efforts to map the human genome have greatly contributed to the identification of the genetic basis of many diseases. None-theless, there are major technical impediments to successful implementation of gene transfer, challenges like those inherent to classical intracellularly-targeted drugs (Table 2). Site-specific delivery, and control of gene catabolism, gene expression and gene deletion are major challenges that remain to be resolved.

Objectives of gene therapy have been classified (3) according to the transferred gene's intended role:

- gene replacement in hereditary diseases such as ADA deficiency and cystic fibrosis (e.g. enzyme replacement),
- gene replacement / supplementation for potentiation of host immune defences (e.g. cytokines) against cancer
- gene addition for drug resistance (e.g. multidrug resistance gene) to protect sensitive tissues such as the bone marrow, thereby permitting the use of otherwise toxic doses of a drug,
- gene addition for drug sensitivity (e.g. viral thymidine kinase gene to induce selective cell sensitivity to ganciclovir) in a cell that would normally be non-responsive to this drug, and,
- gene addition to disable abnormal DNA (e.g. HIV-DNA in host DNA is abnormal and can be treated as a genetic disease, this therapy would be directed towards T-cells).

Replacement gene therapy is particularly attractive for treating congenital disorders arising from absence or deficiency in expression of a gene, whereas introduction of new genes is a common objective in gene therapy of cancer. Importantly, current ethical considerations strictly limit human studies to somatic cell therapy.

Gene therapy begins with selection and isolation of the desired gene(s) from an eukaryotic, prokaryotic or viral donor. The naked gene is a charged strand of DNA strand that is readily degraded by circulating nucleases. This gene must be inserted into a delivery vector that will protect it and facilitate its movement through biological membranes and into the nucleus. A number of the obstacles to gene delivery are similar to the obstacles faced by other drugs (Table 2).The delivery options are outlined in Scheme 1; detailed discussion of the transfection vectors and the molecular engineering leading to a suitable plasmid are beyond the scope of this paper.

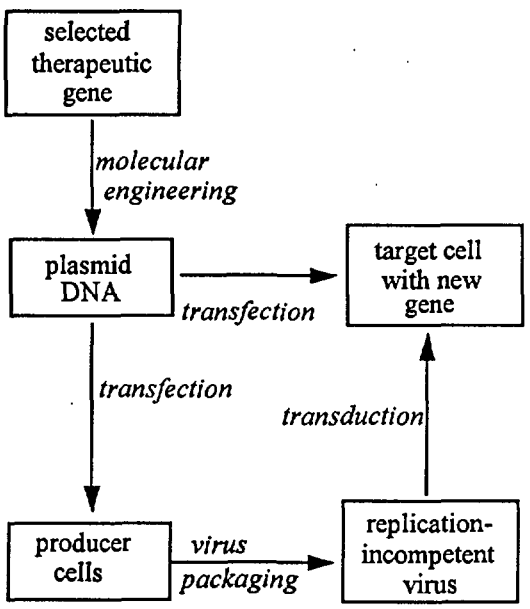

Scheme 1. Approaches to gene delivery to target cells.

There are several classes of vectors for gene delivery. Non-viral vectors have a large DNA-carrying capacity. They are non-immunogenic and non-infectious, but they are inefficient and non-selective in delivering the DNA to the target. Non-viral vectors include cationic liposomes, molecular conjugates, macro-molecular and ionic complexes (e.g. using lipids, charged carbohydrates and even inorganic salts) and the 'gene gun' which literally shoots the DNA into the cell.

The most popular and effective delivery vectors to date are retroviruses and adenoviruses that have been engineered to render them replication incompetent. Retroviruses insert their DNA directly into the DNA of dividing cells that they have invaded, but they have a limited DNA loading capacity (6-7 kb), and they transfect only actively dividing host cells. Adenoviruses carry larger DNA loads (15-25 kb) and are not cell cycle selective, but they do not actively insert their DNA into host DNA, thereby giving

rise to transient gene transfer. Because adenoviruses are cytoplasmic they are less likely to become infectious through the development of replication competency, but their immunogenecity raises an additional challenge to their use as vectors.

Gene transfer can be effected *in vitro* or *in vivo*. For *in vitro* transfer, the therapeutic gene is inserted into target cells (e.g. cord blood stem cells for a blood cell disease) isolated from the patient. After *in vitro* replication these homologous transformed or transfected cells are injected back into the donor patient at the appropriate tissue site. For *in vivo* delivery, the gene-carrying vector is injected (plasmid or engineered virus) or implanted (producer cell) into the target tissue *in situ*.

Interested readers are referred to reviews by Whartenby *et al* (3) and Anderson (4) for orientations to the literature.

3. GENE THERAPY IMAGING

Why use imaging in gene therapy?

When one considers the current methodologies of gene therapy, a number of uncertainties become apparent. Imaging is perhaps the only clinically-acceptable method available to deal with concerns related to delivery, transfer and expression of therapeutic somatic genes:

- *Site-specific delivery*: Systemic, but even stereotactic, administration of the vector creates the possibility of multiple, unwanted sites of transfer. Loss of efficacy and unexpected toxicity are the main consequences of delivery to non-target tissues.
- *Gene transfer*: From the viewpoint of clinical outcomes, gene expression will predicate successful treatment. However, transfer may be successful, but expression may be blocked. Knowledge of such occurrences are of critical importance in research leading to development of the proposed gene therapy protocol.
- *Expression*: If the transferred gene is not expressed, there can be no therapeutic benefit. Overexpression could present complications, depending on the role of the gene product.

These three issues can be addressed very explicitly by tissue biopsy together with immunohistochemical and nucleic acid analyses using the appropriate molecular probes. Unfortunately, biopsy is invasive and often not feasible because of the anatomical location and number of biopsies required. Also, biopsy provides discrete information relevant only to the biopsy sample itself, so that any heterogeneity in distribution may result in over- or under-estimation in the measurement. In sharp contrast, all sites are accessible simultaneously through imaging, and the signal volume-averaging properties insure that subject only to signal intensity, all sites will be sampled.

The utilization of a suicide gene as a reporter gene has an additional value in that there is no easy way to eliminate cells that proliferate as a result of gene transfer if there were to be a need to do so, other than with a suicide gene.

Clearly, the major role of imaging is to monitor the gene therapy protocol, alerting the therapist of impending risk, predicting therapeutic efficacy and indicating when no further improvement is to be expected.

4. CURRENT RESEARCH IN GENE THERAPY IMAGING

Two imaging modalities are currently of interest for gene therapy imaging. Beta-galactosidase has been investigated (5) as an enzyme target for Magnetic Resonance Imaging (MRI), and other targets such as tyrosinase are certain to emerge (6). Nuclear medicine approaches, using planar, SPET and PET imaging are the most common technologies at the present time, and will be discussed in greater detail in this paper. Current molecular targets for gene therapy imaging include therapeutic enzymes, receptors and nucleic acids encoded by the gene; of these, the enzyme-orientated projects are furthest advanced. There are three gene therapy enzyme-imaging projects that are based on the 'gene addition for drug sensitization' concept. *In vitro* and *in vivo* imaging of the herpes simplex virus

type-1 thymidine kinase (HSV-1 tk^+) has been the main enzyme target.

Virus encoded HSV-1 tk^+ was initially identified as an enzyme target for imaging herpesvirus infections, using radiolabelled nucleoside analogues (7-9) Selective phosphorylation in HSV-1-infected tissue, enhanced through intracellular metabolic trapping of phosphorylated metabolites formed the basis for this approach. The underlying principle, insertion of the viral gene (HSV-1 tk^+) into target tissues is now harnessed for suicide gene therapy. In essence, the only difference is that in viral disease the virus inserts its entire genome into that of the host, whereas in gene therapy, only the gene encoding for HSV-1 tk^+ is inserted (10). With the development of new gene expression targets (e.g. cytokines, receptors), it is likely that the suicide drug sensitizing gene will be replaced by other gene product targets. However, their roles as reporter genes remains of great interest. The radiopharmaceuticals used for their detection (enzyme substrates) are small, chemically-defined molecules that are highly diffusible and readily prepared, making them ideal for practical application in the clinic.

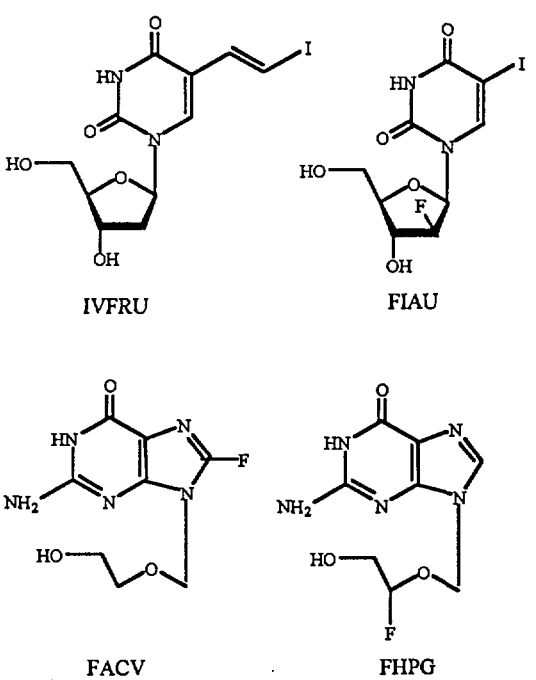

Figure 1. Nucleosides for imaging HSV-1 tk^+ expression in HSV-1 tk^+ gene therapy.

Current HSV-1 tk^+ -based gene therapy imaging studies are based on the radiotracers ^{123}I-IVFRU (11-13), ^{124}I-FIAU (14, 15), ^{18}F-FHPG (16) and ^{18}F-FACV (17) (Figure 1).

A second gene therapy enzyme target proposed was fungal cytosine deaminase using ^{18}F-5-FCT as the reporting radiopharmaceutical (18). This system is complicated by substrate catabolism and is therefore not expected to be viable with currently available radiopharmaceuticals. A bacterial reductase enzyme (19) for use in combination with the hypoxia imaging agent ^{123}I-IAZA (20) is another system that has been proposed recently (21).

These approaches are based on the use of genes that function as therapeutic suicide genes (negative selectable markers) when transferred into cells and combined with therapeutic drugs that are highly-specific substrates of the gene-encoded enzyme. The principles of suicide and reporter gene function are depicted in Scheme 2.

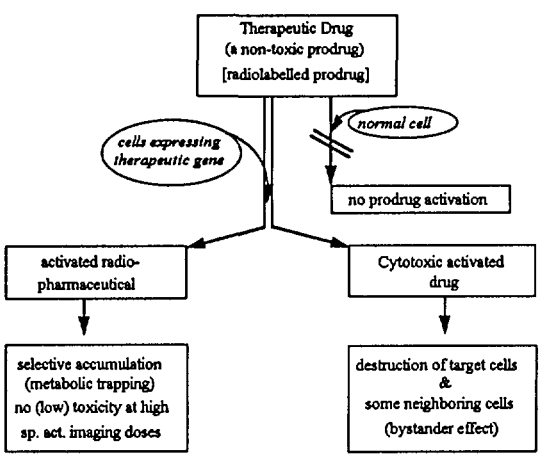

Scheme 2. Selective activation of prodrugs by enzymes encoded by suicide (reporter) genes, forming active drugs (radiopharmaceuticals) that are metabolically trapped.

The suicide gene product (e.g. HSV-1 tk^+) converts a non-toxic prodrug (e.g. IVFRU) into a toxic metabolite (e.g. IVFRU-5'-phosphate). Cells genetically modified to express these genes essentially commit metabolic suicide in the presence of the convertible prodrug. The prodrugs are essentially non-toxic before conversion, but highly toxic in cells that express the suicide gene. If metabolic conversion of the prodrug produces a polar or otherwise poorly

diffusible drug product, metabolic trapping is possible. If the prodrug is radioactive, then there will be an accumulation of radioactivity in the transformed cells, thus enabling imaging. Since unique metabolic pathways are seldom present in diseased cells, metabolic pathways present in bacteria, viruses or fungi have been exploited as targets.

5. CONCLUSIONS

Nuclear medicine has developed a focus on molecular targets, using both biological and chemical radiopharmaceuticals to obtain functional images. Gene therapy is a new treatment modality that can initiate or enhance the expression of unique molecular targets. Imaging these gene therapy targets will provide essential prognostic information critical to the assessment of both efficacy and untoward effects. Imaging based on the HSV-1 tk^+ gene, although still experimental, is the most advanced among three or four gene therapy imaging targets identified to date. For further information, a recent, detailed review (22) of gene therapy imaging is recommended.

6. ACKNOWLEDGEMENTS

Dr. Kevin Morin and Prof. Edward Knaus are gratefully acknowledged for their collaborative efforts to initiate and develop gene therapy imaging at the University of Alberta.

7. REFERENCES

1. Silvester DJ, White ND. Nature 200, 1963, 65-66.
2. Friedman, T. Nature Medicine 2, 1996, 144-147.
3. Whartenby KA, Marrogi AJ, Freeman SM. Drugs 50, 1995, 951-958.
4. Anderson WF. Sci. Amer. September, 1995, 124-128.
5. Moats RA, Fraser SE, Meade TJ. Angewandte Chemie Int. Ed. 36, 1997, 726-731.
6. Jimbow, K. personal communication.
7. Saito Y, Price RW, Rottenberg DA *et al.* Science 217, 1982, 1151-1153.
8. Saito Y, Rubenstein R, Price RW *et al.* Ann. Neurol. 15, 1984, 548-559.
9. Tovell DR, Samuel J, Mercer JR *et al.* Drug Des. Del. 3, 1988, 213-221.
10. Moolten FL. Cancer Res. 46, 1986, 5276-5281.
11. Iwashina T, Tovell DR, Xu L *et al.* Drug Des. Del. 3, 1988, 309-321.
12. Morin KW, Wiebe LI, Knaus EE. Nucl. Med. Commun.. 1997, in press.
13. Morin KW, Atrazheva ED, Knaus EE, Wiebe LI. J. Med. Chem.. 40, 1997, 2184-2190.
14. Tjuvajev JG, Stockhammer G, Desai R, *et al.* Cancer Res. 55, 1995, 6126-6132.
15. Tjuvajev JG, Finn R, Watanabe K *et al.* Cancer Res. 56, 1996, 4087-4095.
16. Alauddin MM, Conti PS, Mazza SM *et al.* Nucl. Med. Biol. 23, 1996, 787-792.
17. Barrio JR, Namavari M, Satyamurthy N *et al.* J. Nucl. Med. 37, 1996, 193P.
18. Haberkorn U, Oberdorfer F, Gerbert J, et al. J Nucl Med. 37, 1996, 87-94.
19. Bridgewater JA, Springer CJ, Knox RJ *et al.* Eur. J. Cancer 31A, 1996, 2362-2370.
20. Urtasun RC, Parliament MB, McEwan AJ *et al.* Br. J. Cancer 74, 1996, S209-S-212.
21. Wiebe LI, Knaus EE, Morin KW, McEwan AJ. U.S. Provisional Patent, 1997.
22. Wiebe LI, Morin KW, Knaus EE. Quart. J. Nucl. Med. 41, 1997, 79-90.

APPENDIX A. VOCABULARY

- *cloning vectors:* usually plasmid or bacteriophage, used to transport genes; may be amphotropic or ecotropic
- *expression:* cellular production of the gene-encoded product; see *transcription* and *translation*
- *gene transfer:* insertion of a new gene into a host cell; see *transduction* and *transfection*
- *plasmids:* small, autonomously replicating DNA molecules
- *reporter genes:* used to confirm successful transfer of a gene cassette
- *transcription:* synthesis of RNA from DNA
- *transduction:* acquisition and transfer of eucaryotic genes by retroviruses
- *transfection:* incorporation of the gene into the eukaryote cell via non-viral vectors
- *translation:* RNA-encoded protein synthesis
- *vectors* (*transfer vectors*): materials used to transfer the gene into the host cell.

AU9817386

New Research Heavy-Water Reactors with the Capacities 25 MWt and 100 MWt for the Production of Radionuclides with High Specific Radioactivity.

Report for Second International Conference on Isotopes,
Sydney, Australia, October 12-16,1997

G.V.Kiselev, L.A.Myrtsimova, O.V.Shvedov
State Scientific Center of the Russian Federation
Institute of Theoretical and Experimental Physics
117261 Moscow, Russia, B.Cheremushkinskaya, 25
phone/fax:(095)9306130
e-mail:kiselev_g@vitep5.itep.ru

Abstract

Main amount of radionuclides is produced by the use of research nuclear reactors. But these reactors have in the main multiple-function applications: neutron investigations, experimental grounding of fuel for the power reactors, production of radionuclides and so on. It is special reactor for the production of different radionuclides. It is formulated the requirements to the reactor for the production of radionuclides.
Information about the design and performance of research heavy-water reactors HWR-25 and HWR-100 is given. Reactor HWR-25 has the capacity 25 MWt and maximal thermal neutron density flux in the reflector is $4{,}6.10^{14}$ $cm^{-2}s^{-1}$. Burn-up of fuel is 50%, duration of the campaign is 105 days. Reactor HWR-100 has the capacity 100 MWt and maximal thermal neutron density flux in the reflector is approximately $1{,}2.10^{15}$ $cm^{-2}s^{-1}$ .Reactors both have a large amount of channels for the place of target for the production of radionuclides.

1. Introduction

At modern level of industrial production, agriculture, science, medicine the need for radionuclide is not reduced, and an achievement of high specific activity for some of them is necessary. In SSC RF ITEP during almost 40 years a research heavy-water reactor HWR with thermal power 2.5 MWt was maintained, on which significant quantity of radionuclides for Moscow region was made. In last years in SSC RF ITEP the group of the experts carryed out the investigations, concerning the opportunities of radionuclides production in nuclear reactor for various purposes. This group has published significant amount of results which have formed the basis for the formulation of the requests to special isotope reactor. At the same time follows to take into account requirement for realization of the scientific investigations, if isotope reactor is constructed in research centre. In SSC RF ITEP settlement researches in the field of nuclear physics and radiation material investigations and simultaneous radionuclides production were conducted. The choice of heavy water as moderator of neutrons is explained it large diffusion length and, hence, the opportunity of the organization significant irradiation volume.

In present report results of settlement neutron research of two heavy-water reactor parameters are submitted. Comparison of use heavy-water and light-water coolants was in addition conducted.

2.Conceptual design (brief description).

The main requirements to the design of HWR-25 and HWR-100 are:

-the opportunity of fundamental and applied investigations on nuclear physics and nuclear engineering;

-the opportunity of radionuclides production with high specific activity;

-the provision of current level of safety, reliable operation and the possibility of decomissioning.

Reactor assignment - to receive a high thermal neutrons flux for physical, material and other researches and for radionuclides production. For this purpose a reactor with compact core and heavy-water coolant and moderator was considered, so that the neutron flux was maximum in reflector, where experimental channels are placed.

Two design Bureau were developed the designs of these reactors. First designer was research and Developing Institute of Power Technology (RDIPT, Moscow) which was developed the project HWR-25. RDIPT had been finishing the technical design HWR-25 with loop layout of reactor till 1990 (Fig.1). According to this design HWR-25 is the reactor of channel-vessel type with heavy-water as moderator and coolant of first curcuit and lower delivery of coolant. In emergency case of loss of integrity for vessel and input pipe of first circuit and loss of coolant it needs to provide ccooldown of core by the use of external source of coolant, for instance, light water. In connection with that it is necessary to make the special tank with emergency store of coolant.

Second designer was Experimental Bureau of Building Machinery (EBBM, N.Novgorod) which was carried out the design of HWR-100. EBBM was investigated 2 versions of research HWR-100: 1. loop layout; and 2. integral layout to compare the level of their safety and to satisfy to current requirements of reliable operation. The loop layout is shown at Fig.2. The conceptual investigation of EBBM tetifies more increasing level of safety for this HWRM which quit satisfies to current requirements than the version of RDIPT. For instance, the probability for accident with loss of integrity for vessel and input pipe of first circuit and loss of coolant is very low in connection with jacket of vessel and upper delovery. Of course there is natural circulation of coolant to remove the residual heat. Of course, there is natural circulation of colant of first circuit and so on. According to my private point of view one can be to recommend for next stage of development.

3. Results of neutron-physical calculations.

3.1. Reactor geometry. The core contains multiring heat-producing assemblies as fuel channels (FC), located in units of hexagonal lattice. The central cell is free. The core is placed in tank with heavy-water moderator by a diameter 200 cm and height (between plates) 180 cm. Core height is 60 - 80 cm. In the centre of each fuel assembly a burning absorber (Gd) or tube can be placed.

Regulation system organs (two AR - automatic regulators, 6 CR - compensating ones, 3 ER - emergency rods) are located outside of core in reflector on distance ~31cm from reactor centre. AR are executed from stainless steel, their sizes were chosen such, that the efficiency did not exceed the β, CR and ER contain a strong absorber (B, Cd, Eu) and their efficiency is determined by the outside radius. The axial experimental channels (EC) have diameters of 50 mm (number is equal to 37) and 100 mm (number is equal to 6). Horizontal EC pass on different level in radial reflector. Main characteristics of HWR-25 and HWR-100 are given in Table 1.

Table 1. Characteristics of HWR-25 and HWR-100 reactors

Reactor	HWR-25	HWR-100
Power, Mwt	25	100
Lattice pitch, cm	11	8
Core height, cm	63.5	60 - 80
Channel area	47.8	47.8
U-235 load, g/cm	5.795	6.725
Total U-235 load, kg	6.624	12.1 - 16.1
Heat-remover share in lattice, %	24	43
Fuel channels amount	18	30
Spectrum hardness(core middle)	0.17	0.54
Temperature effect without exp.channels, 1/grad (coolant/coolant+moderator)	$(-0.5.10^{-4})$ $(-2.2.10^{-4})$	$(-0.3.10^{-4})$ $(-0.9.10^{-4})$
Maximum undisturbed flux in reflector, 10^{14} cm^{-2} s^{-1}	5.3	20 - 18
Campaign duration (with campaign refueling), d	105	20 - 46
Experimental channels number	43 axial and 11 radial	

3.2. Calculation technique. The reactor heterogeneous calculation includes the following stages:

a). Detailed multigroup (24 groups in epithermal and 10 - in thermal spectrum) calculation of geometry-power neutron distribution in multizoned cylindrical cell [1] with allowance made for changes of fuel and burning absorber during lifetime;

b). Reactor volume is made of cells, containing channels of a different type (FC, regulation organs, EC, reflector etc.). For each cell are calculated Λ - matrix, representing a set characteristics, used in reactor calculation;

c). 4 groups three-dimensions reactor calculation, enabling to determine effective multiplication factor also with axial and radial distributions of neutron flux [2].

3.3. Calculation results. The following reactor characteristics were determined:

- Critical load;
- Neutron flux distribution in reactor volume;
- Fuel channels (FC) and regulation rods (RR) effectivities;
- Reactivity balance;
- Reactivity effects connected with change of temperature and light water adding;
- Exit to stationary mode, power drop and reactor shutdown;
- Composition of unloaded fuel, calculation of temporary storehouse for used FC.

3.4. Comparison of two versions of cooling for heavy-water reactor.

Question is of interest how quantities of a core load and neutron flux will be changed if to use as a coolant light water instead of heavy one. For solution of this problem rather simple estimated calculations were made whith two coolant types of a core disregarding of such features of a reactor, as availability of a plenty of experimental channels, non-uniform burnup of fuel etc. At given stage of calculation it is possible to assume, that all these questions have to be decided irrespective of a coolant choice.

Light water in core of small volume results in essential lower of a neutron spectrum hardness, that is accompanied by improvement of the neutron balance and increase of K_{eff}. The share of capcured neutrons in coolant is greater, causing to fall K_{eff}, but also - to change the neutron flux distribution not only in core, but also in reflector.

To receive close values K_{eff} in reactor with different coolants, it is necessary to reduce the FC number or to reduce an uranium core load in each FC.

In Table 2 values of Keff received for different core configurations (with the same core U-235 load in FC) with light-water and heavy-water coolants are compared. The calculations were made with allowance for 7 harmonics on height. We shall note, that in considered reactor the dependence of results on harmonics number is very essential and has a different sign for two kinds of a coolant (with heavy-water - factor of duplication decreases at increase of number of harmonics, with light-water - increases).

On the Table 2 data it is possible to see that all versions with heavy-water coolant have about identical and required excess criticality. It was chosen the version with N(FC) = 30 - is rather high so it was possible to remove required power. However for version with light water as a coolant K_{eff} is too great even for reduced FC number.

Table 2. Dependence of multiplication factor of a reactor on core configuration

Version	1	2	3	4	5	6	7	8
Coolant			D_2O			H_2O		
N(FC)	24	30	30	36	24	30	30	18
N(central zone)	37	61	7	1	37	61	7	19
K_{eff}	1.198	1.200	1.202	1.187	1.291	1.291	1.387	1.280

The similar calculations were made for reactor with reduced U-235 load in FC (β - is share of an initial core load) when the core contains 30 FC and is cooled by light water. The dependence K_{eff} from U-235 load in FC is resulted in Table 3. The number of cells in the core centre, free from FC, was equal to N (central zone) = 7, though the final choice should be made depending on requests to quantity of a neutron flux. For that purpose optimisation calculations would be necessary. In Table 3 multiplication factors for the cell with fuel (K(FC)) are indicated also. Version 1 in Table 3 is the same as 7 in Table 2.

Table 3. Multiplication factors in cell and reactor depending on relative U-235 load in FC β.

Version	1	2	3	4
β	1	0.8	0.6	0.4
K(FC)	1.747	1.730	1.696	1.623
K_{eff}	1.387	1.361	1.317	1.235

At given stage of calculation we shall accept for comparison versions 3 from Table 2 and 4 from Table 3. The divergence in values K_{eff} makes 3 % that will not affect essentially comparison of neutron flux distributions and their quantities in reactor reflector.

An average neutron flux on fuel in core is proportional to the relation of reactor power to core load and makes, accordingly:

D_2O - coolant - F(fuel)= $1.6.10^{14}$ cm^{-2} s^{-1},

H_2O - coolant - F(fuel)= $3.3.10^{14}$ cm^{-2} s^{-1}.

Increase of a flux in 2 times in case of light water cooling results in appropriate reduction of campaign duration, increasing of fuel price and operating ratio of power lower.

The distribution of flux density on reflector was determined on quantities of activation in cells, containing, besides D_2O, small impurity of the activator (for example, U-235), practically not influencing on reactor criticality. Received results are illustrated on Fig. 3. The quantities of of flux density are referred to average flux on fuel. Distance from centre of a core is measured in a lattice pitch.

So it has appeared that in heavy-water reflector around of a compact core, exsess of neutron flux density makes in relation to flux on fuel about 8.5 (with heavy-water coolant) and 1.75 (with light-water coolant), and in central zone - 9.6 and 2.2, accordingly. A loss in a flux quantity in case of light-water coolant use makes more than 2.

As following step it is necessary to consider influence of experimental channels to neutron flux for two types of a coolant. From total of reasons it is represented, that this influence will be stronger in version with light water, and the losses of a neutron flux will only increase.

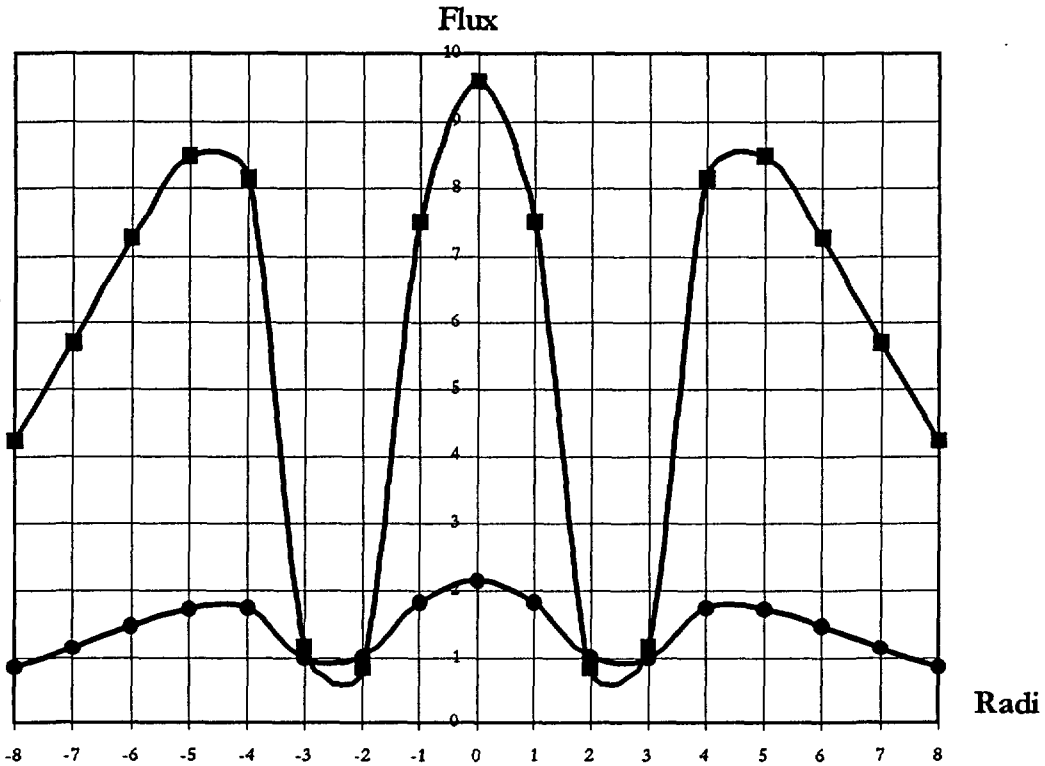

Fig. 3. Radial neutron flux distribution

4. Opportunity of the isotops program realization

High-flux reactors of an offered type are permitted to irradiate some nuclides in reflector, where neutron flux yas a maximum, and to place targets in rather large volume. The limitation connected only with necessity to avoid strong blocking of targets. The degree of flux neutron depression is determined by quantity of an irradiating material and should be designed for particular program in addition.

As target nuclide were considered Co-60, Ir-192 and Mo-99, while its production (in particular - Co) high neutron flux is necessary. The values of specific activity of targets, core load of starting nuclide and productivity and complete amount of activity in year of an irradiation are calculated. It is supposed, that for share of targets in reactor can be spent 8 % of a reactivity (see [2,3]).

In table 4 results of calculations for Co-60 are submitted (capture cross-section was accepted equal to 37 b, thickness of targets - 0.5 mm).

Table 4. Co-60 production.

Reactor	HWRM-25			HWRM-100	
Neutron flux in reflector,	$5.10^{14} cm^{-2}s^{-1}$			10.10^{14} $cm^{-2}s^{-1}$	
$\square_{irrad.}$, year	1	1.25	1.5	0.5	0.75
Q_{Co}, Cu/g	410	475	530	420	560

m_{Co}, g	330			660	
A_{Co}, □Cu/year	135	125	115	555	495

In table 5 similar results for Ir-192 (capture cross-section was accepted equal to 1000 b, target diametrs - 0.5 and 1 mm, isotopic composition - natural and enriched up to 100 % Ir-191).

Table 5. Ir-192 production.

Reactor	HWRM-25				HWRM-100			
Neutron flux in reflector	2.10^{14} cm^{-2} s^{-1}							
Target dimensions,mm	0.5		1.0		0.5		1.0	
T_{irrad}, day	30	60	30	60	30	60	30	60
Q_{natur}, Cu/g	616	760	470	650	616	760	470	650
$Q_{100\%}$, Cu/g	1200	1600	400	660	1200	1600	400	660
m, g	100				400			
A_{atur},KCu/g	740	455	565	390	2960	1820	2260	1560
$A_{100\%}$,KCu/g	1440	960	480	395	5760	3840	1920	1580

At last, in table 6 the same quantities for Mo-99 are indicated. Calculations were made in assumption that the neutron spectrum hardness is equal to 0.02 (effective capture cross-section for Mo-98 is 0.27 b), material of a target - MoO_3, average chorde is equal to 20 mm (plate by thickness 10 mm or cylinder by a diameter of 20 mm); enrichment 100 %. The time of an irradiation - 7 days.

Table 6.

Reactor	HWRM-25	HWRM-100
Neutron flux in reflector	5.10^{14}cm^{-2}s^{-1}	10.10^{14}cm^{-2}s^{-1}
Q, Cu/g	12	23
m, kg	75	150
A_{Mo},MCu/year	45	90

5.Conclusion.

Calculation results permit to make the following conclusions.

- The reactor, loaded with FC accompanied with burning absorber - Gd with ~30% FC reloading on each third of campaign time has stable significance of multiplication factor. The Keff change during campaign time is minimum and does not exceed on estimations 3%, if to choose the correct radius of Gd rod.
- When reactor power is equal to W = 25 MWt maximum undisturbed neutron flux density in reflector F (refl) = $5.3 .10^{14}$ cm^{-2}s^{-1}. Average on campaign duration and on core volume neutron flux density is F (FC) = $1.6.10^{14}$ cm^{-2}s^{-1}. The campaign duration is equal to 105 d. When reactor power W = 100 MWt maximum undisturbed neutron flux density in reflector is equal to 20.10^{14} cm^{-2}s^{-1}, the average on fuel is $2.75.10^{14}$ cm^{-2}s^{-1}. Duration of campaign is about 20 - 40 d.
- Change of multiplication factor at RR dropping makes about 16 %, including ~7 % is because of ER.
- Approached account of experimental channels has shown, that their effectivity is about 6 %. This quantity should be adjusted on critical assembly.
- Temperature effect in reactor with heavy-water coolant - negative and equal to $\Delta k/\Delta t$ =
- (0.9 - 1.6) 10^{-4} 1/^{0}C.

- Light-water effect in heavy-water coolant - positive; at small impurity of H_2O (C~1 %) it is equal to $\Delta k/\Delta C$ 0.4, and then falls up to $\Delta k/\Delta C$ 0.05. Additions of water simultaneously in coolant and the moderator does not almost influence factor of duplication, but results in appreciable reduction of a flow of neutrons in reflector (on ~ 20 % on first added percent (interest) of water and on ~ 5 - 7 % on following 3 %.

Comparison of two versions of cooling of a heavy-water reactor has shown that a loss in maximum value of undisturbed neutron flux in reflector in case of light-water coolant makes more than 2. Simultaneously a flux on fuel will twice increase and that will result in reduction of campaign duration, rise in fuel making prise and reduction of capacity factor.

An irradiation in heavy-water high-flux reactor reflector of such starting materials as Co-59, Ir-191, Mo-98 permits to receive nuclide with high specific activity.

Reference.

1. Burmistrov A.I. Kochurov B.P. Spatial-energy neutron distribution in cylindrical cell of a reactor (program TRIFON).M., Preprint ITEP, 1978, 107.

2. Malofeev V.M. 3-dimensional calculation method of heterogeneous reactor in dipole approximation. M., Preprint ITEP, 1987, 73.

Current Status and Trends of Cooperation on Radiotracer and NCS Technologies

J THERESKA
IAEA,RIPC, Industrial Applications and Chemistry Section
Wagramer strasse 5, P.O. Box 100, A-1400, Vienna, Austria

SUMMARY. Considerable progress has already been made in promoting the industrial applications of radioisotopes both in developed and developing countries. The economic benefits of the technology have been amply demonstrated. There is now a need to upgrade the capability of radiotracing and radiogauging groups in developing countries, to consolidate and systematize existing know-how, and to promote research and development to extend further the capabilities of the radiotracer and Nucleonic Control Systems (NCS) technologies.
The chief objectives of further cooperation should be:
-to further develop and refine radiotracer and NCS methodologies, new radiotracer and sealed sources, data processing and interpretation with special reference to complex industrial processes;
-to develop, test and intercompare standard software packages for tracer data processing and modeling and for design and calibration of nucleonic gauges,
-to provide relevant information packages and technical guidelines which may be readily disseminated among developing countries to promote wider use of the technologies and to facilitate their use by the industrial end users.

1.INTRODUCTION

Radiotracers and nucleonic gauges first began to be used in industry some forty years ago. Since then, there has been a continuous expansion in their usage so that, today, teams around the world are actively promoting and developing both the theory and the practice of tracing and gauging methods.
The success of radioisotope applications is due primarily to the ability, conferred by the unique properties of radioactive materials, to collect data which cannot be obtained by other investigative techniques.
The cost effectiveness of radiotracer applications should be widely promulgated to encourage industrialists to take full advantage of the technology. Probably, an average benefit to cost ratio of 20:1 is reasonably representative. There are few short-term investments which will give a return of this magnitude (1).
Nucleonic gauges or Nucleonic Control Systems (NCS) have been widely used in developed countries by industry to improve the quality of product, optimize and improve regulation of the process, save energy and materials. It is considered (2) that NCS technology is by far the most requested among other nuclear techniques which have been used in the industries of developed countries. Their economic benefits have been demonstrated and recognized by industry.
The paper reviews the current status and trends of cooperation on radiotracer and NCS technologies, pointing out that there was an extremely strong case, on economical, social and technical grounds for a further research and development in the field of the industrial application of these advanced and competitive technologies.

2. RADIOTRACER TECHNOLOGY AND METHODOLOGY

2.1 State of the art

Radiotracer methodology, generally comprises four interrelated aspects of the application, namely: experimental design,

data acquisition, data treatment and data interpretation. The sophisticated modeling capability, which is now available to many radiotracer groups, is fundamentally changing the way radiotracers are being applied to industrial and environmental problems, focusing on their verification role to computational modeling for solving industrial problems.

There has been a significant improvement in radiotracer methodology and technology covering design of experiment; selection of appropriate radiotracer, injection method, and digital data acquisition techniques. The theory of residence time distribution (RTD) is considered to be developed and in almost all applications this methodology is used to obtain necessary information.

Some specific areas needing mention are:

-digital data acquisition systems coupled with PC for data processing and visualization;

-a number of radioisotope generators for radiotracer tests in remote areas or in countries where there is no nuclear reactor;

-combination of radiotracers tests with measurements carried out by sealed sources to get more technological information;

-growing interest in flow-pattern recognition (emission and absorption tomography) using gamma camera or multiple counter systems.

2.2 Trends

In detail, trends can be found in the different aspects of radiotracer applications.

In the field of methodology, developments are related on the one hand to a research and development activity for localization and visualization of flow, and on the other hand to the determination of the sensitive volume of a detector (data acquisition, modeling, prediction). This work will greatly enhance the method from a scaling-up point of view, the long term aim being the development of an expert system and for the interpretation of data.

Concerning hardware and experiment implementation, development of injector technology is important, for reasons of performance (shorter injection pulses of gas, liquid and solid) and for safety (remote injection systems).

In the field of data acquisition and data processing, including deconvolution, the trend is to make use of commercial hardware and software developments throughout the world (new generation of computers, very efficient mathematical and data acquisition commercial software). Data interpretation and flow monitoring can be considered at different levels of complexity, according to what is requested by the end-user. The first step is temporal moment analysis of the RTD. The trend is to use and customize available software. The second step is to interpret curve shape either by peak decomposition (from a chromatographic or a spectroscopic point of view) or either by chemical engineering system analysis (different arrangements of plug flow and perfect mixers). The trend here is also to make use of software developments, especially of commercial software. The next step is the use of more complex flow structure modeling in the framework of RTD (IAEA Computer Manual Series 11) (3). The final step is the combination of tracer data with computer fluid dynamics (CFD), in order to make use of the tremendous mathematical development in this field in describing more precisely flow structure and flow to visualization (Finite element methods).

2.3 Target application areas

The IAEA "Guidebook on Radioisotope Tracers in Industry" (Vienna, 1990) (4) discussed radiotracer applications in twelve industrial sectors which were believed to be potential growth areas for radiotracer applications.

It is timely to review that expectation. Although radiotracers are applied widely across a broad industrial spectrum it is fair to comment that growth has been demonstrated, primarily, in four main sectors: Petroleum, Petrochemicals, Minerals Processing and Waste-Water

Treatment. Petroleum, Petrochemicals and Minerals Processing units are widespread throughout the developed and the developing world. Generally, the operating units are large-scale and continuously operating. There are huge financial penalties associated with unscheduled shut-downs. The benefits conferred by radiotracer technology in terms of on-line fault diagnosis and process optimization are very large indeed and the incentive for these industries to apply the technology is clear.

The incentives in the case of Waste-Water treatment plants are somewhat different. Though it is undoubtedly true that there are financial benefits associated with the applications of radiotracer technology on such units the primary benefit is not monetary. Rather, it is the improvements in health, social hygiene and environmental conservation which are more important and this is especially relevant in developing countries.

a. Petroleum Industry

The applications of radiotracer technology are widespread throughout Oil Refineries Word-wide and this industry is one of the main users, and beneficiaries of the technology.

Economically, the most important operating unit in a refinery is the Fluidized Catalytic Cracking Unit (FCCU), the function of which is to upgrade the "heavy" components of the oil to gasoline. Technically, this is also the most complex unit, involving as it does the interaction of multiple phases: solid catalyst, vaporized feedstock steam and air. Because of the construction and extreme operating conditions of FCCUs, the only effective way to study their behavior is through the application of radioisotope technology. This, then, is the primary target area for radioisotope applications in the short to medium term.

b. Petrochemical Complexes

The Petrochemicals Plant lies immediately downstream of the Oil Refinery and in many developing countries, construction of the two types of facility is proceeding in parallel. Like refineries, petrochemicals plants are generally continuously operating and technically complex. Thus, high economic benefits may be realized by the applications of radiotracer techniques on petrochemicals units. Though radiotracers are useful in solving a wide range of problems, the economic benefits become more pronounced the further "upstream" they are applied. This means that studies of the cracking furnace, primary fractionator and gas separation chain are of the highest potential value.

c. Minerals Processing

This generic heading covers an enormous range of industries. Minerals processing plants, in one form or another are to be found in practically every country in the world and in many cases they are major contributors to national economies.

Though the range of minerals which are extracted and processed is extremely wide, there are certain processes found throughout the industry, such as Comminution, Classification, Flotation, Homogenization.

These processes involve two (or in some cases three) phase flow and are notoriously difficult to control. Radiotracer technology is of proven benefit in contributing to the understanding of these processes and it is believed that radioisotope applications may be refined and extended to further benefit the industry.

d. Waste-water Treatment Plants

As has been stated, the primary justification for concentrating attention on this sector is based upon health and environmental considerations, rather than purely on economic benefit per se. Additionally there are opportunities to extend the technology in terms of understanding both the macroscopic and near-field behavior of such systems. Modeling by CFD together with radiotracer verification of the models will be a powerful tool, aiding both the design

and performance optimization of waste-water treatment systems.

2.4 Topics for a CRP

The following Coordinated Research Programme (CRP) is proposed :
"Radiotracer technology for engineering unit operations studies and unit process optimization"
The CRP will cover the following topics:
a).Improvement in Radiotracer Methodology, including:
-Development of new radiotracers.
-Improved systems for tracer injection.
-Evaluation of new radiation detectors.
-Use of sealed source techniques to provide data complementary to that obtained from radiotracer studies.
-Development of expert systems.
b).Data Acquisition, Processing and Evaluation
-Definition and characterization of the "sensitive detection volume" of radiation detectors for the proper design of experiments and the evaluation of the data.
-System analysis through the decomposition of detector response curves.
-Intercomparison of software for radiotracer applications.
-Utilization of finite element methods for flow structure visualization.
-Computational modeling and radiotracer verification for solving complex industrial problems.
c). Applications: Formulation of guidelines for radio tracer studies of complex processes:
-Fluidized Catalytic Cracking Reactors
-Coke formation and plant malfunction
-Comminution, classification, flotation and homogenization
-Separation efficiency and particle cut size in cyclones
-Monitoring the efficiency of waste-water treatment plants
-Nucleation and growth in crystallizers.

3.NUCLEONIC CONTROL SYSTEMS

3.1. State of the art and trends

There are several hundred thousand of nucleonic gauges installed in industry all over the world. The major users in industry are petroleum and petrochemical industries, iron and steel plants, mineral ore and raw materials processing, paper and plastics sectors.
The NCS are available from several manufactures; competitiveness obliges them to continually improve their equipment using the latest technology but also not to disclose their know-how. In many cases, developing countries are facing difficulty in developing their capability and experience on NCS.
The emerging new applications of NCS in industry, focused on multi-beam interactions with multiphase medium, have improved on-line performance (accuracy) minimizing geometrical and compositional variations.
There is apparently the trend of introducing low and ultra low radiation nucleonic gauges especially in mining industry.
There is trend to recommend procedures for quality control certification of NCS according to ISO standards.
The important subjects for the further cooperation among laboratories from developed and developing countries are the optimal design and calibration in radiogauging, and the quality control certification according to ISO standards.
Expert systems for the conception and optimal design of industrial gauges based on beta, gamma or x-ray, and on fast or thermal neutrons transmission and scattering, as well as multibeam and multienergy gauges for measurement of parameters of multi-phase systems are requested. Their aim is to optimize the different components of a transmission or scattering gauge (radioactive source, detector, electronic device, collimator and shielding), taking into account parameters and constraints linked to the configuration (nature and composition of materials, presence of shields and walls,..), as well as users requirements (accuracy, counting time, beam collimation, duration of tests).

At any rate is believed that the emerging practice in this field is the use of Monte Carlo simulation for both design and calibration.

3.2 Topics for a CRP

The following Coordinated Research Programme (CRP) might be taken in consideration in the near future:

' Multibeam radiogauging for multi-phase systems studies'.

This potential CRP may cover the following topics:

a).Improvement in radiogauging methodology, including:

. Development of new sealed sources,

.Improved collimating and detection system,

. Combination of nuclear radiation beams (neutron-gamma, gamma-gamma, gamma - x, etc.) and nuclear radiation with other beams (microwave and infrared),

.Development of experts systems for optimal design and calibration.

b).Applications: Formulation of guidelines and software for radiogauging studies of industrial processes:

. neutron gauges for level and interface measurement and explosives/landmines and drugs detection,

. dual X-ray transmission and backscatter gauge for minimizing the effect of sheet composition and geometrical variations on the thickness measurement,

. multi beam X-ray profile gauges and on line X-ray image processing for pipe inspection,

.development of nucleonic suspended sediment concentration gauging,

.case studies from petroleum industry (off-shore and on-shore), mineral ore processing, pulp and paper and plastic industries, pipe, tank and vessels inspection in petroleum refineries, etc.

.recommendation of procedures for quality control evaluation and standardization according to ISO standards.

4. CONCLUSIONS

a. Over the years, the Agency has invested heavily in the development and promulgation of radioisotope applications in industry. Excellent work has been carried out in a number of centers and the high benefit to cost ratio of such applications is beyond doubt. It is recommended that the knowledge and experience which has been gained should be consolidated and disseminated to IAEA Member States in a systematic way.

b.The IAEA Coordinated Research Programme to further the development of these technologies is fully justified.

To upgrade the capability of radiotracing and radiogauging groups in developing countries, to consolidate and systematize existing know-how, and to promote research and development to extend further the capabilities of the technologies, the following CRPs should be promoted:

-Radiotracer technology for engineering unit operations studies and unit process optimization,

-Multi-beam radiogauging for multi-phase systems studies.

c. The IAEA should provide relevant information packages and technical guidelines which may be readily disseminated among developing countries to promote wider use of the technology and to facilitate its use by the industrial end users.

d. Synergism and close interaction with connected disciplines: nuclear medicine and gamma scanning in industry, because of the requirement of similar tools and approaches for data processing, visualization and standardization.

e. The preliminary results of emission and absorption tomographies are encouraging. It could be recommended the topics for future review as potential CRPs when more information has been accumulated.

ACKNOWLEDGMENT

Many known experts have contributed for the preparation of this paper. I would like to thank them for relevant information provided on current status and trends of radiotracer and nucleonic gauge technologies. I would like to express my gratitude to:
Mr. Airey P. and Mr. Charlton J.S. from Australia, Mr. Boutaine J-L and Mr.Vitart X. from France, Mr. Rao S.M. from India, Mr. Gardner R. from USA, Mr. Salgado J. from Portugal, Mr. Chmiliewski A. from Poland and Mr. Shirakawa from Japan, and to all experts participated in two important meetings the IAEA organized recently on evaluation of radioisotope technologies.

REFERENCES

1. Emerging New Applications of Radiotracers in Industry, IAEA, CM Report, 3-6 June 1997, p.1-10

2. Evaluation of IAEA Sub-programme on Industrial Applications of Radioisotopes and Radiation, IAEA, CM Report, PPAS External Review, 25-27 September 1996, p. 1-19.

3. Residence Time Distribution Software Analysis, Computer Manual Series No.11, IAEA, 1996.

4. Guidebook on Radioisotope Tracers in Industry, Technical Reports Series No.316, IAEA, Vienna, 1990

AU9817388

Uptake and distribution of ^{191}Pt in patients undergoing therapy with cisplatin.

Areberg J[1], Björkman S[2], Einarsson L[4], Frankenberg B[1], Lundqvist H[4], Mattsson S[1], Norrgren K[1], Scheike O[3] and Wallin O[2]

[1] Department of Radiation Physics, [2] Hospital Pharmacy and [3]. Department of Oncology, Malmö Uninversity Hospital, Sweden
[4] The Svedberg Laboratory, Uppsala, Sweden

Introduction

At the University Hospital in Malmö, Sweden, we are studying the distribution of cytostatic agents in the patient, during and after the treatment. Having this knowledge, we think it is possible to optimise the drug delivery to the tumour and minimise the adverse effects of the cytostatic agent. The treatment will then be more individualised, which hopefully will give better result.

Cisplatin is a cytostatic agent widely used in chemotherapy. The antitumour activity of cisplatin was discovered by Rosenberg et al. (1) in the late 1960:s and the agent has been used in the clinics since the middle of the 1970:s. It has been most successful in the treatment of testis cancer (germ cell tumours), where today more than 90 % of the patients treated are cured. It is also used to treat ovarian, oesophageal, small cell lung, head and neck and bladder cancers.

Renal failure was early considered as the most severe adverse effect of the treatment with cisplatin. Today, the patients are hydrated in connection with the infusion of cisplatin and the toxicity to the kidneys is smaller. Other side-effects are ototoxicity, myelosuppression, nausea and vomiting.

The cisplatin molecule, *cis*-dichlorodiammineplatinum(II), is an inorganic compound which consists of a platinum atom surrounded by two chloride ions and two ammonia ligands in *cis*-configuration.

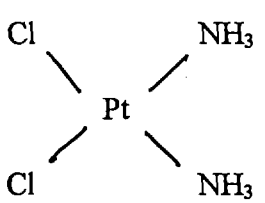

Figure 1. *Cis*-dichlorodiammineplatinum(II)

By synthesising radioactive cisplatin, the distribution and uptake of the drug in the patient can be studied. This has been done in our case by synthesising cisplatin containing trace amounts of the radioactive isotope ^{191}Pt.

Methods

^{191}Pt was produced by irradiating stable gold with protons, with energies 70-75 MeV. ^{191}Pt decays, with a half-life of 2.9 days, to the stable isotope ^{191}Ir. Among the emitted photons, the characteristic x-rays with energies 63-73 dominate. Also conversion electrons and Auger electrons are emitted in the decay.

The synthesis of ^{191}Pt-cisplatin, performed under aseptic conditions, was started from $^{191}PtCl_4$(IV). Carrier in the form of non-radioactive $PtCl_4$(IV) was then added. To reduce Pt(IV) to Pt(II), hydrazine was used. The synthesis, proceeded as described by Hoeschele et al. (2), was going on for eight hours and the yield of the radioactivity was in the range 10-35 %.

To check the identity, the purity and the concentration of the synthesised product, HPLC was used. Sterility and absence of pyrogens was checked. The activity and the radionuclidic purity was controlled with a high pure Ge-detector.

The in-house synthesised cisplatin was mixed with ordinary and composed as maximum of ten percent of the total amount given. The mixture was given intravenously to the patient during a two-hour infusion. The patient was hydrated with physiological saline before and after the infusion of cisplatin. The urine from the patient was collected for the first 48 hours after the start of the infusion.

Imaging was performed using a gamma camera, equipped with a high energy collimator due to the presence of the high energy photons. The 20 % energy window was centred at 70 keV. Static images over the thorax region and the tumour region as well as whole-body scanning were performed directly, one day and in some cases, depending on the condition of the patient, up to ten days after the end of the infusion. The administered activity was in the range 31-50 MBq.

Eleven patients, 7 male and 4 female, have so far been included in the study. Their age varied between 32 and 72 years. The diagnoses were one testis, two bladder, three oral and five lung cancers. All eleven patients gave their written consent to take part in the study, which was approved by the Human Research Ethics Committee of Lund University, the Swedish Medical Products Agency and the Isotope Committee of Malmö University Hospital.

Results

About one percent of the activity of the final product was in the form of ^{188}Pt. Impurities such as ^{191}Au and ^{188}Ir were present at the start of the synthesis but were not carried through and were not found in the final product. All batches tested were found to be sterile and in absence of pyrogens.

The organ who showed the highest uptake of platinum was the liver. Maximum fractional uptake was on average 9 % of the platinum administered, corresponding to 5.5 % per kg liver tissue. Maximum fractional uptake in the kidneys was 0.5 % of the platinum administered, corresponding to 1.8 % per kg kidney tissue. Uptake of platinum was also visible in the gall bladder, spleen, gastro-intestinal tract, neck and mediastinum and uro-genital region.

For two patients, the visualisation of platinum in areas corresponding to tumour sites could easily be seen. For two other patients, an uptake was visible but not so obvious as in the former cases. The tumour sites were verified with CT-images or bone-scan images, examinations performed close in time to the ^{191}Pt-cisplatin study. For the other seven patients, the concentration of platinum in the tumour was not high enough for visualisation.

There was an initial, rapid excretion of platinum via the urine. Already at four hours after the start of the infusion, 15 to 45 % of the administered platinum had been excreted. After 48 hours, the amount of platinum excreted varied between 28 and 62 %.

Discussion

The uptake of platinum in the liver seen in our images is consistent with data reported by Smith et al. (3). The uptake in the kidney was lower than expected from earlier XRF measurements (4) but consistent with other studies using radioactive cisplatin (5, 6). The uptake of platinum into the gall bladder and the gastrointestinal tract indicates that part of the platinum was excreted into the gastrointestinal tract and not only through the kidneys.

The uptake of cisplatin into a tumour is determined by a number of factors. Although uptake of cisplatin by a tumour is not a guarantee for a cytotoxic effect, the drug cannot be effective if it does not reach the tumour in sufficient concentration. We have shown that by using radioactive cisplatin, visualisation of platinum in tumour tissue is possible.

References

1. Rosenberg B, Van Camp L, Trosko JE, Mansour VH (1969) Platinum compounds: A new class of potent antitumour agents. Nature 222:385

2. Hoeschele JD, Butler TA, Roberts JA, Guyer CE (1982) Analysis and refinement of the microscale synthesis of the ^{195m}Pt-labeled antitumor drug, cis-dichlorodiammineplatinum(II), cis-DDP. Radiochimica Acta 31:27

3.Smith HS, Taylor DM (1974) Distribution and retention of the antitumor agent ^{195m}Pt-cis-dichlorodiammine-platinum (II) in man. J Nucl Med 15(5): 349

4. Jonson R, Börjesson J, Mattsson S, Unsgaard B, Wallgren A (1991) Uptake and retention of platinum in patients undergoing cisplatin therapy. Acta Oncologica 30(3): 315

5. Owens SE, Thatcher H, Sharma H, Adam N, Harrisson R, Smith A, Zaki A, Baer JC, McAuliffe CA, Crowther D, Fox BW (1985) *In vivo* distribution studies of radioactively labelled platinum complexes; cis-dichlorodiammine platinum (II), cis-trans-dichlorodihydroxy-bis-(isoproplamine) platinum (IV), dis-dichloro-bis-cyclopropylamine platinum (III), and cis-diammine 1,1-cyclobutanedicarboxylate platinum (II) in patients with malignant disease, using a gamma camera. Cancer Chemother Pharmacol 14: 253

6. Stewart DJ, Mikhael NZ, Nanji RC, Nair RC, Kacew S, Howard K, Hirte W, Maroun JA(1985) Renal and hepatic concentrations of platinum: Relationship to cisplatin time, dose and nephrotoxicity. J Clin Onc 3(9): 1251

Development of New Target Materials for the Production of Tc-99m Generators by Column Chromatography

* M. A. ROUF, A. HAQUE,** H. MATSUOKA, K. HASHIMOTO

* Institute of Nuclear Science & Technology, Atomic Energy Research Establishment, P. O. Box 3787, Dhaka 1000, Bangladesh.

** Department of Radioisotopes, Japan Atomic Energy Research Institute, Tokai-mura, Naka-gun, Ibaraki-ken, 319-11 Japan.

SUMMARY. Three different types of new gel targets as column matrix have been developed for the production of Mo-99/Tc-99m generators by column chromatography. A good number of samples are prepared from these targets at different pH and drying conditions before irradiation in a nuclear reactor. In the chromatographic generator G4 type of columns have been used with neutral alumina as column bed. Physiological saline is used as eluent. Samples having pH 5.5 and dried at 70^{0}C for 24 hrs, 48 hrs and samples having pH 2.75 and dried at 70^{0}C for 6 hrs, 24 hrs are seemed good giving the yield of Tc-99m 85%, 73%, 77.6% and 79.6% respectively. Further research of the new targets regarding optimization of elemental ratio, pH and drying condition is required to use them as column matrix to prepare Tc-99m chromatographic generator.

1. INTRODUCTION. Technetium-99m has been attained a unique position as a radiotracer (1,2) in the field of nuclear medicine. Chemical forms of Tc-99m are most widely used for radionuclidic imaging of brain, liver, lung and skeleton. Tc-99m labelled radiopharmaceuticals for both static and dynamic studies of renal and cardiac pathology have already been developed. Such widespread application demands simple Tc-99m production methods. They should yield appropriate quantities of Tc-99m at a reasonable cost and in a readily usable form of high purity.

At present Tc-99m is mainly obtained from generators based on column chromatography using Mo-99 of very high specific activity from fission or by high flux neutron irradiation of MoO_3 (3,4). In column chromatography $^{99}MoO_4^{2-}$ from fission produced Mo-99 is adsorbed on acidic alumina and $^{99m}TcO_4^-$ is eluted with physiological saline (0.9% NaCl solution). Tc-99m is also obtained from the selective extraction of $^{99m}TcO_4^-$ (5,6) into organic solvents or sublimation of Tc_2O_7 (7,8,9,10) to a little extent in some generator systems from Mo-99 of relatively low specific activity, produced from direct neutron activation of molybdenum targets. A low temperature (380-410°C) sublimation procedure has been described (11) by L. Zsinka using a new target prepared from Titanium Tetrachloride ($TiCl_4$), and Ammonium Hepta Molybdate [$(NH_4)_6Mo_7O_{24}.2H_2O$] but with a low yield (25-40%) of Tc-99m.

Evans et al have developed a procedure (12) of converting Mo-99 of low specific activity into an insoluble gel matrix of Zirconium Molybdate from Zirconium Oxychloride ($ZrOCl_2.8H_2O$) and Molybdenum Trioxide (MoO_3) which has been used as column matrix for preparing a column type generator of Tc-99m.

In the present study, we have developed new gels and investigated the possibility of preparing a gel type column chromatographic generator of Tc-99m from low specific Mo-99 by the direct irradiation of the pre-formed (13,14) gel. The irradiated gel has been used as column matrix and irradiated in the reactor only for 5 minutes at a neutron flux of $3x10^{13}$ n/cm^2.sec with 250-350 μCi of Mo-99 radioactivity. It has not yet been irradiated in the reactor under high flux, long time and high dose of Mo-99.

The results obtained so far from the new gels have been found encouraging with respect to % yield of Tc-99m, radionuclidic and radiochemical purities.

2. MATERIALS AND METHODS.

Preparation of Targets. The new gel has been prepared from Molybdenum Trioxide (MoO_3), Titanium Tetrachloride ($TiCl_4$) and Ammonium meta Vanadate (NH_4VO_3). Another gel has also been prepared for column chromatographic generator from Molybdenum Trioxide (MoO_3), Zirconium-oxychloride ($ZrOCl_2.8H_2O$) and Ammonium meta Vanadate (NH_4VO_3).

Target A

Target A was prepared according to the following procedures:

Solution (1). 1.15 g of NH_4VO_3 was dissolved in 150 ml water by heating and stirring.

Solution (2). 11.45 g of MoO_3 was dissolved in a minimum volume of 1:1 NH_4OH by heating and stirring.

Solution (3). 10.8 ml of $TiCl_4$ was taken in a beaker and was diluted with 20 ml of 1:1 HCl. The soln. was filled into a burette.

Solution (1) in a 400 ml beaker was placed on a magnetic stirrer and heater. Soln.(2) was added to it and heated to 60^0C with stirring. Soln. (3) was then added dropwise to this mixed solution with vigorous stirring. A heavy yellow precipitate was formed. The complete precipitation was checked by adding a few drops of $TiCl_4$. The reaction temperature was maintained at 60^0C for 10 minutes. The pH of the mixing solution was adjusted to 5.5 by 1:1 NH_4OH. The precipitate was stand overnight. The next day, it was filtered by vacuum. The precipitate was dried at room temp. for 24 hrs and again dried at 70^0C for 6 hrs. At this drying condition the target could be stored for a long time.

Six samples were prepared from this target at different pH and drying conditions for irradiation in the reactor.

The content of Mo, Ti and V in this target was 34.1%, 13.3% and 2.0% respectively as measured by ICP-AES (Inductively Coupled Plasma-Atomic Emission Spectrometry) at Analytical Chemistry Laboratory in Japan Atomic Energy Research Institute (JAERI).

Target B

Target B was prepared according to the following and procedures:

Solution (1). 1.15 g of NH_4VO_3 was dissolved in 150 ml of water by heating and stirring.

Solution (2). 8.46 g of MoO_3 was dissolved in a minimum vol. of 1:1 NH_4OH by heating and stirring.

Solution (3). 6.48 ml of $TiCl_4$ was taken in a beaker and was diluted with 20 ml of 1:1 HCl. The solution was filled into a burette.

The preparation procedures were the same as those adopted in the preparation of target A except the pH. The pH was adjusted to 3.7.

Two samples were prepared from this target at different pH and drying conditions for irradiation in the reactor.

The content of Mo, Ti and V in this target was 28.7%, 12.0% and 1.8% respectively as measured by ICP-AES (Inductively Coupled Plasma-Atomic Emission Spectrometry) at Analytical Chemistry Laboratory in Japan Atomic Energy Research Institute.

Target C

Target C was prepared according to the following procedures:

Solution (1). 0.575 g of NH_4VO_3 was dissolved in 75 ml of water by heating and stirring.

Solution (2). 1.8 g of MoO_3 was dissolved in a minimum vol. of 1:1 NH_4OH with heating and stirring.

Solution (3). 3.53 g of $ZrOCl_2.H_2O$ was dissolved in 20 ml of 1:4 HCl.

The preparation procedures were the same as those adopted in the preparation of target A except soln. (3) and the pH. The pH was adjusted to 7.5.

Three samples were prepared from this target at different ratios of Mo, Zr, and V, pH and drying conditions as indicated in the experimental results.

The content of Mo, Zr and V in this target was 15.8%, 25.0% and 6.4% respectively as measured by ICP-AES (Inductively Coupled Plasma-Atomic Emission Spectrometry) at Analytical Chemistry Laboratory in Japan Atomic Energy Research Institute.

Irradiation of Targets.

The targets were irradiated for 5 min in JAERI JRR-4 reactor. Co-Al alloy wire (Co: 0.475%) and Cd pipe (thickness: 0.5mm) were used as a neutron flux monitor for the calculation of Mo-99 radioactivity. Cooling time was 72 hrs.

Estimation of Mo-99 Radioactivity.

The Mo-99 radioactivity of the sample was determined in comparison with standard value. The standard values, determined by the irradiation in JRR-4 for 5 min of standard sample (Target A, Mo(34.1%) with a Co-Al neutron flux monitor, were 0.534 mCi/mg.Mo and 123.35 dps/mg.Co-Al at EOB. The Mo-99 radioactivity of the sample was calculated from the following equation :

Radioactivity of Mo-99 = 0.534 x Weight of target (mg) x Mo(%) of target/100 x Co-60 radioactivity of Co-Al neutron flux monitor (dps/mg.Co-Al)/123.35.

Preparation of Generator.

The chromatographic column (20mm x 100mm : G4 filter) was prepared using neutral activated alumina. The irradiated gel is loaded in a G-4 type of chromatographic column with glass frit. The column is previously packed with neutral alumina (Al_2O_3) to a height of 5 cm and Tc-99m is eluted by 0.9% NaCl solution.The irradiated target was put on top of the alumina bed and then the column was eluted with 0.9% sodium chloride solution at the rate of 2.5 ml/min. The particle size of the target before irradiation is chosen in the range of 3-5 mm. Smaller particles requires much more time to elute Tc-99m from the column. The elution is done by external pressure and the rate of elution is maintained to 2.5 ml per minute. Higher elution rate may produce channel in the alumina and there would be chance of Mo-99 breakthrough in Tc-99m..

Measurement of Radioactivity.

A calibrated high-purity Ge detector equipped with a 4096-channel pulse-height analyzer was used for the measurement of radionuclidic purity. The activity of Tc-99m was measured in a radioisotope dose calibrator (Aloka IGC-3).

Expt. No. 1.

Target A. Two samples (a,b) were irradiated in this experiment. After irradiation the samples were cooled for 72 hrs and loaded in the columns. Elutions were taken with 0.9% NaCl solution. The first elution with 10 ml saline was discarded. The 2nd and 3rd elutions were collected and measured for Tc-99m.

a) Sample wt. 2.205 g, pH 5.5, dried at 70°C for 6 hrs.The Mo-99 radioactivity at the end of irradiation was 330 μCi.The sample was eluted for two days but discontinued for low yield.

Table 1. Elution of Tc-99m by column chromatography.

Elution	Mo-99(μCi)	Tc-99m(μCi)	Measured Tc-99m(μCi)	% Yield
1st day	155	146	81	52
2nd day	120	114	68	59

b) Sample wt. 2.335 g, pH 5.5, dried at 70°C for 24 hrs.The Mo-99 radioactivity at the end of irradiation was 321 μCi.

Table 2. Elution of Tc-99m by column chromatography.

Elution	Mo-99(μCi)	Tc-99m(μCi)	Measured Tc-99m(μCi)	% Yield
1st day	151	141	118	84
2nd day	117	111	96	87
3rd day	91	86	75	87
4th day	71	67	57	85
5th day	55	52	46	88

Target C. One sample (a) was irradiated in this experiment.

a) Sample wt. 2.237 g, pH 7.5, dried at 70°C for 6 hrs.The Mo-99 activity at the end of irradiation was 178 μCi.

Table 3. Elution of Tc-99m by column chromatography.

Elution	Mo-99(μCi)	Tc-99m(μCi)	Measured Tc-99m(μCi)	% Yield
1st day	83	78	55	70
2nd day	64	61	40	66
3rd day	50	47	31	65
4th day	39	37	27	73
5th day	30	29	21	72

Expt. No. 2.

Target A.

Three samples (a,b,c) were irradiated in this experiment. Each column was eluted for three times. Elution volume was lowered to 5 ml which was 10 ml in Expt.No. 1. Eluent was 0.9% NaCl + 1 mg $NaNO_3$/ml of 0.9% NaCl soln. First 5 ml of the eluent was used for pretreatment of the hard sample and was discarded. Second and third elutions were collected and measured.

a) Sample wt. 2.007 g, pH 2.75, dried at 70°C for 6 hrs.The Mo-99 activity at the end of irradiation was 256 μCi.

Table 4. Elution of Tc-99m by column chromatography.

Elution	Mo-99(μCi)	Tc-99m(μCi)	Measured Tc-99m(μCi)	% Yield
1st day	121	114	88	77
2nd day	94	89	64	72
3rd day	73	69	54	78
4th day	56	54	43	79
5th day	44	41	34	82

b) Sample wt. 2.100 g, pH 2.75, dried at 70°C for 24 hrs.The Mo-99 activity at the end of irradiation was 292 μCi.

Table 5. Elution of Tc-99m by column chromatography.

Elution	Mo-99(μCi)	Tc-99m(μCi)	Measured Tc-99m(μCi)	% Yield
1st day	137	127	88	68
2nd day	106	101	77	76
3rd day	82	78	64	82
4th day	64	61	51	84
5th day	50	48	42	88

c) Sample wt. 2.008 g, pH 5.5, dried at 70°C for 48 hrs.The Mo-99 activity at the end of irradiation was 341 μCi.This sample was pretreated by the eluent for 10 min before elution.

Table 6. Elution of Tc-99m by column chromatography.

Elution	Mo-99(μCi)	Tc-99m(μCi)	Measured Tc-99m(μCi)	% Yield
1st day	161	151	110	73
2nd day	125	119	87	73
3rd day	97	92	67	73
4th day	75	72	53	74
5th day	58	55	41	75

Expt. No. 3.

Target A and Target C. Two samples were irradiated in this experiment. One from target A (a) and the other from target C (b). Eluent was 0.9% NaCl solution. Both the samples were pretreated with saline for 5 min before actual elution.

a) Target A. Sample wt. 2.003 g, pH 2.75, dried at 70°C for 48 hrs. The Mo-99 activity was 359 μCi at the end of irradiation.

Table 7. Elution of Tc-99m by column chromatography.

Elution	Mo-99(μCi)	Tc-99m(μCi)	Measured Tc-99m(μCi)	% Yield
1st day	169	158	109	69
2nd day	130	124	90	72
3rd day	101	96	74	77
4th day	78	74	59	80
5th day	61	58	45	78

b) Target C. Sample wt. 2.015 g, pH 4.8, dried at 70°C for 12 hrs. The Mo-99 activity at the end of irradiation was 188 μCi. The ratio of Mo, Zr and V in this target was 1.35:1.0:0.25.

Table 8. Elution of Tc-99m by column chromatography.

Elution	Mo-99(μCi)	Tc-99m(μCi)	Measured Tc-99m(μCi)	% Yield
1st day	88	83	68	82
2nd day	71	67	69	Mo-99 break through

Expt. No.4.

Target B. Two samples were irradiated in this experiment (a,b).

a) Sample wt. 2.021 g, pH 3.7, dried at 70°C for 12 hrs. The Mo-99 activity at the end of irradiation was 259 μCi. Eluent was physiological saline. The sample was pretreated for 5 min before elution.

Table. 9. Elution of Tc-99m by column chromatography.

Elution	Mo-99(μCi)	Tc-99m(μCi)	Measured Tc-99m(μCi)	% Yield
1st day	148	138	115	83
2nd day	115	109	84	77
3rd day	89	85	67	79
4th day	69	66	48	74
5th day	54	51	39	77

b) Sample wt. 2.013 g, pH 3.7, dried at 70°C for 24 hrs. The Mo-99 activity at the end of irradiation was 258 μCi. Eluent was physiological saline. The sample was pretreated for 10 min before elution.

Table 10. Elution of Tc-99m by column chromatography.

Elution	Mo-99(μCi)	Tc-99m(μCi)	Measured Tc-99m(μCi)	% Yield
1st day	146	137	104	76
2nd day	113	108	86	79
3rd day	88	84	66	79
4th day	68	65	45	69
5th day	53	50	31	62

Expt. No. 5.

Target C. One sample was irradiated in this experiment (a).

a) Sample wt. 2.033 g, pH 6.25, dried at 70°C for 12 hrs. The Mo-99 activity at the end of irradiation was 185 μCi. The ratio of Mo, Zr and V in this sample was 1.35:1.25:0.25. The sample was pretreated for 15 min with 5 ml of saline.

Table 11. Elution of Tc-99m by column chromatography.

Elution	Mo-99(μCi)	Tc-99m(μCi)	Measured Tc-99m(μCi)	% Yield
1st day	87	81	54	67
2nd day	67	64	52	81
3rd day	52	49	40	81
4th day	40	38	31	82
5th day	31	30	24	80

3. RESULTS AND DISCUSSION.

Five experiments (irradiations) have been carried out with the new targets. The experimental results are shown in the tables above. The radionuclidic purity was found quite satisfactory and the radiochemical purity was > 99%. Neutral alumina is taken in the column as because no elution is possible through acidic alumina and poor elution is obtained from basic alumina. The pH of the eluted Tc-99m is found 6-7. The radionuclidic and radiochemical purity of the produced Tc-99m were checked by gamma spectrometry and paper chromatography

Samples at different pH, drying conditions are irradiated to see the effect of pH and water content in the target on elution efficiency of Tc-99m. It has been observed that pH of the sample, drying conditions and water content in the target have definite role on elution efficiency of Tc-99m in this type of column chromatographic generator.

The principle of elution of Tc-99m from this type of target is the diffusion of Tc-99m through the surface of the target. So, the surface characteristics of the newly developed targets are very important. Because the easy diffusibility of Tc-99m through the target surface depends on the pH and the drying conditions of the target.

Around pH 2-4, the surface becomes hard and less penetrating to Tc-99m (difficult to diffuse Tc-99m) with saline. Also the same is true if the target is dried for more than 24 hrs or so at 70°C.

The targets can be stored for long time by drying them at 70°C for 6 hrs after room temperature drying. But before irradiation they have to be dried at 70°C for the desired duration.

It is observed that targets of lower pH (2-4) are harder than those of pH (5-7). The samples having lower p^H need about 15 minutes of pretreatment with saline before the actual elution of Tc-99m. On the other hand, samples having higher pH need only 5 minutes of pretreatment before the actual elution.

However, the lower pH samples after adding saline remains in the same (3-5 mm) crystalline size, but samples of higher pH break to smaller pieces by the addition of saline for elution. Nevertheless, the sample having pH 5.5 and dried at 70°C for 24 hrs (Target A) is giving the best performance. The other sample, Target C (expt.5) having pH 6.5 and dried at 70°C for 12 hrs also gives good result.

The results obtained from sample a) and b) of expt. 2 are interesting. The % yield of Tc-99m is found to increase at the end of the week which is not usually the case in commercially available Tc-99m chromatographic generators. This sample could also be a useful target.

The role of vanadium in the target is seemed to enhance the elution efficiency by easing the diffusion of Tc-99m through the target surface. Also by the addition of small quantity of vanadium, the amount of Mo content in the target might have increased to 33 - 34 %.

4. CONCLUSION.

The elution efficiencies obtained from the new targets containing Mo, Ti and V are seemed very much promising to produce Tc-99m by column chromatography from low specific activity of Mo-99. Though the results are preliminary, the new target prepared from MoO_3, $TiCl_4$ and NH_4VO_3 in the ratio 1.01:1.25:0.125 having the pH 5.5 and dried at 70°C for 24 hrs could be an important target.

The target from Mo, Ti and V is sufficiently porous to permit ready elution of Tc-99m and which is stable under irradiation and elution conditions. The conditions of preparation are critical, particularly the pH, drying temperature and duration of drying.

The incorporation of vanadium in the gel targets has not been done by anyone before. The results obtained so far are found comparable to some literatures (15,16) and sometimes even higher. Radiopharmaceuticals have not yet been prepared from this Tc-99m.

Subject to satisfactory performance under high activity of Mo-99, the new gel generators could be an impotant alternative to fission based Mo-99 generators.

5. REFERENCES.

1. L. Szirtes. Izotoptechnika 18 (1975) 5/18, N. S. A. 31 (1975) No. 32668.
2. M. Radwan, K. Zelany, S. Myczkoski. Rap. Inst. Fiz. Tech. Jad. AGH 1976, INT - 92 - 1, pp 71/92, C. A. 89 (1978) No. 222776, INT - 92 - 1 (1976) 71/92, Prog. Nucl. Tech. Appl. Sci. Ind. Proc. Polish Symp., Zakopane 1975, pp 71/92, INS Atomindex 8 (1977) No. 281514.
3. Boyd, R. E., Hetherington, E. L. R., Moore, P. W. " Radio-nuclide Generator Technology ". Radiopharmaceuticals and Labelled Compounds Conference, Tokyo, October 22 - 26, 1984, IAEA, Page 79.
4. The Special Position of Tc-99m in Nuclear Medicine, Radionuclides Production, Vol. II, Frank Helus, CRC Press, Chapter 4, 1983, Page 125.
5. Lathrop, K. A. Preparation and Control of Tc-99m Radiopharmaceuticals. Radiopharmaceuticals from Generator Produced Radionuclides. Proc. Panel, Vienna 1970, IAEA, Vienna (1971) 39.
6. Mani, R. S., Narashimhan, D. V. S. Development of Kits for Short-Lived Generator Produced Radioisotopes. Radiopharmaceuticals and Labelled Compounds, IAEA and WHO, Copenhagen, 1973, 141.
7. Boyd, R. E., Robson, J. The Production of Tc-99m. Radioisotope Production (Rep. Study Group Mrg. Lucas Heights, Australia, June 1968), IAEA - 110, IAEA, Vienna (1969) 187.

8. Boyd, R. E. Radiopharm. Labelled Compounds, Proc., Copenhagen 1973, Vol. 1, pp 3/26; C. A. 81 (1974) No. 98188.
9. K. Motojima, M. Tanase. Intern. J. Appl. Radiat. Isotop. 28 (1977) 485/9.
10. Zsinka, L., Kern, J. New Portable Generator For the Sublimation of Tc-99m. Radiopharmaceuticals and Labelled Compounds, October 22 - 26, Tokyo, 1984, Page 95.
11. Zsinka, L. Tc-99m Sublimation Generators. Invited Review Paper at the Seminar on Radionuclide Generator Technology, October 13-17, 1986, IAEA, Vienna.
12. Evans, J. V., Moore, P. W. et al. Proceedings of World Congress of Nuclear Medicine and Biology, Held in Paris, August, 1982, p 1592.
13. Ramamoorthy, N., Vanaja, P. et al. Studies on the Preparation of Tc-99m Generators Based on Neutron Irradiation of Metallic Molybdate. International Symposium on Artificial Radioactivity, Pune, India, January, 1985.
14. Mani, R. S., Vanaja, P., et al. Development of a Gel Type Generator for Tc-99m. IAEA's Research Co-ordination Meeting, Bangkok, Thailand, November, 1985.
15. J. V. Evans, P. W. Moore, M. E. Shying and J. M. Sodeau. Zirconium Molybdate Gel as a Generator for Tc-99m - The Concept and its Evaluation. Int. J. Radiat. Isot. Vol.38, No. 1, pp 19-23, 1987.
16. P. W. Moore, M. E. Shying et al. Zirconium Molybdate Gel as a Generator for Tc-99m - High Activity Generators. Int. J. Appl. Radiat. Isot. Vol. 38, No. 1, pp 25-29, 1987.

AU9817390

TDPAC–Studies of Macrocyclic Ag–Thiocrownethers: Molecular Stability of Radiopharmaceuticals

B. CTORTECKA, W. TRÖGER, and T. BUTZ
Fakultät für Physik und Geowissenschaften, Universität Leipzig
Linnéstraße 5, D-04103 Leipzig, Germany

R. ALBERTO, D. ANGST, and P.A. SCHUBIGER
Radiopharmazie, Paul-Scherrer-Institut, Villigen, Switzerland

SUMMARY. The nuclear quadrupole interaction of $^{111}Ag(\beta^-)^{111}Cd$ monitored by time differential perturbed angular correlation of γ–rays was employed to perform coordination studies of $[Ag]^+$ complexes with macrocyclic thiocrownethers. These studies were performed with crystallized complexes as well as with frozen solutions of the dissolved complexes at picomolar $[Ag]^+$ concentrations. Dissolving the crystallized complexes leads to changes of the coordination sphere of the bound metal ion. The ring size of the macrocyclic thiocrowns as well as the the pH influence the coordination and the chelating ability of $[Ag]^+$. These studies aim at a rational design of highly inert $[Ag]^+$ complexes to allow the application of ^{111}Ag in the targeted radioimmunotherapy of cancer.

1. Introduction

Radioactive isotopes (e.g. ^{32}P, ^{67}Cu etc.) are used for systemic targeted radiotherapy of a disease (mostly cancer) in which a radioisotope is selectively taken up due to the high affinity of either the radionuclide or its carrier to the affected tissue. Pure or almost pure β^- emitters are most widely used due to the convenient range of β^- radiation in tissue (few mm) which allows to deposit most or even all radiation to the treated tissue [1,2]. Therefore, ^{111}Ag ($\tau_{1/2}$ = 7.5 d) which decays with 93% probability via a β^--decay to the groundstate of ^{111}Cd (see figure 1) would be a useful therapeutic isotope [2]. Since ^{111}Ag exhibits no tissue selectivity, it has to be conjugated to a carrier such as peptides, hormones or antibodies which can be used for tumour targeting. The carriers are labelled with a chelating agent containing the radioisotope. In the case of ^{111}Ag derivatized hexadendate macrocyclic thiocrownethers are used as chelating ligands which can be coupled to antibodies [3]. Structural information on the metal coordination in the concentration regime of trace amounts used for clinical application is needed to optimize rationally the molecular stabiltity of the radiopharmaceutical. In order to obtain structural information at these extremely low concentration levels the nuclear quadrupole interaction (NQI) of the nuclear probe $^{111}Ag(\beta^-)^{111}Cd$ determined via time differential perturbed angular correlation (TDPAC) of γ–rays can be used. Here, we report on our coordination studies of the $[Ag]^+$ complexes with the macrocyclic thiocrownethers (18S6), (18S6-OH), (19S6-OH), and (20S6-OH)(see figure 2) by ^{111}Ag–TDPAC. These results have to be compared with available X-ray structures of the crystallized complexes (see figure 2).

2. Experimental

2.1 TDPAC

The ^{111}Ag ($\tau_{1/2}$ = 7.5 d) transmutes via a β^-decay into ^{111}Cd and feeds the 95–247 keV γ–γ–cascade used for the TDPAC. This cascade is populated by $\approx$ 0.2 % of all decays only (see figure 1)[4].

For randomly oriented nuclear spins - as it is the case in the present studies - each γ-quantum is emitted isotropically. However, the coincidence countrate of the first γ-quantum (γ_1 = 95 keV) and the second γ–quantum (γ_2 = 247 keV)is anisotropic, i.e. it depends on the angle between both emitted γ-quanta. The reason for this anisotropy is the conservation of angular momentum for each of the decay processes. The intermediate level (I = 5/2) of the γ-γ-cascade has

a half-life of $\tau_{1/2} = 85(5)$ ns and a nuclear quadrupole moment of $Q = 0.83(13)$ barn [5]. If the nucleus interacts via its quadrupole moment with an electric field gradient, the angular correlation between both γ-rays is periodically perturbed due to the nuclear spin precession. Hence, the time resolved coincidence countrate can be written as [6]:

$$W(\vec{k_1}, \vec{k_2}, t) \sim e^{t/\tau_N}(1 + A_{22}G_{22}(t) \cdot P_2(\cos\theta) + \ldots), \quad (1)$$

Here, the vectors $\vec{k_1}$ and $\vec{k_2}$ are the emission directions of γ_1 and γ_2 with θ denoting the angle between them, τ_N is the nuclear lifetime ($\tau_N = \tau_{1/2}/ln2$), A_{22} denotes the anisotropy ($A_{22} = 13$ % [7]), $G_{22}(t)$ is the perturbation function and P_2 is a Legendre polynomial. The perturbation function for pure NQI and $I = 5/2$ can be written as [8]:

$$G_{22}(t) = \sum_{i=0}^{3} f_i(\eta)\cos(\omega_i(\eta)t). \quad (2)$$

Here, $f_i(\eta)$ are intensities which depend on the asymmetry parameter η of the electric field gradient tensor (EFG) and which have well-defined values for a given η. The asymmetry parameter is defined as:

$$\eta = (V_{xx} - V_{yy})/V_{zz}, \quad |V_{xx}| < |V_{yy}| < |V_{zz}| \quad (3)$$

where V_{ii} denote the EFG-tensor components in the principal coordinate system. The frequencies $\omega_i(\eta)$ are related to the energy splittings between the sublevels with $m = \pm 5/2, \pm 3/2, \pm 1/2$. The connection to $\nu_Q = eQV_{zz}/h$, the nuclear quadrupole coupling constant, is given as follows [8]:

$$\nu_Q = \frac{10\omega_1}{\sqrt{3}\alpha \cdot \pi \sin\frac{\arccos\beta}{3}}$$
$$\text{with } \alpha = \sqrt{\tfrac{28}{3}(3+\eta^2)} \text{ and } \beta = \tfrac{80(1-\eta^2)}{\alpha^3} \quad (4)$$

Note, that $\omega_3 = \omega_1 + \omega_2$ by definition. Hence, there are two parameters (ω_1, η) to be extracted for a unique probe geometry. In the case of a superposition of several probe geometries, each site is characterized by its pair of (ω_1, η). Additionally, a Lorentzian frequency distribution δ due to slightly inequivalent probe geometries is allowed for. The populations of different sites are treated as adjustable parameters. In practice, solid angle correction factors reduce A_{22} (also treated as a free parameter). Furthermore, the finite time resolution of the spectrometer of about 850 ps FWHM has to be taken into account. Since the γ–γ–cascade is populated by 0.2 % of all decays only, an extremely efficient spectrometer such as the TDPAC-Camera [9] is required.

2.1. Isotope and Sample Preparation

The extraction of ^{111}Ag from neutron irradiated natural Pd is described in detail in [10]. The main contamination is the stable silver isotope ^{109}Ag (10 - 100 times the amount of ^{111}Ag). On the average $\approx$ 100 MBq are obtained from 100 mg irradiated natural Pd. For the preparation of the macrocyclic thiocrownether ligands see [3,11].

For the experiments described here, a ligand solution of methanol (ligand concentration 10 mM) was incubated first with ^{111}Ag solution ($\approx$ 10 MBq, volume $\approx$ 300 μl) and then stoichiometric amounts of [Ag][CF_3SO_3] or [Ag][tosylat] as carrier were added. After 30 to 90 minutes incubation time, small crystals of the Ag complexes were obtained within a few days by slow diffusion of diethylether into methanol [3]. The sample temperatures during the TDPAC measurements are given in table 1. After the TDPAC measurement of the polycrystalline [Ag(18S6-OH)][CF_3SO_3] these crystals were dissolved in about 500 μl of dimethylsulfoxide (DMSO) and the frozen solution was measured at −51°C.

In the case of [Ag(18S6)]$^+$ 50 μl of a ligand solution (tetrahydrofurane (THF), ligand concentration 3 mM) was given to 100 μl ^{111}Ag solution of HNO_3 (0.01 M) at pH = 0.5, for pH = 7 the HNO_3 solution was neutralized by adding $NaHCO_3$ solution (1 M). In both cases **no** carrier was added (n.c.a.).

3. Results

Table 1 summarizes the NQI parameters yielded by a least squares fitting analysis of the performed TDPAC experiments presented in figures 2 – 5.

Figure 3 shows the observed TDPAC time spectra and their Cosine transforms of crystallized thiocrownethers with varying ring-size: [Ag(18S6-OH)][CF_3SO_3], [Ag(19S6-OH)][tosylat], and [Ag(20S6-OH)][CF_3SO_3]. Only the [Ag(18S6-OH)][CF_3SO_3] shows a unique NQI with negligible frequency distribution indicating that there is one distinct coordination of the $[Ag]^+$ ion. In the case of [Ag(20S6-OH)][CF_3SO_3], two different NQIs with frequency distributions are observed. Here, $[Ag]^+$ is coordinated in two main geometries which exhibit a certain site variability. The medium sized [Ag(19S6-OH)][tosylat] shows only one main geometry with a quite high site variability as indicated by the considerable frequency distribution of ≈ 7 %.

In figure 4, the TDPAC spectra of the crystallized [Ag(18S6-OH)][CF_3SO_3] complex together with the spectra of the in complex dissolved in THF are shown. In order to avoid reorientational motions of the dissolved complex the solution was frozen at -51 °C; the crystallized complex was measured at the same temperature to facilitate a comparison of the data. Both spectra show a unique NQI within the instrumental line width of ≈ 20 Mrad/s. Dissolving the crystallized complex leads to a significantly lower frequency ω_1 and lower asymmetry parameter η. Obviously, this reflects the influence of the counterions.

In figure 5, the TDPAC spectra of the complexation of $[Ag]^+$ by the ligand (18S6) at pH = 0.5 and pH =7 in frozen THF are shown. No carrier was added (n.c.a.). Compared to the TDPAC time spectra presented above these spectra show a reduced amplitude (≈ 1.5 % at pH = 7; ≈ 3.5 % at pH = 0.5) of the signal and a baseline shifted to negative values, especially at pH = 7. These effects are due to an incomplete complexation of the $[Ag]^+$ ions. Assuming an effective anisotropy of ≈ 5 % due to our sample detector geometry, at pH = 7 only about 1/3 and at pH = 0.5 about 2/3 of the $[Ag]^+$ ions are complexed by the ligand. This illustrates drastically the influence of the pH on the $[Ag]^+$ complexation. It should be mentioned that at pH = 0.5 the NQI parameters of the $[Ag(18S6)]^+$ are almost identical to those of the dissolved [Ag(18S6-OH)][CF_3SO_3] complex.

4. Discussion

It has to be pointed out that in the decay of ^{111}Ag a β^- decay precedes the γ–γ–cascade used for TDPAC experiments. Therefore, these experiments have to be discussed with respect to the response of the coordination sphere to the nuclear transmutation $[^{111}Ag]^+ \rightarrow [^{111}Cd]^{2+}$ and the concomitant β^--recoil ($E_{recoil,max} \approx 6$ eV). The TDPAC spectra of $[Ag(18S6\text{-}OH)]^+$ and $[Ag(18S6)]^+$ complexes show no line broadening indicating that there are no after-effects due to the nuclear decay of ^{111}Ag. Obviously, the reorganisation of the electron shell is completed before the TDPAC measurement takes place and – furthermore – the β^- recoil is not sufficient to kick out the $[^{111}Cd]^{2+}$ of its coordination sphere. It has to be noted that despite of the nuclear transmutation and the valence change, both isotopes - $[^{111}Ag]^+$ and $^{111}Cd^{2+}$ – exhibit the same electron configuration $[Kr]4d^{10}$. To withstand the β^- recoil is a rigorous test for the stability of the coordination sphere. Evidently, the (18S6)-ligand (with and without hydroxyl group) complexes the metal best compared to (19S6-OH) and (20S6-OH) ligand.
Plotting the observed NQI parameter in a so-called Czjzek plot [12], which is essentially a linear plot of one EFG component (V_{xx}) versus a linear combination of V_{zz} and V_{xx} (see figure 6), reveals that the NQI parameters are found approximately on straight lines of constant V_{zz} which can be assigned to octahedral and tetrahedral coordination geometries.

This site assignment is based on the fact that coordination geometries with higher coordination numbers tend to have lower V_{zz}–values and on X-ray studies of the crystallized complexes [3]. Due to the frequency distribution of octahedral as well as of tetrahedral sites a certain variability of their coordination sphere has to be presumed. In [3],

it is suspected from $^{1}H/^{13}C$ NMR solution experiments that the $[Ag]^+$ coordination spheres in $[Ag(19S6\text{-}OH)]^+$ and $[Ag(20S6\text{-}OH)]^+$ switch between six–fold and four–fold binding ("fluxional behaviour"). Whether the observed frequency distribution in the TDPAC experiments arises from such a fluxionality of the metal sites has to be clarified by temperature dependent TDPAC experiments.

The comparison of the crystallized and dissolved $[Ag(18S6\text{-}OH)][CF_3SO_3]$ complex elucidates the influence of the counterions of the metal coordination sphere. The dissolved complex displays a lower frequency and a considerable lower asymmetry parameter indicating a somewhat more relaxed coordination geometry compared to the crystalline state. TDPAC studies on the [Ag(18S6-OH)] ligand (data not shown) with $[CF_3SO_3]^-$ and [tosylat] as counterions proved unambiguously that counterions may have a quite important influence on the coordination structure of the metal center. The same holds true for the hydroxyl group: whereas X-ray crystallographic data on $[Ag(20S6)\text{-}OH][BF_4]$ show two distinct coordinations - an octahedral and a tetrahedral one - the TDPAC spectra of $[Ag(20S6)][BF_4]$ (data not shown) display an unperturbed spectrum with no indication of any distinct metal coordination sphere.

Last but not least, a significant pH dependence of the complexation of $[Ag]^+$ by the ligand (18S6) was observed in the experiment where no carrier was added. Having in mind the experiments with the dissolved $[Ag(18S6\text{-}OH)][CF_3SO_3]$ complex, there are two explanations for this effect: (i) as already suspected, the hydroxyl group has some influence on the metal coordination and therefore on the chelating ability of the ligand, too; (ii) unintentional side reactions are competing with the complexation of $[Ag]^+$. In any case, the final reason for this behaviour is essential to create reliable radiopharmaceutical kits for clinical applications.

Summing up, we have proved that TDPAC with the nuclear probe $^{111}Ag(\beta^-)^{111}Cd$ is well suited to achieve a better understanding of the stability of $[Ag]^+$ complexes even with trace amounts of $[Ag]^+$. Whereas conventional analytical methods like thin layer chromatography, high performance liquid chromatography, or even capillary zone electrophoresis just give the percentage of bound or unbound radioisotope, TDPAC additionally elucidates the molecular origin of this behaviour.

These studies have now to be extended using body liquids as solvents in order to probe the molecular integrity as closely as possible to in-vivo conditions.

Acknowledgement. We are very grateful for the technical support of Dr. M. Rösseler and his group during the measuring times at the Control Area (Permoserstraße 15, Bld. 4.0, 04318 Leipzig) of the Leipzig University.

References

[1] C.A. Hoefnagel, *Eur. J. Nucl. Med.* 18 (1991) 408-431

[2] P.A. Schubiger, R. Alberto, and A. Smith, *Bioconjugate Chem.* 7(1996)165-179

[3] R. Alberto, W. Nef, A. Smith, Th.A. Kaden, M. Neuburger, M. Zehnder, A. Frey, U. Abram, and P.A.Schubiger, Inorg. Chem. 35 (1996) 3420 and references therein

[4] C.M. Lederer, J.M. Hollander, I. Perlman, "Table of Isotopes", John Wiley & Sons, New York, London, Sydney, 1968

[5] P. Herzog, K. Freitag, M. Reuschenbach, H. Walitzki, *Z. Phys.* (1980) 13

[6] T. Butz, *Z. Naturf.* 51a (1996) 396–410 and references therein.

[7] H. Hass and D.A. Shirley, *J. Chem. Phys.* 58 (1973) 3339

[8] T. Butz,*Hyp. Int.* 52 (1989) 189-228

[9] T. Butz, S. Saibene, Th. Fraenzke, and M. Weber, *Nucl. Inst. Meth.* A284 (1989) 417

[10] R. Alberto, P. Bläuenstein, I. Novak-Hofer, A. Smith, and P.A. Schubiger *App. Radiat. Isot.* 43 (1992) 869-872,

[11] A.J. Blake, R.O. Gould, A.J. Holder, T.I. Hyde, M. Schröder, *Polyhedron* 8 (1989) 513-518

[12] T. Butz, M. Ceolin, P. Ganal, P. Schmidt, M.A. Taylor, and W. Tröger, *Pysica Scripta* 54 (1996) 234–239

Ag thiocrownether	ω_1 [Mrad/s]	η	δ [%]	V_{zz} [10^{21} V/m^2]	sample no.
[Ag(18S6-OH)][CF_3SO_3] polycrystalline sample, 22°	166.9(2)	0.399(2)	0.3(1)	7.60	1
[Ag(19S6-OH)][tosylat], polycrystalline sample, 22°	209.5(8)	0.536(7)	6.7(5)	8.68	2
[Ag(20S6-OH)][CF_3SO_3], polycrystalline sample, 24°C,					
1^{st} site, pop.: 45(14)%	180(2)	0.58(2)	4.5(6)	7.24	3'
2^{nd} site, pop.: 55(14)%	231(2)	0.66(1)	3.7(7)	8.78	3"
[Ag(18S6-OH)][CF_3SO_3], DMSO, -51°C	149.5(5)	0.186(9)	0 fixed*	7.62	4
[Ag(18S6-OH)][CF_3SO_3], polycrystalline sample, -51°C	165.6(3)	0.399(3)	0 fixed*	7.55	5
$[Ag(18S6)]^+$, n.c.a., THF, -70°C, pH=7.0	174(3)	0.50(3)	4(2)	7.41	6
$[Ag(18S6)]^+$, n.c.a., THF, -70°C, pH=0.5	146(1)	0.12(3)	3.3(8)	7.60	7

* kept fixed during the fit

Table 1: NQI parameters of the investigated $[Ag]^+$ thiocrownether complexes.

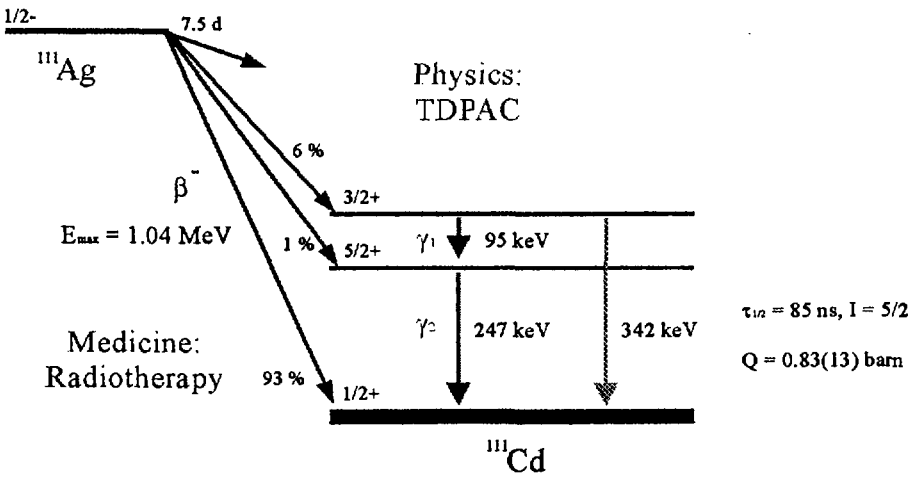

Figure 1: Simplified decay scheme of ^{111}Ag [4].

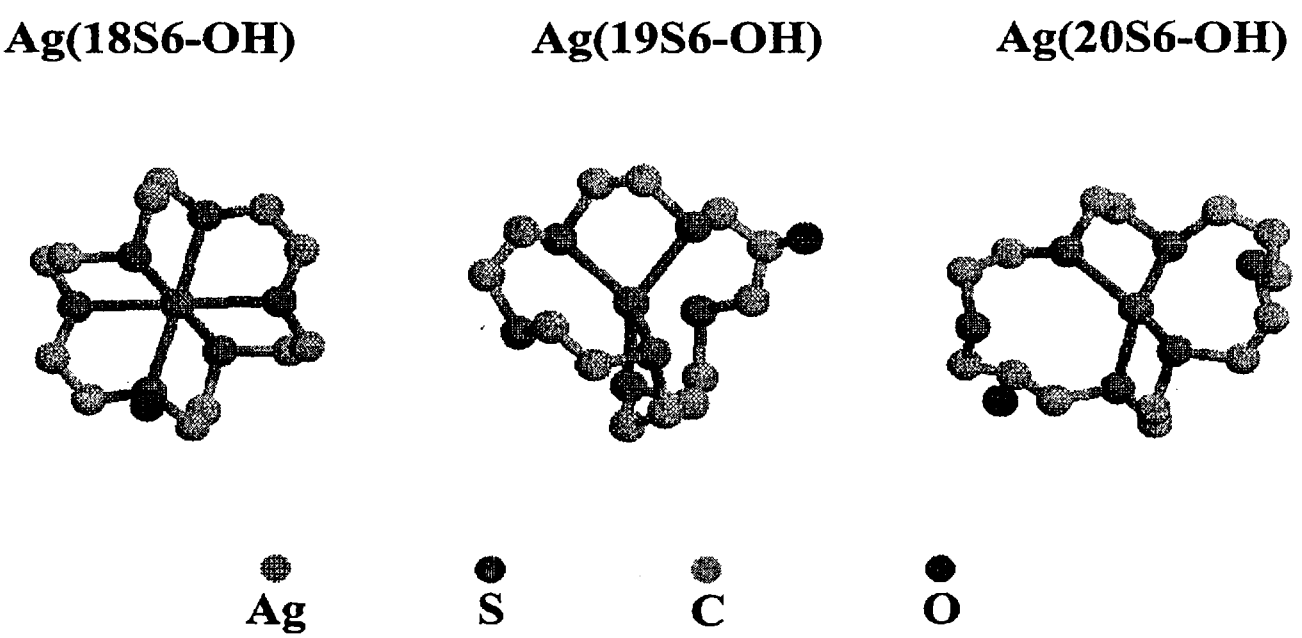

Figure 2: $[Ag]^+$ thiocrownether complexes: $[Ag(18S6\text{-}OH)]^+$ (left), $[Ag(19S6\text{-}OH)]^+$(middle), $[Ag(20S6\text{-}OH)]^+$(right) [3]. Only the $[Ag]^+$ centers without the hydrogen atoms and without the counterions are shown. The OH-group can be used as linker to a convenient tumour seeking agent.

141 89/51

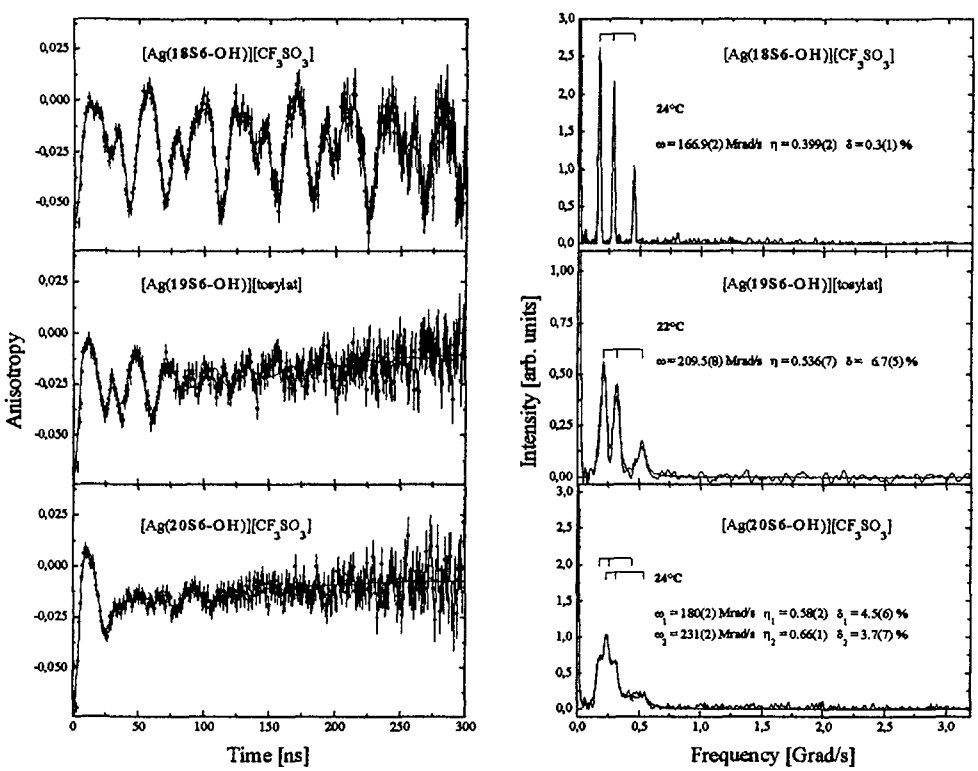

Figure 3: TDPAC time spectra (left) and their Cosine transforms (right) of $[Ag]^+$ crown thioethers with different ring sizes (polycrystalline samples).

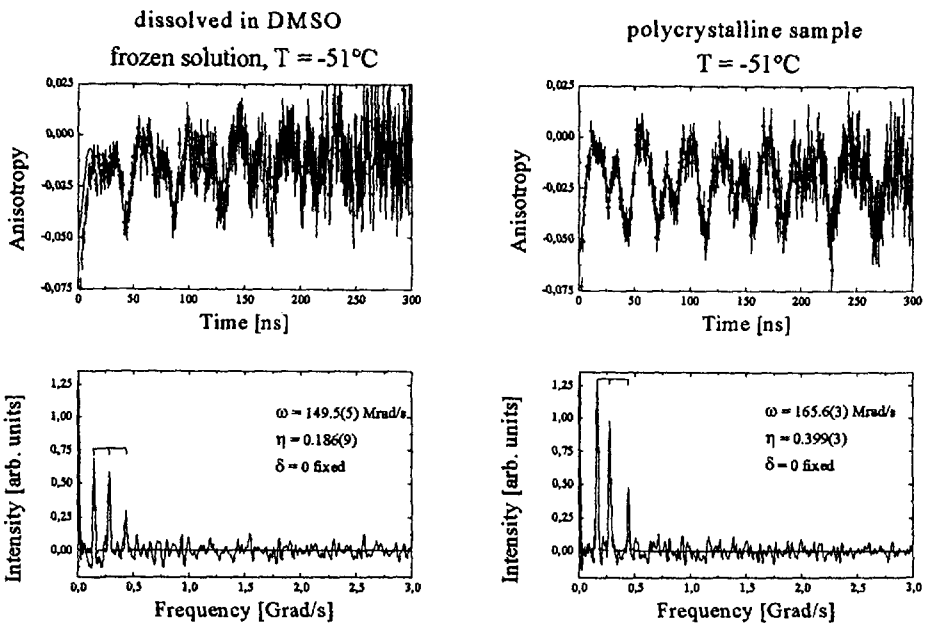

Figure 4: TDPAC time spectra (top) and their Cosine transforms (bottom) of [^{111}Ag(18S6-OH)] [CF_3SO_3] in frozen DMSO solution (left) and in the polycrystalline state (right).

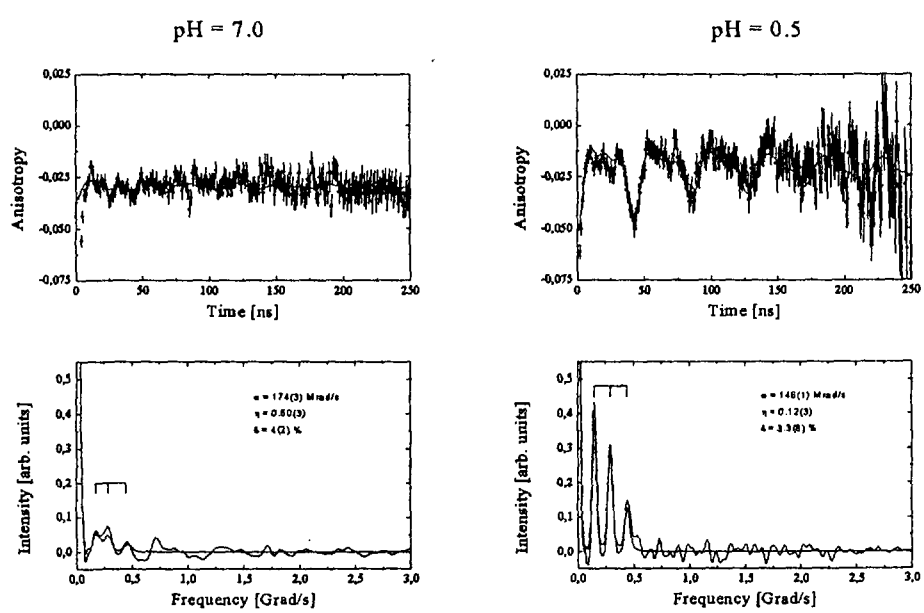

Figure 5: TDPAC time spectra (top) and their Cosine transforms (bottom) n.c.a [^{111}Ag(18S6-OH)]$^+$ at pH = 7 (left) and pH = 0.5 (right) in frozen DMSO solution (T = -70°).

89/51

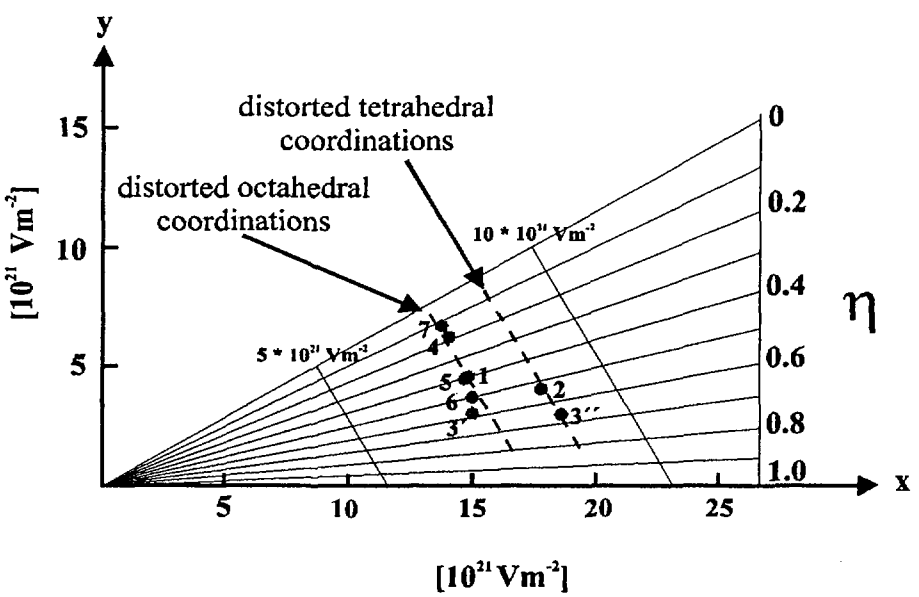

Figure 6: Czjzek diagram (abscissa: $x = 2|2V_{zz} + V_{xx}|/\sqrt{3}$, ordinate: $y = -2V_{xx}$, units: 10^{21} Vm^{-2}) of the investigated macrocyclic $[Ag]^+$-thiocrownethers. For the sample numbers and the corresponding NQI parameter see table 1. The straight lines for V_{zz} = const. (V_{zz} = $5 \cdot 10^{21}$ Vm^{-2}, $10 \cdot 10^{21}$ Vm^{-2}) and for η = const. ($\eta = 0,\ 0.1,\ \ldots,\ 1$) are indicated.

Radiotracers for In Vivo PET Imaging of Acetylcholinesterase in the Brain

M.R. KILBOURN, S.E. SNYDER, T. NGUYEN, R.A. KOEPPE, K.A. FREY, AND D.E. KUHL

Division of Nuclear Medicine, Department of Internal Medicine, University of Michigan Medical School, Ann Arbor, MI, U.S.A.

SUMMARY. As potential in vivo imaging agents for the enzyme acetylcholinesterase (AChE), a series of N-([^{11}C]methyl)-4-piperidinol esters and N-([^{11}C]methyl)-nipecotic acid esters have synthesized and examined in vivo in mouse and monkey brain. The radiolabeled nipecotic esters are not cleaved in vivo by brain enzymes. The N-([^{11}C]methyl)-4-piperidinol esters (acetyl, propionyl and isobutyryl) are cleaved in brain in proportion to regional concentrations of AChE, with the metabolic product N-([^{11}C]methyl)-4-piperidinol trapped in the tissues. The esters are also cleaved by blood AChE, producing low to zero blood levels at short periods (40-60 min) after radiotracer injection. Regional hydrolysis rates (combined forward rate constants, k_3) for these radiotracers can be calculated using a simplified analysis of tissue-time activity curves, without a need for determining metabolite-corrected plasma levels. These radiolabeled esters form a new approach to the measurement of in vivo function of AChE in the mammalian brain.

INTRODUCTION

Acetycholinesterase (AChE) functions as the primary mechanism for degradation of the neurotransmitter acetylcholine. An extremely fast and efficient enzyme, acetylcholinesterase is an integral part of the cholinergic system, and has thus been the target of insecticides, chemical warfare agents and most recently therapeutic approaches to Alzheimer's disease (AD). The proposed involvement of a cholinergic deficit in AD (1) has created great interest (and a considerable market) for new drugs intended to alter the functioning of the cholinergic system, including the raising of acetylcholine levels by inhibition of the major degradative enzyme, AChE (2).

Developing a new drug which inhibits AChE in a test tube is relatively straightforward: demonstrating that the same drug in an animal or a human patient inhibits AChE is considerably more challenging. Combining a measure of the baseline enzyme activity of AChE in the human brain of AD patients, and changes in that activity with drug treatments, would significantly improve our understanding of the functioning of the enzyme (and the benefits of drug treatment) in that devastating disease. We and others have recently embarked on the development and implementation in humans of in vivo Positron Emission Tomographic (PET) imaging methods for the measurement of AChE in the brains of living subjects (3-10). We report here a structure-activity study of potential radiolabeled esters intended to non-invasively measure AChE enzymatic activity.

EXPERIMENTAL

Radiochemical Syntheses

The esters shown in Fig. 1 were prepared in no-carrier-added form by the alkylation of the appropriate N-desmethyl precursors (4-piperidinol esters and nipecotic acid esters) using [^{11}C]methyl triflate and the procedure reported previously (3).

Blood Metabolite Analyses.

Samples of human and rat blood were collected in heparinized tubes. Radiolabeled esters [^{11}CPMP] or [^{11}C]iBMP) were added, the samples rapidly mixed, and timed

aliquots removed for analysis by thin layer chromatography. TLC was done on silica gel plates using 10% methanol in dichloromethane (with a trace amount of ammonium hydroxide) as developing solvent. Radioactivity distribution on the TLC plates was determined using a Berthold linear scanner. This TLC system cleanly separates the authentic esters ($R_f > 0.6$) from the radiolabeled hydrolysis product, N-[^{11}C]methyl)piperidinol ($R_f = 0.1$).

Mouse brain biodistribution studies.

Regional mouse brain biodistribution studies were done in female CD-1 mice (20-25 g; Charles Rivers). Animals were anesthetized with diethyl ether, and radiotracers injected via the tail vein. Animals were allowed to awaken. At designated time points, animals were again anesthetized and killed by decapitation. A sample of blood was collected, and the brain excised and dissected into samples of striatum, cortex, hippocampus, hypothalamic region, and cerebellum. Tissue samples were then weighed and counted: carbon-11 was determined using an automated γ-counter. Data were calculated as percent injected dose per gram of tissue (%ID/g).

PET Imaging Studies

Imaging studies of the time-dependent distribution of radioactivity in the brain after bolus i.v. radiotracer injection were done in a single nemistrina macaque monkey, using a PCT 4600A scanner and procedures previously reported (7). The kinetic rate constant for in vivo hydrolysis of the esters, k_3, was estimated using an analysis technique based on the shape of the tissue time-radioactivity curves for various brain regions (4).

RESULTS AND DISCUSSION

Acetylcholinesterase is a very effective enzyme for the hydrolysis of the neurotransmitter acetylcholine, as reflected in an extremely rapid turnover rate measured in vitro. In this study, we have examined how changes in structure of potential ester substrates impacts on the in vitro and in vivo hydrolysis by cholinesterases of the blood and brain.

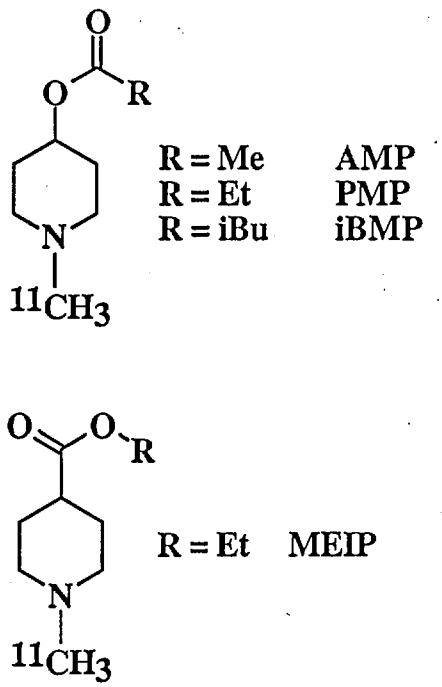

Fig. 1. Structures of radiolabeled esters .

Blood Cholinesterase Activity

The blood is a rich source of cholinesterases, with high concentrations of acetyl-cholinesterase in the red cells, and butyrylcholinesterase in the plasma. Not surprisingly, the piperidinol esters such as [^{11}C]PMP and [^{11}C]iBMP are rapidly hydrolyzed in the blood, producing the radiolabeled metabolite N-[^{11}C]methy-lpiperidinol. Direct comparison of the rates of hydrolysis of these two esters in rat blood shown complete hydrolysis of both by 60 minutes, but faster hydrolysis of [^{11}C]PMP (Fig. 2). This is consistent with the reported faster rate of hydrolysis of [^{11}C]PMP by rat brain cortical acetylcholinesterase (5).

In human blood, [^{11}C]PMP hydrolysis is also rapid and essentially complete by 60 minutes in vitro (Fig. 3). More importantly, the rate of tracer metabolism in the blood is also very rapid after bolus intravenous injection in man, such that the residual amounts of authentic tracer are very low (< 5%) at times greater than 60 minutes.

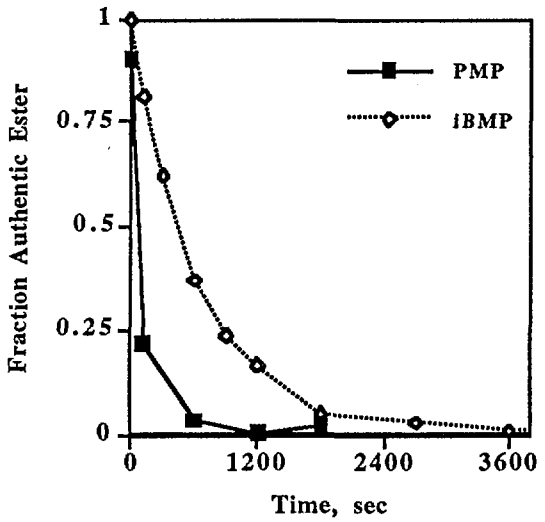

Fig. 2. Metabolite studies of in vitro rat blood metabolism of [^{11}C]PMP and [^{11}C]iBMP. Fraction of authentic at various time points was determined by TLC analysis

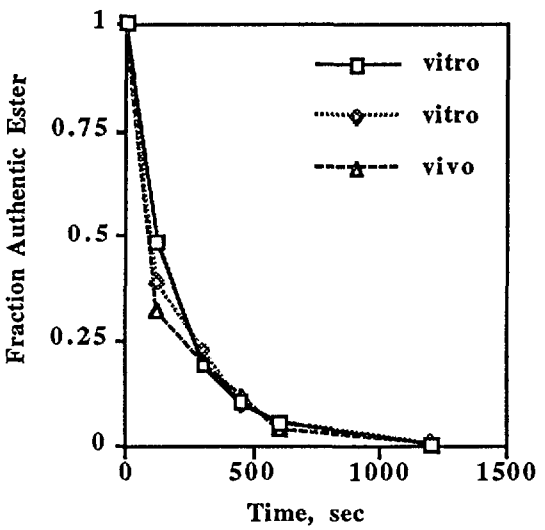

Fig. 3. Metabolite studies of human blood metabolism of [^{11}C]PMP. Data are shown for two in vitro studies and one in vivo study. Fraction of authentic ester (1 = 100% ester) at various time points was determined by TLC analysis.

Mouse Brain Biodistribution Studies.

Upon hydrolysis of these radiolabeled esters by brain cholinesterases, the hydrolysis product N-[^{11}C]methylpiperidinol is effectively trapped. At later time points, the distribution of trapped radioactivity reflects the relative proportions of acetyl-cholinesterase in different brain regions. The time-dependent concentrations of radioactivity in mouse striatum and cortex for the radiolabeled esters [^{11}C]PMP, [^{11}C]iBMP, and [^{11}C]MEIP are shown in Fig 4.

The nipecotic acid ester, [^{11}C]MEIP, shows no retention in the mouse brain, and essentially 99% of the radioactivity initially taken up into the brain washes out within a 30 minute time period. This is consistent not only with no hydrolysis of the ester by any esterases (including AChE), but no significant binding to any other sites in the brain. A comparison of the structures of [^{11}C]MEIP and [^{11}C]PMP shows that they are reverse esters, that is, they differ only by the relative positions of the carbonyl and ester oxygens. This demonstrates that there is structural specificity to the hydrolysis of [^{11}C]AMP (and [^{11}C]iBMP and [^{11}C]PMP) by the cholinesterases, likely due to a required spacing between the heteroatoms of the ester function and the nitrogen of the piperidine ring.

Monkey PET imaging Studies.

The mouse studies suggest a significant difference between the in vivo hydrolysis rates for the different piperidinyl esters, but obtaining complete pharmacokinetic data in mice is time and resource consuming. Such pharmacokinetic studies are, however, relatively simple using PET and primates. In Fig 5. are shown the tissue time-activity curves for [^{11}C]PMP and [^{11}C]iBMP in a monkey brain following bolus intravenous injections of the radiotracers. As can now be clearly seen, there is quite a difference between the two radiotracers: for [^{11}C]iBMP, which has a slower rate of hydrolysis (as measured in vitro), there is a less complete retention of the hydrolysis product in the striatum and the cortex. Estimates of the rates of hydrolysis, obtained using a new method of curve shape analysis, (4) support a quantitative difference between the radiotracers, with striatal hydrolysis rates for [^{11}C]PMP estimated to be 0.075 min^{-1}, and for [^{11}C]iBMP a slower rate of 0.044 min^{-1}.

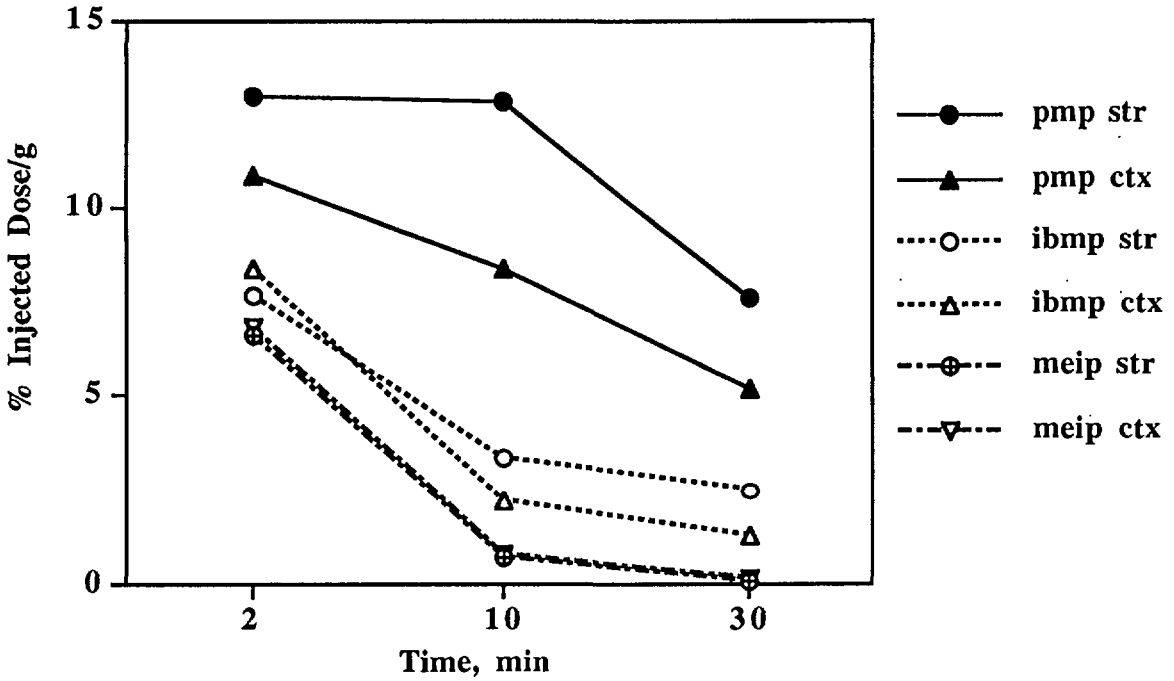

Fig. 4. Tissue concentrations of radioactivity in mouse brain striatum (str) and cortex (ctx) following bolus intravenous injections of [^{11}C]PMP, [^{11}C]iBMP, and [^{11}C]MEIP.

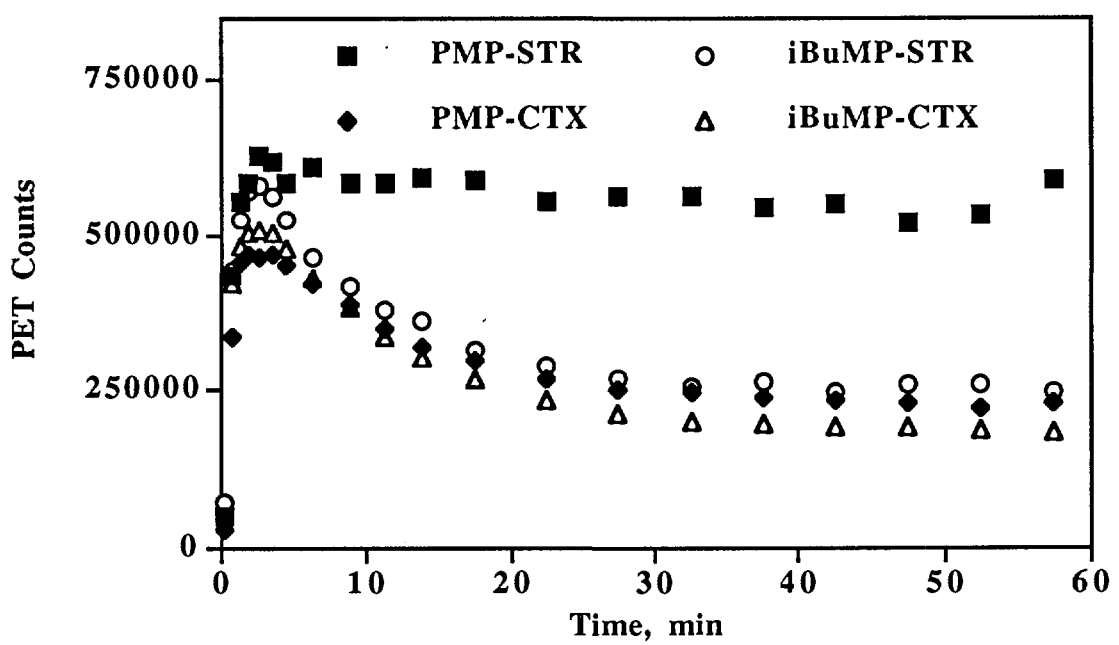

Fig. 5. Tissue time-activity curves obtained from PET imaging of radioactivity distribution in monkey brain follwoing administration of [11C]PMP or [11C]iBMP. Data are shown for the striatum (STR) and the cortex (CTX) for each radiotracer.

CONCLUSIONS

Piperidinyl esters, such as [^{11}C]AMP, [^{11}C]PMP, and [^{11}C]iBMP, can be utilized as in vivo substrates for acetylcholinesterase. External imaging of the pharmacokinetics of these radiotracers, using PET, provides a method for estimating regional brain rates of acetylcholinesterase activity. Recent studies have demonstrated the utility of this approach to the studies of this important enzyme in elderly patients and Alzheimer's disease patients (9,10). Future applications of this approach to the study of neurodegenerative disease, and therapeutic approaches to these diseases, can be expected.

ACKNOWLEDGMENTS.

This work was supported by grants from the National Institutes of Health (NS 24896 and T-32-CA09015) and the Department of Energy (DE-DE-FG021-87ER60561).

REFERENCES

1. Atack, J.R., Perry, E.K., Bonham, J.R., Candy, J.M. and Perry, R.H. Molecular forms of acetylcholinesterase and butyrylcholinesterase in the aged human central nervous system. J. Neurochem. 1986: 47, 263-277.

3. Bormans, G., Sherman, P., Snyder, S.E. and Kilbourn, M.R. Synthesis of carbon-11 and fluorine-18 labeled 1-methyl-4-piperidyl-4-fluorobenzoate and their biodistribution in mice. Nucl. Med. Biol. 1996: 23, 513-517.

2. Freeman, S.E. and Dawson, R.M. Tacrine: a pharmacological review. Prog. Neurobiol. 1991: 36, 257-277.

4. Frey, K.A., Koeppe, R.A., Kilbourn, M.R., Snyder, S.E., and Kuhl, D.E. PET quantification of cortical acetylcholinesterase inhibition in monkey and human. J. Nucl. Med. 1997: 38, 146P.

5. Irie, T., Fukushi, K., Akimoto, Y., Tamagami, H. and Nozaki, T. Design and evaluation of radioactive acetylcholine analogs for mapping brain acetylcholinesterase (AChE) in vivo. Nucl. Med. Biol. 1994: 21, 801-808.

6. Irie, T., Fukushi, K., Namba, H., Iyo, M., Tamagami, H., Nagatsuka, S., and Ikota, N. Brain acetylcholinesterase activity: validation of a PET tracer in a rat model of Alzheimer's disease. J. Nucl. Med. 1996: 37, 649-655.

7. Kilbourn, M.R., Snyder, S.E., Sherman, P.S., and Kuhl, D.E. In vivo studies of acetylcholinesterase activity using a labeled substrate, N-[^{11}C]methylpiperidin-4-yl propionate. Synapse 1996: 22, 123-131.

8. Koeppe, R.A., Frey, K.A., Snyder, S.E., Kilbourn, M.R., and Kuhl, D.E. Kinetic analysis alternatives for assessing AChE activity with N-[C-11]methylpiperidinyl propionate (PMP): to constrain or not to constrain? J. Nucl. Med. 1997: 38, 198P.

9. Kuhl D.E., Koeppe, R.A., Snyder, S.E., Minoshima, S., Frey, K.A. and Kilbourn, M.R. Mapping acetyl-cholinesterase in human brain using PET and N-[C-11]methylpiperidinyl propionate. J. Nucl. Med. 1996: 37, 21P.

10. Iyo M., Namba H., Fukushi K., Shinotoh H., Nagatsuka S., Suhara T., Sudo Y., Suzuki K., and Irie T. Measurement of acetylcholinesterase by positron emission tomography in the brains of healthy controls and patients with Alzheimer's disease. Lancet 1997: 349, 1805-1809.

A New Optical Fiber Method for Neutron and γ-Ray Flux Distribution Measurements in Narrow Space

C. MORI, A. URITANI, K. KAGEYAMA, Y. MAKIBAYASHI, T. SUZUKI, H. SAKAI, H. MIYAHARA, S. SHIROYA[1], T. MISAWA[1], and I. KIMURA[1]
Department of Nuclear Engineering, Nagoya University, Chikusa-ku, Nagoya 464-01, Japan
[1] Research Reactor Institute, Kyoto University, Kumatori, Sennan-gun, Osaka-hu 590-04.

SUMMARY. A new method has been developed for the measurement of neutron flux distribution and γ-ray flux distribution in extremely narrow space by using an optical fiber with which a mixture of ZnS(Ag) scintillator, neutron converter and adhesive paste was painted on the tip of the fiber. The outer diameter of the detector can be down to 1 mm, and the thickness of the scintillator mixture painted is about 0.3 mm. Since the diameter is very thin, it can be inserted into very narrow spaces such as those between reactor fuel elements, or between shielding materials. The fiber can be driven by an automatic driving unit. The geometrical distribution of neutron flux can be measured in a very short time of about 10 minutes or so and with fine position resolution of less than 1 mm by using a neutron converter such as ^{6}Li, ^{235}U, or ^{232}Th in the mixture. This method was applied to obtain thermal neutron flux distribution and fast neutron one in critical assembly and research reactor. The distribution of γ-rays can also be obtained by using only ZnS(Ag) scintillator or CsI(Tl) scintillator, which was applied to obtain γ-ray intensity distributions.

1. INTRODUCTION

The measurements of geometrical distributions of thermal and high energy neutrons in critical assemblies or research reactors are important in the fields of reactor experiment, neutron physics or reactor physics. γ-ray intensity distributions are also desirable to be obtained in γ-ray irradiation facilities or high energy accelerator rooms. Radiation shielding experiment also needs such measurements. Usually the measurements for neutrons in experimental reactors or critical assemblies are carried out by gold wire activation method which takes many hours and whose position resolution is not so good, i.e. more than ~5 mm or so.

We found that even a very small amount of neutron converter mixed with scintillator, which is painted on the tip of an optical fiber, can detect neutrons under the pulse height discrimination against γ-rays as shown by Mori et al (1),(2). Then we developed a new system for the measurement of flux distributions of thermal neutrons and fast neutrons using optical fiber, which can be inserted into very narrow space down to 2 mm or so. This paper reviews the new techniques of the measurement of thermal and fast neutrons and γ-rays in a critical assembly.

2.OPTICAL FIBER DETECTOR WITH ^{6}Li CONVERTER

Scintillation powder ZnS(Ag) and neutron converter LiOH of enriched ^{6}Li (95%) were mixed with adhesive paste with weight ratio of 1:1:2 and painted with a thickness of about 0.3 mm on the tip of plastic fiber with a core diameter of 1mm and with an outer polythene cover diameter of 2.5 mm. The scintillation pulses by ^{6}Li(n, α)T reaction with Q-value of 4.78 MeV can be selected with pulse height discriminator from the pulses by γ-rays, i.e. actually by electrons with energy dissipation of at most ~0.4MeV in the detector part.

The new simple detector with an outer diameter of 2.5 mm was tried to measure the neutron flux distribution in the core of Kyoto University Critical Assembly (KUCA) with 25 fuel elements F shown in Fig. 1. Each fuel element has a shape of 5cm×5cm×150cm with fuel part of 43.36 cm at the central part and with polythene moderator parts at the upper and the lower parts. In the experiments, the fiber was inserted beforehand deep into a narrow gap hole appeared at the four adjacent corners of four fuel elements and then pull it up automatically with a fiber driver controlled by a computer.

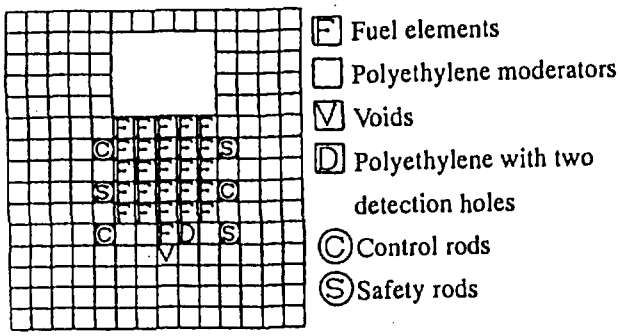

Fig. 1. Core structure of Kyoto University Critical Assembly KUCA (top view).

Figure 2 (a) shows the configuration of each fuel element which is consisted of various cell components and each cell is consisted of uranium part and polythene part. Figure 2 (b) shows the distribution of thermal neutrons obtained by the fiber method (open circles) for 20 minutes measurement by inserting the fiber detector into the very narrow space between the fuel elements and the distribution obtained by gold wire activation method (full circles) for (4~5)×2 hours. The both are similar , but not exactly the same due to the difference of the neutron energy dependence of the cross sections for nuclear reactions. Figure 2 (c) shows the distribution of the enlarged portion from 67 cm to 94 cm in the part of (b). The fine structure of the neutron flux distribution due to the fine structure of the fuel element configuration is shown, which shows the position resolution is less than 1mm.

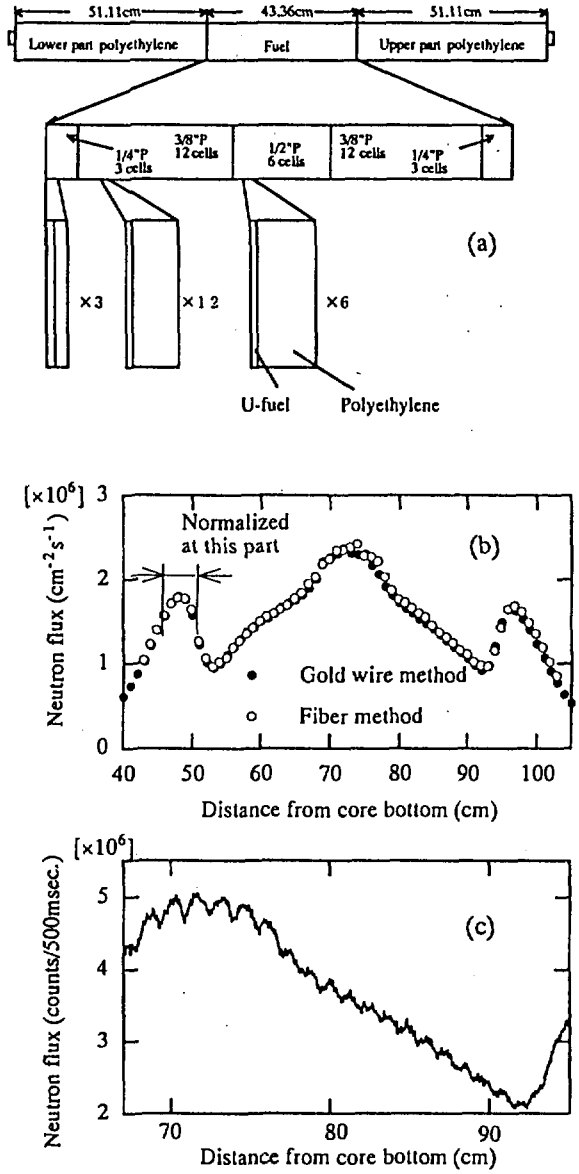

Fig. 2. A fuel element structure of KUCA and an expanded views of the parts (a), thermal neutron flux distribution obtained with ^{6}Li fiber method and gold wire activation method (b) and the fine structure (c) of the distribution at a part of (b).

3. OPTICAL FIBER DETECTORS WITH ^{235}U AND ^{232}Th CONVERTERS

When nuclear fission reaction can be used, the pulse height wouldbe very large due to the large kinetic energy ~170MeV of fission fragments compared with ^{6}Li reaction, so that the

discrimination from pulses of γ -ray interactions will be easier and clearer. Enriched ^{235}U (16 %) converter was used by mixing with ZnS(Ag) and the paste with weight ratio of $1(UO_2):1:2$ and by painting it on the tip of a quartz fiber with core diameter of 600 μ m and outer diameter of 2.5mm. The sensitivity of the detector is smaller than ^{6}Li method by about 2 decades, which means ^{235}U method will be useful in the intense field of thermal neutrons.

Thorium-232 has nuclear fission reaction cross section only for fast neutrons with the energy more than about 1.1 MeV and the natural abundance of the nucleus is 100%. We tried to use this convertor (ThO_2) for the measurement of fast neutron distribution.

The nuclear fission detectors ^{235}U and ^{232}Th were used for the measurements of thermal and fast neutrons in KUCA with the core construction being slightly different from the construction used with ^{7}Li detector shown in

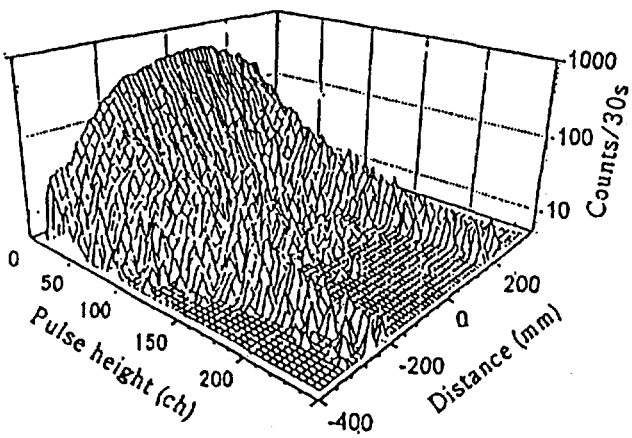

Fig. 3. Pulse height distributions obtained with ^{235}U(16% enriched) converter at various positions.

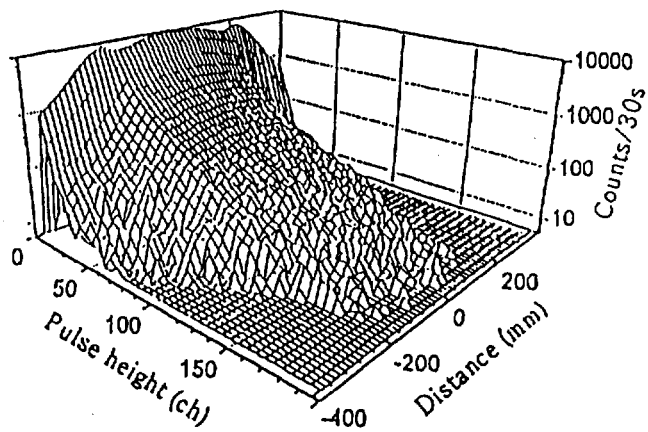

Fig. 5. Pulse height distributions obtained with ^{232}Th converter at various positions.

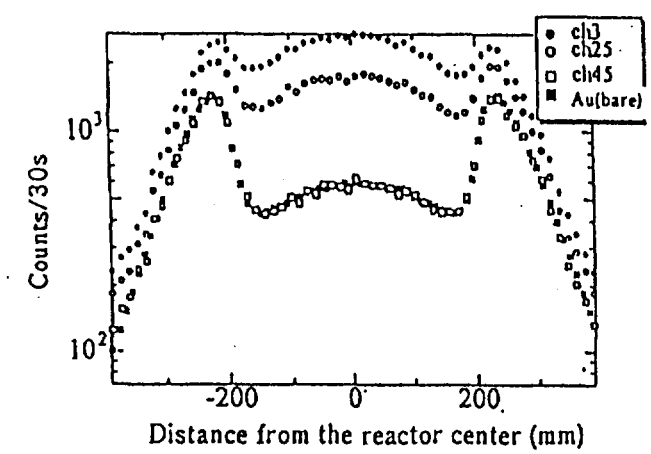

Fig. 4. Thermal neutron flux position distributions obtained with ^{235}U converter and gold wire activation method. The parameter is pulse height discrimination level (channel number)

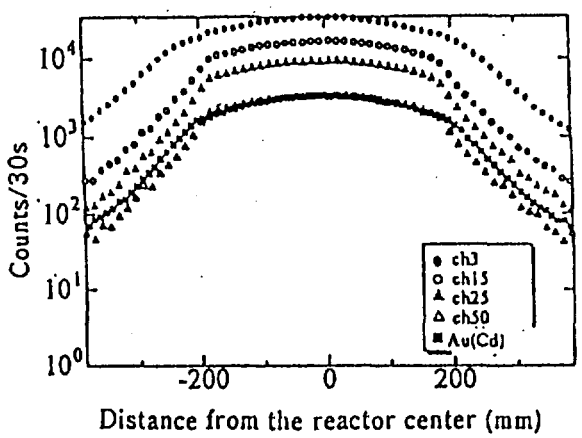

Fig. 6. Fast neutron flux distributions obtained with ^{232}Th converter and gold wire activation method with Cd sheath.

Fig.1. In this case pulse height distributions were measured for 30 seconds at each 1 cm different point. Figure 3 shows three dimensional expression of the pulse height distributions measured with ^{235}U detector at different distance from the vertical center of the core element.

Figure 4 shows position distributions of thermal neutrons obtained from Fig.3 by setting the discrimination levels at different pulse height channels, 3, 25, or 45. The distributions with discrimination channels 3 and 25 include γ-ray intensities because of too low level of the discrimination. The figure includes the distribution obtained by gold wire activation method normalized at one of the peak points of the distribution at 45 channel discrimination, which shows fairly good agreement between ^{235}U method and Au wire method.

Figure 5 shows three dimensional expression of the pulse height distributions measured with ^{232}Th detector at different distance from the core center.

Figure 6 shows position distributions of fast neutrons obtained from Fig.5 by setting the discrimination levels at different pulse height channels, 3, 15, 25, 50 and together with gold wire activation method covered with a Cd sheath to cut thermal neutrons. The distribution with channel 3 contains γ-ray intensity. The intensity ratios at each distance for channel 25 and channel 50 are same, which means the distributions with the discrimination channel more than about 25 show nuclear fission intensity distribution of ^{232}Th by fast neutrons. There are difference between the distributions of channel 50 and Au wire with Cd sheath at the both skirt parts, which come from the giant resonant cross section of Au for activation at 4.9eV neutrons being largely present at the polythene moderator regions.

Position distribution of γ-ray intensity can be measured by ZnS(Ag) scintillator without neutron convertor on the tip of quartz fiber, which was shown by Mori et al (3).

4. SUMMARY

Neutron detector of an optical fiber painted with the mixture of ZnS(Ag) scintillator and neutron converter on the tip of it is very useful for quick and precise measurement of the geometrical distribution of neutron flux in a narrow space with 1~3 mm gap in, for example, critical assemblies or other neutron generation facilities by automatically scanning the detector along the narrow gap using a fiber driver controlled with a computer.

Thermal neutrons can be detected by ^{6}Li converter with high sensitivity and by enriched ^{235}U converter for rather intense neutron flux. Fast neutrons can be detected by ^{232}Th converter which can detect fast neutrons with the energy more than 1.1 MeV.

The measurement time is short, 10~20 minutes depending on the flux intensity and the kind of detector, and the position resolution is very good, ~ 1 mm. By changing the kind and the content of the convertor, this method can be applied to the measurement of neutrons over wide ranges of intensity and energy.

ACKNOWLEDGEMENTS

This work was partly supported by a Grant-in Aid for Scientific Research from the Ministry of Education and Culture and was performed under The Joint Research Programs of Kyoto University Critical Assembly, Yayoi Reactor of The University of Tokyo and Rikkyo University Reactor.

REFERENCES

(1) Mori,C, Osada,T, Yanagida,K, Aoyama,T, Uritani,A, Miyahara,H, Yamane,Y, Kobayashi, K, Ichihara,C, and Shiroya,S, Simple and Quick Measurement of Neutron Flux Distribution by using an Optical Fiber with Scintillator, J. Nucl. Sci. & Technol., 31(1994)248.

(2) Mori,C, Mito,Y, Kageyama,K, Takenaka,Y, Yanagida,K, Uritani,A, Miyahara,H, Wu,Y, et al., Simple, Quick and Precise Measurement of In-Core Neutron Flux Distribution by using Optical Fiber with Scintillator, Proc. 9th Int. Symp. on Reactor Dosimetry (Prague, Sep., 1996)

(3)Mori,C, Y, Kageyama,K, Mito,Y, Takenaka, Y, Yanagida,K, Uritani,A, Miyahara,H, Wu,Y, et al., Measurement of In-Core Gamma-Ray Flux Distribution by using Optical Fiber with Scintillator, Proc. 9th Int. Symp. on Reactor Dosimetry (Prague, Sep., !996)

Highly Accurate Determination of Relative Gamma-Ray Detection Efficiency for Ge Detector and Its Application

H MIYAHARA, C MORI, M A LUDINGTON[*1]
R F FLEMING[*2] and Y K DEWARAJA[*2]
Department of Nuclear Engineering, Nagoya University,
Furo-cho, Chikusa-ku, Nagoya, 464-01, Japan,
Albion College, Albion, Michigan 49224, USA[*1],
and University of Michigan, Phoenix Memorial Laboratory, Ann Arbor,
Michigan 48109-2100, USA[*2]

SUMMARY The objective of this work is to determine the relative gamma-ray detection efficiency for an HPGe detector with the uncertainty approaching 0.1%. We used some nuclides which emit at least two gamma-rays with energies from 700 to 1400 keV for which the relative emission probabilities are known with uncertainties much smaller than 0.1%. This work also shows that accurate determination of the relative gamma-ray emission probabilities for other nuclides can be possible by using the determined highly accurate detection efficiency curve.

1. INTRODUCTION

When quantitative measurements of γ-rays using high purity germanium (HPGe) detectors are made for a large variety of applications, accurate knowledge of γ-ray detection efficiency is required. There are two kinds of γ-ray detection efficiency, total efficiency and full energy peak efficiency (peak efficiency), and the peak efficiency is usually important in various measurements. The peak efficiency is classified into the absolute peak efficiency and the relative one.

If the absolute peak efficiency is calibrated, the emission rates of γ-rays from sources can be determined quickly. The absolute peak efficiencies are determined from measuring standard sources with known disintegration rates. The uncertainties of the absolute peak efficiencies depend mainly on the uncertainties of the disintegration rates, and it is difficult to obtain sources with certainties better than 1%. Therefore, the absolute peak efficiencies have the uncertainties more than 1%.

On the other hand, the relative peak efficiencies are used for the determination of intensity ratios for plural samples and for comparison to the standard source. The relative peak efficiencies are determined from measurements of the sources emitting multi-γ rays with accurately known emission probabilities. In this case, the uncertainties of them depend mainly on the uncertainties of the emission probabilities and the uncertainties are almost about 1% or more except for some particular nuclides. Therefore, the relative peak efficiencies also

show usually the uncertainties more than 1%. One method to improve the certainties of relative peak efficiencies is to obtain many data points using many sources. Another method is to measure certain nuclides that emit γ-rays with intensity ratios of much better than 0.1% [1].

2. METHOD TO DETERMINE RELATIVE PEAK DETECTION EFFICIENCY WITH HIGH ACCURACY

The method used in this paper is to calibrate using sources with highly accurate emission probabilities. Therefore, requirements for the nuclides are following.
(1) Two or more γ-rays are emitted.
(2) The γ-ray emission probabilities are very close to unity.
(3) The internal conversion coefficients are negligibly small.
(4) The energy interval of two γ-rays is proper.
Namely, the emission probabilities of almost unity assure very small uncertainties for those, and the negligible internal conversion coefficients certify the γ-ray emission probabilities of almost unity. Considering various conditions, the small energy interval of two γ-rays gives small uncertainties of the corrections, but too short energy interval shows large uncertainty of slope of the detection efficiency line that is determined from the peak intensity ratio and energy ratio.

When the measurements are carried out using nuclides satisfying these conditions, good certainties must be obtained from the small difference of correction for both γ-rays. The corrections are necessary for the differences of emission probability, self-absorption and cascade summing. However, the chance coincidence is very nearly equal for both γ-rays, because the random summing resolving time is statistically equal for both. The cascade summing depends on the total detection efficiency, so the measurements must be carried out at a large distance between the source and detector for small correction. Small correction for self-absorption is attained for effectively thin source considering γ-ray energy. Namely, measurements must be carried out at an enough large source-detector distance using thin sources.

It is widely used to obtain peak intensity that the measured data in a peak region are fitted with an analytical function assumed for the calculation of the peak area. On the other hand, summation method is easy in evaluation and gives the area with enough certainty for the well-resolved peak with high signal-to-noise ratio and a slowly varying continuum. The spectral analysis described by Helmer [2] was introduced in this study.

After obtaining peak intensities, the relative peak efficiencies are expressed as a function of energy, and the function allows the estimation of the peak efficiency at energy where measured point are absent. In the energy range 300 to 3000 keV the logarithms of the peak efficiencies are linearly related to the logarithms of their corresponding energies. We have been using the polynomial function for both logarithms of energy and peak efficiency [3].

3. EXPERIMENT

Four nuclides satisfying the requirements described in section 2 were measured in this experiment. They are ^{46}Sc, ^{48}Sc, ^{60}Co and ^{94}Nb, and Table 1 shows the energies and γ-ray emission probabilities. These decay data are obtained from IAEA report [4] except for ^{48}Sc of which the data are described in Nuclear Data Sheets [5]. Using these nuclides, the energy range covered extends from 702 keV for ^{94}Nb to 1333 keV for ^{60}Co.

Table 1 The energies and γ-ray emission probabilities of the nuclides used in the present experiment.

Nuclide	Half-life (day)	Energy (keV)	Emission probability
^{46}Sc	83.79(4)	889.3 1120.5	0.999844(16) 0.999874(11)
^{48}Sc	2.0279	983.5 1312.1	1.0011(58) 1.0011(71)
^{60}Co	1925.5(5)	1173.2 1332.5	0.99857(22) 0.99983(6)
^{94}Nb	$7.3(9)\times10^{6}$	702.6 871.1	0.9979(5) 0.9986(5)

Table 2 The results of intensities for ^{46}Sc, ^{60}Co and ^{94}Nb and the intensity ratios.

Run number	Peak area (σ)		Intensity ratio(σ)
^{46}Sc	889.3 keV	1120.5 keV	
1	19.029(21)	16.397(19)	1.1605(19)
2	18.929(21)	16.332(19)	1.1590(19)
3	18.854(21)	16.264(19)	1.1592(19)
4	18.715(21)	16.158(18)	1.1583(18)
5	18.712(21)	16.115(18)	1.1612(18)
Mean			1.1596(6)
Weighted mean	18.8478(94)	16.2532(83)	1.1596(8)
^{60}Co	1173.2 keV	1332.5 keV	
1	25.415(22)	23.365(20)	1.0878(13)
2	25.414(22)	23.379(20)	1.0870(13)
3	38.964(26)	35.862(25)	1.0865(10)
Mean			1.0871(4)
Weighted mean	29.931(14)	27.535(13)	1.0870(7)
^{94}Nb	702.6 keV	871.1 keV	
1	2.3380(33)	2.0377(30)	1.1474(23)
2	5.8883(83)	5.1266(76)	1.1486(24)
3	5.8695(83)	5.1212(76)	1.1461(23)
4	5.8846(83)	5.1269(76)	1.1478(23)
Mean			1.1475(6)
Weighted mean	4.2511(30)	3.7048(27)	1.1475(12)

Sources of ^{46}Sc, ^{48}Sc and ^{60}Co were prepared by irradiation in the Ford Nuclear Reactor at the University of Michigan and ^{94}Nb sources were prepared by irradiation in the NIST reactor. The reactions are $^{45}Sc(n,\gamma)^{46}Sc$, $^{51}V(n,\alpha)^{48}Sc$, $^{59}Co(n,\gamma)^{60}Co$ and $^{93}Nb(n,\gamma)^{94}Nb$. Only V_2O_5 powder sample was irradiated at in-core position for the availability of the maximum fast neutrons. The disintegration rates of the sources were appropriately distributed from 10 to 150 kBq. The typical source was a thin metal foil with a diameter of about 2 mm and a thickness of 0.025-0.13 mm sandwiched by polyester films with a thickness of 7.3 mg·cm^{-2}. The source of ^{48}Sc was sandwiched with the same films after precipitation on a filter paper with a diameter of 6 mm by vacuum suction.

The sources were measured using a closed-end coaxial HPGe detector (Canberra model GC 7020) mounted ultra low-background cryostat. The detector head locates in a lead shield box with thickness of 15 cm, but measurements were carried out in a condition of no top shield because of under-construction. The sources were placed in an open-end lucite disk which was positioned in a lucite holder and measured at a distance of 40 cm referred to the detector end cap and along the central axis of the detector. The detector was operated with a high voltage of 4.5 kV and the signals from the detector were treated by a shaping time of 6 μs. The pulse heights of amplified signals were analysed by APTEC PCMCA/WIN soft loaded on a GATEWAY 2000 Work Station.

4. RESULTS OF RELATIVE PEAK DETECTION EFFICIENCY

Table 2 shows the results for ^{46}Sc, ^{60}Co and ^{94}Nb. For ^{48}Sc measurements of thirty times of 10000 sec were carried out, so the results were not shown in Table 2 but shown in Fig. 1. The mean value and standard deviation of the intensity ratios was 1.2064 ± 0.0036 and the uncertainty of each run was distributed from 0.0036 to 0.0067, then the uncertainty of each measurement seems to be evaluated correctly. Final intensity ratios corrected for the self-absorption, cascade summing and γ-ray emission probabilities are listed in

Table 3. Figure 2 shows the slope to energy relation and the linear relation is recognised at least up to the 1121 keV point. Beyond this energy the slope changes slowly and these results show that the third-order polynomial function is proper.

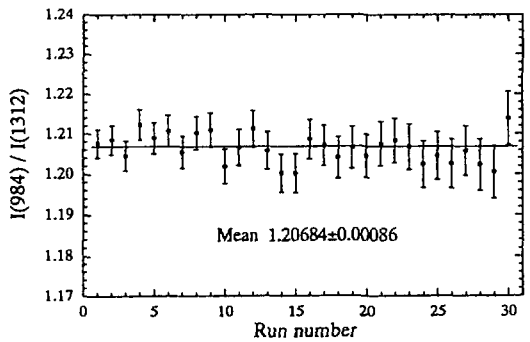

Fig. 1 The results of intensities for ^{48}Sc.

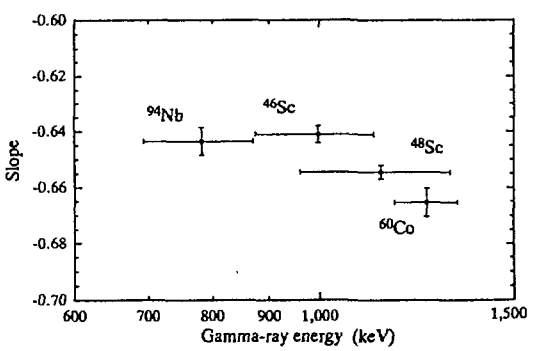

Fig. 2 The slope to energy relation expressed in both logarithmic scales. The linear relation is recognised at least up to the 1121 keV.

First, the data of ^{46}Sc and ^{94}Nb were fitted linearly on both logarithmic scales by the least squares method, and the data of 983.5 keV γ-rays for ^{48}Sc was normalised on the line. Next, the parameters of a third-order polynomial function were determined using these data and those of ^{60}Co by the least squares method. The results of the fitting and the deviation of the data from the fitting function are presented in Fig. 3.

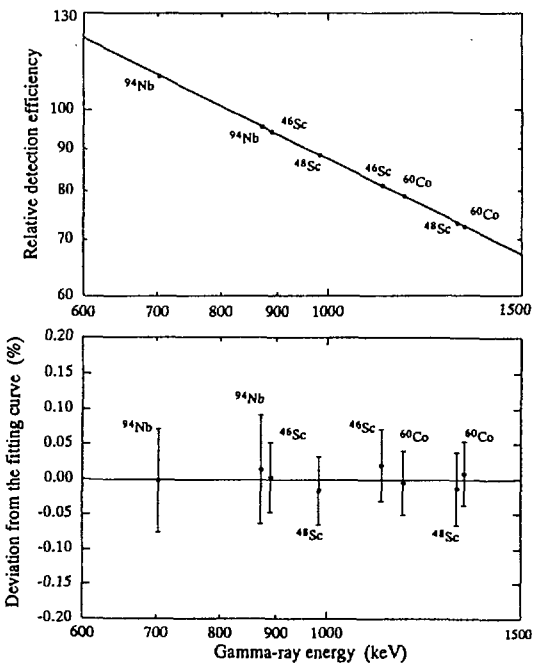

Fig. 3 The results of the fitting and the deviation from the fitting function.

5. EMISSION PROBABILITIES OF THE 1038 AND 1213 KEV γ-RAYS FOR ^{48}Sc

As the relative peak efficiency can be

Table 3 Final intensities corrected for self-absorption, cascade summing and γ-ray emission probabilities.

Nuclide	^{46}Sc	^{48}Sc	^{60}Co	^{94}Nb
Eγ1	889.277(3)	983.526(12)	1173.238(4)	702.645(6)
Eγ2 (keV)	1120.545(4)	1312.120(12)	1332.502(5)	871.119(4)
Peak area ratio	1.15964(82)	1.20684(86)	1.08700(70)	1.14748(123)
Total correction factor	1.00009	1.00067	1.00126	1.00075
Relative efficiency	1.15974(82)	1.20765(86)	1.08837(70)	1.148342(123)
Log(Iγ1/Iγ2)	0.06436(31)	0.08194(31)	0.03678(28)	0.06007(47)
Log(Iγ1/Iγ2)/Log(Eγ1/Eγ2)	-0.6411(31)	-0.6545(25)	-0.6653(50)	-0.6436(50)

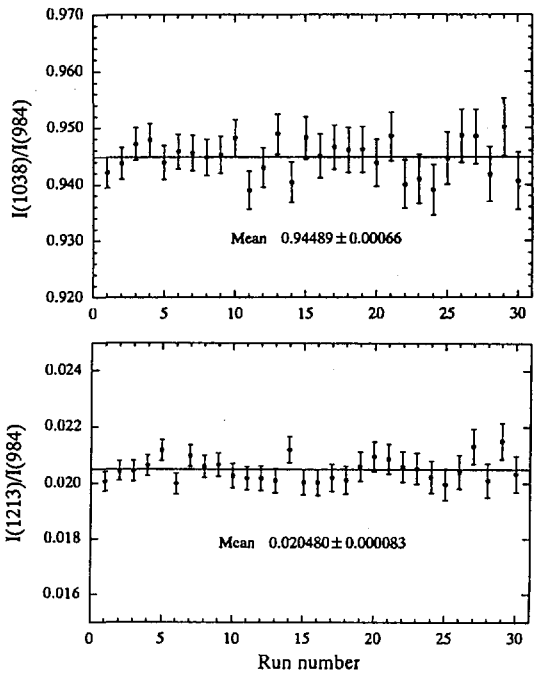

Fig. 4 The intensity ratios of the 1037.5 and 1212.9 keV γ-rays to the 983.5 keV γ-rays.

precisely obtained from the fitting function, the emission probabilities of the 1037.5 and 1212.9 keV γ-rays were determined with very high accuracy as an example of application. In this case, those for the 983.5 and 1312.1 keV γ-rays are assumed to be determined accurately. Figure 4 shows the intensity ratios of the 1037.5 and 1212.9 keV γ-rays to the 983.5 keV γ-rays. The final results obtained from these intensities are shown in Table 3, and the emission probabilities of the 1037.5 and 1212.9 keV γ-rays are 0.97770±0.00079 and 0.02345 ±0.00017, respectively.

6. DISCUSSION

The results obtained in the present measurement show that the relative peak efficiencies are obtainable with uncertainties less than 0.1% as seen in Fig. 3. One of the reason to have been obtained the very highly accurate relative peak efficiency is use of the nuclides with the γ-ray emission probabilities of near unity and the other is the method to accurately calculate the peak area. Particularly in the case of the nuclides satisfying the conditions mentioned in section 2, the uncertainties for γ-ray emission probabilities can be reduced to be less than 0.01%. Four nuclides used in this measurement satisfy the above conditions. The present method of the peak area evaluation shows smaller systematic uncertainty than the method attached to APTEC PCMCA. In the latter method, the left and right boundaries of a peak are defined and a linear continuum is estimated under the peak. Assumption of the linear continuum gives no serious effect for peak area determination with an uncertainty of 1% order in the case of slowly varying continuum, but affects for evaluation with uncertainty of 0.1% order, particularly in the case that a large slope exists on the continuum.

As the chance coincidence is equal for both γ-rays, the effect to the relative intensity determination is negligible. The effect of the cascade summing was avoided by the large source-detector distance location. The correction for self-absorption of ^{48}Sc attained absolutely about 0.5% for 983.5 keV γ-rays, but the relative correction factor was less than 0.1%.

As shown in Table 3, when the emission probability of the 983.5 keV γ-rays is assumed to be 0.999876 under consideration of the internal conversion coefficient of 1.24×10^{-4}, the total transition probability of the 1312.1 keV is given to be 1.00002±0.00082. This value shows the accuracy of the relative peak efficiency. Furthermore, the sum of the 1037.5 and 1212.9 keV transitions is 1.00125 ± 0.00080, and that this value agrees with unity within the uncertainty shows also the appropriateness of the results.

The emission probabilities of the 1037.5 and 1212.9 keV γ-rays are shown with the evaluated values in Table 4. The evaluated

values in Nuclear Data Sheets are based on the results by Meyer and his group [8-10], and the recent values for the 1037.5 and 1212.9 keV γ-rays are 0.976±0.005 and 0.0238±0.0004, respectively. Comparing his relative detection efficiency curves to the present one, the high accuracy of the present results is reasonable.

within the uncertainty which means that the certainties of the results are high and the accuracy have been improved considerably. To expand the energy region of highly accurate detection efficiency curve is future subject and the expansion to higher and lower energy region will lead to further wide applications.

Table 4 The measured and evaluated emission probabilities of the 1037.5 and 1212.9 keV γ-rays for ^{48}Sc.

Gamma-ray energy (keV)	1037.5	1212.9	Reference
Nuclear Data Sheets (1978) [7]	0.975(3)	0.0238(2)	Jackson, Henry, Meyer J. Inorg. Nucl. Chem. (1976) [8]
Nuclear Data Sheets (1985) [6]	0.975(5)	0.0238(4)	Meyer Priv. Comm. (1978) [9]
Nuclear Data Sheets (1993) [5]	0.976(5)	0.0238(4)	Meyer Fizika (Zagreb) (1990) [10]
Present work (1996)	0.9777(8)	0.0235(2)	

7. CONCLUSION

The relative full energy peak detection efficiencies were given very accurately as a function in the energy range from 702 keV of ^{94}Nb to 1333 keV of ^{60}Co. This result was obtained from the measurements of the nuclides emitting two γ-rays with the emission probabilities of almost unity, ^{46}Sc, ^{48}Sc, ^{60}Co and ^{94}Nb. It is important in the measurement that various corrections are small. A third-order polynomial function on both logarithmic scales of energy and efficiency was fitted to the data, and the peak efficiency predicted at certain energy from covariance matrix showed the uncertainty less than 0.05% except for near 700 keV.

As an application, the emission probabilities of the 1037.5 and 1212.9 keV γ-rays were determined using the function of the highly precise relative peak efficiency. Those were 0.97770 ± 0.00079 and 0.02345 ± 0.00017 for the 1037.5 and 1212.9 keV γ-rays, respectively. The sum of these probabilities is very close to unity

REFERENCES

[1] A.I. Hawari and R.F. Fleming, Nucl. Instr. and Meth., A353 (1994) 106-108.

[2] R.G. Helmer, Nucl. Instr. and Meth., 199 (1982) 521-529.

[3] H. Miyahara, K. Usami and C. Mori, Nucl. Instr. and Meth., A374 (1996) 193-196.

[4] IAEA, "X-ray and gamma-ray standards for detector calibration" (IAEA-TECDOC-619, Vienna, 1991).

[5] T.W. Burrows, Nucl. Data Sheets, 68 (1993) 1-115.

[6] D.E. Alburger, Nucl. Data Sheets, 45 (1985) 557-699.

[7] J.R. Beene, Nucl. Data Sheets, 23 (1978) 1-70.

[8] S.V. Jackson, E.A. Henry and R.A.Meyer, J. Inorg. Nucl. Chem., 38 (1976) 1099-1101.

[9] private communication from Meyer to Burrows (1978).

[10] R.A. Meyer, Fizika(Zagreb), 22 (1990) 153-182.

New Pulse Shape Analysis Method with Multi-Shaping Amplifiers

H SAKAI[*1], A URITANI[*1], Y TAKENAKA[*2], K INOUE[*1], C MORI[*1] and T IGUCHI[*1]

[*1] Department of Nuclear Engineering, School of Engineering, Nagoya University
Furo-cho, Chikusa-ku, Nagoya 464-01, Japan

[*2] Toyota Soft Engineering
Sakae 2-3-31, Naka-ku, Nagoya 460, Japan

SUMMARY. This paper describes a novel pulse-shape-analysis method that uses 'similarity' to recognize an individual pulse shape. We obtain four pulse heights by using four linear amplifiers with different shaping time constants. We treat a combination of the four pulse heights as a pattern vector. A similarity of the pulse shape can be obtained by comparison between the pattern vector and a discriminant vector which was given in advance. Each pulse shape is analyzed by using the similarity. The method has been applied to the improvement of characteristics of a CdZnTe semiconductor detector. The characteristics of the energy spectrum of the CdZnTe detector such as a photopeak efficiency or a peak-to-valley ratio are improved after the correction procedure with the similarity.

1. INTRODUCTION

A digital pulse-shape-analysis method became popular in the field of radiation measurement with recent development of digitizers. In these digital pulse-shape-analysis methods, pulse shapes are analyzed by using many algorithms such as a neural network (1,2), template matching (3), fitting with an appropriate function (4), a Fast Fourier Transformation (5) and other methods (6-8). Digital pulse-shape-analysis is potentially superior to an analog counterpart. However, it takes too much time to obtain the pulse shape data and analyze them. In the present study, we used an analog system instead of a digital one. We used four parallel linear amplifiers with different time constants. We treated a combination of four pulse heights obtained with the four linear amplifiers as a vector. The combination for the individual pulse shape was analyzed by using the similarity of each vector. Although a very detailed feature of a pulse shape could not be extracted, this method is superior to the digital method in the simplicity and the speed of the data processing.

2. SIMILARITY

A similarity has been used in the field of pattern recognition. The similarity is used to recognize a pattern when a pattern can be expressed as a vector. The similarity $S(\mathbf{X},\mathbf{Y})$ is defined as follows;

$$S(\mathbf{X},\mathbf{Y}) = \frac{(\mathbf{X},\mathbf{Y})}{|\mathbf{X}||\mathbf{Y}|}$$

$$= \cos\theta \cdots\cdots\cdots\cdots (1),$$

where $\mathbf{X}$ is a pattern vector to be identified and $\mathbf{Y}$ is an appropriate discriminant vector, $(\mathbf{X},\mathbf{Y})$ is the scalar product, $|\mathbf{X}|$ and $|\mathbf{Y}|$ are the norms of the vectors and θ is the angle between the two vectors. The similarity indicates the closeness of the two patterns. We used the angle θ as an index of the closeness of pulse shapes instead of the similarity itself.

Fig. 1 shows the examples of pattern vectors. In a digital system, a pattern vector is taken as $\mathbf{A} = (a_1, a_2, \cdots, a_n)$, where $a_1, a_2, \cdots, a_n$ are pulse amplitudes at $t = t_1, t_2, \cdots t_n$. In an analog system, a pattern vector is taken as $\mathbf{A}' = (a_1', a_2', \cdots, a_n')$, where $a_1', a_2', \cdots, a_n'$ are pulse amplitudes when the pulse is shaped by the linear amplifiers with different shaping time constants of $\tau_1, \tau_2, \cdots, \tau_n$. The pulse height after shaping with time constant τ would have roughly the information of pulse height of original pulse at the time of τ, hence $\mathbf{A}$ and $\mathbf{A}'$ have nearly the same information about the pulse shape if both dimensions are the equal.

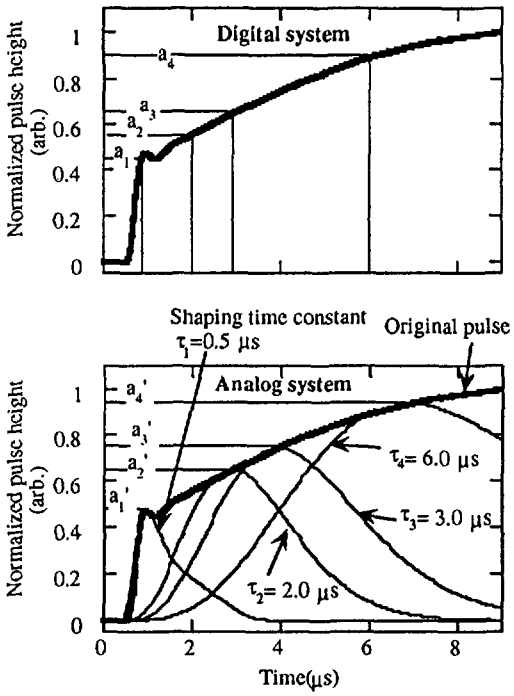

Fig. 1 Examples of the pattern vectors.

3. CdZnTe SEMICONDUCTOR DETECTOR

This method was applied to the improvement of characteristics of a gamma-ray energy spectrum of a CdZnTe semiconductor detector. A CdZnTe semiconductor detector has prominent properties as a radiation detector (9-11). The high atomic numbers indicate a larger detection efficiency for X or gamma rays than that of other semiconductor detectors such as Si or Ge. The large forbidden band gap energy permits room temperature operation. Needlessness of a cooling system permits the CdZnTe detector to be applied to compact use such as a field work or a medical application. However, as with other compound semiconductor materials, the pulse shapes from the CdZnTe detector differ from event to event depending on the positions of radiation interaction because of the different mobilities of the holes and electrons (12,13), and the short life time of the holes for trapping in the bulk. The typical pulse shapes from the CdZnTe detector used in the present study are shown in Fig. 2. The different pulse shapes yield different degrees of ballistic deficits, i.e., different pulse heights even for the same energy deposition. Consequently, the energy spectra of the CdZnTe detector become unusual shapes with low energy tails below photopeaks as shown in Fig. 3. There are several approaches for solving these problems

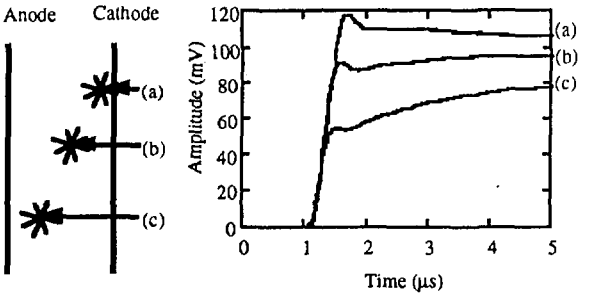

Fig. 2 Output pulses of the preamplifier for gamma rays interacting (a) near the cathode; (b) at the intermediate position and (c) near the anode. The overshoot features are due to the characteristics of the preamplifier.

such as unipolar charge sensing with coplanar electrodes (14,15) and risetime discrimination (16). Many other approaches have been done for improving characteristics of other compound semiconductor detectors such as a CdTe (1,3,17,18) or a HgI_2 (19) one that shows the same tailing effect due to the same reason. We tried to correct each pulse height through the analysis of the pulse shapes with the similarity.

4. EXPERIMENTAL SETUP

Fig. 4 shows a schematic diagram of an experimental setup. Signals from a CdZnTe (eV Products 180.5.5.5s, 5 × 5 × 5 mm) are shaped with four linear amplifiers with time constants of 0.5, 2, 3 and 6 μs, hence the pattern vector was four-dimensional. The pulse amplitudes of the output signals from the linear amplifiers were digitized by Wilkinson-type ADCs. The sets of four pulse amplitudes were stored on a personal computer. The signal processing by using the similarity was done with the personal computer after the measurement.

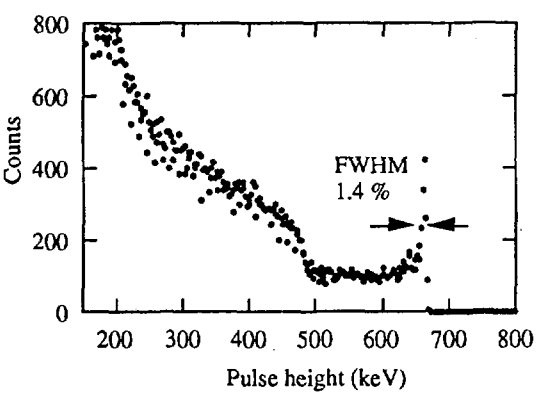

Fig. 3 Energy spectrum for ^{137}Cs gamma rays.

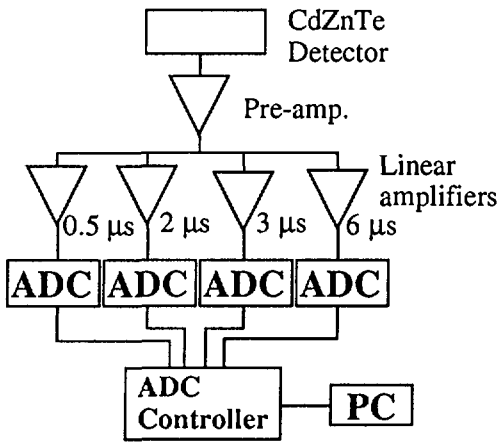

Fig. 4 Schematic diagram of an experimental setup.

5. RESULTS AND DISCUSSION

In the first step of the processing with the similarity, we must choose a proper discriminant vector. The relations between the pulse height and the angle θ for two discriminant vectors obtained by the measurement of a ^{137}Cs gamma-ray source are shown in Fig. 5. For the correction of the pulse shape dependence of the pulse height with the angle θ, the angle θ must be independent of the pulse height. If the vector was not properly chosen, the starting point of the compton edge for 662 keV gamma rays was not found at the same angle of the starting point of the photopeak for 662 keV gamma rays as shown in Fig. 5 (a). With this relation, the angle was not independent of the pulse height. If the discriminant vector was properly chosen, the starting point of the compton edge for 662 keV gamma rays was found at the same angle of the starting point of the photopeak for 662 keV gamma rays as shown in Fig. 5 (b). The best discriminant vector was obtained by trial and error.

We obtained the angle θ with the proper discriminant vector. The shift of the photopeak indicated the relation between the correction factor of the pulse height and the angle θ as shown in Fig. 6. By using this relation, the ballistic deficits of the pulse heights can be compensated. The corrected energy spectrum is shown in Fig. 7. The spectrum was fairly improved. However, there still remains a broad skirt under the photopeak. This is because the pulse heights whose events occur at a certain distance from the cathode suffer fluctuations due to trapping and detrapping of the holes, as well as their deficiency.

Fig. 8 shows the energy spectra for ^{137}Cs gamma rays when the angles were 19.5 and 22.6 degree. The energy resolution (FWHM) of the photopeak for 662 keV gamma rays worsened with increase of the angle θ as shown in Fig. 9. The threshold value for the angle θ was determined by weighing the relative importance of the photopeak efficiency and the energy resolution. In Fig. 7, we discarded the events with large angle more than 22.6 degree. The area under the photopeak for the 662 keV gamma rays drastically increased

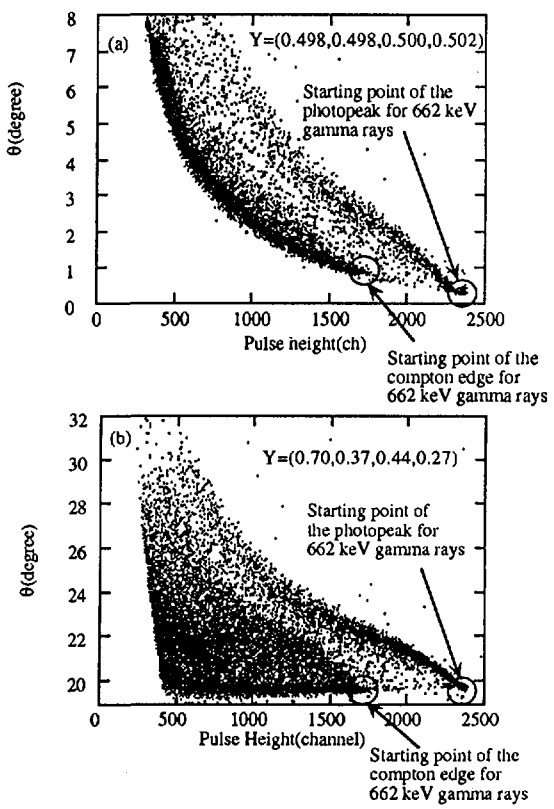

Fig. 5 Relation between the pulse height and the angle θ for the several discriminant vectors obtained by the measurement of a ^{137}Cs gamma ray source, using (a) a proper discriminant vector and (b) an improper one.

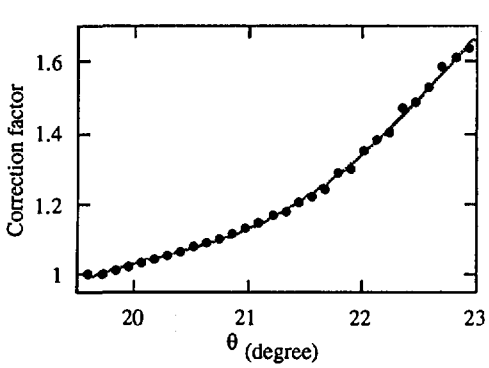

Fig. 6 Relation between correction factor of the pulse height and the angle θ.

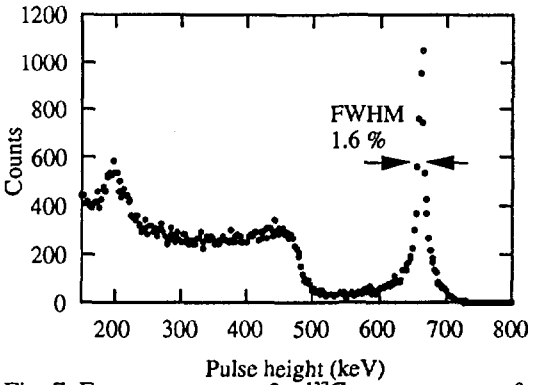

Fig. 7 Energy spectrum for ^{137}Cs gamma rays after the correction procedure.

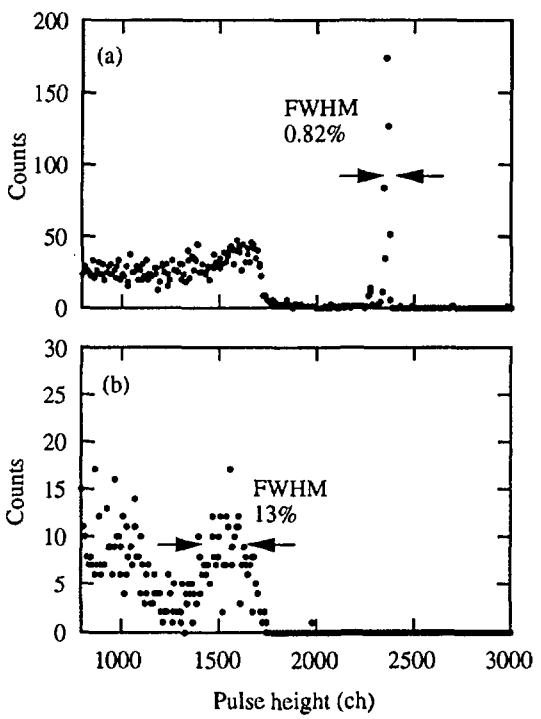

Fig. 8 Energy spectra for ^{137}Cs gamma rays for the angles (a) 19.5 and (b) 22.6 degree.

from 838 to 9,200 events. Although the energy resolution of the photopeak for the 662 keV gamma rays worsened from 1.4 % to 1.6 %, the peak-to-valley ratio defined as a ratio of the count at 662 keV to that at 550 keV, that was the index of the separation of the photopeak, drastically increased from 4.0 to 37.

The events with large θ contained much fluctuations in pulse heights due to the trapping of the holes. Hence the energy spectrum is expected to be further improved when the threshold of the angle θ is lowered. The spectrum, where the events with the angles larger than 20.0 degree were discarded, is shown in Fig. 10. The area under the photopeak for the 662 keV gamma rays decreased to 1,124 events from

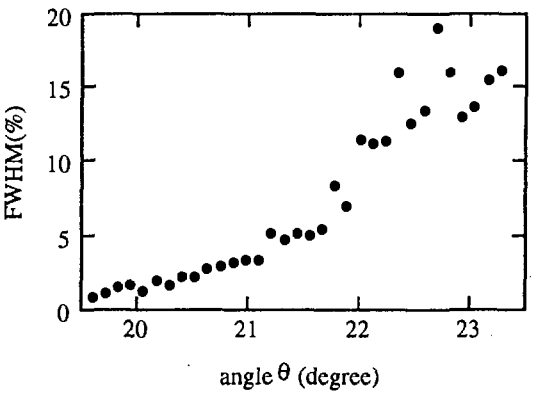

Fig. 9 Energy resolution of the photopeak for 662 keV gamma rays vs. the angle θ.

the spectrum of Fig. 7. However, the area increased from the original spectrum of Fig. 3. The energy resolution of the photopeak for the 662 keV gamma rays was improved to 0.92 % and the peak-to-valley ratio increased to 164. Even the escape peak was observed. Table 1 summarizes the characteristics of these spectra. The relation between the energy resolution and the number of the events used after the correction procedure is shown in Fig. 11. The threshold of the angle θ must be determined by weighing the relative importance of the photopeak efficiency and the energy resolution.

It must be emphasized that this method can be used as a real time processing method for each pulse after obtaining the proper discriminant vector.

6. CONCLUSIONS

A novel pulse-shape-analysis method using the similarity of pulse shapes was presented. The method was applied to the improvement of the energy spectrum characteristics of the CdZnTe

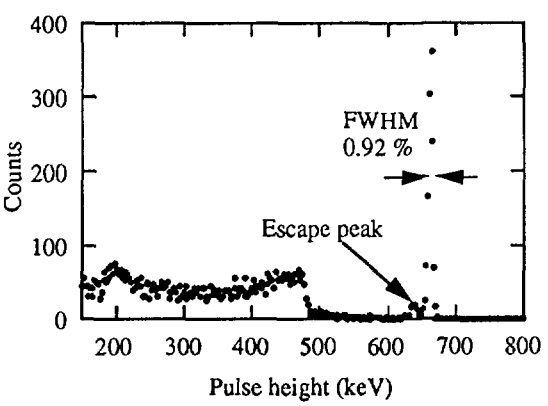

Fig. 10 Energy spectrum for ^{137}Cs gamma rays after the correction procedure by discarding the events with angles larger than 20.0 degree.

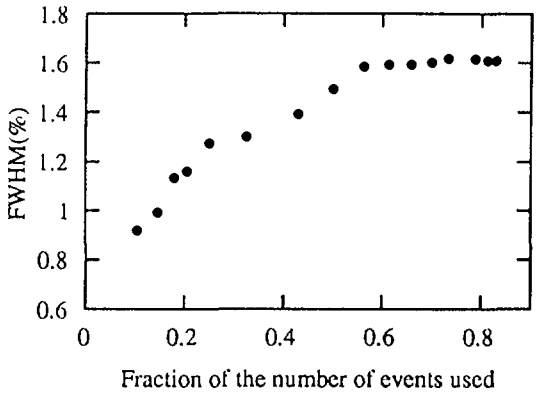

Fig. 11 Relation between the energy resolution and the number of the events used.

semiconductor detector. The energy spectrum has been improved with the increased photopeak efficiency and the better peak-to-valley ratio. The threshold of the angle θ must be determined by weighing the relative importance of the photopeak efficiency and the energy resolution. This method is simple and useful for pulse shape analysis, which can be used for many other applications.

REFERENCES

(1) H. Sakai, A. Uritani, K. Inoue, Y. Takenaka and C. Mori, J. of Radioanal. Nucl. Chem. **205** (1996) 147.

(2) H. Sakai, A. Uritani, K. Inoue, Y. Takenaka and C. Mori, Nucl. Instr. and Meth. **A385** (1997) 335.

(3) H. Takahashi, D. Fukuda, T. Kurahashi, T. Iguchi and M. Nakazawa, Nucl. Instr. and Meth. **A380** (1996) 381.

(4) J.M. Los Arcos and E. Garcia-Torano Nucl. Instr. and Meth. **A339** (1994) 99.

(5) A. Uritani, O. Kubota, Y. Takenaka and C. Mori, Nucl. Instr. and Meth. **A351** (1994) 598.

(6) G. Betuccio, E. Gatti, M. Sampietro, P. Rehak and S. Rescia, Nucl. Instr. and Meth. **A351** (1992) 271.

(7) H. Takahashi, J. Kawarabayashi, T. Iguchi and M. Nakazawa, IEEE Trans. Nucl. Sci. **NS-40** (1993) 626.

(8) H. Takahashi, J. Kawarabayashi, T. Iguchi and M. Nakazawa, Nucl. Instr. and Meth. **A353** (1994) 164.

(9) J.F. Butler, C.L. Lingren and F.P. Doty, IEEE Trans. Nucl. Sci. **NS-39** (1993) 605.

(10) M. Schieber, J.C. Lund, R.W. Olsen, D.S. McGregor, J.M. Van Scyoc, R.B. James, E. Soria and E. Bauser, Nucl. Instr. and Meth. **A377** (1996) 492.

(11) K.B. Parnham, Nucl. Instr. and Meth. **A377** (1996) 487.

(12) R.C. Whited and M.M. Schiber, Nucl. Instr. and Meth. **162** (1979) 114.

(13) E. Sakai, Nucl. Instr. and Meth. **196** (1982) 121.

(14) P.N. Luke, IEEE Trans. Nucl. Sci. **NS-42** (1995) 207.

(15) P.N. Luke and E.E. Eissler, IEEE Trans. Nucl. Sci. **NS-43** (1996) 1481.

(16) A. Niemelä, H. Sipilä and V.I. Ivanov, Nucl. Instr. and Meth. **A377** (1996) 484.

(17) L.T. Jones and P.B. Woollam, Nucl. Instr. and Meth. **124** (1975) 591.

(18) M. Richter and P. Siffert, Nucl. Instr. and Meth. **A322** (1992) 529.

(19) A. Beyerle, V. Gerrish and K. Hull, Nucl. Instr. and Meth. **A242** (1986) 443.

Table 1 Summary of the characteristics of the energy spectra for ^{137}Cs gamma rays.

	Energy resolution FWHM(%)	Photopeak area (counts)	Peak-to-valley ratio	Total events
Before correction	1.4	838	4.0	82,703
Maximum angle θ 22.6 degree	1.6	9,200	37	63,143
Maximum angle θ 20.0 degree	0.92	1,124	164	8,706

Research Achievements in Bangladesh Agriculture using Nuclear Techniques

M A SATTAR
Bangladesh Institute of Nuclear Agriculture
Mymensingh-2200, Bangladesh.

SUMMARY. Nuclear techniques have been successfully used in Bangladesh agriculture in the development of many technologies that are environment-friendly and contributing to the national economy. Low input - and stress tolerant - crop varieties of rice, jute, mustard, chickpea, mungbean, blackgram and tomato, high BNF potential (Ndfa) rhizobial biofertilizers, many soil-water management practices including uptake efficiencies of fertilizer nutrients for various crops, irrigation scheduling, water requirements, residual effect of legumes to succeeding cereal, development of suitable tillage practices, food preservation techniques, means of livestock improvement, etc. are the important achievements that imparted a tremendous impact on agricultural development with less pressure on the environment. The paper also discusses the constraints related to nuclear research and highlights the prospects for its further development in Bangladesh.

1. INTRODUCTION

The beginning of the application of atomic energy for peaceful uses dates back to 1923 and the work of G.V. Hevesy, which signified the start of isotope application in soil and crop research (I). With the establishment of International Atomic Energy Agency on July 29, 1957 the work on this arena of science got momentum worldwide. In Bangladesh, application of isotopes and ionizing radiations in agricultural research has been initiated in 1961 at the Atomic Energy Agricultural Research Centre (AEARC), Dhaka under the then Pakistan Atomic Energy Commission (2). In July 1972, an institute was established as Institute of Nuclear Agriculture (INA) as a constituent institute of Bangladesh Atomic Energy Commission(BAEC) and was shifted from Dhaka to its present site in Mymensingh in 1975. Later the institute's activity was strengthened, separated from BAEC and made an autonomous research organization as Bangladesh Institute of Nuclear Agriculture (BINA) under Ministry of Agriculture on July 1, 1982. Since then the institute has been working on different disciplines of agricultural science viz. Plant Breeding, Soil Science, Crop Physiology, Plant Pathology, Entomology, Irrigation and Water Management, Agronomy, Training, Communication and Publication, etc. The other major institutes that are involved in nuclear agriculture research are Institute of Food & Radiation Biology and Bangladesh Agricultural University.

A good amount of work has been done with nuclear technique in Bangladesh agriculture. It is not possible to review all the works done, but some important research achievements made in the field of mutation breeding, soil fertility, food preservation and animal husbandry are briefly reviewed in this article.

2. DEVELOPMENT OF CROP VARIETIES

Sixteen crop varieties have been developed (2,3,4) using ionizing radiations either directly or by crossing with the irradiated mutant line that included three varieties of rice (Iratom 24, Iratom 38 and Binasail), two varieties of jute (Atompat-38 and Binadeshipat-2), one variety each of chickpea (Hyprosola), mungbean (Binamoog-2) and blackgram (Binamash-1) and four varieties each of mustard (Safal, Agrani, Binasarisa-3 and Binasarisa-4) and tomato (Anobik, Bahar, Binatomato-3 and Binatomato-4). The varieties are high yielder (10-20%) than their respective mother varieties, most of them (all the three rice varieties, chickpea variety Hyprosola, mungbean variety Binamoog-2 and mustard varieties Agrani, Binasarisa - 3 and

Binasarisa-4) mature 2-4 weeks earlier and resistant to diseases common to mother and/or popular variety.

The rice variety Binasail has got late planting potential and hence useful in flood rehabilitation programme. It is also tolerant to brown plant hopper. The jute variety Atompat - 38 has stiff stem and therefore has lesser possibility of lodging or breaking during stormy weather. It is tolerant to stem rot disease (*Macrophomina phaseolina*) and gives improved quality of fibre. The chickpea variety, Hyprosola contains 4% higher protein in the seed than mother variety Faridpur -1. It has shown field tolerance to root rot and *Alternaria* leaf spot disease and pod borer insect *Heliothis helicoverpa*. The mustard varieties Agrani and Safal do not lodge under high input condition and have tolerance to aphid and *Alternaria* blight. The Binamoog-2 is a bold seeded summer mungbean tolerant to weather damage caused by excessive rain and splitting of the pod. All pods of this variety mature at a time. It is also tolerant to yellow mosaic virus and *Cercospora* leaf spot. The blackgram variety Binamash-1 is tolerant to yellow mosaic virus and *Cercospora* leaf spot. The tomato variety Anobik is a dwarf variety, does not lodge, and contains more vitamin c. Bahar variety is characterized by its larger fruit size, fleshy, tasty and contains less number of seeds. The mutagenic agent (radiation or chemical mutagen) used to develop the mutant varieties with their mother variety/line and the year of release by the National Seed Board are given in Table 1.

3. SOIL FERTILITY AND PLANT NUTRITION TECHNOLOGIES

It has been observed through tracer studies that nitrogen is deficient in all soils of Bangladesh, phosphorus and sulphur status is below critical level in many areas and potassium is deficient in terrace and piedmont areas. Calcareous and HYV rice soils are deficient in zinc. Gray brown terrace soils of Madhupur and grey floodplain soils of Mymensingh and Jamalpur are deficient in molybdenum. Copper deficiency has also been observed in some soil series.Results from these studies are being utilized in formulating, updating and refining fertilizer recommendation guide for use by the farmers (5, 6, 7, 8).

Studies with ^{15}N isotope showed that nearly 70% of applied N is lost if applied in the soil surface and only 35-40% of it is utilized by rice crop. Nitrogen use efficiency can be enhanced considerably if applied at 8-10 cm depth. About 25-50% nitrogen fertilizer can be saved if applied by this method. Two split application of urea, one-half before planting and the other half at 45-50 days after planting have been found useful for increased yield of rice and jute. Ammonium sulphate and urea behaved similarly as a source of N in rice fields with respect to timing and placement while sodium nitrate was found inefficient as a source of N (9,10).

Use of ^{32}P indicated that phosphorus use efficiency of crops is enhanced if applied in the soil surface and hoed in before planting of seeds. Sodium bicarbonate extractable phosphorus has shown highest correlation with 'A' values. Direct application of rock phosphate is not suitable in the calcareous and saline soils while in acid soils, it is more effective as compared to triple super phosphate (TSP). It was found that 1270 kg sugar mill waste (press-mud) and 180 kg TSP were equally effective as sources of phosphorus. Thus a considerable amount of TSP can be saved if press-mud is applied in the soils of sugar mill area.. Surface placement of phosphatic fertilizer was superior to shallow or deep placement. Mixing ammonium sulphate with super phosphate stimulated P uptake by rice crop from applied fertilizer. Rubidium-86 tracer studies indicated that the annually flooded floodplain soils do not need immediate application of potash fertilizer. But the terrace soils of Madhupur and Barind area would require supplemental potash for increased crop production. It has been proved that phosphate, sulphur and zinc fertilizers applied in the first crop of a cropping sequence remains unutilized in a considerable amount and become available to succeeding crops. Thus the fertilizer need of

the next crops of a cropping pattern may be reduced. Nitrogen utilization in the first, second and third crops were found to be 36, 9 and 2%, respectively (7, 8, 11).

Irrigation scheduling and water requirement of HYV rice, wheat, chickpea, lentil and mustard have been made for the soils of Ishurdi, Bogra,, Madhupur and Satkhira area based on monitoring the changes in water content of the soil profile using neutron moisture meter (12,13). Minimum tillage for wheat cultivation by planting seeds in furrows made by country plough in between the lines of preceding rice crop has been recommended for the floodplain soils having water table at a shallow depth and where transplanted *aman* rice is harvested late (early to mid December). Deep tillage beyond 15 cm depth coupled with one or two irrigation has been found to increase wheat yield by about 20% in the heavy textured soils of Madhupur and Bogra area (14,15,16).

Using ^{15}N-isotope dilution technique seven high biological nitrogen fixation potential (Ndfa) rhizobial inoculants have been developed for seven leguminous crops that are being used in the demonstration trials by Department of Agricultural Extension since 1989. The yield increase due to use of these

Table 1. Crop varieties developed with the help of induced mutation and released by National Seed Board for commercial cultivation.

Crop	Variety Name	Physical/chemical mutagen	Mother variety	Year of release
Rice	Iratom-24	300 Gy	IR 8	1975
	Iratom-38	300 Gy	IR 8	1975
	Binasail	250 Gy	Nizersail	1987
Jute	Atompat-38	900 Gy	D - 154	1988
	Binadeshipat-2	NaN_3	CVL-1(BJRI line)	1997
Chickpea	Hyprosola	200 Gy	Faridpur-1	1981
Mungbean	Binamoog-2	Hybridization	Mutant MB-55 (4) x V-2773 (AVRDC line)	1994
Blackgram	Binamash-1	600 Gy	Local cultivar (BINA Acc. B-10)	1996
Mustard				
B. campestris	Safal	700 Gy	Advanced line YS-52	1991
	Agrani	700 Gy	Advanced line YS-52	1991
B. napus	Binasarisa-3	700 Gy	Nap-3	1997
	Binasarisa-4	700 Gy	Nap-3	1997
Tomato				
(winter)	Anobik	200 Gy	Local variety	1975
	Bahar	Hybridization	Anobik x Oxheart	1992
(summer)	Binatomato-2	Hybridization	Advanced line S_1 x Bahar	1997
	Binatomato-3	Hybridization	Advanced line S_1 x Bahar	1997

inoculants ranged from 15-40% in lentil, 20-45% in chickpea, 18-35% in mungbean, 25-45% in cowpea, 40-80% in *Sesbania*, 20-40% in groundnut and 75-200% in soybean (17). It was also observed that these local inoculants are better than the exotic strains and that the mixed culture inoculants are superior to single cultures (18,19). The success of the biofertilizer technology has led to the development of a Pilot Project by the Government and a model project by IAEA to creat awareness among the farmers and generate interest among industrialists for mass scale use of biofertilizer in the country.

4. FOOD PRESERVATION TECHNIQUES

Significant advances have been made in applying the radiation techniques to reduce post-harvest food losses and ensure microbiological safety for consumption of food materials. A gamma radiation dose of 0.50 kGy was found suitable for disinfestation of commercial quantities of pulses, oil seeds and tobacco leaves irrespective of varietal differences (20). Laminated gunny bags with additional 0.5 mm thick polyethylene pouches containing the pulses inside were observed to be adequate for irradiation and storage at ambient condition (20 - 35°C, 60-90% relative humidity). Significant reduction of losses was observed on 7-8 months storage of the irradiated samples. A dose of 0.04-0.08 kGy could inhibit sprouting in onions. Sprouting in potatoes could be inhibited at 0.10 kGy. Dried and cured fishery products could be infested of insects at a dose of 0.30 kGy (21). Sun-dried fish (moisture content 18% or below) packaged in high density polyethylene pouches and placed in ply-wood cartoon boxes was irradiated to 1 kGy with effective disinfestation and reduction of microbial load in both 100g laboratory samples and 20 kg commercial bags. The irradiated samples were also found to be of superior quality in physical appearance and organoleptic evaluations (22). Consumers preferred irradiated potatoes although some remarks on colour were received. An industrial enterprise has successfully marketed good quality chips made from irradiated potatoes. The success of food irradiation technology in this country has generated lot of interest among industrial entrepreneurs. A large multipurpose commercial radiation plant has already started its operation for processing foods and medical supplies since 1993.

DDT is a banned item in the country. But while monitoring of pesticide residues in food and environment indicated rampant misuse and overuse of agrochemicals in agriculture and post harvest food storage. Contamination of dried fish with alarming concentrations of DDT (upto 96 ppm) were observed following usage of this persistant organochlorine insecticide during sun-drying and storage. In a marine microcosm experiment conducted in aquaria, it was found that ^{14}C-DDT metabolized to DDE and DDD, and the reduction in ^{14}C-DDT in one component (water) resulted in an increase in other components. (sediment, algae and mussel) (23,24).

Using sterile insect technique Huda et al (25) were successful in the control of a blowfly (*Lucilia cuprina*), a serious pest that infest fishes while sun drying in 3 off- shore islands of Cox's bazar. They reported that male flies could be sterilized at 3 krad and female flies at 2.5 krad without any adverse effect on the adult emergence and longevity.

5. LIVESTOCK IMPROVEMENT

The improved feeding strategies and utilization of locally available low quality feed stuff were suggested by several workers on the basis of experiments conducted with nuclear technique (^{51}Cr-EDTA). Chaudhury (26) reported that water hyacinth in combination with rice straw and concentrated mixture (70% wheat bran + 30% oil cake) showed better results in respect of dry matter consumption, body weight gain, digestibility of dry matter, organic matter, nitrogen free extract, ether extract and total digestible nutrient in cattle. Addition of salt further increased the above parameter. Addition of *dhaincha (Sesbania)* significantly improved the digestibility of crude fibre. The efficiency of rice straw utilization was found improved due to inclusion of banana plant, azolla, sweet potato leaves, legumes and other grasses (27, 28).

Improvement of rice straw digestibility due to feeding of urea-molasses mineral block (UMB) together with rice straw which in turn also improved reproductive performance (29, 30).

Using ^{125}I-labelled progesterone Alam et al. (31) and Ghosh and co-workers (29) reported that supplementation of UMB increased body weight of Zebu cows by 4.8% during 3-month period after calving. Analysis of milk progesterone also showed that the block (UMB) alters body weight loss, resulting in an earlier resumption of ovarian cyclicity in postpartum Zebu cows. Alam et al (31) reported highly significant positive correlation between the changes of plasma and milk progesterone concentrations. Shamsuddin et al. (32) found radio-immunoassay of hormones as an effective tool to monitor the reproductivity in cattle. The technique can be reproducibly used to control the success of artificial insemination for the development of cattle by improving the breeds.

6. CONSTRAINTS TO NUCLEAR RESEARCH

Research work using nuclear techniques needs specialized equipment, supply of stable and radio-isotopes and skilled manpower to work with. Since nucleonic equipments or their accessories and the isotopes are not produced in the country, the long procedure to procure such items hamper the work seriously. It takes long time to clear equipment and chemicals from the custom authority which affects durability of the items specially short-lived radio-isotopes and temperature sensitive chemicals. Shortage of manpower on these specialized technical activity and for maintenance of the equipment, unavailability of foreign currency to the institutes involved in nuclear research, fear among the general mass on the development of nuclear establishments in the country and hence little allocation of fund in this sector, etc., are the main bottlenecks to foster the activity. A pragmatic plan is yet to develop to extract the benefit from this technology.

7. FUTURE PROSPECTS

Bangladesh is dominantly an agricultural country with more than 120 million population over an area of about 148,000 square kilometer. Like most other developing countries it is a resource-poor country burdened with over-population, food shortage, poverty, malnutrition, mass illiteracy and energy crisis. Hence, the development of appropriate technology using techniques with greater efficiency is more needed here than anywhere else to cope with the increasing demand of food in years to come .

Nuclear techniques now a days are being widely used in both developing and developed countries to solve many serious problems hampering health, agriculture and industrial development. The techniques are proved to be highly effective, do certain jobs better, easier, quicker, quantitatively accurate and direct. Some measurements could not be done at all without the use of isotopes as there are no alternative methods available. The successful application of these techniques can contribute significantly to the sound development of technologies that are economically feasible, environment-friendly and sustainable.

8. RECOMMENDATION

Bangladesh is basically a food deficit country and the gap between the need and the production (which is around 2-5 million tons per annum) is usually met up by imports. The demand for food due to increasing population will be more than double by 2025 and then rise at least another 50% by 2050. To cope with the increasing demand of food, nuclear techniques must be widely used to develop suitable technology. Research capabilities need to be strengthened substantially to address the issue. Strong Government commitment is essential to foster the activity. Increased international cooperation are of utmost importance to establish nuclear facilities and their effective utilzation.

REFERENCES

1. Hera, C. IAEA Bull., IAEA, Vienna, 1995, 37(2), 36.
2. Anonymous, Institute of Nuclear Agriculture, Bangladesh Atomic Energy Commission, 1977.
3. Anonymous, BINA, Bangladesh Institute of Nuclear Agriculture, Mymensingh, 1994.

4. Shaikh, M.A.Q., Ali, M.I., Hossain, M. and Jalaluddin, M. Bangladesh J. Environ. Sci., 1997, 3 (1), 17-29.
5. Ali, M.I., Bhuiya, E. H., Rahman, M. M., Badruddin, M. and Habibullah, A.K.M., INA Res. Report No. 40, 1981.
6. Rahman, L., Ahmed, Sultana., Dutta, R. K. and Muslimuddin, M. Progress Report presented at FAO/IAEA research coordination meeting on micronutrient studies held in Indonesia, 1978.
7. Ali, M. I. Paper presented at 14th Senior Staff Course held at Bangladesh Public Adminis. Training Centre, Savar, Dhaka during Dec. 21 to Mar. 8, 1992, pp. 36.
8. Rahman, S.M. Soil Sci. Bull., Dhaka Univ., 1992, 1, pp.30-35.
9. Karim, M., Rahman, S.M., Ahmed, F., and Patwary, S.U. Geoderma, 1972, 7, 121-131.
10. Akanda, M.R.U. Eunus, M., Islam, M.A. and Ali. M.I. Bangladesh J. Agric. 1986, 11: 39-43.
11. Patwary, S.U., Haq, Q., Badruddin, M. and Rahman, L. Bangladesh J. Nucl. Agric., 1987, 3, 1-7.
12. Rahman, S.M., Patwary, S. U. and Ahmed, Sultana. Bangladesh J. Nucl. Agric. 1987, 3, 8-13.
13. Habibullah, A. K. M., Rahman, S. M., Enayetullah, M. Sikder, D.H., Biswas, M.R. and Idris, M. *In:* Isotopes and Radiotion in Research on Soil Plant Relationships. 1979, IAEA-SM-235/3, 235-245.
14. Rahman, S. M. and Islam, A. Ann. Agric. Res., 1989, 10(1), 67-72.
15. Rahman, S.M. and Khalil, M..I. Pakistan J. Sci. Ind. Res., 1993, 36(9), 369-372.
16. Patwary, S.U., Haque, Q., Podder, A.K., Uddin, B. and Habibullah, A.K.M. BINA Res. Report. No. BINA/S.Sc./41, 1984.
17. Sattar, M. A., Podder, A. K. and Chanda, M. C. *In:* Proc. Intern. Symp. Biological N_2 fixation Associated with Rice, held at Dhaka. (Rahman, M. ed.), 1996, Kluwer Academic Publishers, DPSS 70, pp 15-20.
18. Sattar, M.A., Quader, M.A. and Danso, S..K.A. Soil Biol. Biochem.1995, 27(4/5), 725-727.
19. Sattar, M. A., Podder, A. K. and Danso, S. K. A. Bangladesh J. Sci. Res. 1990, Special issue, 73-80.
20. Bhuiya, A. D., Ahmed, M., Rezaur, R., Nahar, G, Huda, S. M. S. and Hossain, S.A.K.M. *In:* Proc. Final RCM on Insect Disinfestation of Food and Agricultural Products by Irradiation organized by joint FAO/IAEA Division, Beijing, May 25-29 (1987), 1991, IAEA-RC-273.3/2,pp. 27-50.
21. Ahmed, M., Karim, A., Quaiyum, M.A, Bhuiya, A.D., Matin, M.A. , Siddiqui, A.K. and Hossain M.M. IAEA Technical Bull. Series No. 303, 1989, pp. 29-75.
22. Shahjahan, R. M, Saha, A. K. and Bhuiya, A.D. Bangladesh J. Zool., 1996, 24(1), 39-44.
23. Matin, M .A., Hoque, E., Khatoon, J., Rahman, S., Malek, M.A., Aminuddin, M. and Rahman, M, *In:* Environmental Behaviour of Crop Protection Chemicals, 1997, IAEA, Vienna, IAEA-SM-343. pp. 279-287.
24. Matin, M.A. Trends anal. chem., 1995, 14(10), 468-473.
25. Huda, S.M.S., Bhuiya, A.D., Rezaur, R. and Ahmed, M., Nucl. Sci. & Appl. 1983,14(A), 70-73.
26. Chaudhury, R. P,. M. Sc. Ag. Thesis, Deptt. Animal Nutrition, BAU, Mymensingh, 1979.
27. Tareque, A. M. M. *In:* Isotope Aided Studies on Non-protein Nitrogen and Agro-Industrial By-Products Utilization by Ruminants. 1987, IAEA STI/PUB/748 pp. 129-142.
28. Tareque, A. M. M. Bangladesh Vet. J. 1986, 20(1-2), 33-38.
29. Ghosh, A., Alam, M. G. S. and Akbar, M.A. Anim. Reprod. Sci., 1993, 31, 61-67.
30. Khan, M. A. S. and Ahmed, A.R. BAU Res. Prog., 1995, 9, 298-305.
31. Alam, M. G. S., Yeasmin, F. and Ghosh, A. Bangladesh Vet. J. 1993, 24-26(1-4), 46-50.
32. Shamsuddin, M., Bhuiyan, M. M. U. Chanda, P.K., Alam, M.G.S. and Abedin, J., Proc. Symp Reproductive Health Management in Ruminants, held at BAU, Mymensingh, 1997, pp. 21-33.

Studies on the Competitive Sorption of Divalent Metal Ions to Natural Soil Samples Using a Multitracer Technique

Ryoko Fujiyoshi, Hiroyuki Hirashima and Sadashi Sawamura

Faculty of Engineering, Hokkaido University, Sapporo 060 Japan

Summary

Sorption of divalent zinc and/or manganese ions have been investigated on the surface soil samples using a radiotracer technique in order to elucidate competitive sorption processes. Quite different properties appeared among those metal ions used either independently or simultaneously as a tracer. Proton exchange process may be important for the Zn(II) sorption, whereas a solid-solution partition is supposed to control the Mn(II) uptake, when each of them was examined independently as a sorbate. In contrast, simultaneous use of those tracers to a soil suspension had great effects on the result ; the maximum sorption (A_m) of Zn(II) increased , and Mn(II) behaved like a sorbate which tends to occupy specific sites of the soil surfaces. Those results indicate that the sorption of minor and/or trace elements to natural soils would not be evaluated only by using a series of single sorbate experimental data.

Introduction

The fate of various pollutants like heavy metals and radionuclides released into the aquatic environment depends on the 'in situ' conditions , such as temperature, pH, redox potential, water flow, existence of scavengers etc. , as well as on the physicochemical properties of the pollutants themselves.

The present authors studied the sorptive behavior of Zn(II) in various natural solid samples including lake and marine sediments by radiotracer technique(1,2). They obtained the results on the zinc sorption which occurs competitively with protons in the aqueous media. There are several candidates of natural solid phases which could be a proton donor or acceptor, such as hydrous iron oxides, clay minerals and also organic substances. Importance of the organic matter as a scavenger of trace elements has been pointed out by many people, and several models have been proposed to predict the fate so far, for

example, by Kinniburgh et al(3). Equilibrium consideration and matrix effects in the solution system are two serious problems to be solved.

The present authors have studied competitive sorption among several divalent metal ions to natural soils using a multitracer technique which is considered to be useful to evaluate relative importance of the sorption without serious matrix effects. This time they will report a result on the sorption of binary systems with Zn-65 and/or Mn-54 as a tracer.

Experimental

Reagents and materials

Soil samples. The surface soil samples used in this study were collected between June and September 1996 at five different sites around Sapporo City(Hokkaido, Japan).

Figure 1 shows the sampling locations. The samples were dried at 110°C and then ground to a homogeneous powder.

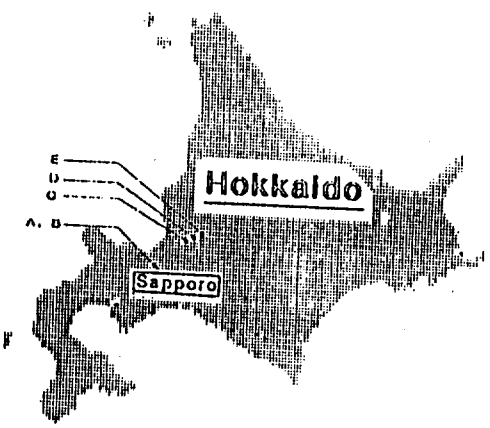

Figure 1 Sampling location of the soils.

The reagents used were purchased from Wako Pure Chemical Industries(Japan) and were of analytical reagent grade.

Zinc-65 and Manganese-54 were obtained from the Japan Radioisotope Association as chlorides in 0.5M hydrochloric acid. The nominal specific activities for Zn and Mn were 113 and 7.30 MBq/mg, respectively with a radionuclidic and radiochemical purity of 99.00%.

The tracer solutions were prepared by mixing aliquots of either Zn-65 or Mn-54 stock solution and of a standard solution of each metal ion(1g/dm^3) to yield a specific activity of 2.31GBq/g.

Instruments

NaI(Tl) scintillation counting system(Aloka ARC301C); x-ray diffractometer(Mac Science MXP); centrifuge(Kokusan Partner 3); ion analyzer(Orion EA940); pH meter(Horiba D-12); mechanical shaker(Yamato Model SA-31); Thermal analyzer(Shimazu DTA-50 and Shimazu TG-50).

Procedure

The sorption experiments were carried out according to the procedure described by the present authors(1,2) previously. A soil sample(20 mg) was weighed and transferred to a centrifuge tube (10 cm^3). The total volume of the suspension was adjusted to 10 cm^3 with distilled water. A small amount of Zn-65

and/or Mn-54 tracer solutions (both 925 kBq/cm^3, 1-15 μ l) was added to the suspension, which was shaken for 30 min with a mechanical shaker. In order to evaluate the time required for the sorption equilibrium to be reached, the pH change of the soil suspension with time was monitored at 20 °C. The solid-solution ratio in the whole experiments was set to be 20 mg/10 cm^3 considering the amount of Zn(II) or Mn(II) remaining in the solution after each run to be measured with certain accuracy. After centrifugation, an aliquot (5 cm^3) of the supernatant solution was pipetted into a vial and the Zn-65 and/or Mn-54 activities of the liquid phase were measured in a NaI(Tl) scintillation counter with the counting efficiencies of 1.31% at γ energy of 1115 keV for Zn-65 and of 3.54% at 835 keV for Mn-54, respectively, where the energy window for counting was set to be 5% for both nuclides. Several standards of known activity were used to evaluate data obtained.

The cation exchange capacity(CEC) of the soil sample was measured electrochemically with an ammonia electrode(Orion 95-10). All the cation exchange sites of a sample in an aqueous suspension were substituted with NH_4^+ ions, and after centrifugation, the residue was treated with 0.1M NaCl solution. The amount of NH_4^+ ions released by the exchange with Na^+ ions was determined electrochemically.

According to the method byWong et.al.(4), the organic contents of the soil samples were estimated from the weight loss in ignition at 450 °C for 24 hours.

Powder x-ray diffraction analyses were carried out on individual samples to identify the crystalline minerals by a random orientation method.

Results and discussion

Soils are mixtures of various mineral and organic components which could scavenge toxic trace pollutants discharged to ground surface through atmospheric precipitation and water streams. The scavenging capacity is supposed to be quite different among soils with different physicochemical properties.

Powder x-ray diffraction analyses gave several peaks due to crystalline quartz present in all samples. Some types of clay minerals and also hydrous iron oxides in amorphous state would probably exist in those samples according to the results by Sakaguchi(5).

Table 1 lists the water content(%), weight loss in ignition(%) and ammonia content(mg/100g) of the soils examined. The water and ammonia contents are relatively high in Sample C collected from a peatland(Tsukigata district in Hokkaido).

Radiometric sorption experiments were then carried out on those samples using Zn-65 and /or Mn-54 as a tracer. The metal ions are supposed to compete each other to occupy specific sites on the soil surfaces. Experimental results were summarized in Table 1.

Table 1 Summary of data obtained from all soil samples(A, B, C, D and E).

Sample No	A	B	C	D	E
Water content /%	25.7	35.2	84.5	18.5	24.8
Ignition weight loss /%	10.3	9.0	9.2	3.4	3.7
Ammonia NH_3 g /100g	0.60_5	0.90_3	2.23_6	1.28_1	0.57_9
Suspension pH	6.99	7.84	4.52	5.45	5.97
CEC /mmo /100g	18.8	7.74	13.3	6.12	10.9
A_m(Zn) /mmol /100g *	0.34_8	0.38_4	0.19_8	0.18_3	0.30_4
$[Mn]_{soil}$/ $[Mn]_{aq}$ /mgcm^{-3}*	2.56	11.4	0.68_1	1.06	7.27
A_m(Zn) /mmol/100g(Mn)**	1.50	3.00	2.53	2.00	0.49_0
A_m(Mn) /mmol/100g(Zn)**	0.41	1.28	0.52_8	0.58_7	0.22_9

* Single sorbate system
** Double sorbate system

Zn(II) sorption. Sorption isotherms fit to the Langmuir equation which provides the amount of Zn(II) at the maximum sorption(A_m) corresponding to 100 percent surface coverage by Zn(II) ions. They were in the range between 0.18 and 1.38 mmol/100g dry soil, and much smaller(< a few %) than the corresponding CEC values of individual samples. Only a part of the total sites for the sorption would be occupied by Zn(II) ions. The A_m values were positively correlated with the equilibrium pH values of the soil suspensions in all cases. The results indicate that the zinc sorption occurs competitively with protons in the liquid phase.

Mn(II) sorption. Divalent manganese ions behaved quite differently from Zn(II) ; almost all Mn(II) ions present in the soil suspension initially disappeared to be with the solid phases. The isotherms for the Mn(II) did not fit to the Langmuir equation. Divalent manganese species may be stable thermodynamically under pH and redox conditions of the present soil solution systems. As predicted from a p ϵ -pH diagram for manganese, $Mn(OH)_2$ is likely to exist in a soil suspension with pH higher than 7.5. It is in the case of Sample B, where most Mn(II) in the suspension disappeared after the sorption equilibrium. The peatland soil(sample C) with lower pH did not incorporate much amount of Mn(II) from the liquid phase.

Simultaneous Zn(II) and Mn(II) sorption. Both tracers were added to a soil suspension simultaneously. The A_m values for Zn(II) were obtained from the isotherms of individual samples. They were consistently higher than those obtained in the previous systems free from Mn(II), and were much

smaller than the corresponding CEC values in all cases. Manganese ions added to the soil suspension clearly affect the Zn(II) behavior in the sorption process. There seems to be no regularity among the degree of A_m increases for Zn(II) sorption in the presence of Mn(II). For example, in Sample B with high pH, Mn(II) ions trapped on the soil surfaces may provide additional sites for Zn(II) to occupy. In contrast, the A_m value of Sample C did not change appreciably regardless whether Mn(II) was present in the system or not .

Peculiar properties also appeared on the Mn(II) sorption, when Zn(II) coexisted in the soil suspension. As in the case of Zn(II) sorption, the Langmuir equation is applicable to fit data obtained for all samples. The result indicates that Zn(II) ions may play a role to make Mn(II) occupy some specific sites of the soil surfaces in order. The A_m values thus obtained for Mn(II) sorption were much smaller than the corresponding CEC values in all samples.

It seems to be very difficult to evaluate the whole system just as it is, and to make a suitable model to predict the fate of pollutants. However, the present radiometric approach to the zinc and/or manganese sorption may have at least an advantage which is to prevent the results from suffering serious matrix effects often occur in usual techniques.

On the evaluation of the sorption equilibria, there are many data which showed the equilibrium to be far more attained in the real systems. They may be true, as a whole, since a trivial event would cause quite serious problems. It is our approach to deal an edge of the phenomena; to evaluate capacities of the sorption on individual components of various natural samples.

Conclusion

Divalent zinc and manganese behave quite differently as a sorbate to natural soil samples. It may be partly caused by the $p\epsilon$-pH dependence of Mn(II) species in the present soil solution systems. Manganese hydroxide is possibly to be formed in a soil with high pH. In contrast to Mn(II) which is a minor component of soils, there exists some specific sites for Zn(II) ions to be sorbed. They may be ion(proton) exchangeable in character. Those findings suggest that much data are necessary for evaluating the fate of pollutants with certain models.

References

1. Fujiyoshi R., Gomei T. and Katayama M. Sorption of Zn(II) on marine sediments by a sequential extraction(1996) Appl. Radiat. Isot. 47, 165- 169.
2. Fujiyoshi R., Gomei T. and Sawamura S. Sorptive behavior of Zn(II) on a lake sediment by sequential extraction-radiotracer technique(1997) Talanta (in press).
3. Kinniburgh D. G., Milne, C. J., Benedetti M., Pinheiro J. P., Filius J., Koopal L. K. and

97/19

Van Riemsdijk W. H. Metal ion binding by humic acid: application of the NICA -Donnan model(1996) Environ. Sci. Technol. 30, 1687-1698.

4. Wong C. S., Chin Yu-P. And Gschwend P. M. Sorption of radon-222 to natural sediments. (1992) Geochim. Cosmochim. Acta 56, 3923-3932.
5. Sakaguchi Y. "Geology of the Peatland"(1980) Tokyo Daigaku Shuppankai(Tokyo), in Japanese.

Application of Oxygen and Carbon Isotopes as Evidence for Alteration in Carbonates

MOHAMMAD H. ADABI[1, 2] and J.C. VAN MOORT[1]

1) Geology Department, University of Tasmania, GPO Box 252-79, Hobart, Tasmania, Australia.

2) Geology Department, University of Mashhad, Mashhad, Iran.

SUMMARY

Dolomite alteration studies involving oxygen and carbon isotopes, elemental analysis and EPR spectroscopy were carried out for the large stratabound carbonate replacement tin deposit at Renison Bell, Tasmania, Australia. The Renison sequence generally consists of three main dolomite horizons and siliciclastic sediments of Neoproterozoic age. Alteration in the three dolomite horizons resulted from the passage of magmatic hydrothermal fluids through major faults and fractures.

The heaviest $\delta^{18}O$ (-2.5‰ PDB) and $\delta^{13}C$ (+4.1‰ PDB) values are in the least-altered dolomite, whereas, highly altered dolomites are more depleted in both $\delta^{18}O$ (-21‰ PDB) and $\delta^{13}C$ (-5.1‰ PDB) values. The Mg contents decrease with increasing lighter $\delta^{18}O$ and $\delta^{13}C$ values, whereas, Fe and Sr concentrations increase with lighter $\delta^{18}O$ values, due to alteration. EPR intensity of the Mn^{2+} sextet is high in the more altered dolomite, which corresponds to the lighter $\delta^{18}O$ values. In contrast, in the least-altered dolomites, the EPR intensity is low and $\delta^{18}O$ values are more enriched.

1. INTRODUCTION

Renison, the largest primary tin producer in Australia, is situated at Renison Bell, Tasmania, at latitude 41° 47' S, and longitude 145° 26' E (Fig. 1). Little is known about the elemental composition and isotopic values ($\delta^{18}O$ and $\delta^{13}C$) of these carbonate rocks.

The $\delta^{18}O$ and $\delta^{13}C$ values of carbonates, together with major and minor elements and EPR studies can provide useful criteria to determine the extent of carbonate alteration and the temperature range for carbonate replacement mineralisation. Depletion in Mg, Sr, Fe and $\delta^{18}O$ and $\delta^{13}C$ values may assist differentiation of least-altered from highly altered dolomites. High Sr contents and heavy $\delta^{18}O$ and $\delta^{13}C$ values of least-altered dolomites may reflect original carbonate compositions, whereas, Mn and Fe concentrations can typically increase and $\delta^{18}O$ and $\delta^{13}C$ values decrease during alteration of unaltered dolomites (Veizer, 1; Adabi, 2).

2. GEOLOGY OF THE RENISON DISTRICT

The Renison mine sequence consists mainly of the Neoproterozoic Success Creek Group and the Crimson Creek Formation. The Renison deposit at the mine area occupies the upper part of the Success Creek Group and the lower part of the Crimson Creek Formation (Fig.2). The Success Creek Group consists of a thick (~1000 m) shallow shelf sequence of siliciclastic facies hosting the No.2 (5-30 m) and No.3 (up to 15 m) dolomites of the Renison Mine Sequence (Patterson et al., 3; Morrison, 4). These dolomites consist of dolomicrite, dolomicrosparite, dolosparite, and abundant vein and saddle dolomite (Adabi et al., 5). The Success Creek Group is conformably followed by a thick succession of relatively shallow marine carbonates, siliciclastics and volcaniclastics of the Crimson Creek Formation (~5000 m, Kitto, 6). The Crimson Creek Formation hosts the No.1 dolomite horizon (8-25 m, Morrison, 4).

Carbon isotope chemostratigraphy supports the Neoproterozoic age of about 570-820 Ma for the Crimson Creek Formation and Success Creek group respectively (Adabi, 7). The Renison mine sequence is intruded by the Devonian Pine Hill Granite, south-east of Renison Bell (Cannard, 8; Kitto, 6, Fig. 2).

Regional fault structures at Renison are attributed to a tensional regime associated with emplacement of the Upper Devonian Pine Hill Granite (Fig. 2; Lea, 9). The Mine Sequence is disrupted by at least three major groups of mineralised faults formed during the forceful emplacement of the Pine Hill Granite (Kitto, 6). These are: 1) the Federal-Bassett Fault (FBF) and Blow fault Complex (BFC), 2) the Transverse Faults which are also called the Shear Faults, 3) a series of north-south striking faults which form minor horst and graben structures. The Federal-Basset Fault (FBF) is a major feeder fault in the mine area and has an inferred strike length of several tens of kilometres, along the north-eastern margin of the Pine Hill Granite (Lea, 9; Kitto, 6).

3. MINERALISATION AT RENISON

Mineralisation resulted from the passage of hydrothermal fluids, sourced from the Devonian Pine Hill Granite, through major fault structures, partially replacing the three dolomite horizons and forming a cassiterite-rich pyrrhotite orebody (Holyland, 10; Kitto, 6; Adabi et al, 5). The No.2 and No.3 dolomite horizons were heavily mineralised, particularly at the intersections of major fault structures in close proximity to hydrothermal feeders, whereas the No. 1 dolomite contains only minor mineralisation of economic grade (Holyland, 10; Cannard, 8; Kitto, 6). The Federal-Bassett Fault (FBF) was the primary structural control on distribution of ascending magmatic hydrothermal fluids at Renison (Kitto, 6, Adabi et al., 5).

4. OXYGEN AND CARBON ISOTOPES

Renison dolomites have gone through minor to major alteration after deposition. Therefore, samples were grouped into less recrystallised and strongly recrystallised dolomites.

Carbon and oxygen isotope values for both less recrystallised and strongly recrystallised Renison dolomites show a positive correlation (Figs. 3 A, B). The heaviest $\delta^{18}O$ and $\delta^{13}C$ values are -2.5‰ PDB and 4.1‰ PDB, respectively. The $\delta^{13}C$ values, in both less recrystallised and strongly recrystallised samples, decrease from 4.1 to -5.1‰ PDB with increasingly lighter $\delta^{18}O$ values due to alteration by magmatically derived hydrothermal fluids. Overlapping $\delta^{18}O$ and $\delta^{13}C$ fields for Renison carbonates with the Devonian magmatic dolomite field support a magmatic source from the Devonian Pine Hill Granite for the hydrothermal fluids (Fig. 4). $\delta^{18}O$ values in dolomites from strongly recrystallised samples (-2.5 to -21‰ PDB) are lighter on average than less recrystallised dolomites (-2.7 to -15‰ PDB; Figs. 3 A, B). Dolomicrites (<5μm to ~16μm in size) have the heaviest $\delta^{18}O$ and $\delta^{13}C$ values, whereas dolomicrosparites (recrystallised dolomicrites, ~16μm to ~62μm) are more depleted in both $\delta^{18}O$ and $\delta^{13}C$ (Figs. 3 A, B). In strongly recrystallised samples, dolomicrosparites and coarsely crystalline dolomites (~250μm to 1 mm) can be markedly depleted in both $\delta^{18}O$ and $\delta^{13}C$ (Fig. 3 B). Dolosparites (~16μm to ~250μm) and vein dolomites (>250μm), both precipitates, have light $\delta^{18}O$ and $\delta^{13}C$ values in less recrystallised dolomites (Fig. 3 A) and moderate to light $\delta^{18}O$ and $\delta^{13}C$ values in strongly recrystallised dolomites (Fig. 3 B). The wide variation in $\delta^{18}O$ and $\delta^{13}C$ values is mainly dependent on proximity to fractures, faults or mineralisation.

5. ISOTOPES AND ELEMENTAL COMPOSITION

The alteration of dolomites can be deduced from variations in concentrations of Mg, Sr, Mn and Fe, and $\delta^{18}O$ and $\delta^{13}C$ values.

Mg contents of the Renison carbonates decrease with increasingly lighter $\delta^{18}O$ values (Figs. 5 A, B). An apparent correlation between Mg and $\delta^{18}O$ (PDB and SMOW) values in the various dolomite types exists in the less recrystallised carbonates, from dolomicrite, to dolomicrosparite, to dolosparite, to vein dolomite (Fig. 5 A). Dolomicrosparites dominate in the strongly recrystallised Renison dolomites and show a trend similar to the less recrystallised dolomites (Fig. 5 B). In less recrystallised and strongly recrystallised Renison carbonates, dominated by dolomicrosparite, Sr and Fe concentrations increase with lighter $\delta^{18}O$ values (Figs. 5 C, D). A negative correlation between both Sr and Fe contents and $\delta^{18}O$ values, with r^2 values of 0.75 and 0.78 respectively reflects the systematic increase in both Sr and Fe, due to alteration.

Mg contents of the Renison dolomites decrease with increasingly lighter $\delta^{13}C$ values (Figs. 6 A, B). The decreases in both Mg and $\delta^{13}C$ values in medium to coarsely crystalline dolomites are due to alteration. These trends

are similar to Mg- $\delta^{18}O$ bivariate plots. There is no correlation between Na and Sr contents versus $\delta^{13}C$ values in less recrystallised and strongly recrystallised dolomites. In strongly recrystallised Renison dolomites, Mn and Fe concentrations increase with lighter $\delta^{13}C$ values. Appreciable gains in Fe and Mn in altered dolomites are due to their reaction with hydrothermal fluids in an anaerobic environment.

6. OXYGEN ISOTOPES AND ELECTRON PARAMAGNETIC RESONANCE (EPR)

Randomly dispersed Mn in dolomite causes a strong EPR signal (Schindler and Ghose, 11). Room temperature X-band powder EPR spectroscopy showed a marked increase of the Mn^{2+} signal in dolomite on approach of the mineralization. The intensity of the EPR signal correlates negatively with the $\delta^{18}O$ values of the dolomites (Fig. 7).

7. EQUILIBRIUM TEMPERATURES

$\delta^{18}O$ values of dolomites can be used to determine the equilibrium temperatures responsible for alteration. Calculation of depositional temperatures from early *diagenetic* dolomite values (-2.5 to -8‰ PDB) using the $\delta^{18}O$ value of -4.9‰ SMOW (Irwin, 12) gives temperatures around 20° C for heavy $\delta^{18}O$ values of Renison dolomites.

Calculation of $\delta^{18}O$ temperatures for *hydrothermal* solutions, using $\delta^{18}O_{fluid}$ (magmatic) values of +9‰ SMOW (Kitto, 6), indicate a range of depositional temperatures up to 350° C (Fig. 4). These temperatures are similar to those obtained for mineralising fluids at Renison based on fluid inclusion studies (Patterson et al., 3; Holyland, 10; Kitto, 6).

8. CONCLUSIONS

Elemental and isotopic compositions ($\delta^{18}O$ and $\delta^{13}C$), along with EPR studies indicate that Renison carbonates have been altered mainly by hydrothermal alteration which has progressively obliterated original carbonate compositions. The variations in the intensity of the alteration, which is shown by the wide ranges in $\delta^{18}O$ and $\delta^{13}C$ values and major and minor element concentrations, is mainly dependent on proximity to fractures, faults or mineralisation.

The wide range in $\delta^{18}O$ and $\delta^{13}C$ values and Mg, Sr, Fe and Mn concentrations in the Renison carbonates from least to most altered indicates that fluid infiltration has occurred. Fluid infiltration resulted in diagenetic dolomite being recrystallised to dolomicrosparite and coarsely crystalline dolomite. The less recrystallised dolomite generally contains relatively more Mg, less Mn and Fe, and heavier $\delta^{18}O$ and $\delta^{13}C$ values than strongly recrystallised samples. The heaviest $\delta^{18}O$ and $\delta^{13}C$ values are in the least-altered dolomicrite, whereas, the lightest isotopic values are in vein dolomites.

Variation in carbonate $\delta^{13}C$ values from -5.1 to 4.1‰ and the linear trend between $\delta^{18}O$ and $\delta^{13}C$ values are due to

alteration by magmatically derived hydrothermal fluids. Overlaping $\delta^{18}O$ and $\delta^{13}C$ fields for Renison carbonates with the Devonian magmatic dolomite field support a magmatic source for the hydrothermal fluids. $\delta^{18}O$ values of least-altered dolomite correspond to formational temperatures of ~20° C, whereas, $\delta^{18}O$ values of altered Renison carbonates indicate that they were magmatically derived hydrothermal fluids of ~ 350° C. These temperatures are similar to those obtained from fluid inclusion studies.

The EPR intensity is high in the more altered dolomites and $\delta^{18}O$ values are more depleted, whereas, in the least-altered dolomites, the EPR intensity is low and $\delta^{18}O$ values are more enriched.

REFERENCES

1- VEIZER, J., 1983. Chemical diagenesis of carbonates: theory and application of trace element technique: Stable Isotopes in Sedimentary Geology: Soc. Econ. Palaeont. Mineral. Short Course No.10, p. 3-1 to 3-100.

2- ADABI, M.H., 1997b. Sedimentology and geochemistry of Upper Jurassic (Iran) and Precambrian (Tasmania) carbonates. Unpub. Ph.D. thesis, Univ.Tasmania, 470p.

3- PATTERSON, D.J., OHMOTO, H.H., and SOLOMON, M., 1981. Geologic setting and genesis of cassiterite-sulfide mineralisation at Renison Bell, western Tasmania: Econ. Geology, v. 76, p. 393-438.

4- MORRISON, G.W., 1982. Stratigraphy and sedimentology of the Renison mine sequence: Unpub. Rept. Renison Ltd, 102p.

5- ADABI, M.H., RAO, C.P., and KITTO, P.A., 1996. The source of hydrothermal fluids responsible for carbonate alteration, Renison, Tasmania, Australia: 13th Geol. Conv. Austral (abst), p. 7.

6- KITTO, P.A., 1994. Structural and geochemical controls on mineralization at Renison, Tasmania: Unpub. Ph.D. thesis, Univ. Tasmania, 484p.

7- ADABI, M.H., 1997a . Application of carbon isotope chemostratigraphy to the Renison dolomites (Tasmania, Australia): a Neoproterozoic age: Australian. Jour. Earth Sci., v. 44 (in press).

8- CANNARD, C., 1991. Renison Bell Tin Mine ore reserves report: Unpub. Rep., Renison, Ltd., 143p.

9- LEA, J.R., 1991. Renison mine lease exploration: Models, concept, interpretation and future directions: Unpub. Rept. Renison Ltd., 60p.

10- HOLYLAND, P., 1987. Structure and hydrodynamics of the Renison Tin Mine: Unpub. Ph.D. thesis, Univ. Queensland, 258p.

11- SCHINDLER, P., and GHOSE, S., 1970. Electron paramagnetic resonance of Mn^{2+} in dolomite and magnesite and Mn^{2+} distribution in dolomites: Am. Miner., v. 55/11-12, p. 1889-1896.

12- IRWIN, H., 1980. Early diagenetic carbonate precipitation and pore fluid migration in the Kimmeridge Clay of Dorset, England: Sedimentology, v. 27, p. 577-591.

13- JONES, M., and EVANS, D., 1985. Trace elements and stable isotope variations in rocks of the Renison Mine Sequence: Unpub. Rept. Renison Ltd., 34p.

14- ZEMPOLICH, W.G., WILKINSON, B.H., and LOHMANN, K.C., 1988. Diagenesis of Late Proterozoic carbonates: the Beck Spring Dolomite of eastern California: Jour. Sed. Petrology, v. 58, p. 656-672.

15- COLLINS, P.L.F., 1981. The Geology and genesis of the Cleveland tin deposit, western Tasmania: fluid inclusion and stable isotopes studies: Econ. Geology, v. 76, p. 365-392.

Figure Captions

Figure 1. Regional geology of western Tasmania and the location of the Renison tin mine within the Paleozoic Dundas Trough.

Figure 2. Schematic cross section of the Renison deposit showing the distribution of stratabound carbonate-replacement tin deposits (modified after Cannard, 8).

Figure 3. $\delta^{18}O$ and $\delta^{13}C$ values in less recrystallised (A) and strongly recrystallised (B) Renison dolomites. Strongly recrystallised dolomites exhibit the lightest $\delta^{18}O$ and $\delta^{13}C$ values, whereas least-altered dolomicrites exhibit the heaviest $\delta^{18}O$ and $\delta^{13}C$ values.

Figure 4. Carbon isotope versus oxygen isotope covariance diagram for the Renison carbonates. Comparisons are made between Renison carbonate types (this study), bulk carbonates (Patterson et al., 3; Jones and Evans, 13; Holyland, 10), with unaltered dolomites from the late Proterozoic of California (Zempolich et al., 14) and Devonian hydrothermal dolomites from the Cleveland Mine, Tasmania (Collins, 15). Temperature calculations are discussed in the text.

Figure 5. Mg, Sr and Fe values, relative to oxygen isotope compositions. (A-B), Mg versus $\delta^{18}O$ values in less recrystallised and strongly recrystallised Renison dolomites, respectively. Decrease in both Mg and $\delta^{18}O$ values are the result of alteration effects. (C-D), Sr and Fe versus $\delta^{18}O$ values in strongly recrystallised Renison dolomites, respectively. Increases in Sr and Fe concentrations with lighter $\delta^{18}O$ values are the result of alteration.

Figure 6. Mg versus $\delta^{13}C$ values in less recrystallised (A) and strongly recrystallised (B) Renison dolomites. Note decrease in both Mg and $\delta^{13}C$ values are the result of alteration effects.

Figure 7. EPR intensity versus $\delta^{18}O$ values. Note in the least-altered dolomicrites the EPR intensity is low and $\delta^{18}O$ values are more enriched.

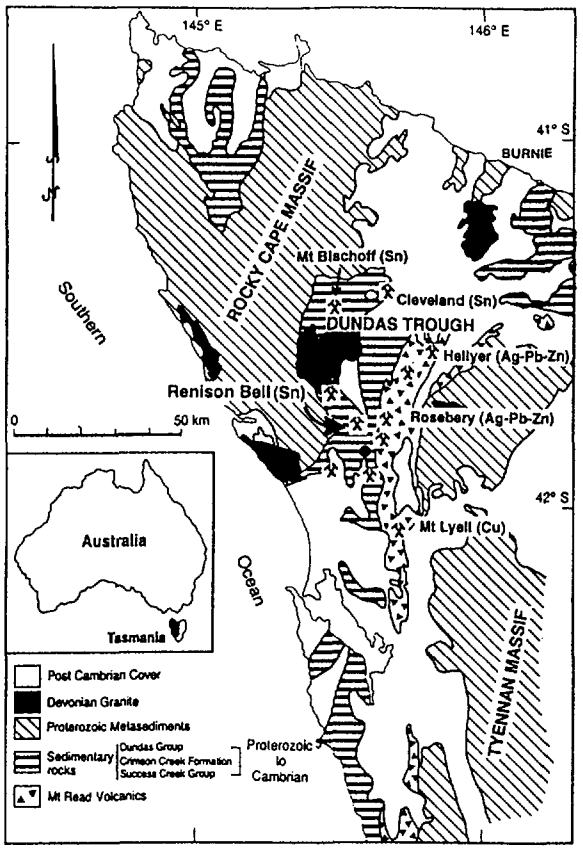

Fig 1

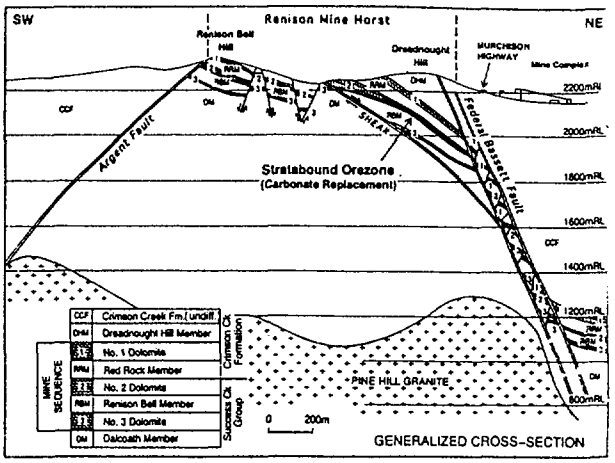

Fig 2

Fig 3 →

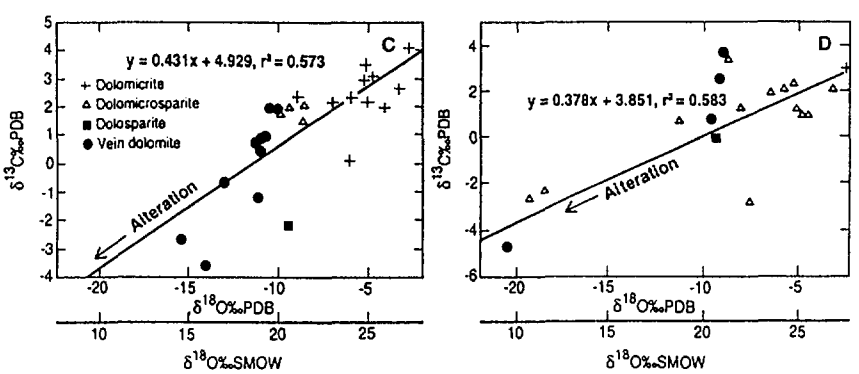

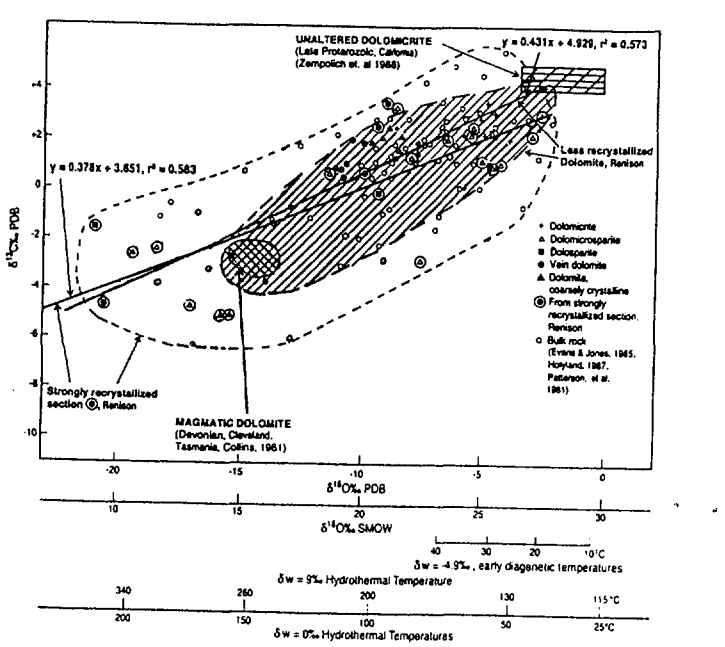

Fig 4

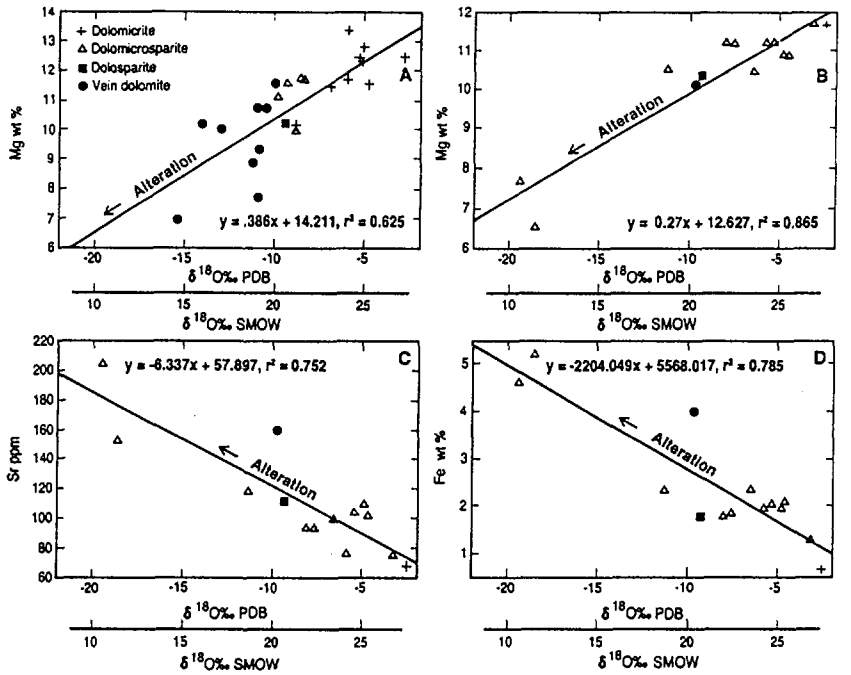

Fig 5

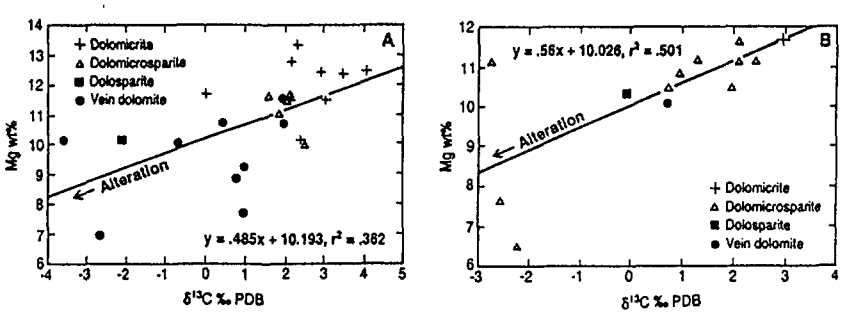

Fig 6

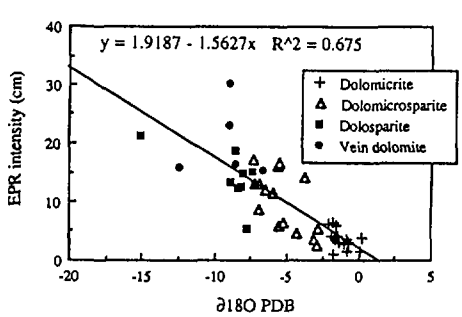

Fig 7

Application of Radioisotope Au-198 to Radiometrical Field Investigation of Spraying Machine

W GORACZKO, E KOCZOROWSKA
Radio- and Photo-chemistry Department, Technical University Poznan
60-965 Poznan, Piotrowo 3, Poland
GORACZKO@SOL.PUT.POZNAN.PL

SUMMARY. An article shows application of radioisotope Au-198 to radiometrical field testing of spraying machine. In the research was tested the Polish suspenioned tractor OZS-400 type spraying machine. The machine worked in two different variants : without and with the beam stabilization (oscilatory stabilization).

1. INTRODUCTION

The radioisotope method of estimation functionality of the spraying machine was based on the measurement of a quantity of the radioisotope labeled liquid in the field. This method was based on the linear relation between the quantity of the sprayed liquid and measured frequency range.
Lab experiments confirmed the right choice of the radioisotope Au-198 ($t_{1/2}$=2.7 days, Eγ =0.67 MeV). As a chemical form of this radionuclide I used the water solution of chlorauric acid (i.e.$H^{198}AuCl_4$)(1). For detection a typical collimated scintillation probe with NaJ(Tl) crystal was employed. The lead collimator was deliminated the probe "field of view" to 100 cm^2.
The labelling process has been realized in the field. I was put the radioactive preparation into the machine tank where it was mixed automaticaly. Finally I received the water solution with the equal concentration of the radioisotope tracer in the whole tank capacity.
In the research was tested the Polish suspensioned tractor OZS-400 type spraying machine. This machine had the following parameters : width of beam - 12 m, quantity of the spray nozzles - 24, spray nozzle distance - 0.5 m, spray nozzle type - TEEJET 1104 splot spray nozzle, tank capacity - 400 liters, travelling speed of the machine - 5.6 km/h, wind velocity - 0.0 m/s.

2. FIELD TESTING

To decrease the total radioactivity of the preparation a half of the spraying beam was tested only.
The testing field was devided into three parts. In the first one the tractor with the spraying machine was started, accelerated and stabilized (setting parameters of spraying process). The liquid was sprayed in the middle part. The third part was the final one (2).
The radiometrical data were measured in the middle part only. To estimate an influence of a terrain configuration on the sprayed liquid distribution in the ground a hole was graved (depth - 0.20 m, tractor wheel width). This obstacle was simulated the change of a terrain topography. The good work of the spraying machine was characterized by the independence of the sprayed liquid distribution in the terrain configuration (good machine reacted immediately on the ground topography and had a negative influence on the spraying process.
The spraying machine was tested in two different variants of work : 1 - without the beam stabilization (undetachable beam - field no.1); 2 - with the beam stabilization (oscilatory stabilization - field no.2).
Finally I received two populations of radiometrical data (in each field). Statistical sizes of each population were 700 unitary measuring points.

3. RESULTS AND DISCUSSION

Figure 1 shows an example of frequency range variations which have been measured in parallely (a) and perpendicularly (b) to the tractor direction movement (only for variant 1, i.e. field no.1).

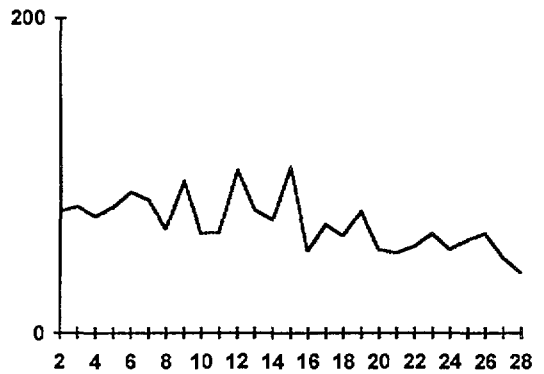

Figure 1a. Frequency range variation profile (parallely-field no.1)

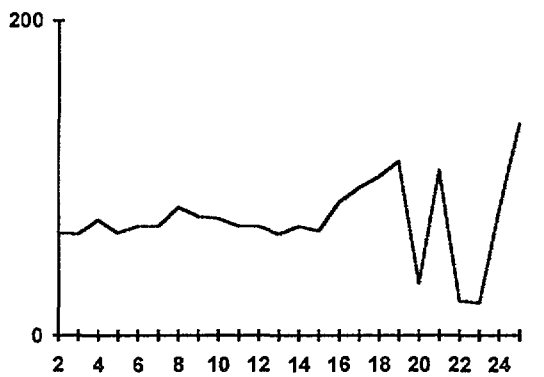

Figure 1b. Frequency range variation profile (perpendicularly-field no.1)

Axonometric projections of the frequency range distribution (quantity - of the sprayed liquid) are shown in Figure 2 (field no.1) and Figure 3 (field no.2). Whole population has been analised statistically.

In this way statistic parameters of the real distribution of sprayed liquid have been qualified. It has appeared thet the analized sample of variant 1 (field no.1) belongs to the beta-distribution.

Figure 2 shows that the tested spraying machine worked very unstable, however did not record clear influence of the obstacle.

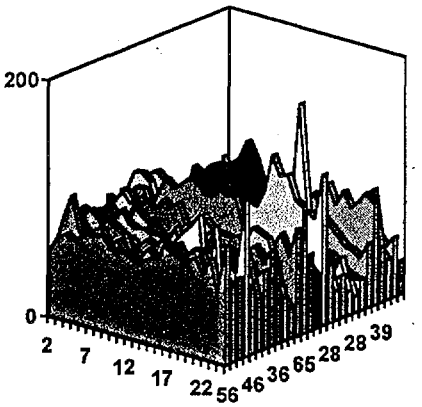

Figure 2.Axonometric projection of the frequency range distribution - field no.1

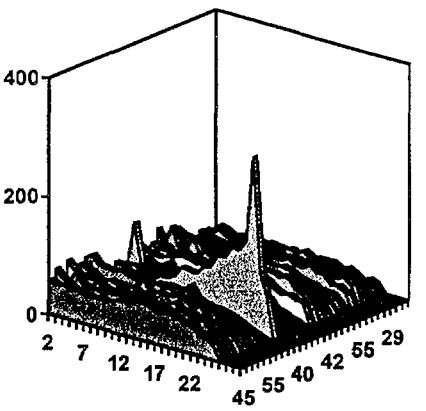

Figure 3.Axonometric projection of the frequency range distribution - field no.2

The spaying machine in variant 2 (field no.2; i.e. with the beam stabilization) worked quite differently. In Figure 3 is shown that the obstacle has been clearly recorded (increasing of frequency range - i.e. increasing quantity of the sprayed liquid). It is the unfovourable result. On the other hand the stabilization process of the beam was very fast - and it was favourable. Just 0.5 m beyond the obstacle the beam was stabilized. In this variant real distribution parameters of the sprayed liquid belonged to the t-Student one.

In Figure 4 and Figure 5 have been shown two examples of real herbicide distributions which have been analyzed for two different types of spraying machines (i.e. Figure 4 - the spraying machine with the beam stabilization on the dual trapezium, and Figure 5 - the oscilatory stabilization). In both cases the spraying machines worked properly (in according to the

agricultural rules). Negative influences of the terrain obstacle have not been found.

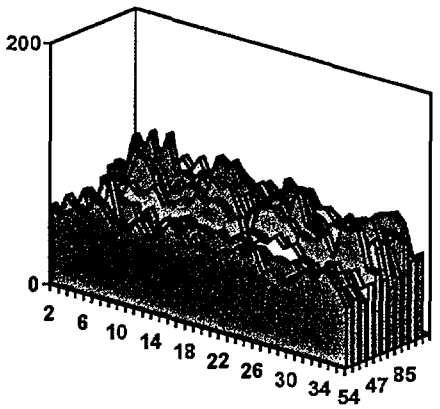

Figure 4.Real herbicide distribution - dual trapezium stabilization.

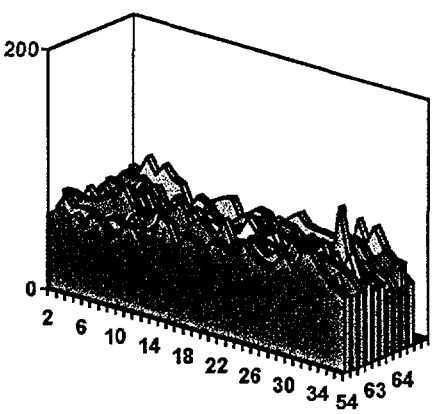

Figure 5. Real herbicide distribution - oscilatory stabilization.

4. REFERENCES

1.Goraczko W, Koczorowska E, Radioisotope Method of Investigation of Agriculture Machines on Field Testing, Technical University Poznan Report, 1992-1996.
2.Goraczko W, Koczorowska E, Radioisotope Testing Method of the Spraying Machine Functionality, Technical University Poznan Report, 1992-1996.

Imaging Tissue Hypoxia: clinical and pre-clinical experience with ^{123}IAZA

LEONARD. I. WIEBE
Noujaim Institute for Pharmaceutical Oncology Research,
Faculty of Pharmacy and Pharmaceutical Sciences,
University of Alberta, Edmonton, Canada T6G 2N8

SUMMARY. Nitroimidazole radiosensitizers were developed to enhance the efficacy of radiotherapy. This chemical class of compounds has more recently gained attention as scintigraphic markers of tissue hypoxia when labelled with gamma-emitting radionuclides. The initial orientations of imaging applications were towards radiobiological hypoxia, with covalent binding of activated intermediates occurring at O_2 concentrations below 1000 ppm. More recently, hypoxia imaging with agents such as ^{123}I-IAZA has been applied to a number of clinical pathologies, including peripheral vascular disease associated with diabetes, rheumatoid arthritis, stroke, myocardial ischaemia, brain trauma and oxidative stress. The current status of hypoxia selective radiopharmaceuticals is outlined, with special reference to ^{123}I-IAZA.

1. INTRODUCTION

The *oxygen effect* in radiation biology refers to the contribution of molecular oxygen to the lethal effects of low linear-energy-transfer (LET) ionizing radiation. Oxygen-deficient cells require approximately three times more low LET radiation for a lethal effect than is required to kill oxygenated cells, an effect attributable in part to the reaction of O_2 with molecular free radicals. Radiation generates high concentrations of molecular free radicals, solvated electrons, hydrogen radicals and hydroxy radicals. These can in turn react with O_2 to produce oxygen radical anion (superoxide), peroxy radicals and other reactive species which can then bind to sensitive molecules in the cell (adduct formation). In this way the radiation damage is immobilized, and the adducts prevent or inhibit normal homeostatic repair mechanisms.

Many radiosensitizers mimic this effect of adduct formation under reducing conditions. The reductive binding of nitroimidazoles (Scheme 1) is a radiosensitization process (O_2 mimicry) that also results in their hypoxia-selective accumulation(1). Adduct formation in hypoxic tissue is the basis for radiotracer accumulation in target tissues, whereas selectivity is attributable to the formation of chemically-reactive species under reducing conditions in the viable but oxygen deficient cell. As shown in Scheme 1, the first-electron reduction is a reversible process, thereby making the ultimate binding dependent on the absence (low concentration) of oxygen.

Tissues are hypoxic if O_2 levels are below normal, but not at zero (anoxia). Oxygen levels fluctuate among and within the tissues, even under excellent perfusion, so that there is no universal base-line criterion. For example, radiobiological hypoxia (reduced radiosensitivity) occurs at O_2 levels below 1000 ppm, but metabolic effects due to higher (but sub-normal) O_2 levels may be evident in some tissues (2).

In contrast to the case for radiosensitizers, where reducing equivalents (electrons) may be produced in high flux through the interaction of therapeutic x- / γ-radiation with cell constituents (mainly water), hypoxia-sensitive radiopharmaceuticals must be reduced by metabolically-derived

electrons (3). Flavin-dependent cytochrome P450 reductase and related enzymes including xanthine and aldehyde oxidases, and quinone oxidase are thought capeable of carrying out the activation (reduction to reactive species) step.

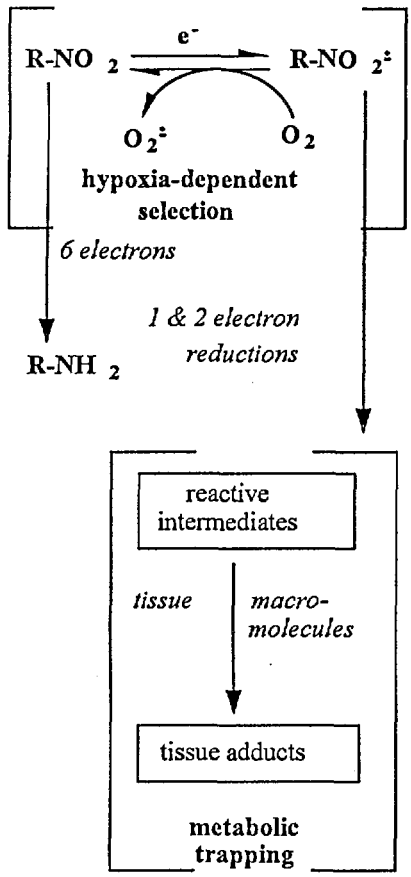

Scheme 1. Reductive activation and binding of nitroimidazole radiosensitizers.

The reductive activation process is dependent on the flow of electrons, derived from intermediary metabolism of glucose, down the cytochrome chain. The electrons flow from low electron potentiall to more electron-affinic species (Scheme 2). Normally, O_2 is the end recipient, but in its absence, other molecules can accept and be reduced by these electrons. The cell must be viable, even if oxidatively quiescent, to carry out this function. Indeed it is this property that makes hypoxia imaging a valuable diagnostic tool, enabling the diagnostician to discriminate between dead and potentially salvageable tissue.

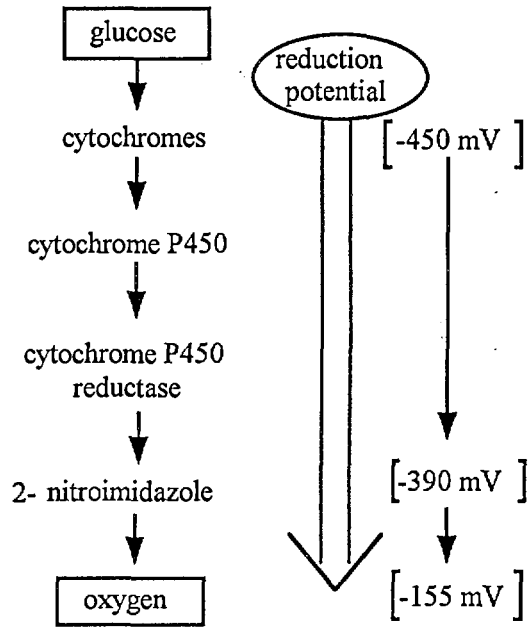

Scheme 2. Electron flow along the flavin-cytochrome system, leading to metabolic reduction of 2-nitro-imidazoles in viable tissue.

2. DESIGN CONSIDERATIONS FOR HYPOXIA RADIOTRACERS

In 1981 Chapman postulated that scintigraphic imaging of tumour hypoxia using gamma-emitting nitroimidazole radiosensitizers would be a useful predictive assay for radiation therapy planning (4). Considerations for the design of these imaging agents are briefly outlined in the following paragraphs.

Electron affinity and water-lipid partition (*P*) have been identidied as the critical properties that govern efficacy and toxicity of nitroimidazole radiosensitizers, and most investigators developing radiopharmaceuticals for imaging hypoxia apply these principles. If the electron affinity of the tracer for the first, single-electron, reduction step (first electron reduction potential at neutral pH, E^1_7) is too great, approaching that of O_2 (-155 mV), then selectivity for hypoxia will be diminished; if it is not sufficiently electron-affinic ($E^1_7 < -450$ mV), then sensitivity will be lost. This step is critical, since it is reversible by O_2 and is therefore responsible for selective binding to only

those tissues that are O_2 deficient. The E^1_7's of most 2-nitroimidazoles lie around -390 mV, an electron affinity considered to be optimal for both selectivity and sensitivity (5).

An equally important property is the compound's ability to permeate tissues. The combination of extra- and intracellular water, and hydrophobic plasma membranes, dictates that the molecules must have some lipophilicity (6). However, if they are too lipophilic (octanol:water partition coefficient $P > 10$), they will dissolve in lipoidal tissues and delineate areas that are not necessarily hypoxic (false positive images). If they are too hydrophilic ($P < 0.1$), they may not diffuse readily through cell membranes and they are likely to be cleared very rapidly via the kidney, severely reducing the amount of tracer available for metabolic activation and hypoxia-dependent binding (low signal intensity).

Of course, there are other biological properties that must be considered. Protein binding may have an effect on both clearance and diffusion from the central compartment (blood) to tissues. Strong protein binding of the radiopharmaceutical or any of its radiolabelled metabolites will result in prolonged clearance times, thereby delaying or preventing imaging because of poor signal-to-background ratios. The route of elimination is also important, with renal clearance and urinary excretion being preferred over hepato-biliary clearance because of radiation dosimetry and imaging complexity considerations. Similarly, metabolism other than reduction will complicate any interpretation of the image because of differences between the radiopharmaceutical and its metabolite(s) with respect to whole-body tracer kinetics, microkinetics (intracellular dynamics) and even metabolic binding. Finally, the acidity (pKa) of the molecule will reflect the influence of the pH gradient across the plasma membrane, with weakly acidic or weakly basic compounds concentrating as a result of ionization in either extracellular or intracellular fluid, leading to ionic trapping and overestimation of hypoxia.

Of the radiohalogen family, ^{123}I and ^{18}F have the most acceptable properties for imaging, in terms of photon energy, photon flux, decay half-life and radiation dosimetry. Other radiohalogens ($^{124/125/131}I$; ^{82}Br) and ^{99m}Tc, have been proposed for and/or used in the synthesis and pre-clinical evaluation of potential hypoxia radiotracers. For information on hypoxia-selective imaging agents other than ^{123}I-IAZA, readers are referred to reviews by Nunn *et al* (7) and Wiebe and Stypinski (8).

3. 1-β-D-(5-IODO-5-DEOXYARABINO-FURANOSYL)-2-NITROIMIDAZOLE (AZOMYCIN ARABINOSIDE; IAZA)

The radioiodinated 2-nitroimidazoles (azomycin derivatives) comprise the main body of literature that deals with agents for scintigraphic detection of tissue hypoxia. Their E^1_7's lie within the range for O_2-reversible reductions to occur, so the main challenge in molecular design is to adjust metabolic (non-reductive) and pharmacokinetic properties. Misonidazole (Miso) remains the reference compound against which the sensitizing properties of radiosensitizers are compared. Unfortunately, it is not a potential radiopharmaceutical because it does contain elements that have a suitable gamma-emitting radioisotope.

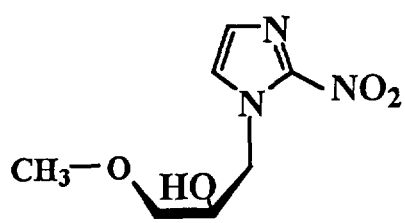

MISONIDAZOLE

The radiohalogenated azomycin nucleosides were selected for on the basis of their relatively low lipophilicity, with the benefit of several side-chain hydroxyl groups to counteract the lipophilic effects of iodine.

The synthesis of 1-β-D-(5-iodo-5-deoxyarabino-furanosyl)-2-nitroimidazole (azomycin arabino-side; IAZA) was initially reported in 1991 (9).

IAZA is more lipophilic (P = 4.98) than the sensitizer misonidazole (P = 0.41) (10), and than azomycin riboside (P = 2.1) (11), the first reported compound of this class.

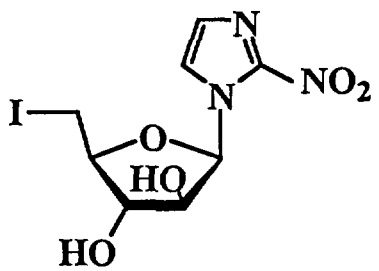

IAZA

IAZA was found to undergo *in vitro* hypoxia-dependent adduct formation at a higher rate than misonidazole, and although it was found to be almost 10 times more effective as a radiosensitizer, it was also almost 10 times as cytotoxic (Mannan *et al* 1991). Since toxicity is not a concern at the low doses used in scintigraphic imaging, IAZA was considered to be highly suitable for this purpose.

^{125}IAZA was found to undergo minimal deiodination and metabolic degradation *in vivo* in the EMT-6 murine tumour model. ^{123}IAZA scintigrams taken 8 h post-injection in this model showed good uptake by the tumour and rapid whole-body background clearance, so that favourable tumour:blood ratios provided usable images within 4-6 h. In non-thyroid-blocked animals, thyroid and stomach were visible on the late time interval scintigrams (9).

IAZA has been used for imaging in a variety of experimental and clinical pathologies. In photodynamic therapy (PDT) of a rat Dunning prostate tumour model, ^{123}IAZA localized in regions of PDT-induced hypoxia, with inverse correlation to ^{99m}Tc-HMPAO uptake, to provide evidence of hypoxia-selective binding for ^{123}IAZA (12). A dual radionuclide autoradiographic study of cerebral occlusion in rats depicted uptake of ^{125}IAZA in ischaemic areas and mutually exclusive uptake of ^{99m}Tc-HMPAO in well-perfused regions (13). Preliminary imaging studies in a surgical model of canine myocardial ischaemia showed uptake of ^{123}IAZA in *ex vivo* images but not in *in vivo* images taken 4 h after dosing (14). ^{123}IAZA and ^{99m}Tc-pertechnetate have also been used in models of non-steroidal anti-inflammatory drug (NSAID) damage to the intestinal epithelium and of adjuvant-induced arthritis in rats, in which scintigraphy showed abnormal and contrasting biodistribution patterns for these tracers. The relationships of these changes to hypoxia is under continuing investigation (15).

4. CLINICAL ^{123}IAZA IMAGING

High diffusibility into poorly-vascularized (ischemic) tissues, high reductive binding rate, moderately rapid clearance from blood, rapid total body clearance and minimal loss of radiolabel have been used to rationalize the clinical utilization of ^{123}IAZA for clinical hypoxia imaging. ^{123}IAZA-based investigations of regional hypoxia in cancer (16-18), diabetes (19), arthritis (20), brain trauma (21) and exercise-stress(22) pathologies have been reported.

It is understandable, given the role of tumour hypoxia in radiation curability of some human tumours, that the largest number of patients studied with ^{123}IAZA have oncological disease. This work has focused on patients with head and neck primaries and/or metastases, including small cell lung cancer, squamous cell carcinomas, glioblastomas and soft-tissue sarcoma. About 40% of the tumours were found to be hypoxic, based on ^{123}IAZA uptake. This data has been reported in detail.(16, 18). In addition, in a correlative study of ^{123}IAZA and ^{99m}TcHMPAO uptake, an inverse relationship was observed between uptake of the hypoxia (^{123}IAZA) and perfusion (^{99m}TcHMPAO) markers. In a small follow-up study to determine the prognostic potential of hypoxia with respect to radiation therapy responsiveness, 0 of 4 ^{123}IAZA-avid tumours showed control 3 months after therapy, whereas 5 of 9 non-avid tumours were still controlled 3 months after treatment. More recently, patients with other tumours, including prostate and breast cancers and melanoma have

been imaged to determine the range of solid tumours likely to accumulate the hypoxia marker (23) and a detailed prospective follow-up study is underway in conjunction with a radiation therapy protocol (24).

Diabetes mellitus is a prevalent disease in which the acute symptoms are usually managed by insulin replacement therapy, but there are complications. Peripheral vascular disease leading to ulceration, infection and even amputation of affected limbs, is currently diagnosed by transcutaneous measurement of limb oxygenation ($TcpO_2$) using oxygen-sensitive surface electrodes. This diagnostic modality measures O_2 concentrations only superficially. It is unable to detect subcutaneous hypoxia and is therefore most effective only late in the disease management process. In an investigation of the lower limbs of diabetic patients, ^{123}IAZA imaging detected regional and focal hypoxia. Correlations to $TcpO_2$ scores and visible lesions indicated that there is a role for ^{123}IAZA as a predictive test to identify problems in underlying tissues that are not otherwise detected until well advanced..

Hypoxia in load-bearing joints results from momentary ischaemia during the pressure interval. Joints with inflammatory effusive synovitis have associated increases in intra-articular pressure. In rheumatoid arthritis, increases in synovial membrane oxygen consumption combine with chronically high intra-articular pressures to create an hypoxic joint. Oxygen measurements in biopsied synovial tissue and in aspirated synovial fluid correlate with low pH, increased lactate, elevated pCO_2, high intra-articular pressure and large synovial fluid volume. Importantly, oxygen concentrations are inversely related to severity of arthritic disease. The radiopharmaceuticals currently used or proposed for imaging the arthritic joint act non-specifically or are targetted at other (not hypoxia) specific markers. In an ongoing clinical study using ^{123}IAZA, there was scintigraphic evidence of arthritic joint hypoxia (17).

^{123}IAZA is also being used clinically to study regional hypoxia associated with brain trauma (18). Preliminary data indicate that ^{123}IAZA uptake occurs in areas in decreased perfusion, and that there may be a complimentary role for hypoxia imaging to verify the viability of poorly-perfused brain tissue.

5. CLINICAL PHARMACOKINETICS AND RADIATION DOSIMETRY OF ^{123}IAZA

In early clinical studies there was some concern about the role of chemical dose on the sensitivity of this diagnostic imaging test *in vivo*, because of confusion in the literature (25) concerning dose dependent pharmacokinetics of misonidazole, together with reported dose-dependent uptake of ^{123}IAZA *in vitro* (9). Although the impact of dose on uptake in hypoxic tissue has not been systematically investigated in patients, radiopharmacokinetics and radiotracer kinetics in humans receiving i.v doses of ^{123}IAZA ranging from 0.1 to 10 mg showed no discernible differences in plasma clearance and whole-body elimination (26). These studies in healthy volunteers confirmed rapid distribution and clearance phases, with extensive urinary clearance (Plate 1). Initial radiation dosimetry estimates indicate an dose of 0.12 mGy/MBq to the bladder wall and 10-fold less to the liver.

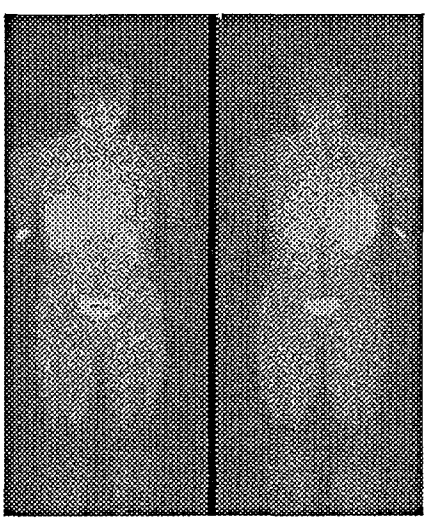

Plate 1. Planar scintigram of a healthy volunteer after injection of ^{123}IAZA (185 MBq as bolus i.v. dose).

6. SUMMARY

The initial application of hypoxia imaging agents was as predictive markers of radioresistant (hypoxic) tumours. Now there is interest in applying this diagnostic procedure not only to detect hypoxic tissues for radiotherapy planning, but to differentiate viable hypoxic tissue from necrotic regions. The differentiation of salvageable hypoxic tissue in a given pathology is an important objective for prognosis and for monitoring therapeutic intervention. Demonstrations of the widespread influence of hypoxia on metabolic processes such as drug resistance (27) continue to create interest in hypoxia imaging to address basic scientific questions.

7. REFERENCES

1. Adams GE, Cooke M.S. Int. J. Radiat. Biol. 15, 1969, 457-471.
2. Hall EJ. Radiobiology for the Radiologist. Harper and Row, Publishers, New York (1978).
3. Biaglow JE, Varnes ME, Roizen-Towle L, Clark EP, Epp ER, Astor MB, Hall EJ. Biochem. Pharmac. 35, 1986, 77-90.
4. Chapman JD, Franko AJ, Sharplin J. Brit. J. Cancer 43, 1981, 546-550.
5. Adams GE, Flockhart IR, Smithen CE, Stratford IJ, Wardman P, Watts ME. Radiat. Res. 67, 1976, 9-20.
6. Brown JM, Workman P. Radiat. Res. 82, 1980, 171-190.
7. Nunn A, Linder K, Strauss HW. Europ. J. Nucl. Med. 1995, 265-280.
8. Wiebe LI, Stypinski D. Quart. J. Nucl. Med. 39, 1996, 270-284.
9. Mannan RH, Somayaji VV, Lee J, Mercer JR, Chapman JD, Wiebe LI. J. Nucl. Med. 32, 1991, 1764-1770.
10. Brown JM, Workman P. Radiat. Res. 82, 1980, 171-190.
11. Jette DC, Wiebe LI, Flanagan RJ, Lee J, Chapman JD. Radiat. Res. 105, 1986, 169-179.
12. Moore RB, Chapman JD, Mercer JR, Mannan RH, Wiebe LI, McEwan AJ, McPhee MS. J. Nucl. Med. 34, 1993, 405-413.
13. Lythgoe MF, Williams SR, Wiebe LI, McEwan AJB, Gordon I. Europ. J. Nucl. Med. 24, 1997, 16-20.
14. Okada R, Johnson G, Edwards B, Mannan RH, McEwan AJB, Wiebe LI. unpublished data.
15. McEwan AJB, Skeith KJ, Mannan RH, Davies N, Jamali F, Schmidt R, Golberg L, Wiebe LI. J. Nucl. Med. 38, 1997, 300P-301P.
16. Parliament MB, Chapman JD, Urtasun RC, McEwan AJ, Golberg L, Mercer JR, Mannan REH, Wiebe LI. Br. J. Cancer 65, 1992, 90-95.
17. Groshar D, McEwan AJB, Parliament MB, Urtasun RC, Golberg LE, Hoskinson M, Mercer JR, Mannan RH, Wiebe LI, Chapman JD. J. Nucl. Med. 34, 1993, 885-888.
18. Urtasun, RC, Parliament MB, McEwan AJ, Mercer JR, Mannan RH, Wiebe LI, Morin C, Chapman, JD. Br. J. Cancer, 74, 1996, S209-S-212.
19. Al-Arafaj A, Ryan EA, Hutchinson K, Mannan RH, Mercer J, Wiebe LI, McEwan AJB. Eur. J. Nucl. Med. 21, 1994, 1338-1342.
20. Skeith KJ, McEwan AJB, Schmidt R, Wiebe LI. unpublished.
21. Vinjamuri S, van den Broek M, Maltby P, Stringer RE, Grime JS, Wiebe LI, McEwan AJ, O'Drisodl K, Critchley M. Europ. J. Nucl. Med. in press, 1997, (abstract).
22. Cwik VA, McEwan AJB, Brooke, MH. Neurology, 45 (Suppl 4), 1995, A446.
23. McEwan AJB, Schmidt R, Wiebe LI. unpublished.
24. Cox P, Levendag PC, Pillay M, Planting AST, Senan S, McEwan AJB, Wiebe LI. unpublished.
25. Wiebe LI, Stypinski D. Quart. J. Nucl. Med. 40, 1996, 270-284.
26. Stypinski D, Wiebe LI, McEwan AJB, Tam YK, Mercer JR, Schmidt RP. (submitted).
27. Sakata K, Kwok TT, Murphy BJ, Laderoute KR, Gordon GR, Sutherland RM. Br. J. Cancer 64, 1991, 809-814.

Quality Control Methods of Strontium Chloride $^{89}SrCl_2$, Radiopharmaceutical for Palliative Treatment of Bone Metastases.

CZ DEPTULA, T KEMPISTY, A MARKIEWICZ, R MIKOLAJCZAK, S STEFAŃCZYK, T TERLIKOWSKA, W ZULCZYK
Radioisotope Centre POLATOM,
05-400 Otwock - Swierk, Poland

SUMMARY

Strontium chloride, $^{89}SrCl_2$, a radiopharmaceutical used for palliative therapy of bone metastases from breast and prostate cancer is produced by irradiation in a nuclear reactor. Radionuclidic purity of the preparation is well over 99.6%. Extraction chromatography on strontium and rare earth elements specific resins is used for separation of the ^{90}Y (daughter of ^{90}Sr) and γ-impurities for the radionuclidic purity analysis of the $^{89}SrCl_2$ solution. Complexometric determination of strontium and argentometric titration of chlorides are used to confirm chemical composition of the preparation and its specific activity. The quality control protocol is established to confirm the suitability of the obtained $^{89}SrCl_2$ as the radiopharmaceutical.

1.INTRODUCTION

^{89}Sr-Strontium chloride is a radiopharmaceutical used for palliative therapy of multiple malignant metastases to the skeleton, mainly from breast or prostate cancer. Therapeutic action of ^{89}Sr is known for over 50 years, as reported by Pecher (1) but its application became popular in recent years because of increasing number of patients suffering from malignant bone neoplasm. In Europe the preparation is offered by Amersham under the name Metastron.

Internal radiotherapy gives a selectively directed and effective radiation dose in the painful osseous metastases whereas the radiation risk to normal tissue is minimal. Several radiopharmaceuticals were used for therapy of bone metastses: ^{32}P, ^{89}Sr, ^{131}I, ^{90}Y (2) and recently ^{186}Re-HEDP and ^{153}Sm-EDTMP (3). Among them ^{89}Sr seems to be the most effective and gives long lasting pain palliation (4). Strontium-89 is practically a pure beta emitting radionuclide (β-particle energy of 1.46 MeV and $T_{1/2}$ = 50.5 days). In bone tissue this radiation penetrates to about 0.8 cm. In normal bones the biological half life of strontium is about 14 days, in malignant bone tissue about 50 days (4). Radiotherapeutic action of $^{89}SrCl_2$ is probably based on irradiation of metastases and surrounding tissue which gives in effect pain palliation (5).

Strontium-89 can be produced either in a cyclotrone or by irradiation of strontium-88 in a nuclear reactor (n,γ reaction). When the latter option is used, depending on the purity of the target material and irradiation parameters several long- and short lived γ-radionuclides can be produced as impurities.

Strontium-90, a β-emiter produced in a secondary reaction (^{89}Sr (n,γ) ^{90}Sr) contributes to the impurities. It accumulates in the bones as well and has a very long ($T_{1/2}$ = 28.5 years) half life. Two parameters, besides its sterility and isotonicity, are critical when the therapeutical usefulness of the preparation is concerned: specific activity and radionuclidic purity. The aim of the work presented below was to establish analytical quality control procedures to confirm the radionuclidic purity as well as chemical composition and specific activity of the $^{89}SrCl_2$ preparation obtained by irradiation in a nuclear reactor.

2.EXPERIMENTAL

2.1.Materials

Strontium-88 carbonate, isotopic enrichment 99.8%, Cambridge Isotope Laboratories, US.

^{90}Sr and ^{90}Y(carrier free), produced at the Radioisotope Centre POLATOM were used for spiking the analysed solutions.

Extraction chromatography resins with organic extractants supported on nonionic acrylic ester polymer:
Sr-Spec : 4',4"(5") di-t-butylcyclohexane-18-crown-6 in N-octanol
RE-Spec : octyl(phenyl) -N,N-diisobutyl carbamoylmethylphosphine oxide [CMPO] in tributyl phosphate (TBP)
Pre-filter material (AmberlitXAD-7)
®Spec resins and pre-filter material are commercially available from EICHroM Industries, Inc. Il.US.
All reagents used were of analytical grade.

2.2.Column preparation
Glass columns of 6 mm internal diameter were filled to about 50 mm height with Spec resin which was preliminary conditioned in the acidic solution for 24 hours. The Sr-Spec resin was prepared in 3M HNO_3 and RE-Spec in 2M HNO_3 according to the suppliers recommendations (6).

2.3. Instrumentation
LSC counter WALLAC (LKB) with application of liquid scintillator Ultima Gold (Hewlett Packard)

Gamma-spectrometer with HPGe detector of 70 cm^3 volume and resolution of 0.8 keV at energy 122keV from ^{57}Co and 1.8 keV at 1332 keV from ^{60}Co. Detection limits for γ-impurities by this apparatus are within $5*10^{-3}$and $5*10^{-5}$ %.

PU 8745 UV/VIS spectrophotometer (Philips)

PGS-2 spectrograph (Carl Zeiss, Jena).

2.4.Method of $^{89}SrCl_2$ preparation
^{89}Sr was obtained by neutron bombardment of $SrCO_3$ (enriched in strontium-88 over 99.8%) in a reactor at 10^{15} $n*cm^{-2}*s^{-1}$ neutron flux. Irradiated target material was dissolved in 1 M HCl, evaporated to dryness and dissolved in water (bulk solution). After correction of specific activity and isotonicity by addition of natural $SrCl_2$ and NaCl the solution was filtered on 0.22μm filter, dispensed into glass vials, sealed and autoclaved.

2.5. ^{90}Y separation from $^{89}SrCl_2$ solution on Sr-Spec and RE-Spec resins.
The solutions to be analyzed on Sr-Spec or RE-Spec were acidified correspondingly to either 3M or 2M with nitric acid. Aliquots of the analysed solution were loaded onto a column, rinsed with an appropriate nitric acid solution and finally a stripping of the column with dilute nitric acid was made. Aliquots of the load, rinse and strip fractions were collected and subjected to analysis by γ or β-counting. The capacity of resin in the column is about 6 mg of Sr while the aliquots of the analysed solution contained up to 3 mg of Sr.
Carrier-free ^{90}Y solution and its mixture with ^{89}Sr bulk solution were analysed on Sr-Spec column. The elution profile of ^{90}Y rinsed with 3M HNO_3 is presented in Figure 1.

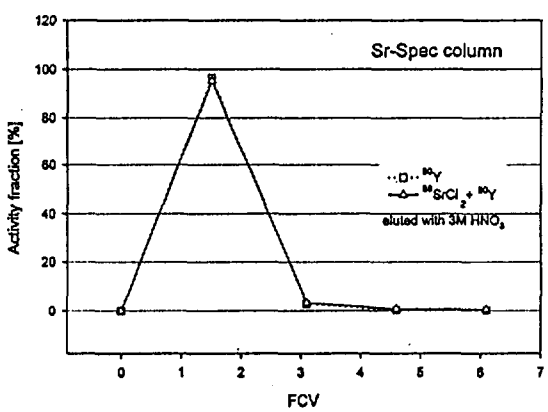

Fig.1 ^{90}Y elution efficiency on Sr-Spec column.

The effluent volume necessary to rinse ^{90}Y loaded as carrier free solution and with addition of strontium carrier was not more than 2ml (up to 3 free column volumes FCV). Fractions eluted with 3M HNO_3 did not contain ^{89}Sr but γ-impurities such as ^{156}Eu, ^{51}Cr, ^{54}Mn, ^{60}Co and ^{65}Zn present in the $^{89}SrCl_2$ solution were eluted together with ^{90}Y. Under these conditions the measurement of ^{90}Y activity by the LSC method was not possible.
RE-Spec resin (RE is for rare earth elements) retains yttrium selectively when eluted with 2M HNO_3. To strip yttrium from the column the eluent is changed to diluted 0.2M HNO_3. Europium isotopes are retained on the RE-Spec column and neither 2M HNO_3 nor 0.2M HNO_3

removes them (see Table 1). Carrier free ^{90}Y solution of known activity was loaded on the RE-Spec column and rinsed with 2M HNO_3. Any ^{90}Y activity was present in the effluent. Then the column was rinsed with 0.2M HNO_3. The elution profile of ^{90}Y from the RE-Spec column is shown in Fig.2. The strip of yttrium from the RE-Spec column is rapid and not more than 8 free column volumes of eluent are needed for its complete recovery.

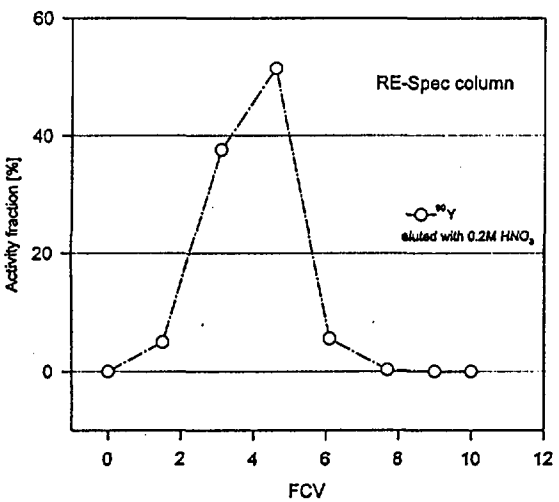

Fig. 2 Recovery of ^{90}Y from the RE-Spec column.

The activities of radionuclides present in the collected fractions of effluent were measured. Five fractions of 1ml volume rinsed with concentrated HNO_3 followed by four fractions of diluted HNO_3 were collected.
As shown in Table 1, bulk $^{89}SrCl_2$ solution loaded on the RE-Spec column is purified from ^{156}Eu and ^{154}Eu, other γ-impurities are eluted with 2M HNO_3 (fractions 1-5) while trace amounts of ^{60}Co and ^{59}Fe (which was previously not observed) are detected next to the ^{90}Y (fractions 6-9).

3. RESULTS

3.1. Determination of the ^{90}Sr in the $^{89}SrCl_2$ solution

The ^{90}Sr activity in the $^{89}SrCl_2$ solution is calculated on the basis of ^{90}Y activity. Prior to the measurement by LSC method ^{90}Y must be separated chemically. The system for separation of ^{90}Y from the $^{89}SrCl_2$ solution is presented in Figure 3.

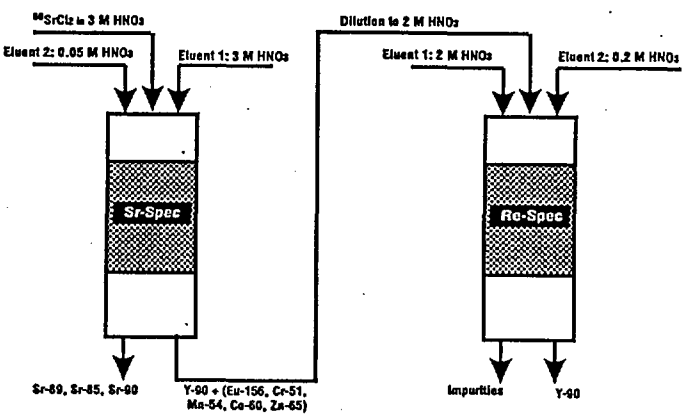

Fig.3 Extraction chromatography system for ^{90}Y separation from $^{89}SrCl_2$ product solution.

Table 1. Radionuclidic impurities determined in fractions of effluent collected during $^{89}SrCl_2$ solution chromatography on RE-Spec column (results obtained by γ-spectrometry)

Radionuclide	Fractions eluted with 2M HNO_3 [kBq]					Fractions eluted with 0.2M HNO_3 [kBq]	RE-Spec resin [kBq]
	1	2	3	4	5	6 - 9	
^{85}Sr	0.44	7.03	0.041				
^{51}Cr	0.37	4.81	0.037	0.012	0.005		
^{60}Co	0.013	0.37	0.003			0.008	
^{65}Zn	0.011	0.28					
^{54}Mn		0.14	0.016				
^{103}Ru	0.004	0.085					
^{159}Fe						0.006	
$^{154}Eu + ^{156}Eu$							103.6

To separate ^{90}Y from the product solution two steps of extraction chromatography are involved. The analyzed solution is first purified from γ-impurities (mostly ^{154}Eu and ^{156}Eu) on the Sr-Spec column. When eluted with 3M HNO_3, the Sr-Spec column retains strontium isotopes while impurities i.e. ^{156}Eu, ^{51}Cr, ^{54}Mn, ^{65}Zn as well as ^{90}Y are removed from the column and the effluent collected. This solution is diluted with water to get 2M HNO_3 environment and then placed on the RE-Spec column. Rinsing with 2M HNO_3 is continued to remove impurities while yttrium is retained. Then ^{90}Y is stripped from the column with 0.2M HNO_3. The fraction containing ^{90}Y is collected for measurement by the LSC method and its activity recalculated for ^{90}Sr and related to the ^{89}Sr activity in the original sample. The results of the ^{90}Sr determinations varied in the range from $1.9*10^{-4}$ % to $2.1*10^{-4}$%.

3.2. Determination of $^{89}SrCl_2$ chemical composition

The chemical concentration of strontium in the product is determined by complexometry with arsenazo III. In acetone solution Sr^{+2} forms with arsenazo III a complex which maximum absorbance can be measured at 640 nm (7). The assay of chlorides is determined by potentiometric titration with silver nitrate (8) The sum of chlorides coming from $SrCl_2$ and NaCl present in the solution is determined.
The chemical purity of the preparation is measured by DC graphite spark spectrography. With this technique the limits for contamination with the following elements: As, Ba, Cd, Pb and Te are 5 μg/ml of each and summaricaly not more than 10μg/ml.

4. DISCUSSION OF RESULTS

The radionuclidic purity of the radiopharmaceutical (when γ-impurities are concerned) can be determined directly in the product solution by γ-spectrometry but the activity of ^{90}Sr by β-counting is not measureable against ^{89}Sr. We proposed the indirect method of ^{90}Sr determination by separation of yttrium-90 which is in equilibrium with ^{90}Sr and can be separated chemicaly from the parent nuclide.
The decay scheme of ^{90}Sr is as follows:

$$^{90}Sr \xrightarrow[28y]{\beta^-(0.54MeV)} {}^{90}Y \xrightarrow[64.0h]{\beta^-(2.28MeV)} {}^{90}Zr$$

This reaction is widely used for production of carrier-free ^{90}Y. The chemical separation techniques used by different authors were: solvent extraction (9,10), precipitation (11) and various forms of chromatography (12,13,14). The properties of solid phase extraction chromatography on Spec resins were used for ^{90}Y separation. Extraction chromatography combines the advantages of solvent extraction (selectivity) and ion exchange chromatography (ease of use). The Sr and RE-Spec resins are stable and easy to regenerate. The effect of resins irradiation was carefuly studied by Horowitz (15) and their stability proved. The organic extractant is well bound to the supporting resin and if freed can be removed from the effluent when passing it through a bed of uncoated nonionic acrylic ester polymer (pre-filter material from Eichrom).
The contamination with ^{90}Sr determined in the $^{89}SrCl_2$ solution at the value of about $2*10^{-4}$ % conforms with the data published by Laing et all (5) and with the value calculated on the basis of activation parameters.
When the radionuclidic purity measurements in the bulk solution indicate relatively high level of γ-impurities (<0.4% relative to ^{89}Sr is the upper limit for the product) it is possible to extend the period of cooling the short lived radionuclides (shorter than that of ^{89}Sr). Among the radionuclides detected in the bulk solution only the half lifes of ^{54}Mn(312,5d), ^{60}Co(1926d) and ^{65}Zn(244d) are longer than that of ^{89}Sr. Cooling might be practical when the level of the impurities is at the limit, when it is higher the benefit of increase in radionuclidic purity is counterweighed by loss of ^{89}Sr activity.
The possibilities of the technology optimization in the aim to reduce contamination with γ-radionuclides were carefully studied (data not shown). The radionuclidic purity of the obtained preparation is about 99.9%. The γ-impurities determined are: ^{85}Sr at the level of 0.09 - 0.1% and ^{65}Zn, ^{51}Cr, ^{54}Mn, ^{60}Co, ^{188}Re at the level of $1*10^{-2}$ to $1*10^{-4}$%.
The quality of the obtained product was investigated. Table 2 specifies the tests included into quality control procedure of $^{89}SrCl_2$ as well as the results of the determinations performed on the 3 production batches.

Table 2. Quality control protocol of the 3 production batches of $^{89}SrCl_2$.

TESTS	SPECIFICATIONS	Batch 1A	Batch 1B	Batch 2A
Identification: Characters	clear, colourless liquid	complies	complies	complies
spectra identification	β-ray spectrum E_{max} = 1.49 MeV γ-ray spectrum E_{max} = 910 keV	complies	complies	complies
pH	4 - 7	5.5	5.5	6.0
Radionuclidic purity	γ-impurities < 0.4%	≤ 0.1	≤ 0.1	≤ 0.1
	^{90}Sr	$2.0*10^{-4}$	$1.97*10^{-4}$	$2.04*10^{-4}$
Radioactive concentration	37.5 MBq/ml	37.5	37.5	37.5
Chemical purity	not more than 10 μg/ml of: Cd, Ba, As, Te, Pb,	< 10	< 10	< 10
Assay:				
strontium chloride	10.8 - 19.4 mg/ml	10.8	11.3	10.9
sodium chloride	0 - 3.0 mg/ml	2.9	2.9	3.0
Specific activity	3.5 - 6.3 MBq/mg Sr	6.2	6.3	6.2

The $^{89}SrCl_2$ preparation forms a sterile and isotonic water solution. The specific activity of $^{89}SrCl_2$ falls in the range from 3.5 to 6.3 MBq/mg Sr while chemical concentration of strontium is about 10.8 mg/ml and NaCl about 3.0 mg/ml. The radionuclidic purity with respect to γ-impurities is not less than 99.6%. The radioactive concentration is 37.5 MBq/ml which gives a standard single patient dose of 150 MBq in 4 ml solution. The preparation is stable over the period of not less than 4 weeks. After this time the ^{89}Sr activity decreases by about 32% of its initial value and the specific activity decreases to its lower limit but the therapeutical usefulness of the preparation is not lost.

5. CONCLUSIONS

The obtained solution of $^{89}SrCl_2$, produced by irradiation of $^{88}SrCO_3$ in a nuclear reactor fulfills the requirements of a medical preparation. The radionuclidic purity of the preparation with respect to γ-impurities is about 99.9%. ^{90}Sr strontium assay in the $^{89}SrCl_2$ solution determined by its daughter nuclide ^{90}Y separation on the selective extraction chromatography resins is at the level of $2*10^{-4}$% and the toxicological risk from contamination with this isotope can be neglected.

References

1. Pecher C.: Univ. Calif. Publ. Pharmacology **11**, 1942, 117-149
2. Reddly E.K. et all.: J. Nucl. Med. Assoc. 7, 1986, 27-32
3. Volkert W.A. et all: Drugs of Future. **14**, 1989, 779-881
4. Bloke S.M. et al.: European J. Nucl. Med. **12**, 1986, 447-454
5. Laing A.H.: The British Journal of Radiology, **64**, 1991, 816-822
6. Eichrom Analytical Products Description, Eichrom Industries Inc., 1995
7.Marczenko Z.: Spektrofotometryczne oznaczanie pierwiastków.PWN;Warszawa 1979
8. European Pharmacopoeia 3rd edition,1997.
9. Peppard D.F. et all.: J. Inorg. Nucl. Chem. **5**, 1957, 141-144
10. Goldin A.S. and Velten R.J.: Anal. Chem. **33**, 1961, 149-152
11. Kanapilly G.M. and Newton G.J.: Int. J. Appl. Radiat. Isot. **22**, 1971, 567-575
12. Suzuki Y.: Int. J. Appl. Radiat. Isot. **15**, 1964, 599-602
13.Sraba W.J. et all: Int.J. Appl. Radiat. Isot. **29**, 1978, 91-94
14. Dietz M.L. and Horowitz E.P.: Appl. Radiat. Isot. **9**, 1992, 1093-1101
15. Horowitz E.P. et all: Analytica Chimica Acta, **266**, 1992, 25-29

^{149}Terbium, a novel α-emitter for Radioimmunotherapy

Imam, SK[1], Allen, BJ, Goozee, G, Sarkar, S*, and **Henniker, AJ.

Department of Biomedical Physics Research, St. George Cancer Care Centre, Kogarah
[1]Now at Department of Nuclear Medicine & Clin. Ultrasound, Liverpool Hospital, Liverpool
*School of Medical Radiation Technology, University of Sydney, Cumberland Campus
** Department of Haematology, ICPMR, Westmead Hospital, Westmead.

Abstract

Due to the endowed physical properties, like short range, high energy α-particles with high linear energy transfer (LET) and high relative biological effectiveness (RBE), the α-emitters are particularly promising in the treatment of micrometastases by killing cells in transit (Go phase) and in preangiogenic lesions sparing normal cells and bone marrow (the dose limiting organ), if conjugated to a 'smart' carrier (radioimmunoconjugate, RIC).

^{149}Tb, the α-emitting radiolanthanide was successfully produced on tandem accelerator at ANU by irradiating ^{152}Nd and studied by us for the first time for its possible use in the treatment of cancer with its high α-energy of 4.0 MeV, high LET of 143 keV/μm and high RBE of 3.

^{152}Tb, a predecessor of ^{149}Tb, alongwith another lanthanide, ^{153}Sm, were used for optimising the technique for radiolabelling anti-melanoma and anti-leukaemia antibodies, viz, 9.2.27 and WM-53, respectively, by virtue of bifucntional chelators, like cyclic anhydride of diethylene triamine pentaacetic acid (cDTPAa) or 1,4,7,10-tetraazacyclo-dodecane-N,N',N",N"'-tetraacetic acid (DOTA) derivative.

The RIC was subjected to quality control based on radiochemical purity, serum stability, and flow-cytometry studies. The biological effectiveness of these conjugates was evaluated by in vitro and in vivo experiments. The former was based on cell survival study by ^{3}H-thymidine incorporation test, and the latter by looking at the biodistribution in tumour models in nude mice using melanoma cell lines MM-138.

The results were encouraging and the ^{149}Tb-RIC could possibly emerge as a promising modality for the treatment of micrometastases of melanoma and the cell purging for leukaemia.

Introduction

We intend to study the possibility of α-RIT with Tb-149 which is an α- emitter with a short half-life of 4.15 hr. Radiolanthanides have common chemical properties and can be used for radiolabelling monoclonal antibodies (MoAbs) for targeted cancer therapy. Two, primarily beta-emitting radiolanthanides, namely, ^{153}Samarium and ^{152}Terbium, have been investigated for radiolabelling of the anti-melanoma antibody 9.2.27 using a bifunctional chelator, the bicyclic anhydride of diethylene triamine pentaacetic acid (cDTPAa).Tb-149 has identical chemistry to Tb-152, and as a radiolanthanide is expected to have a similar radiolabelling chemistry to Sm-153. We have initiated this preliminary study with β-emiters Tb-152 (β^+) and Sm-153 (β^-) which have longer $t_{1/2}$ enabling us to optimise radiolabelling techniques, and also have appropriate γ-energy for imaging.

In contrast to the β- and γ-emitters, the physical properties of α-emitters offer a greatly improved level of selectivity in RIT. Tb-149, an α-emitting radiolanthanide, has been shown to be the most appropriate radiolabel for radioimmunoconjugation (RIC) for the treatment of disseminated tumours and microscopic metastases (Allen and Blagojevic, 1996) because of the:

- high α-energy of about 4.0 MeV
- short range of 28 μm
- high linear energy transfer (LET) of 143 keV/μm
- higher relative biological effectiveness (Allen and Blagojevic 1996).

These attributes lead to the deposition of a much greater fraction of total energy into cancer cells if a *smart* carrier is employed. Very few nuclear hits are required to kill the cells in transit (which may be in the Go phase), preangiogenic and subclinical lesions (Allen et al, 1996). The α-radionuclides are also expected to spare normal stem cells as only a narrow strip of marrow would be irradiated by the short range alphas if deposition of separated Tb occurs on the surface of trabecular bone.

Table 1: Properties of radiolanthanides

Radionuclide & Decay		*Half-life (hr)*	*E_α (MeV)*	*E_β (MeV)*	*E_γ (MeV)*
Tb-149	α	4.15	3.967	-	0.165, 0.352
Tb-152	β^+	17.5	-	2.80	0.344, 0.511
Sm-153	β^-	46.8	-	0.81,0.71, 0.64	0.103

Materials

Tb-152 was produced on the tandem accelerator at ANU using a beam of C-12 ions on a Nd-142 target Goozee et al 1996). Sm-153 was procured from the Australian Radioisotopes (ANSTO).
The bifuctional chelator, cDTPAa was purchased from Aldrich and the anti-melanoma antibody 9.2.27 was generously provided by the Reisfeld's Laboratory, Scripps Research institute, La Jolla, California, USA (Morgan et al 1981) through the John Hunter Hospital, Newcastle. The melanoma antibody WM-53 as well melanoma cell lines MM-138 and MM-170, and the leukaemia cell line HL-60 were provided by the Department of Haematology, Westmead Hospital.

Methods

The irradiated source was transported from ANU to Sydney, dissolved in concentrated HNO_3 and the separation of Terbium from reaction products was done on an anion exchanger, Aminex using α-hydroxy butyric acid as an eluent (Sarkar et al 1996).

a) Prelabelling approach:
A suspension of cDTPAa in $CHCl_3$ (1mg/mL) was made and an aliquot of that was evaporated in a ReactiVial under stream of Nitrogen gas. Then, Tb-152 or Sm-153 in 0.2M NaAc buffer (pH 5.5) was incubated at 37 °C for 30 min, purified on chelex column and eluted with NaAc buffer. The eluate was then conjugated with 2 mg of MoAb 9.2.27 in NaAc or bicarbonate buffer (alkaline pH) by incubating for 1 h at 37 °C. The radioimmunoconjugate (RIC) was purified on P6DG column using the respective buffer.

Conventional approach:
The chelator was first conjugated with the protein in NaAc or bicarbonate buffer (alkaline pH), purified on P6DG column using the respective buffer and then radiolabelled with Tb-152 or Sm-153. The RIC was purified on P6DG column.

The quality control of the resulting radioimmunoconjugate (RIC) included the determination of radiochemical purity using instant thin layer chromatography (ITLC)-SG/0.1M HCl, and protein estimation using ELISA plate reader. The in vitro studies comprised serum stability, cell affinity and cell binding assays. The biological effectiveness of the RIC was evaluated in vitro by cell survival studies based on ^{3}H-thymidine incorporation using human melanoma cells, MM-138. Biodistribution studies in nude mice were performed to determine the uptake in tumour xenografts.

^{3}H-thymidine incorporation test:
Method a) 100 µL cells + 10 µL (1 µCi) ^{3}H-thymidine + 15 µL RIC, incubated for 4 days at 37 °C, harvested and counted the strips in a beta counter.

Method b) 100 µL cells + 15 µL RIC, incubated for 1 h at 4 °C, washed twice with PBS/2% FCS, plated out in triplicates, incubated for 4 days at 37 °C, added 10 µL (1 µCi) ^{3}H-thymidine, reincubated at 37 °C overnight, harvested and counted.

Cell affinity study: It was done by flowcytometry using labelled and unlabelled antibody 9.2.27 with MM-138 cell line after 30 min incubation at 4 °C.

Cell binding assay: The same number (0.9 million) of MM-138 cells (for specific binding) and HL-60 (leukaemia cells for non-specific binding) were incubated with the same amount of RIC (16 MBq) for 45 min at 37 °C. After two washings with PBS, the pellets and their respective pooled supernatants were counted for radioactivity.

Results

a) Tb-152:
Prelabelling: Protein recovery 56%; Labelling 60%.
^{3}H-thymidine: Inhibition due to RIC 31%.
Conventional: Protein recovery 61%; Labelling 30%.

b) Sm-153:
Prelabelling: Protein recovery 94 %; Labelling 71%.
^{3}H-thymidine: 50% inhibition.
Conventional: Protein recovery 97%; Labelling 47%.
Cell affinity: Unlabelled Ab= 98%; Radiolabelled Ab= 93%.
Cell binding: Binding with MM-138 = 35.23 %
Binding with HL-60 (non-specific control) = 9.47 %
Nett specific binding = 25.76 %

Table 2: Parameters of radiolabelled immunoconjugates

Method	*Radioisotope*	*Protein recovery*	*Labelling efficiency*	*^{3}H-thymidine Inhibition*
Prelabelling	Tb-152 Sm-153	50 % 94 %	60 % 71 %	31 % 50 %
Conventional	Tb-152 Sm-152	61 % 97 %	30 % 47 %	- 72 %

Table 3: Cell affinity and binding for Sm-RIC

	Unlabelled MoAb 9.2.27	*Radiolabelled MoAb 9.2.27*	
Affinity	98 %	93 %	
		Cells	*Supernatant*
Cell binding: MM-138 specific		35 %	65 %
HL-60 non-specific		9 %	91 %
Nett Specific		**26 %**	

Animal studies: A tail vein injection of 50 μL RIC lead to a tumour uptake of 12% in a nude mouse model having a subcutaneous tumour with MM-138 cells.
Serum stability: RIC at room temperature(RT): 3-5.8% leaching after 95h, RIC w/serum: 11% leaching at RT and 33.5% leaching at 37°C after 20 h.

Discussion

The encouraging results so obtained support the use of these RICs for combined radioimmunoscintigraphy (RIS) and radioimmunotherapy (RIT) by virtue of their inherent soft gamma and strong beta emissions.

A partially successful radiolabelling of antimelanoma antibody with Tb-152 and Sm-153 was achieved, giving 72% inhibition of DNA synthesis, 12% tumour uptake of the Sm-RIC in a nude mouse model, and 25 % specific cell binding for MM-138 appear to be encouraging results for the proposed α-RIT program. However, further endeavours are needed to improve the existing radiolabelling efficiency in order to explore the great potential of Tb-149 for cancer therapy.

A 5% loss of affinity of the RIC to cancer cells and 11% leaching of radiolabel in human serum after 20 hr at room temperature are within acceptable limits.

Conclusion

We have radiolabelled an antimelanoma antibody with the two radiolanthanides, Tb-152 and Sm-153. We expect Tb-149 to behave likewise to form a RIC for α-RIT. Further studies are needed to optimise labelling with these 3 lanthanides in order to determine the therapeutic efficacy of Tb-149.

References

1. Allen, BJ and Blagojevic, N, Alpha and beta-emitting radionuclides in targeted cancer therapy, 1996, Nucl. Med. Comm. 17:40-47.

2. Allen, BJ, Goozee, G, Imam, SK, Sarkar, S, Leigh, J, and Beyer, GJ, Targeted cancer therapy: the potential role of Tb-149, 1996, Proc. VI Ann. Symp. on Radiopharmaceutical Dosimetry, Gatlinburg, Tenn., USA

3. Goozee, G, Allen, BJ, Imam, SK, Sarkar, S, and Leigh, J, Tandem accelerator production of Tb-149 for targeted cancer therapy, AINSE Radiation Science Conference "RADIATION'96".

4. Morgan, AC, Gallaway, DR, and Reisfeld, RA, Production and characterisation of monoclonal antibody to a melanoma specific glycoprotein, Hybridoma 1:271, 1981.

5. Sarkar, S, Allen, BJ, Goozee, G, and Imam, SK, Radiochemical separation of Tb-149 after tandem accelerator production, AINSE Radiation Science Conference "RADIATION'96".

Production and Separation of Terbium-149,152 for Targeted Cancer Therapy

S SARKAR[1], B J ALLEN[2], S IMAM[2], G GOOZEE[2], J LEIGH[3], H. MERIATY[4]

[1]School of Medical Radiation Technology, Faculty of Health Sciences, The University of Sydney, East Street, Lidcombe2141
[2]St George Cancer Care Centre, Gray Street, Kogarah 2217
[3]Department of Nuclear Physics, Australian National University
[4]ANSTO, PMB 1, Menai 2234, NSW

SUMMARY. This work concerns the production and separation of small amount of Terbium-149,152 (^{149,152}Tb) from natural Neodymium (^{nat}Nd) and Praseodymium-141 (^{141}Pr) for in-vitro studies. Carbon-12 (^{12}C) was used as projectile to produce ^{149,152}Tb through ^{142}Nd(^{12}C,5n)^{149}Dy$\rightarrow$^{149}Tb, ^{141}Pr(^{12}C,4n)^{149}Tb, ^{142}Nd(^{12}C,2n)^{152}Dy$\rightarrow$^{152}Tb and ^{141}Pr(^{12}C,n)^{152}Tb reactions. This new class of isotopes have unique physical, chemical and nuclear properties and potential applications for radionuclide therapy and diagnosis. In this study thin-target catcher foil and thick target radiochemical techniques were employed to determine the yield. Appropriate radiochemical separation techniques have been used to separate other lanthanides, from terbium, produced by secondary reactions. Optimum experimental conditions for the production of useful quantities of ^{149,152}Tb and carrier free separation of terbium are discussed.

Introduction

The efficacy of radionuclides for therapy and diagnostic purposes depends on their physical, chemical and nuclear properties. Traditionally beta-emitting radionuclides such as iodine-131 (^{131}I), yttrium-90 (^{90}Y) and samarium-153 (^{153}Sm) are used in radionuclide therapy. Beta-emitting radionuclides are effective in palliative treatment but not for controlling cancer. Recently, alpha-emitting radionuclides have gained importance for their potential application to targeted cancer therapy (1,2) because of their short range and high Relative Biological Effectiveness.

Selection of the production process of the desired radionuclide is crucial since a number of parameters are to be considered including target(s), projectile(s), energy of the projectiles, reaction cross section, required specific activity produce and postirradiation examination. In this work the production and separation of ^{149,152}Tb from ^{nat}Nd, ^{142} Nd (enriched) and ^{141}Pr are discussed. Terbium-149 is produced from ^{142}Nd(^{12}C,5n) ^{149}Dy$\Rightarrow$^{149}Tb and ^{141}Pr(^{12}C,n)^{152}Tb reactions. Statistical model calculation shows that ^{142}Nd produces higher yield than ^{141}Pr for ^{149,152}Tb. Praseodymium-141 is naturally monoisotopic but neodymium has a number of naturally occurring stable isotopes : ^{142}Nd(27.2%), ^{143}Nd(12.2%), ^{144}Nd(23.8%), ^{145}Nd(8.3%), ^{146}Nd(17.2%), ^{148}Nd(5.7%), ^{150}Nd(5.6%). ^{142}Nd has the highest abundance among all the naturally occurring neodymium isotopes. Because of the presence of different stable isotopes of neodymium other than ^{142}Nd a number of other lanthanides, apart from ^{149,152}Tb, are produced by the secondary reactions. In order to remove the undesired secondary lanthanides an efficient radiochemical separation method is essential. High Performance Liquid Chromatography is appropriate for this purpose since it reduces the separation time and terbium can be separated in a carrier free state. Optimum experimental conditions for the production and separation of ^{149,152}Tb are discussed. Relevant nuclear data are given in Table 1.

Table 1. Relevant nuclear data of ^{149}Tb and ^{152}Tb

Radionuclide	Half-life	E_γ (keV)	Branching Ratio (%)	E_α (MeV)	Branching Ratio (%)	$E_{\beta+}$ (MeV)	Branching Ratio (%)
Tb-149	4.1 h	165, 352	26.6, 33.2	3.97	16.7	1.8	4
Tb-152	17.5 h	344	66.5			2.8	13

Experimental

Methods and materials: a) *Thin Targets*. The thin metal targets, both praseodymium and neodymium, were rolled from small pieces of metal cut from larger pieces. The metal was rolled thin, then weighed and its area (usually 1 cm ^{2}) was estimated with graph paper in order to determine the thickness in mg. cm^{-2}. The target was mounted in a copper frame or onto a copper block which could act as a heat sink as it itself was fixed to a water-cooled block. The irradiation conditions are given in Table 2.

Table 2: Typical irradiation conditions for ^{141}Pr and ^{nat}Nd targets

Beam ion (projectile)	Beam energy (MeV)	Target	Target thickness (mg.cm^{-2})	Irradiation time	Beam current (nA)
C-12	66	Pr-141	1.2	30-60 min	600
C-12	100	Nd-nat	28	4-15 hrs	300

For thin-targets, the catcher foil technique was used. The thin target, of typical thickness of 0.8-1.0 mg cm^{-2} , was placed in the beam line wrapped with an aluminium catcher foil, of thickness of 1.3-1.6 mg cm^{-2} , to collect the recoiled products. The typical energy loss in the thin target was around 2 MeV. After irradiation the aluminium catcher foil was removed from the target and subjected to alpha and gamma spectrometry using Silicon Surface Barrier Detector (manufactured at Australian National University) and High Purity Germanium (HPGE) detector (EG&G Ortech, Model GEM-13180). The alpha spectrometer was calibrated with a standard ^{241}Am source and the HPGE detector was calibrated with the standard ^{152}Eu and ^{137}Cs sources. A PC-based program (PCMCA, by Aptec) was used for storing and analysing data.

b) *Thick Targets*. For thick target experiment, the irradiated target was dissolved in about 0.5 ml of 6M nitric acid and the sample was evaporated to dryness subsequent to a number of non-destructive γ-spectroscopy measurements to determine the chemical yield. The residue was taken in about 0.5 ml of 0.16 M α-hydroxyisobutyric acid (α-HIBA). The solution was passed through a cation exchange column (Aminex A5, length- 60 mm, diameter - 3 mm, particle size ~ 13 μm). The pH of the eluent, α-HIBA, was 5 adjusted by aqueous ammonia. Terbium was eluted with α-HIBA under pressure of 5-7 kgf/cm^2 at a flow rate of 0.5 ml/min and the separated fractions were subjected to gamma spectrometry to check the radionuclidic purity. The terbium fractions were dried up gently and heated to about 450 °C to destroy the Tb-isobutyrate complex. Finally, the residue was dissolved and taken in a suitable medium, dilute nitric or hydrochloric acid, and was used for labelling of antibodies (3).

103/23

Results and Discussion

The variation of yields of ^{149}Tb from ^{141}Pr and ^{nat}Nd is presented in Fig 1. From the figure it is evident that the praseodymium target exhibits a relatively sharp peak at 66 MeV compared with the natural neodymium target which is much broader because of secondary reactions occurring concomitantly on other stable isotopes of neodymium yielding ^{149}Tb eg. ^{142}Nd(^{12}C,5n)^{149}Dy $\Rightarrow$ ^{149}Tb (peak at 95 MeV), ^{144}Nd(^{12}C,7n)^{149}Dy $\Rightarrow$ ^{149}Tb (peak at 120 MeV). Figure 1 also shows that ^{nat}Nd target would produce higher yields for terbium in comparison to ^{141}Pr target. Therefore, the production of ^{149,152}Tb from ^{nat}Nd is emphasised. (Fig 1)

Figure 2 shows the variation of relative activity of ^{149}Tb and ^{152}Tb as a function of irradiation time. From the figure it is clear that shorter irradiation time of less than six hours would minimise the presence of ^{152}Tb in ^{149}Tb. Conversely, to attain higher yields of ^{152}Tb, irradiation time greater than 8-10 hours would be favourable. Thus a long irradiation and long decay time would enhance the production of ^{152}Tb. (Fig 2)
The amount of ^{149}Tb produced from various forms of targets is compared in Table 3. Given that we can achieve beam currents of 200-350 nA, this gives a maximum saturated activity of ^{149}Tb of 98 μCi. From the table it can be inferred that neodymium metal is suitable for the production of ^{149}Tb. The amount of ^{152}Tb produced from ^{nat}Nd target was found to be about 4 mCi.

Table 3. Saturated activities of ^{149}Tb obtained from different targets

Target	Tb-149 saturated activity (μCi/μA)
Enriched Nd-142	240
Nd metal	239
Pr-metal	72

Forty eluted fractions each of 0.5 ml was collected for the separation of terbium from other lanthanides and the target. Terbium was detected in fractions number 14-19 at 7-10 minutes of retention time. The results of separation are presented in Fig 3. From the chromatogram it can be noticed that there is slight overlapping of dysprosium at the tail of the terbium peak. If one or two fractions of terbium peak are discarded, terbium can be obtained with higher purity. The separation profiles suggest satisfactory separation of terbium from other lanthanides applying the physico-chemical conditions described in this work. The chemical yield was determined by comparing the activity of the non-destructive measurement and the chemically separated sample by γ-spectroscopy and was found to be approximately 96%. (Fig 3)

Conclusion

The results of this study demonstrates that useful quantities of ^{149,152}Tb can be produced by Tandem accelerator from ^{141}Pr and ^{nat}Nd targets. The separation method described here was found to be appropriate for separation of terbium from other lanthanides. The quantity of ^{149}Tb present during the production of ^{152}Tb and vice-versa could be controlled by adjusting the irradiation time. Further studies are going on for the refinement of the experimental parameters to optimise the production and separation of ^{149,152}Tb, and their application to therapeutic and diagnostic purposes.

Acknowledgment

One of the authors, S Sarkar, is thankful to the Cumberland Research Grant of the University of Sydney for the partial financial support to this work.

References

1. Willbur D S; Potential use of alpha emitting radionuclides in the treatment of cancer. Antibody Immunoconjugate Radiopharm 1991, **4**, 85-97.
2. Allen B J, Blagojevic N; Alpha and beta-emitting radiolanthanides in targeted cancer therapy: the role of terbium-149. Nucl. Medicine Communication 1996, **17**, 40-47.
3. Imam S K et al.; In vitro and in vivo studies with Tb-152 and Sm-153 radioimmunoconjugate of the antimelanoma antibody 9.2.27. 4th World Congress on Melanoma, Sydney, June 10-14 1997. Melanoma Res, 7 suppl, 1997, S35

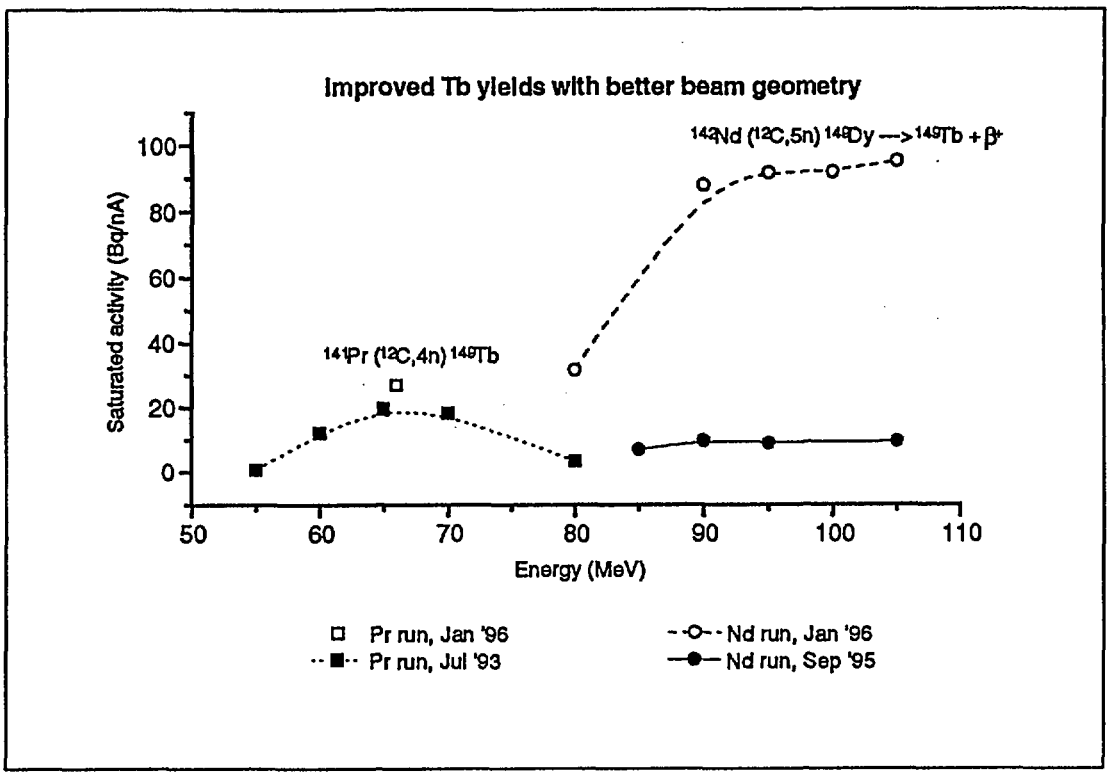

Figure 1. Comparisons of yields from Pr and natural Nd targets. The importance of having good beam geometry is demonstrated by the different results obtained for Nd runs

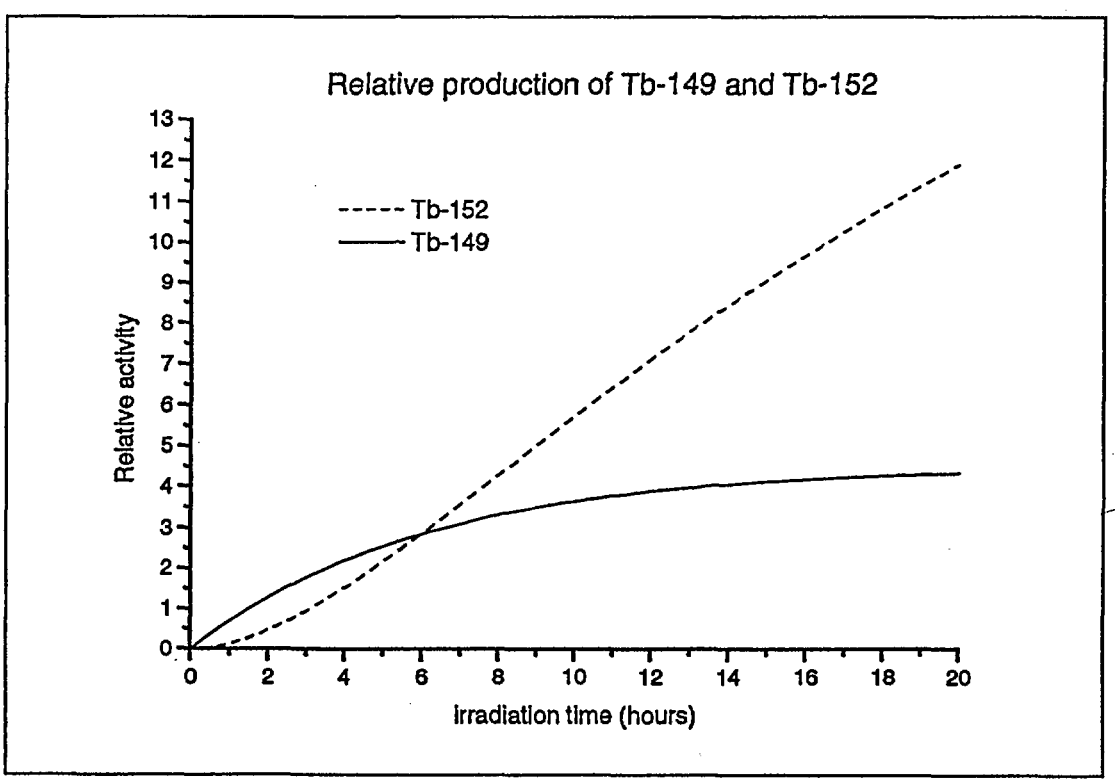

Figure 2. Model of increasing presence of Tb-149 in Tb-152 with time

Separation Profiles of Terbium, Dysprosium and Gadolinium

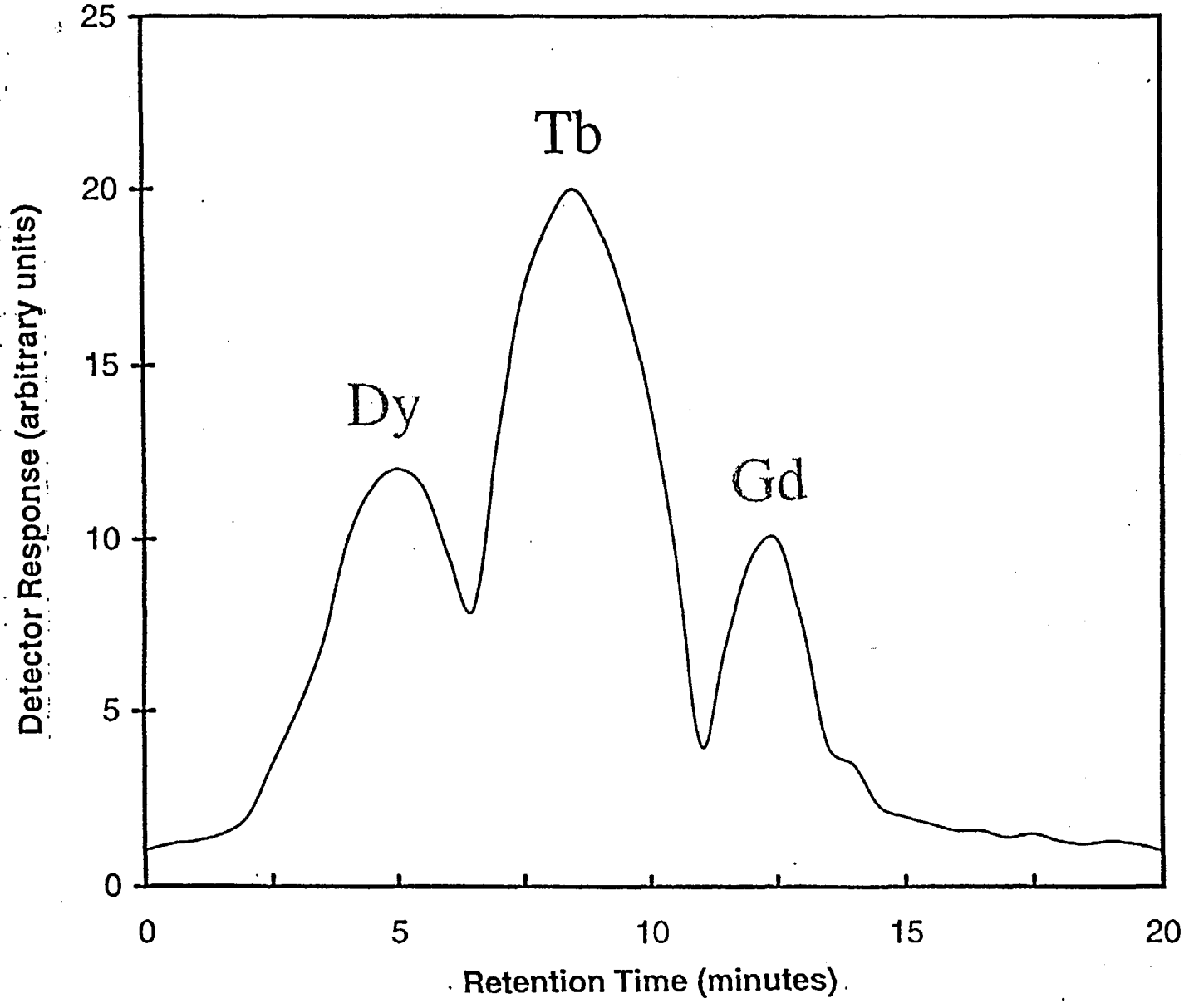

Figure 3. Separation profiles of Tb, Dy and Gd

Applications of Radioisotopes in Industry and Healthcare in Vietnam

N. N. DIEN, N. H. QUANG
Nuclear Research Institute, Dalat, Vietnam

SUMMARY. Applications of radioisotopes have significant meaning in economic development, people health protection, as well as in scientific research in Vietnam. Radioisotopes have been used in various fields, especially in industry and health care. In this paper the present status and main applications of radiation and radioactive isotopes in industry and healthcare in Vietnam are reported.

In order to monitor and control industrial processes, the sealed source and radioactive tracer techniques have been utilized. Nucleonic control devices and gauges have been used in various industrial factories: liquid level gauges in steel industry, cement and beverage factories; density and moisture gauges in paper industry, etc. Tracer technique and sealed source applications have also been utilized for trouble-shooting and process control in industrial production plants and in the petroleum industry.

For medicine purpose, two departments of nuclear medicine were primarily established at the beginning of the 1970's. Up to now more than twenty nuclear medicine departments have been set up and equipped with advanced equipment. Main activities are focused on thyroid function studies, nuclear cardiology, brain scans, gastrointestinal studies, bone scans, etc. Radioisotopes and radiopharmaceuticals used in these departments are imported or produced at the Dalat nuclear research reactor. This reactor is today an important scientific tool in Vietnam for developing nuclear techniques and radioisotope applications for socio-economic progress. Utilization of the Dalat research reactor for radioisotope production is summarized in this paper.

1. INTRODUCTION

Nuclear technique was applied in Vietnam at the early 1950's by using sealed sources for diagnosis and therapy in the medicine field. But its applications were rapidly expanded only after the 1960's by using sealed source techniques in industry, in nuclear medicine as well as in scientific research. Tracer technique applications in medicine for diagnosis, therapy and biology research were started in 1971 based on the establishment of two nuclear medicine departments with relatively little equipment. For nuclear diagnostic, there were a rectilinear scanner, a renograph and some radiometers for measurements of thyroid uptake. Ten years later, especially after 1984 when the Dalat research reactor was reconstructed, the number of nuclear medicine departments were increased, some modern equipment have been acquired.

At that time, in the field of industry only sealed source techniques were utilized in the production sectors, such as paper factories, cement factories and in petroleum companies. It is estimated that there are some tens of such factories and companies where radiation sources have been used. Nowadays both sealed source and tracer techniques are utilized in industrial production plants, but the second one is still under development and poor in applications.

2. CURRENT STATUS AND MAIN ACTIVITIES IN INDUSTRY

At the present time, there are a lot of factories where nucleonic control systems (NCS) are utilized. But it is still difficult to make a statistics of the operating NCS systems in Vietnam. Moreover, most of industrial production factories in Vietnam were established by turnkey contracts with foreign companies. In that situation we tried to obtain

some degree of participation, for example in civil engineering and construction, or in some low-grade technology industry, so NCS and related systems for controlling and monitoring automatic processes are completion equipment in the technological lines. In general, the present status of NCS installations can be estimated as follows: some hundreds of liquid level gauges; about one hundred of density and moisture gauges; about 50 thickness gauges and a number of well logging units. They are installed and operated at the cement, paper and beverage factories, steel industry and in petroleum companies. In that case, the factory's technicians are responsible for the operation and maintenance works, while the repairing and renovation works are carried out by NCS specialists who usually work for the nuclear research institutions and have a good knowledge of nuclear technique applications.

For the last few years, attention was paid to the design and construction of domestic nucleonic gauges. A series of nucleonic gauges have been developed at various nuclear organizations in the country. Domestic products are focused on liquid level gauges used in beverage factories and glass production industry, basis weight and moisture gauges for paper industry, weight scales for on-line measurement of the material weight as well as ash content and the moisture levels in coal, etc.

For monitoring and detecting liquid level, one-level and two-level gauges were designed and manufactured. As usual, gamma ray absorption method is used successfully for liquid level gauges of sealed tanks and vessels. In this case, ^{137}Cs or ^{60}Co sources with relatively energetic gamma rays and NaI(Tl) or GM detectors are usually utilized. Digital electronics parts are designed based upon programmable logic controllers (PLC) or multi-purpose interface cards connected to personal computers (PC).

In order to measure the weight of materials as well as the ash content and moisture levels in coal, the on-line radiometric conveyor weight scale based on transmission technique with ^{137}Cs source was designed and manufactured. It is well known that in the region of 0.5 - 5 MeV, Compton effect is the main process and the total cross section is a function of density ρ as described by formula: $\sigma = \sigma_k \rho (Z/A) L_A$ (where $L_A = 6.023.10^{23}$; σ_k - cross section of Compton effect). Information about transmitted radiation from counter is collected and stored into a PC, where processing and calculation procedures are realized. Based on specialized programmes and calibration curves, these gauges can be used for weight measurement of different materials, such as rock, soil, sand, cement, etc. as well as for measuring ash content of coal.

A paper basis weight monitoring gauge based on backscattering method using Am-241 source with gamma ray energy of 60 KeV was designed and installed in a paper-making factory as prototype. A PC-based system is utilized for on-line measurements, calculations as well as control of experimental processes. The measuring range is 20 - 600 g/m^2.

Gamma ray radiography is one of the most popular applications of the sealed source techniques in industry. Activities in this field have been carried out successfully during the past fifteen years for inspection of various types of welded structures.

It is easy to recognize that research and application of radiation technology are a very important in peaceful uses of nuclear energy in Vietnam as radiation has been utilized in a wide variety of fields such as industry, agriculture, medical treatment and scientific research.

The first research ^{60}Co irradiator with activity of 16.5 kCi was installed and put into operation in 1981 at the Dalat Nuclear Research Institute. Based on this facility the R&D programmes on radiation chemistry, radiation sterilization, food irradiation and biomass conversion have been established and carried out during the last fifteen years. Research activities in radiation chemistry have been carried out in radiation polymerization, radiation crosslinking of polyethylene and natural rubber, radiation vulcanization of natural rubber latex, preparation of wood-polymer composite, etc. The results obtained from the researches will be used for industrial applications of radiation technology in the near future. These investigations have led to knowledge and experience accumulation in a very promising field serving the industry development of our country. Basing on the

obtained results, feasibility studies for the first industrial irradiation centre in the Ho Chi Minh city were carried out a few years ago. This industrial irradiation centre equipped with ^{60}Co source of 300 kCi activity is under construction and will start its operation in the next year.

Compared to the sealed source techniques, radiotracer applications are still poor. The main reason is that activities in tracer technology have just begun since the last decade. Some applications of tracer technology have been carried out successfully during the last few years. The most remarkable activities in this field were concentrated in sedimentology and hydrology studies based on national research projects, technical co-operation projects of IAEA, as well as contracts with end-users. Most of the current sedimentology studies are involved with the optimization of dredging operations or the verification of transport models of bed sediments at the shipping access channels of Hai-phong harbour. ^{46}Sc and ^{192}Ir labelled sands produced at Dalat reactor have been utilized as radioactive tracers to conduct field experiments. Applications of tracer techniques in hydrology have permitted us to solve a number of problems in the field of water resource assessment and hydraulic construction. ^{131}I solution has been used for these studies.

In industry, several experiments using radiotracer techniques for studying material mixing/blending processes were done at a glass production factory a few years ago. The three main parameters of interest in mixing are maximum obtainable homogeneity, optimum mixing time and segregation. Basing on the obtained results, we could utilize these techniques to respond to the requirements of industry in the near future.

For trouble-shooting assessment purposes, studies on leak detection and blockage location in buried pipelines and other industrial systems were carried out several years ago. But so far these studies do not find wide applications in local industry.

It is necessary to emphasize that, the applications of radiotracer for studying industrial processes in Vietnam are not strongly developed yet. In order to realize this task, tracer users must be trained to acquire necessary knowledge on modelling applications such as resident time distribution, flow rate, mixing studies, etc. Since the beginning of the 1990's, some members of our staffs have been sent abroad to attend training courses on industrial applications of radiotracers.

3. CURRENT STATUS AND MAIN ACTIVITIES IN MEDICINE

Up to now, there are more than twenty nuclear medicine departments in Vietnam. Some of them have been equipped with modern equipment and are in good working condition. The number of SPECT, gamma cameras increased from one in 1992 to more than ten nowadays. Main activities in nuclear medicine field comprise the following:

1. Thyroid Function Studies and Therapy

Diagnoses of thyroid disease are being the main activities in all nuclear medicine departments in Vietnam. The measurements of thyroid uptake have been performed almost with ^{131}I isotope, which are imported or produced at the Dalat reactor. The in-vitro diagnostic method is still restrained due to lack of equipment and the irregular supply of radioimmunoassay kits for T_3, T_4, TSH. In recent years, the thyroid uptake and the thyroid scanning with ^{99m}Tc have been performed in some nuclear medicine departments equipped with gamma camera or SPECT. Moreover, the radionuclide therapy of Graves's disease with ^{131}I isotope has been realized in some nuclear medicine departments and hundreds of Graves's disease patients are treated successfully every year.

2. Nuclear cardiology

Nuclear cardiology is a quite new technique in Vietnam. In some modern hospitals where gamma camera or SPECT is available, two procedures have been developed for cardiology studies: the first-pass study and the equilibrium gated blood pool study. The imaging and non-imaging results such as end-diastolic volume, end-systolic volume, ejection fraction, wall motion, chamber size, emptying and filling rates, emptying and filling times, regurgitation index, etc. have given new

significant information for the estimation of cardiac status.

3. Brain Scans

Nuclear brain scanning has been performed in some nuclear medicine departments. The radiopharmaceuticals used were ^{99m}Tc-DTPA and ^{99m}Tc-pertechnetate. The nuclear brain imaging can help us to distinguish malignant tumour meningeoma from other brain tumour, such as astrocytoma, glioblastoma, etc. This method is non-invasive and the obtained results can reach a high estimation in clinical practice.

4. Gastrointestinal Studies

The quantitative studies of gastrointestinal function were developed in the past few years at some departments of nuclear medicine. Gastric motility, gastric emptying studies and scintigraphic measurement of hepatic function have been performed by gamma camera and SPECT. Gamma camera and SPECT imaging provide useful information about a variety of important diseases, such as liver cirrhosis, hepatic tumour and other complications of malaria or viral hepatitis.

There were some investigations of alpha-feto-protein on chronic liver disease patients. However, this procedure cannot be widely applied because of the high cost and irregular delivery of imported RIA-kits.

5. The Genitourinary System

Nuclear medicine diagnoses in renal disorders have become a routine technique and are highly valued. With multi-probe system for radiorenography with ^{131}I - Hippurat produced at the Dalat reactor, two renograms were simultaneously registered and analyzed with or without computer assistance. In other departments equipped with gamma camera or SPECT, new methods for renal study have been performed. The renogram is useful in measuring the contribution of each kidney to total renal function. It is becoming a standard technique for evaluating renal function.

6. Bone Scans

Nuclear bone scanning can give good results although it is recently applied in Vietnam. The radiopharmaceuticals used are ^{99m}Tc-diphosphonate and ^{99m}Tc-pertechnetate produced at the Dalat reactor. The tracer is taken up by osteoblastic activity and is also dependent on bone blood flow. The three-phase study comprises a flow phase, a blood pool image and standard static views. The sensitivity of bone scanning in detecting osseous metastases is about 98 percent.

It is well known that industrial application of radiation sterilization is expanding throughout the world. Recognizing this application, the R&D programmes on radiation sterilization of medical disposables and pharmaceuticals produced in Vietnam have been carried out in co-operation between nuclear research institutions and medicine facilities including medical factories and hospitals. Medical products to be sterilized in the past fifteen years include surgical gloves, plastic syringes, serum packaging, gauze, cotton, etc. and several kinds of pharmaceuticals such as traditional drug, physiological saline, lactate ringer, etc. These medical disposables and pharmaceuticals are sterilized at the ^{60}Co irradiator in the Dalat Nuclear Research Institute and at the irradiation centre in Hanoi. In the framework of an IAEA technical co-operation project entitled "Food irradiation", the Hanoi irradiation centre equipped with a semi-commercial scale irradiator of ^{60}Co source with 110 kCi activity has been established and put into operation since July 1991. Although the facility was designed for food preservation purpose, it has been successfully used as a multi-purpose one. Besides food preservation, sterilization of medical products, disinfestation of medicinal herbs, modification of polymeric materials, etc. studies on gamma sterilized human tissue for surgical treatment have been also carried out at this centre. The results obtained show that freeze drying and radiation sterilization were successfully applied for the production of such tissue grafts as biomembrane and human bone. The achievement in tissue graft preservation and applications for health care in Vietnam during the past ten years are considerable.

4. UTILIZATION OF THE DALAT REACTOR FOR RADIOISOTOPE PRODUCTION

The Dalat reactor was inaugurated in March 1984 and has been operated since then

to realize objectives in the fields of radioisotope production, neutron activation analysis, scientific research and training. For optimal utilization of such low power reactor, its core is equipped with more neutron irradiation channels and with a neutron trap at the center of the core for improving thermal neutron flux. In addition, the reactor characteristics are more useful as far as radioisotope production and neutron activation analysis are concerned, i.e., the cadmium ratio in neutron irradiation positions being rather high in the neutron trap and in the rotary specimen rack and rather low in the fast neutron irradiation channels. For radioisotope production the neutron trap and 40 holes of rotary specimen rack are used for thermal neutron irradiation and one vertical channel for fast neutron activation.

Since its reconstruction and inauguration, the Dalat reactor has been operating for a total duration of more than 18,000 hrs (approximately 1350 hrs per year) mostly at nominal power of 500 kW. The main regime of operation is 100 hrs of continuous run every three or four weeks, largely for radioisotope production and neutron activation analysis. The remaining time is devoted to maintenance work or to short runs for physics experiments. About 90 percent of reactor operation time is utilized for production of radioisotopes and radiopharmaceuticals for nuclear medicine, agriculture, oil exploitation, sedimentology and hydrology studies and other scientific research. The radioisotope production at the Dalat reactor has concentrated on the following radionuclides:

- ^{32}P in injectable orthophosphate solution and ^{32}P applicator for skin disease therapeutics

- ^{131}I in NaI solution

- ^{99}Mo - ^{99m}Tc generator

- ^{51}Cr in injectable sodium chromate solution and Cr-EDTA

- Other radionuclides such as ^{60}Co, ^{65}Zn, ^{64}Cu, ^{24}Na, ^{86}Rb, ^{46}Sc, ^{71}Ge, ^{55}Fe, ^{192}Ir, etc., have also been produced in small amounts when requested.

In order to support the application of ^{99m}Tc isotope in clinical diagnosis, the preparation of radiopharmaceuticals for labelling with ^{99m}Tc (kit) has been started in parallel with the development of ^{99m}Tc generator systems. The following kits are regularly prepared at the Dalat reactor: Phytate, Gluconate, Pyrophosphate, Citrate, DMSA, HIDA, DTPA, Maccroggregated HSA and EHDP. The annual production rate is about 1000 bottles for each kit which is equivalent to 5000 diagnosis doses.

The annual amount of radioisotopes produced at the Dalat reactor has generally increased with time. Up to now the total output has reached more than 1300 Ci. The yearly amount of radioisotopes produced at the Dalat reactor is about 150 Ci and is not enough to meet the needs of society, especially in medicine field. So, a large quantity of radioisotopes for medicine purpose has to be imported every year.

5. CONCLUSION

The applications of radiation and radioactive isotopes are a very important in peaceful uses of nuclear energy in Vietnam, and have made substantial contributions towards improving not only the national living standard, but also the public acceptance of nuclear power programme. This is because radioisotopes have been utilized successfully in various socio-economic fields, especially in industry, agriculture and health care. During the last ten years, based on national research projects in the nuclear field and through the technical co-operation projects of IAEA, a number of nuclear laboratories and facilities have been set up and equipped with necessary equipment, a large number of nuclear scientists and technicians have been educated and trained. Since then, due to the successfully economy reform and renovation, the growth rate of GDP and the national living standard rapidly increase, we are convinced that Vietnam will soon to strengthen nuclear technology to meet the needs of society and to introduce nuclear power for ensuring the country's future development.

6. REFERENCES

[1] Nguyen Nhi Dien, Current status on application of NCS and Tracer Technology in Vietnam. 3rd National Co-ordinator Meeting on NCS and TT, India, 22-26 April 1996.

[2] Nguyen Xuan Phach, Nuclear Applications in Medicine. National Seminar, on nuclear power introduction and public information, Hanoi, 4-5 October 1995.

[3] Le Van So, Utilization of Nuclear Research Reactor in Vietnam. Experts Group Meeting on optimal utilization of research reactor for radioisotope production, Japan, 23-27 October, 1995.

[4] NRI - Ten years of edification and maturation 1984-1994. Activity Report of the Dalat Nuclear Research Institute, Dalat, November 1994.

[5] Proceedings of the First National Conference on Nuclear Physics and Techniques, Hanoi, 14-15, May 1996.

[1] New Therapeutic Agent for Radiation Synovectomy----- Preparation of ^{166}Ho-EDTMP-HA Particles

H.S. Bai [1] X.H. Jin J. Du F. Wang D.M. Chen H.Q. Fan Z. Cheng J.R. Zhang
Isotope Department , China Institute of Atomic Energy ,
P. O. Box 275 (58), Beijing ,102413

SUMMARY In order to treat the patient with inflammation synovial disease, Hydroxyapatite particle (HA) was labeled with ^{166}Ho by EDTMP. Radiolabeling efficiency was more than 95%, the particle size of ^{166}Ho-EDTMP-HA was mainly at range of 2-5μm, absorbed capacity of HA particle was 5mg Ho/g HA. In vitro stability studies showed that the loss rates of ^{166}Ho-EDTMP-HA particle incubating over a period of 72 hr in the normal saline and 1% BSA solution at 37 ^{0}C respectively were less than 2%. The tissue distribution and extra-articular leakage were investigated following injection of ^{166}Ho-EDTMP-HA particles into the knee of normal rabbits. The experimental result indicated that extra-articular leakage of ^{166}Ho-EDTMP-HA was 0.32% I. D. at 48hr postinjection, most of ^{166}Ho activity from the knee joint was excreted in the urine in form of ^{166}Ho-EDTMP. ^{166}Ho-EDTMP-HA as a potential therapeutic agent for radiation synovectomy had the value of clinical research.

1. INTRODUCTION

Fellinger et al reported first radiation synovectomy that is the ablation of inflamed synovium by means of intra-articular injection of a beta -emitting radionuclide in colloidal or particulate form [1] . This technique was extensively used in Europe and obtained good therapeutical result . Radiation synovectomy is a noninvasive therapy for rheumatoid arthritis that had been investigated as an alternative to surgical synovectomy . It has some advantage , such as short hospitalization , low reoccurance rate and good synovectomy result [2,3,4] . Radiation synovectomy was performed with ^{90}Yand ^{198}Au-colloid and obtained an encouraging therapeutical result in the clinic [5,6] . However, it exited a major problem with ^{90}Y and ^{198}Au-colloid for radiation synovectomy----undesirable leakage of radioactivity from jiont, this is possible due to the relatively small size (60-100 nm) and unstability of radiocolloid used. Therefore, the particulate carrier for beta-emitting radionuclides in radiation synovectomy was further improved and optimized.

Hydroxyapatite (HA) , a natural component of bone, has good biocompatibility with soft tissue, and is biodegraded into calcium and phosphonate in vivo at 6 weeks postinjection[7] ; HA is readily prepared from common chemical process and formed into particle of the desired size range in the controlled process. HA has high in vitro and vivo stability. Therefore , HA would make as a new particulate carrier for bate-emitting in radiation synovectomy. The articles on labelling HA particle with ^{153}Sm and ^{186}Re had been published[8-12] , their extra-articular leakage lowed apparently (

[1] Correspondence: Bai Hongsheng, China Institute of Atomic Energy, P.O. Box 275(58), 102413, Beijing. P.R.China E-mail: Jinxh@mipsa.ciae.ac.cn

0.16%-0.28% and 1.65%-3.05% respectively) comparing with radiocolloid and radiolabeling FHMA. In addition, it was concluded that radioactive leakage from the joint can be reduced with the utilization of a radionuclide with short half-life since a greater fraction of decay occurs before possible leakage from joint. ^{166}Ho (t1/2 26.9hrs, beta energy =1.84Mev and range in tissue=8.5mm) was a more practicable chioce. This paper discussed mainly labelling condition , particle size distribution , stability in vitro , biodistribution in the normal rabbit and extra-articular leakage.

2. MATERIAL and METHOD

2.1 Reagent and Instrument: Hydroxyapetite (HA) (biogical department , China institute of science, Shanghai); EDTMP (Tokyto chemical industry company, Japan); Holmium oxide (China rare earth company); HCl and NaOH (A.R.) (Beijing chemical reagent factory); normal saline (Shijiazhuang manufacture medicine factory). JGL-168 high speed plat centrifuge (Shanghai Anting science instrument factory); JHR-4 controlled -temperature instrument (Hebei Huanghua instrument factory); Model 110-2 electric balance (Shanghai balance factory); RM-905 Radioisotpe activity calibrator (China scientific dose institute); Model FH-408 calibrator (Beijing nuclear instrument factory).

2.2 Method

2.2.1 Preparation of $^{166}HoCl_3$

20mg of holmium oxide (spectrum purity) was weighted, and put into small aluminium can, then sealed. It was irradiated for 7-8days in the neutron flux ϕ=7-8$\times10^{13}$n/cm^2·sec . The irradiated target was dissolved with 10ml of 1 mol/l HCl solution and evaporated to nearly dryness. After cooling to room temperature, it was dissolved with 10ml deionized water and determined its radioactivity, its specific activity was 140mCi/mg Ho.

2.2.2 Labeling HA particle with ^{166}Ho

Radiolabeling of HA particles was divided into two steps. Preparation of ^{166}Ho-EDTMP was followed by the incubation of ^{166}Ho-EDTMP with the HA particles.

2.2.2.1 Preparation of ^{166}Ho-EDTMP

1ml of $HoCl_3$ solution (1mg/ml) and 100μl $^{166}HoCl_3$ solutions as radiotracer were added together in the vial, then added equimolar EDTMP solution and mixed completely. The pH value of the mixture was adjusted to 8.0-9.0 with 2mol/l NaOH solution , the mixture heated for 60min at water bather . The radiolabeling efficiency of ^{166}Ho-EDTMP was determined with Bio-Rex 70 cation ion exchange resin and normal saline as eluent, its radiolabeling efficiency was more than 95%.

2.2.2.2 Preparation of ^{166}Ho-EDTMP-HA

1ml of above solution was added into small centrifuge tube containing 100mg of HA particle, sealed and vibrated for 15 minutes on the micromixer at room temperature. Radiolablled HA particle washed with deionized water. Radiolablled HA particle was separated from free ^{166}holmium to determine labeling efficiency. Its radiolabeling efficiency was calculated according to the formula as following:

Labeling efficiency (%)= [1-radiocounts of the supernatant fluid/total radiocounts of HA particle and supernatant fluid]×100%

2.2.3 Control experiment

To determine the biological fate of radionuclde that was injected into knee joint in form of ^{166}Ho-EDTMP(not bound to HA). The control studies were performed in six normal rabbits (weight 3.5 kg or so) following injection of ^{166}Ho-EDTMP (7.4 MBq, 0.2mCi) into knee joint. Two rabbits killed at 12hr , 24hr and 48hr postinjection respectively , took out major organ , collected blood and urine, and determined their radiocounts.

1.2.4 Biodistribution of ^{166}Ho-EDTMP-HA in the normal rabbits

Tissue distribution of ^{166}Ho-EDTMP-HA was investigated in the normal rabbits following injection of the radiolabeling particle into knee joint. Two rabbits killed at 12hr , 24hr and 48hr postinjection respectively , took out major organ , collected blood and urine, determined their radiocounts. Extra-articular leakage was calculated as sum of all activity in major organs , total urine excreted and the activity remaining in the circulating blood at the time of sacrifice.

3. RESULT

3.1 Size distribution of radiolabeled HA particle

After the radiolabeling particle decaying ten half-lives, it was diluted with deionized water, the size distribution of radiolabeling particle was determined with optical microscope. The result was shown in the figure1. The figure 1 indicated that the size of radiolabeling HA particle distributed mainly at range of 2-5μm (85%).

Figure1 size distribution of Radiolabeling HA particle

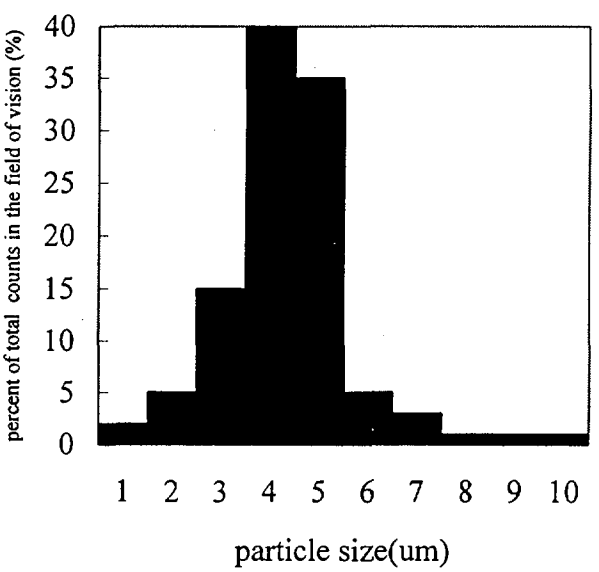

3.2 Determination of HA absorbed capacity

^{166}Ho-EDTMP solution with different quantity of Holmium was added to the vial containing 100mg of HA particle, and vibrated for 15 minutes at different reaction temperature. After cooling to the room temperature, its radiolabeling efficiency was determined using centrifuge method. The experimental result was shown in the figure 2. Figure 2 showed that radiolabeling efficiency decreased with Holmium quantity increasing; its absorbed capacity of HA particle increased with reaction temperature

increasing; The absorbed capacity of HA particle was 5mg Ho/mg HA at room temperature.

Figure 2. Effect of Ho quantity on radiolabelling efficiency

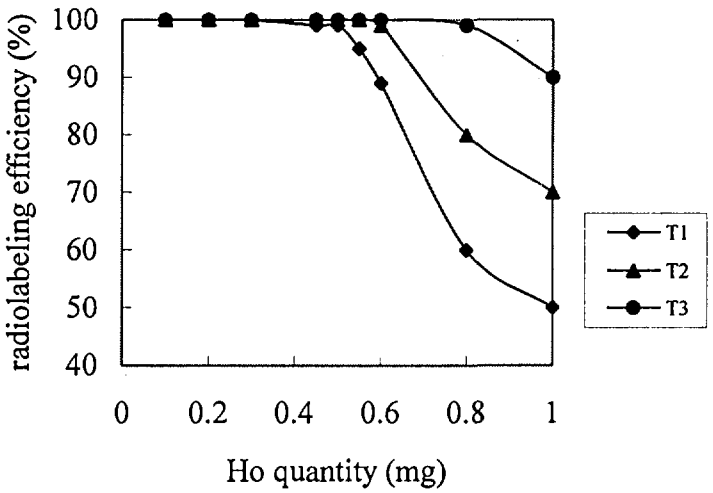

T1---room temperature T2---50-60 ^{0}C T3----80-90 ^{0}C

3.3 Effect of quantity of EDTMP on radiolabeling efficiency

^{166}Ho-EDTMP with different mole ratio (EDTMP/Ho) was added to the vial containing 100mg of HA particle, HA particle was labeling with ^{166}Ho and determined labeling efficiency according to the method (2.2.2) . The result was shown in the figure 3. Figure 3 indicated that labeling efficiency decreased with mole ratio of EDTMP/Ho increasing , when mole ratio of EDTMP/Ho was equal to 8:1, the radiolabeling efficiency was akin to zero. This revealed that ^{166}Ho-EDTMP was bound to HA by EDTMP, ^{166}Ho-EDTMP competing with free EDTMP chelator was bound to HA particle.

3.4 Effect of vibration time and pH value on labeling efficiency

According to method (2.2.2) , HA particle was with ^{166}Ho by EDTMP at the different vibration time and pH value, radiolabeling efficiency was determined using centrifuge method . The experimental result was shown in the figure 4. Figure 4 exhibited that the labeling efficiency was more than 95% under condition of vibration time 15 minutes and pH 6.0-8.0. Under extremely acidic condition (pH 1-2) , HA particle itself was dissolved .

3.5 In vitro stability study

In vitro stability was investigated with ^{166}Ho-EDTMP-HA particle incubating respectively in the 2ml of normal saline and 1% BSA solution at 37 ^{0}C . At various times, radiolabeling particle was separated from free ^{166}Ho via centrifugation to determine radiochemical purity. The stability of ^{166}Ho-EDTMP-HA was listed in the table1. The data of table1 showed that no dissociation of activity from radiolabeling particle was observed in the normal saline and 1% BSA solution over a period of 72hr, its radiochemical purity was more than 98%. This exhibited high stability in vitro of ^{166}Ho-EDTMP-HA.

Table1. Radiochemical purity of ^{166}Ho-EDTMP-HA in the normal saline and 1% BSA solution at different incubation time

incubation time(hr)	12	24	36	48	60	72
normal saline	0%	0%	0.5%	1.0%	1.2%	1.3%
1% BSA solution	0%	0%	0.3%	1.1%	1.5%	2.0%

Figure3. Effect of mole ratio of EDTMP/Ho on radiolabeling efficiency

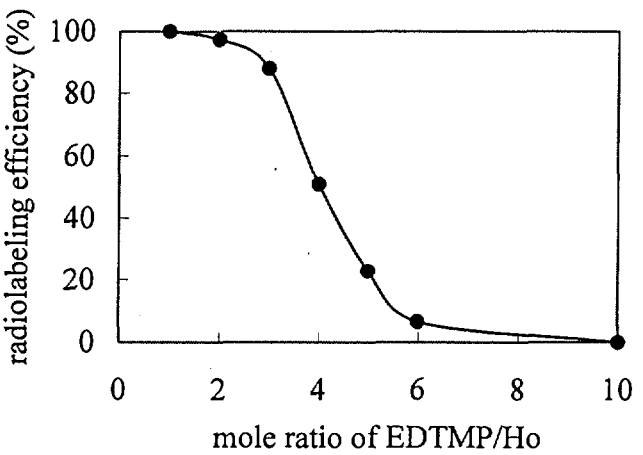

Figure 4. Effect of pH and vibration time on radiolabeling efficiency

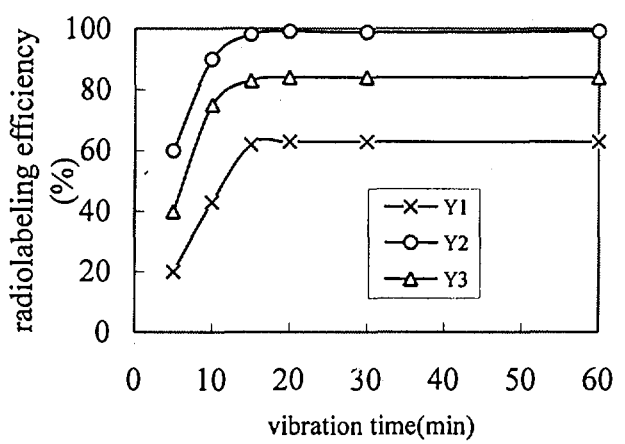

Y1--3.0-4.0 Y2---6.0-8.0 Y3---10.0-11.0

3.6 Control study

The extra-articular leakage of radionuclide following injection of ^{166}Ho-EDTMP (not bound to HA particle) into knee joint of normal rabbits is listed in the table 2. Results are expressed as the percent of injected dose (% I. D.) . A large amount of ^{166}Ho activity (50%) was excreted in the urine within 48 hr of administration, but the

radioactivity of ^{166}Ho in the blood was extremely (0.2%). Based on tissue distribution studies , 22% of the ^{166}Ho activity was retained in the body , of which a significant amount (17%) was found in the bone and uptake of ^{166}Ho activity in the liver was 5% at 48 hr postinjection. Control studies showed that 28% of activity was found in the joint space, and the most of activity leaking from the joint was excreted in the urine.

Table 2. Biodistribution in vivo of ^{166}Ho-EDTMP in normal rabbits (n=2, % I.D.)

organ	12hr	24hr	48hr
urine	43.50	6.00	0.50
blood	0.10	0.12	0.02
liver	0.50	1.50	3.00
kidney	0.50	0.10	0.05
other organ	-	-	18.56
total leakage	-	-	72.56

3.7 Biodistribution of ^{166}Ho-EDTMP-HA in normal rabbits.

The tissue distribution and extra-articular leakage of ^{166}Ho activity following injection of ^{166}Ho-EDTMP-HA particle into the knee joint is listed in the table 3. Total cumulative leakage in the normal rabbits was 0.213% at 24hr post-injection and 0.32% at 48hr post-injection. The most of ^{166}Ho activity leaking from joint was excreted in the urine in form of ^{166}Ho-EDTMP. All organs showed no significant accumulation of ^{166}Ho activity . The extremely small ^{166}Ho activity leaking from joint was seen in the liver and bone.

Table3. Tissue distribution of ^{166}Ho-EDTMP-HA particle in the normal rabbits (n=2, % I.D.)

organ	12hr	24hr	48hr
urine	0.075	0.028	0.009
blood	0.001	0.001	NS
liver	0.005	0.025	0.035
lung	0.000	0.000	0.000
spleen	0.003	0.003	0.000
kidney	0.002	0.001	0.008
lymph	0.0005	0.0003	0.000
rear leg	99.85	99.80	99.50
femur	0.023	0.014	0.008
total leakage	0.139	0.213	0.32

4. DISCUSSION

4.1 HA particle , as a natural component of bone was known to have good compatibility with soft tissue and biodegrade into calcium and phosphate in vivo . It was readily prepared from common chemical and formed into particles of desired size range in a controlled process. It had high stability in vitro and vivo. Therefore, HA particle used in this study appeared to be a very attractive carrier for use in radiation synovectomy.

4.2 The two-step procedure desired this study (preparation of an intermediate radiochemical form ^{166}Ho-EDTMP, followed by labeling of the hydroxyapatite)

offered a fundamental advantage over previous one-step reaction that have been used to prepare radiolabeling colloid. In two-step method, the particulate carrier can be carefully prepared controlled its physical properties (such as particle size), before radiolabeling occurred, then the radiolabeling procedure could be independently optimized . The optimal labeling condition at room temperature was pH 6.0-8.0 and vibration time 15minutes. The absorbed capacity of HA particle at room temperature was 5 mg Ho/g HA particle and size of radiolabeling particle was at range of 2-5μm that is suitable for therapy of radiation synovection.

4.3 ^{166}Ho-EDTMP-HA particle demonstrated high in vitro stability in either normal saline or 1% BSA solution, but unstability under extremely acidic condition (pH=1-2) because of dissolution of HA particle. ^{166}Ho activity was bound to HA particle by EDTMP that has high affinity for HA particle and form into very stable complexation with ^{166}Ho under neutron condition. Therefore , the activity of ^{166}Ho washed off particle until the HA particle itself dissolved and absorbed rate of HA particle decreased with EDTMP quantity increasing possible due to competition of free EDTMP chelator and ^{166}Ho-EDTMP.

4.4 The control studies performed with ^{166}Ho-EDTMP not bound to HA particle provided information on the distribution of radioactivity that would occur upon leakage of the radiochemical compound from joint. At 48hr postinjection, 50 % of ^{166}Ho activity was excreted in the urine , uptake of liver was 5% I.D. The rest activity of ^{166}Ho was retained in the bone and joint space. This revealed that activity leaking from knee joint was excreted in the urine in form of ^{166}Ho-EDTMP and this tended to minimize any irradiation exposure to normal tissue caused by leakage.

4.5 Tissue distribution and extra-articular leakage investigated following injection of ^{166}Ho-EDTMP-HA particle into knee joint of normal rabbits showed that the extra-articular leakage was 0.213% and 0.32% at 24 hr and 48hr postinjection respectively, the total cumulative activity of ^{166}Ho in the urine was 0.16% at 48hr post-injection , most of ^{166}Ho activity leaking from knee joint was excreted in the urine. Therefore, its short half-life, its extremely low leakage from the joint and it's even distribution throughout the synovium make this agent attractive for use in radiation synovectomy.

Reference

1. Fellinger K, Schmid J. Wien Z Inn Med, 1952:33:351.
2.Geens S, Clayton M, Leidhiodt J., et al. J. Bone Joint Surg 1969:51A:626-642.
3. Sledge CB, Zuckerman JD, Zalutsky MR, et al. Arthitis and Rheumatism. 1986, 29 : 153-159.
4. Taylor AR, Harbison JS, Pepler C., Ann Rheum Dis. 1972: 31:159-161.
5. Ansell BM, Crook A, Mailard JR. Ann Rheum Dis, 1963:22:435-439.
6. Gumpel JM, Beer TC, Crawley JCW. Br J. Radiol, 1975: 48:377-381.
7.Shortkroff S, Mahmood A, Sledge CB. J Nucl Med, 1992:33:937.
8. Brodak JW, Chinen LK, Deutsch E. J Nucl Med, 1992:33:980.
9. Macro Ch, Shankar VA, Stanley J. J Nucl Med, 1993:34:1536-1542.
10. Jin H.X, Liu Y M, Du J., Isotope, 1994:7:92-97.

Separation of Rare Earths and Transuranium Elements from Spent Nuclear Fuel Solution by High Performance Liquid Chromatography

S SARKAR[1], A OHUCHI[2]

[1]School of Medical Radiation Technology, Faculty of Health Sciences, The University of Sydney, East Street, Lidcombe, NSW 2141

[2]Nippon Nuclear Fuel Development Co., Ltd, 2163 Narita-cho, Oarai-machi, Ibaraki-ken, 311-13 JAPAN

SUMMARY. This work concerns the separation of rare earths (RE), uranium and transuranium elements (TUE) from spent nuclear fuel solution by high performance liquid chromatography (HPLC). Ammonium lactate was used as an eluent. Optimum physico-chemical conditions such as temperature, pH of the eluent etc. are established by simulated experiment and these conditions have been applied for the separation of RE and TUE from spent nuclear fuel solution. Satisfactory separation is achieved at pH of 3.5 and temperature of 80°C. Coulometry, beta-gamma counting, alpha- and gamma-ray spectroscopy were used to detect the nuclides. The elution behaviour of plutonium as a function of pH and temperature studied using tracer is also presented. Uranium and plutonium show clear separation from americium and curium. The applicability of the method, developed in this work, for the analysis of spent nuclear fuel solution is discussed. An attempt has also been made to correlate the retention behaviour of lanthanides and actinides with their corresponding ionic radii.

Introduction

Analysis of irradiation products in spent nuclear fuels is of great importance in nuclear power programs for the calculation of burnup, the problems in waste treatment, and examination of the build-up of transuranium elements. Because of the prominence of the lanthanide group within the fission products and the unusually high neutron cross sections of some of the individual nuclides, the growth of lanthanide separation knowledge has been greatly stimulated by the increasing demands of nuclear technology. Usually lanthanides are used for burnup measurement and among them ^{148}Nd is widely used as a burnup monitor of nuclear fuel by standard method (1). In nuclear fuel analysis, radionuclides under consideration for separation include TUE (Np, Pu, Am, Cm), the high heat producing fission products (^{90}Sr, ^{137}Cs), long-lived soluble fission products (^{99}Tc, ^{129}I) and the strategic metals (Ru, Rh, Pd). Selection of suitable separation procedure is rather complicated because of the multiple constituents of the spent fuel solution. The application of HPLC for the separation of RE from nuclear fuel has been reported by several authors (2,3). Most of the reported works used α-hydroxyisobutyric acid as eluent for the separation of RE.

The aim of this study is to develop a convenient separation procedure for RE, uranium and TUE (Pu, Am, Cm) by studying the optimum physico-chemical conditions. Ammonium lactate was chosen as eluent because it provides efficient separation of the RE with the usual decrease in retention as the ionic radius of the element decreases. The influence of different parameters such as pH of the eluent, temperature and concentration of the matrix element (uranium) was investigated. The experimental conditions were established using a mixture of fourteen lanthanides plus yttrium and uranium of known concentration. The behaviour of plutonium was examined using plutonium tracer. The application of this method to

nuclear fuel solution analysis is also discussed.

Experimental

a. *Apparatus*. The HPLC system consists of an eluent pump (Hitachi Intelligent Pump, Model L-6210) with gradient programmer, a ceramic sample injector with 20 µl loop, a dynamic mixer, a column oven (Model L-5020, Hitachi Ltd.), a constant potential coulometer (Model D-630, Hitachi Ltd.) and a fraction collector (Model L-5200, Hitachi Ltd.). The column used for separation was 10 cm x 5 mm i.d. packed with cation exchange resin, Hitachi Gel #2618 of particle size of 10 µm. A high purity germanium detector (EG & G ORTECH), a beta-gamma counter (Eberline) and a silicon surface barrier detector (Toshiba Ltd.) were used for the identification of radionuclides.

b. *Method*. Stock solutions of lanthanides, yttrium, and uranium were prepared by dissolving known quantity of their corresponding oxides in dilute nitric acid. Plutonium tracer and nuclear fuel solution were also taken in dilute nitric acid. The eluent was 2, 3 and 6% ammonium lactate (by volume) . The eluent was degassed, and filtered through 0.45 µm membrane filter before use. The pH of the eluent was adjusted by ammonium hydroxide and/or dilute nitric acid.

A known amount of the sample was prepared in the eluent. The column was conditioned with the eluent for about 50-60 minutes prior to loading the sample. A 10 µl of the sample was injected through the sample injector and the concentration gradient program was run from 2-6% (by vol.) ammonium lactate at a flow rate of 0.5 ml/min and pressure of 9-11 kgf/cm^2.

Results and Discussion

Migration of a solute through a column depends on the equilibrium distribution of the species between the stationary and mobile phases. Retention is therefore controlled by the factors which affect the distribution including the composition and pH of the mobile phase, the nature of the stationary phase and the temperature. In liquid chromatoghraphy three sets of interactions such as solute-mobile phase, solute-stationary phase and mobile phase-stationary phase need to be optimized to achieve satisfactory separation. Change in mobile phase composition is recommended to obtain the correct balance of interaction. In gradient elution the mobile phase composition is changed so that an increase in strength causes a decrease in retention. The results of different physico-chemical conditions studied on the separation of RE, uranium and TUE are described below.

1. *Effect of pH*. The pH of the mobile phase significantly influences retention time which decreases with the increase of pH owing to greater complexing ability of lactate. Figure 1 shows the variation of retention time of several lanthanides (La, Ce, Nd, Eu, Yb), uranium and plutonium as a function of pH. (Fig) The results are from the run at 80 °C since at this temperature separation characteristics become better (see next section). The retention time falls sharply, especially for lighter lanthanides, at lower pH (3.0-3.5) following a gradual decline in the pH range of 4.0-5.0, and then the retention time attains a plateau at higher pH of 5.0-6.0. Uranium elutes with heavier lanthanides at pH≥4.5 suggesting suitable separation of lanthanides from uranium at lower pH. Plutonium also elutes with heavier lanthanides in the studied pH range but shows clear separation from uranium. The overlapping of the elution profiles of plutonium with those of heavier lanthanides does not seem to cause any notable effect since the amount of heavier lanthanides produced in irradiated fuel is nearly zero and plutonium can easily be detected by its characteristics alpha-radiation. Considering the separation characteristics of all the elements studied in

this work pH of 3.5 was used in the subsequent experiment.

2. *Effect of Temperature.* A possible influence of temperature on chromatographic selectivity is said to improve the column efficiency with the increase in temperature due to the reduction of eluent viscosity and an increase in solute diffusivity. The variation of retention time of RE, uranium and plutonium is shown in Figure 2 as a function of temperature at pH of 3.5. From Fig 2 it is apparent that the overall separation feature becomes better at 70-90 °C. Therefore, 80 °C was used as working temperature. (Fig 2)

3. *Effect of uranium concentration on the separation of the lanthanides.* For the separation of lanthanides from nuclear fuel the study of the effect of concentration of uranium deserves special interest since uranium is the matrix element. The extent of interference of the matrix element would determine the necessity of preseparation of uranium from from other irradiated products of the nuclear fuel. Analysis time can be saved if there is no preseparation step involved. The effect of uranium concentration on the mutual separation of REE was investigated over the concentration range of 70-700 μg (300-3000 nmol)of uranium and no appreciable effect was observed in the range of 70-220 μg (300-900 nmol). This effect was determined based on the full width at tenth maximum (FWTM) of the elution profile as a function of uranium concentration as presented in Figure 3. The FWTM is expressed in term of retention time (RT). The elution profile of uranium broadens and overlaps with those of heavier lanthanides (up to Er) at uranium concentration higher than 220 μg. Above the concentration of 535 μg, the FWTM of uranium profile could not be determined accurately because of anomalous tailing, and therefore, the variation of FWTM above this concentration is assumed to follow the broken line in Fig 3. Generally for analytical purpose, a small amount, below the interference level found in this study, of uranium fuel is used. If only lighter lanthanides are of interest for separation the interference of uranium can be overlooked since the amount of heavier lanthanides in nuclear fuel is negligible. (Fig 3)

4. *Elution profiles.* The separation profiles of rare earths and uranium obtained at pH of 3.5 and temperature 80 °C are shown in Figure 4. The profiles demonstrate clear mutual separation of the constituents used in cold experiment (not using nuclear fuel solution). In the cold run the elements were detected by coulometry. We applied the optimum physico-chemical conditions, established by the cold experiment, to separate RE and TUE from nuclear fuel solution. The separation profiles of the constituents of nuclear fuel are shown by the broken curves. Ru-106 was eluted at 4 minutes of retention time, ^{90}Y at 32 minutes, $^{134,137}Cs$ at 45 and 49 minutes, $^{154,155}Eu$ at 50 minutes. Ruthenium shows broadening in the elution profile probably because of the presence of its multiple oxidation states. Plutonium exhibits two elution peaks: one at 12 minutes and the other at 27 minutes. 75% of plutonium elutes at 12 minutes and the rest at 27 minutes. Uranium elutes around 9 minutes which is 7 minutes earlier than that observed in the cold experiment. Curium elutes at 52 minutes and americium at 53 minutes and their elution profiles overlap each other. In this study uranium and plutonium separate clearly from americium and curium. (Fig 4)

5. *Correlation of retention time with ionic radii of lanthanides and actinides.* It is instructive to see the correlation of retention time with the ionic radii since retention time is related to ionic radii. The results are presented in Figure 5. Lanthanides show consistency with retention time with ionic radii profiles though the results of Tb^{3+}-Ho^{3+} are somewhat deviated from the normal trend. The profiles of Cm^{3+} and Am^{3+} are compatible. Plutonium retention shows complex behaviour since elution profiles at two different retention times indicate the presence of two species. The plutonium species at 12 minutes RT can be thought of Pu^{4+} because of its closeness with the ionic radii (IR) profiles. If we utilise the normalisation factor of 0.64, obtained from [RT of Pu^{4+}/IR of Pu^{4+}] RT and IR of Pu^{4+}, to UO_2^{2+} the retention time of uranium becomes about 9 minutes which in good agreement with the experimental observation. This consistency with uranium results supports the assumption of plutonium species eluted (Fig 5)

at 12 minutes as Pu^{4+}. On the other hand plutonium species eluted at 27 minutes could not be ascertained although this result is in agreement with the tracer experiment. It can be mentioned that the plutonium tracer was kept in very dilute solution of nitric acid (0.07 M) and it can be thought that plutonium might undergo hydrolysis or polymerisation under this condition. The present results also suggest the possibility of disproportionation of plutonium at some stage of the experiment. To confirm this argument further details study on plutonium are required.

Conclusion

The results of the present work demonstrate the applicability of the method described here for analysing nuclear fuel solution.

References

1. ASTM, E321-69, 1969, p 1045.
2. Knight et al.; Dynamic ion exchange chromatography for determination of number of fissions in thorium-uranium dioxide fuels. Anal Chem, 1984, **56**, 474-478.
3. Raaphorst van J G, Haremaker H; A rapid chemical separation procedure for the determination of burnup of nuclear fuel. J Radioanal Chem, 1979, **53**[1-2], 71-80.

106/39

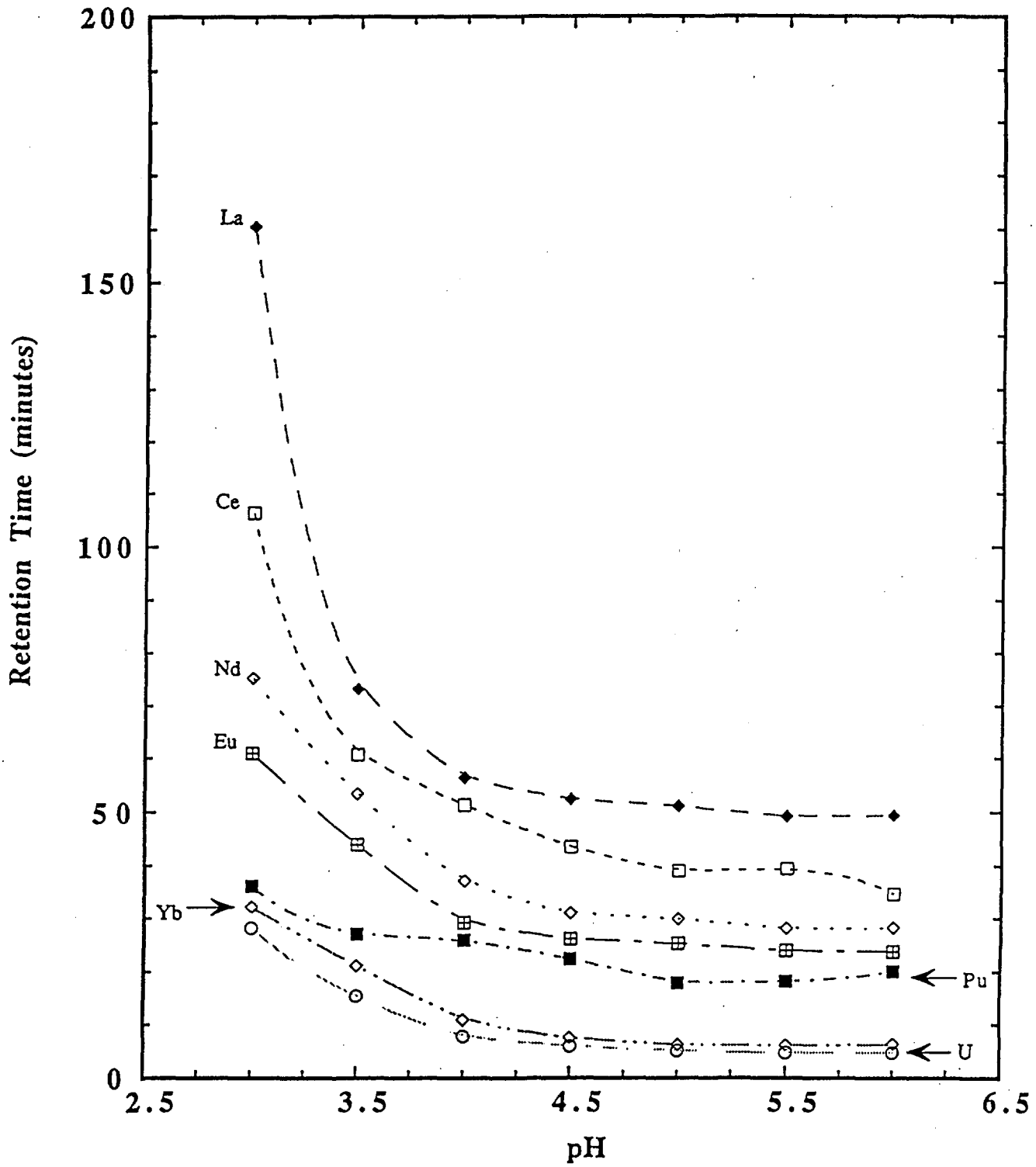

Fig 1. Variation of retention time as a function of pH

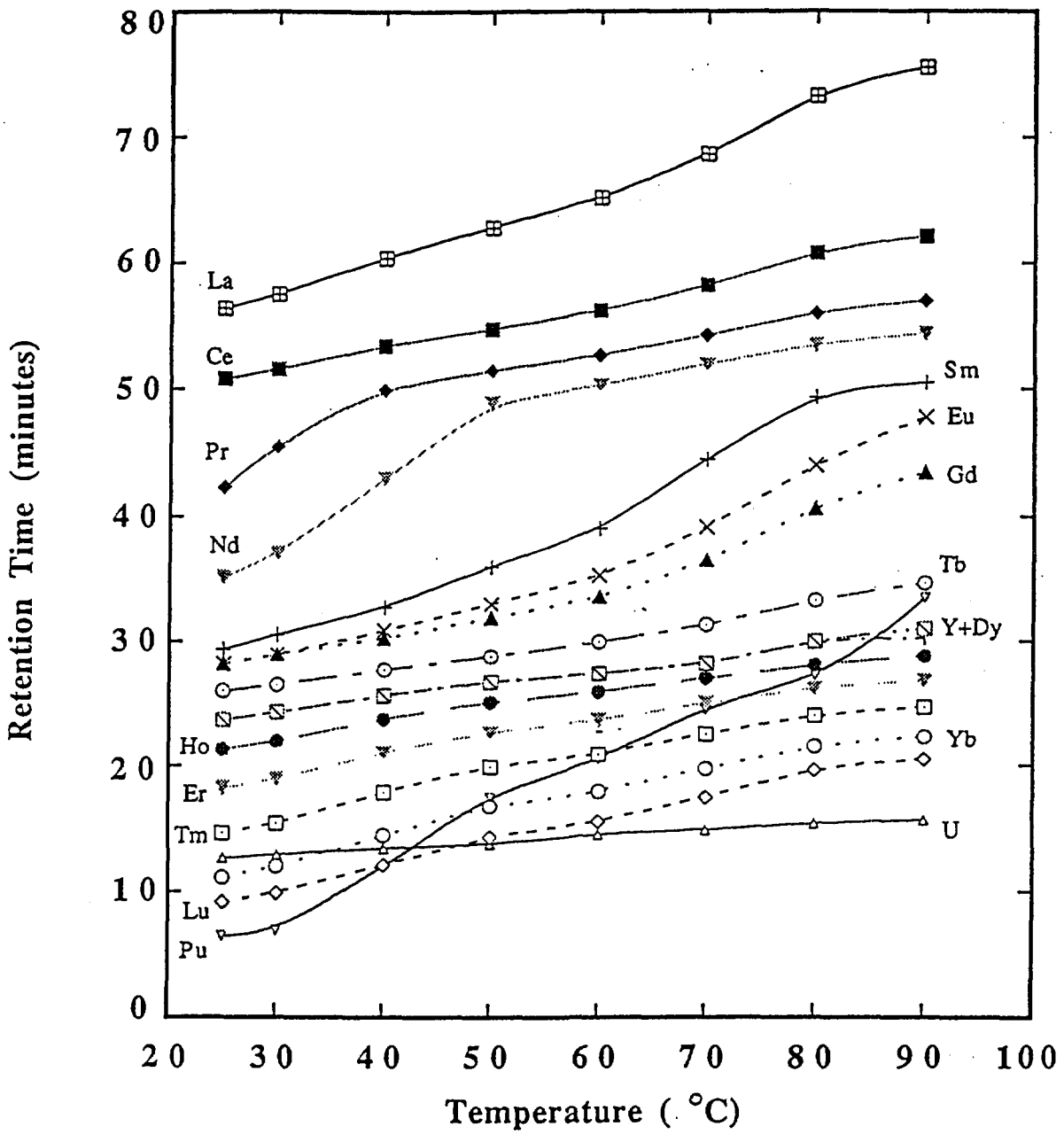

Fig 2. Variation of Retention time as a function of temperature

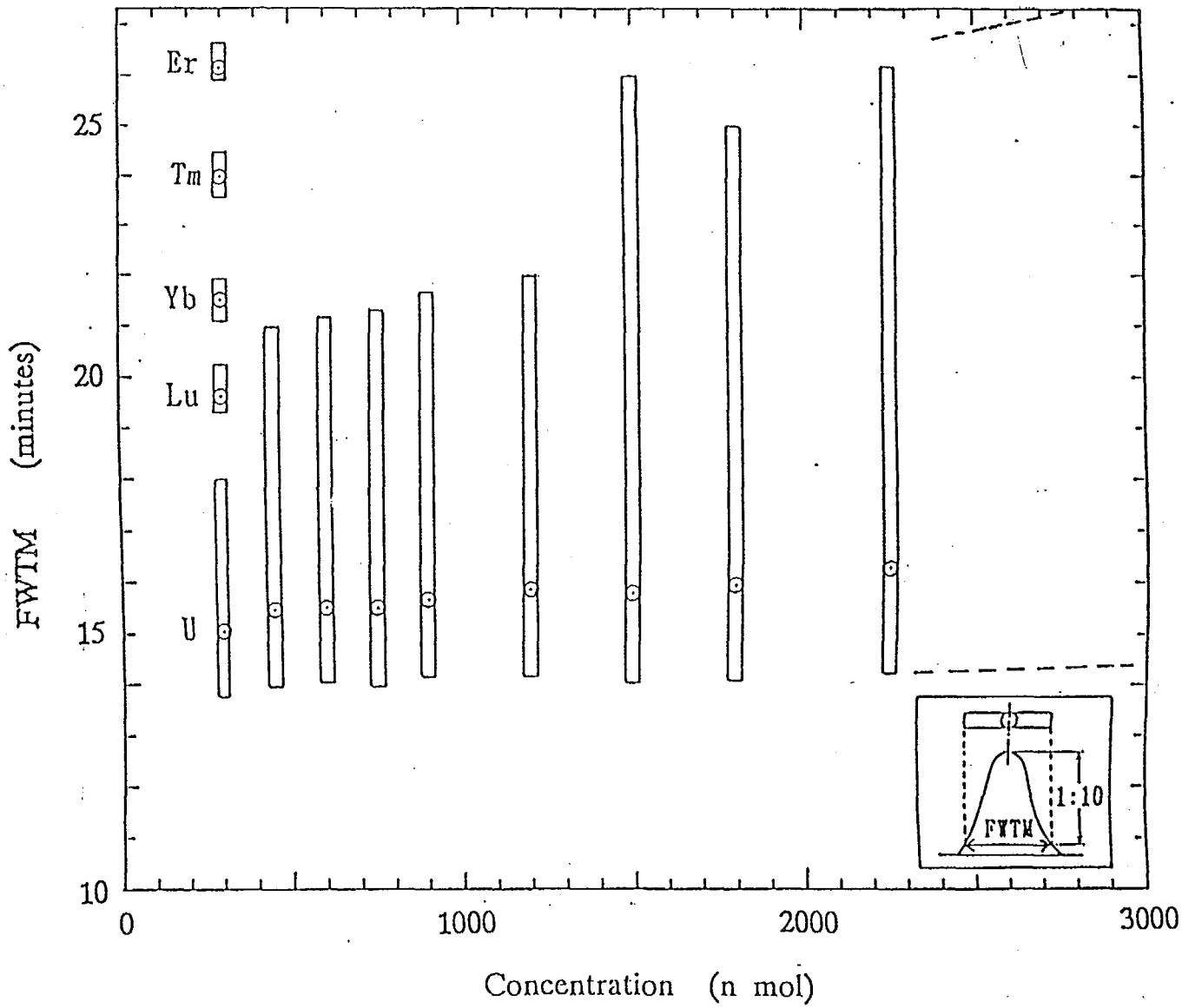

Fig 3. Variation of the FWTM of uranium elution profile as a function of uranium concentration (see text for details)

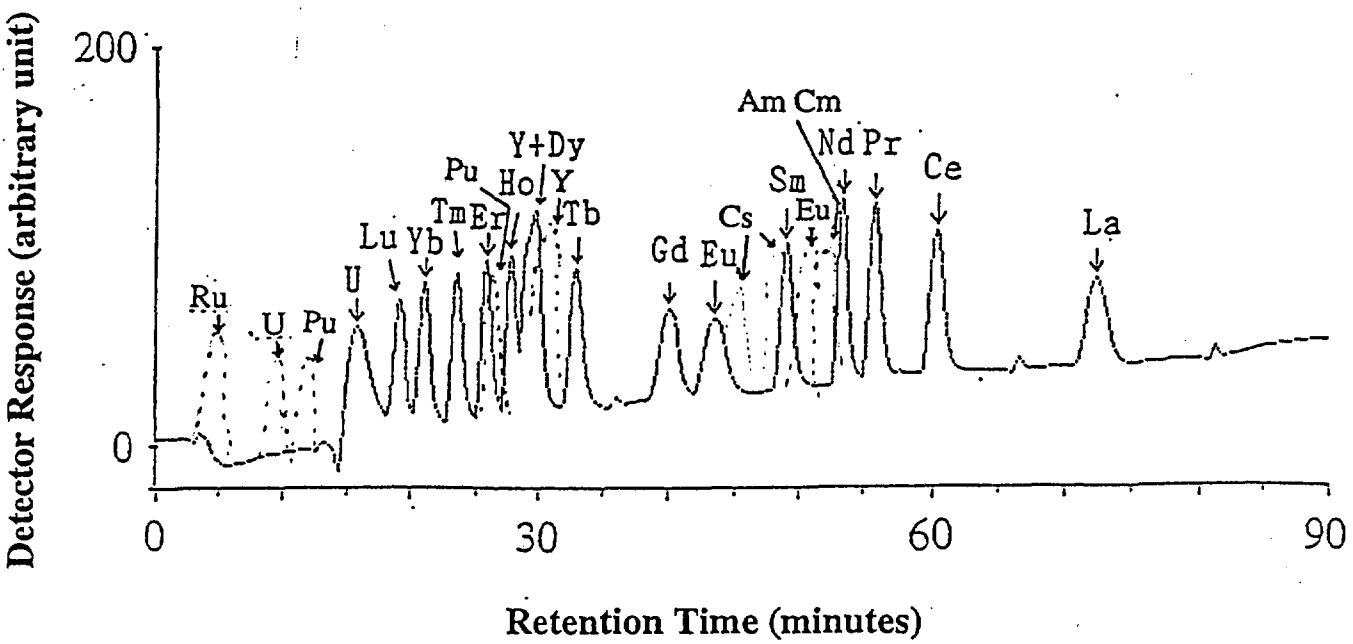

Fig 4. Elution profiles of RE, uranium, Ru, Cs and TUE. The elution profiles for the constituents a separated from nuclear fuel, shown by broken curves, are for eye guide (see also text)

THIS PAGE IS MISSING IN THE

ORIGINAL DOCUMENT

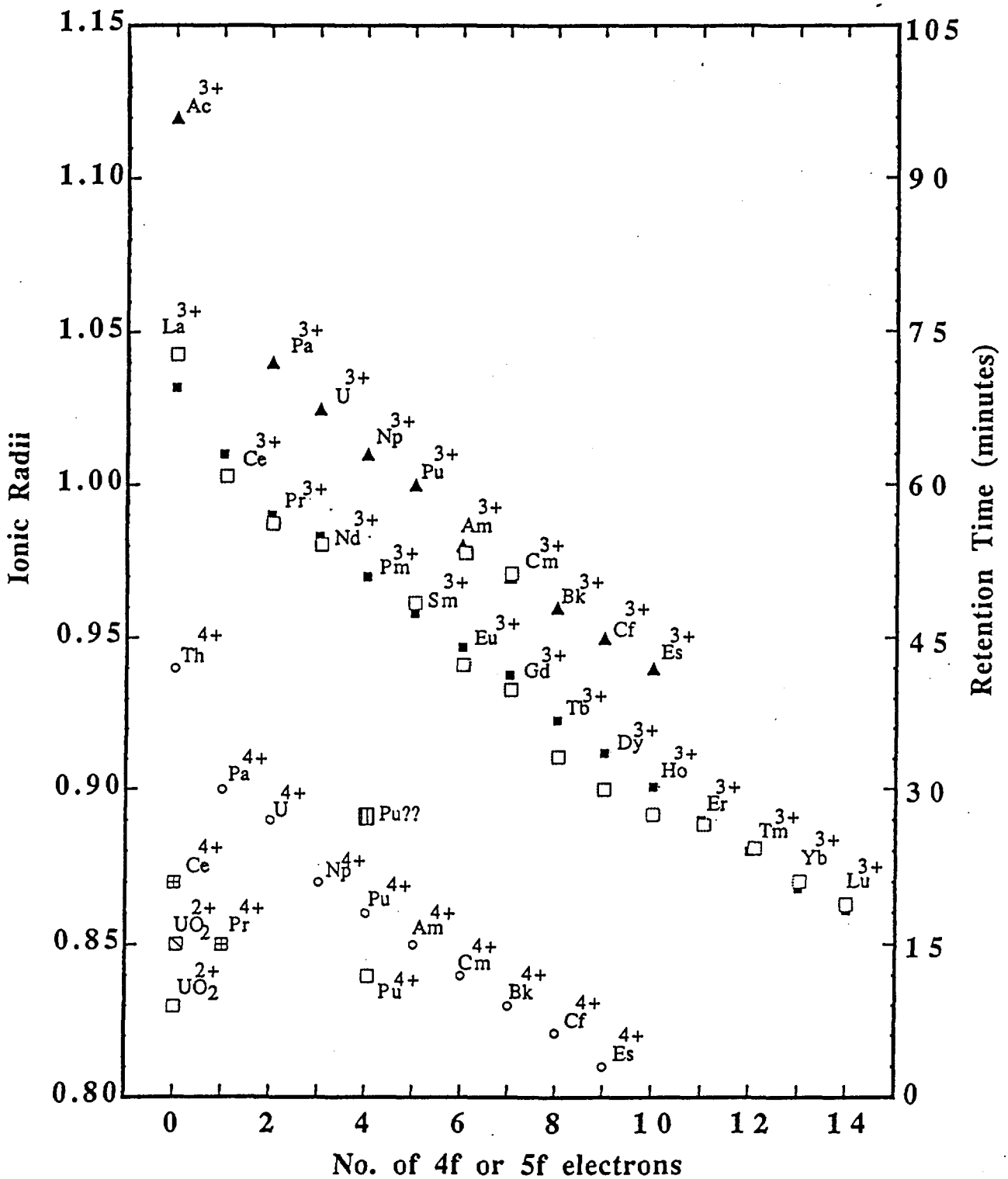

Fig 5. Correlation of retention time with ionic radii. Open and slashed squares denote the retention time and the rest symbols for the ionic radii. For uranium the slashed square stands for the retention time observed in simulated experiment.

AU9817406

A Computerised Radioactive Effluent Monitoring System for a Medical Cyclotron Complex

BHASKAR MUKHERJEE
ANSTO, Safety Division, Radiation Protection R&D Section
PMB 1, Menai, NSW 2234, Australia

SUMMARY. In July 1993 a computerised effluent monitor for the real-time estimation of the stack releases of short lived positron emitting gaseous radiopharmaceuticals has been installed at the 30 MeV Medical Cyclotron Facility of the Australian Nuclear Science and Technology Organisation (ANSTO). Recently an electronic weather station consisting of an anemometer, a wind-vane and a wind temperature indicator have been added to the existing monitoring system. The activity concentration of the radioactive stack releases at selected critical receptor locations in the close vicinity of the cyclotron complex was calculated in real-time by implementing a simple "Gaussian Plume" type atmospheric dispersion model. The stack release concentration and weather data were used in this model calculations in a spreadsheet environment. In this paper the principle and important results of the computerised real-time stack effluent monitoring system operating at our cyclotron facility are presented.

1. INTRODUCTION

Short lived positron emitting gaseous radiopharmaceuticals such as $^{11}CO_2$ ($T_{1/2}$ = 20 min), $^{13}NH_3$ ($T_{1/2}$ = 13 min), ^{18}F ($T_{1/2}$ = 109 min, as ^{18}F-Fluorodeoxyglucose in liquid form) and ^{123}I ($T_{1/2}$ = 13.6 h), in the form of $Na^{123}I$ (liquid) are routinely produced by the 30 MeV H^- ion Medical Cyclotron of the Radio-pharmaceutical Division of ANSTO. During the handling and chemical processing in sterile automatic chemistry cells a fraction of the radioactive inventory is released into the atmosphere through the main stack of the cyclotron facility. The activity concentrations of the atmospheric release of radioactive gases are strictly limited by regulations (1, 2) imposed by the Environmental Protection Authority (EPA). Hence, the installation of a suitable effluent detector for the real-time estimation of the stack discharges during the entire radioisotope production and handling process became mandatory. A smart effluent monitoring system based on a small flow-through detector-chamber and a datalogger has been developed at the Health Physics laboratory of our cyclotron facility and installed in July 1993 (3).

Recently an anemometer, a wind-vane with optoelectronic transducers and a wind temperature indicator have been added to the existing stack monitoring system thus, enabling the datalogger to retrieve the stack release and weather data simultaneously.

The deposited activity concentration at selected "Critical-Receptor-Locations" in the immediate vicinity of the cyclotron complex were calculated and displayed on a spreadsheet with the corresponding time of the stack release. A Gaussian-Plume type "Atmospheric-Dispersion-Model", incorporated in the spreadsheet macro program was used to process the atmospheric data such as wind speed, temperature, wind direction and the released activity concentration [$MBqm^{-3}$] from the stack.

2. SYSTEM DESCIPTION

The exhaust air from the radiochemical cells is drawn via a HEPA (High Efficiency PArticulate) filter and released through the stack at a rate of 10 m^3s^{-1} (Figure 1). From the lower section of the stack an air sample is drawn via the stack monitor and returned to the exhaust air stream. The stack monitor includes a flat (25 mm diameter) flow-through chamber (4.5 ml) attached to a NaI scintillation detector (5 cm × 5 cm dia.) interfaced to a Single Channel Analyser (SCA). The air containing radioactive effluent residing in the chamber is sampled every minute by the datalogger. The analog voltage output (mV) of the SCA, proportional to instantaneous activity concentration is linearised and converted to activity concentration [$MBqm^{-3}$] using a set

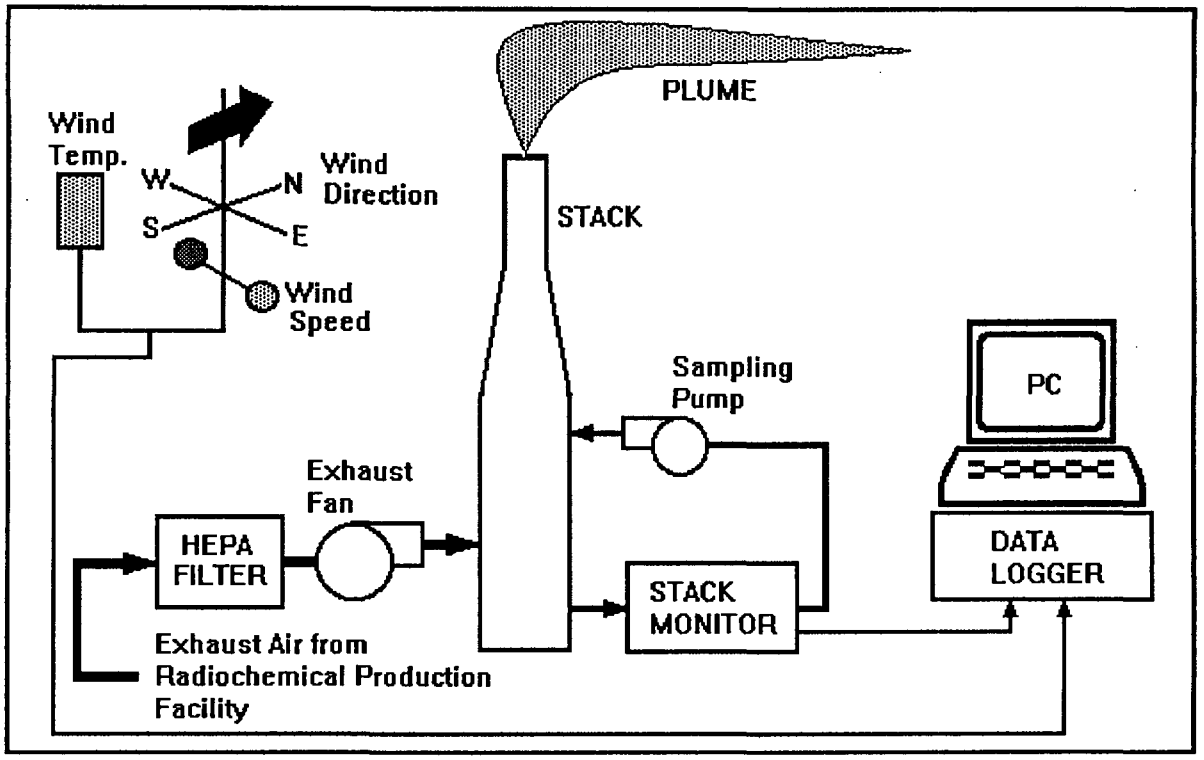

Figure 1: Schematic diagram of the stack monitoring system at the cyclotron radioisotope production facility of ANSTO showing the electronic weather station, HEPA Filter, exhaust fan, sampling pump, flow meter, stack monitor and the datalogger connected to a host PC. The diagram is explained in the main text.

of calibration polynomials. A spreadsheet macro program on a personal computer (PC) with a 133 MHz central processing unit (CPU) and a 100 MB (Mega Byte) hard disc was implemented for data processing.

3. STACK DISCHARGE EVALUATION

The activity concentration a_t of the effluent in the detector at the instant t (duration = 1 minute) is given as:

$$a_t = k(v_t) \qquad (1)$$

where, v_t and $k(v_t)$ are the output voltage sampled by the datalogger and the calibration polynomial respectively.

The total activity (q) released during the period of a single production run (t) is given as:

$$q = \Sigma a_t \, r \, t \qquad (2)$$

where, Σa_t, r and t are the integrated activity concentration, stack flow rate (m^3s^{-1}) and the duration of release respectively. In Figure 2 the activity rate of released ^{18}FDG is shown as function of time (3).

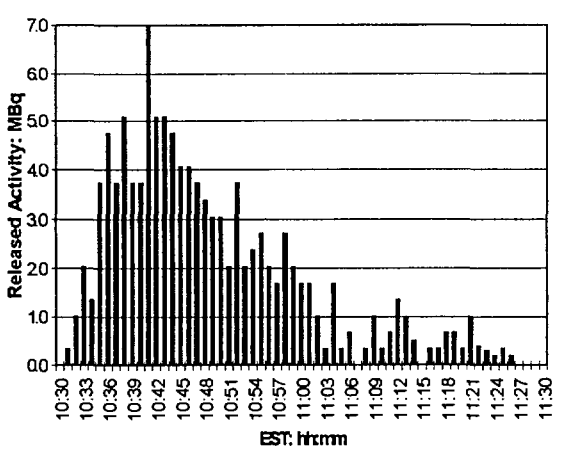

Figure 2: Shows the activity [MBq] of ^{18}FDG vapour released through the main stack of the cyclotron facility during the radiochemical processing and handling in the morning hours between 10.30 AM - 11.30 AM. The total released activity was found to be 111 MBq.

4. ATMOSPHERIC DISPERSION

The stack emission is dispersed from its release point to the neighborhood due to the movements of the air. The typical pathways of atmospheric dispersion is shown in Figure 3.

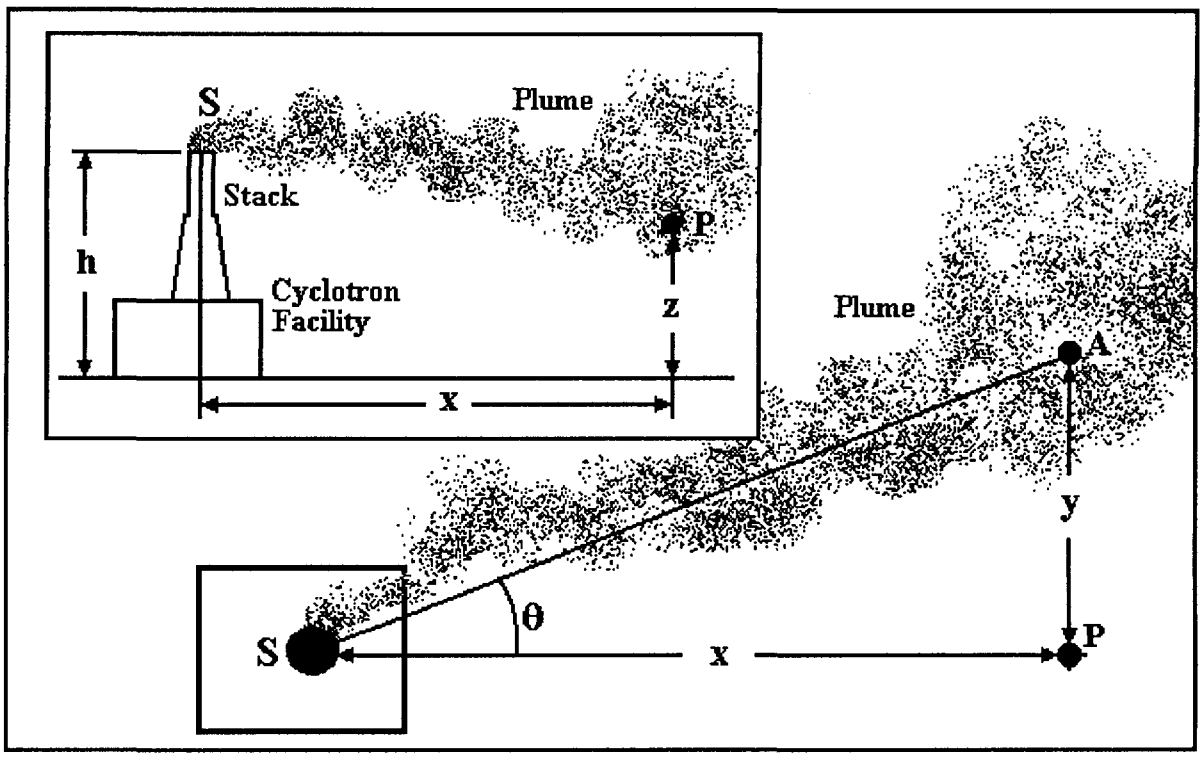

Figure 3: Schematic diagram showing the important aspects of the atmospheric dispersion model for the plume released from the cyclotron facility stack. The emission source (stack), receptor, plume core, downwind distance, crosswind distance and the wind direction are indicated as S, P, A, x, y and θ respectively. The stack (h) and receptor (z) heights are shown in the upper picture (inset).

The steady state atmospheric dispersion of the released radioactivity is described by the "Gaussian Plume Model"(4):

$$X(x,y,z) = Q/(2\pi\sigma_y\sigma_z u)[A+B]C \quad (3)$$

where,

X = Activity concentration at critical receptor location [$MBqm^{-3}$]

Q = Radioactivity release rate from the stack [$MBqs^{-1}$]

σ_y = Horizontal dispersion parameter [m]

σ_z = Vertical dispersion parameter [m]

u = Wind speed [ms^{-1}] and,

$$A = \exp(-(h + z)^2/2\sigma_z^2) \quad (4)$$

$$B = \exp(-(h - z)^2/2\sigma_z^2) \quad (5)$$

$$C = \exp(-y^2/2\sigma_y^2) \quad (6)$$

where,

h = Stack height [m]

y = Cross wind distance [m]

z = Receptor height [m]

The horizontal (σ_y) and vertical (σ_z) dispersion parameters as a function of downwind distance at different atmospheric stability conditions (Pasquill-Gifford Stability Classes) have been published elsewhere (4). The atmospheric stability classes are divided in seven categories:

Class A: Extremely Unstable

Class B: Moderately Unstable

Class C: Slightly Unstable

Class D: Natural Stability

Class E: Slightly Stable

Class F: Moderately Stable

Class G: Very Stable

5. RESULTS

The activity concentration [$MBqm^{-3}$] of the ^{18}FDG deposition at the ground level (z = 0) critical receptor situated at 110 meters from the Cyclotron stack was calculated using equations 3, 4, 5 and 6. The radioactivity release and atmospheric data was retrieved from the datalogger and processed using a spreadsheet macro program and shown in Table 1.

Table 1: Showing the result-printout of the spreadsheet macro program developed for the real-time estimation of atmospheric dispersion of ^{18}FDG vapour released from the automatic chemistry (production) cell. The atmospheric data (columns 2, 3 and 4) was sampled in every minute and averaged over the interval of 15 minutes by the datalogger. The radioactivity release data in column 5 was derived from the original data (Figure 2) sampled in every minute. The diffusion time of the plume to reach the critical receptor was not calculated. Hence, the effect of the radioactive decay of ^{18}F ($T_{1/2}$ = 109 minute) on the deposited activity concentration has been ignored. The Pasquill-Gifford Classification Factor ands the horizontal (σ_y) and vertical (σ_z) dispersion factors were extrapolated from the literature data (4).

Atmospheric Dispersion of 18-FDG Vapour Released from the NMC Stack

Date: 3 June 1997
Critical Receptor: Queen Mary Building
Distance from the Stack: 110 m
Pasquill-Gifford Classification Factor: C
Horizontal Dispersion Factor (σ_y): 12 m
Vertical Dispersion Factor (σ_z): 7 m
Stack Height (from ground level): 10 m
Receptor Height (from ground level): 0 m

EST hh:mm	Av. Wind Temp: [°C]	Av. Wind Speed: [ms^{-1}]	Av. Wind Dir: [deg]	Act. Release Rate: [MBqs^{-1}]	Act. Deposition: [MBqm^{-3}]
10:30	23.4	1.51	62	3.33E-04	5.05E-07
10:45	23.9	1.33	70	6.15E-02	1.90E-04
11:00	24.6	1.26	20	4.92E-02	5.44E-05
11:15	25.2	0.82	28	1.37E-02	2.38E-05
11:30	24.9	2.25	64	5.33E-03	5.98E-06

6. CONCLUSION

The spread of gaseous radioactive effluent released from the stack of a radioisotope production facility via atmospheric diffusion process constitutes a critical radiological /epidemiological problem. This paper highlights a simple and reliable technique for the estimation of atmospheric diffusion of the radioactive vapours released from a medical cyclotron complex in real-time. A datalogger interfaced to custom designed radioactive gas monitors (developed at our Health Physics laboratory) and a popular spreadsheet package running on a 133 MHz Personal Computer was used. This method is based on the "Gaussian Plume-Diffusion Model" and the "Pasquill-Gifford" atmospheric stability factor. User-friendly animated mimics display the weather data as well as the released activity concentrations on the computer screen.

This computerised real time radioactive effluent monitoring system is well suited to predict the value of the deposited activity concentration at critical receptor locations within 1000 m from the stack in an urban environment (present case). At longer distance, the air turbulence caused by the neighbouring buildings of different heights as well as non-uniform terrain structure would result in a high uncertainty of the predicted activity concentration value.

7. REFERENCES

1. Birattari, C., Ferrari, A., Parnell, C. J. and Silari, M., 1987, Radiation Protection Dosimetry, Vol 19(3), pp183-186.
2. Kopeikin, I. N., Serezhnikov, S. V. and Stepanov, V.E., 1993, Radiation Protection Dosimetry, Vol 46(2), pp79-88.
3. Mukherjee, B., 1995, Proceeding 14th International Conference on Cyclotrons and their Applications, Cape-Town, South Africa, October 8-13, pp 334-337.
4. Shleien, B.1994. The Health Physics and Radiological Health Handbook, 2nd Ed, Scienta Inc, Silver Spring, MD.

Development of a New Hydrogen Gauge using a Small Neutron Source

I. ISHIKAWA, N. TACHIKAWA
Japan Atomic Energy Research Institute
Oarai, Higashi-Ibaragi-gun, Ibaraki-pref. 311-13 JAPAN
H. TOMINAGA
Institute of Radiation Measurements
Tokai, Naka-gun, Ibaraki-pref. 319-11 JAPAN
M. AZUMA
Shinko Mex, Ltd.
Kanazawa-cho, Kakogawa-shi, Hyogo-pref. 675-01 JAPAN

Most of industrial nuclear gauges are based on the use of radiation transmission through matter. In moisture gauges for a big volume of object, a simple technique of neutron moderation is usually employed. Neither technique could be applied to determination of hydrogen or its compounds in a small volume of metallic sample.

A new technique has been developed for measuring the thickness of a thin layer of 30-200 μm thick plastic, which is sandwiched with two sheets of 0.6-4.2mm in total thickness. In this complex steel plate as a new material with the properties of suppressing vibration and preventing noise in some portions of buildings etc., the measurement of the plastic layer thickness and its homogeneity is needed for quality control, whereas there has been so far no nondestructive measurement technique. To obtain a sufficient sensitivity in the thickness measurement, a source-sample-detector arrangement and its surrounding structure were specially devised, where multiple scattering of neutrons and efficient generation of slowed-down neutrons from the plastic layer of a sample were utilized.

In a final design of the measuring head of the thickness gauge, two iron blocks as fast-neutron reflectors were placed on both the upper and lower sides of a ^{252}Cf neutron source with a small gap. An appropriately thick polyethylene sheet(3mm) as a neutron moderator was placed on one side of the gap. A ^{3}He proportional counter was located close to the ^{252}Cf source. A sample to be measured was inserted into the gap.

In the structure described above, at the first glance, the polyethylene sheet may look like an unfavorable choice that merely increases the background in the neutron counting, since its thickness is larger than one order of magnitude over that of the plastic to be measured. In practice, however, the sheet plays an important role in generating thermal neutrons efficiently from the plastic to be measured owing to multiple reflection of neutrons through the sheet and sample in the gap with the aid of iron reflectors. A precision of about 10 μm was attained in a 1 minute measurement with a ^{252}Cf source of 40MBq.

The new technique developed may be applicable also to the determination of a trace amount of hydrogen in a small sample of various materials.

Radioisotopic Determination Methods of Sulfur Dispersion and Sulfur Blooming in Rubber Compounds. Part II.

E. KOCZOROWSKA, W. GORĄCZKO
Radio- and Photochemistry Department, Technical University Poznań
60-965 Poznan, Piotrowo3, Poland
GORACZKO@SOL.PUT.POZNAN.PL

SUMMARY. : Radioisotope methods have been analysed to study the sulfur dispersion and sulfur blooming in rubber compounds. These methods can be applied to investigate physical and chemical processes in rubber and to optimize technical conditions of tire production.

1.INTRODUCTION

In the manufacturing processes of rubber goods, particularly tires, it is important to retain the tack building of materials to be stable and determined according to technological speciffications, since weak tack causes great difficulties during the building of the tires and theirs deteriorations. Such deterioration appears as the bubbles between layers of the tire body and unsymmetrical location of the elements, etc. The migration of sulfur and other ingredients would form the so - called blooming on the surface of semi-finished raw rubber products. The ratio of ingredients in the recipe and the methods of preparation besides storage conditions of a compound and further processing play an important role here.

In the present work, an attempt was made to estimate the influence of selected technological factors on the kinetics of sulfur blooming.

Rubber compounds containing soluble sulfur and insoluble Crystex sulfur were made for such investigations.

2.Experiments.

The radioactivity of the ^{35}S isotope introduced into rubber compounds has been measured by volumetric and surface methods. The soluble sulfur and insoluble sulfur Crystex were activated by neutrons in quartz capsules. [1,2,3].

The radioactivity sulfur was mixed with sulfur that was usually used in industry to obtain a homogeneous mixture. The methods of the radiation intensity measurements were chosen from these reported in the literature, which are:

- liquid scintillates,
- the proportional flow- throuhh counter 2 π,
- the Geiger-Muller counter,
- the autoradiographic method.

3. Results and Discussion.

The above-described methods were used in a number of experiments performed in laboratory and industriel scales to estimate the dispersion degree of sulfur and the sulfur blooming in rubber compounds. The analysed factors affecting the dispersion and blooming were the tipe of compounds, number of passes through a mixing mill gap, temperature of the batch at the time of introduced curatives, conditions of the vulcanization, time and storage temperature, different kind of sulfur.

During experiments on an industrial scale the samples were taken at different stages of the process: 1- from the discharde mill under the mixer, 2, 3- from two subsequent homogenizing mills, 4- from the extruded tread. The obtained variation coefficients proved that the considered technological process does not provide a satisfactory distribution of curatives in the rubber compounds during production but the scatter of intensity results decreases after subsequent technological operations. Data are plotted in Figure 1.

Visible sulfur blooming on the surface of the rubber compound samples containing labelled soluble sulfur stored at temperatures of 20 and 40°C (Fig. 2 and 3). At 42°C (Fig. 4) the processes occuring here are the reverse of blooming. It is confirmed by the fact that at a storing temperature of 60°C (Fig. 5) the decrease in concentration of the soluble sulfur on the surface is very sharp. At a storage tempereture of 20°C no essential change of concentration of the insoluble sulfur Crystex OT 33 was noticed (Fig. 6).

We showed that up 40°C the blooming of soluble sulfur on the rubber compounds surface is observed. At higher temperatures this bloom gradually disappears. Why ? To answer this question additional experiments on sublimation and oxidative degradation of sulfur during storage at different

temperatures were performed. The mass decrement was analysed by the radioisotopic (^{35}S) and gravimetrical method. Taking into account that in the rubber compound the sulfur concentration is smaller than during discussed above model experiments, the influence of sulfur sublimation and oxidation on the surface concentration of sulfur is too small to change substantially our conclusions shown in the Figs 2-6 and previous results of experiments of blooming process.

These problems are to be solved in the future.

4. References

1. J.Komosiński and E. Koczorowska: Radioisotope Investigation of Sulfur Dispersion in Rubber Mix. Isotopenpraxis, **26** (2), 81-84, 1990.

2. B.Jurkowski, E.Koczorowska, W.Gorączko, J.Manuszak: Ocena możliwości pomiaru metodą radioizotopową wpływu warunków sporządzania mieszanek gumowych na wykwitanie siarki. Polimery (in Polish), **37** (4), 163-166, 1992. Full English translation: Int.Polymer Sci. Technol. (UK), **20**, (1), T/82-T/85, 1993.

3.B.Jurkowski, E.Koczorowska, W.Gorączko and J.Manuszak: Radioisoto-pic Determination methods of Sulfur Dispersion and Sulfur Blooming in Rubber Compounds. J. Appl. Pol. Sci. 59, 639-645, 1996.

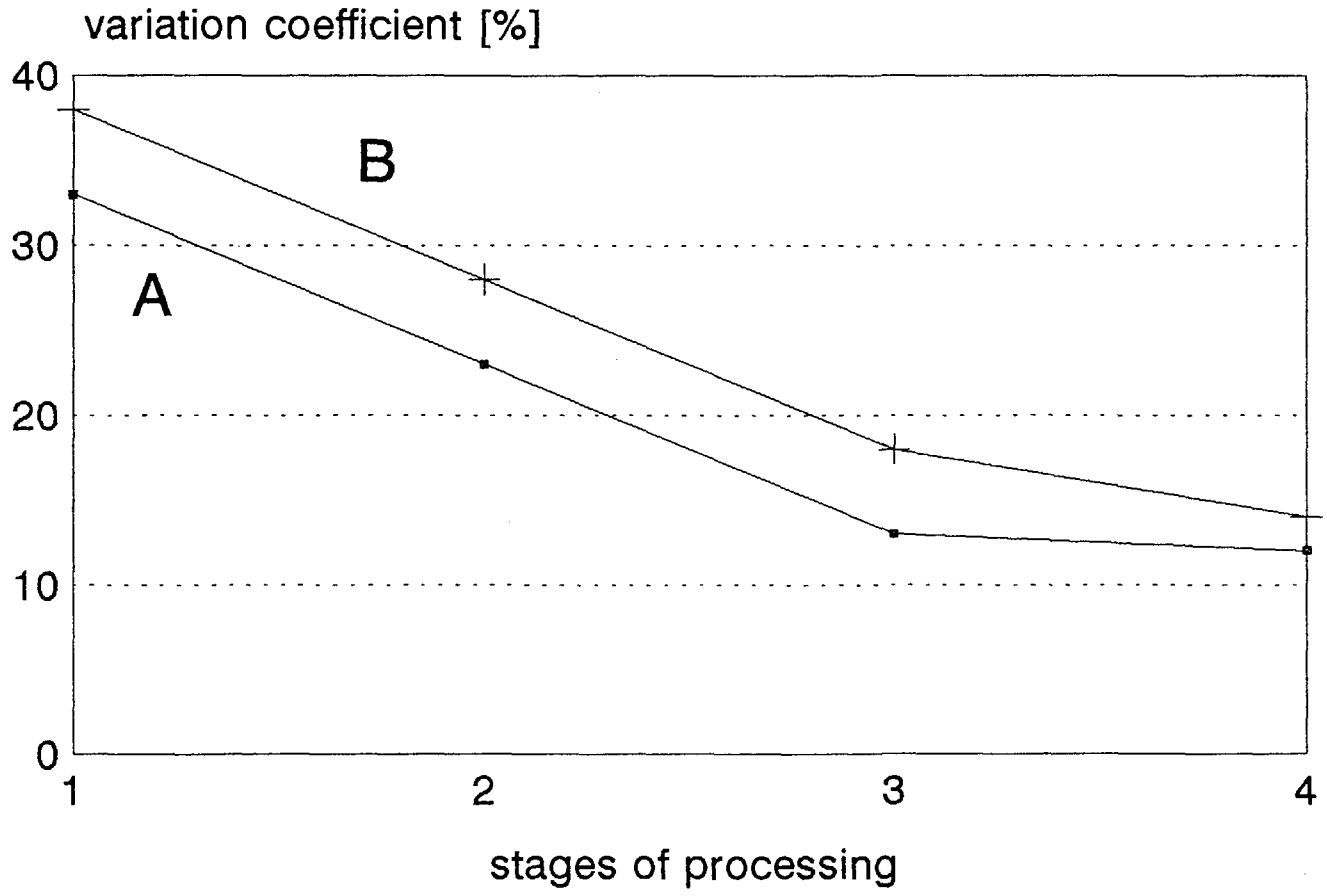

Fig.1 Comparison of variation coefficient at different stages of tire production.
A-intensity of radiation measured by G-M counter.
B-intensity of radiation measured by flow-through counter.

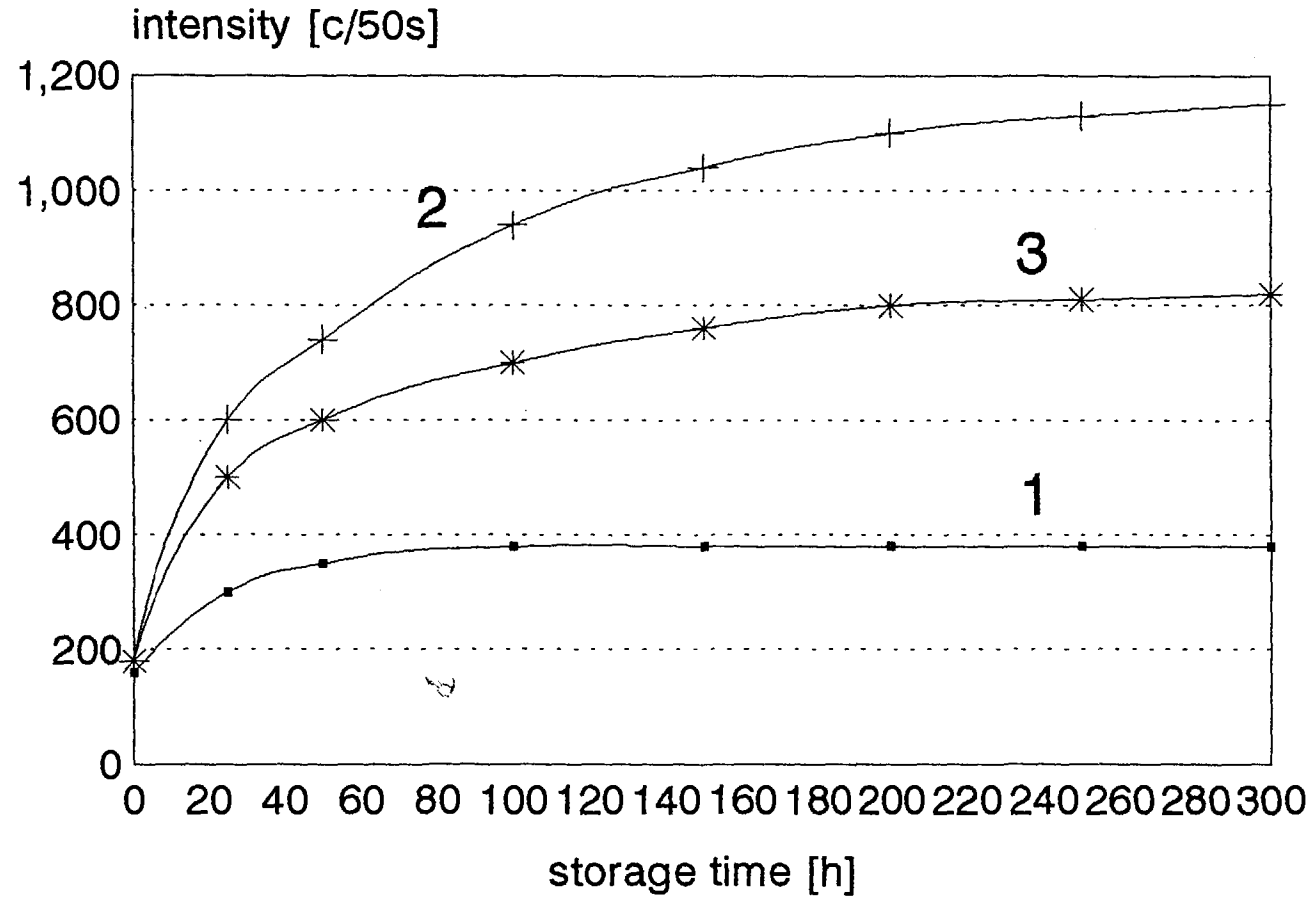

Fig.2 Rubber compounds stored at 20°C.
1-mixing at 106°C, 2-mixing at 125°C,
3-mixing at 145°C.

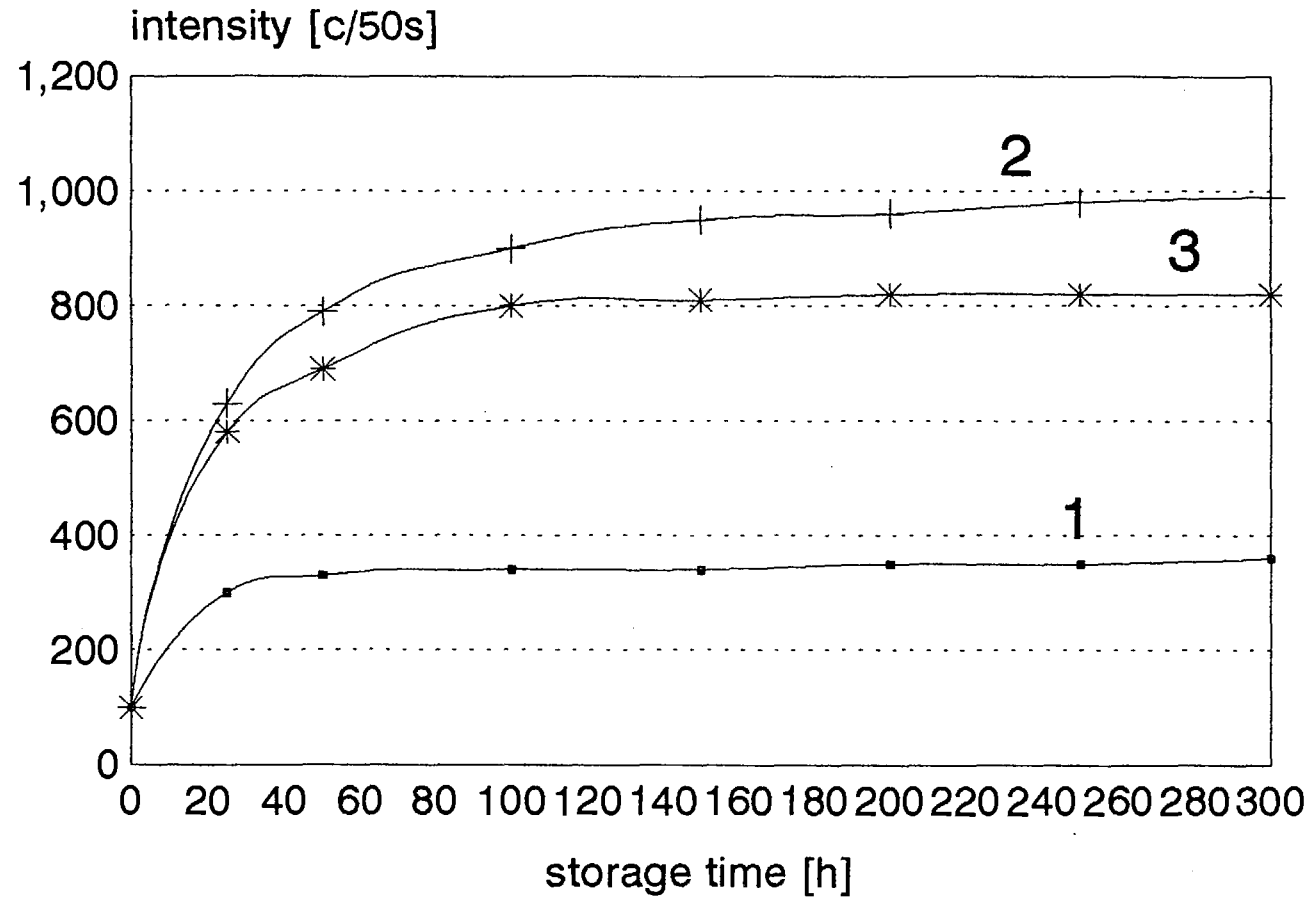

Fig.3 Rubber compounds stored at 40°C.
1-mixing at 106°C, 2-mixing at 125°C,
3-mixing at 145°C.

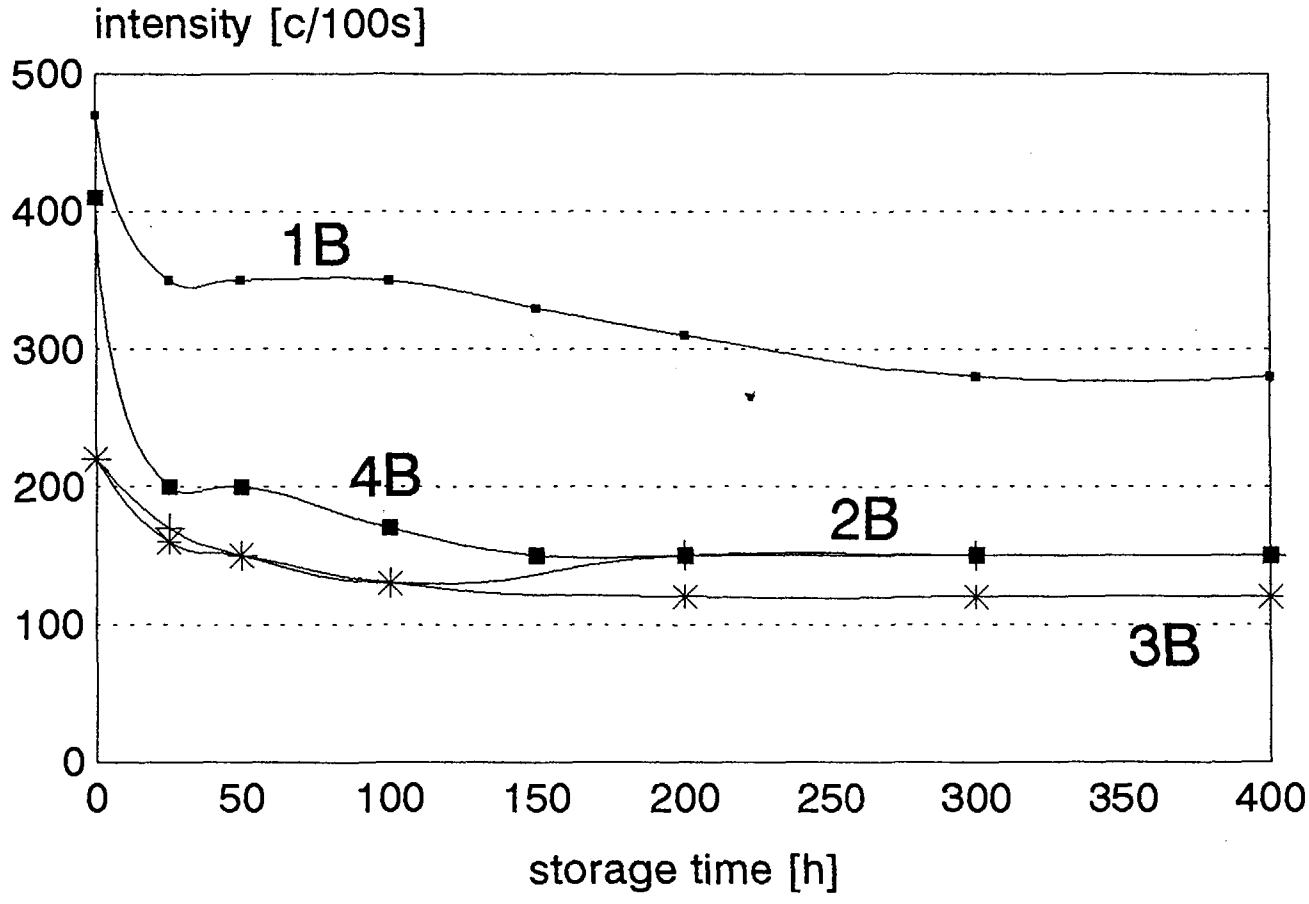

Fig.4 Rubber compounds stored at 42°C.
1B-soluble sulfur, mixing at 106°C,2B-Crystex, mixing at 106°C,
3B-Crystex, mixing at 158°C,4B-soluble sulfur, mixing at 158°C.

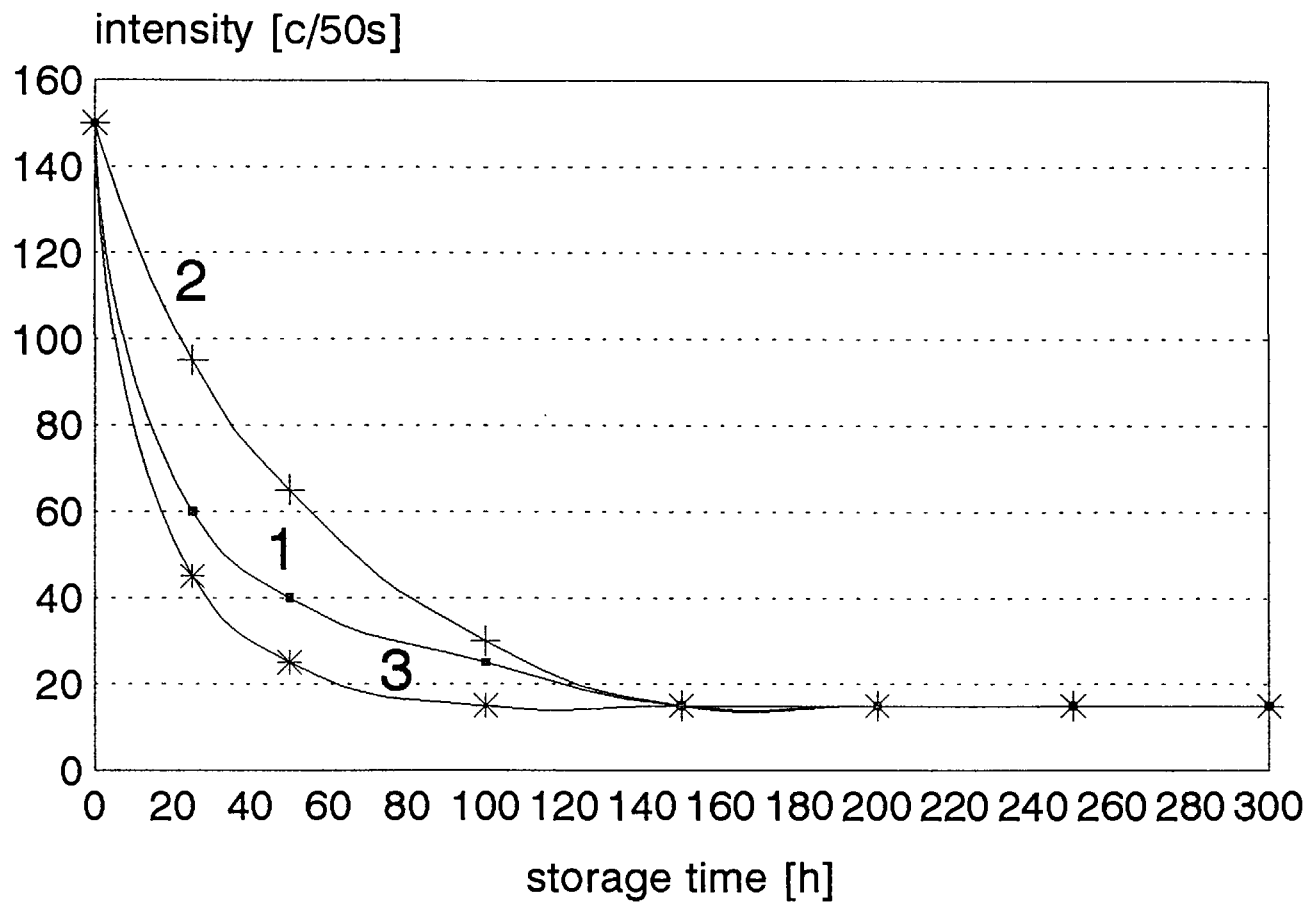

Fig.5 Rubber compounds stored at 60°C (soluble sulfur).
1-mixing at 106°C, 2-mixing at 125°C,
3-mixing at 145°C.

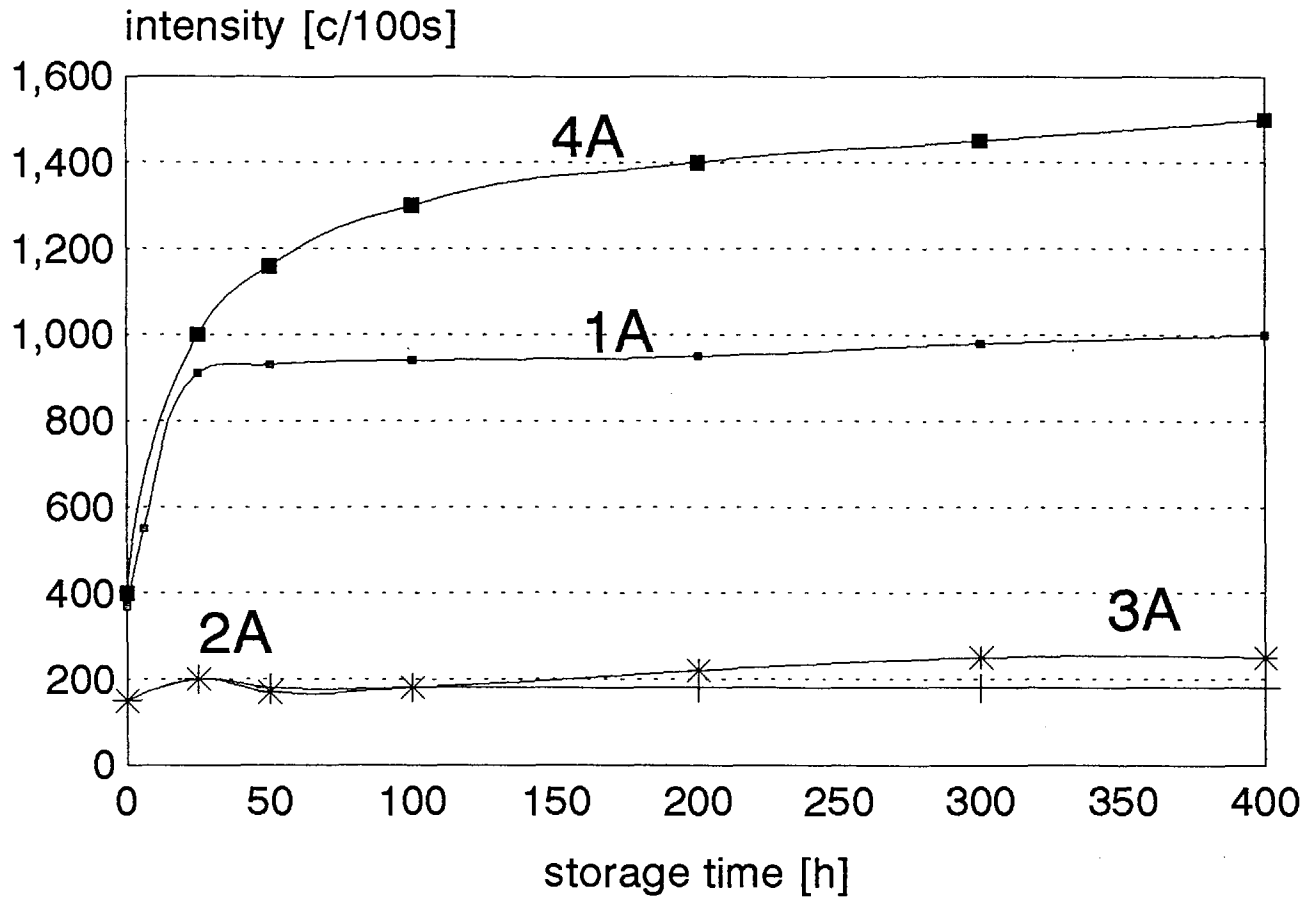

Fig.6 Rubber compounds stored at 20°C.
1A-soluble sulfur,mixing at 108°C, 2A-Crystex,mixing at 106°C,
3A-Crystex,mixing at 158°C, 4A- soluble sulfur,mixing at 158°C.

Paper 110/148

C-13 Isotopic Studies of the Surface Catalysed Reactions of Methane

MERVYN A LONG, SIMON J X HE and MOSES ADEBAJO
School of Chemistry, University of New South Wales
Sydney, NSW 2052, Australia

Zeolitic type materials, by virtue of the acidic nature of their surfaces exhibit catalytic activity for promoting tritium isotope exchange reactions between tritium gas or water and many organic molecules, including hydrocarbons. Many organic substrates may be tritium labelled in this way.

The question as to whether or not methane gas may be activated on the surface of a zeolitic type catalyst, such that it directly methylates a suitable aromatic hydrocarbon at temperatures around 400°C is of considerable interest. Related to this reaction, but at higher temperatures, is the direct formation of benzene from methane in the presence of these catalysts. Controversy exists in the literature on the former reaction, and ^{13}C isotope studies are being used to resolve the question.

The interest in this reaction arises because the utilisation of methane, in the form of natural gas, in place of hydrogen for direct coal liquefaction would have major economic advantage. For this reason the ability of methane to methylate aromatic compounds, which are considered to be models for coal, is being studied.

Isotope studies in this area have contributed significantly to an understanding of the methylation reactions. The paper describes experiments utilising methane-^{13}C, which show that methylation of aromatics such as naphthalene by the methane^{13}C is catalysed by microporous, Cu-exchanged SAPO-5, at elevated pressures (6.8 MPa) and temperatures around 400°C. The mass spectrometric analysis and n.m.r. study of the isotopic composition of the products of the methylation reaction demonstrate unequivocally that methane provides the additional carbon atom for the methylated products. Thermodynamic calculations predict that the reaction is favourable ag high methane pressures under these experimental conditions. The mechanism as suggested by the isotope study is discussed.

The catalysts which show activity for the activation of methane for direct methylation of organic compounds, such as naphthalene, toluene, phenol and pyrene, are substituted aluminophosphate molecular sieves, ElAPO-5 (where El=Pb, Cu, Ni and Si) and a number of metal substituted zeolites. Our earlier tritium studies had shown that these catalysts will activate alkanes, at least as far as isotope hydrogen exchange reactions are concerned.

Excitation Functions of Deuteron Induced Nuclear Reactions on ^{nat}Mo up to 21MeV : an Alternative Route for the Production of ^{94m,99m}Tc and ^{99}Mo.

M.SONCK[1]*, S.TAKÁCS[2], F.SZELECSÉNYI[2], A.HERMANNE[1] and F.TÁRKÁNYI[2]

[1]Vrije Universiteit Brussel, Cyclotron Department, Laarbeeklaan 103, 1090 Brussel, Belgium
[2]Institute of Nuclear Research of Hungarian Academy of Sciences, 4001 Debrecen, Hungary
*Aspirant Fonds voor Wetenschappelijk Onderzoek (FWO), 1000 Brussel, Belgium

SUMMARY. Cross sections of deuteron induced nuclear reactions on natural molybdenum have been studied in the frame of a systematic investigation of charged particle induced nuclear reactions on metals for different applications. The excitation functions of ^{92m,95}Nb-, ^{93,94g,94m,95g,95m,96,99m}Tc- and ^{99}Mo were measured up to 21MeV deuteron energy by using stacked foil technique and activation method. The goal of this work was to find which of the reactions can be recommended for monitoring the performance of deuteron beams and to study the production possibility of the medical important ^{94m,99m}Tc- and ^{99}Mo-nuclides. Production of ^{99m}Tc and ^{99}Mo is of importance for their use in nuclear medicine, whereas ^{94m}Tc is of interest regarding quantification of kinetics of well-established ^{99m}Tc-radiopharmaceuticals (see e.g. Denzler et al. (1)).

1. INTRODUCTION

The importance of ^{99m}Tc for nuclear medicine is well known, with almost 90% of the nuclear medicine studies utilising this nuclide. Currently ^{99m}Tc is produced through the mother isotope ^{99}Mo which is a fission product with $T_{1/2}$=66h. Today's world's need of ^{99}Mo is produced in a small number of research reactors which have been in operation for a considerable time and are due for refurbishment or decommissioning. Although at present there is still an overproduction capacity, future problems with the availability of ^{99}Mo can be expected if no new dedicated reactors are licensed rapidly. This leads to a search for alternative production techniques for ^{99m}Tc of which direct cyclotron production and indirect production by cyclotron-driven subcritical assemblies are the most important ones. In this paper we will focus on the possibilities of direct production by deuteron beams of ^{99m}Tc as well as the possible use for beam monitoring of the many other nuclides induced in ^{nat}Mo.

2. EXPERIMENT

Irradiations were carried out with the external beams of the VUB CGR 560 and the ATOMKI MGC 20E cyclotron. Stacks containing up to 16 foils of 12μm thick ^{nat}Mo foils (Goodfellow-99.9% purity) were irradiated for about 1 hour with 200nA deuteron beams of 10, 16 and 21MeV primary energies. The beam current was kept constant during each irradiation and was measured in a Faraday-cup. The target holder was equipped with a special "long" collimator and a secondary electron suppressor. The irradiation set-up, the experimental technique, data acquisition and data evaluation were the same or similar as described earlier by us (2, 3). The initial energy of the particles was determined with an accuracy of ±0.3MeV by time-of-flight method at the Brussels cyclotron (3) and ±0.2MeV by an analysing magnet for irradiations in Debrecen. The effective "on target" energy for each foil was determined using the energy-range formula and tables of Andersen and Ziegler (4). The activity of the irradiated foils was measured without chemical separation by high resolution gamma-ray spectrometry. The decay of the activity of the samples was followed by measuring each sample several times. All given cross sections are production cross sections and are hence calculated for ^{nat}Mo. The decay data of the investigated isotopes and the Q-values of the contributing processes were taken from Browne

et al. (5). The average error on the cross section values varies from 10% to 15% and was obtained by quadratic summation of the individual errors.

3. RESULTS AND DISCUSSION

When bombarding ^{nat}Mo with deuteron beams up to 21MeV, several reaction processes are taking place and contribute to the simultaneous formation of the γ-emitting ^{92m,95}Nb-, ^{93,94g,94m,95g,95m,96,99m}Tc- and ^{99}Mo-nuclides. Some of these reactions are measured for the first time and all are measured here for the first time up to 21MeV. This paper will concentrate on the production routes for ^{99m}Tc ($T_{1/2}$=6.01h), ^{99}Mo ($T_{1/2}$=2.75d) and ^{94m}Tc ($T_{1/2}$=52min) and on the possibilities of monitoring deuteron beams by threshold reactions induced in Mo. Only a very limited number of reference curves were found in literature, all limited to 13MeV deuteron energy. In the overlapping energy regions our data are mostly in good agreement with the available literature data.

3.1 ^{92m}Nb ($T_{1/2}$=10.15d)

The results obtained for the formation of ^{92m}Nb are shown in Figure 1. The pictured cross section values were calculated from a spectroscopic analysis performed after a rather long cooling time (>30 days). The 99.0% abundant 934.5keV γ-line was used to characterise this nuclide.

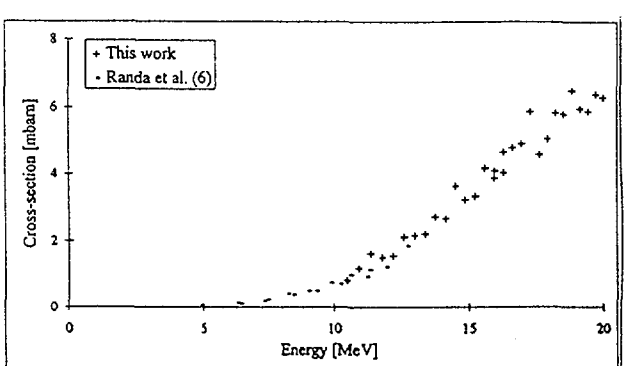

Figure 1 Cross section for ^{nat}Mo(d,x)^{92m}Nb.

The only reference found in literature with respect to this excitation curve, published by Randa et al. (6), is in good agreement with our results. Our measurements show a nearly linear behaviour in the observed energy range and the cross section reaches 7mbarn at 20MeV deuteron energy. The contributing reactions in this energy region are ^{94}Mo(d,x) (mainly ^{94}Mo(d,α) with Q=+8.6MeV), ^{95}Mo(d,x) (mainly ^{95}Mo(d,αn) with Q=+1.2MeV), ^{92}Mo(d,2p) with Q=-1.9MeV, ^{96}Mo(d,x) (mainly ^{96}Mo(d,α2n) with Q=-7.9MeV) and ^{97}Mo(d,x) (mainly ^{97}Mo(d,α3n) with Q=-14.7MeV).

As no cross section extremum is reached in the observed energy band, the excitation function of this reaction does not allow monitoring of deuteron beams without independent energy calibration of the beams. Furthermore additional and independent measurements are needed for this purpose.

3.2 ^{95}Nb ($T_{1/2}$=34.97d)

As both ^{95g}Tc and ^{95m}Tc (see 3.6 and 3.7) are formed besides ^{95}Nb, as these three nuclides decay finally to ^{95}Mo and as no chemical separation is performed on the irradiated samples, the characteristic γ-lines of ^{95}Nb will be contaminated by contribution from ^{95g}Tc and/or ^{95m}Tc. To solve this a long cooling time (>30 days) was used to allow decay of ^{95g}Tc ($T_{1/2}$=20h). The 765.8keV γ-line was then used in which the only direct contributions are due to ^{95}Nb (99.79%) and ^{95g}Tc (94.0%) and not to ^{95m}Tc. As ^{95m}Tc has several unique characteristic lines (e.g. 582.1keV, 31.4%) and as all directly formed ^{95g}Tc has decayed, the contribution of ^{95g}Tc (resulting from the isomeric decay of ^{95m}Tc) to the 765.8keV line can be calculated, yielding the number of counts resulting from the decay of ^{95}Nb. The results of these calculations are shown in Figure 2.

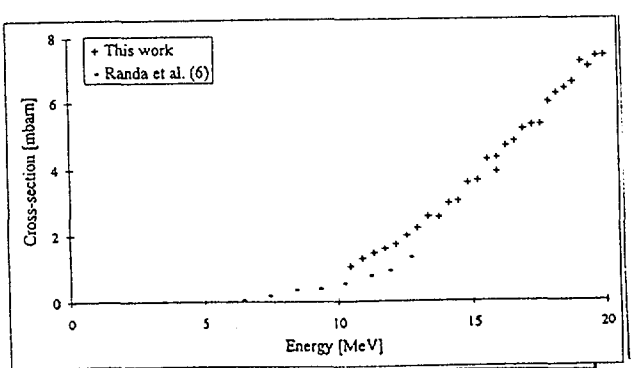

Figure 2 Cross section for ^{nat}Mo(d,x)^{95}Nb.

Like in the previous case only one literature references by Randa et al. (6) could be found for this excitation curve, giving slightly lower cross section values. The main contributing

reactions are ^{97}Mo(d,α) with Q=+10.0MeV, ^{98}Mo(d,αn) with Q=+1.3MeV, ^{95}Mo(d,2p) with Q=-2.4MeV, ^{96}Mo(d,^{3}He) with Q=-3.8MeV and ^{100}Mo(d,α3n) with Q=-12.9MeV. At 20MeV deuteron energy a cross section of 8mbarn is reached after a near linear behaviour.
As no other data on this reaction are available and as no extremum is reached in the studied energy band, monitoring deuteron beams is not possible using this reaction.

3.3 ^{93}Tc ($T_{1/2}$=2.75d)

After total decay of ^{93m}Tc ($T_{1/2}$=43.5min) the results for the production of ^{93}Tc are shown in Figure 3 where the undisturbed 1363.1keV (66%) and the 1477.2keV (9.6%) γ-lines were used to characterise the ^{93}Tc-isotope.

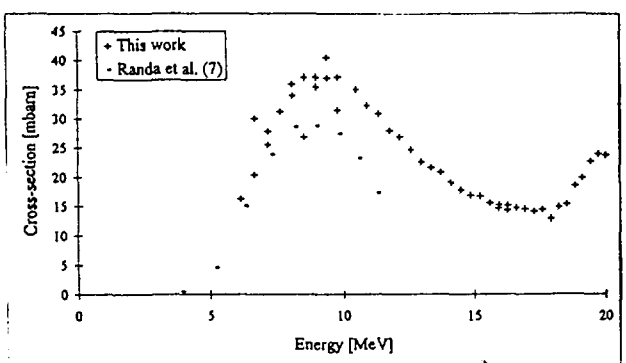

Figure 3 Cross section for ^{nat}Mo(d,x)^{93}Tc.

The 2 contributing reactions which can be clearly observed in Figure 3 are ^{92}Mo(d,n) with Q=+1.9MeV and ^{94}Mo(d,3n) with Q=-15.9MeV.
One reference was found in literature (Randa et al. (7)) giving cross section results for the formation of ^{93g}Tc and ^{93m}Tc by (d,n)-reactions separately. These two production channels were added together appropriately yielding the curve in Figure 3. Our measurements show a higher cross section value for the (d,n)-reaction than those from Randa et al. (7) in the overlapping energy region.
The form of the curve allows its use for deuteron beam monitoring although additional measurements are certainly needed to confirm the current available data.

3.4 ^{94g}Tc ($T_{1/2}$=4.883h)

As ^{94g}Tc has several unique γ-lines (e.g. 916.1keV, 7.6%) and as ^{94m}Tc shows no isomeric transition, the cross section for the production of ^{94g}Tc can be directly calculated from γ-spectrometric analysis after a short cooling time (a couple of hours). Results are shown in Figure 4 where 2 contributing reactions can be observed : ^{94}Mo(d,2n) with Q=-7.3MeV and ^{95}Mo(d,3n) with Q=-14.6MeV. Two sets of literature data were found (Randa et al. (7) and Alexandrov et al. (8)) with results in very good agreement with our data. A cross section value of 100mbarn is reached at 20MeV deuteron energy.
The change in the slope of the excitation curve between 12 and 14MeV allows the use of this reaction for beam monitoring.

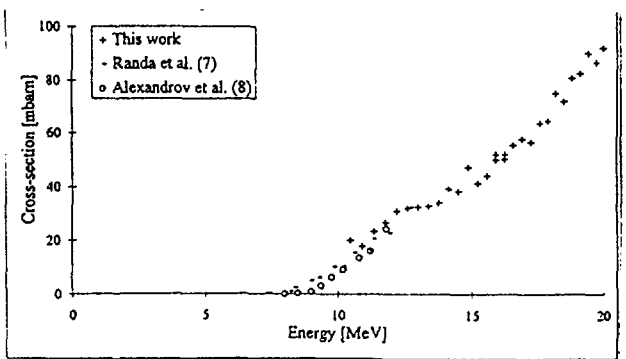

Figure 4 Cross section for ^{nat}Mo(d,x)^{94g}Tc.

3.5 ^{94m}Tc ($T_{1/2}$=52min)

After a short cooling time (1 to 2 hours) the activity of ^{94m}Tc can be calculated from the 871.1keV (94.2%) or the 1521.6keV (4.5%) γ-line. The first line is contaminated with ^{94g}Tc (99.9%), while the second one contains contributions of ^{93}Tc (23.9%). The contributions of both ^{93}Tc and ^{94g}Tc can be calculated based on the presence of their unique lines (see 3.3 and 3.4), the abundance of the different lines and the detector efficiency at these γ-lines. As a result of these correction calculations a larger scatter on the results can be expected as is seen from Figure 5.

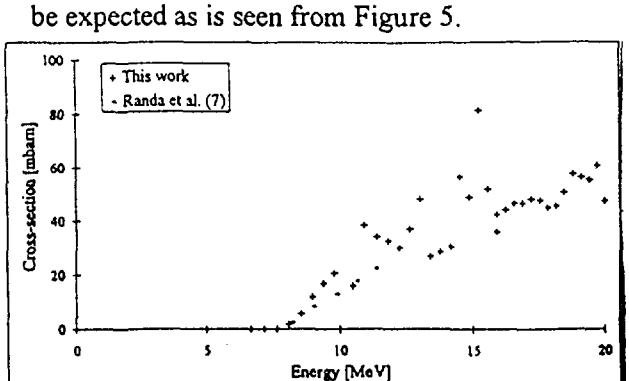

Figure 5 Cross section for ^{nat}Mo(d,x)^{94m}Tc.

The excitation curve (Figure 5) shows two contributing reactions : ^{94}Mo(d,2n) (Q=-7.3MeV) and ^{95}Mo(d,3n) (Q=-14.7MeV), where the (d,2n) reaction on the less abundant ^{94}Mo (9.25%) reaches a maximal cross section value near 16MeV, making this the optimal production path using deuteron induced reactions below 21MeV. From our measured cross section values a yield of 67.5mCi/μAh is calculated for the energy range 12-17MeV. Contamination can be expected through the ^{94}Mo(d,n)^{95g,95m}Tc processes (Figure 6 and 7) and the main contamination arises from ^{95g}Tc ($T_{1/2}$=20h). The data from Alexandrov et al. (7), obtained on partly enriched ^{94}Mo, show that the contribution of ^{94}Mo(d,n) to the total formation of ^{95g}Tc decreases strongly at 12MeV incident deuteron energy where reactions on other Mo-isotopes take over. At the high energy side ^{93}Tc-contamination can occur through the ^{94}Mo(d,3n) process (Q=-15.9MeV) (Figure 3), limiting the incident deuteron energy to 17MeV. Another contaminating nuclide is ^{94g}Tc (Figure 4) with a maximal cross section value derived from our measurements on ^{nat}Mo of 45mbarn, leading to the conclusion that the production of ^{94m}Tc through deuteron induced reactions is only possible with low isotopic purity. The ^{94}Mo(p,n)^{94m}Tc production channel is hence to be preferred both for the resulting purity, as is shown by Rösch et al. (9), as for the total yield according to both Denzler et al. (1) and Rösch et al. (9). The ^{92}Mo(α,2n)^{94}Ru→^{94m}Tc will result in even higher purity, however the total yield for this process is considerably lower based on the results of Denzler et al. (1). Production based on the ^{93}Nb(^{3}He,2n) reaction is not an alternative due to the important isotopic contamination with ^{93g,93m,94g}Tc and due to the rather low yield as shown by Denzler et al. (1).

3.6 ^{95g}Tc ($T_{1/2}$=20.0h)

Figure 6 shows the results of the cross section calculation for the formation of ^{95g}Tc. The results were obtained after a cooling time of 1 to 2 hours and are corrected for the small amount of ^{95g}Tc produced by the isomeric transition ^{95m}Tc→^{95g}Tc.

Contributing reactions are ^{94}Mo(d,n) with Q=+2.7MeV, ^{95}Mo(d,2n) with Q=-4.7MeV and ^{96}Mo(d,3n) with Q=-13.9MeV. Two sets of literature data were found (Randa et al. (7) and Alexandrov et al. (8)). The results of Randa et al. (7) were, like ours, obtained on ^{nat}Mo and both sets are in very good agreement with each other, where as the data of Alexandrov et al. (8) were gathered on partly enriched ^{94}Mo and hence only include the ^{94}Mo(d,n)-reaction with almost no contribution from the ^{95}Mo(d,2n)-process.

The change in slope of the excitation curve at 12MeV would make this reaction suitable for monitoring deuteron beams. However extra measurements are still needed to confirm the current available data.

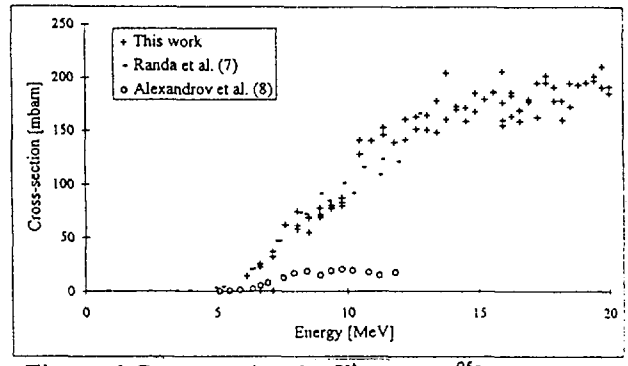

Figure 6 Cross section for ^{nat}Mo(d,x)^{95g}Tc.

3.7 ^{95m}Tc ($T_{1/2}$=61d)

After a long cooling time (>30days) the results shown in Figure 7 were obtained for the formation of ^{95m}Tc. Direct calculation of the cross section is possible from the unique γ-lines of this isotope (e.g. 582.1keV, 31.4%).

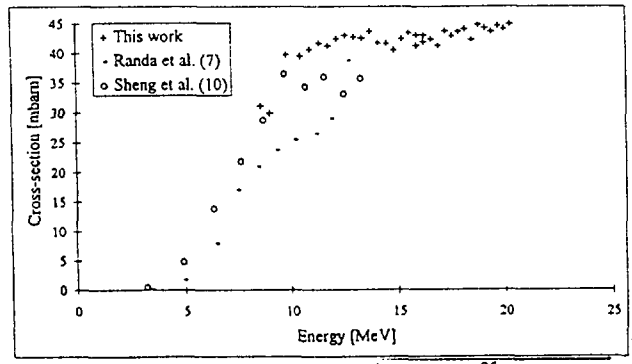

Figure 7 Cross section for ^{nat}Mo(d,x)^{95m}Tc.

Again two sets of literature data were found (Randa et al. (7) and Cheng et al. (10)). Data from Cheng et al. (10) are in agreement with our results although our cross section values tend to be slightly higher. The excitation curve given by Randa et al. (7) has a clearly different

shape although these results were obtained in comparable experimental conditions.
The same contributing reactions as in the ^{95g}Tc case can be observed and due to the change in slope of the curve around 12MeV this reaction can be used for monitoring purposes.

3.8 ^{96}Tc ($T_{1/2}$=4.28d)
After a long cooling time (>30days) the activity of ^{96}Tc can be calculated from the 812.5keV (82%) or the 849.9keV (98%) γ-lines. Results are shown in Figure 8 together with the 2 sets of literature values published by Randa et al. (7) and Cheng et al. (10). Both literature sets are in reasonable good agreement with our data. Contributing reactions are ^{95}Mo(d,n) with Q=+3.2MeV, ^{96}Mo(d,2n) with Q=-6.0MeV and ^{97}Mo(d,3n) with Q=-12.8MeV together with the isomeric transition of ^{96m}Tc. The ^{96m}Tc-nuclide was not found during this study what is probably due to the low γ-abundance in the energy region between 50keV and 2000keV and the rather short half life ($T_{1/2}$=51.5min).

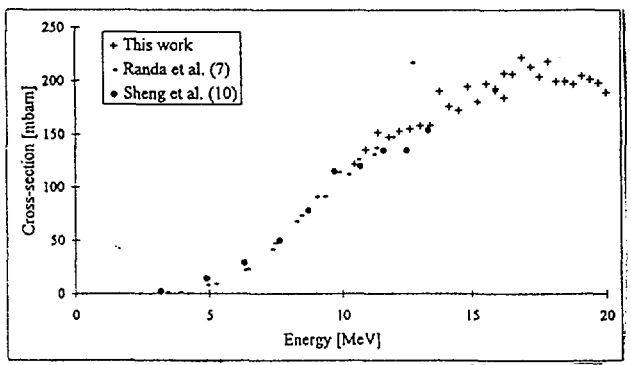

Figure 8 Cross section for ^{nat}Mo(d,x)^{96}Tc.

3.9 ^{99m}Tc (direct formation) ($T_{1/2}$=6.006h)
After a short cooling time (1 to 2 hours) the activation of ^{99m}Tc can be obtained from the 140.5keV (87.2%) γ-line. The fraction due to the directly formed ^{99m}Tc is obtained by subtracting the contribution of the coupled reaction ^{99}Mo→^{99m}Tc.

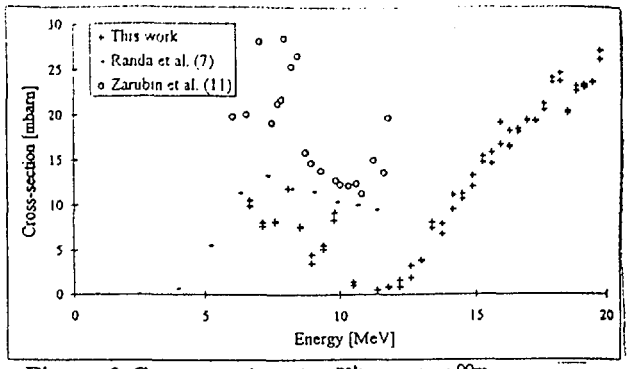

Figure 9 Cross section for ^{nat}Mo(d,x)^{99m}Tc.

In Figure 9 two contributing reactions to the formation of ^{99m}Tc can be observed : ^{98}Mo(d,n) (Q=4.1MeV) and ^{100}Mo(d,3n) (Q=-10.1MeV), showing a maximal cross section value measured on ^{nat}Mo of 16mbarn (at 7MeV), respectively 35mbarn (at 21MeV). The optimal production path for ^{99m}Tc based on deuteron induced reactions is hence the ^{100}Mo(d,3n) process with a maximal cross section $\sigma_{max}\approx$365mbarn in the studied energy interval. Our results are in good agreement with the values reported by both Randa et al. (7) and Zarubin et al. (11) (Figure 9) except for the values at lower energy where the values reported by Zarubin et al. (11) are considerably higher than what is reported by Randa et al. (7) and in this work.

Contaminating nuclides in the ^{100}Mo(d,3n)-process are ^{99}Mo (natural decay to ^{99m}Tc) and short lived nuclides (^{100,101}Tc, ...). From our measured cross section values a direct production yield of 12.4mCi/μAh in the 11-21MeV energy interval is calculated. A larger value is expected for higher incident energies. It can hence be concluded that the direct production of ^{99m}Tc is only economically possible at high energy deuteron beams, but is only practical if daily production facilities are available on site.

3.10 ^{99}Mo ($T_{1/2}$=2.7477d)
When a cooling time of a couple of hours is used, the production of ^{99}Mo can be calculated directly from the 181.1keV (6.07%) or the 739.5keV (12.14%) γ-lines. Results are shown in Figure 10.

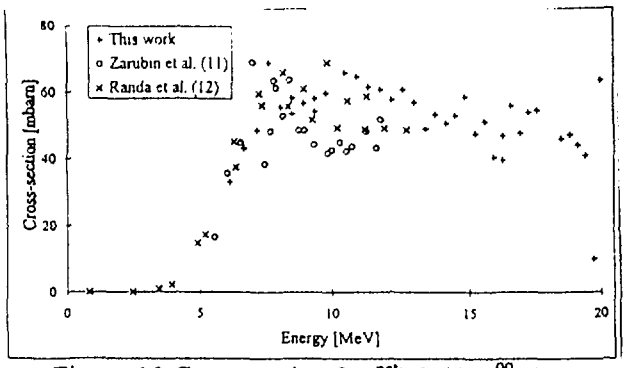

Figure 10 Cross section for $^{nat}Mo(d,x)^{99}Mo$.

Several contributing reactions can be observed : $^{98}Mo(d,p)$ (Q=3.7MeV), $^{100}Mo(d,x)$ and decay from ^{99}Nb formed by $^{100}Mo(d,x)$-processes (Figure 10). The maximal cross section for the $^{98}Mo(d,p)$ reaction is 240mbarn, while we find ≈600mbarn for the $^{100}Mo(d,x)$-reaction, which decreases only slowly with higher deuteron energy due to the contributions of $^{100}Mo(d,t)$ (Q=-2.0MeV), $^{100}Mo(d,dn)$ (Q=-8.3MeV) and $^{100}Mo(d,p2n)$ (Q=-10.5MeV). This reaction can hence be used in a very wide energy band and will be the preferred reaction path. From the point of the radionuclidic purity no real problem is to be expected as all possible contaminating nuclides are naturally removed by decay. Only at higher deuteron energy the production of ^{97m}Tc through a (d,5n) reaction could be a problem, making chemical purification necessary. This reasoning is clearly based on the use of highly enriched ^{100}Mo (+99%), as otherwise numerous contaminating nuclides could be formed in considerable amounts on the other isotopes present.

From the measured cross section values a production yield of 2.5mCi/μAh can be calculated for a 320μm thick target irradiated at 21MeV deuteron energy. Production of a 2Ci generator is hence possible with 8.3h of irradiation time at a current of 100μA on target, making deuteron induced threshold reactions on ^{100}Mo not a real alternative for fission production of ^{99}Mo despite the physical and chemical feasibility.

4. CONCLUSION

In conclusion to the previous discussions we can state that deuteron induced production of $^{94m,99m}Tc$ and ^{99}Mo on Mo-isotopes is no real alternative. ^{94m}Tc can only be produced with low isotopic purity and a rather low yield whereas, according to Rösch et al. (9), proton induced reactions on ^{94}Mo will result in better isotopic purity and higher yield. Direct production of ^{99m}Tc is possible but only at high deuteron energies and is only practical if daily production facilities are available on site. In order to cover the current weekly world need of ^{99}Mo by deuteron induced reactions, over 1000 dedicated accelerators are needed, making the production of ^{99}Mo by deuteron induced reactions on highly enriched ^{100}Mo not a real alternative to the fission production of ^{99}Mo.
The status of the data is still rather poor and only very limited data are currently available. Additional measurements are hence required before using reactions on Mo for monitoring deuteron beams.

References

(1) F.O.Denzler, F.Rösch, S.M.Qaim, Radiochim. Acta, 68, pp. 13, 1995.
(2) F.Tárkányi, F. Szelecsényi, P.Kopecký, J. Appl. Radiat. Isot., 42, pp. 513, 1991.
(3) M.Sonck, J.Van hoyweghen, A.Hermanne, J. Appl. Radiat. Isot., 47, pp. 513, 1996.
(4) H.H.Andersen, J.F.Ziegler, Hydrogen Stopping Powers and Ranges in All Elements, Pergamon Press, 1977.
(5) E.Browne, R.B.Firestone, Table of Radioactive Isotopes, Wiley, 1986.
(6) Z.Randa, K.Svoboda, Int. J. Appl. Rad. Isot., 28, pp. 555, 1977.
(7) Z.Randa, K.Svoboda, J. inorg. Nucl. Chem., 38, pp. 2289, 1976.
(8) J.A.Alexandrov et al., Bull. Russian Ac. Sciences, 39, pp.103, 1975.
(9) F.Rösch, S.M.Qaim, Radiochim. Acta, 62, pp. 115, 1993.
(10) Sheng et al., NST-004, 9008.
(11) P.P.Zarubin et al., Bull. Russian Ac. Sciences, 42, pp.145, 1978.
(12) Z.Randa, K.Svoboda, J. inorg. Nucl. Chem., 39, pp. 2121, 1977.

Isotope Anomalies in Oxygen Isotope Exchange Equilibrium Systems

MASAHIRO KOTAKA
Research Laboratory for Nuclear Reactors, Tokyo Institute of Technology
2-12-1 O-okayama, Meguro-ku, Tokyo 152-8550, Japan

SUMMARY. Equilibrium constants of the oxygen isotope exchange reactions between diatomic oxides were calculated in a wide temperature range on the basis of quantum statistical mechanics. Oxygen isotope separation factors were also calculated about the oxygen isotope exchange equilibrium systems which contained some of the above isotope exchange reactions. Many equilibrium constants and the separation factors showed anomalous mass effects. It can be concluded that some oxygen isotopic exchange equilibria cause the isotope anomalies.

1. INTRODUCTION

It has long been believed that any isotopic exchange equilibria can not produce the isotope anomalies, because isotope effects in isotopic exchange equilibria studied with different isotopes of the same element are a monotonic function of the isotopes' relative mass differences.

Recently, however, anomalous mass effects, which do not fit the above rule of the isotope effects have been found in some equilibrium systems(1 - 8).

The objective of the present work is to shed light on the isotope anomalies and the anomalous mass effects in the oxygen isotope equilibrium systems, according to the calculations of the equilibrium constants for oxygen isotopic exchange reactions between diatomic oxides, and the calculations of the oxygen isotope separation factors between two phases.

2. CALCULATION

An equilibrium constant(K) for an isotopic exchange reaction between diatomic species A and B,

$$A_1 + B_2 = A_2 + B_1 \qquad (1)$$

can be written in terms of the reduced partition function ratios$\{(s_2/s_1)f\}$ for chemical species A and B,

$$K = (s_2/s_1)f[A_2/A_1] \,/\, (s_2/s_1)f[B_2/B_1] \qquad (2)$$

where the subscripts 1 and 2 refer to the light and heavy isotopic species, respectively(9).

With the approximations that the vibrational motion is harmonic, that the rotational and translational motions are clasical, and that there is no rotational-vibrational interaction, the reduced partition function can be presented by

$$(s_2/s_1)f = [u_2\exp(-u_2/2)\{1 - \exp(-u_1)\}]/ [u_1\exp(-u_1/2)\{1 - \exp(-u_2)\}] \quad (3)$$

Here $u = h\nu/kT$, where ν refers to a normal mode vibrational frequency, h is Plank's constant, k Boltzmann's constant, and T the absolute temperature.

Equilibrium constants(K65, K67, K68, and K69) of ^{16}O - ^{15}O, ^{16}O - ^{17}O, ^{16}O - ^{18}O, and ^{16}O - ^{19}O oxygen isotopic exchange reactions between diatomic oxides were calculated in a wide temperature range by the equations 2 and 3. The vibrational frequencies used in the calculations were determined on the basis of the force constants which were obtained from the frequencies observed.

An equilibrium constant of isotope exchange reaction is a function of temperature, force constants of the molecules contained in the reaction, and masses of atoms in the molecules, according to the equations 2 and 3. When the equilibrium constants of ^{16}O - ^{17}O, ^{16}O - ^{18}O, and ^{16}O - ^{19}O oxygen isotope exchange reactions between OH and the other diatomic oxide(MO) showed the anomalous mass effects, the force constants of MO were calculated as a function of atomic mass of M in the temperature range 50 - 2000 K by the Newton Raphson method.

Oxygen isotope separation factors S6j(j = 5, 7, 8, 9) between the first phase and the second phase defined in the following equation.

S6j = {(Total amount of ^{1j}O in the second phase) / (Total amount of ^{16}O in the second phase)} / {(Total amount of ^{1j}O in the first phase) / (Total amount of ^{16}O in the first phase)}
; j = 5, 7, 8, 9 (4)

When CO and OH were in the first phase, SiO, AlO, FeO, and MgO were in the second phase, oxygen isotope separation factors(S65, S67, S68, and S69) between the two phases were calculated by the following equation 5, according to the theory of two phase distribution of isotopes(10).

$$S6j = \{X_{SiO}/K6j(SiO) + X_{AlO}/K6j(AlO) + X_{FeO}/K6j(FeO) + X_{MgO}/K6j(MgO)\}/\{X_{OH} + X_{CO}/K6j(CO)\} \quad j = 5, 7, 8, 9 \quad (5)$$

X_{MO} ; Mole fraction of MO in each phase

K6j(MO) ; K6j between OH and MO

3. RESULTS AND DISCUSSION

Many equilibrium constants calculated showed the anomalous mass effects. For example, the equilibrium constants for the oxygen isotope exchange reactions between OH and the diatomic oxides(MO) showed the anomalous mass effects, and had the cross over temperatures and the mass independent fractionation(MIF) temperatures, when M was Li, Na, K, Rb, Be, Mg, Ca, Sr, Ba, Sc, Y, Ti, Zr, V, Cr, Mn, Fe, Co, Ir, Ni, Pt, Cu, Ag, Zn, Al, Ga, In, Ge, Sn, Pb, As, Sb, Bi, Se, Te, F, Cl, Br, I, La, Ce, Pr, Eu, Tb, Lu, Th, and U(47 elements). The force constants of these forty seven diatomic oxides were smaller than that of OH. The cross over temperature is that temperature at which the logarithm of an equilibrium constant changes sign. The MIF temperature is that temperature at which

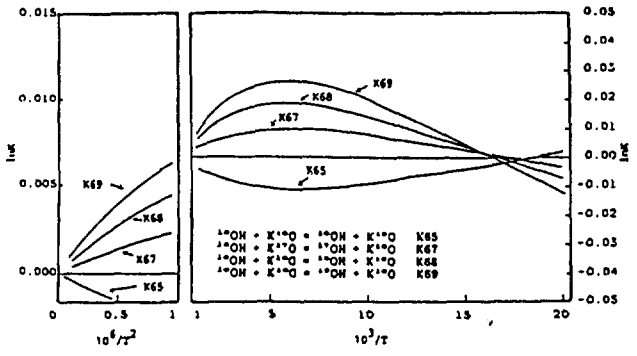

Figure 1 lnK for the Oxygen Isotope Exchange Equlibria $^{16}OH + K^*O = {}^*OH + K^{16}O$ vs. $10^6/T^2$(left), $10^3/T$(right). $^*O = {}^{15}O, {}^{17}O, {}^{18}O, {}^{19}O$

an equilibrium constant is equal to the other one.

Figure 1 shows the temperature dependence of equilibrium constants for the oxygen isotope exchange reactions between OH and KO. The reactions are

$$^{16}OH + K^{15}O = {}^{15}OH + K^{16}O \quad K65$$
$$^{16}OH + K^{17}O = {}^{17}OH + K^{16}O \quad K67$$
$$^{16}OH + K^{18}O = {}^{18}OH + K^{16}O \quad K68$$
$$^{16}OH + K^{19}O = {}^{19}OH + K^{16}O \quad K69$$

For the reactions, there are the cross over and MIF temperatures and three maxima and one minimum of the equilib -rium constants. The cross over temperature increases with the mass of the isotopomer ; lnK67=0 at 57.8K and lnK68= 0 at 59.3K. The curves for lnK67, lnK68, and lnK69 cross one another above the cross over temperatures. The value of ln K67 is equal to that of lnK68 at 60.9K Below this temperature lnK67 is larger than lnK68. The value of logarithm of equilibrium constant at the maximum increases with the mass difference between the isotopes in the exchange reaction.

We have also studied the mass dependence of oxygen isotope exchange equilibria between OH and eleven diatomic oxides (BO, CO, NO, O_2, SiO, PO, SO, NbO, HfO, TaO, and WO) whose force constants were larger than that of OH. These equilibria showed no anomalous mass effects. The heavy oxygen isotope concentrated in the eleven diatomic oxides in preference to OH at all temperatures.

When the equilibrium constants of $^{16}O - {}^{17}O$, $^{16}O - {}^{18}O$, and $^{16}O - {}^{19}O$ oxygen isotope exchange reactions between OH and the other diatomic oxide (MO) showed the anomalous mass effects, the force constants of M-O were calculated as a function of atomic mass of M and temperature. As the result we found the following. The M-O force constant depended on the atomic mass of M, particulary below mass 20. The force constant increased with decreasing the atomic mass of M. The cross over and MIF temperatures increased with the force constant.

We have studied the oxygen isotope separation factors(S65, S67, S68, and S69) between the first phase(OH and CO) and the second phase(SiO, AlO, FeO, and MgO) as a function of temperature and the mole fractions of OH and CO, the mole fractions of four oxides in the second phase being kept constant at 0.25, respectively. The results are given in Figure 2. For the separation factors, there are cross over temperatures, MIF temperatures, maxima, and minima, when the mole fraction of OH is 1.00, 0.60, or 0.50. The cross over temperature of a separation factor is that temperature at which the logarithm of a separation

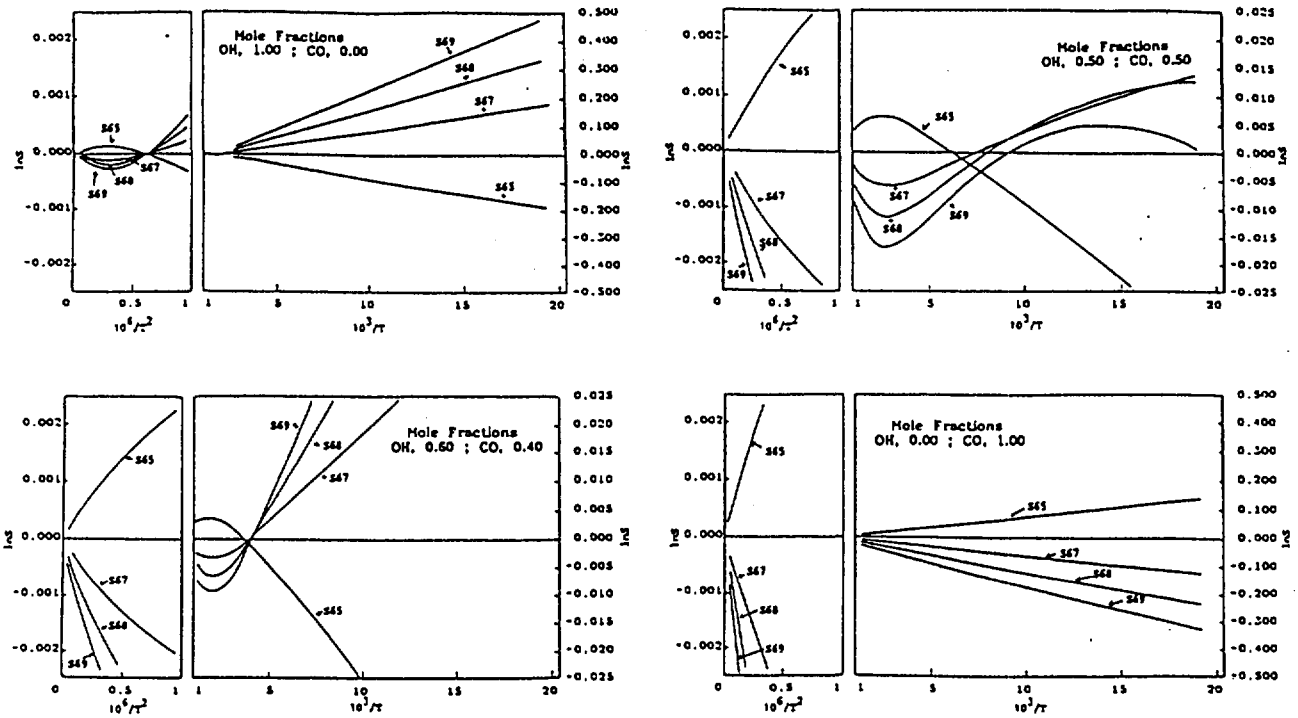

Figure 2 Logarithms of Oxygen Isotope Separation Factors between First Phase(OH and CO) and Second Phase(SiO, AlO,FeO, and MgO) vs. $10^6/T^2$(left), $10^3/T$(right).

The mole fractions of four oxides in the second phase were kept constant at 0.25.

factor changes sign. The MIF temperature of a separation factor is that temperature at which a separation factor is equal to the other one. The results are reasonable, because in the two phases there are the oxygen isotope exchange equilibria which have the anomalous mass effects. The temperature dependence of the separation factors widely varies with the mole fraction of OH.

In Figure 3 we plot lnS67 against lnS68 as the mole fraction of OH being 0.5, and then the values of lnS67, lnS68, and the ratios are given in Table 1. The value of lnS68/lnS67 should be 1.885 because the value of lnK68/lnK67 is 1.885, according to the high temperature approximation for the equilibrium constant of isotopic exchange reaction(11). However, the ratios obtained widely varies with temperature. For example, at

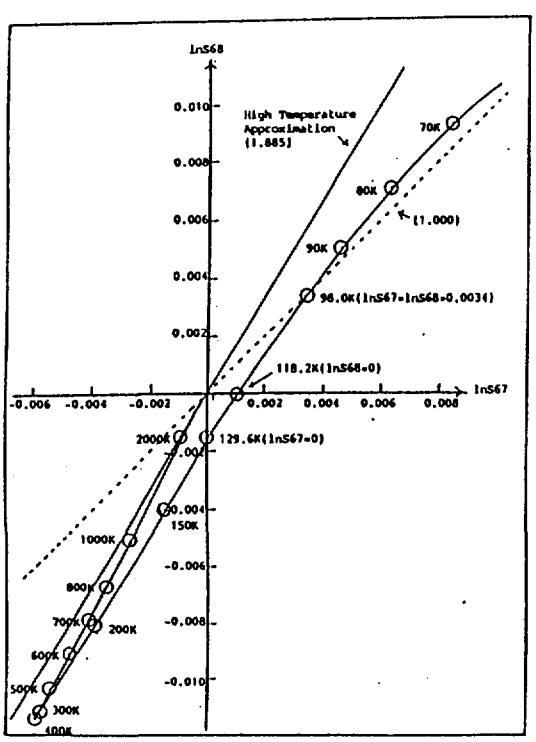

Figure 3 Plot of lnS67 vs. lnS68 for Oxygen Isotope Exchange Equilibrium System between First Phase(OH and CO) and Second Phase (SiO, AlO, FeO, and MgO) The mole fraction of OH was 0.5.

Table 1 Temperature Dependence of lnS67, lnS68, and the Ratio for Oxygen Isotope Exchange Equilibrium System between First Phase(OH and CO)and Second Phase(SiO, AlO, FeO, andMgO) The mole fraction of OH was 0.5.

T(K)	lnS67	lnS68	lnS68/lnS87
50.0	0.0139	0.0127	0.914
60.0	0.0109	0.0114	1.046
80.0	0.0063	0.0071	1.127
98.0	0.0034	0.0034	1.000
118.2	0.0010	0.0000	0.000
129.6	0.0000	-0.0016	--
140.0	-0.0008	-0.0029	3.625
150.0	-0.0015	-0.0040	2.667
300.0	-0.0058	-0.0113	1.948
1000.0	-0.0027	-0.0051	1.889

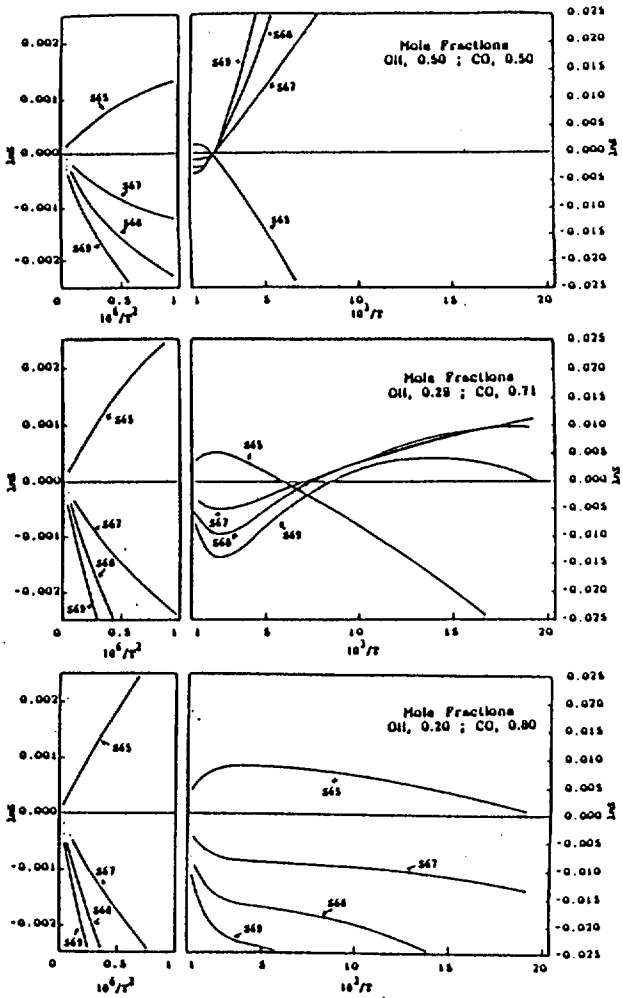

Figure 4 Logarithms of Oxygen Isotope Separation Factors between First Phase (OH and CO) and Second Phase(SiO) vs. $10^6/T^2$(left), $10^3/T$(right).

98.0 K the value of lnS67 is equal to that of lnS68, 0.0034. As a result, both oxygen isotopes ^{17}O and ^{18}O are enriched in the second phase by the same separation factor. In the range below 98.0 K to 50 K the value of lnS67 is almost equal to that of lnS68. Therefore oxygen isotopes^{17}O and ^{18}O are also enriched in the second phase by about the same separation factor in this range. At 129.6 K ^{18}O is enriched in the first phase, whereas ^{17}O is not enriched in both the first phase and the second phase, since the value of lnS68 is -0.0016 and the value of lnS67 is 0.0000. Therefore the oxygen isotope anomalies can occur in the two phases at these temperatures.

When only SiO was in the second phase, and OH and CO were in the first phase, we also studied the oxygen isotope separation factors between the two phases. The results are given in Figure 4. Although there is no oxygen isotopic exchange equilibrium with the anomalous mass effects in the two phases, the oxygen isotope separations have the cross over temperatures, the MIF temperatures, maxima, and minima, when the mole fraction of OH is 0.50 or 0.29.

Whether the oxygen isotopic exchange equilibria in two phases have the cross over temperatures, the MIF temperatures, maxima, and minima, or not, the oxygen isotope separation factors between the two phases show the anomalous mass effects on certain conditions. Therefore the exchange equilibria can produce the oxygen isotope anomalies under the conditions.

4. CONCLUSION

It can be concluded from the results obtained in the present work that some oxygen isotopic exchange equilibria cause the anomalous mass effects, the anomalous oxygen isotope separation factors, and then the oxygen isotope anomalies.

ACKNOWLEDGMENT

The author would like to express his sincere gratitude to Mrs. Sachiyo Kotaka for her encouragement in the present work.

REFERENCES

1) Kotaka M., Okamoto M., and Bigeleisen J., J. Amer. Chem. Soc., 114, 6436 - 6445(1992).
2) Kotaka M. and Bigeleisen J., 9th International Symposium on Nuclear Chemistry, Radiochemistry and Radiation Chemistry, Cuernavaca, Mexico, NR - 15 (1992).
3) Kotaka M. and Bigeleisen J., 37th Symposium on Radiochemistry, 2A15, 68 - 69(1993).
4) Bigeleisen J., J. Amer. Chem. Soc., 118, 3676-3680(1996).
5) Bigeleisen J., Proc. Natl. Acad. USA, 93, 9393 - 9396(1996).
6) Kotaka M., 1996 Annual Meeting of the Geochemical Society of Japan, 4C08 (1996).
7) Kotaka M., 1996 Fall Meeting of the Atomic Energy Society of Japan, J31 (1996).
8) Kotaka M., 18th Grain Formation Workshop, 1 - 4(1996).
9) Bigeleisen J. and Mayer M. G., J. Chem. Phys., 15, 261-267(1947).
10) Kakihana H., Takahashi K., and Yato Y., J. Nucl. Sci. Tech., 5, 93-97(1968).
11) Bigeleisen J., Proceedings of the International Symposium on Isotope Separation, North - Holland Publishing Co., Amsterdam, 121-157(1958).

Application of 1-(3,4-dimethylphenyl)-dodecanedione-1,2-dioxime (MFDDO) to Substoichiometric Extraction and Determination of Nickel (II) by the Isotope Dilution Method.

ZBIGNIEW GÓRSKI, WIESŁAW GORĄCZKO

Radio- and Photo-chemistry Department
Technical University of Poznań, Poland
Email: ZGORSKI@SOL.PUT.POZNAN.PL

SUMMARY. The conditions of MFDDO in toluene solution for substoichiometric extraction of nickek(II) from aqueous phase are described. This procedure allows the determination of 0.03-60 μg/mL of nickel(II) in 1 mL samples by the isotope dilution of $^{63}Ni(II)$, to within ± 2 to ± 0.2 % standard error, respectively.

1.INTRODUCTION

Investigations of the physicochemistry and analytical applicatins of new oxime derivatives synthesized in our Institute (1-5) have disclosed that those derived from 1-(3,4-dimethylphenyl)-dodecanedione-1,2-dioxime (fig.1)form very stable chelates with nickel(II).

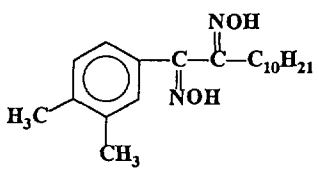

MFDDO

Fig.1. 1-(3,4-dimethlphenyl)-dodecanedione-1,2 dioxime

The stable nickel chelates are composed of one nickel cation and two ligand molecules.

$$Ni^{2+} + 2MFDDO \rightarrow 2H^{+} + Ni(MFDDO)_2$$

Non-aqueous solutions containing these oximes in excess appeared to be useful for extraction of trace amounts of nickel(II) from an aqueous phase for subsequent determination of this metal by electrothermal atomic absorption (4). The results encouraged us to extend the investigations to extraction conditions in which not the extractant, but the metal in question remained in a stoichiometric excess. Such a substoichiometric extraction procedure would make possible the determination of nickel(II) by isotope dilution (6,7). The purpose of the present study was to find proper conditions under which a constant amount of nickel(II) could be transferred to the organic phase by a given volume of dilute MFDDO solution.

2.EXPERIMENTAL

The experiments were designed to investigate the effects of the concentration and proportion of ammonium and codium hydroxides in the

aqueous phase upon the efficiency and kinetics of extraction of small quantities (0.03-60μg/mL) of nickel(II).

MATERIALS

MFDDO was synthesized in our Institute as described previously (4). It was then dissolved in toluene to obtain 10^{-6} to 4×10^{-4} M extracting solutions which were used throughout the study. Radioactive $^{63}NiCl_2$, specific activity 25-370 GBq/g Ni and of 99.9% radiochemical purity, was purchased from the Polish Nuclear Research Center in Swierk. Non-radioactive nickel(II) chloride, nitric acid and sodium hydroxide were Suprapur reagents from E. Merck, Germany. Hydrochloric acid, ammonium hydroxide, toluene and methanol, of the A. R.-grade (POCH, Poland), were additionally purified by distillation prior to use. All aqueos solutions were prepared using double-distilled and deionized water. The scintillattion coctail was prepared by dissolving 4.8 g 2,5-diphenyloxazole (PPO), 0.2 g 1,4-bis-2-(phenyloxazoyl)-benzene (POPOP) and 4 g silica gel AEROSIL™ per liter of toluene. The both scintillators was purchased from J. T. Baker Chem. Co., U.S.A.

EQUIPMENT

The extractions were performed in 20 mL glass or polyethylene vials with Teflon-sealed caps, which were shaken mechanically by the Premed Medical Shaker, typ 327 (Premed, Poland). All vials and glassware were prewashed befor use with nitric and hydrochloric acids followed by extensive rinsing with water of the highest purity grade. Radioactivity of ^{63}Ni was measured by means of liquid scintillation counting in the Beckman LS-100C (U.S.A.) counter, within the $^{3}H + {}^{14}C$ channel and 1% 2δ counting error.

METHOD

Figure 2 shows idea of the method. Into tuo similor samplees, measured (Y) and standard (Y_s), which contein respectivelly Ni_x and Ni_s of nickel ions is adding the same, well-known quantitie of ^{63}Ni ($X=X_s$). After mixing the same ralne of sample ase mesured. Fromradioactivity ratioo can be calculate the concentration of Ni. Realisation of this idee demands execute the procedure showing on the fig.3. The mathematical equation is correct, when the concentrations both in measured sample and standard sample are equal.The coctail (Peterson and Green(8)) with silica gel Aerosil™ (fig. 4) can be used for measurent radiactivity of solution.. Traditional (Kasprzak and Sunderman(9)) coctail (fig.5.) is not reliable (chargiund during time of measurement).

3.RESULTS

This method has been used for measurement of Ni(II) concentration in human urine and blood's serum.

probe	result [ng Ni/cm^3]
human urine	4,2 ± 0,06
human blood's serum	11,7 ± 0,07

Results as an averege been received from 5 independent analysis.

Coufodence intervals: α= 0,99.

Notice: urine and serum from different donors.

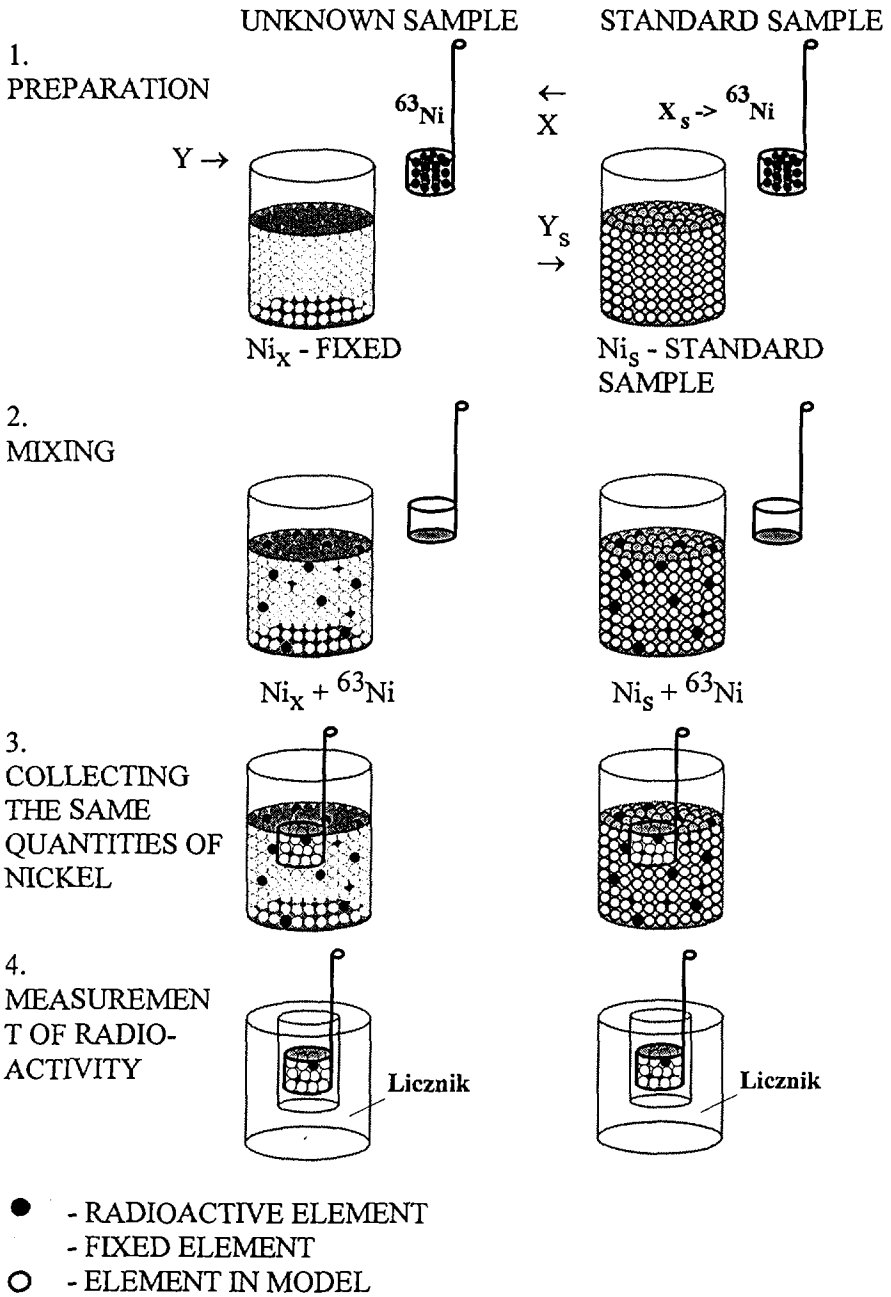

Fig.2. Idea of the method

REALISATION

1-ST STEP.

Mineralisation

to 1 cm^3 of sample add 0,6 cm^3 of mineralisation mixture (HNO_3 + H_2SO_4 + $HClO_4$) , collng to white smolce

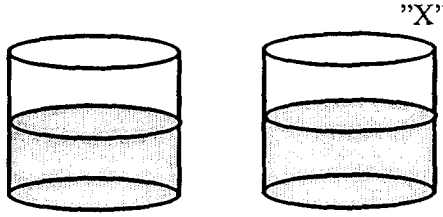

4 to 6 h

SECOND STEP

Fixing

a. Adding 2 cm^3 of $^{63}Ni(FDDO)_2$ solution in hexane and 0,1 cm^3 10M HCl

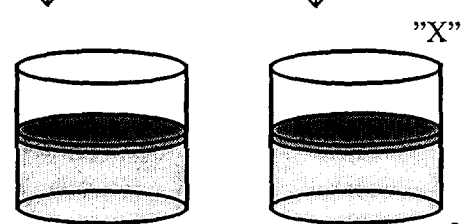

Breaking of complex and dilution

closed and shake 0,5 h

b. Adding 0,2 cm^3 0,7M NH_4OH and 0.3 cm^3 11,7M NaOH

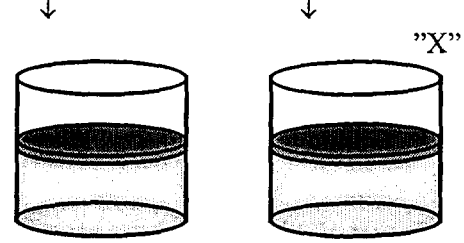

Complex Re-creating after dilution

closed and shake 0,5 h

c. collecting and measurement of radioactivity of 0.1 cm^3 $^*Ni(FDDO)_2$ solution

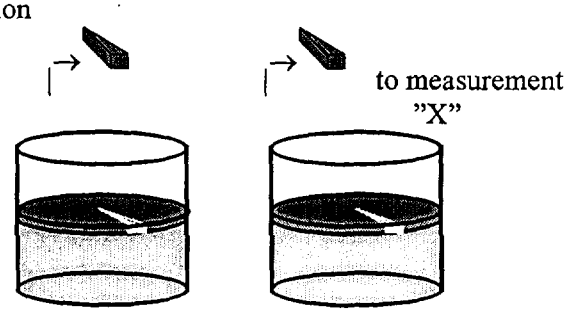

d. result calculating

$$Y_x = Y_s * a_x/a_s$$

Fig.3. Realisation of the method MFDDO.

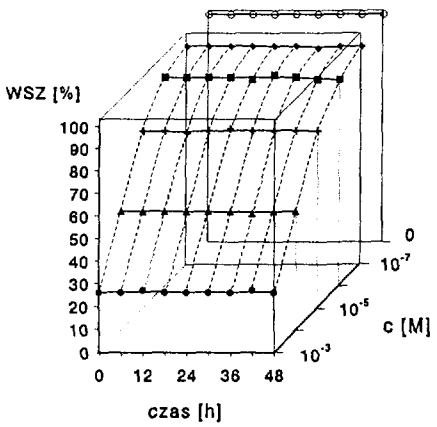

Fig. 4. Counting yield (WSZ) as a function of time adsorption $Ni(FDDO)_2$ for different concentration. Coctail (Peterson and Green[2]) with silica gel (Aerosil™); 4 g PPO, 0.1 g POPOP, 340 cm^3 Triton X-100, 20 g Aerosil ™, per liter of toluene).

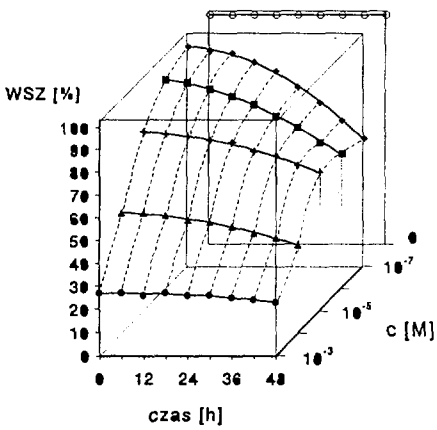

Fig.5. Counting yield (WSZ) as a function of time adsorption $Ni(FDDO)_2$ for different concentration. Traditional (Kasprzak and Sunderman[1]) coctail; 6 g PPO, 0.2 g POPOP per liter of toluene .

4. REFERENCES

1. Kiciak S. **Chem. Anal.** Warsaw 23, 384 (1978).
2. Kiciak S. **Chem. Anal.** Warsaw 23, 615 (1978).
3. Lewandowski A., Kostański M. And Kiciak S. **Chem. Anal.** Warsaw 24, 596 (1979).
4. Kasprzak K. S., Stoeppler M., Górski Z. And Kopczyński T. **Chem. Anal.** Warsaw 27, 115 (1982).
5. Kasprzak K. And Górski Z. **Int. J. Appl. Radiat. Isot.** 34, 1640 (1983).
6. Tölgyessy J., Braun T. And Kyrš M. *Isotope Dilution Analysis* (Akademiai Kiado, Budapest, 1972).
7. Růžička J., Starý J. *Substoichiometry in Radiochemical Analysis* (Pergamon Press, Oxford 1966).
8. Petterson M. S. and Greene R. C. **Anal. Chem.** 37, 854, (1965).
9. K. S. Kasprzak: **Pure Appl. Chem.**, 51, 1375, (1975).

267

An Approach to Peat Formation Period on Both Coast of Fildes Strait, Antarctica

ZHANG WENFEN
CHANGCHUN INSTITUTE OF GEOGRAPHY, CAS, CHANGCHUN 130021, CHINA

SUMMARY: This paper carries out how to use radiocarbon (^{14}C) to study the peat age. The research area of the item is China Great Wall Station in Antarctica and nearby area(both coast of Fildes Strait). We study more than ten ^{14}C samples of Antarctica and contrast with the peat samples of other areas. The authors find out the difference of peat formation period between the pole and other areas.

1. PEAT FORMATION PERIOD ON BOTH COAST OF FILDES STRAIT

This study approaches the peat age on both coast of Fildes Strait, that is Fildes Peninsula at King George Island of South Shetland Islnads, the northern peninsula in Nelson Island and Ardley Island.

Ten wetland peat samples were analyzed. The determined results show that the age of peat at China Great Wall Station located in Fildes Peninsula was 2750symbol 177 \f "Symbol" \s 11±}110 a B.P., the profile was at subsurface 40-42 cm, consists of grey-mud and peat together with big stones. Below the subsurface 37 cm there were nearly peat sandwiched with mud and stone, reflecting that the peat depositing environment at that time was unstable. The sample taken from 26-27 cm in the very profile was peat of freezing layer, the ^{14}C age was 2360symbol 177 \f "Symbol" \s 11±}100 a B.P. It is inferred from peat homogeneity, that the depositing environment at that time was quite stable, The profile's surface plants are *Calliergidium austro-stramineum, Polytrichastrum alpinum*(Hedw.) G. Sm. and *Dreanocladus A.*

The first sample of Ardley Island was taken from 20-32 cm deep, the peat ^{14}C age was 1860symbol 177 \f "Symbol" \s 11±}100 a B.P.. It was a peat layer with small amount of debris, above the peat layer, 14-20 cm was freezing peat, 10-14 cm was yellow-brown peat, 0-10 cm was moss layer, consisting of *Calliergidium austro-stramineum* and *Drepanocladus*. The sampling site was at the highest plane near the east coast, the ground slope was 0-5symbol 176 \f "Symbol" \s 11°} , the profile of 0-7 cm sampled on February 17 had been freezing phase. The sampling site of the second sample in Ardley Island was a gentle slope. The sample taken on February 11 from subsurface 20-35 cm, was freezing peat, the peat ^{14}C was 1630symbol 177 \f "Symbol" \s 11±}130 a B.P., below 35 cm was mineral, 9-20 cm brown humid unfreezing peat, 0-9 cm living moss layer, consisting of *Chorisodontium aciphyllum*(Hook. f. et Wils.) Borth. etc. The wetland in whole Ardley Island is developed well. The proportion of wetland area in Ardley Island is larger than that in Fildes Peninsula and that in the northern peninsula to the north of Nelson ice cap.

The ^{14}C age of Xiangxi peat in Fildes Peninsula is 950symbol 177 \f "Symbol" \s 11±}100 a B.P.. The sampling site was on the upper part of south slope, the slope is 38-40symbol 176 \f "Symbol" \s 11°}, the peat was 13 cm thick, the buried depth was 5-18 cm. The vegetation is *Polytrichastrum alpinum*(Hedw.) G. Sm., *Bartramia patens* Brid, and small amount of *Drepanocladus*, as well as several kinds of lichen.

The sampling site of No.22 sample is comparatively particular, located in the cape of the southmost of Sancha coast along Fildes west coast, about 3000 m from the ice cap, 40 m above sea level, stagnant water 0 cm, the plant is dominated by *Drepanocladus*, 5 cm high, the cover degree is 60 %, the peat is 5 cm thick, under thepeat layer is yellow-brown sand filling between

big stones. Although the peat is only 5 cm thick, the peat ^{14}C age is 260symbol 177 \f "Symbol" \s 11±}100 a B.P.

Among the determination of the peat samples, the deposition ages of 4 peat sites are comparatively new. They are 1) Nelson periglacial brook valley wetland 400 m from Nelson ice cap, 2) wetland on north slope of Nelson Island 1400 m away from Nelson ice cap, 3) seashore wetland of Biology cove 20 m from seashore, 4) Collins periglacial meltwater lakeshore wetland 450-500 m from Collins ice cap.

Although Nelson periglacial valley wetland is 400 m away from Nelson ice cap, there is peat layer in wetland, the buried depth is 5-8 cm, 8-12 cm is weathering matter and debris layer, the peat ^{14}C age is 1.040symbol 177 \f "Symbol" \s 11±}0.11 a B.P., the peat-forming plant is *Calliergon stramineum*(Brid.)Kindb. As to the wetland on north slope of Nelson Island, the slope is 10-20symbol 176 \f "Symbol" \s 11°}, the determined peat depth is 8-10 cm, the ^{14}C age is 1.294symbol 177 \f "Symbol" \s 11±}0.012 a B.P., 10-18 cm is sand and stone, below 18 cm is weathering stone, the maximum section area of the stone is 10cmsymbol 180 \f "Symbol" \s 11×}17 cm and 5 cmsymbol 180 \f "Symbol" \s 11×}6 cm, the peat-forming plant of the wetland is *Drepanocladus* and *Brachythecium subplosum*(Hook. f.et Wils) Jaeg. In seashore wetland of Bilogy cove, the peat develops on black fine sand, the buried depth is 10-12 cm, the ^{14}C age is 1.126symbol 177 \f "Symbol" \s 11±}0.011 a B.P., the peat-forming plant is *Drepanocladus uncinatus*(Hedw.)Warnst. In Collins ice-meltwater lakeshore wetland, the buried depth of the peat is 5-12 cm, below 12 cm is stone, the peat ^{14}C age is 1.049symbol 177 \f "Symbol" \s 11±}0.011 a B.P.. the peat-forming plant is *Calliergon sarmentosum*(Wahlenb.) Kindb. and *Drepanocladus*.

2. ICE AREA DISTRIBUTION OF EARTH SURFACE AND TREND OF PEAT ACCUMULATION AFTER I

2.1 Ice area distribution in polar and sub-polar regions

The wetland distribution in polar and sub-polar regions is closely related to ice melting environment. The present ice cap area in all continents in the Northern Hemisphere corresponds to 7.175% of the maximum ice cap area in glacial epoch, that in the Southern Hemisphere corresponds to 89.182%(1). The first flash deterioration of climate in Antarctica occurred in the end of Eocene epoch (38Ma B.P.)when shallow-water environment appeared between Australia and Antarctica. Antarctic climate began vicious circle, the present climate pattern was formed in the end of the Oligocene Epoch when Deleic Strait formed between South America and Antarctica(23.5 Ma B.P.)(2) and deep-water current of rim-Antarctica formed. From the model of growth and decline of Antarctic ice cap (Payne A J, Sugden D.E et al., 1989), it can be found that the present stable ice cap formed in 6500 a B.P.(3)

2.2 Peat accumulation in the polar and sub-polar regions after ice melting

Global climatic fluctuation is the decisive factor to form concentrative peat-forming period. With the climatic cold-warm fluctuation caused by ice age and interglacial period there appeared a trend that climatic zone on the earth moved towards low latitude and low elevation or towards high latitude and high elevation. At the same time, tectonic change of the earth itself, and continentality had certain interference and change to this trend. Global peat-forming period is basically consistent with sub-interglacial epoch and post-glacial period, corresponding to 1-2(symbol 180 \f "Symbol" \s 11×}10^4) years, while peat-forming sub-period controlled by zonality and regionality only had a year scale of 2-4(symbol 180 \f "Symbol" \s 11×}10^3) years. the analysis of stratum data show that the peat concentrative zone in the Northern Hemisphere is located at the edge of continental ice cap alternation of glacial and interglacial epoch directly controlled peat mire development. This paper only contrast the peat formation ages and rates after ice melting in last glacial period.

From the Late Pleistocene to paleo-holocene(4), with glacier retreaing, peat mire began to develop. From about 11000-12000 a B.P., Minnesota in north America, European part and north of west Siberia of Russia etc. began to lie in ice lake after cap melting, and began organic matter accumulation. In the first turn of the Yellow River on the east edge of the Qinghai-Xizang Planteau, China, there was peat of 12330symbol 177 \f "Symbol" \s 11±}215 a B.P.. At the same time, Harberton bog (lat. 54symbol 176 \f "Symbol" \s 11°} 52symbol 162 \f "Symbol" \s 11′} S, ,long 67symbol 176 \f "Symbol" \s 11°} 53symbol 162 \f "Symbol" \s 11′} W) at the south end of south America began to accumulate organic snady silt from 13000 a B.P.(buried depth was 9.5m). According to the study of Rabassa et al.(5) in the south end of south America in 14670 and 13000 a B.P. warmer climate made *Nothofagus* forest quickly develop. This kind of forest expasion was from the maximum edge in last glacial epoch to ice retreating zone, in 11500 a B.P. and 11200 a B.P. the climate got colder, the forest retreated, tundra expanded (nearly in 11000-10500 a B.P.).

From the Early Holocene to the Middle Holocene was the flourishing period of peat mire development. In the Early to Middle Holocene(10000-3000 a B.P.) temperature was higher, especially in Atlantic period(7500-5000 aB.P.) with high temperature and humid climate, peat mire widely developed, for example, paludification occurred commonly near 70symbol 176 \f "Symbol" \s 11°} N. In England low-land peat accumulation began from 7000 a B.P., high-land peat began to accumulate from 5000 a B.P. After glacier retreat of northwest Europe in Province of North Karelia (61symbol 176 \f "Symbol" \s 11°} 45symbol 162 \f "Symbol" \s 11′} -63symbol 176 \f "Symbol" \s 11°} 55symbol 162 \f "Symbol" \s 11′} N, 28symbol 176 \f "Symbol" \s 11°} 15symbol 162 \f "Symbol" \s 11′}-31symbol 176 \f "Symbol" \s 11°} 35symbol 162 \f "Symbol" \s 11′} E) large-scale paludification occurred on vast low-land. In pre-boreal period(about 10000-8000 a B.P.) peat accumulated quickly and eutrophic fen prevailed. In sub-boreal period (5000-2500 a B.P.), paludification increased again and

developed towards high bog. Patvinsuo peat in east Finland began to form in *Betula-Pinus* period(9000-8000 a B.P.), the mire vegetation grew on the earth after ice cap melting. In 5500 a B.P. spruce invaded Piipsanneva(64symbol 176 \f "Symbol" \s 11°} 20symbol 162 \f "Symbol" \s 11'} N) peatland in west Finland formed about 7000 a B.P. the deepest peat was 4.9 m, main types were *Carex* peat and *Sphagnum* peat, ash content was only 2%-6%. The northern part of European section and west Siberia area in Russia, moss peat, herb-moss peat and wood-herb peat developed in pre-boreal period and boreal period(9800-7700a B.P.). In Atlantic period and subboreal period(7700-2500 a B.P.) in the Middle Holocene, weak decomposed *Sphagnum fuseum* peat developed, the accumulation thickness was 1.8 m (0.2 limiting layer and 1.6 m weak decomposed layer) in northwestern part of European section in Russia, the accumulation rate was 0.346 mm/a, in west Seberia, there was 2-4.5-m weak decomposed *Sphagnum fuseum* peat, the accumulation rate was 0.625 mm/a.

Over the past 5000 years, North America peatlands have rapidly developed under the influence of a variety of climatic, biotic and geologic factors. They are commonly found in a wide range of environments including the polar tundra regions of the upper latitudes; boreal forest and humid temperate prairie regions of the mid-and upper mid-latitudes; coastal areas of the Atlantic and North Pacific Oceans; sub-tropical savanna areas of the Southeast United States; and Alpine settings throughout mountainous Canada and the United States. Rates of peat accumulation vary according to environmental conditions during peat formation. It is estimated that the average rate of peat accumualtion is 0.6-0.7 mm/a for Canadian peatlands and 0.3-0.4 mm/a for the United States's peatlands(6).

During the period of the Early Holocene, South America climate got drier and warmer than the present, peat developed in alternative zone of forest and steppe , detritus peat, except volcanic and sandwich, nearly successively accumulated, the accumulation rate was 0.865 mm/a.

Over sub-Atlantic period (2500-) of the Late Holocene, in Province of North Karelia, fen developed towards high bog. Patvinsuo wetland *Sphagnum* mostly began to grow about 2500 a B.P.. At the same time, in western part of European section and west Seberia in Russia, *Sphagnum fuseum* developed well, the accumulation thickness was 1.25-1.5 m and 3-3.5m, the accumulation rate was 0.55 mm/a and 1.3mm/a, respectively.(4)

Towards the Late Holocene, the climate moved to cooler and wetter conditions, permiting the development of closed forest environments and the accumulation of *Sphagnum* peat in shallow depressions and small pond and lakes. A comparison between palynological sections of forest bogs and steppe bogs indicates that the more arid environments, located farther from the maritime influence , resulted in a slower more recent climatic response to environmental variations, with a time delay of the order of 2000 to 3000 years(4,5).

The mean annual peat accumulation rate has been estimated by Rabassa et al.(5) at 0.5 mm/a, based on the correlation between depth and the radiametric dating of specific layers. Some values show a significant increase in the relationship of accumulation rate with time during the Late Glacial and the Late Holocene. Towards 10000 a B.P., the accumulation rate reached up to 2.0 mm/a, whereas around 3000 a B.P. it varied between 2.0 and 3.0 mm/a.

3. CHARACTERISTICS OF PEAT FORMATION PERIOD ON BOTH COAST OF FILDES STRAIT

Peat is the accumulation of plant residues, the age is its experienced time after it basically stop the exchange with atmosphere, hydrosphere, lithosphere and bioshpere. Because peat mainly consists of organic matter and it is in a relatively closed system nearly without exchange with outside environment, both credibility and comparbility of the peat ^{14} C age are comparatively high. Comparing peat formation period on both coast of Fildes Strait with other areas, the characteristics of the Antarctic peat formation period are summarized as follows:

Antarctic peat began to form in the middle and late periods of the Late Holocene, especially late period, the lag section of peak period of peat formation of warm temperate zone, that is the stage that peat accumulation in the frigid zone was still in peak period. Since the Late Holocene with climate getting cold and wet, in peat accumulation regions in middle latitude after peat accumulation peak period in sub-boreal period(Q_4^2)(5000-2500 a B.P.), peat accumulation peak period began to reduce in sub-Atlantic period (Q_4^3)(2500 aB.P.. According to 121 peat ^{14}C dating of 10 provinces in cold-temperate zone in China, 42.15% of peatland began to accumulate in sub-boreal period, 22.31% in sub-Atlantic period(7). But sub-Atlantic period of the Late Holocene, was an important peat-forming period for sub-frigid and cold-temperate zones, which is proved from the peat accumulation rate of Arctica and Anrarctica mentioned above. ^{14}C ages of 2750 a B.P., 2360 a B.P., 1860 a B.P. and 1630 a B.P. basically occurred between glacial advanced events in 3500 a B.P., 3000 a B.P., 2500 a B.P., 2000 a B.P. in the Northern hemisphere. Comparison of lasting section of little ice age of East Asia, European section of Russia, North America, Arctica and the Southern Hemisphere, which is from Wang Shaowu (1995) can also confirm the basic consistence of the earth ice age. And comparing with research results of Man Zhimin, Zhang Xiugui(11) it can be confirmed that there was a law that peat formation age since 1000 a B.P. in Antarctic region (950 a B.P., 260 a B.P. and some modern carbon) appeared in the period that lasting stage of the Little ice age just ended.

Frontal surface Precipitation formed by meeting of oceanic air-mass of Antarctic nearshore zone and polar air-mass and topographic precipitation formed by moist air-mass carrying from coastline to inland 100 m (1000 a s.l.) due to topography enforcing lift, can make water within air-mass lose 2/3, even to 97%(12). Wetlands can only develop in the regions with allowable heat and water. Therefore, Antarctic peat only limited in nearshore icefree zones with good water supply, temperature enough to plants growth and accumulating residues.

In general, peat accumulation period in Antarctic region is from late period of the Holocene (3000 a B.P.). Peat(modern carbon) accumulation rate of 1.973-3.659 mm/a has certain error influenced by living moss layer, so only for reference. Peat accumulation rate of non-modern carbon is 0.114-0.323 mm/a, the accumulation rayeis lower, the lowest one is smaller than that of 67symbol 176 \f "Symbol" \s 11°} 33symbol 162 \f "Symbol" \s 11'} N. According to Ren Zhenqiu's (1993) prediction of climate on peat development, from present to the end of this century, air temperature will continue to rise, by the year 2020, the winter solstice revolution radius will prolong(960000 km), there will be a trend of climate getting cold in the early 22 century, the climate will get warmer, in the middle 22 century, air temperature will sharply drop. If these temlperature changes do not have an impact on the Antarctic wetland development essentially peat will continuously accumulate.

REFERENCES

1. Li Rushen. Statistic data of physical geography, Beijing Shangwu Press. 1984, p 347.
2. Li Haomin.Early tertiary palaeoclimate of King George island, Antarctica, Antarctic Research, 3(4), 1991, p18-23.
3. Payne A.J. Sugden D.E. Modeling the growth and decay of the Antarctic Peninsula ice sheet. Quaternary Research, 31(2), 1989, p 119-134.
4. Chai Xiu. Peatland. Beijing: Geological Publishing House. 1990, p 154-170.
5. Jorge Rabassa, et al. The peat bogs of Tierra Del Fuego, Argentina. Global Resources, Lappalainen E.(ed.). p 261-266.
6. Thomas J. Malterer. General Review of North American peatland(mires). Global Peat Resources, Lappalainen E.(ed.), p 241-242.
7. Zhang Wenfen. The contrast of period and rate of peat accumulation in cold regions, China. Quaternary Correlation Between South and North China and Globe Change. Guangzhou: Guangdong Higher Education Press. 1993, p 31.
8. De Geer E. H. Skandinavians geokronologi, Geol. Foren. Forhandl., (GFF), 76, Stockholm, 299-329.
9. Bryson R. A., Wendland W.A., Ives J.D. et al. Radiocarbon isochrones on the distintegrataion of the Laurentide ice sheet, Arctic and Alpine Res.(II), Boulder, Colorado, p 1-114.
10. Li Shijie. Evolution of glacier, periglacier and lakes and climatic environment in the Qinghai-Xizang Plateau since last glacial epoch. Quaternary Correlation Between South and North China and Globe Change. Guangzhou: Guangdong Higher Education Press, 1993. p 121-122.
11. Zhang Lansheng. Research on the past life-supporting environment change of China. Beijing: Ocean Press. 1993, p 95-104, 138-146, 169-180.
12. Qin Dahe et al. Distribution law of symbol 100 \f "Symbol" \s 11δD value in 25-cm snow layer in Antarctica. Scientia Sinica (series B) 35(7), 1992, p 768-776.